

AD-A114 831

PURDUE UNIV LAFAYETTE IN SCHOOL OF MECHANICAL ENGINEERING F/G 21/5
EFFECT OF WATER ON AXIAL FLOW COMPRESSORS. PART II. COMPUTATION--ETC(U)
JUN 81 T TSUCHIYA, S N MURTHY F33615-7A-C-2401

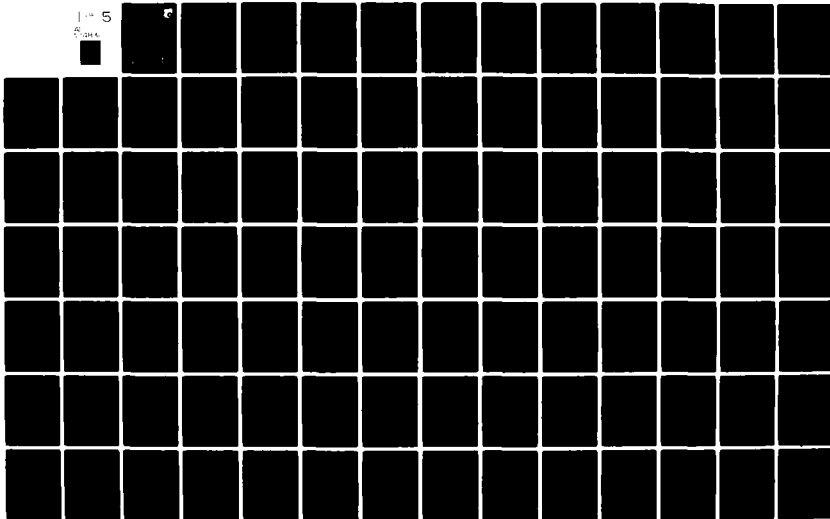
UNCLASSIFIED

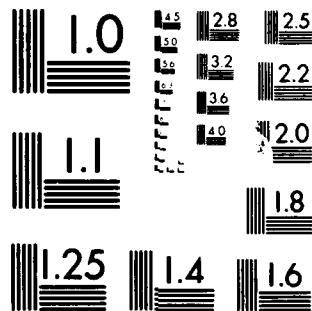
AFWAL-TR-80-2090-PT-2

NL

1-5

5-10





MICROCOPY RESOLUTION TEST CHART
NATIONAL BUREAU OF STANDARDS 1963-A

AFWAL-TR-80-2090



EFFECT OF WATER ON AXIAL FLOW COMPRESSORS

PART II COMPUTATIONAL PROGRAM

AD A114831

T. Tsuchiya
S.N.B. Murthy

Purdue University
School of Mechanical Engineering
West Lafayette, Indiana 47907

June 81

TECHNICAL REPORT AFWAL-TR-80-2090, PART II
Final Report for Period 15 December 1977 - 30 September 1980

DTIC FILE COPY

Approved for public release; distribution unlimited.

AERO PROPULSION LABORATORY
AIR FORCE WRIGHT AERONAUTICAL LABORATORIES
AIR FORCE SYSTEMS COMMAND
WRIGHT-PATTERSON AIR FORCE BASE, OHIO 45433

DTIC
ELECTE
MAY 24 1982
S D E

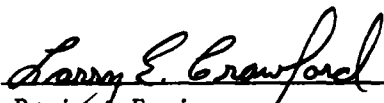
82 05 24 048

NOTICE


When Government drawings, specifications, or other data are used for any purpose other than in connection with a definitely related Government procurement operation, the United States Government thereby incurs no responsibility nor any obligation whatsoever; and the fact that the government may have formulated, furnished, or in any way supplied the said drawings, specifications, or other data, is not to be regarded by implication or otherwise as in any manner licensing the holder or any other person or corporation, or conveying any rights or permission to manufacture use, or sell any patented invention that may in any way be related thereto.

This report has been reviewed by the Office of Public Affairs (ASD/PA) and is releasable to the National Technical Information Service (NTIS). At NTIS, it will be available to the general public, including foreign nations.

This technical report has been reviewed and is approved for publication.

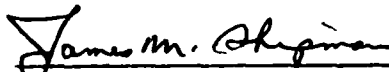


Project Engineer
LARRY E. CRAWFORD
Compressor Research Group



WALKER H. MITCHELL
Chief, Technology Branch

FOR THE COMMANDER



JAMES M. SHIPMAN, MAJOR, USAF
Deputy Director
Turbine Engine Division
Aero Propulsion Laboratory

"If your address has changed, if you wish to be removed from our mailing list, or if the addressee is no longer employed by your organization please notify AFWAL/POTX, W-PAFB, OH 45433 to help us maintain a current mailing list".

Copies of this report should not be returned unless return is required by security considerations, contractual obligations, or notice on a specific document.

Unclassified

SECURITY CLASSIFICATION OF THIS PAGE (When Data Entered)

REPORT DOCUMENTATION PAGE		READ INSTRUCTIONS BEFORE COMPLETING FORM
1. REPORT NUMBER AFWAL-TR-80-2090	2. GOVT ACCESSION NO.	3. RECIPIENT'S CATALOG NUMBER
4. TITLE (and Subtitle) Effect of Water on Axial Flow Compressors Part II Computational Program		5. TYPE OF REPORT & PERIOD COVERED Final Report 1-1-78 - 6-1-81
		6. PERFORMING ORG. REPORT NUMBER
7. AUTHOR(s) T. Tsuchiya and S.N.B. Murthy		8. CONTRACT OR GRANT NUMBER(s) F33615-78-C-2401
9. PERFORMING ORGANIZATION NAME AND ADDRESS Purdue University School of Mechanical Engineering West Lafayette, IN 47907		10. PROGRAM ELEMENT, PROJECT, TASK AREA & WORK UNIT NUMBERS Project 3066 Job Order No. 30660454
11. CONTROLLING OFFICE NAME AND ADDRESS Aero Propulsion Lab. Air Force Wright-Aeronautical Laboratories Air Force Systems Command Wright-Patterson Air Force Base, Ohio		12. REPORT DATE June 1981
14. MONITORING AGENCY NAME & ADDRESS (if different from Controlling Office) NASA-Lewis Research Center 21000 Brookpark Road Cleveland, Ohio 44135		13. NUMBER OF PAGES 264
		15. SECURITY CLASS. (of this report) Unclassified
		15a. DECLASSIFICATION/DOWNGRADING SCHEDULE
16. DISTRIBUTION STATEMENT (of this Report) Approved for Public Release; Distribution Unlimited		
17. DISTRIBUTION STATEMENT (of the abstract entered in Block 20, if different from Report)		
18. SUPPLEMENTARY NOTES		
19. KEY WORDS (Continue on reverse side if necessary and identify by block number) Water Ingestion Propulsion Control Axial Compressors Rain Effects Gas Turbine Engines Flight Control Two-phase Flow Compressor Performance		
20. ABSTRACT (Continue on reverse side if necessary and identify by block number) The subject of air-water mixture flow in axial compressors of jet engines is of practical interest in two contexts of water ingestion: during take-off from rough runways with puddles of water and during flight through rain storms. The change in the compressor performance in turn produces changes in the performance of other components and of the engine as a whole. During the current investigation, (i) an analysis of the effects of water ingestion into a compressor has been carried out leading to the development of a predictive code, the PURDUE-WICSTK program and (ii) a series of tests have been carried		

DD FORM 1 JAN 73 1473

EDITION OF 1 NOV 65 IS OBSOLETE
S/N 0102-LF-014-6601

Unclassified

SECURITY CLASSIFICATION OF THIS PAGE (When Data Entered)

Unclassified

SECURITY CLASSIFICATION OF THIS PAGE (When Data Entered)

7out on a small test compressor with mixtures of gases (containing methane gas to simulate steam) and with air-water droplet mixtures. The experimental results have been compared with predictions. It is concluded that the basic effects of water ingestion into compressors arise through (2) blockage, (b) distortion and (c) heat and mass transfer processes, the changes in blade aerodynamic performance being relatively small. In the case of a compressor of small mass flow and pressure ratio and high operating speed, increased quantities of water ingestion give rise to large quantities of water in the tip region. When the pressure ratio and air mass flow are large and the operating speed is correspondingly small, there arises a possibility of water evaporation, especially towards the hub, which gives rise to changes in gas phase mass flow and temperature. The changes in compressor performance are large at high speeds and high flow rates; there also arises a change in the surge characteristics. In light of the nature of changes produced by water ingestion, a preliminary analysis has been carried out on the possible changes in engine performance.

Accession For	
NTIS GRA&I	<input checked="checked" type="checkbox"/>
DTIC TAB	<input type="checkbox"/>
Unannounced	<input type="checkbox"/>
Justification	
By	
Distribution/	
Availability Codes	
Dist	A



Unclassified

SECURITY CLASSIFICATION OF THIS PAGE (When Data Entered)

FOREWARD

This final report presents the results of research undertaken at Purdue University under Air Force Contract No. F33615-78-C-2401. The effort was sponsored by the Air Force Aero Propulsion Laboratory, Air Force Systems Command, Wright-Patterson Air Force Base, Ohio, under Project/Task/Work Unit 3066/04/54, with Mr Larry E. Crawford, AFAPL/TBC, as Project Engineer. This work was jointly sponsored by NASA-Lewis Research Center, Cleveland, Ohio.

Two earlier publications of direct relevance to the project are as follows:

- i) "Water Ingestion into Axial Flow Compressor", Report No. AFAPL-TR-76-77, August, 1976 and
- ii) "Analysis of Water Ingestion Effects in Axial Flow Compressors", Report No. AFAPL-TR-78-35, June, 1978.

The research reported in the current report pertains to a further development of a prediction code for the performance of an axial compressor with water ingestion, experimental studies on a small engine-driven axial compressor with water ingestion and an analysis of the results.

The final report consists of three parts, Part I entitled Analysis and Predictions, Part II entitled Computational Program and Part III entitled Experimental Results and Discussion. Each part is presented in a separate volume.

Dr Bruce A. Reese, currently Chief Scientist at the Arnold Engineering Development Center, Arnold Air Force Base, who was Professor and Head, School of Aeronautics and Astronautics, Purdue University, up to June 30, 1979, participated in the conduct of research from January, 1978 until June 30, 1979.

The Drive Engine and the Test Compressor provided by the Air Force for the experimental studies under this project were manufactured by the Detroit Diesel Allison of Indianapolis. They refurbished the units during this program under a subcontract. In that work and in a variety of ways, the DDA and several of their personnel have been most helpful and have given their time and advice generously to the investigators.

TABLE OF CONTENTS

PAGE

LIST OF FIGURES - - - - -	ix
LIST OF TABLES - - - - -	xxv
NOMENCLATURE - - - - -	xxvii
SUMMARY - - - - -	xxxix
CHAPTER I: Introduction - - - - -	1
1.1 Objectives and scope of the investigation - - - - -	7
1.2 Effects of water ingestion - - - - -	12
1.3 Implications of models - - - - -	15
1.4 Organization of report - - - - -	17
CHAPTER II: Air-water mixture flow in a compressor - - - - -	19
2.1 Performance parameters - - - - -	19
2.2 Two phase flow aerothermodynamic model for compressors - - - - -	33
2.3 Compressor performance calculation - - - - -	38
2.4 Scaling of compressor performance with two phase flow - - - - -	41
2.5 Engine performance scaling - - - - -	46
CHAPTER III: Models for limiting cases - - - - -	49
3.1 Model for gas mixture flow calculation - - - - -	49
3.2 Model for air-water droplet mixture flow with small droplets - - - - -	50
3.3 Model for air-water droplet mixture flow with large droplets - - - - -	55
3.4 Model for air-water droplet mixture flow with instantaneous evaporation of water - - - - -	59

TABLE OF CONTENTS (continued)

	<u>PAGE</u>
CHAPTER IV: Analytical results for Test Axial Flow Compressor- -	61
4.1 Predicted performance with air-methane mixture- - - - -	62
4.2 Predicted performance with small droplets- - - - -	65
4.3 Performance prediction with large droplets - - - - -	69
4.4 Performance prediction with local injection and instantaneous evaporation of water - - - - -	73
4.5 Predicted performance with air-water droplet mixture flow with evaporation- - - - -	75
4.6 Overall Test Compressor performance- - - - -	77
CHAPTER V: Engine operation with water ingestion- - - - -	81
5.1 Criteria for equilibrium running - - - - -	83
5.2 Gas generator nozzle matching- - - - -	87
5.3 Radial distortion effects- - - - -	89
FIGURES - - - - -	95
APPENDIX 1: Detail of Test Compressor and Drive Engine - - - - -	241
APPENDIX 2: Effective droplet diameter for different processes- - - - -	257
APPENDIX 3: Characteristic Lengths and Times - - - - -	267
APPENDIX 4: Aerothermodynamic equations for two phase flow in compressors- - - - -	285
APPENDIX 5: Modification of UD-0300 Program Code - - - - -	327
APPENDIX 6: Calculation procedure for air-methane mixture- - - - -	333
APPENDIX 7: Performance calculation procedure for air-water mixture flow with small droplets - - - - -	341

TABLE OF CONTENTS (concluded)

	<u>PAGE</u>
APPENDIX 8: Performance calculation procedure for air-water mixture flow with large droplets - - - - -	361
APPENDIX 9: Calculation procedure for local injection and instantaneous evaporation of water - - - - -	371
APPENDIX 10: Calculation procedure for air-water droplet mixture flow with evaporation- - - - -	375
APPENDIX 11: Functional expressions for thermo- physical properties- - - - -	377
REFERENCES - - - - -	383

LIST OF FIGURES

<u>Figure</u>	<u>Page</u>
1.1 Droplet Size Distribution in Rain	96
2.1 Acoustic Speed in Droplet-Laden Air Flow.	97
2.2 Local Impingement on Compressor blade	98
2.3 Streamlines (Model for Droplet Motion).	99
2.4 Droplet Radial Location in Rotor.	100
2.5 Critical Weber Number and Stability Number vs. Droplet Diameter.	101
3.1 Model for Motion of Large Droplet	102
4.1.1 Effect of Methane Content on Overall Total Pressure Ratio.	103
4.1.2 Effect of Methane Content on Overall Total Temperature Ratio	104
4.1.3 Effect of Methane Content on Overall Total Adiabatic Efficiency.	105
4.1.4 Effect of Methane Content on Stage Total Pressure Ratio (Stage 1, 2, 3)	106
4.1.5 Effect of Methane Content on Stage Total Pressure Ratio (Stage 4, 5, 6)	107

<u>Figure</u>	<u>Page</u>
4.2.1 Effect of Water Content on Overall Total Pressure Ratio ($D_0 = 20 \mu\text{m}$, $T_{01} = 20^\circ\text{C}$, 100 % Rotor Speed) . . .	108
4.2.2 Effect of Water Content on Overall Adiabatic Efficiency ($D_0 = 20\mu\text{m}$, $T_{01} = 20^\circ\text{C}$, 100 % Rotor Speed)	109
4.2.3 Effect of Water Content on Overall Temperature Rise of Gas Phase and Droplet ($D_0 = 20 \mu\text{m}$, $T_{01} = 20^\circ\text{C}$, 100 % Rotor Speed)	110
4.2.4 Change of Water Content at Tip along Compressor Stages ($D_0 = 20 \mu\text{m}$, $T_{01} = 20^\circ\text{C}$, 100% Rotor Speed). .	111
4.2.5 Temperature Change of Gas Phase and Droplet along Compressor Stages ($D_0 = 20 \mu\text{m}$, $T_{01} = 20^\circ\text{C}$, 100% Rotor Speed)	112
4.2.6 Effect of Water Content on Overall Total Pressure Ratio ($D_0 = 20 \mu\text{m}$, $T_{01} = 20^\circ\text{C}$, 90% Rotor Speed)	113
4.2.7 Effect of Water Content on Overall Adiabatic Efficiency ($D_0 = 20 \mu\text{m}$, $T_{01} = 20^\circ\text{C}$, 90% Rotor Speed)	114
4.2.8 Effect of Water Content on Overall Temperature Rise of Gas Phase and Droplet ($D_{01} = 20 \mu\text{m}$, $T_{01} = 20^\circ\text{C}$, 90% Rotor Speed)	115
4.2.9 Change of Water Content at Tip along Compressor Stages ($D_0 = 20 \mu\text{m}$, $T_{01} = 20^\circ\text{C}$, 90% Rotor Speed) . .	116
4.2.10 Temperature Change of Gas Phase and Droplet along Compressor Stages ($D_0 = 20 \mu\text{m}$, $T_{01} = 20^\circ\text{C}$, 90% Rotor Speed)	117

<u>Figure</u>	<u>Page</u>
4.2.11 Effect of Water Content on Overall Total Pressure Ratio ($D_0 = 20 \mu\text{m}$, $T_{01} = 20^\circ\text{C}$, 80% Rotor Speed)	118
4.2.12 Effect of Water Content on Overall Adiabatic Efficiency ($D_0 = 20 \mu\text{m}$, $T_{01} = 20^\circ\text{C}$, 80% Rotor Speed)	119
4.2.13 Effect of Water Content on Overall Temperature Rise of Gas Phase and Droplet ($D_0 = 20 \mu\text{m}$, $T_{01} = 20^\circ\text{C}$, 80% Rotor Speed)	120
4.2.14 Change of Water Content at Tip along Compressor Stages ($D_0 = 20 \mu\text{m}$, $T_{01} = 20^\circ\text{C}$, 80% Rotor Speed)	121
4.2.15 Temperature Change of Gas Phase and Droplet along Compressor Stages ($D_0 = 20 \mu\text{m}$, $T_{01} = 20^\circ\text{C}$, 80% Rotor Speed)	122
4.2.16 Effect of Water Content on Overall Total Pressure Ratio ($D_0 = 20 \mu\text{m}$, $T_{01} = 40^\circ\text{C}$, 100 % Rotor Speed)	123
4.2.17 Effect of Water Content on Overall Adiabatic Efficiency ($D_0 = 20 \mu\text{m}$, $T_{01} = 40^\circ\text{C}$, 100% Rotor Speed)	124
4.2.18 Effect of Water Content on Overall Temperature Rise of Gas Phase and Droplet ($D_0 = 20 \mu\text{m}$, $T_{01} = 40^\circ\text{C}$, 100% Rotor Speed)	125
4.2.19 Change of Water Content at Tip along Compressor Stages ($D_0 = 20 \mu\text{m}$, $T_{01} = 40^\circ\text{C}$, 100% Rotor Speed)	126

<u>Figure</u>		<u>Page</u>
4.2.20	Temperature change of Gas phase and Droplet along Compressor Stages ($D_0 = 20\mu\text{m}$, $T_{01} = 40^\circ\text{C}$, 100% Rotor Speed)	127
4.2.21	Effect of Water Content on Overall Total Pressure Ratio ($D_0 = 20\mu\text{m}$, $T_{01} = 40^\circ\text{C}$, 90% Rotor Speed)	128
4.2.22	Effect of Water Content on Overall Adiabatic Efficiency ($D_0 = 20\mu\text{m}$, $T_{01} = 40^\circ\text{C}$, 90% Rotor Speed)	129
4.2.23	Effect of Water Content on Overall Temperature Rise of Gas Phase and Droplet ($D_0 = 20\mu\text{m}$, $T_{01} = 40^\circ\text{C}$, 90% Rotor Speed).	130
4.2.24	Change of Water Content at tip along Compressor Stages ($D_0 = 20\mu\text{m}$, $T_{01} = 40^\circ\text{C}$, 90% Rotor Speed).	131
4.2.25	Temperature Change of Gas Phase and Droplet along Compressor Stages ($D_0 = 20\mu\text{m}$, $T_{01} = 40^\circ\text{C}$, 90% Rotor Speed)	132
4.2.26	Effect of Water Content on Overall Total Pressure Ratio ($D_0 = 20\mu\text{m}$, $T_{01} = 40^\circ\text{C}$, 80% Rotor Speed)	133
4.2.27	Effect of Water Content on Overall Adiabatic Efficiency ($D_0 = 20\mu\text{m}$, $T_{01} = 40^\circ\text{C}$, 80% Rotor Speed)	134
4.2.28	Effect of Water Content on Overall Temperature Rise of Gas Phase and Droplet ($D_0 = 20\mu\text{m}$, $T_{01} = 40^\circ\text{C}$, 80% Rotor Speed).	135
4.2.29	Change of Water Content at Tip along Compressor Stages ($D_0 = 20\mu\text{m}$, $T_{01} = 40^\circ\text{C}$, 80% Rotor Speed).	136

<u>Figure</u>		<u>Page</u>
4.2.30	Temperature Change of Gas Phase and Droplet along Compression Stages ($D_0 = 20\mu\text{m}$, $T_{01} = 40^\circ\text{c}$, 80% Rotor Speed).	137
4.3.1	Effect of Water Content on Overall Total Pressure Ratio ($D_0 = 600\mu\text{m}$, $T_{01} = 20^\circ\text{c}$, 100% Rotor Speed)	138
4.3.2	Effect of Water Content on Overall Adiabatic Efficiency ($D_0 = 600\mu\text{m}$, $T_{01} = 20^\circ\text{c}$, 100% Rotor Speed).	139
4.3.3	Effect of Water Content on Overall Temperature Rise of Gas Phase and Droplet ($D_0 = 600\mu\text{m}$, $T_{01} = 20^\circ\text{c}$, 100% Rotor Speed).	140
4.3.4	Change of Water Content at Tip along Compressor Stages ($D_0 = 600\mu\text{m}$, $T_{01} = 20^\circ\text{c}$, 100% Rotor Speed)	141
4.3.5	Temperature Change of Gas Phase and Droplet along Compressor Stages ($D_0 = 600\mu\text{m}$, $T_{01} = 20^\circ\text{c}$, 100% Rotor Speed)	142
4.3.6	Effect of Water Content on Overall Total Pressure Ratio ($D_0 = 600\mu\text{m}$, $T_{01} = 20^\circ\text{c}$, 90% Rotor Speed)	143
4.3.7	Effect of Water Content on Overall Adiabatic Efficiency ($D_0 = 600\mu\text{m}$, $T_{01} = 20^\circ\text{c}$, 90% Rotor Speed).	144
4.3.8	Effect of Water Content on Overall Temperature Rise of Gas Phase and Droplet ($D_0 = 600\mu\text{m}$, $T_{01} = 20^\circ\text{c}$, 90% Rotor Speed).	145
4.3.9	Change of Water Content at Tip along Compressor Stages ($D_0 = 600\mu\text{m}$, $T_{01} = 20^\circ\text{c}$, 90% Rotor Speed).	146

<u>Figure</u>	<u>Page</u>
4.3.10 Temperature Change of Gas Phase and Droplet along Compressor Stages ($D_0 = 600\mu\text{m}$, $T_{01} = 20^\circ\text{c}$, 90% Rotor Speed)	147
4.3.11 Effect of Water Content on Overall Total Pressure Ratio ($D_0 = 600\mu\text{m}$, $T_{01} = 20^\circ\text{c}$, 80% Rotor Speed).	148
4.3.12 Effect of Water Content on Overall Adiabatic Efficiency ($D_0 = 600\mu\text{m}$, $T_{01} = 20^\circ\text{c}$, 80% Rotor Speed)	149
4.3.13 Effect of Water Content on Overall Temperature Rise of Gas Phase and Droplet ($D_0 = 600\mu\text{m}$, $T_{01} = 20^\circ\text{c}$, 80% Rotor Speed)	150
4.3.14 Change of Water Content at Tip along Compressor Stages ($D_0 = 600\mu\text{m}$, $T_{01} = 20^\circ\text{c}$, 80% Rotor Speed)	151
4.3.15 Temperature Change of Gas Phase and Droplet along Compressor Stages ($D_0 = 600\mu\text{m}$, $T_{01} = 20^\circ\text{c}$, 80% Rotor Speed)	152
4.3.16 Effect of Water Content on Overall Total Pressure Ratio ($D_0 = 600\mu\text{m}$, $T_{01} = 40^\circ\text{c}$, 100% Rotor Speed).	153
4.3.17 Effect of Water Content on Overall Adiabatic Efficiency ($D_0 = 600\mu\text{m}$, $T_{01} = 40^\circ\text{c}$, 100% Rotor Speed)	154
4.3.18 Effect of Water Content on Overall Temperature Rise of Gas Phase and Droplet ($D_0 = 600\mu\text{m}$, $T_{01} = 40^\circ\text{c}$, 100% Rotor Speed).	155
4.3.19 Change of Water Content at Tip along Compressor Stages ($D_0 = 600\mu\text{m}$, $T_{01} = 40^\circ\text{c}$, 100% Rotor Speed).	156

<u>Figure</u>		<u>Page</u>
4.3.20	Temperature Change of Gas Phase and Droplet along Compressor Stages ($D_0 = 600\mu\text{m}$, $T_{01} = 40^\circ\text{C}$, 100% Rotor Speed)	157
4.3.21	Effect of Water Content on Overall Total Pressure Ratio ($D_0 = 600\mu\text{m}$, $T_{01} = 40^\circ\text{C}$, 90% Rotor Speed).	158
4.3.22	Effect of Water Content on Overall Adiabatic Efficiency ($D_0 = 600\mu\text{m}$, $T_{01} = 40^\circ\text{C}$, 90% Rotor Speed).	159
4.3.23	Effect of Water Content on Overall Temperature Rise of Gas Phase and Droplet ($D_0 = 600\mu\text{m}$, $T_{01} = 40^\circ\text{C}$, 90% Rotor Speed).	160
4.3.24	Change of Water Content at Tip along Compressor Stages ($D_0 = 600\mu\text{m}$, $T_{01} = 40^\circ\text{C}$, 90% Rotor Speed).	161
4.3.25	Temperature Change of Gas Phase and Droplet along Compressor Stages ($D_0 = 600\mu\text{m}$, $T_{01} = 40^\circ\text{C}$, 90% Rotor Speed).	162
4.3.26	Effect of Water Content on Overall Total Pressure Ratio ($D_0 = 600\mu\text{m}$, $T_{01} = 40^\circ\text{C}$, 80% Rotor Speed).	163
4.3.27	Effect of Water Content on Overall Adiabatic Efficiency ($D_0 = 600\mu\text{m}$, $T_{01} = 40^\circ\text{C}$, 80% Rotor Speed).	164
4.3.28	Effect of Water Content on Overall Temperature Rise of Gas Phase and Droplet ($D_0 = 600\mu\text{m}$, $T_{01} = 40^\circ\text{C}$, 80% Rotor Speed).	165

<u>Figure</u>	<u>Page</u>
4.3.29 Change of Water Content at Tip along Compressor Stages ($D_0 = 600\mu\text{m}$, $T_{01} = 40^\circ\text{C}$, 80% Rotor Speed)	166
4.3.30 Temperature Change of Gas Phase and Droplet along Compressor Stages ($D_0 = 600\mu\text{m}$, $T_{01} = 40^\circ\text{C}$, 80% Rotor Speed)	167
4.4.1 Effect of Location of Evaporation on Overall Total Pressure Ratio (100% Rotor Speed, $T_{01} = 90^\circ\text{C}$)	168
4.4.2 Effect of Location of Evaporation on Overall Adiabatic Efficiency (100% Rotor Speed, $T_{01} = 90^\circ\text{C}$)	169
4.4.3 Effect of Location of Evaporation on Stage Total Pressure Ratio (100% Rotor Speed, $T_{01} = 90^\circ\text{C}$)	170
4.4.4 Effect of Location of Evaporation on Temperature Change along Compressor Stages (100% Rotor Speed, $T_{01} = 90^\circ\text{C}$)	171
4.4.5 Effect of Location of Evaporation on Overall Total Pressure Ratio (90% Rotor Speed, $T_{01} = 90^\circ\text{C}$)	172
4.4.6 Effect of Location of Evaporation on Overall Adiabatic Efficiency (90% Rotor Speed, $T_{01} = 90^\circ\text{C}$)	173
4.4.7 Effect of Location of Evaporation on Stage Total Pressure Ratio (90% Rotor Speed, $T_{01} = 90^\circ\text{C}$)	174
4.4.8 Effect of Location of Evaporation on Temperature Change along Compressor Stages (90% Rotor Speed, $T_{01} = 90^\circ\text{C}$)	175

Figure	Page
4.4.9 Effect of Location of Evaporation on Overall Total Pressure Ratio (80% Rotor Speed, $T_{01} = 90^{\circ}\text{C}$)	176
4.4.10 Effect of Location of Evaporation on Overall Adiabatic Efficiency (80% Rotor Speed, $T_{01} = 90^{\circ}\text{C}$)	177
4.4.11 Effect of Location of Evaporation on Stage Total Pressure Ratio (80% Rotor Speed, $T_{01} = 90^{\circ}\text{C}$)	178
4.4.12 Effect of Location of Evaporation on Temperature Change along Compressor Stages (80% Rotor Speed, $T_{01} = 90^{\circ}\text{C}$)	179
4.4.13 Effect of Location of Evaporation on Overall Total Pressure Ratio (100% Rotor Speed, $T_{01} = 70^{\circ}\text{C}$)	180
4.4.14 Effect of Location of Evaporation on Overall Adiabatic Efficiency (100% Rotor Speed, $T_{01} = 70^{\circ}\text{C}$)	181
4.4.15 Effect of Location of Evaporation on Stage Total Pressure Ratio (100% Rotor Speed, $T_{01} = 70^{\circ}\text{C}$)	182
4.4.16 Effect of Location of Evaporation on Temperature Change along Compressor Stages (100% Rotor Speed, $T_{01} = 70^{\circ}\text{C}$)	183
4.4.17 Effect of Location of Evaporation on Overall Total Pressure Ratio (90% Rotor Speed, $T_{01} = 70^{\circ}\text{C}$)	184
4.4.18 Effect of Location of Evaporation on Overall Adiabatic Efficiency (90% Rotor Speed, $T_{01} = 70^{\circ}\text{C}$)	185

Figure	Page
4.4.19 Effect of Location of Evaporation on Stage Total Pressure Ratio (90% Rotor Speed, $T_{01} = 70^{\circ}\text{C}$)	186
4.4.20 Effect of Location of Evaporation on Temperature Change along Compressor Stages (90% Rotor Speed, $T_{01} = 70^{\circ}\text{C}$)	187
4.4.21 Effect of Location of Evaporation on Overall Total Pressure Ratio (80% Rotor Speed, $T_{01} = 70^{\circ}\text{C}$)	188
4.4.22 Effect of Location of Evaporation on Overall Adiabatic Efficiency (80% Rotor Speed, $T_{01} = 70^{\circ}\text{C}$)	189
4.4.23 Effect of Location of Evaporation on Stage Total Pressure Ratio (80% Rotor Speed, $T_{01} = 70^{\circ}\text{C}$)	190
4.4.24 Effect of Location of Evaporation on Temperature Change along Compressor Stages (80% Rotor Speed, $T_{01} = 70^{\circ}\text{C}$)	191
4.5.1 Effect of Evaporation on Overall Total Pressure Ratio ($T_{01} = 90^{\circ}\text{C}$, $x_{v,o} = 0.025$)	192
4.5.2 Effect of Evaporation on Overall Adiabatic efficiency ($T_{01} = 90^{\circ}\text{C}$, $x_{v,o} = 0.025$)	193
4.5.3 Effect of Evaporation on Temperature Change of Gas Phase and Droplet along Compressor Stages ($T_{01} = 90^{\circ}\text{C}$, $x_{v,o} = 0.025$)	194
4.5.4 Effect of Evaporation on Mass Flow Rate of Liquid Phase at Tip along Compressor Stages ($T_{01} = 90^{\circ}\text{C}$, $x_{v,o} = 0.025$)	195

<u>Figure</u>	<u>Page</u>
4.5.5 Effect of Evaporation on Mass Flow Rate of Gas Phase at Tip along Compressor Stages ($T_{01} = 90^{\circ}\text{C}$, $x_{v,0} = 0.025$	196
4.5.6 Effect of Evaporation on Overall Total Pressure Ratio ($T_{01} = 90^{\circ}\text{C}$, $x_{v,0} = 0.43$).	197
4.5.7 Effect of Evaporation on Overall Adiabatic Efficiency ($T_{01} = 90^{\circ}\text{C}$, $x_{v,0} = 0.43$).	198
4.5.8 Effect of Evaporation on Temperature Change of Gas Phase and Droplet along Compressor Stages ($T_{01} = 90^{\circ}\text{C}$, $x_{v,0} = 0.43$).	199
4.5.9 Effect of Evaporation on Mass Flow Rate of Liquid Phase at Tip along Compressor Stages ($T_{01} = 90^{\circ}\text{C}$, $x_{v,0} = 0.43$)	200
4.5.10 Effect of Evaporation on Mass Flow Rate of Gas Phase at Tip along Compressor Stages ($T_{01} = 90^{\circ}\text{C}$, $x_{v,0} = 0.43$)	201
4.5.11 Effect of Evaporation on Overall Total Pressure Ratio ($T_{01} = 90^{\circ}\text{C}$, $x_{v,0} = 0.55$).	202
4.5.12 Effect of Evaporation on Overall Adiabatic Efficiency ($T_{01} = 90^{\circ}\text{C}$, $x_{v,0} = 0.55$).	203
4.5.13 Effect of Evaporation on Temperature Change of Gas Phase and Droplet along Compressor Stages ($T_{01} = 90^{\circ}\text{C}$, $x_{v,0} = 0.55$).	204
4.5.14 Effect of Evaporation on Mass Flow Rate of Liquid Phase at Tip along Compressor Stages ($T_{01} = 90^{\circ}\text{C}$, $x_{v,0} = 0.55$).	205

<u>Figure</u>		<u>Page</u>
4.5.15	Effect of Evaporation on Mass Flow Rate of Gas Phase at Tip along Compressor Stages ($T_{01} = 90^{\circ}\text{c}$, $x_{v,0} = 0.55$)	206
4.5.16	Effect of Evaporation on Overall Total Pressure Ratio ($T_{01} = 85^{\circ}\text{c}$, $x_{v,0} = 0.43$).	207
4.5.17	Effect of Evaporation on Overall Adiabatic Efficiency ($T_{01} = 85^{\circ}\text{c}$, $x_{v,0} = 0.43$).	208
4.5.18	Effect of Evaporation on Temperature Change of Gas Phase and Droplet along Compressor Stages ($T_{01} = 85^{\circ}\text{c}$, $x_{v,0} = 0.43$)	209
4.5.19	Effect of Evaporation on Mass Flow Rate of Liquid Phase at Tip along Compressor Stages ($T_{01} = 85^{\circ}\text{c}$, $x_{v,0} = 0.43$)	210
4.5.20	Effect of Evaporation on Mass Flow Rate of Gas Phase at Tip along Compressor Stages ($T_{01} = 85^{\circ}\text{c}$, $x_{v,0} = 0.43$)	211
4.6.1	Effect of Water Ingestion on Overall Total Pressure Ratio ($D_0=20\mu\text{m}$, $T_{01} = 20^{\circ}\text{c}$).	212
4.6.2	Effect of Water Ingestion on Overall Temperature Rise of Gas Phase ($D_0= 20\mu\text{m}$, $T_{01} = 20^{\circ}\text{c}$)	213
4.6.3	Effect of Water Ingestion on Overall Temperature Rise of Droplet ($D_0 = 20\mu\text{m}$, $T_{01}= 20^{\circ}\text{c}$)	214
4.6.4	Effect of Water Ingestion on Work Done ($D_0 = 20\mu\text{m}$, $T_{01} = 20^{\circ}\text{c}$).	215

<u>Figure</u>	<u>Page</u>
4.6.5 Effect of Water Ingestion on Overall Total Pressure Ratio ($D_0 = 20\mu\text{m}$, $T_{01} = 40^\circ\text{C}$)	216
4.6.6 Effect of Water Ingestion on Overall Temperature Rise of Gas Phase ($D_0 = 20\mu\text{m}$, $T_{01} = 40^\circ\text{C}$)	217
4.6.7 Effect of Water Ingestion on Overall Temperature Rise of Droplet ($D_0 = 20\mu\text{m}$, $T_{01} = 40^\circ\text{C}$)	218
4.6.8 Effect of Water Ingestion on Work Done ($D_0 = 20\mu\text{m}$, $T_{01} = 40^\circ\text{C}$)	219
4.6.9 Effect of Water Ingestion on Overall Total Pressure Ratio ($D_0 = 600\mu\text{m}$, $T_{01} = 20^\circ\text{C}$)	220
4.6.10 Effect of Water Ingestion on Overall Temperature Rise of Gas Phase ($D_0 = 600\mu\text{m}$, $T_{01} = 20^\circ\text{C}$)	221
4.6.11 Effect of Water Ingestion on Overall Temperature Rise of Droplet ($D_0 = 600\mu\text{m}$, $T_{01} = 20^\circ\text{C}$)	222
4.6.12 Effect of Water Ingestion on Work Done ($D_0 = 600\mu\text{m}$, $T_{01} = 20^\circ\text{C}$)	223
4.6.13 Effect of Water Ingestion on Overall Total Pressure Ratio ($D_0 = 600\mu\text{m}$, $T_{01} = 40^\circ\text{C}$)	224
4.6.14 Effect of Water Ingestion on Overall Temperature Rise of Gas Phase ($D_0 = 600\mu\text{m}$, $T_{01} = 40^\circ\text{C}$)	225
4.6.15 Effect of Water Ingestion on Overall Temperature Rise of Droplet ($D_0 = 600\mu\text{m}$, $T_{01} = 40^\circ\text{C}$)	226

<u>Figure</u>	<u>Page</u>
4.6.16 Effect of Water Ingestion on Work Done ($D_0 = 600\mu\text{m}$, $T_{01} = 40^\circ\text{C}$)	227
4.6.17 Effect of Initial Water Content and flow rates on Compressor Performance (100% Rotor Speed, $\phi_0 = 0.52$)	228
4.6.18 Effect of Initial Water Content and Flow rates on Compressor Performance (80% Rotor Speed, $\phi_0 = 0.46$)	229
5.1 Simple Constant Geometry Jet Engine	230
5.3.1 Radial Displacement of Water Droplet Due to Centrifugal Effect ($D_0 = 20\mu\text{m}$)	231
5.3.2 Radial Displacement of a Water Droplet Due to Centrifugal Effect ($D_0 = 600\mu\text{m}$)	232
5.3.3 Change of Mass Flow Rate of Water at Hub along Compressor ($D_0 = 20\mu\text{m}$)	233
5.3.4 Change of Mass Flow Rate of Water at Hub along Compressor ($D_0 = 600\mu\text{m}$)	234
5.3.5 Geometry of Test Compressor	235
5.3.6 Variation of Mass Flow Rate of Gas Phase in Different Compressor Stages ($D_0 = 20\mu\text{m}$)	236
5.3.7 Variation of Mass Flow Rate of Gas Phase in Different Compressor Stages ($D_0 = 600\mu\text{m}$)	237
5.3.8 Variation of Mass Flow Rate of Liquid Phase in Different Compressor Stages ($D_0 = 20\mu\text{m}$)	238
5.3.9 Variation of Mass Flow Rate of Liquid Phase in Different Compressor Stages ($D_0 = 600\mu\text{m}$)	239

<u>Figure</u>		<u>Page</u>
A.1.1	Performance Characteristics of Test Compressor (1st Stage)	246
A.1.2	Performance Characteristics of Test Compressor (2nd Stage)	247
A.1.3	Performance Characteristics of Test Compressor (3rd Stage)	248
A.1.4	Performance Characteristics of Test Compressor (4th Stage)	249
A.1.5	Performance Characteristics of Test Compressor (5th Stage)	250
A.1.6	Performance Characteristics of Test Compressor (6th Stage)	251
A.1.7	Performance Characteristics of Test Compressor (Overall)	252
A.1.8	Throttle (Annulus) Area.	254
A.2.1	Comparison of Mean Diameters	260
A.3.1	Evaporation Time With Negligible Relative Velocity Effect.	279
A.3.2	Evaporation Time With Effect of Relative Velocity ($D = 15\mu\text{m}$)	282
A.3.3	Evaporation Time With Effect of Relative Velocity ($D = 80\mu\text{m}$)	283
A.3.4	Evaporation Time With Effect of Relative Velocity ($D = 800\mu\text{m}$).	284
A.4.1	Intrinsic Coordinate System.	312
A.4.2	Cylindrical Coordinate System.	314
A.5.1	Calculation Procedure For Prediction of Fluid Outlet Angle and Total Pressure Loss Coefficient.	332

<u>Figure</u>		<u>Page</u>
A.6.1	Overall Calculation Procedure for Air-Methane Mixture	339
A.8.1	Model for Motion of Large Droplet.	364
A.11.1	Saturation Specific Humidity vs Temperature	381
A.11.2	Latent Heat vs Temperature	382

LIST OF TABLES

<u>Table</u>	<u>Page</u>
1.1 Comparison of Properties for Steam and Methane	11
2.1 Summary of Effective Mean Diameter	25
4.1.1 Calculation Conditions for UD-0300 Program Code	64
4.2.1 Calculation Conditions for Small Droplets (20 μm) . . .	66
4.2.2 Predicted Performance Parameter for Small Droplets (20 μm)	68
4.3.1 Calculation Conditions for Large Droplets (600 μm) . .	70
4.3.2 Predicted Performance Parameter for Large Droplets (600 μm)	72
4.4.1 Calculation Conditions for Local Injection and Instantaneous Evaporation of Water	74
4.5.1 Calculation Conditions for Air-Water Droplet Mixture Flow with Evaporation	76
4.6.1 Conditions for Overall Performance Calculation	78
4.6.2 Predicted Overall Performance Parameter	79
A.1.1 Test Compressor Design Velocity Diagram Values	243
A.1.2 Symbols for Test Compressor Design Velocity Diagram Values	244

<u>Table</u>	<u>Page</u>
A.1.3 Test Compressor Design Data (Rotor)	245
A.1.4 Test Compressor Design Data (Stator)	245
A.2.1 Example of Droplet Size Distribution	259
A.3.1 Characteristic Lengths and Times for Test Compressor	268
A.3.2 Injector Characteristics (Capacity and Spray Angle) Example I	269
A.3.3 Injector Characteristics (Capacity and Spray Angle) Example II	270
A.3.4 Spray Characteristics (Droplet Sizes) Example I	271
A.3.5 Spray Characteristics (Droplet Sizes) Example II	272
A.3.6 Characteristic Times for Various Processes	275
A.6.1 Coefficients for Calculation of Ψ , η , and τ	338
A.11.1 Coefficients for c_p Calculation	378
A.11.2 Molecular Weight, Gas Constant, Specific Heat Ratio	378

NOMENCLATURE

Symbol

A	area
a	acoustic speed
a_g	acoustic speed in gaseous phase
C	water concentration per unit volume
C_d	nozzle discharge coefficient
C_D	drag coefficient
C_w	water vapor concentration
C_{wb}	water vapor concentration at droplet surface
c	blade chord length
c_p	specific heat at constant pressure
c_{p_a}	specific heat at constant pressure for air
$c_{p_{air}}$	specific heat at constant pressure for air
\bar{c}_{p_B}	average specific heat at constant pressure for burner
\bar{c}_{p_C}	average specific heat at constant pressure for compressor
\bar{c}_{p_T}	average specific heat at constant pressure for turbine
$c_{p_{methane}}$	specific heat at constant pressure for methane
c_{p_m}	specific heat at constant pressure for mixture
c_{p_v}	specific heat at constant pressure for water vapor
c_w	specific heat of water
c_s	humid heat for air-water mixture
D	diameter of droplet

Symbol

D_{ab}	mean diameter of droplet (a,b=0,1,2,3)
D_d	average droplet diameter
D_e	effective mean diameter
D_{eq}	equivalent diffusion ratio
D_{eq}^*	equivalent diffusion ratio at minimum loss
D_{ij}	mean diameter of droplet (i,j=0,1,2,3)
D_v	diffusivity
d	diameter of droplet
d_{max}	diameter of largest stable droplet
dH_g	rise in total enthalpy of gaseous phase (per unit mass of gaseous phase)
dS'	rise in entropy of gaseous phase (per unit volume of mixture)
dS_D	rise in entropy of D-droplet (per unit volume of mixture) due to wall shear on D-droplet
dS_{Dd}	rise in entropy of D-droplet (per unit volume of mixture) due to relative motion between D-droplet and d-droplet
dS_{Dg}	rise in entropy of D-droplet (per unit volume of mixture) due to relative motion between D-droplet and g-droplet
dS_d	rise in entropy of d-droplet (per unit volume of mixture) due to wall shear on d-droplet
dS_{dD}	rise in entropy of d-droplet (per unit volume of mixture) due to relative motion between d-droplet and D-droplet
dS_{dg}	rise in entropy of d-droplet (per unit volume of mixture) due to relative motion between d-droplet and gaseous phase
dS_g	rise in entropy of gaseous phase (per unit volume of mixture) due to wall shear on gaseous phase

Symbol

dS_{gd}	rise in entropy of gaseous phase (per unit volume of mixture) due to relative motion between gaseous phase and d-droplet
dS_{gD}	rise in entropy of gaseous phase (per unit volume of mixture) due to relative motion between gaseous phase and D-droplet
dq_{Dd}	heat transfer between D-droplet and d-droplet (per unit volume of mixture)
dq_{Dg}	heat transfer between D-droplet and gaseous phase (per unit volume of mixture)
dq_{dD}	heat transfer between d-droplet and D-droplet (per unit volume of mixture)
dq_{dg}	heat transfer between d-droplet and gaseous phase (per unit volume of mixture)
dq_{gD}	heat transfer between gaseous phase and D-droplet (per unit volume of mixture)
dq_{gd}	heat transfer between gaseous phase and d-droplet (per unit volume of mixture)
e_d, e_D	internal energy of droplet (per unit mass of liquid phase)
e_g	internal energy of gaseous phase (per unit mass of gaseous phase)
$e_g(T_d), e_g(T_D)$	internal energy of gaseous phase (per unit mass of gaseous phase) at the local droplet temperature
F_B	dissipative body force
F_D	drag force
F_{IgD}	force (per unit volume of mixture) acting upon the gaseous phase due to D-droplet
F_{Igd}	force (per unit volume of mixture) acting upon the gaseous phase due to d-droplet
f	fuel-air ratio (Chap. V)
f	ratio of drag coefficient and Stokes' drag coefficient (Appendix 3)
$f(D)$	percent number of droplet with a diameter within certain size increment

Symbol

g_c	Newton constant relating force and mass
\bar{H}	rise in total enthalpy across the stage
\bar{H}	effective enthalpy change which under isentropic conditions produces the same stagnation pressure change as the actual enthalpy change
H_{rel}	total enthalpy of mixture based on relative velocity
H_v	latent heat of vaporization
h	heat transfer coefficient
h_c	convection heat transfer coefficient
h_g	enthalpy of the gaseous phase (per unit mass of the gaseous phase)
$h_g(T_d), h_g(T_D)$	enthalpy of the gaseous phase (per unit mass of the gaseous phase) at the local droplet temperature
h_m	mass transfer coefficient
i	incidence
i^*	incidence at minimum loss
K	thermal conductivity
K_a	thermal conductivity of air
K_d	thermal conductivity of gaseous film surrounding an evaporating droplet
K_v	thermal conductivity of water vapor
k	thermal conductivity
k_g	thermal conductivity of gaseous phase
\bar{L}	total losses per unit volume of mixture
L_D	losses associated with the D-droplet
L_d	losses associated with the d-droplet
L_g	losses associated with the gaseous phase

Symbol

M_{av}	average molecular weight between droplet and surrounding air
M_1	blade inlet Mach number
\dot{m}	mass flow rate
\dot{m}_{eD}	evaporation rate (per unit volume of mixture) of D-droplet
\dot{m}_{ed}	evaporation rate (per unit volume of mixture) of d-droplet
mw	molecular weight
$(mw)_{air}$	molecular weight of air
$(mw)_{methane}$	molecular weight of methane
N	number of droplets per unit normal projected area at inlet (Chap. III)
N	rotor rotational speed (Chap. IV)
N^*	cumulative number fraction of droplet below diameter D in the spectrum
N_d	number of droplet
Nu	Nusselt number
n_{tot}	total number of droplet
$(n_{tot})_e$	total number of droplet corresponds to effective mean diameter
P	pressure
P_{01}	compressor inlet total pressure
\bar{P}	total work input per unit volume of mixture
\bar{P}_D	external shaft work (per unit time per unit volume of mixture) done on the D-droplet
\bar{P}_d	external shaft work (per unit time per unit volume of mixture) done on the d-droplet
\bar{P}_g	external shaft work (per unit time per unit volume of mixture) done on the gaseous phase
Pr	Prandlt number

Symbol

P_{ref}	reference pressure
P_w	vapor pressure in fluid flowing around droplet
P_{wb}	vapor pressure at droplet surface
\dot{Q}_{gD}	heat transfer rate (per unit volume of mixture) from the gaseous phase to the D-droplet
\dot{Q}_{gd}	heat transfer rate (per unit volume of mixture) from the gaseous phase to the d-droplet
R	gas constant
\bar{R}	universal gas constant
R_a	gas constant of air
Re	Reynolds number
R_g	gas constant of gaseous phase
R_m	gas constant of mixture
R_u	universal gas constant
R_v	gas constant of vapor
r_{tip}	radius of blade tip
S	gap between blades
Sc	Schmidt number
Sh	Sherwood number
SN	stability number
T	temperature
T_{01}	compressor inlet total temperature
T_{av}	average temperature between droplet surface and surrounding gas
T_D	temperature of D-droplet
T_d	temperature of d-droplet
T_{dD}, T_{Dd}	average temperature between d-droplet and D-droplet

Symbol

T_g	temperature of gaseous phase
T_{gd}, T_{dg}	average temperature between gaseous phase and d-droplet
T_{gD}, T_{Dg}	average temperature between gaseous phase and D-droplet
T_{ref}	reference temperature
T_s	saturation temperature
T_w	temperature of water droplet (Appendix 3)
T_w	vapor temperature in fluid flowing around droplet (Appendix 7)
T_{wb}	vapor temperature at droplet surface (Appendix 7)
\bar{U}	local blade rotational velocity vector
U_{tip}	blade tip speed
u_D	velocity of D-droplet
u_d	velocity of d-droplet
u_g	velocity of gaseous phase
\bar{V}	absolute velocity vector
V_0	relative velocity of flow approaching the blade
V_d	velocity of droplet
V_g	velocity of gaseous phase
V_r	relative velocity between droplet and surrounding gas
V_z	axial velocity
$v_g(T_d), v_g(T_D)$	specific volume of vapor at the local droplet temperature
v_p	specific volume of water at the local droplet temperature
W	specific humidity
W_s	specific humidity for saturated air
\bar{W}	relative velocity vector
We	Weber number

Symbol

We_{crit}	critical Weber number
W_I	overall impingement rate (per unit area per unit time); $W_I = W_{I_1} + W_{I_2}$
W_{I_1}	average impingement rate (per unit area per unit time) at the stagnation region
W_{I_2}	average impingement rate (per unit area per unit time) aft of the stagnation region
W_r	relative velocity between gaseous phase and droplet
x	methane content
x_a	mass fraction of air
x_g	mass fraction of gaseous phase
x_v	vapor content
$x_{v,0}$	vapor content at compressor inlet
x_w	water content
$x_{w,0}$	water content at compressor inlet
$x_{w,tip}$	water content at blade tip
x_{w1}	mass fraction of water which does not impinge upon the blade surface
x_{w2}	mass fraction of water which impinge on the blade surface and rebounds
x_{w3}	mass fraction of water which is re-entrained from the trailing edge

Greek Letters

α_D	volume fraction of D-droplet
α_d	volume fraction of d-droplet
α_g	volume fraction of gaseous phase
β	local impingement efficiency (Chap. I)
β	inclination of flow with respect to axial direction (Chap. III)

Greek

β_1	inlet flow angle
β_2	outlet flow angle
β_1^*	inlet flow angle corresponds to minimum loss
β_2^*	outlet flow angle corresponds to minimum loss
β_{1c}	inlet flow angle at choking
β_{1s}	inlet flow angle at stall
β_{1ref}	inlet flow angle corresponds to minimum loss
β_{2ref}	outlet flow angle corresponds to minimum loss
γ	ratio of specific heats
γ_g	ratio of specific heats for gaseous phase
γ_m	ratio of specific heats for mixture
ΔH_c	heating value of fuel
ΔH_v	latent heat of vaporization
$(\Delta H_0)_1$	work input to gaseous phase
$(\Delta H_0)_2$	work input absorbed by water droplets which do not impinge upon blade surface
$(\Delta H_0)_3$	work input absorbed by water droplets which impinge upon blade surface, adhere to form a film and are re-entrained from the trailing edge
$(\Delta H_0)_4$	work input absorbed by droplets which impinge upon blade surface and rebound
ΔP_{OD}	pressure loss due to D-droplet
ΔT_g	rise in overall temperature of gaseous phase
$(\Delta T_g)_{ht}$	drop in temperature of gaseous phase due to heat transfer
$(\Delta T_g)_{wk}$	rise in temperature of gaseous phase due to work done
ΔT_w	rise in overall temperature of droplet
$(\Delta T_w)_{ht}$	rise in temperature of droplet due to heat transfer

Greek

$(\Delta T_w)_{wk}$	rise in temperature of droplet due to work done
δ	corrected pressure (Chap. IV, V)
δ	deviation (Appendix 4)
δ^*	deviation corresponds to minimum loss
ϵ	desired accuracy
η	compressor adiabatic efficiency
η_B	efficiency of combustor
η_M	mechanical loss in power balance equation
θ	inclination of the surface to the direction normal to the axial direction (Chap. I)
θ	corrected temperature (Chap. IV, V)
$\frac{\theta}{c}$	ratio of wake momentum thickness and chord length
$(\frac{\theta}{c})^*$	ratio of wake momentum thickness and chord length corresponds to minimum loss
λ	work done factor
μ_e	effective coefficient of viscosity
μ_f	viscosity of liquid phase
μ_g	viscosity of gaseous phase
ρ	density
ρ_a	density of air
ρ_d, ρ_D	density of water at the local droplet temperature
ρ_D'	bulk density of D-droplet (mass of D-droplet per unit volume of mixture); $\rho_D' = \alpha_D \rho_w$
ρ_d'	bulk density of d-droplet (mass of d-droplet per unit volume of mixture); $\rho_d' = \alpha_d \rho_w$
ρ_f	density of liquid phase
ρ_g	density of gaseous phase

Greek

ρ'_g	bulk density of gaseous phase (mass of gas per unit volume of mixture); $\rho'_g = \alpha_g \rho_g$
$\rho_g(T_d), \rho_g(T_D)$	density of vapor at the local droplet temperature
ρ_w	density of water
σ	surface tension of droplet (Appendix 3)
σ	solidity (Appendix 4)
σ_{ij}	stress tensor
τ	equivalent temperature ratio
τ_I	inertial relaxation time
τ_T	thermal relaxation time
τ_{rup}	droplet rupture time
Φ	viscous dissipation function
ϕ	flow coefficient
ψ	equivalent pressure ratio
ω	rotor angular velocity
$\bar{\omega}$	total pressure loss coefficient
$\bar{\omega}_{min}, \bar{\omega}^*$	total pressure loss coefficient corresponds to minimum loss

Subscript

cr	pertaining to critical value
d	pertaining to droplet
f	pertaining to fuel (Chap.V)
l	pertaining to liquid phase
g	pertaining to gaseous phase
ht	pertaining to heat transfer
hub	pertaining to blade hub

Subscripts

in	pertaining to compressor inlet
out	pertaining to compressor outlet
ref	pertaining to reference value
t	pertaining to stagnation property
tip	pertaining to blade tip
v	pertaining to vapor
w	pertaining to water or liquid phase
wk	pertaining to work done
0	pertaining to stagnation property
0	pertaining to initial value
2	pertaining to compressor inlet
3	pertaining to compressor outlet
4	pertaining to turbine inlet
5	pertaining to turbine outlet
6	pertaining to nozzle inlet
7	pertaining to nozzle throat

Super Script

*	pertaining to the design point (Chap. IV)
*	pertaining to minimum loss (Appendix 5)
-	pertaining to average (Chap. V)

SUMMARY

An analysis of the performance of an axial flow compressor operating with (a) mixtures of gases and (b) air-water droplet mixtures has been developed. In the case of mixtures of gases, account has been taken of the changes in molecular weight and ratio of specific heats. In the case of two phase flow, the major processes of interest are (i) droplet-blade interaction, (ii) droplet heating, (iii) droplet centrifuging and (iv) droplet break-up. The PURDU-WICSTK program developed for the prediction of compressor performance has been utilized to obtain the performance of a Test Compressor. A three-dimensional streamline computer code, the UD-0300, has also been modified and exercised in the case of compressor operation with mixtures of gases.

Water ingestion into the compressor of an aircraft gas turbine engine affects the performance of the engine, and a preliminary analysis of the nature of the effects has also been conducted.

CHAPTER I

INTRODUCTION

Water ingestion into an aircraft gas turbine arises due to two circumstantial reasons:

- (1) wheel-generated spray clouds entering the engine inlet during take-off and landing from a rough runway with puddles of water; and
- (2) rain, occasionally mixed with hail, entering the engine inlet during various parts of a flight in a rain storm.

A number of studies (Refs. 1-6) have shown that adverse effects can arise in engine performance due to such ingestion of water at engine inlet, when the engine has been designed for operation with air flow. In particular the engine may surge and may suffer blow-out or unsteadiness in the main burner or the after-burner. Simple corrective steps, such as resetting the throttle, have generally been ineffective in overcoming the problems of loss of power and nonsteady behaviour of the engine. In the case of wheel-spray ingestion, it has again become clear that basic changes in engine installation may be necessary in relation to inlets and landing wheels.

In the current investigation, there is no particular emphasis on the precise cause for the presence of water at the engine inlet. Water is assumed to enter the compressor along with air in droplet form. The droplet (nominal) diameters may be in the range of 20 to 1,300 microns. The water content by weight may be in the range of 2.5 to 15.0 per cent. In case of rain through which an aircraft may have to fly (Refs. 7-9) the droplet sizes may be of the order of 100 to 1,500 microns, although 3,000 micron size droplets have also been reported (Fig.1.1). On the

other hand, 15.0 per cent of water by weight is probably to be considered as a large amount of ingestion into the inlet, corresponding to flight through storm conditions. Under such extreme conditions there may also be hail and snow ingestion into the engine. However, only water ingestion effects are examined here.

A comprehensive investigation of the problem of water ingestion into engines during flight should take into account details of the engine, its installation and the engine and aircraft controls. In the current investigation attention is focussed on the engine and its control.

Furthermore, it is felt that the response of the compressor in the engine to water ingestion plays a determining and crucial role in the response of the engine as a whole in view of two considerations.

- (1) The compressor receives the ingested water directly and, as a rotating machine, is most strongly affected by the ingested water, and also changes the "state of water" before the fluid enters the burner.
- (2) The compressor performance most directly affects the operating point of the engine under steady and transient state conditions.*

However, the compressor performance is affected by the presence of an inlet through the changes in the flow field introduced by it, especially the distortion of the compressor inlet flow field. While noting such strong interaction between the inlet and the compressor flow fields, the

* It may be pointed out that the operating point of an engine is determined by the matching between all of the components of the engine. Thus, the swallowing capacity of the turbine and nozzle, for example in a simple jet engine, at a given engine speed and turbine entry temperature, determine the engine operating point on the compressor map. However, any changes in the compressor outlet conditions affect the engine operating point most directly with a given turbine and nozzle. In particular, during water ingestion, the compressor map becomes completely changed, causing at least a change in the surge margin for a possible operating point and, in extreme cases, a total mismatch between the components. Even with a turbine and nozzle that have variable-area capability, it may become necessary to regulate the compressor outlet conditions independently.

most important aspect of the problem of water ingestion into an engine is still considered to be that pertaining to changes in the compressor performance itself.

In the case of turbofan engines, the air-water mixture upon entering the inlet becomes divided between the fan and the compressor. In particular cases, the compressor stream may have a different water content and droplet size distribution from that of the compressor stream in the absence of a fan. The effects of water ingestion are important both in the fan and the core engine compressor, although, perhaps, more so in the latter. When there is an after-burner in the fan stream or when a "mixing" nozzle is employed, water ingestion into the fan stream may, however, become critically important.

From practical operational and design points of view, the effects of water ingestion in a compressor are as follows:

- (1) changes in temperature ratio, pressure ratio and efficiency of the compressor;
- (2) changes in surge line and operating line, and therefore the surge margin under given operating conditions;
- (3) blade deformation and erosion due to impact of droplets;
- (4) blade and casing deformation due to differential thermal expansion under transient conditions;
- (5) oscillation of pressure ratio and flow; and
- (6) changes in dynamic loading including aero-elastic effects.

For given entry conditions, the response of the compressor is determined by the following:

- (1) compressor geometry;
- (2) blade loading;
- (3) machine rotational speed; and
- (4) parameters of the engine of which the compressor is a part.

The latter pertain to engine matching and should include not only the steady state performance parameters but also the mechanical, aerodynamic and thermal inertia of the various components of the engine

under transient conditions. It should be noted that in particular cases, the engine components may include a fan, an after-burner or a second nozzle as part of the engine.

In establishing the response of a compressor to water ingestion, it seems therefore useful to divide the total problem into two parts.

- (1) The compressor as a machine itself; and
- (2) The compressor as a part of the engine system.

In that fashion, one can separate the problems associated with engine matching (steady or transient) from those dependent upon the design of the compressor itself. Once the latter have been understood in detail, the engine as a whole may be studied from a system point of view. This is the approach adopted in the current investigation, since it is also especially convenient in conducting experimental studies.

A number of parameters pertaining to the air-water mixture entering a compressor during water ingestion are the following:

- (1) amount of water approaching and actually entering a blade row as a fraction of the total mass flow of fluid entering compressor;
- (2) form in which water is present, film and droplets;
- (3) temperature and pressure of air, temperature of water and temperature of machine;
- (4) vapor content;
- (5) turbulence; and
- (6) distortion, radial and circumferential.

Water vapor is always present in air-water mixtures ingested into an engine. The water vapor content changes in the compressor because of changes in pressure and temperature and because of transfer processes between the two phases. In particular, in a multi-stage compressor of large pressure ratio, there is a possibility of some of the water reaching local saturation temperature and undergoing a phase change due to boiling causing addition of large quantities of vapor to the gas phase.

It will be observed that each of the afore-mentioned six parameters changes after each blade row and the cumulative changes are therefore especially significant in a multi-stage machine. Furthermore, both time-dependent changes during sudden and sporadic ingestion, as well as steady state changes, as, for example, may arise in a laboratory experiment, need consideration. Thus, a detailed study of this problem should result in the determination and verification of methods for establishing (a) the changes in the performance of a compressor with water ingestion and (b) the changes in the state of fluid between the inlet and the outlet of the compressor. Such a study requires investigations both on a single row of blades (stationary and rotating) as well as on a unit with several rows of blades, under steady, transient, and distorted flow conditions. The latter is a means of establishing the response of a blade row to the flow generated by a preceding row. Furthermore, in order to examine the occurrence and effects of phase change in a blade row, the entry conditions to the blade row have to be selected such that they are suitable for such phase change. In a multi-stage compressor of large pressure ratio, there is, of course, a considerable change in air temperature at design conditions.

However, at this stage there are still considerable problems in conducting detailed measurements of two-phase flows in rotating machinery. It has therefore been felt in this investigation that one should aim at establishing overall performance changes and fluid flow changes in a compressor for given entry conditions of state of the two-phase fluid. Once such overall changes are established and related to verifiable models for performance prediction, it is felt one can proceed to more detailed measurements and modeling.

For a given compressor, the variables of interest during water ingestion are the following:

- (1) speed of the machine;
- (2) throttle setting;
- (3) stagnation pressure
- (4) temperature of air and water;

- (5) amount of water as a fraction of total mixture flow;
- (6) droplet size and number density distribution, and
- (7) vapor content.

The variables (3) to (7) have a spanwise and circumferential distribution at compressor inlet, which may or may not be uniform.

The overall performance parameters of a compressor with two-phase flow are the following:

- (1) pressure ratio temperature ratio and efficiency;
- (2) changes in total water content and droplet size across the compressor; and
- (3) changes in vapor content across the compressor.

Each of these varies along the span of a compressor blade. Both the measurements and prediction of these is beset with considerable difficulties at this time. In particular the determination of water and vapor content and of droplet size distribution requires further advances in instrumentation, data acquisition and data processing.

On establishing and demonstrating predictive methods for the estimation of such overall performance parameters for a compressor, an analysis can be carried out for an engine operating with water ingestion. Under steady conditions, the equilibrium running of a simple engine depends upon the following parameters:

- (1) engine speed;
- (2) mass flow;
- (3) compressor performance with air-water mixture;
- (4) ratio of turbine entry temperature to inlet temperature;
- (5) turbine operational point (choked or unchoked); and
- (6) thrust nozzle geometry.

Regarding the latter, a fixed geometry thrust nozzle with a constant area turbine restricts the number of variables for equilibrium running of a simple engine to a single parameter, namely engine speed or mass flow. In a variable geometry engine which permits changes in area of the turbine and the thrust nozzle, one can select, at least in principle, three variables independently for equilibrium running: engine speed, mass flow and turbine entry temperature.

An analysis of steady state equilibrium running of an engine with water ingestion can be expected to reveal the following:

- (1) whether equilibrium running is feasible under a given set of operating conditions,
- (2) changes in surge margin, and
- (3) effect of fuel scheduling and bleed of working fluid.

The latter, along with other aspects of engine operation, is dependent upon the type of engine control incorporated in the system.

Even when attention is focussed on the performance of a compressor by itself, several aspects of the performance may come to light only when it is operated as a part of an engine. However, if engine matching and its effect on compressor performance are not included, one can test a compressor as a separate unit by driving it, for example, with an aerodynamically-independent drive engine. This has been the basis for experimental studies in the current investigation.

1.1 Objectives and Scope of the Investigation

The principal objectives of the present investigation are as follows:

- (1) Establishment and demonstration of a predictive method for the calculation of the performance of an isolated compressor driven by an external drive unit and operating with air-water mixture flow; and
- (2) Obtaining and correlating experimental data on a multistage compressor with air-water mixture flow.

In both of the above, the vapor content of the mixture is taken into account, both initial humidity and changes in vapor content due to phase change of water droplets.

The other objectives of the present investigation are as follows:

- (1) Determination of the manner in which engine performance becomes affected by water droplet ingestion into the engine compressors; and

- (2) Providing a review of instrumentation suitable in compressors.

1.1.1 Analytical-Predictive Investigations

The analytical-predictive investigations are divided into two parts; (1) investigation on the performance of a compressor with water ingestion, and (2) analysis of a simple gas turbine engine with water ingestion.

Part I: Performance of Compressor with Water Ingestion

The analytical-predictive investigations on performance of compressor with water ingestion are divided into three parts:

- (1) Setting up the general aero-thermodynamic equations for compressor with air-water mixture flow and deduction of a one-dimensional model.
- (2) Establishing one-dimensional models for the estimation of performance of a compressor in four limiting cases as follows:
 - (i) Ingestion of mixtures of gases directly into a compressor at inlet, without water droplets.
 - (ii) Ingestion of small droplets that can be assumed to follow gas motion and hence absorb angular momentum.
 - (iii) Ingestion of large droplets that can be assumed to move with equal probability in all directions and that cause a loss of compressor performance due to drag forces acting on them; and
 - (iv) Injection of water with sudden phase change into steam at an appropriate stage in the compressor.
- (3) Adapting and exercising a three-dimensional streamline computer code, the UD-0300 computer code (Ref.10), for the case of direct ingestion of mixtures of gases into a compressor.

Part II: Analysis of Gas Turbine Engine with Water Ingestion

The objectives of Part II are as follows:

- (1) Establishing a model for steady state engine matching with water ingestion; and
- (2) Establishing a model for calculation of flight performance with water ingestion.

1.1.2. Experimental Investigation

The experimental investigations have been conducted on a specially built Test Compressor. The experimental investigations may be divided into the following three parts:

- (1) Tests with air as the working fluid;
- (2) Tests with air-methane mixture as the working fluid; and
- (3) Tests with air-water droplet mixture as the working fluid.

The Air Force System Command has provided the Test Compressor and a T-63 Drive Engine for the experimental investigations. The predictive methods developed for estimating compressor performance with two phase flow have also been employed to calculate the performance of the Test Compressor.

Details regarding the Test Compressor and Drive Engine are provided in Appendix 1 to this Report.

The Test Compressor, it will be observed, has several limitations:

- (1) the annulus and the blade heights are small and only overall performance parameters at one or at most two radial locations at the exit plane can be measured.
- (2) the overall pressure and temperature ratios, even at design point, are too small to cause evaporation of more than 2.5 per cent of water (by weight) although the inlet temperature is raised to as high a value as 185°F (85°C); and
- (3) the compressor assembly permits little flexibility in locating instrumentation, especially at the compressor exit.

Since the Test Compressor casing has a plastic coating that does not

withstand high temperatures, the Test Compressor has been tested at low inlet temperatures in the range of 70°F to 100°F (about 20°C to 40°C). Such inlet temperatures do not cause water evaporation within the Test Compressor. The test program has therefore been conducted in two parts:

- (1) With a mixture of gases to simulate air-steam mixture flow corresponding to (a) high humidity in the air and (b) operation of different stages with air-steam mixture following complete evaporation of water, and
- (2) With air-water droplet mixture flow.

In examining the effects of presence of water vapor on a compressor performance, it is clear that another gas, such as methane, can be substituted for water vapor so long as the desired similarity laws with respect to Reynolds and Mach numbers, are satisfied. A comparison of properties for steam and methane is presented in Table 1.1. In view of the similar properties, experimental studies have been undertaken in this investigation utilizing air-methane mixtures.

The tests with air-water droplet mixtures have been conducted utilizing the following variables: mixture temperature, mixture composition and droplet size.

1.1.3 Measurements and Predictions

The results of the experimental investigation have been compared with prediction from models from the point of view of examining selected assumptions introduced in the models. It is clear that in view of limitations on the feasibility of measurements and the nature of assumptions introduced in modeling, comparison of analytical predictions with experimental results is restricted to certain overall performance parameters. In particular, the effects of mechanical-aero-thermodynamic interactions are established indirectly from overall compressor performance parameters and changes in water and vapor content.

TABLE 1.1

COMPARISON OF PROPERTIES FOR STEAM AND METHANE

	Steam	Methane
Chemical Formula	H ₂ O	CH ₄
Molecular Weight	18.016	16.043
Specific Heat at Constant Pressure		
(Btu/lbm-°F)	0.445**	0.531*
(kJ/kg-°C)	1.863**	2.223*
Ratio of Specific Heats*	1.329**	1.304*
Enthalpy Increase		
(Btu/lbm)	62.70 ⁺	69.96 ⁺
(kJ/kg)	145.84 ⁺	162.73 ⁺

* pressure = 1 atm; temperature = 78°F (26°C)

** pressure = 1 atm; temperature = 212°F (100°C)

⁺ pressure ratio, $P_{02}/P_{01} = 2.6$; $T_{01} = 68°F (20°C)$

1.1.4 Measurement Techniques

A brief review of instrumentation suitable for use in axial flow compressors and cascades operating with two phase fluid flow has been undertaken.

Two important overall performance parameters in compressors are the stagnation pressure ratio and the stagnation temperature ratio. A probe for the measurement of stagnation pressure in two phase flow has been developed. Its possible use in a compressor flow field has been examined. The development of a similar probe for the measurement of stagnation temperatures has been considered.

1.1.5 Engine Performance

The engines considered are those that have been designed for air flow through the inlet. Engines in which there may be injection of water at gas flow part locations beyond the compressor or in other stream such as fan ducts or after-burners are not under consideration. Specifically water ingestion effects have been examined in the case of simple turbo-jet and turbo-fan engines that have originally been designed for air flow operation only. Thus (a) the adverse flow effects due to water ingestion and (b) possible methods of mitigating such effects are of interest.

The response of an engine to water ingestion depends upon the following:

- (a) component geometrical constraints;
- (b) component performance characteristics; and
- (c) nature of control incorporated into the engine.

The performance characteristics that are of major interest are the following:

- (a) Changes in component performance characteristics due to water injection, in particular the compressor;
- (b) Changes in operating characteristics of engine under conditions of equilibrium running;

- (c) Changes in surge margin; and
- (d) Limiting conditions of operation.

The foregoing have been analyzed in order to establish general performance trends without reference to specific engine configurations.

It may be noted that, because of the aero-thermo-mechanical processes arising on account of water ingestion, one may also expect, at least in extreme cases, aero-elastic processes becoming significant. However, the manner in which flutter, for example may be altered during two phase flow in compressors is not included for study in the current investigation.

1.2 Effects of Water Ingestion

The two critical factors during water ingestion may be said to be the following: (a) the aero-thermo-mechanical processes associated with two phase flow and (b) the centrifugal action on droplets in the compressor. The first of these includes droplet disintegration and evaporation processes. The latter gives rise to a change in gas phase mass flow as well as reduction in gas phase temperature. The centrifugal action introduces a radial distortion in the flow and fluid properties, and the distortion changes in every stage of a multistage compressor. In particular, the spanwise distribution of the composition and properties of the fluid, in terms of air, water vapor and water droplets (both content and size distribution), undergoes changes continuously along the compressor flow path. The effects (a) and (b) should be examined in a compressor in relation to the following:

- (i) Formation of a water film in the tip region, that may flow into the diffuser;
- (ii) Possibility of choking hub sections and stalling tip sections with redistributed gas and liquid phase mass flow; and
- (iii) Nonuniform distribution of water vapor in the radial direction.

The foregoing will in turn affect engine performance depending

upon engine-matching and the type of control in the engine.

In order to reduce the effects of water ingestion, one can consider the following in order of increasing complexity.

- (i) Bleeding of gas or liquid phase flow at appropriate locations in the compressor;
- (ii) Resetting stator blades;
- (iii) Modifying engine control; and
- (iv) Introduction of variable geometry nozzle and also turbine.

The results of some preliminary studies on bleeding and also gas injection have been reported in Ref. 11.

1.2.1. Relation to Other Two-Phase Flow Problems in Turbo-Machinery

The current investigation deals with air-water droplet mixture ingestion into engines. On the other hand there has also been considerable interest in the problem of dust particle ingestion into engines (Refs. 12-13). In the latter case the principal interest is in erosion of blades and nozzles, although there is some loss in aerodynamic performance.

It is generally considered that the solid particulates may agglomerate but not disintegrate during dust ingestion. Furthermore the heat and mass transfer processes between the two phases are considered negligible.

Solid particulates are also of interest in certain rocket motor nozzle and plume flows (Refs. 14-16). In this case, in addition to erosion and particulate drag effects it is generally necessary to take into account heat and mass transfer processes, as well as condensation, solidification and other phase change processes. However, in this case there is not strong centrifugal action, although there may be some swirl in the flow.

The low pressure stages of a steam turbine (Refs. 17-19) may

operate, as is well known, with steam-water droplet mixture, the droplets arising through condensation. However, in this case, while erosion, loss of aerodynamic performance, and consequences of strong centrifugal action are important, one does not have the problems of stalling and surging. A compressor is prone to surging and the surge margin with respect to operating line when it is part of an engine is an extremely important parameter in engine operation. Hence the problem of water ingestion into an engine compressor attains a level of complexity and significance much larger than the two phase flow problem in steam turbines. One should also note that a turbine is basically a nozzle, while a compressor flow (both past a blade and through a blade passage) involves diffusion and complicated blade wake interactions.

The current investigation does not take into account geometrical changes in a compressor because of, say, differential contraction of rotor and casing upon water ingestion. In general one can expect a change in clearance between rotor and stator. If a compressor has been designed with optimum clearance, one has to examine both aerodynamic and mechanical effects caused by changes in clearance. This aspect of water ingestion should be examined in relation to the general problems of gas flow path integrity (Ref. 20).

While nonsteady state operation is not considered in the current investigation, one of the most important aspects of water ingestion into compressors and engines is transient state operation. The aero-thermo-mechanical interactions including differential contraction of casing and rotor under transient conditions are significant in evolving various means of reducing the effects of water ingestion.

Finally, it is recognized that the entry conditions into a compressor are not uniform radially and circumferentially. The effects of distortion with respect to pressure, temperature, velocity and turbulence continue to be a subject of concern even with air flowing alone (Ref. 21). During water ingestion, one can expect, in general, distortion both at entry and to the compressor and at entry to each stage. The sensitivity

of an engine to water ingestion should include consideration of inlet distortion with regard to water content and water droplet size distribution. This problem has been entirely neglected in the current investigation. It may be pointed out that even under uniform inlet flow conditions, radial distortion, of course, arises within the compressor due to centrifuging and heat and mass transfer processes.

1.3 Implications of Models

The models derived in the current investigation may be divided into four groups:

- (i) Model for the calculation of stage performance with air flow.
- (ii) Model for droplet motion across a blade row.
- (iii) Model for centrifuging of water, and
- (iv) Model for heat and mass transfer processes, including droplet disintegration.

Experimental investigations have been conducted in order to determine overall compressor performance changes for given initial and operating conditions. A comparison between predictions and measurements therefore yields no detailed verification of the models. It is in any case doubtful if detailed verification of all aspects of the models can be obtained even if one attempted additional measurements.

The performance of a compressor stage with two phase flow depends upon the following parameters:

- (i) geometrical design of blade and blade passage,
- (ii) spacing between blade rows,
- (iii) leading and trailing edge geometry,
- (iv) casing geometry,
- (v) rotor and stator blade junctions,
- (vi) incoming flow conditions, and
- (vii) operating speed and throttle setting.

The foregoing determine (a) the stage work input, (b) the states

of gas and liquid phases, (c) the efficiency of compressor, (d) the redistribution of water and vapor and (e) limiting condition of steady state operation of compressor. When the compressor is part of an engine, the operating characteristics of all other components of the engine and of the engine as a whole are also determined by the compressor design and initial conditions. It is clear that while the models developed can be employed to determine the performance of any compressor under a set of reasonable operating conditions, there is need to establish relations that can be employed to scale the performance of a compressor with respect to design, initial and operating conditions. Such scaling laws have to be based on characteristic lengths, characteristic times, and blade, blade passage and blade row characteristics of the compressor and, when the compressor is part of an engine, the characteristics of other components such as diffuser, burner, turbine and nozzle. Under certain assumptions an attempt has been made to establish scaling laws for both a compressor and a simple jet engine.

1.4 Organization of Report

The final report is being issued in three parts:

Part I: Analysis and Predictions

Part II: Computational Programs and Measurement
Techniques, and

Part III: Experimental Results and Discussion

This report constitutes Part I of the Final Report. Chapter I is the introduction. Chapter II is devoted to a discussion of model for air-water droplet mixture flow in a compressor, and Chapter III presents the models employed for the calculation of various limiting cases. The results of calculations on the Test Compressor are presented in Chapter IV. Chapter V presents an analysis of engine operation with water ingestion.

CHAPTER II

AIR-WATER MIXTURE FLOW IN A COMPRESSOR

One of the central features of water ingestion into compressors is that water is predominantly in discrete droplet form, although some of the water may move in the form of a film at least over short distances on the blades and the casing walls. A second important feature is that the droplets or the film may undergo both change of form as well as of phase along the flow path. Those processes lead to a span-wise redistribution of water and vapor content across the compressor. Thirdly, the presence of discrete droplets and water vapor in air changes substantially the acoustic speed in the medium, and hence the flow Mach number (Ref. 22). The acoustic speed in a droplet-laden air flow is presented graphically in Fig. 2.1 for standard atmospheric conditions. The acoustic speed decreases initially as liquid volume fraction increases. Fourthly, the motion and transport processes of the air-water droplet mixture are dependent upon the following: (1) the interactive gravitational and centrifugal flow fields; (2) the characteristic length and time scales typified by various characteristic parameters such as Reynolds number of flow, Reynolds number of droplets, and blade-casing clearance; and (3) the flow Mach number. Finally, the turbulent characteristics and nonuniformities in the flow are affected by the presence of droplets.

2.1 Performance Parameters

The overall performance of a compressor is given by the following parameters: (a) pressure ratio, (b) temperature ratio, (c) efficiency, and (d) the surge mass flow at different speeds. In the case of

two phase flow, the following additional parameters are of interest: (a) change of vapor content, (b) change of water content, and (c) change in droplet size and number distribution.

Considering the blades in any stage of a multistage compressor, the performance depends upon the blade characteristics, inter-blade space geometry, casing geometry and the inter-row spacing geometry. It has been established practice with air flow in a compressor to correlate experimental data on pressure rise coefficient and loss coefficient, as well as deviation and diffusion factors, based on blade profile shape, incidence angle and flow Mach number (Refs.23 and 24). During water ingestion changes can be expected to arise in air mass flow rate, work done on air, diffusion, boundary layer characteristics and wake characteristics. The major performance parameters that reflect those changes are those mentioned earlier for the case of (one phase) air flow and those pertaining to the state of air-water droplet mixture. The air-water mixture undergoes changes across a stage in (a) vapor content, (b) water content, and (c) water droplet size and number distribution.

The central uncertainty in regard to each of those is that droplets impinge on physical surfaces (one or more times on any given surface in a specific part of the machine), rebound, break-up, possibly form films and become re-entrained into blade wakes. A film has its own characteristics including break-up, droplet formation and film reformation. These processes affect each of the flow and transfer processes as well as the state of air-water droplet mixture. It is clearly impossible to adapt air flow cascade data for direct application to air-water mixture flow. In principle, with adequate detailed investigations on cascades and compressor stages, it may be possible to separate the principal effects during water ingestion into a compressor as follows:

- (1) blade passage effects;
- (2) impingement and associated effects;
- (3) heat and mass transfer effects;
- (4) centrifugal force effect; and
- (5) droplet break-up processes.

The five effects become strongly inter-related in any compressor stage because of the presence of a finite gap-chord ratio of blades, a finite aspect ratio of blades, and rotation.

In the case of a single wing or bluff body, such as a fuselage, impingement of water droplets has been studied in the past with reference to the following parameters (Refs.25 and 26):

- (a) droplet trajectory parameter for which the scaling parameter is based on a simple momentum balance for individual droplets;
- (b) capture parameter, defined by CV_0 , where C is the water concentration per unit volume and V_0 is the velocity of ingestion relative to the body; and
- (c) thermal parameters based on heat and mass transfer.

The trajectory parameter is in the nature of an inertia parameter. In the case of a duct-like configuration, a scooping ratio or capture efficiency has been defined to extend the application of trajectory parameter and capture parameter.

In the case of a compressor, while one may still utilize the concept of a scooping ratio at the inlet, the trajectory or inertia parameter and the thermal parameters are also governed by the presence of blades and by rotation. Once the droplets impinge on the blades other processes have to be taken into account such as rebound, motion on the surface of blade in the form of film and reingestion of the film into blade wake. Meanwhile the flow over the surface of the blade and in the blade passage undergo profound modifications. There is probably little relation between cascade characteristics as they may have been established with air flow and the characteristics as obtained with two phase flow (Refs.17 & 27). The blade boundary layer, the secondary flows and the wake will undoubtedly change with two phase flow. A variety of assumptions, therefore, are required at this stage in setting up a model for two phase flow in a rotating cascade of blades: regarding scooping of droplets; impingement, motion over blade surfaces and reingestion; profile and secondary losses and wake characteristics.

Each of the foregoing is affected by rotation, and resulting centrifugal action, in rotors. Centrifugal action arises both over the surface of blades and also in the blade passages due to the whirl component of mixture velocity. In general, it introduces a spanwise or radial distortion in the composition of the mixture and the flow field, that have profound consequences on compressor, and eventually engine, performance.

It is also important to recognize here that the mechanical and aerothermodynamic interactions between a compressor and two phase flow also involve various processes at the casing wall and the "inner wall" of the compressor. In view of the nature of centrifugal action on droplets, the casing wall boundary layer and its relation to rotor blade clearance become especially significant. A film formation with repeated break-up and reformation is very plausible in a compressor, especially a multistage compressor.

The film formation and accumulation of water in the tip region generally affect:

- (a) the blade tip mass flow and pressure losses,
- (b) the casing boundary layer losses, and
- (c) heat and mass transfer processes.

In view of lack of adequate data, modeling in this region has to be based (currently) largely on heuristic reasoning.

Some sophisticated models exist (Refs. 12 - 13) for the calculation of solid particle trajectories in blade passages. However, empirical rules have to be introduced into the calculations for particle drag, rebound, motion on the boundary layer and reingestion into wakes. The most significant conclusion from such studies is that the effect of particulates is much greater in regard to blockage and flow path than in regard to pressure loss. This has important implications for air-water droplet mixture motion since it will be found later in this Report that the redistribution of water content, the changes in droplet size and number density, and the phase change have much greater effect

on performance than droplet drag.

In applying such sophisticated models for the case of air-water droplet mixtures, one has to introduce several assumptions regarding droplet impact and heat and mass transport processes possibly leading to phase change. While some simple models are available for these processes, considerable empiricism becomes necessary in incorporating them into the droplet-associated processes in compressor blade rows.

It is felt that, from the point of view of overall performance estimation, a parametric study based on assumptions regarding (a) droplet trajectory, (b) droplet drag, and (c) droplet impact, rebound and reingestion processes may be adequate at this stage. This is especially so in view of the limited measurements that are feasible in a small compressor such as the Test Compressor and the limited opportunities for verification of various aspects of more sophisticated models.

Even in the limited framework of establishing overall performance changes due to water ingestion, one has to take into account at least the following:

- (1) the relations between droplet size distribution and various processes in a compressor;
- (2) the droplet impingement, rebound and reingestion;
- (3) the action of centrifugal force;
- (4) the heat and mass transfer processes leading to vaporization; and
- (5) the droplet break-up.

Each of those aspects of the problem is discussed in the following before discussing a simplified model for two phase flow in a compressor.

2.1.1 Effective Mean Diameter of Droplets

In dealing with an air-water droplet mixture, it is necessary to observe that a spectrum of droplet sizes exists in any given spray. The existence of such a spectrum of droplet sizes should be taken into

account in analyzing the flow, transport, and compressor processes. Questions then arise pertaining to the following:

- (1) Method of including the spectrum of sizes, and
- (2) Method of taking into account the various droplet related processes along the flow path in the compressor.

Regarding the flow and transport processes, one can proceed in one of two ways:

- (1) The spray can be divided into a number of classes of nominal sizes which together make up the spray. Each class is considered as governed by appropriate flow and transport equations (Ref. 28).
- (2) The spray, when it is nearly homogeneous, can be considered in terms of a single effective mono-dispersed spray that is equivalent to the given spray with respect to a chosen process (Ref. 17).

The latter is especially useful when the spray employed is nearly homogeneous during a laboratory experiment. Considering various processes such as droplet motion, droplet break-up, and transport processes, one can determine an effective mean diameter that is the most appropriate for each process. Then the effective mean diameter applicable to a given process should be used in the process. The method is also useful in selecting injectors for the experiment. Various injectors that yield the same effective mean diameter for a given process, but with variations in their actual output of droplet sizes, can be considered as equivalent with respect to that process. A discussion on the determination of effective mean diameters for various processes is provided in Appendix 2. The effective mean diameters corresponding to selected processes during air-water droplet mixture flow in a compressor are presented in Table 2.1.

In conducting experiments, one can compare the performance of a given compressor with respect to a chosen process by utilizing injectors that have different effective mean droplet diameters corresponding to

TABLE 2.1

SUMMARY OF EFFECTIVE MEAN DIAMETER

Process	Effective Mean Diameter Based on Surface Area	Effective Mean Diameter Based on Volume
1. Drag Force		
$Re < 1.9$	D_{21}	D_{31}
$550 < Re < 2.0 \times 10^5$	-	D_{32}
2. Centrifugal Force	D_{32}	-
3. Heat Transfer	D_{21}	D_{31}
4. Mass Transfer	D_{31}	D_{31}
5. Droplet Deformation and Break-up	D_{21}	D_{31}

that process. One can also examine with a given compressor and given injectors the manner in which various processes are affected by the droplet size and number density distribution.

2.1.2 Droplet Impingement

An extension of the concept of capture parameter originally defined for a single body (Ref. 26) can be applied to a cascade of blades.

Referring to Fig. 2.2, droplet impingement on a blade can be divided into (1) impingement at the stagnation region and (2) impingement aft of the stagnation region. For part (1) the local impingement efficiency, defined by

$$\beta = \frac{dy}{ds}$$

is taken to be equal to unity. Thus the average impingement rate (per unit area per unit time) is given by the relation,

$$W_{I1} = CV_0\beta = CV_0 ,$$

where C is the water concentration per unit volume and V_0 is the velocity of flow approaching the blade. The stagnation region is assumed to be normal to the axial direction.

For impingement aft of the stagnation region, the local impingement efficiency is taken to be equal to $(\cos \theta)$ where θ is the inclination of the surface to the direction normal to the axial direction. Thus, the average impingement rate is given by the relation,

$$W_{I2} = CV_0\beta = CV_0 \cos \theta .$$

The overall impingement rate is then equal to W_I , given by

$$W_I = W_{I1} + W_{I2} .$$

In applying the foregoing to blade rows in a compressor, the velocity of interest is that relative to the blade row under consideration. However, all of the droplets cannot be expected to move with a

single velocity in direction or in magnitude. At this time there are neither theoretical nor experimental methods that are adequately reliable for measuring droplet size and velocity in the range of droplet sizes of interest in this investigation. Accordingly, the following assumptions are introduced.

- (1) During entry to the first stage of a compressor, the droplets have the same velocity as the gas phase at a chosen location; and
- (2) During entry into one of the succeeding stages, there is always a well-defined relation between droplet velocity and gas phase velocity.

Implications of these assumptions are discussed further in Section 2.

In calculating the total impact, rebound and reingestion of droplets, the following assumptions are employed.

- (1) Referring to Fig. 2.3, the total number of droplets impacting a blade in a row of blades is reckoned as equal to the number of droplets impacting the pressure and suction surfaces of two neighboring blades in the region of flow between the two stagnation streamlines, $A1_1$, $B2_2$, for the two blades under consideration. The streamline directions are nothing but the directions of relative velocity of droplets at entry to the blade row under consideration. The total number of droplets impacting the surfaces of the two blades is taken as the total number of droplets impacting a blade.
- (2) It is assumed that a fraction of the droplets that impact is rebound, noting that the fraction is an unknown parameter.
- (3) The rebound droplets are then assumed to rejoin the droplets in the blade passage and move along with the gas phase.
- (4) The balance of droplets that do not rebound are then assumed to become subjected to the rotational speed of the blades (and hence to centrifugal force action) and become reingested into the main stream in the blade wake. Starting with small relative velocity with respect to gas phase, the droplets can

be expected to attain equilibrium with the gas phase after some acceleration in the wake.

- (5) The droplet trajectories upon leaving a blade are assumed to follow the gas phase outlet angle at the trailing edge of the blade, based on the premise that the droplets should leave the blade in a region that is of the nature of a boundary layer. The droplet trajectory at the trailing edges of blades is also shown in Fig. 2.3. This type of assumption on droplet and gas phase outlet angle neglects the mutual interaction between the two phases and is therefore strictly in error insofar as estimate of deviation angle of mixture is concerned.

In view of paucity of data on the foregoing processes and the unreliability of analytical methods, various fractions of rebound and reingested droplets are treated as parameters in setting up limiting cases for performance calculation in Chapter III of this Report.

The proposed estimates of impact, rebound and reingestion have also an effect on the energy input into the working fluid. Droplets of different sizes can be expected to follow different trajectories with different relative velocities with respect to gas phase, as stated earlier. It is therefore again necessary to divide the total work input (into the fluid mixture) between the gas and droplet phases on a parametric basis. The method of undertaking this in limiting cases is also described in Chapter III of this Report.

Although there is no energy input into the working fluid in a stator, all of the processes associated with droplet impact have to be treated in the same manner as in a rotor. However, since the pressure loss due to droplets is small and it is assumed that droplet outlet angle is the same as gas outlet angle at the trailing edge of a blade, one can introduce the simplification that a stator blade can be treated in isolation insofar as impact-associated processes are concerned. This is equivalent to uncoupling the effects of a finite gap-chord ratio, aspect ratio and twist in the blade on the gas and droplet phases.

2.1.3 Centrifugal Force

A whirl component of velocity exists everywhere in a compressor. It arises from the turning of the flow over a blade section and is further increased by the wheel speed of the rotors. Centrifugal action gives rise to a redistribution of a single phase fluid when there is a nonuniform radial distribution of mass flow in the compressor annulus, which in turn arises because of nonuniform distribution of velocity and density. In the case of two phase flow with droplets, the droplets suffer a much greater centrifugal action than the gas phase, and the redistribution of droplets due to centrifugal action affects the overall performance of a compressor in regard to every process associated with two phase flow.

A model for the calculation of centrifugal force effects is developed as follows.

- (1) While centrifugal action arises everywhere, it is assumed that it is sufficient to consider the effects of centrifugal force action only at the exit of a row of blades, that is in the inter-blade row spacing.
- (2) Centrifugal action is calculated by dividing the annulus height or the blade span into a series of radial sections and then dividing each radial section into a series of axial sections (Fig. 2.4). The displacement of droplets in each section is then integrated over a desired length along the compressor and the redistribution of droplets established at the end of the chosen length. The length chosen is the largest chord of a blade or, in other cases, the length equal to the chord and a fraction of the inter-blade row spacing on either side of the blade under consideration.
- (3) As stated earlier, in Section 2.2 on droplet impingement, some of the droplets can be expected to move over the blade surfaces while the rest (being the larger fraction) move in the gaseous stream. Centrifugal action is always associated with droplets moving over the surfaces of rotor blades. On

the other hand, for the droplets moving in the gas stream, centrifugal action is associated with droplets depending upon whether they are assumed to move largely with the gas phase or independently.

In regard to the foregoing assumptions, certain limiting cases are identified and discussed in Chapter III of this Report.

2.1.4 Effect of Phase Change and Presence of Water Vapor

An important aspect of air-water droplet mixture flow in compressors is the possibility of water undergoing a change of phase in the compressor. A compressor (operating, as an ordinary gas turbine compressor does, without intercooling) can increase the temperature of air substantially when it is a high pressure ratio machine. Depending upon the flow speeds and physical dimensions involved, there may be adequate time for appreciable heat transfer between the gaseous and liquid phases. It is then of interest to establish the effects of the presence of water vapor in appreciable quantities with or without (liquid) water depending upon the extent of vaporization.

In establishing a model for phase change, two processes have to be considered:

- (1) Mass transfer in order to reach equilibrium with respect to humidity at the local gas phase pressure and temperature; and
- (2) mass transfer due to vaporization.

In the length of time required for gas phase motion across a blade row, the mass transfer due to the humidity equilibrating process is, in general, extremely small and negligible. Regarding vaporization, while the liquid phase temperature increases in each stage to some extent along with the gas phase temperature, vaporization requires that:

- (a) water should reach local boiling point; and
- (b) there must be adequate heat transfer from gas phase to liquid phase to provide the needed latent heat.

To a large extent, whether vaporization occurs or not depends upon the following:

- (1) Air-water droplet mixture inlet conditions, particularly the temperature;
- (2) Performance of compressor (pressure ratio and efficiency);
- (3) Water droplet characteristics;
- (4) Water and vapor content in mixture; and
- (5) Droplet residence time in the compressor.

The consequences of phase change are as follows:

- (1) Change in gas phase mass;
- (2) Change in gas phase composition and temperature;
- (3) Change in liquid phase mass;
- (4) Change in specific heat and specific heat ratios of gas phase; and
- (5) Change in acoustic speed of the medium.

Those changes cause performance changes in the compressor, which in turn have an important effect on engine performance.

It may be pointed out that phase change during water ingestion introduces a change in gas phase temperature that does not arise during ingestion of dust-laden air. The latter, of course, introduces other complexities such as accumulation on physical surfaces and wear of blades.

2.1.5 Droplet Break-up

In general, droplets may undergo agglomeration or break-up and also there may arise condensation of vapor into droplets, although the latter is unlikely with the steady increase of pressure and temperature within the compressor. Droplets may also become formed in unstable sizes following film break-up. Finally, when film or droplets become reingested into blade wakes, the droplets may be in unstable sizes before they attain reasonable equilibrium with the gas phase. It is assumed throughout this investigation that the equilibrium state

of a droplet is governed by whether a critical value of Weber number has been reached at certain chosen locations in the compressor. The droplet size is adjusted accordingly.

The Weber number is defined as follows and represents a balance of some of the forces acting on the droplet.

$$We = \frac{\rho_g (V_g - V_d)^2 d}{\sigma g_c}$$

where ρ_g is the gas phase density, d , the droplet diameter, σ , the surface tension, V_g , the gas phase velocity, and V_d , the droplet velocity.

For nonviscous fluids, the critical value of the Weber number above which a droplet breaks up is about 12 (Ref. 29). Liquid viscosity apparently has a stabilizing effect which is scaled by the stability number, SN, whose definition is given by

$$SN = \mu_f^2 / \rho_g \sigma d g_c$$

where μ_f is liquid viscosity. The results of some experimental data have been represented by the equation, namely,

$$We_{crit} = 12 [1 + (SN)^{0.36}] ,$$

for values of stability number less than 5 (Ref. 29). The relationship between the droplet diameter and the critical Weber number and the stability number is shown in Fig. 2.5.

Using the value of critical Weber number, the largest stable droplet diameter can be expressed as follows:

$$d_{max} = \frac{We_{crit} \sigma g_c}{\rho_g (V_g - V_d)^2}$$

In the case of droplets that re-enter the stream at the trailing edge of the blade, it is a reasonable assumption that in the vicinity of the blade trailing edge, the droplet velocity is zero. The maximum possible droplet diameter is then given by the relation as follows.

$$d_{\max} = \frac{We_{\text{crit}} \sigma g_c}{\rho_g V_g^2}$$

A model for droplet size adjustment is developed as follows.

- (1) While droplet size may change everywhere, it is assumed that it is sufficient to adjust droplet size only at the exit of a row of blades, that is in the inter-blade row spacing.
- (2) Droplet size is changed if the critical value of Weber number is exceeded.
- (3) Droplets have been assumed to rebound, in part, following impingement on a blade surface. It is assumed that the rebound droplets have a pre-assigned change of size, for example, zero change; and
- (4) Droplets, following reingestion into a wake, are analyzed along with the rest of the droplets for change of size at the exit of a blade row or in the inter-blade row spacing.

The foregoing have been taken into account in the development of certain limiting cases in Chapter III of this Report.

2.2 Two-Phase Flow Aero-thermodynamic Model for Compressors

The aero-thermodynamic flow equations for two phase flow in compressors have been derived, largely based on Refs. 30 and 11, and presented in Appendix 4. The main features pertaining to two phase flow, that have been included in deriving those equations, are as follows:

- (1) The working fluid is assumed to consist of air, water vapor and two classes (by size, designated small and large) of droplets;
- (2) The gas phase is considered to be a mixture of air and water vapor, and is assumed to be a perfect gas continuum. They are assumed thoroughly mixed and assumed to move together in thermodynamic equilibrium so that differential diffusion rates

may be neglected on a scale large compared to the droplet dimensions and so that one may consider wherever necessary transport properties of the mixture rather than those of the two components.

- (3) The liquid droplets are assumed finely divided so that any volume element considered contains many droplets; then the droplets may be treated from a continuum viewpoint. This clearly does not hold on a scale comparable to the droplet dimensions, but the major length scale of the current problem is large compared to the droplet dimensions.
- (4) Two exceptions to the continuum assumption for the particulate liquid phase arise in the accounting of (a) the viscous interaction force between the droplet and gas phase, and (b) the interfacial heat and mass transfers.
- (5) Droplets are assumed to be not numerous enough to give rise to a pressure force component.
- (6) It is assumed that while the droplet and gas are two continua, co-existing in space and interacting with each other through the transfer of heat, mass, and momentum, the droplets are assumed sufficiently separated so that the local field of one droplet does not interact with the field of another droplet.

The equations are developed in both intrinsic and cylindrical coordinate systems in a rotating frame of reference.

The balance equations required for the analysis of compressor flow fields are the balance equations for mass, momentum and energy and also the radial equilibrium or another equation to replace it to yield spanwise variations (Ref. 23).

The flow field in a compressor is generally turbulent although some relaminarization - transition-like processes (Ref. 31) - may be occurring over blade surfaces. The viscous forces associated with the gas and liquid phases have been based on an effective eddy viscosity coefficient for the gas phase in the model developed here.

In accounting for compressibility effects in high speed compressors, one has to recognize the change in acoustic velocity introduced by the presence of droplets. The acoustic velocity is reduced greatly and the Mach number becomes increased (Ref. 11).

A general flow field calculation of two phase flow in an axial flow compressor requires solution of three-dimensional flow equations. One should then be able to obtain both the gas phase and liquid phase trajectories in the blade passages and inter-blade row spacing. However, in evolving such a model there will still be considerable uncertainties regarding the following:

- (1) droplet impact and rebound processes;
- (2) droplet motion along the surface of a blade, especially in the presence of secondary and centrifugal forces;
- (3) droplet reingestion into the wake of a blade and the development of the wake in the inter-blade passage; and
- (4) redistribution of water content and size following each blade row.

Each of the foregoing is of fundamental importance in predicting the compressor flow field. However, there are no specific analyses or experimental data to take those processes into account.

Even when axisymmetric or one-dimensional approximation is employed, the foregoing droplet-associated processes may only be taken into account on a parametric basis.

In the current state of knowledge of two-phase flows in compressors, it is felt that calculations based on one-dimensional flow approximation should be performed and examined before proceeding to extensive models.

2.2.1 One-dimensional Approximation

Based on the aero-thermodynamic equations in a rotating frame of reference for two-phase flow in axial flow compressors, equations based on one-dimensional approximation have been deduced and presented in

Appendix 4 of this Report.

It will be observed that under one-dimensional approximation the flow is assumed to be uniform over any part of the span selected for consideration and variations of the flow parameters in the radial and tangential (whirl) directions are entirely neglected. This is equivalent to specifying a location in the span of a blade for entry and exit of a streamline and assuming continuity with respect to the axial component of velocity. The work input in a rotor is obtained by the use of the Euler turbine equation.

It is common practice to apply the one-dimensional flow analysis to the mean sections of compressor stages in succession starting at the inlet to the compressor and ending at its last stage. In view of the importance of compressibility in air flow compressors, the area changes across and between blade rows is taken into account.

In the case of two phase flow, because of the action of centrifugal force, there arises a concentration of water in the tip region of a blade and a depletion of water at the hub. The difference in concentration of water between the hub and the tip introduces differences in every aspect of compressor performance at the two sections. Among other things, for example, there may arise large differences in acoustic velocity and hence in Mach number.

The question therefore arises whether tip and hub sections are not more important than the mean section under two phase flow conditions. Even within the framework of one-dimensional approximation, it appears that performance at those two sections should be compared with the mean section performance.

In the discussion of limiting cases pertaining to the Test Compressor in Chapter III of this Report, attention has been concentrated entirely on the tip sections, corresponding to the region of constant outer diameter of Test Compressor annulus.

2.2.2 UD-0300 Code Modification for Mixtures of Gases

Water vapor is always present in a mixture of air and water droplets. It is in general, therefore, necessary to consider the gas phase as consisting of a mixture of air and water vapor. This is especially so when the water begins to undergo a change of phase and introduces large quantities of vapor into the gas phase. (It may also be pointed out that the change of phase of water itself is governed by the presence of water vapor, for example, high temperature, saturated air permitting little evaporation of water even when the temperature is raised.)

An interesting case of operation of a compressor operating entirely with a mixture of air and water vapor arises when the water in the initial mixture undergoes complete change of phase at some station along the compressor path. This leads to (a) a reduction in gas phase temperature, (b) an increase in vapor content and (c) the consequent changes in the medium properties. It is then of interest to develop a calculation procedure for the flow of a mixture of gases following the station where complete evaporation occurs. Various schemes for the calculation of compressor performance with gas flow continue to become available (Ref. 32) and they may be easily modified for use with mixtures of gases accounting for changes in molecular weight and ratio of specific heats.

The UD-0300 Code for compressor flow calculations (Ref. 10) has been developed for air flow based on the axisymmetric theory of Wennerstrom (Ref. 30) for air flow in compressor. This program has been modified (Ref. 11) for use with gases other than air, in particular air-steam mixture. The detailed procedure for calculations utilizing the modified UD-0300 Code is presented in Appendix 5.

The modified UD-0300 Code can be used in the following cases.

- (1) flow of humid air;
- (2) air-steam mixture, with steam entering at the inlet along with air or after complete evaporation of water;

- (3) water entering the compressor at a suitable location where it undergoes instantaneous and complete evaporation; and
- (4) mixture of air and methane flowing through the compressor.

It may be recalled that the relevant physical properties of steam and methane are sufficiently close that it is of interest in certain cases to perform calculations and also experiments for air-methane mixtures.

The UD-0300 Code is an expensive computer program for operation on a routine basis. The modified UD-0300 program is only recommended for specific calculations the results of which may be compared with those obtained utilizing, for example, one-dimensional flow approximation. This is the manner in which the UD-0300 Code has been utilized here. A further discussion on this is provided in Chapter III of this Report.

2.3 Compressor Performance Calculation

The overall performance of a compressor operating with two phase flow can be obtained in one of two ways: (1) by analyzing and calculating the detailed two phase flow field with work input in the rotors or (2) by first establishing the individual stage characteristic with the most essential features of two phase flow taken into account and then correcting the stage exit flow conditions for other more difficult aspects of two phase flow. Although the basic fluid mechanical equations have been deduced and presented in Appendix 4 for two phase flow with droplets in a compressor, it is clear that a very large number of assumptions pertaining to a variety of processes are required before one can solve the flow equations to any degree of satisfaction. Many of the assumptions may not even be verifiable on their own. In view of this, the approach adopted in the current analysis is the more simplified one, the second of the afore-mentioned approaches.

The simplified approach consists of the following:

- (1) For given initial conditions into a blade row, the state of the fluid (the two phase flow mixture) is established at the

exit of the blade row without detailed modeling of two phase flow processes but taking into account (a) the blockage for air flow introduced by the presence of droplets and (b) the apportionment of work input between the gas and liquid phases, where necessary. This is equivalent to treating the mixture as a continuum in the blade passage but neglecting the processes associated with the presence of discrete droplets, the centrifugal force effects and the heat and mass transfer effects.

- (2) Droplet impact, rebound and reingestion processes are partially included in the foregoing work input calculation through assumptions relating to the number of droplets that may need to be taken into account in the apportionment of work input. The droplet impact and associated processes are also taken into account in calculating (a) the reingestion of droplets into wakes and (b) the effects of centrifugal force action. Finally, those processes are also taken into account, if only indirectly, in adjusting droplet size where necessary.
- (3) The action of centrifugal force is introduced at the exit plane of a stage to determine the redistribution of water content along the blade span.
- (4) Heat and mass transfer processes are included at the exit plane of the stage to determine the "final" temperature and mass fraction of the gas and liquid phases.
- (5) The droplet size at the exit conditions of the stage is adjusted based on droplet equilibrium related to Weber number.
- (6) Based on steps (1) to (5) of the foregoing, one has at the exit of a stage all of the properties of two phase fluid flow. In essence, one has superposed the effects of a number of processes at the stage exit. These conditions are then adjusted, taking into account the area change in the inter-stage spacing, to obtain the entry conditions for the next stage.
- (7) Each of the following stages is then examined on the same bases to obtain the compressor exit flow conditions.

It may be observed in the foregoing that, for most of the processes, a stage of a compressor is the relevant unit of compressor to carry out the calculations. In a few cases, a blade row is the more natural unit taking into account also the inter-blade row space and the processes therein.

2.3.1 Effect of Droplet Size

All of the two phase flow processes depend at every station in the compressor upon the water content and the droplet size. The latter signifies either a nominal size assigned to the droplets in the spray or the various specially determined effective diameters pertinent to different processes. In all cases, one recognizes the presence of a spectrum of sizes and a radial distribution of water content and number density of droplets. The various aero-thermo-mechanical processes associated with droplets can be expected to vary differently and independently with respect to water content and droplet size distribution. In general, increasing water content should affect various aspects of a compressor performance increasingly. The same may not be said with respect to droplet size.

It has, therefore, been considered useful to introduce a classification of sprays into those that consist of "small" droplets and those others that consist of "large" droplets. It is assumed that the small droplet class generally contains small droplets that move with the gas phase with negligible relative velocity. Rain water, even in mist form or even during condensation, may be found under stable conditions only at much larger sizes. However, as a limiting case, the small droplet spray has been postulated to examine the effect of droplet size. On the other hand, the large droplet class is assumed to contain generally larger droplets that can be expected to move largely independent of the gas phase motion.

The two classes of droplets are distinguished further as follows:

- (1) Small droplets, in view of their motion being related to gas

phase motion, absorb some of the work input in rotors and therefore undergo a rise in temperature. Small droplets cause relatively little drag loss. Large droplets, on the other hand, absorb no work input but give rise to drag losses.

- (2) Small droplets suffer centrifugal action both over the surface of blades and in the blade passages, while large droplets may become subjected to centrifugal force only so long as they are on the surfaces of a blade.
- (3) Heat and mass transfer processes arise in both cases, although the magnitude of heat transfer and the resulting change in temperature are different in the two cases because of differences in surface area and volume.

These factors have been taken into account in evolving limiting cases in Chapter III of this Report.

2.4 Scaling of Compressor Performance with Two Phase Flow

The various processes of interest in a compressor during water ingestion are as follows:

- (1) air compression;
- (2) droplet ingestion and its motion;
- (3) absorption of angular momentum by droplets;
- (4) droplet impingement, rebound, break-up, and entrainment;
- (5) film formation and its flow;
- (6) film break-up, reformation of film, formation of droplets, and entrainment from film;
- (7) centrifuging in multiple-curved and rotating passages;
- (8) gravitational action;
- (9) droplet drag;
- (10) film friction
- (11) aerodynamic losses;
- (12) droplet heating;

- (13) droplet vaporization; and
- (14) film vaporization.

Each of the foregoing have characteristic lengths and times that should be considered in relation to the characteristic lengths and times of the compressor. The relations between the two sets of characteristic lengths and times determine the rules for scaling water ingestion effects in different compressors.

Scaling laws for compressor performance with air (single phase) flow are generally well-known (Refs. 23 and 24). In the case of two phase flow, the following additional considerations arise:

- (1) mechanical interactions between droplets and compressor;
- (2) centrifugal force effects;
- (3) aerodynamic phenomena resulting from interactions between droplet and gaseous medium; and
- (4) heat and mass transfer processes.

These processes are strongly interconnected. In particular, the mechanical interactions and centrifugal force effects affect the other two processes. There is considerable uncertainty in regard to the effect of the four processes, since both experiment and analysis are extremely challenging in each case. In order to analyze and to scale the motion of two phase fluid flow in blade passages and over the surface of blades, one needs to have adequate data on the mechanical interactions between blades and droplets. Similarly, in order to scale the deviation and the growth of the (momentum thickness of the) boundary layer over the blade surface, one has to have data concerning the mechanical interactions, and also the flow separation, wake formation and wake growth in the case of two phase fluid flow. Centrifugal force effects and heat and mass transfer processes introduce additional complications.

In considering scaling of compressor performance, one has to consider (a) a single blade, (b) a cascade with finite gap-chord ratio, (c) a blade row in an annulus of finite aspect ratio, (d) a rotor with rotation and work input and (e) two neighboring rows of blades with a finite spacing between them.

The performance of a single blade may be scaled in the same form as that of a wing (Refs. 25 and 26). The presence of droplets in the flow affect (a) the pressure distribution over the blade, (b) the boundary region in the vicinity of the blade and (c) the wake formation. For a given incidence and flow Mach number, one may recognize those in terms of deviation, deflection and losses, using standard compressor cascade terminology. In addition to the foregoing, the state of the fluid also undergoes a change with respect to droplet size distribution between the front and rear of the blade. The change can be related to impingement, rebound, reingestion and droplet size adjustment processes. The principal interest is in the state of the fluid immediately after it has left the trailing edge of the blade. The major uncertainty is the state of the wake in two phase flow. No scaling rules can be given for this. In a given case, if impingement, rebound and reingestion are treated parametrically, the size of droplets in the wake can be established on the basis of equilibrium of forces using the Weber number criterion. Scaling, with respect to the redistribution of water content and droplet size, is the most difficult in every aspect of two phase flow through compressors. Considerable experimental studies are required before useful correlations can be obtained.

In the case of a cascade with finite gap-chord ratio, for a given water content and droplet size distribution in the inlet flow, one can obtain rules for the variation of deviation, deflection and losses with incidence and flow Mach number. The losses may in turn be expressed in terms of diffusion factor and the momentum boundary layer thickness, for example. Proceeding next to a blade row in an annulus of finite aspect ratio, the foregoing rules have to be combined with the design rules utilized for blade design along its span. The finite aspect ratio gives rise to secondary flows, in addition to hub and tip losses. There will also arise a redistribution of water content and droplet size along the blade span at the trailing edge because of induced whirl component.

Next, in the case of a rotor with rotation and work input, one has to take into account, in addition to the various features of a stator flow field, (a) the rise in the temperature of water and of gas, (b) the

change in vapor content, and (c) the centrifugal action induced by the wheel speed. These processes can be scaled based on the laws of heat and mass transfer, and of centrifugal action. However, these processes are again strongly coupled to the droplet mechanical interaction processes. If the droplet dynamics in the rotor can be parametrized, then one can scale the other droplet associated processes.

Finally, a compressor always has some inter-blade row spacing. One has to scale the processes in that region in terms of a short duct with three-dimensional, rotational, wake-like flow in it. In view of the extremely complicated nature of the flow processes in the inter-row spacing (because of the strong interaction between blade rows), it appears that the best approach at the current stage is to include the inter-row spacing with the blade rows. Thus the changes in pressure loss and state of the air-water mixture flow are analyzed as follows: (i) deflection and diffusion are analyzed across the leading and trailing edges of the blade row; and (ii) the changes in the state of the fluid are established between sections located at the middle of the inter-row spacings upstream and downstream of the blade row under consideration. In the case of the first blade row in a compressor, the upstream section may be chosen half-a-chord width upstream of the leading edge of the blade row.

2.4.1 Characteristic Lengths and Times

The following lengths are of interest during two phase flow in a compressor.

- (1) compressor inlet diameter;
- (2) height and aspect ratio of blades;
- (3) distribution of chord and gap-chord ratio of blades in a row and along the compressor;
- (4) distribution of height and aspect ratio of blades along the compressor;
- (5) distribution of tip clearance of rotors along the compressor;
- (6) lengths of blade rows including inter-row spacings along the compressor;

- (7) overall length of the compressor; and
- (8) droplet size and number density distribution.

The following times are of interest:

- (1) air residence time in (a) blade rows, (b) stages, and (c) compressor;
- (2) droplet residence time in (a) blade rows, (b) stages, and (c) compressor;
- (3) inertial relaxation time;
- (4) thermal relaxation time;
- (5) mass transfer relaxation time;
- (6) droplet rupture and reformation times;
- (7) time for blade passage in various blade rows along the compressor; and
- (8) time for one revolution of the compressor.

The principal lengths and times for the Test Compressor are given in Appendix 3.

2.4.2 Scaling Parameters

In order to compare the overall performance of a compressor under given operating conditions (flow coefficient and rotational speed) with two different values of (a) water content, and (b) droplet size, one can employ the following scaling parameters:

- (1) mass fraction of water;
- (2) Ratios of D_{21} , D_{31} , and D_{32} in the spray at entry;
- (3) ratio of heat input required to evaporate all of the water to the work input into the compressor, while operating at the same operating conditions with air;
- (4) Mach number of mixture at inlet; and
- (5) Reynolds number of droplets at entry based on a mean diameter of droplets.

This method of scaling is based on the following reasoning: (a) the mass fraction of water and the Mach number of the mixture at inlet determine the mass flow rate of gas phase at a given flow coefficient;

(b) Items (2), (3), (4), and (5) determine the drag loss, the heat and mass transfer processes and the amount and state of water at a stage outlet and also at compressor outlet.

2.5 Engine Performance Scaling

The general procedure for scaling of installed engine performance under test-bed and installed conditions is discussed in Ref. 33. Engine performance may be scaled among engines of the same class and size taking into account airplane and installation parameters.

The airplane characteristics may generally be presented as a series of plots of dimensionless drag versus Mach number utilizing dimensionless lift as a parameter, each plot applying to a chosen value of the ratio of Reynolds number and Mach number. There is considerable ambiguity about the Reynolds number to be employed. However, the ratio of Reynolds number to Mach number may prove to be a weak variable in a given class and size of airplanes.

The engine characteristics are generally supplied in the form of a series of plots of thrust versus Mach number with air flow and thrust specific fuel consumption as parameters, each plot applying to a chosen altitude. One can re-examine such data in terms of a dimensionless thrust, corrected for the overall efficiency of conversion of available energy, and Mach number. But a further parameter then becomes necessary to account for changes with altitude. Such a parameter may be taken to be the ratio of Reynolds number to the characteristic tip speed of the compressor in the engine. In a given class and size of engines such a parameter may be considered as a weak variable, but appreciable differences arise if very small engines, of vastly different type or geometry and engines designed for high altitude or maneuverability are sought to be compared.

Finally, the engine and the airplane need to be matched. The scaling of a matched system may be examined with reference to the performance characteristics of an installed engine. The matching plot may consist of nondimensional thrust versus Mach number with nondimensional lift as a parameter. However, such a plot may only be used for comparing

systems of similar size and class.

During water ingestion into engines, scaling is of interest in two cases:

- (i) a given engine ingests two different air-water mixtures while operating under the same fuel-throttle and thrust setting; and
- (ii) the same air-water mixture is ingested by two different engines of nearly the same class and size and under similar operating conditions.

The principal engine performance parameters are the following.

- (a) Thrust
- (b) Fuel consumption per unit of thrust per unit of time, and
- (c) Surge margin.

In the case of operation with air, the performance of a simple jet engine can be related to the following.

- (a) Mach number of the air flow in the capture area ahead of the engine.
- (b) Engine operating rotational speed, corrected for inlet temperature.
- (c) Ratio of turbine entry temperature to compressor entry temperature.

The engine performance depends upon whether it is a fixed or variable geometry machine and also on the nature of control incorporated into the engine. In general, the fuel flow rate is employed to regulate the rotational speed, and in a variable geometry engine, the turbine entry temperature may be regulated by change of nozzle area.

During water ingestion into an engine through the compressor, the amount of water ingested, under a variety of droplet size distributions, can be expected to affect the following.

- (a) Mach number for mixture flow in the capture area ahead of the engine

- (b) Air flow into the engine
- (c) Compressor outlet temperature and pressure
- (d) State of the fluid at the exit of the compressor
- (e) Turbine entry temperature corresponding to a fuel mass flow rate, and
- (f) Turbine exit temperature and pressure, which in turn are very nearly the thrust nozzle entry temperature and pressure.

Since the two engines under consideration are assumed to be operating under nearly the same conditions, the Mach number of mixture at entry to the engines should be the same for the same mass fraction of water ingested into the engines. Hence, considering the changes in performance (just mentioned) during water ingestion, the scaling parameters become the following.

- (a) Ratio of turbine entry temperature to mixture temperature at entry to engine, and
- (b) Engine pressure ratio.

Thus, changes in thrust, specific fuel consumption and surge margin can be scaled with respect to the following.

- (a) Mach number of mixture entering the engine
- (b) Ratio of turbine entry temperature to mixture temperature at entry to engine, and
- (c) Engine pressure ratio

These parameters serve to compare the performance of a given engine, at two different conditions of operation, as well as to compare two engines of the same class and approximate size.

CHAPTER III

MODELS FOR LIMITING CASES

The limiting cases investigated are as follows:

- (1) gas mixture flow; the fluid is gas phase only throughout the compressor.
- (2) air-water droplet mixture flow: with the droplets (small in size) following the gas flow path and absorbing work input along with the gaseous phase.
- (3) air-water droplet mixture flow: with the droplets (large in size) moving independently of the gas phase, with equal probability of motion in all directions, and
- (4) air-water droplet mixture flow: with the droplets undergoing sudden evaporation at a particular stage.

These four limiting cases are discussed in detail in the following.

3.1 Model for Gas Mixture Flow Calculation

It has been considered of interest in the current investigation to determine the effect of water vapor on the compressor performance because water vapor is always present in air. Another circumstance in which a gaseous mixture of air and steam arises in a compressor is when, during water ingestion, the conditions become favorable for complete evaporation of water at a location within the compressor. The presence of water vapor gives rise to changes in (1) molecular weight, (2) specific heats, and (3) acoustic speed of the medium. In the present investigation, methane is substituted for water vapor during

some of the experiments, based on similarity laws. Calculations have therefore been performed for both air-steam and air-methane mixtures. The difference between the predicted performance in the two cases has been found to be negligibly small. Performance of the Test Compressor is presented in this Report only for air-methane mixture flow.

Calculations have been performed for air-methane mixture flow utilizing (a) the one-dimensional compressible flow approximation, and (b) the three-dimensional flow UD-0300 Code.

In both cases the gases are assumed to be thoroughly mixed and in thermodynamic equilibrium. Therefore the properties of the mixture can be obtained from the properties of the components of the mixture for given mixture ratios.

In the case of one-dimensional flow approximation, the compressor stage characteristics obtained during tests with air are assumed to be applicable to air-steam and air-methane mixtures. The overall performance of the compressor is obtained by the usual method of stage-by-stage calculation. The calculation procedure is presented in Appendix 6; and thermo-physical properties for the gases are given in Appendix 11.

The procedure for calculations utilizing the UD-0300 Code is given in Appendix 5.

3.2 Model for Air-Water Droplet Mixture Flow with Small Droplets

Small droplets, by definition, belong to the class of droplets that move with negligibly small velocity relative to the gas phase. Therefore, small droplets absorb part of the work input in a compressor and contribute little drag loss. On the other hand, small droplets are assumed to be subjected to heat and mass transfer processes. Finally, the size of small droplets is adjusted at the end of each stage based on Weber number considerations.

The detailed calculation procedure is given in Appendix 7.

The performance calculation is done in two parts.

- (1) The pressure and temperature ratios are calculated in a stage treating the air and droplets as a continuum and utilizing the stage characteristics obtained during tests with air flow.
- (2) All of the processes associated with two phase flow are then taken into account at the exit of the stage. Hence the "final" stage outlet conditions, and also the initial conditions into the next stage, are determined.

The calculations are based on one-dimensional flow approximation and, therefore, can be performed for any chosen section of a stage, with small thickness.

3.2.1 Blockage and Work Input

The presence of droplets introduces a blockage in the flow so that the mass flow of gaseous phase at a particular value of flow coefficient is less than what it would be when there are no droplets. The gaseous phase generally consists of air and water vapor, depending upon the humidity of air.

The work input in a stage has to be apportioned between the gaseous phase and the droplets. The work done on droplets raises the temperature of droplets but does not yield any change in pressure since the droplets are assumed to be not numerous enough to affect the pressure field through random motion.

3.2.2 Mechanical and Aerodynamic Interactions

The following assumptions regarding the mechanical and aerodynamic interactions have been introduced in the model for small droplet calculation.

- (1) The droplets impact the blade surfaces exposed to them in their direction of motion, which is assumed to be the same as that of the gas motion.

- (2) An arbitrary number, such as fifty per cent of the impacting droplets, rebound from the surface. The rebound droplets will then follow the gas phase path in the blade passage along with the droplets that do not impact any surface.
- (3) The impact and rebound of the water droplet do not change its size.
- (4) The droplets that do not rebound from the blade surface suffer centrifugal force action and become displaced spanwise, but are eventually reingested into blade wakes.
- (5) The droplet size of reingested water is determined by consideration of Weber number at the end of each blade row. It is assumed that a droplet on reingestion has zero velocity immediately at blade trailing edge and its size is determined based on the critical Weber number.

The foregoing assumptions are used at the entrance to each stage.

3.2.3 Centrifugal Force Action

The centrifugal force acting on the droplets due to rotor rotation leads to a change in water content of the mixture along the span of the blade. In particular, one is interested in the concentration of water at the tip sections of blades and the depletion of water at the root sections. More generally, the spanwise redistribution of water is required. It may be recalled that the calculations based on one-dimensional flow approximation apply to a particular section of the stage (with a small thickness). The tip section is of interest from several points of view.

The method of incorporating centrifugal action into the model is as follows. The entire blade span is divided into a certain number of sections, one of which is the tip section of the blade. The distance along the chord between the entry and exit section of the blade is also divided into a series of stations. In view of the modeling of mechanical interaction between the droplets and blades in terms of impact, rebound and reingestion into blade wake, it is assumed that centrifugal action

in the case of small droplets applies to all of the droplets that enter the blade passage. Thus, in the present model, centrifugal action is applied both to droplets impinging on the blades and moving over the blade surface into the blade wake, as well as to the droplets moving with the gas phase in the blade passage. Centrifugal action is then imposed on the droplets at each of the blade sections, radially outwards from the hub to the tip and along the chord successively from the entry to the exit section of the blade row under consideration. The foregoing calculation of centrifugal action is completely separated from the other parts of the calculation. It is undertaken after the work done on the gas phase and liquid phase is established. Thus, the redistribution of droplets is determined after the pressure-rise calculation, only at the exit plane of each blade row.

3.2.4 Transport Processes

The transport processes are included only at the exit plane of each blade row. In other words, the step size in the calculation corresponds to one blade row. The gas phase pressure and temperature rise and the liquid phase temperature rise across a blade row under consideration are first determined without taking transport processes into consideration. Then, at the exit plane of the blade row, the heat and mass transfer processes are calculated locally and the following properties are established as entry conditions to the next blade row.

- (1) gas phase temperature;
- (2) liquid phase temperature;
- (3) heat transfer from gas phase to liquid phase, yielding both a reduction in gas phase temperature and an increase in liquid phase temperature; and
- (4) mass transfer from liquid phase to gas phase, yielding the changes in both droplets size and gas phase mass flow rate. In calculating the change in droplet size due to mass transfer, the nominal diameter of all of the droplets is reduced as required.

The major steps in undertaking calculation of phase change because of the equilibrating mechanisms occurring during changes in pressure and

temperature of the gas phase are as follows:

- (1) Determination of gas phase pressure and temperature and liquid phase temperature,
- (2) Determination of time available for equilibration between gas and liquid phases,
- (3) Selection of a model for the equilibrating process, and
- (4) Calculation of heat and mass transfer processes.

Next, consider the heating of droplets; if the temperature attained by the droplet becomes higher than the local boiling point, a phase change due to vaporization of the droplet takes place and the temperature of gas phase drops substantially due to absorption of latent heat by the droplet. The vaporization of droplets is a rate dependent process and several characteristic lengths and times are involved. It is assumed in the present calculation that the drop in the gas phase temperature of droplets exceeds the local boiling point. The major steps in undertaking calculation of water droplet vaporization are as follows:

- (1) Determination of gas phase and water droplet temperature,
- (2) Determination of time which is available for transport processes,
- (3) Calculation of heat and mass transfer processes, and
- (4) Selection of a model for vaporization.

3.2.5 Scheme of Calculation

In summary, the model for calculation with ingestion of small droplets is based on the following scheme of calculation:

- (1) The gas phase pressure and temperature rise and the liquid phase temperature rise are calculated across a blade row in a single step for given initial conditions pertaining to the following:
 - (a) gas phase composition, taking account of initial humidity of air;
 - (b) gas phase pressure and temperature;

- (c) water content and nominal size of water droplets;
and
- (d) rotor rotational speed.

The droplet motion allowing for impact, rebound, and reingestion into blade wake is taken into account in readjusting the gas phase and liquid phase temperature, and in establishing the mean droplet size at the exit of a blade row.

- (2) The redistribution of water content due to centrifugal action is calculated at the exit plane of the blade row under consideration.
- (3) The nominal size of the droplets is adjusted based on the Weber number at the exit plane of the blade row under consideration.
- (4) The heat and mass transfer processes are taken into account at the exit plane of the blade row under consideration.

The foregoing procedure is repeated in each stage of the compressor, after determining the initial conditions for that stage, in order to obtain the cumulative performance of the compressor.

3.3 Model for Air-Water Droplet Mixture Flow with Large Droplets

Large droplets, by definition, belong to the class of droplets that move independently of the gas phase with respect to both magnitude and direction of velocity. Therefore, no part of the work input goes directly into large droplets and, furthermore, losses due to droplet drag have to be accounted for. Large droplets are also subjected to heat and mass transfer processes. Finally, the size of large droplets needs to be adjusted at the end of each stage, based on Weber number considerations.

The detailed calculation procedure is described in Appendix 8.

The performance calculation is done in two parts.

- (1) The pressure and temperature ratios are calculated in a stage

for air utilizing the stage characteristics obtained from experiments.

- (2) All of the two phase flow processes are then incorporated at the exit of the stage. The calculations are based on one-dimensional flow approximation and therefore can be performed for any chosen section of a stage, with small thickness.

3.3.1 Blockage

The presence of droplets introduces a blockage in the flow so that the mass flow of gaseous phase at a particular value of flow coefficient is less than what it would be when there are no droplets. The gaseous phase, in general, contains water vapor.

3.3.2 Mechanical and Aerodynamic Interactions

The most important assumption made in the case of large droplets is that they move with equal probability in all directions. However, in order to obtain a working model for large droplet motion, the model, shown schematically in Fig. 3.1. is used.

A location upstream of the first stage is chosen where it is assumed that the droplets have the same velocity in magnitude as the gas phase but have equal probability of motion in all directions. This section, for example, may be one-half chord upstream of the first blade row. In the case of subsequent stages, this type of reference location is taken simply midway in the stage spacing.

Referring to Fig. 3.1, at the point of consideration on the reference section, a sector of extent π radians is chosen normal to the axial coordinate direction. The droplets moving in this sector are divided into two groups with reference to the gas flow vector. If the gas flow vector is inclined at an angle β with respect to the axial direction, the droplets become divided into two groups, one in the sector of extent β and the other in the sector of extent $(\pi - \beta)$. Then the droplets in the two sectors are assumed to have mean directions of motion, given by

the bisectrices of β and $(\pi-\beta)$ angles. The mean velocity vector of droplets in the β -sector is associated with a fraction of droplets equal to (β/π) of the total in the π radians sector and the other mean velocity vector is associated with a fraction of droplets equal to $[(\pi-\beta)/\pi]$ of the total. Thus, the number of droplets moving with a mean vector direction inclined at an angle $(\beta/2)$ to the gas phase velocity vector, per unit extent of the blade (along its span), is given by $(N\beta S/\pi)$, where N is the number of droplets per unit normal projected area at inlet and S is the gap between blades. Similarly, the number of droplets moving with a mean vector direction inclined at an angle $[(\pi-\beta)/2]$ to the gas phase velocity vector, per unit extent of the blade (along its span) is given by $[N(\pi-\beta)S]/\pi$. Thus the total number of droplets approaching a blade are divided into two groups; and each group is associated with a mean velocity vector oriented with reference to the gas phase velocity vector.

A similar model is adopted at the entry to each stage of the compressor, utilizing the mid-section in the preceding inter-stage space as the reference section.

Once the number and direction of the two subclasses of droplets is determined, the following assumptions are made regarding the impact, rebound and reingestion processes.

- (1) The droplets impact the blade surfaces exposed to them in the two directions of motion determined.
- (2) An arbitrary number, such as fifty per cent of the impacting droplets, rebound from the surface. The rebound droplets have arbitrary directions but the same relative velocity with gas phase, in magnitude, as on impact.
- (3) The impact and rebound of the water droplets do not change their size.
- (4) The droplets that do not rebound from the blade surface suffer centrifugal force action and become displaced spanwise, but are eventually reingested into blade wakes.
- (5) The droplet size of reingested water is determined by consider-

ation of Weber number at the end of each blade row. It is assumed that a droplet, on reingestion, has zero velocity immediately at blade trailing edge and its size is determined on the basis of critical Weber number.

These assumptions are used at the entrance to each stage. They may be compared with the assumptions employed for the case of small droplets in Section 3.2.2.

3.3.3 Droplet Drag

In the case of large droplets, it is necessary to include droplet drag based on the relative velocity between gas phase velocity and droplet. The pressure loss due to droplet drag is introduced at a stage exit after the stage pressure ratio is calculated for the gas phase based on stage characteristics.

3.3.4 Centrifugal Force Action

The method of calculating spanwise redistribution of droplets due to centrifugal force action in the case of large droplets is the same as that described in Section 3.2.3 for the case of small droplets.

It may be noted that, because of the assumption that large droplets have a motion independent of gas phase motion, the gas phase whirl in the blade passages has little influence on droplet motion. Thus, the only large droplets assumed to suffer centrifugal force action are those that remain (without rebounding) on blade surfaces.

3.3.5 Transport Processes

The heat and mass transfer effects are taken into account, at the exit of a stage, in the case of large droplets on the same basis as described in Section 3.2.4 for the case of small droplets.

3.3.6 Scheme of Calculation

In summary, the model for calculation with ingestion of large drop-

AD-A114 831

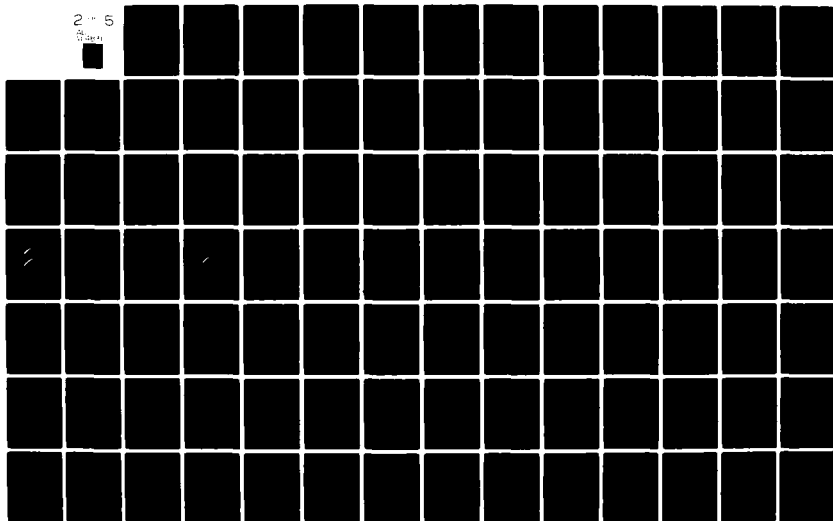
PURDUE UNIV LAFAYETTE IN SCHOOL OF MECHANICAL ENGINEERING F/G 21/5
EFFECT OF WATER ON AXIAL FLOW COMPRESSORS. PART II. COMPUTATION--ETC(U)
JUN 81 T TSUCHIYA, S N MURTHY F33615-70-C-2401

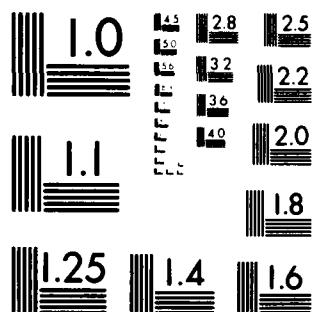
UNCLASSIFIED

AFWAL-TR-80-2090-PT-2

NL

2 5





MICROCOPY RESOLUTION TEST CHART
NATIONAL BUREAU OF STANDARDS 1963-A

lets is based on the following scheme of calculation.

- (1) The gas phase pressure and temperature rise across a stage are calculated in a single step for given initial conditions pertaining to the following:
 - (a) gas phase composition, taking into account the initial humidity of air;
 - (b) gas phase pressure and temperature at entry;
 - (c) blockage introduced by the presence of large droplets; and
 - (d) rotor rotational speed.

The motion of droplets is considered in terms of two subclasses with mean velocities for each. Impact, rebound and reingestion processes are then taken into account in readjusting the gas phase and liquid phase temperature, and in establishing the mean droplet size at the exit of a blade row.

- (2) The redistribution of water content due to centrifugal action is calculated at the exit plane of the blade row under consideration.
- (3) The nominal size of the droplets is adjusted based on Weber number at the exit plane of the blade row under consideration.
- (4) The heat and mass transfer processes are taken into account at the exit plane of the blade row under consideration.

The foregoing procedure is repeated in each stage of the compressor, after determining the initial conditions for that stage, in order to obtain the cumulative performance of the compressor.

The detailed calculation procedure is presented in Appendix 8.

3.4 Model for Air-Water Droplet Mixture Flow with Instantaneous Evaporation of Water

When water droplets evaporate at a certain station in the compressor

it leads to the following: (i) reduction in the temperature of gas phase, (ii) change in the composition and properties of the flowing medium, (iii) change in the operating points of the stages following the position where the water evaporates.

As an illustration the following case may be considered: air-water mixture enters the Test Compressor under a set of initial conditions such that under certain operating conditions, the water undergoes evaporation between the third and the fourth stage. The performance of the compressor becomes affected in the first three stages due to the presence of water ingested with air. It is clear that the performance of stages 4, 5, and 6 are affected because of the evaporation which leads to a reduction in gas phase temperature and addition of water vapor into gas phase. A performance change occurs in each of those stages in the corrected speed, mass flow, pressure ratio, and efficiency, which make up the stage operating point. Thus the overall performance of the compressor also undergoes a change.

As a derivative case of the foregoing, one may consider a simpler case: water at its boiling point corresponding to the pressure at entry to a certain stage is injected at that stage and undergoes immediate and total change of phase. In this case, if for example, water at boiling point is injected at stage 4, stages 1, 2, and 3 operate with air and stages 4, 5, and 6 operate with air-water vapor mixture, the gas phase undergoing a sudden increase in mass flow and a sudden decrease in temperature, both of them due to evaporation of water.

Calculations of Test Compressor performance have been performed in both of the foregoing cases. The detailed calculation procedures are presented in Appendices 9 and 10.

CHAPTER IV

ANALYTICAL RESULTS FOR TEST AXIAL FLOW COMPRESSOR

The performance of the Test Compressor has been calculated under the assumptions of models described in Chapter III.

The performance calculations have been carried out in all of the cases only at the tip section of the Test Compressor. The tip radius is constant in this configuration and, therefore, one-dimensional flow calculations may be applied with some confidence at that section. Furthermore, experimental data obtained in the vicinity of the compressor tip section are probably the most reliable in a small compressor such as the present Test Compressor. Finally, the tip section has the largest amount of water due to centrifuging.

All of the performance calculations have been carried out utilizing the one-dimensional flow approximation. In the case of air-methane mixture flow the UD-0300 code (three-dimensional flow) has also been utilized to calculate the Test Compressor performance at selected conditions of operation.

The results of performance calculations are presented as follows:

- (1) Predicted performance with air-methane mixture: Section 4.1.
- (2) Predicted performance with air-water droplet mixture under the assumption that the droplets are "small": Section 4.2.
- (3) Predicted performance with air-water droplet mixture under the assumption that the droplets are "large": Section 4.3.
- (4) Predicted performance with sudden drop in temperature at a chosen stage of the compressor due to absorption of latent heat for evaporation of water injected at boiling temperature

at that stage: Section 4.4.

This calculation illustrates the change in compressor performance due to reduction in temperature of gas phase at a particular stage in the Test Compressor.

- (5) Predicted performance with air-water droplet ("small droplets") mixture flow at a sufficiently high inlet temperature such that evaporation of water droplets can occur within the compressor: Section 4.5.

This calculation takes into account (a) the absorption of angular momentum by droplets and the resulting heating of droplets, (b) the heating of droplets due to heat transfer between the two phases and (c) evaporation of water wherever the conditions are appropriate.

4.1 Predicted Performance with Air-Methane Mixture

The predicted results for air-methane mixture are presented in Figs. 4.1.1 to 4.1.5. The calculation has been performed at 100 per cent of the design corrected speed. The methane contents investigated are 0.0, 0.02, 0.05, and 0.10, where the definition of methane content is as follows:

$$\text{methane content} = \frac{\text{mass of methane}}{\text{mass of mixture}}$$

Based on unit volume of mixture, the inlet conditions are taken as $T_{01} = 80^\circ\text{F}$ (27°C) and $P_{01} = 14.7\text{ psi}$ ($1.0132 \times 10^5\text{ N/m}^2$).

The predicted results are presented as follows:

Fig. 4.1.1: effect of methane content on overall total pressure ratio;

Fig. 4.1.2: effect of methane content on overall total temperature ratio;

Fig. 4.1.3: effect of methane content on overall adiabatic

efficiency;

Fig. 4.1.4: effect of methane content on stage total pressure ratio (stages 1,2,3); and

Fig. 4.1.5: effect of methane content on stage total pressure ratio (stages 4,5,6).

Each of the foregoing calculations has been performed utilizing the one-dimensional flow approximation. In the case of flow of a mixture of gases, namely the air-methane mixture, calculations have also been performed as stated earlier utilizing the modified UD-0300 program. The results of such three-dimensional flow calculations for selected inlet conditions (Table 4.1.1) are shown in Fig. 4.1.1 along with the predictions based on one-dimensional flow approximation. These calculations serve to illustrate the applicability of the modified UD-0300 program and to compare the predictions based on the two sets of approximations. More extensive three-dimensional flow calculations have not been performed in view of the large costs for exercising the UD-0300 code.

From Figs. 4.1.1 to 4.1.5, the following observations can be made for air-methane mixture flow.

- (1) For a constant initial flow coefficient, overall total pressure ratio decreases as methane content increases.
- (2) For a constant initial flow coefficient, corrected mass flow rate decreases as methane content increases.
- (3) For a constant initial flow coefficient, overall total temperature ratio decreases as methane content increases.
- (4) For a constant initial flow coefficient, there is little change in overall adiabatic efficiency as methane content increases.
- (5) The stage characteristics of Test Compressor are such that the first two stages seem to fall generally into one category and the latter four stages into a second category. Also, it

TABLE 4.1.1

CALCULATION CONDITIONS FOR UD-0300 PROGRAM CODE

	Inlet Temp.		Rotor Speed	Mixture Mass Flow Rate		Methane Content	Corrected Speed	Corrected Mass Flow Rate	
Case	T_{01}		N	\dot{m}		x	$\frac{N}{\sqrt{\theta}}$	$\frac{\dot{m}\sqrt{\theta}}{\delta}$	
	[°F]	[°C]	[RPM]	$[\frac{\text{lbm}}{\delta}]$	$[\frac{\text{kg}}{\delta}]$	[-]	[RPM]	$[\frac{\text{lbm}}{\delta}]$	$[\frac{\text{kg}}{\delta}]$
1	58.7	15.2	51120	3.13	1.36	0.00	51120	3.13	1.36
2	58.7	15.2	51120	3.00	1.30	0.05	51120	3.00	1.30
3	80.0	27.0	52143	3.10	1.35	0.00	51120	3.16	1.38
4	80.0	27.0	52143	3.02	1.32	0.02	51120	3.08	1.34
5	80.0	27.0	52143	3.00	1.30	0.05	51120	3.06	1.33
6	80.0	27.0	52143	2.84	1.24	0.10	51120	2.90	1.26

is observed that the fourth stage characteristic seems to be most sensitive to addition of methane.

- (6) The effect of methane content is much more severe at high mass flow rates.
- (7) The results obtained by utilizing one-dimensional approximation calculation agree reasonably well with those based on three-dimensional UD-0300 code.

4.2 Predicted Performance with Small Droplets

The predicted results for the case of air-water droplet mixture flow with small droplets are presented in Figs. 4.2.1 to 4.2.30. In each of the figures, the gas phase corrected mass flow rate is defined as follows:

$$\text{gas phase corrected flow rate} = \dot{m}_g \sqrt{\theta_g / \delta}$$

where \dot{m}_g is gas phase mass flow rate in lbm/sec or kg/sec, θ_g , the gas phase corrected inlet temperature ($\theta_g = T_{01,g} / T_{ref}$), and δ , the corrected inlet total pressure ($\delta = P_{01} / P_{ref}$), with $T_{ref} = 58.7^\circ\text{F}$ (15.2°C), and $P_{ref} = 14.7 \text{ psi}$ ($1.0132 \times 10^5 \text{ N/m}^2$). The definition of the initial water content is as follows:

$$\text{initial water content} = \frac{\text{mass of water droplets at compressor inlet}}{\text{mass of mixture}},$$

based on unit volume of mixture.

The air-water mixture is assumed to be saturated with water vapor at the local condition of the compressor inlet. The initial droplet diameter is assumed to be 20 μm . The water is redistributed in the compressor due to the centrifugal forces acting on water droplets. The droplet diameter and vapor content vary in the compressor due to the mass transfer and evaporation.

Table 4.2.1 shows the selected conditions for small droplet calculation. In each case, four values of initial water content - 0.00, 0.025, 0.05, and 0.15 - are considered. The results are presented in the following manner for each set of values of the following parameters:

TABLE 4.2.1

CALCULATION CONDITIONS FOR SMALL DROPLETS (20 μm)

Case	Compressor Inlet Temperature	Rotor Rotational Speed
	T_{01}	$\frac{N}{\sqrt{\theta}} / \left(\frac{N}{\sqrt{\theta}} \right)^*$
1	68.0 °F (20.0 °C)	1.00
2	68.0 °F (20.0 °C)	0.90
3	68.0 °F (20.0 °C)	0.80
4	104.0 °F (40.0 °C)	1.00
5	104.0 °F (40.0 °C)	0.90
6	104.0 °F (40.0 °C)	0.80

Note: $\left(\frac{N}{\sqrt{\theta}} \right)^* = 51120$; Design Corrected Speed (RPM)

operational speed, initial temperature and water content.

- (i) overall total pressure ratio, P_{02}/P_{01} , vs. gas phase corrected mass flow rate $(\dot{m}\sqrt{\theta}/\delta)_g$;
- (ii) overall adiabatic efficiency, η , vs. gas phase corrected mass flow rate, $(\dot{m}\sqrt{\theta}/\delta)_g$;
- (iii) overall temperature rise of gas phase, ΔT_g , and of water droplet, ΔT_w , vs. gas phase corrected mass flow rate, $(\dot{m}\sqrt{\theta}/\delta)_g$;
- (iv) temperature of gas phase, T_g , and water droplet, T_w , vs. compressor stage number; and
- (v) water content at blade tip section, $x_{w,tip}$, vs. compressor stage number.

In summary, the predicted performance parameters are presented in Figs. 4.2.1 to 4.2.30 as shown in Table 4.2.2.

From Figs. 4.2.1 to 4.2.30, the following observations can be made for the case of small droplet ingestion.

- (1) For a constant initial flow coefficient, overall total pressure ratio decreases as initial water content increases. The amount of reduction is more severe for higher values of initial flow coefficient.
- (2) For a constant corrected speed, when initial flow coefficient is high, overall adiabatic efficiency decreases as initial water content increases. This trend reverses when initial flow coefficient is low for the same corrected speed.
- (3) For a constant initial flow coefficient, overall temperature rises of both gas phase and water droplet decrease as initial water content increases. The amount of reduction is more severe for higher initial flow coefficient.
- (4) At the outlet of the compressor, temperature of droplets is far below that of gas phase, although water droplet temperature increases due to (i) absorption of angular momentum, and

TABLE 4.2.2

PREDICTED PERFORMANCE PARAMETER FOR SMALL DROPLETS (20 μm)

Compressor Inlet Temperature	Performance Parameter	Rotor 100 %	Rotational 90%	Speed 80%
68.0 °F (20.0 °C)	P_{02}/P_{01}	Fig. 4.2.1	Fig. 4.2.6	Fig. 4.2.11
68.0 °F (20.0 °C)	η	Fig. 4.2.2	Fig. 4.2.7	Fig. 4.2.12
68.0 °F (20.0 °C)	ΔT_g and ΔT_w	Fig. 4.2.3	Fig. 4.2.8	Fig. 4.2.13
68.0 °F (20.0 °C)	T_g and T_w	Fig. 4.2.4	Fig. 4.2.9	Fig. 4.2.14
68.0 °F (20.0 °C)	$x_{w,tip}$	Fig. 4.2.5	Fig. 4.2.10	Fig. 4.2.15
104.0 °F (40.0 °C)	P_{02}/P_{01}	Fig. 4.2.16	Fig. 4.2.21	Fig. 4.2.26
104.0 °F (40.0 °C)	η	Fig. 4.2.17	Fig. 4.2.22	Fig. 4.2.27
104.0 °F (40.0 °C)	ΔT_g and ΔT_w	Fig. 4.2.18	Fig. 4.2.23	Fig. 4.2.28
104.0 °F (40.0 °C)	T_g and T_w	Fig. 4.2.19	Fig. 4.2.24	Fig. 4.2.29
104.0 °F (40.0 °C)	$x_{w,tip}$	Fig. 4.2.20	Fig. 4.2.25	Fig. 4.2.30

Note: (a) The water content is utilized as a parameter.
 (b) Figs. 4.2.1-5, 4.2.6-10, 4.2.11-15, etc. relate to the six cases shown in Table 4.2.1.

- (ii) heat transfer from gas phase.
- (5) Water content at tip increases substantially due to the centrifugal force acting on water droplets.
- (6) Effect of small water droplet ingestion on compressor performance is more severe at high speeds and high mass flow rates than it is at low speeds and low flow rates.

In examining the foregoing, it should be noted that at a given flow coefficient the gas phase corrected mass flow rate decreases as the initial water content is increased. All of the performance predictions have been shown with reference to the inlet gas phase mass flow rate.

4.3 Performance Prediction with Large Droplets

The predicted results for the case of large droplet ingestion are presented in Figs. 4.3.1 to 4.3.30. In each of the figures, the definitions of gas phase corrected mass flow rate and initial water content are the same as those in the case of small droplets. The initial diameter of a large droplet is assumed to be 600 μm .

The six cases investigated are shown in Table 4.3.1. In each case, four values of initial water content - 0.00, 0.025, 0.05, and 0.95 - are considered. The mixture is assumed to be saturated with water vapor at the local condition of the compressor inlet. The results of calculations are presented in the following manner:

- (i) overall total pressure, P_{02}/P_{01} , vs. gas phase corrected mass flow rate, $(\dot{m}\sqrt{\theta}/\delta)_g$;
- (ii) overall adiabatic efficiency, η , vs. gas phase corrected mass flow rate, $(\dot{m}\sqrt{\theta}/\delta)_g$;
- (iii) overall temperature rise of gas phase, ΔT_g , and water droplet, ΔT_w , vs. gas phase corrected mass flow rate, $(\dot{m}\sqrt{\theta}/\delta)_g$;

Table 4.3.1

CALCULATION CONDITIONS FOR LARGE DROPLETS (600 μm)

Case	Compressor Inlet Temperature	Rotor Rotational Speed
	T_{01}	$\frac{N}{\sqrt{\theta}} / \left(\frac{N}{\sqrt{\theta}} \right)^*$
1	68.0 °F (20.0 °C)	1.00
2	68.0 °F (20.0 °C)	0.90
3	68.0 °F (20.0 °C)	0.80
4	104.0 °F (40.0 °C)	1.00
5	104.0 °F (40.0 °C)	0.90
6	104.0 °F (40.0 °C)	0.80

Note: $\left(\frac{N}{\sqrt{\theta}} \right)^* = 51120$; Design Corrected Speed (RPM)

- (iv) temperature of gas phase, T_g , and water droplet, T_w , vs. compressor stage number;
- (v) water content at blade tip sections, $x_{w,tip}$, vs. compressor stage number.

In summary, the predicted performance parameters are presented in Figs. 4.3.1 to 4.3.30 as shown in Table 4.3.2.

From Figs. 4.3.1 to 4.3.30, the following observations can be made for large droplet ingestion:

- (1) For a constant initial flow coefficient, there is little change in overall total pressure ratio as initial water content increases.
- (2) For a constant initial flow coefficient, there is little change in overall adiabatic efficiency as initial water content increases.
- (3) For a constant initial flow coefficient, there is little change in overall temperature rise of both gas phase and droplet as initial water content increases.
- (4) At the outlet of the compressor, the temperature of droplets is far below that of the gas phase. The temperature of droplets changes very little, although droplets receive heat from the gas phase.
- (5) Water content at the tip increases due to centrifugal force acting on droplets. The amount of increase is small compared to that obtained with small droplet ingestion.
- (6) Effect of large water droplet ingestion on compressor performance is more severe at higher speeds and higher mass flow rates.

In examining the foregoing, the following should be noted:

- (1) At a given flow coefficient, the gas phase corrected mass flow rate decreases as the initial water content increases.
- (2) Large droplets do not absorb work input, by assumption.

TABLE 4.3.2

PREDICTED PERFORMANCE PARAMETERS FOR LARGE DROPLETS (600 μm)

Compressor Inlet Temperature	Performance Parameter	Rotor 100%	Rotational 90%	Speed 80%
68.0 °F (20.0 °C)	P_{02}/P_{01}	Fig. 4.3.1	Fig. 4.3.6	Fig. 4.3.11
68.0 °F (20.0 °C)	η	Fig. 4.3.2	Fig. 4.3.7	Fig. 4.3.12
68.0 °F (20.0 °C)	ΔT_g and ΔT_w	Fig. 4.3.3	Fig. 4.3.8	Fig. 4.3.13
68.0 °F (20.0 °C)	T_g and T_w	Fig. 4.3.4	Fig. 4.3.9	Fig. 4.3.14
68.0 °F (20.0 °C)	$x_{w,tip}$	Fig. 4.3.5	Fig. 4.3.10	Fig. 4.3.15
104.0 °F (40.0 °C)	P_{02}/P_{01}	Fig. 4.3.16	Fig. 4.3.21	Fig. 4.3.26
104.0 °F (40.0 °C)	η	Fig. 4.3.17	Fig. 4.3.22	Fig. 4.3.27
104.0 °F (40.0 °C)	ΔT_g and ΔT_w	Fig. 4.3.18	Fig. 4.3.23	Fig. 4.3.28
104.0 °F (40.0 °C)	T_g and T_w	Fig. 4.3.19	Fig. 4.3.24	Fig. 4.3.29
104.0 °F (40.0 °C)	$x_{w,tip}$	Fig. 4.3.20	Fig. 4.3.25	Fig. 4.3.30

Note: (a) The water content is utilized as a parameter

(b) Figs. 4.3.1-5, 4.3.6-10, 4.3.11-15, etc. relate to the six cases shown in Table 4.3.1.

- (3) Only droplets that impact the blades and form a film on them undergo centrifuging, by assumption.

4.4 Performance Prediction with Local Injection and Instantaneous Evaporation of Water

The results of calculation for the case of air-water droplet mixture flow, with instantaneous evaporation of water upon entry into the compressor, are presented in Figs. 4.4.1 to 4.4.24. The various conditions under which the calculations have been performed are shown in Table 4.4.1. In all cases the amount of water undergoing evaporation is taken as 2.5 per cent of the air flow rate. There is no special significance for the choice of 2.5 per cent as the amount of water undergoing evaporation at any selected location. The method of calculation adopted is given in Appendix 9.

In each case, the results of calculations are presented in the following manner:

- (i) Overall total pressure ratio, P_{02}/P_{01} , vs. corrected mass flow rate, $\dot{m}\sqrt{\theta}/\delta$.
- (ii) Overall adiabatic efficiency, η , vs. corrected mass flow rate, $\dot{m}\sqrt{\theta}/\delta$.
- (iii) Changes in individual stage characteristics when evaporation occurs at the designated stage inlet.
- (iv) Total temperature vs. compressor stages.

In (iii), the performance of any stage is denoted by two numbers, X and Y, written as X/Y. The number of the stage under consideration is denoted by X and the number of the stage at which evaporation of water and the consequent reduction in gas phase temperature occur is denoted by Y. The case of just air flow, without injection of any water into the compressor, is denoted by writing Y=0. Thus 5/0 indicates the performance of the 5th stage with air flow only, and 5/4 indicates the performance of the 5th stage with water injection and instantaneous evaporation occurring in the 4th stage. Similarly 4/4 indicates the performance

TABLE 4.4.1

CALCULATION CONDITIONS FOR LOCAL INJECTION
AND INSTANTANEOUS EVAPORATION OF WATER

Case	Inlet Temperature	Rotational Speed
	T_{01}	$\frac{N}{\sqrt{\theta}} / \left(\frac{N}{\sqrt{\theta}} \right)^*$
1	193.4°F (90.0 °C)	1.00
2	193.4°F (90.0 °C)	0.90
3	193.4°F (90.0 °C)	0.80
4	157.4°F (70.0 °C)	1.00
5	157.4°F (70.0 °C)	0.90
6	157.4°F (70.0 °C)	0.80

Note: $\left(\frac{N}{\sqrt{\theta}} \right)^* = 51120$; Design corrected speed

of the 4th stage with evaporation occurring at entry to the 4th stage and 6/4 indicates the performance of the 6th stage with evaporation occurring at entry to the 4th stage.

It should be pointed out here that this part of the investigation pertains entirely to the effect of evaporation of water, leading to a reduction in temperature of the fluid locally, an exchange of mass between the liquid and the vapor phases and consequent change in the molecular weight and specific heat ratio of the gas phase in the compressor. Thus, none of the effects associated with the presence of droplets of water have been included here.

From Figs. 4.4.1 to 4.4.24 the following observation can be made; the evaporation of water droplet and the consequent reduction in gas phase temperature in the compressor improve the overall total pressure ratio but reduce the overall adiabatic efficiency. The magnitude of changes depends upon the inlet temperature, the operational speed and the stage at which evaporation takes place.

4.5 Predicted Performance based upon Air-Water Droplet Mixture Flow with Evaporation

The results of calculations performed at sufficiently high inlet temperatures such that water droplets undergo evaporation in the compressor are presented in Figs. 4.5.1 to 4.5.20. The various conditions under which calculations have been performed are shown in Table 4.5.1. It is assumed in all cases that the droplets belong to the category of small droplets. Thus the assumptions and the general calculation procedure are the same as those discussed in Section 4.4.2 for small droplets. In the earlier calculations discussed in Section 4.4.2, the inlet temperature has been assumed to be small so that no evaporation could occur. But now, the temperature has been taken to be high enough for evaporation to occur.

One important consideration when the inlet temperature is high as

TABLE 4.5.1

CALCULATION CONDITIONS
FOR AIR-WATER DROPLET MIXTURE FLOW WITH EVAPORATION

Case	Rotational Speed $\frac{N}{\sqrt{\theta}} \sqrt{\left(\frac{N}{\sqrt{\theta}}\right)^*}$	Compressor Inlet Temperature T_{01}	Initial Water Content $x_{w,0}$	Initial Vapor Content $x_{v,0}$	Figures
1	1.00	193.4°F(90.0°C)	0.025	0.025	Fig. 4.5.1 to 4.5.5
2	1.00	193.4°F(90.0°C)	0.025	0.43	Fig. 4.5.6 to 4.5.10
3	1.00	193.4°F(90.0°C)	0.025	0.55 ⁺	Fig. 4.5.11 to 4.5.15
4	1.00	193.4°F(90.0°C)	0.025	0.43 ⁺	Fig. 4.5.16 to 4.5.20

⁺ Saturated at compressor inlet.

$\left(\frac{N}{\sqrt{\theta}}\right)^* = 51120$; Design Corrected Speed (RPM)

in the current calculations is the degree of saturation of air. It is therefore a variable in the present calculations. The method of calculation adopted is described in Appendix 10.

The calculated results are presented in the following manner:

- (i) Overall total pressure ratio, P_{02}/P_{01} , vs. gas phase corrected mass flow rate, $(\dot{m}\sqrt{\theta}/\delta)_g$.
- (ii) Overall adiabatic efficiency, η , vs. gas phase corrected mass flow rate, $(\dot{m}\sqrt{\theta}/\delta)_g$.
- (iii) Temperature of gas phase, T_g , temperature of droplet, T_w , the boiling point, T_B , vs. compressor stage number.
- (iv) Mass flow rate of liquid phase at blade tip, $\dot{m}_{w,tip}$, vs. compressor stage number.
- (v) Mass flow rate of gas phase at blade tip, $\dot{m}_{v,tip}$, vs. compressor stage number.

The main observation from Figs. 4.5.1 to 4.5.20 is as follows: The evaporation of water droplets in the compressor improves overall total pressure ratio but reduces overall adiabatic efficiency.

It may be pointed out that a multi-stage compressor yielding a large pressure (and therefore temperature) ratio could cause evaporation of water even when the inlet temperature is low and corresponds to, say, atmospheric conditions. At low temperatures, the saturation value of humidity is also small and therefore there can arise a greater amount of phase change from water to vapor.

4.6 Overall Test Compressor Performance

The overall performance of the compressor for the case of 15 per cent water ingestion has been calculated for conditions as shown in Table 4.6.1. Figures 4.6.1 to 4.6.16 illustrate the performance for various conditions as shown in Table 4.6.2. In each of the figures, the results are presented as follows:

TABLE 4.6.1

CONDITIONS FOR OVERALL PERFORMANCE CALCULATION

Case	Initial Droplet Diameter	Compressor Inlet Temperature (°C)	Rotor Speed $\frac{N}{\sqrt{\theta}} / \left(\frac{N}{\sqrt{\theta}} \right)^*$
1	20 μm	68 °F (20 °C)	1.0, 0.9, 0.8
2	20 μm	104 °F (40 °C)	1.0, 0.9, 0.8
3	600 μm	68 °F (20 °C)	1.0, 0.9, 0.8
4	600 μm	104 °F (40 °C)	1.0, 0.9, 0.8

Note: $\left(\frac{N}{\sqrt{\theta}} \right)^* = 51120$, Design Correct Speed (RPM)

TABLE 4.6.2

Initial Droplet Diameter	Compressor Inlet Temperature	Performance Parameter	No. of Figure
20 μm	68°F (20°C)	Overall pressure ratio	4.6.1
20 μm	68°F (20°C)	Overall temperature rise of gas phase/ inlet temp.	4.6.2
20 μm	68°F (20°C)	Overall temperature rise of droplet/ inlet temp.	4.6.3
20 μm	68°F (20°C)	Work done per unit mass of mixture	4.6.4
20 μm	104°F (40°C)	Overall pressure ratio	4.6.5
20 μm	104°F (40°C)	Overall temperature rise of gas phase/ inlet temp.	4.6.6
20 μm	104°F (40°C)	Overall temperature rise of droplet/ inlet temp.	4.6.7
20 μm	104°F (40°C)	Work done per unit mass of mixture	4.6.8
600 μm	68°F (20°C)	Overall pressure ratio	4.6.9
600 μm	68°F (20°C)	Overall temperature rise of gas phase/ inlet temp.	4.6.10
600 μm	68°F (20°C)	Overall temperature rise of droplet/ inlet temp.	4.6.11
600 μm	68°F (20°C)	Work done per unit mass of mixture	4.6.12
600 μm	104°F (40°C)	Overall pressure ratio	4.6.13
600 μm	104°F (40°C)	Overall temperature rise of gas phase/ inlet temp.	4.6.14
600 μm	104°F (40°C)	Overall temperature rise of droplet/ inlet temp.	4.6.15
600 μm	104°F (40°C)	Work done per unit mass of mixture	4.6.16

- (i) overall pressure ratio, P_{02}/P_{01} , vs. gas phase corrected mass flow rate, $(\dot{m}\sqrt{\theta}/\delta)_g$;
- (ii) ratio of overall temperature rise of gas phase to inlet temperature, $\Delta T_g/T_{01}$, vs. gas phase corrected mass flow rate, $(\dot{m}\sqrt{\theta}/\delta)_g$;
- (iii) ratio of overall temperature rise of droplet to inlet temperature, $\Delta T_w/T_{01}$, vs. gas phase corrected mass flow rate, $(\dot{m}\sqrt{\theta}/\delta)_g$; and
- (iv) work done per unit mass of mixture vs. gas phase corrected mass flow rate.

Overall performance calculations have also been performed for other values of water content, but not shown here. Changes in performance show similar trends at various values of water ingestion.

Figures 4.6.17 and 4.6.18 show the effect of initial water content on (a) the liquid phase mass flow rate at compressor outlet, (b) gas phase mass flow rate at compressor outlet, (c) overall temperature ratio, and (d) overall pressure ratio. The liquid and gas mass flow rates at the inlet to the compressor are also shown for convenience.

CHAPTER V

ENGINE OPERATION WITH WATER INGESTION

The most important feature of an engine operating with water ingestion into its compressor inlet is that the compressor performance becomes altered so completely that the situation is equivalent to operation of the engine with a new compressor even when extreme conditions of operation have not set in. If the compressor surges or the burner suffers a flame-out condition, the engine suffers more severe consequences. However, even with a moderate amount of water ingestion the equilibrium running condition of the engine becomes affected. Depending upon the conditions of operation of the turbine driving the compressor and the thrust nozzle, one may in fact be unable to obtain equilibrium running under a given set of operating and initial conditions: for example, when the turbine or the thrust nozzle remains choked during water ingestion into a simple, constant geometry jet engine.

The manner in which an engine responds to water ingestion depends upon (a) engine design parameters, (b) inlet temperature, (c) vapor and water content at the inlet, (d) conditions of operation and (e) the control scheme included in the engine.

The engine design parameters are (i) component design, (ii) variability of geometry and (iii) performance of various parts of the engine. The water content at the inlet determines the amount of gas phase fluid that enters the compressor at the operating flow coefficient of the compressor, which in turn is a function of the operational condition of the engine.

The control scheme may be based on engine inlet temperature, engine speed, engine pressure ratio, engine temperature ratio or any combination of them. It may regulate the fuel flow rate or the geometry of the engine if there is variable geometry.

The principal performance parameters of interest during water ingestion into engines are (i) the engine operating line, (ii) the surge margin and (iii) the interaction with engine control in operating under equilibrium conditions. In practice these parameters are of interest during transitory conditions. In other words, one has to consider the ingestion of water into the engine under certain operating conditions at a certain instant of time and examine the behavior of the engine, with its control, until a desired equilibrium operating condition is reached. If the time dependent aspects are neglected altogether, say, under the assumption of infinitely slow adjustment from one condition to another, all of the afore-mentioned performance parameters are still of interest. Predictions of performance do become simpler since one does not have to take into account engine inertia, although they are complicated on account of two phase flow effects.

The major two phase flow effects arise through (i) blockage of air flow due to droplets and (ii) distortion of flow at entry to each blade row with respect to (a) water and vapor content, and (b) temperature and pressure distribution, each of them at least in the radial direction. This fact necessitates calculation of spanwise performance of the compressor and the resulting flow into the diffuser. That is a formidable task, as stated earlier, in the case of two phase flow, unless it is carried out under a set of approximations. In any case, one needs to obtain the distortion parameters mentioned earlier and the difference in performance between various sections along the span of the blade for each stage and cumulatively. At a particular condition of operation, it is possible that the root of a blade may be close to stalling with gas phase flow while the tip is close to choking on account of the large amount of water present in that section.

In the current investigation, no experiments have been included on an engine with water ingestion. On the other hand, models have been developed for compressor performance with water ingestion and predictions have been sought to be compared with measurements of overall performance. Accordingly engine performance with water ingestion has been studied only with respect to the following.

- (1) Establishment of equilibrium running conditions with water ingestion into engine inlet.
- (2) Analysis of an engine operating with severe radial distortion in regard to water and water vapor distribution.

In regard to the latter, the equilibrium running of the engine can be examined when the root section is operating, for example, entirely with gaseous phase and the tip section is operating with a large amount of centrifuged water.

A simple constant geometry jet engine, as shown in Fig. 5.1, is examined.

5.1 Criteria for Equilibrium Running

In order to obtain the equilibrium running point, three matching conditions must be satisfied. They are (1) engine shaft speed balance, (2) mass flow rate balance, and (3) power balance.

5.1.1 Engine Shaft Speed Balance

When the compressor and turbine shafts are directly coupled, it follows that:

$$\frac{N}{\sqrt{\theta}_{t4}} = \frac{N}{\sqrt{\theta}_{t2,g}} \sqrt{\frac{T_{t2,g}}{T_{t4}}}$$

where subscripts t, g, 2, and 4 refer to total temperature, gas phase, compressor inlet, and turbine inlet.

5.1.2 Mass Flow Rate Balance

The turbine and compressor inlet mass flow rates can be related as follows.

$$\dot{m}_4 = \dot{m}_2 + \dot{m}_f$$

Since $\dot{m}_2 = \dot{m}_{2,g} + \dot{m}_{2,w}$, one can get

$$\dot{m}_4 = \dot{m}_{2,g} + \dot{m}_{2,w} + \dot{m}_f$$

The mass balance equation can then be written as follows.

$$\begin{aligned} \frac{\dot{m}_4 \sqrt{\theta_{t4}}}{\delta_{t4}} &= \frac{\dot{m}_{2,g} \sqrt{\theta_{t2,g}}}{\delta_{t2}} \sqrt{\frac{T_{t4}}{T_{t2,g}}} \frac{P_{t2}}{P_{t4}} \\ &+ \frac{\dot{m}_4 \sqrt{\theta_{t4}}}{\delta_{t4}} \frac{\dot{m}_2}{\dot{m}_4} \left(\frac{\dot{m}_{2,w}}{\dot{m}_2} + \frac{\dot{m}_f}{\dot{m}_2} \right) \end{aligned}$$

Writing

$$f = \dot{m}_f / \dot{m}_{2,g}, \text{ and}$$

$$x_w = \dot{m}_{2,w} / \dot{m}_2,$$

and noting that

$$\frac{\dot{m}_f}{\dot{m}_2} = (1 - x_w)f, \text{ and}$$

$$\frac{\dot{m}_2}{\dot{m}_4} = \frac{1}{1 + f(1 - x_w)}, \text{ it follows that,}$$

$$\frac{\dot{m}_4 \sqrt{\theta_{t4}}}{\delta_{t4}} = \frac{1 + f(1 - x_w)}{1 - x_w} \frac{\dot{m}_{2,g} \sqrt{\theta_{t2,g}}}{\delta_{t2}} \sqrt{\frac{T_{t4}}{T_{t2,g}}} \frac{1}{(P_{t3}/P_{t2})(P_{t4}/P_{t3})}$$

The combustor and compressor inlet mass flow rates are related by writing

$$\begin{aligned}\dot{m}_3 &= \dot{m}_{2,g} + \dot{m}_{2,w} \\ &= \dot{m}_{2,g}(1 + x'_w)\end{aligned}$$

where $x'_w = \dot{m}_{2,w}/\dot{m}_{2,g} = x_w/(1 - x_w)$

Therefore, one obtains the following.

$$\frac{\dot{m}_3 \sqrt{\theta_{t3,g}}}{\delta_{t3}} = \frac{\dot{m}_{2,g} \sqrt{\theta_{t2,g}}}{\delta_{t2}} \frac{(1 - x_w)^{-1}}{(P_{t3}/P_{t2})} \sqrt{\frac{T_{t3,g}}{T_{t2,g}}}$$

5.1.3 Power Balance

For equilibrium running, the power output of the turbine must match that required by the compressor and any auxiliary load.

Therefore, the power balance equation can be written as follows.

$$\begin{aligned}\dot{m}_4 \bar{c}_{p_T} (T_{t4} - T_{t5}) \eta_M &= \dot{m}_{2,g} \bar{c}_{p_c} (T_{t3,g} - T_{t2,g}) \\ &+ \dot{m}_{2,w} c_w (T_{t3,w} - T_{t2,w})\end{aligned}$$

where η_M is mechanical loss.

Since $\dot{m}_4 = \dot{m}_2 + \dot{m}_f = \dot{m}_{2,g} + \dot{m}_{2,w} + \dot{m}_f$, one can write the power balance equation as follows.

$$\begin{aligned}\left(1 + \frac{\dot{m}_f}{\dot{m}_2}\right) \bar{c}_{p_T} (T_{t4} - T_{t5}) \eta_M &= \frac{\dot{m}_{2,g}}{\dot{m}_2} \bar{c}_{p_c} (T_{t3,g} - T_{t2,g}) \\ &+ \frac{\dot{m}_{2,w}}{\dot{m}_2} c_w (T_{t3,w} - T_{t2,w})\end{aligned}$$

Using the expressions for mass flow ratio, one obtains the following.

$$\begin{aligned} \frac{T_{t4} - T_{t5}}{T_{t4}} = & \frac{1}{\{1 + f(1 - x_w)\} \bar{c}_{pT} \eta_M} \left\{ (1 - x_w) \bar{c}_{pC} \left(\frac{T_{t3,g} - T_{t2,g}}{T_{t2,g}} \right) \right. \\ & \left. + x_w c_w \left(\frac{T_{t3,w} - T_{t2,w}}{T_{t2,w}} \right) \right\} \cdot \left(\frac{T_{t2,g}}{T_{t4}} \right) \end{aligned} \quad (5.1.4)$$

5.1.4 Gas Generator Matching

An equilibrium operating point for a simple, constant geometry gas generator can be obtained by solving simultaneously Eqs. 5.1.1 to 5.1.4, if the compressor, burner and turbine efficiencies and pressure losses in various parts are known. The equilibrium point can be defined, as usual, in terms of the following:

$$\begin{aligned} N/\sqrt{\theta_{t2,g}} \quad , \quad \dot{m}_{2g} \sqrt{\theta_{t2}} / \delta_{t2} \quad , \quad P_{t3}/P_{t2} \quad , \\ T_{t4}/T_{t2,g} \quad , \quad P_{t5}/P_{t2,g} \quad . \end{aligned}$$

In general, it is of interest to determine the fuel flow rate. It can be expressed as follows.

$$\begin{aligned} \dot{m}_f \eta_B \Delta H_C = & \dot{m}_{3,g} \bar{c}_{pB} (T_{t4} - T_{t3,g}) \\ & + \dot{m}_{3,w} c_w (T_s - T_{t3,w}) + \Delta H_v + \bar{c}_{pB} (T_{t4} - T_s) \end{aligned}$$

where T_s is saturation temperature, ΔH_v , latent heat of vaporization, ΔH_C heating value of fuel, and c_w specific heat of water. Using Eq. (5.1.3), this equation becomes the following.

$$\frac{\dot{m}_f}{\delta_{t2} \sqrt{\theta_{t2,g}}} = \frac{\dot{m}_{2,g} \sqrt{\theta_{t2,g}}}{\delta_{t2}} \frac{T_{ref}}{\eta_B \Delta H_C (1 - x_w)} \cdot \left\{ \bar{c}_{pB} \left(\frac{T_{t4}}{T_{t2,g}} - \frac{T_{t3,g}}{T_{t2,g}} \right) \right.$$

+ continued

$$\begin{aligned}
& + \frac{\dot{m}_{3,w}}{\dot{m}_{3,g}} \frac{T_{t2,g}}{T_{t3,g}} \left[c_w \left(\frac{T_s}{T_{t2,g}} - \frac{T_{t3,g}}{T_{t2,g}} \frac{T_{t3,w}}{T_{t3,g}} \right) \right. \\
& \left. + \frac{\Delta H_v}{T_{t2,g}} + \bar{c}_{pB} \left(\frac{T_{t4}}{T_{t2,g}} - \frac{T_s}{T_{t2,g}} \right) \right] \} \quad (5.1.5)
\end{aligned}$$

5.2 Gas Generator Nozzle Matching

The continuity equation for converging nozzle can be written as follows.

$$\dot{m}_6 = A_7 \psi P_{t6} / \sqrt{RT_{t6}} C_d$$

where subscripts 6 and 7 are nozzle inlet and nozzle throat, respectively. C_d is discharge coefficient, and ψ is defined as follows.

$$\psi = \left\{ \frac{2\gamma}{\gamma-1} \left(\frac{P_7}{P_{t6}} \right)^{\frac{2}{\gamma}} \left[1 - \left(\frac{P_7}{P_{t6}} \right)^{\frac{\gamma-1}{\gamma}} \right] \right\}^{1/2}$$

Therefore, the nozzle corrected flow per unit area is

$$\frac{\dot{m}_6 \sqrt{T_{t6}}}{P_{t6} A_7} = \frac{\psi C_d}{\sqrt{R}} \quad (5.2.1)$$

If the nozzle is choked, then

$$\frac{P_{t6}}{P_7} = \left(\frac{\gamma+1}{2} \right)^{\frac{\gamma}{\gamma-1}} \quad (5.2.2)$$

If the nozzle is not choked, then the value of P_{t6}/P_7 is determined by the engine operating point, inlet duct loss, the flight Mach number, and the exhaust duct loss as follows.

$$\frac{P_{t6}}{P_7} = \frac{P_{t6}}{P_0} = \frac{P_{t0}}{P_0} \frac{P_{t2}}{P_{t0}} \underbrace{\frac{P_{t3}}{P_{t2}} \frac{P_{t4}}{P_{t3}} \frac{P_{t5}}{P_{t4}}}_{\frac{P_{t5}}{P_{t2}}} \frac{P_{t6}}{P_{t5}} \quad (5.2.3)$$

where $\frac{P_{t0}}{P_0}$ = flight Mach number effect

$\frac{P_{t2}}{P_{t0}}$ = inlet duct loss

$\frac{P_{t5}}{P_{t2}}$ = engine operating point, and

$\frac{P_{t6}}{P_{t5}}$ = exhaust duct loss.

With the value of ψ determined by P_{t6}/P_7 , the operation of the gas generator at a specified point ($N/\sqrt{\theta_{t2,g}}$, $T_{t4}/T_{t2,g}$) requires a unique nozzle throat area as follows.

$$\begin{aligned} (A_7)_{\text{eff}} = A_7 C_d &= \frac{\dot{m}_6 \sqrt{T_{t6}}}{P_{t6}} \frac{\sqrt{R}}{\psi} \\ &= \frac{\dot{m}_5 \sqrt{T_{t5}}}{P_{t5}} \frac{P_{t5}}{P_{t6}} \sqrt{\frac{T_{t6}}{T_{t5}}} \frac{\sqrt{R}}{\psi} \\ &= \frac{\dot{m}_5 \sqrt{\theta_{t5}}}{\delta_{t5}} \frac{\sqrt{T_{\text{ref}}}}{P_{\text{ref}}} \left(\frac{P_{t5}}{P_{t6}} \right) \sqrt{\frac{T_{t6}}{T_{t5}}} \frac{\sqrt{R}}{\psi} \\ &= \frac{\dot{m}_4 \sqrt{\theta_{t4}}}{\delta_{t4}} \frac{P_{t4}}{P_{t5}} \sqrt{\frac{T_{t5}}{T_{t4}}} \frac{\sqrt{T_{\text{ref}}}}{P_{\text{ref}}} \frac{P_{t5}}{P_{t6}} \sqrt{\frac{T_{t6}}{T_{t5}}} \frac{\sqrt{R}}{\psi} \end{aligned} \quad (5.2.4)$$

5.2.1 Engine Performance Parameters

Based on the foregoing, the following engine performance parameters can be obtained at each equilibrium operating point:

- (i) engine thrust,
- (ii) engine thrust specific fuel consumption, and
- (iii) surge margin.

At each operating point, one can examine the performance of each stage of the compressor and establish whether the stage is tending towards choking or stalling. The overall performance of the compressor may also be examined for similar trends.

5.3 Radial Distortion Effects

The radial distortion introduced by water ingestion arises with respect to the following:

- (1) water content,
- (2) gas phase mixture content,
- (3) gas phase temperature,
- (4) gas phase pressure,
- (5) water temperature, and
- (6) flow Mach number,

at the end of each stage in comparison with the values of some of these parameters during operation with air and also in comparison with the entry conditions. The effects of distortion are important both in the compressor and the engine components following the compressor.

Among the foregoing parameters which may suffer distortion, the spanwise variation of water content along the compressor is especially significant during two phase flow. At some particular stage in a multi-stage compressor, because of centrifugal force and phase change effects, the root section may be entirely devoid of water and the tip

section may have a large amount of water while there is a distribution of water content from root to tip.

In the case of the Test Compressor, the manner in which water becomes centrifuged away from the root section is illustrated in the following figures.

- (i) Fig. 5.3.1, which shows how a particle of water at the hub moves towards the tip at various operating speeds when the flow coefficient is 0.46 and the droplets are small.
- (ii) Fig. 5.3.2, which shows how a particle of water at the hub moves towards the tip at various operating speeds when the flow coefficient is (again) 0.46 and the droplets are large.
- (iii) Fig. 5.3.3, which shows how the mass flow rate of water at the hub changes due to centrifuging along the compressor at various operating speeds when the flow coefficient is 0.46 and the droplets are small.
- (iv) Fig. 5.3.4, which shows how the mass flow rate of water at the hub changes due to centrifuging along the compressor at various operating speeds when the flow coefficient is 0.46 and the droplets are large.

The calculation procedure is that given in Appendix 7 and Appendix 8. Similar predictions can be obtained for other values of flow coefficient.

It may be recalled that centrifuging of water is independent of water content. The difference between Figs. 5.3.1 and 5.3.2 is due to the assumptions made regarding which portions of small and large droplets undergo centrifuging; similarly the difference between Figs. 5.3.3 and 5.3.4. It is also important to recognize the manner in which the hub radius changes while the tip radius is constant (Fig. 5.3.5) in the Test Compressor. Thus, in the case of a compressor with a different geometry and utilizing other assumptions regarding the fraction of droplets that centrifuge, other variations in water content may be obtained along the compressor.

Referring to Fig. 5.3.3, over the range of operating speeds considered, the hub becomes completely depleted of water in the vicinity of the fourth stage. On the other hand, in the case of large droplets, as in Fig. 5.3.4, even at 100 per cent design speed there is some water at the hub all the way up to the sixth stage. At lower speeds, there is a redistribution of water content but there is still an appreciable amount of water at the hub; for example, at 80 per cent design speed, about 40 per cent of the water that entered the hub section at inlet is still present at the hub of the sixth stage.

It may be pointed out that phase change of water to vapor has been taken into account in obtaining the foregoing predictions.

In examining radial distortion effects, a limiting case can be considered, for example, corresponding to operation of the compressor under the conditions employed in obtaining the predictions displayed in Fig. 5.3.3: at design speed, the hub of the compressor is operating entirely with gaseous phase after the fourth stage and the tip section has a substantial amount of water.

The variation of mass flow rates of gas and liquid phases in different stages of the compressor while operating at two different speeds is shown in Figs. 5.3.5 to 5.3.8 for various initial conditions as shown in Table 5.3.1. It will be observed that all of the illustrations are for 15 per cent ingestion of water and apply to the tip section of the compressor. Figures 5.3.5 to 5.3.8 can then be examined in relation to the overall compressor performance maps given in Figs. 4.6.1 to 4.6.16, which also apply to the tip section of the compressor. One can observe in them the extent and nature of the difference between operation with air and with air-water mixture. This difference then affects the equilibrium running of the engine.

5.3.1 Radial Distortion Index for Water Ingestion

A radial distortion index may be postulated for any stage of a compressor, with water ingestion, as the distortion that arises at the exit

TABLE 5.3.1

OPERATING CONDITIONS FOR FIGURES 5.3.5 TO 5.3.8

Initial Droplet Diameter	Compressor Inlet Temperature	Initial Water Content	Rotor Speed	Parameter	Figure
D_0	T_{01}	$x_{w,0}$	$\frac{N}{\sqrt{\theta}} / \left(\frac{N}{\sqrt{\theta}}\right)^*$		
20 μm	68 °F(20 °C)	0.15	0.8,0.9,1.0	$\Delta\dot{m}_g/\dot{m}_{g,in}$	5.3.6
600 μm	68 °F(20 °C)	0.15	0.8,0.9,1.0	$\Delta\dot{m}_g/\dot{m}_{g,in}$	5.3.7
20 μm	68 °F(20 °C)	0.15	0.8,0.9,1.0	$\Delta\dot{m}_w/\dot{m}_{w,in}$	5.3.8
600 μm	68 °F(20 °C)	0.15	0.8,0.9,1.0	$\Delta\dot{m}_w/\dot{m}_{w,in}$	5.3.9

Note: $\left(\frac{N}{\sqrt{\theta}}\right)^* = 51120$; Design Corrected Speed (RPM)

plane of the stage under design conditions (speed and flow coefficient) with a given air-water droplet mixture entering uniformly at the compressor inlet. The design condition may be chosen as either the stage design point or the stage operating point corresponding to engine design point. It may be observed that distortion is defined with respect to compressor inlet conditions rather than the inlet conditions of the stage under consideration. This is essential since in the case of two phase flow the outlet conditions at any stage are affected by the entire compressor section upstream of it. A distortion coefficient for each stage with respect to uniform conditions at its entry may also be defined whenever necessary, but is generally less useful than the overall distortion index up to the stage under consideration.

On the same basis, one may define the cumulative distortion index for a compressor.

Considering various parameters of interest during water ingestion, it is proposed that an overall distortion index be defined as follows.

$$K = K_p + K_T + K_W + K_V + K_M \quad (5.3.1)$$

$$\text{where } K_p = \frac{\sum_{i=1}^n (\bar{P} - P_i) D_i^{-x_1}}{\bar{P} \sum_{i=1}^n D_i^{-x_1}} : \text{total pressure distortion index,}$$

$$K_T = \frac{\sum_{i=1}^n (\bar{T} - T_i) D_i^{-x_2}}{\bar{T} \sum_{i=1}^n D_i^{-x_2}} : \text{total temperature distortion index,}$$

$$K_W = \frac{\sum_{i=1}^n (\bar{X}_W - X_{W,i}) D_i^{-x_3}}{\sum_{i=1}^n D_i^{-x_3}} : \text{water content distortion index,}$$

$$K_V = \frac{\sum_{i=1}^n (\bar{X}_V - X_{V,i}) D_i^{-x_4}}{\sum_{i=1}^n D_i^{-x_4}} : \text{vapor content distortion index,}$$

$$K_M = \frac{\sum_{i=1}^n (\bar{M} - M_i) D_i^{-x_5}}{\sum_{i=1}^n D_i^{-x_5}} : \text{Mach number distortion index,}$$

and the properties P_i , T_i , $X_{W,i}$, $X_{V,i}$, and M_i are total pressure, total temperature, water content, vapor content, and Mach number at radial location D_i . The average is designated by the bar and the weighting factor x_i ($i=1, 2, 3, 4, 5$) is introduced to account for distortion sensitivity.

The overall distortion index is not wholly satisfactory since distortions with respect to each of the selected parameters is given equal weightage in Eq. 5.3.1 and also the various distortions are simply added.

A further simplification can be introduced by considering only the distributions of water content and Mach number. This can be justified by noting that the inlet temperature, flow coefficient and water content largely determine the performance of a compressor at a given speed, including heat and mass transfer processes. One can then modify Eq. 5.3.1 by writing

$$D = K_W + K_M \quad (5.3.2)$$

It may be observed that the radial distortion index serves as a performance parameter in itself. It can also be employed as a means of studying engine and control system performance.

FIGURES

Fig. 1.1 Atmospheric Particle Size Ranges

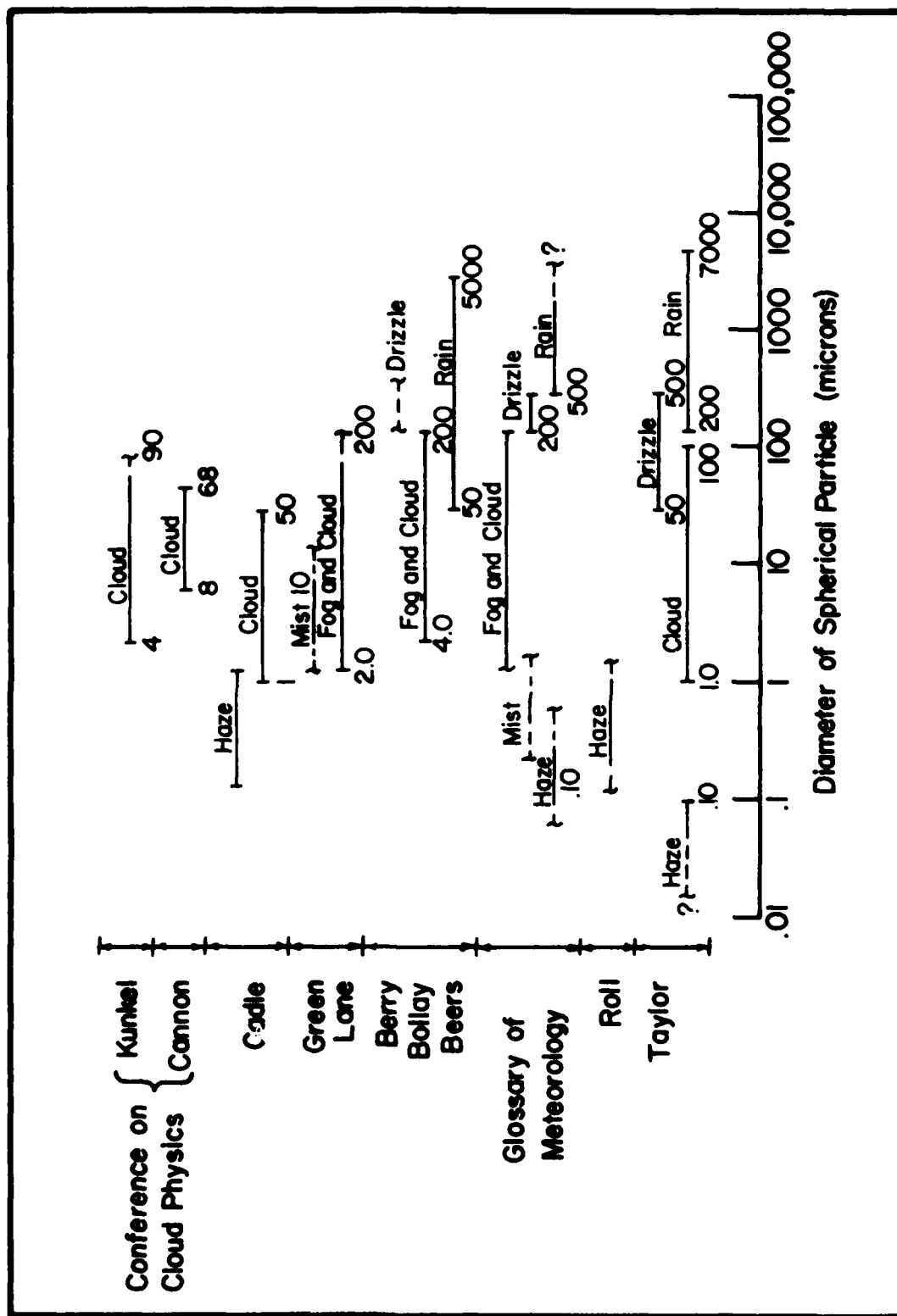
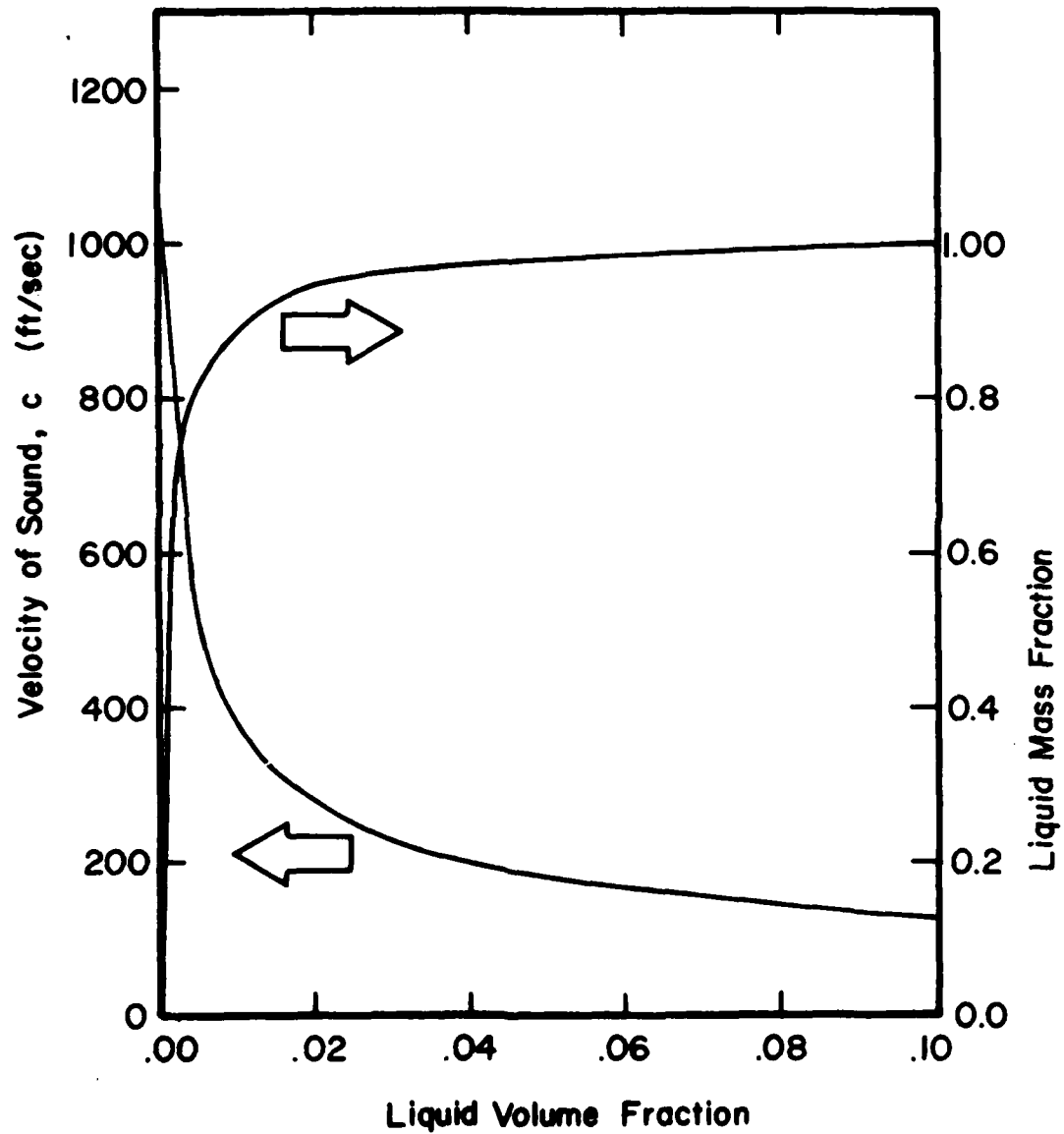


Fig. 2.1
VELOCITY OF SOUND
vs.
LIQUID VOLUME FRACTION
(At Standard Atmospheric Conditions)



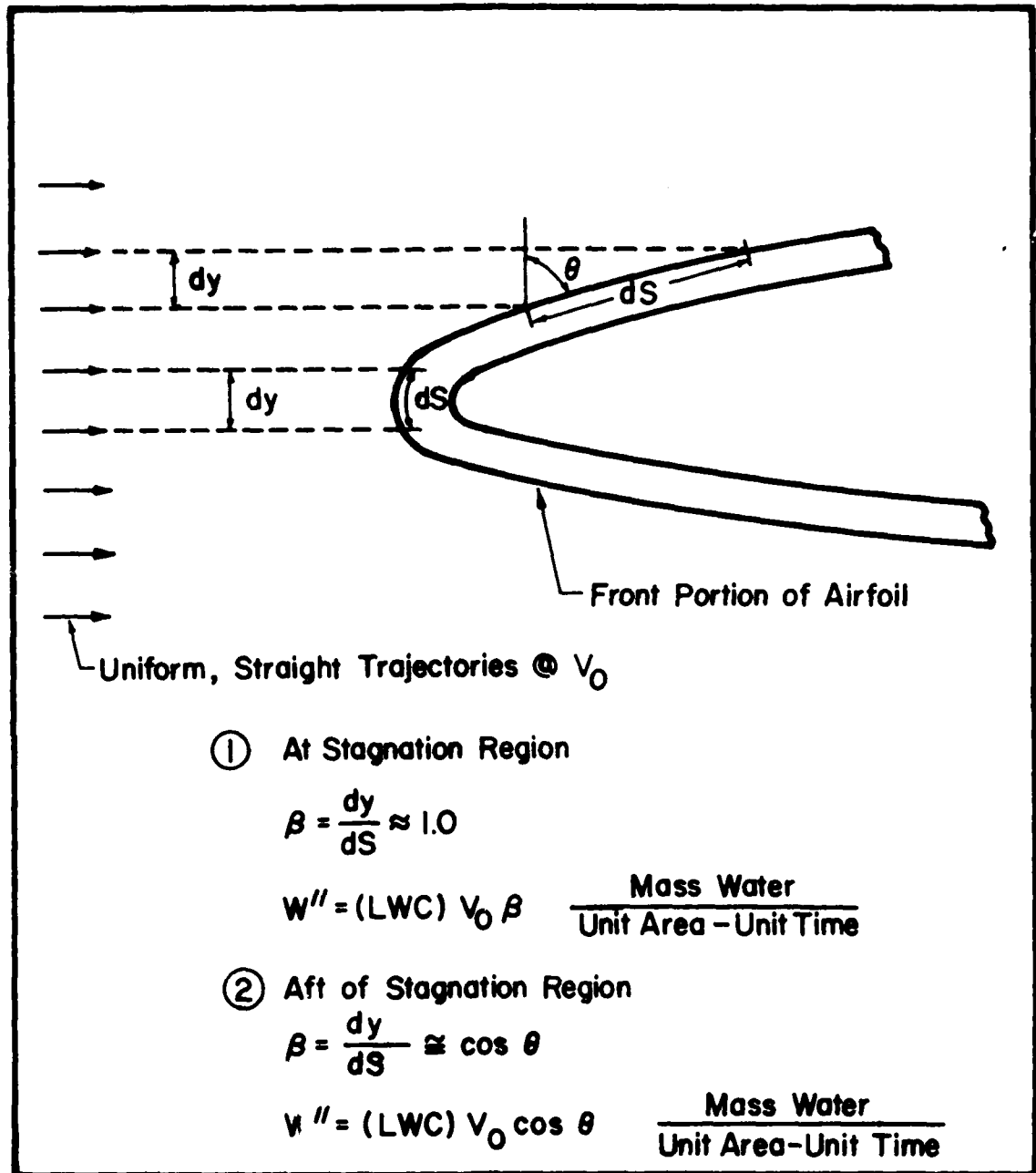


Fig. 2.2 Local Impingement Rates on Compressor Airfoils (Ref. 6)

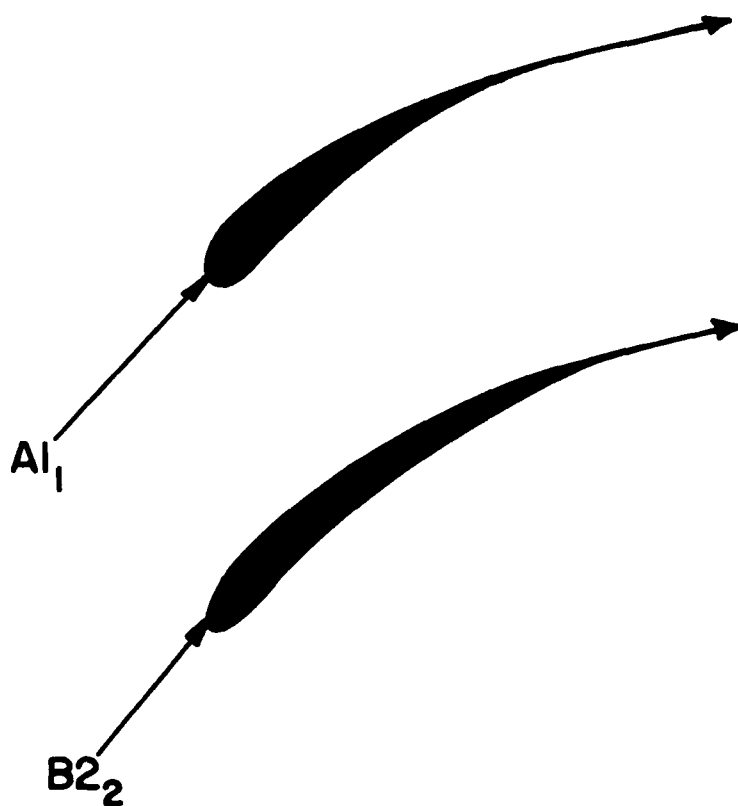


Fig.2.3 Streamlines (Model for Droplet Motion)

Fig.2.4 Droplet Radial Location in Rotor

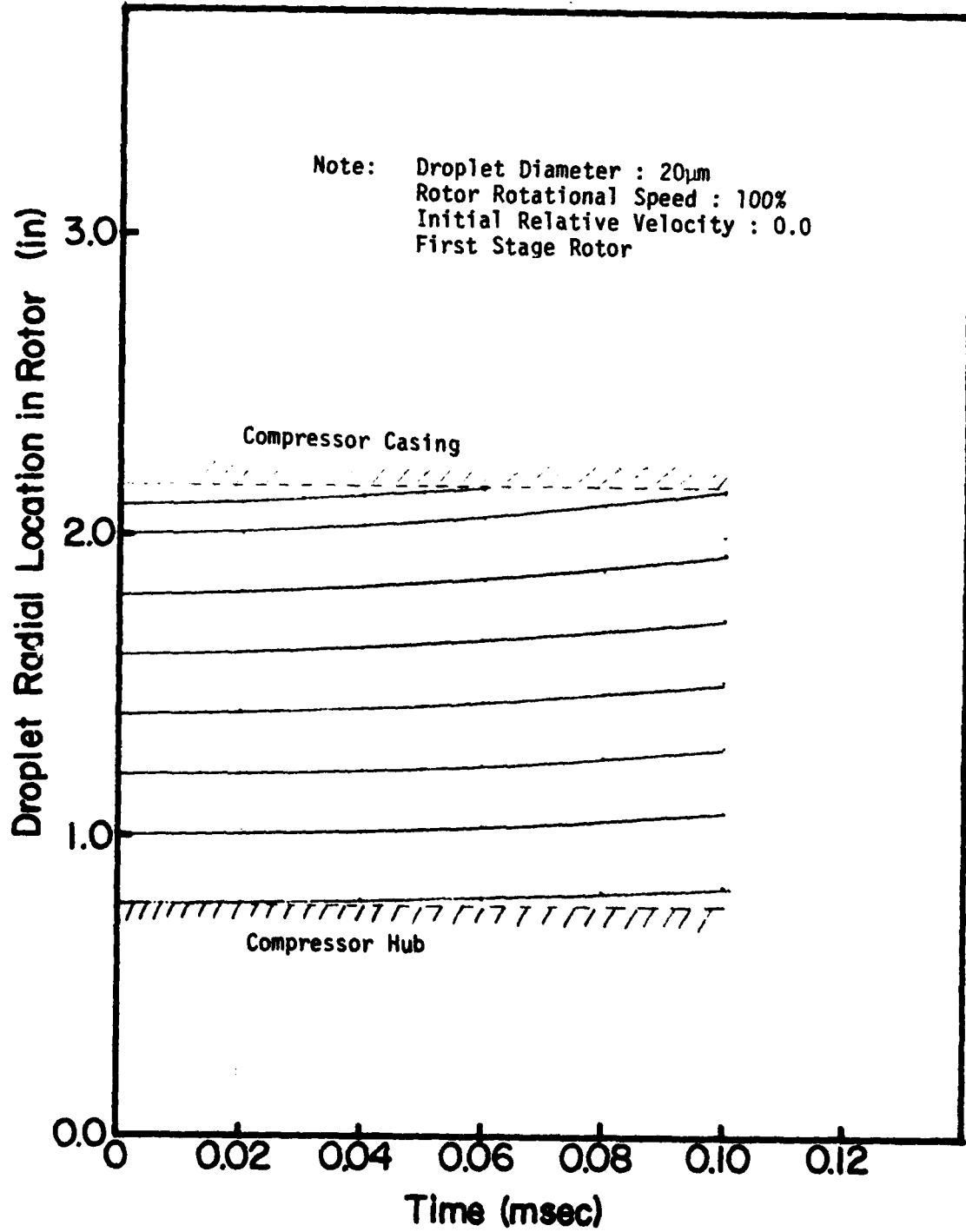
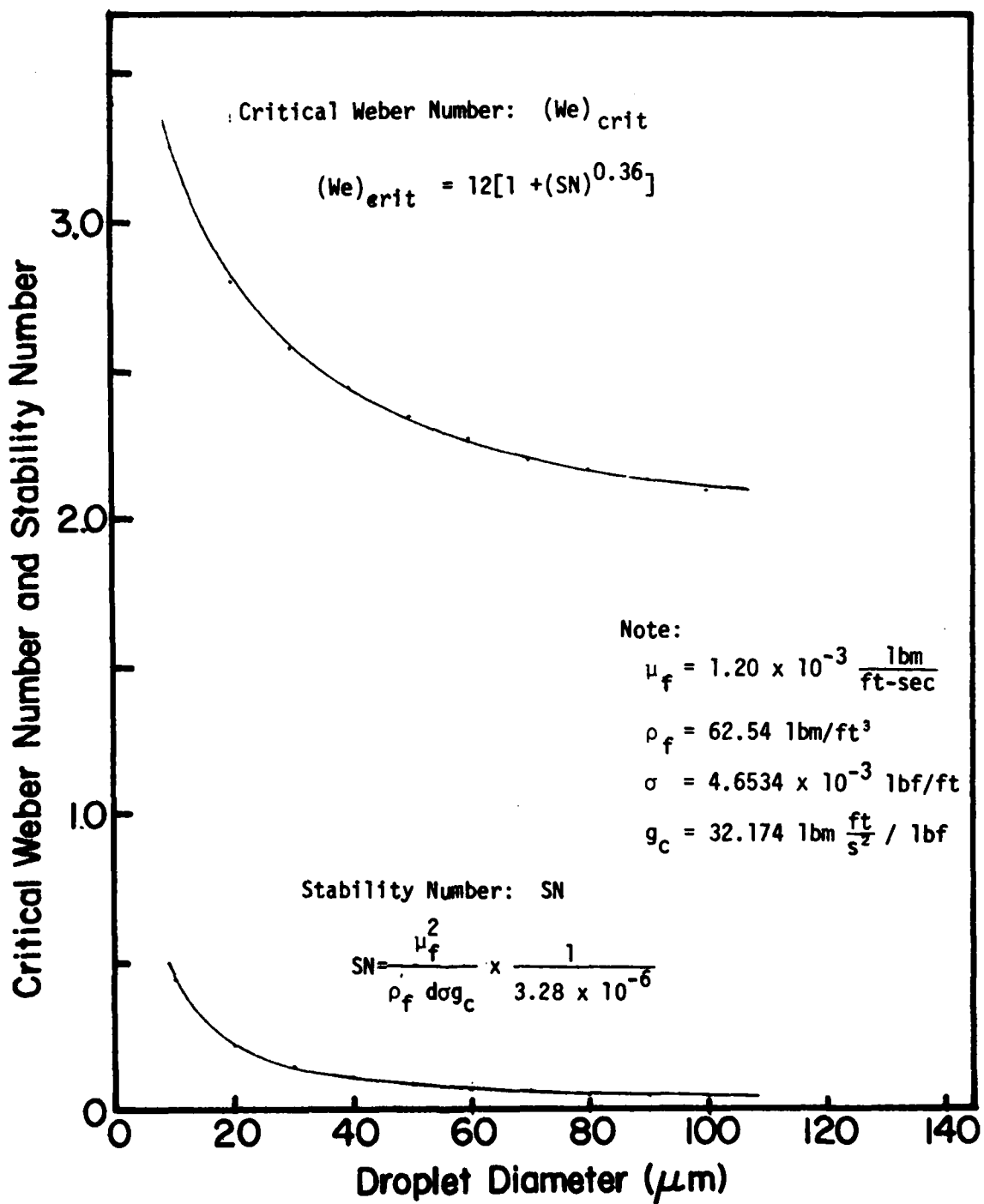


Fig.2.5 Critical Weber Number and Stability Number vs Droplet Diameter



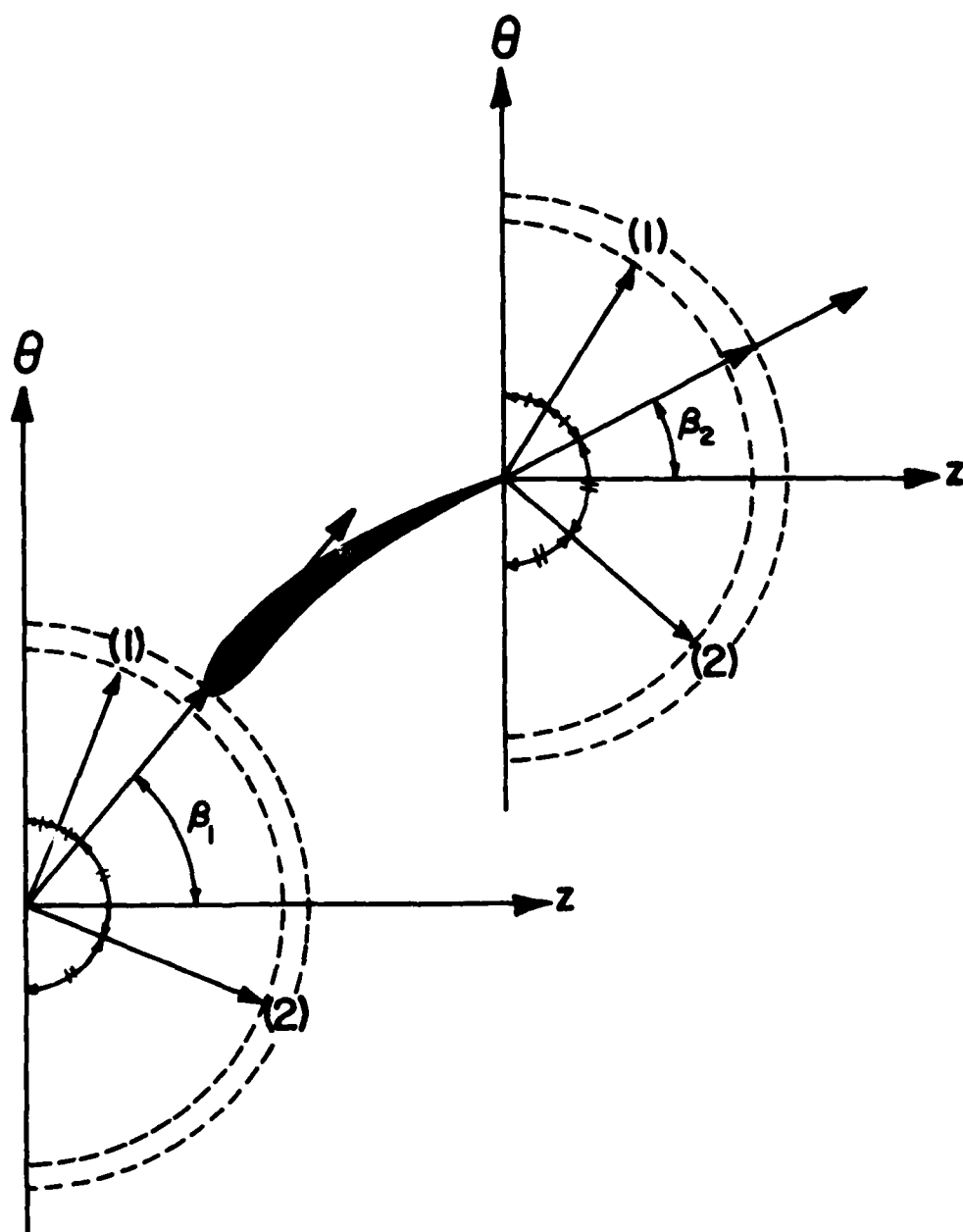
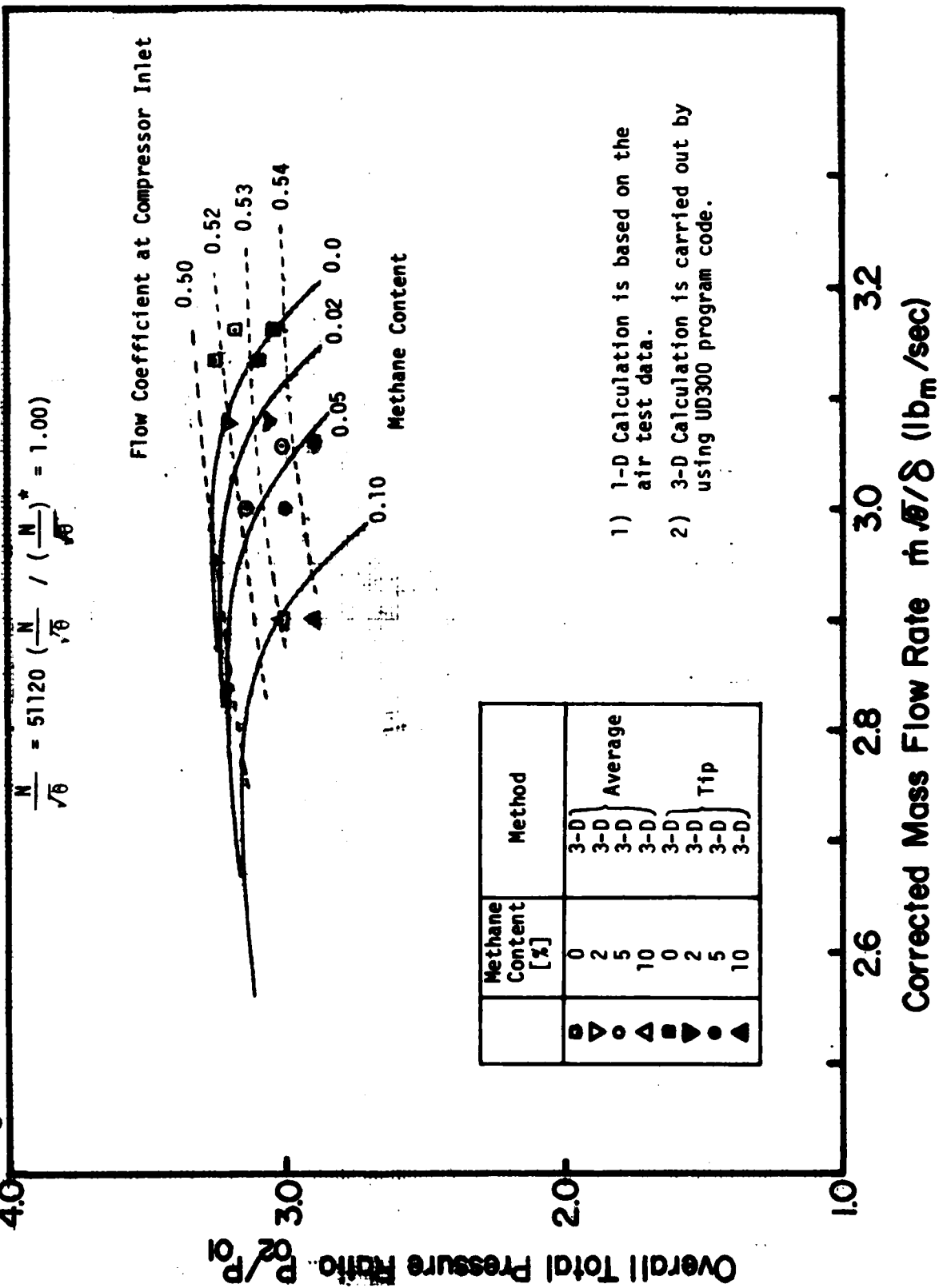


Fig. 3.1 Model for Motion of Large Droplet

Fig. 4.1.1. Effect of Methane Content on Overall Pressure Ratio



- 1) 1-D Calculation is based on the air test data.
- 2) 3-D Calculation is carried out by using UD300 program code.

Fig. 4.1.2 Effect of Methane Content on Overall Total Temperature Ratio

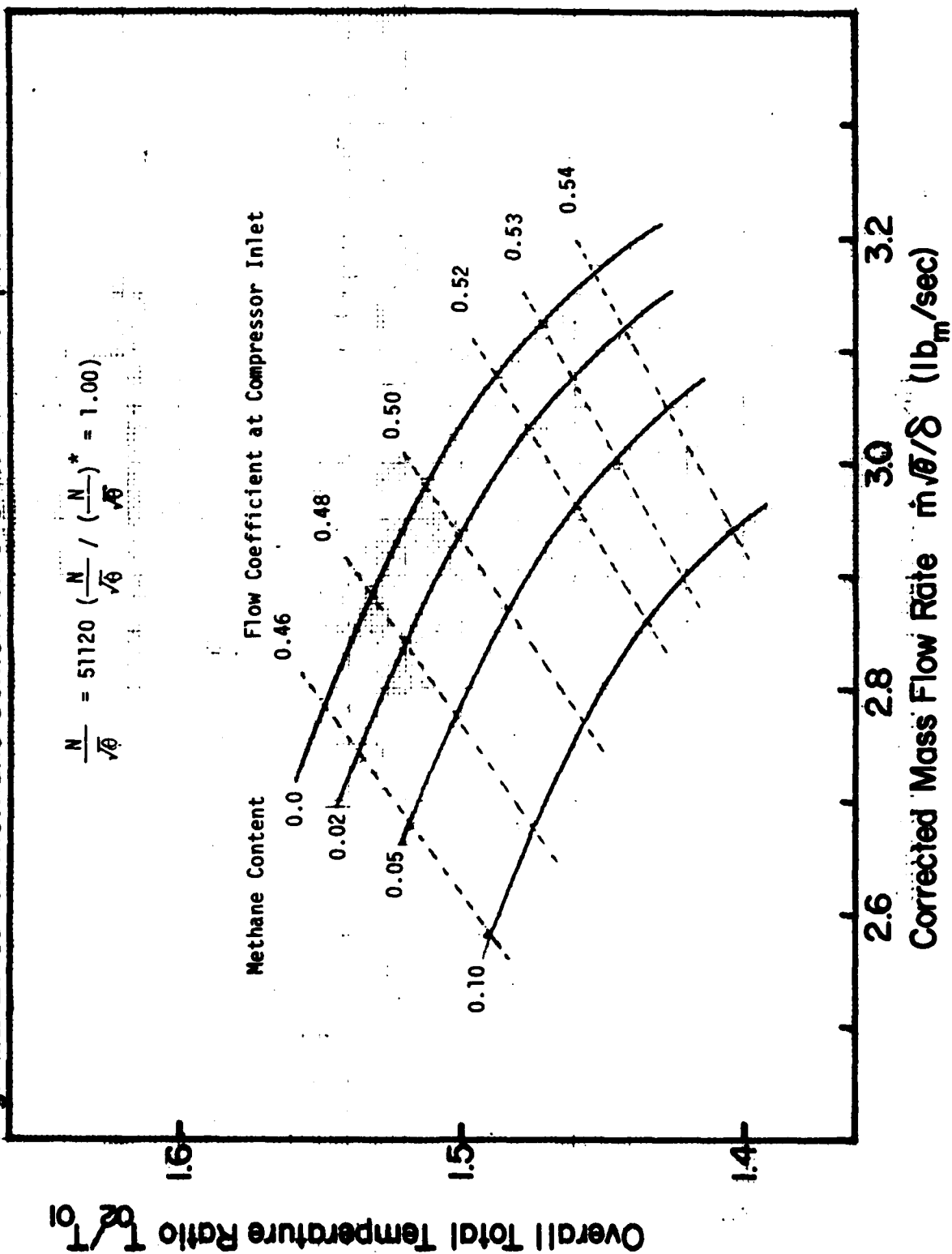


Fig. 4.1.3 Effect of Methane Content on Overall Adiabatic Efficiency

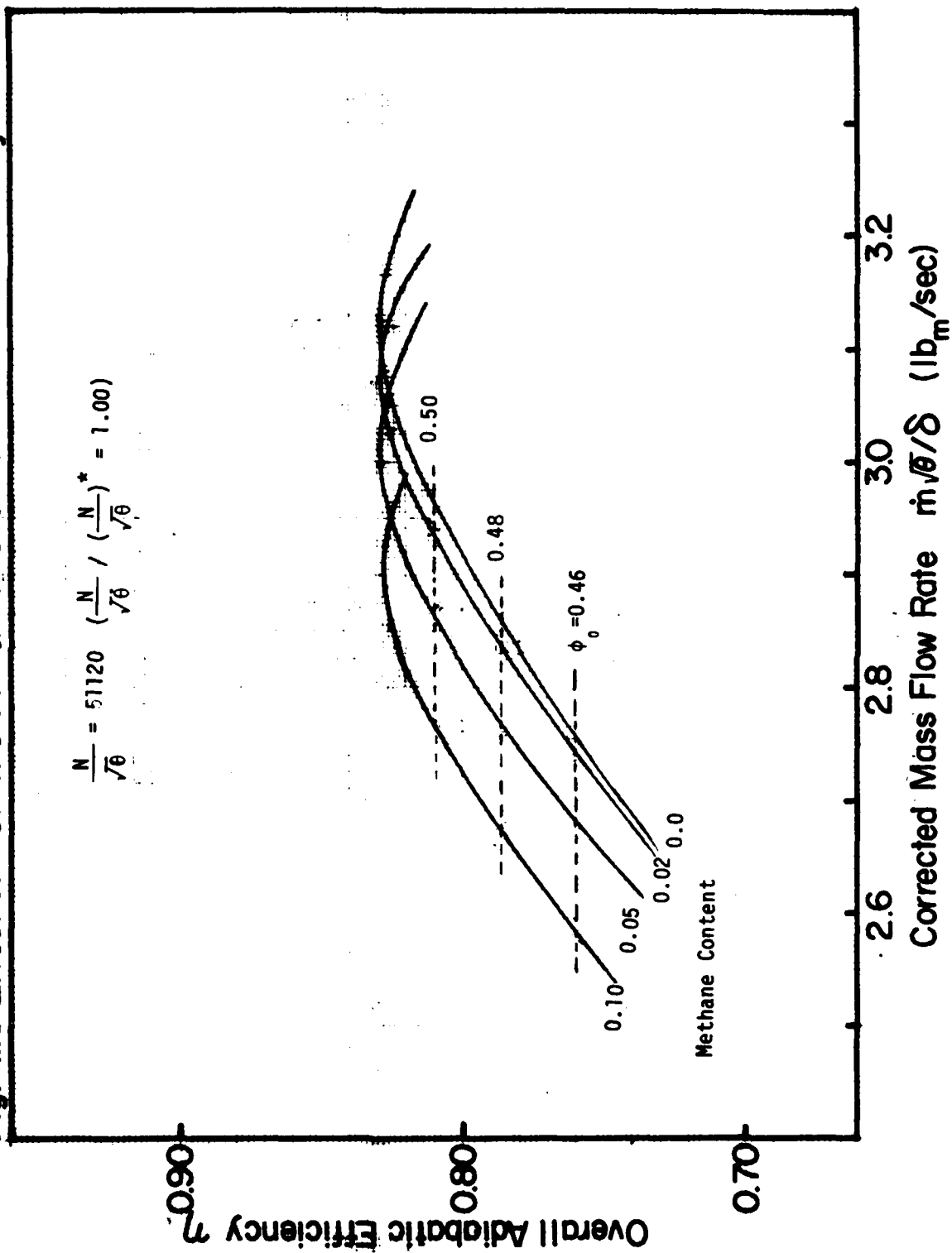


Fig. 4.1.4 Effect of Methane Content on Stage Total Pressure Ratio (Stage 1,2,3)

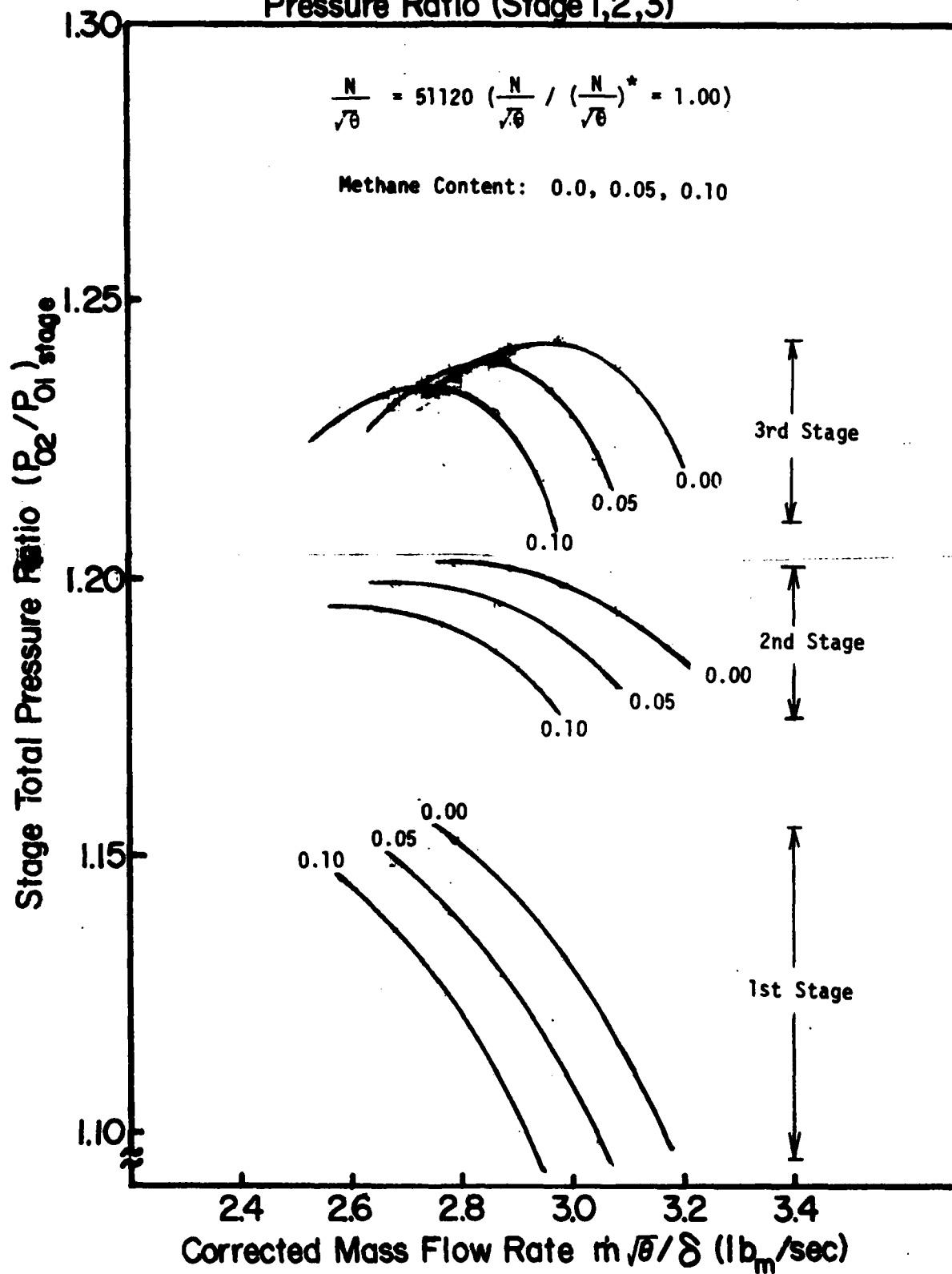
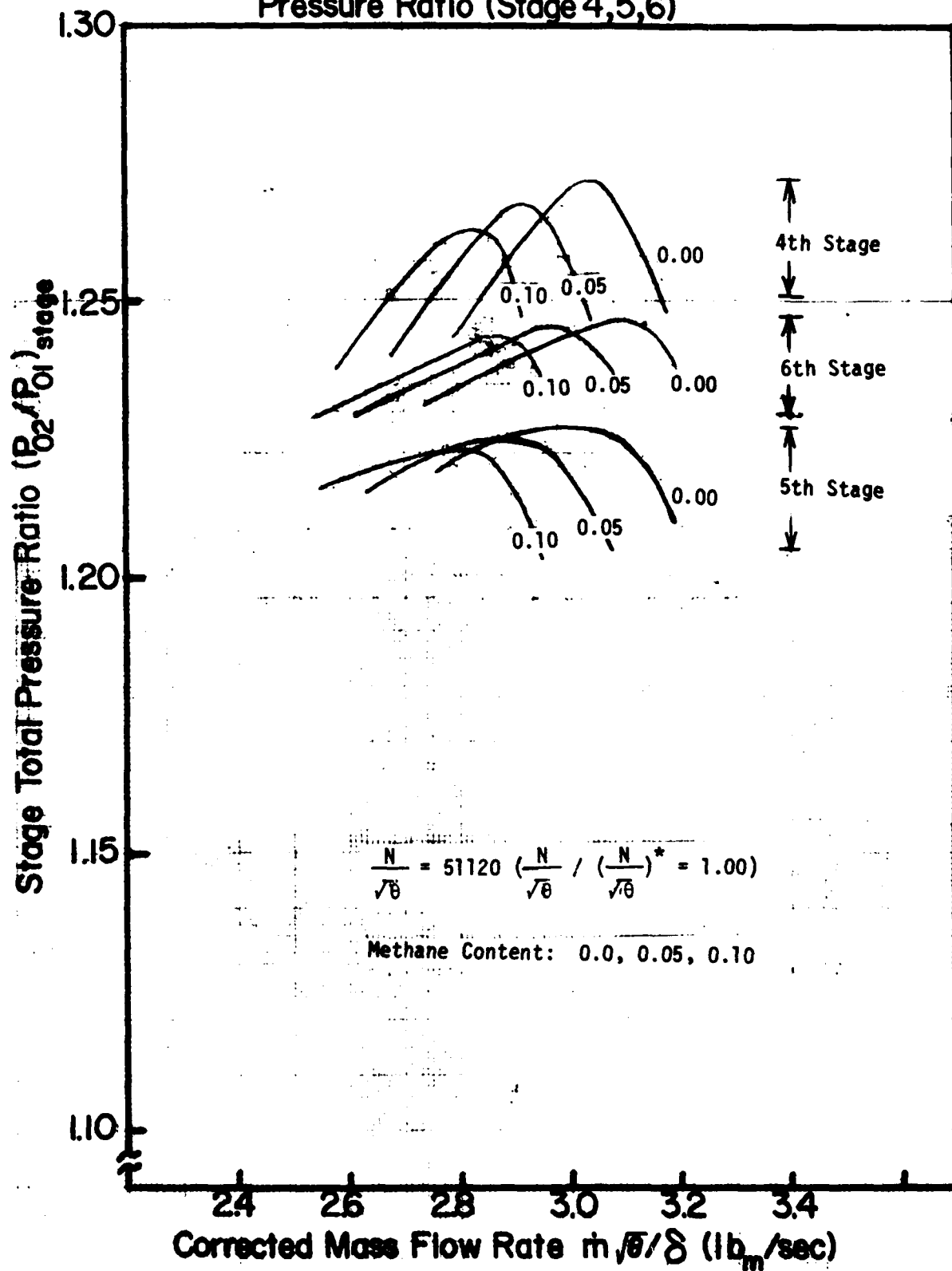


Fig. 4.1.5 Effect of Methane Content on Stage Total Pressure Ratio (Stage 4,5,6)



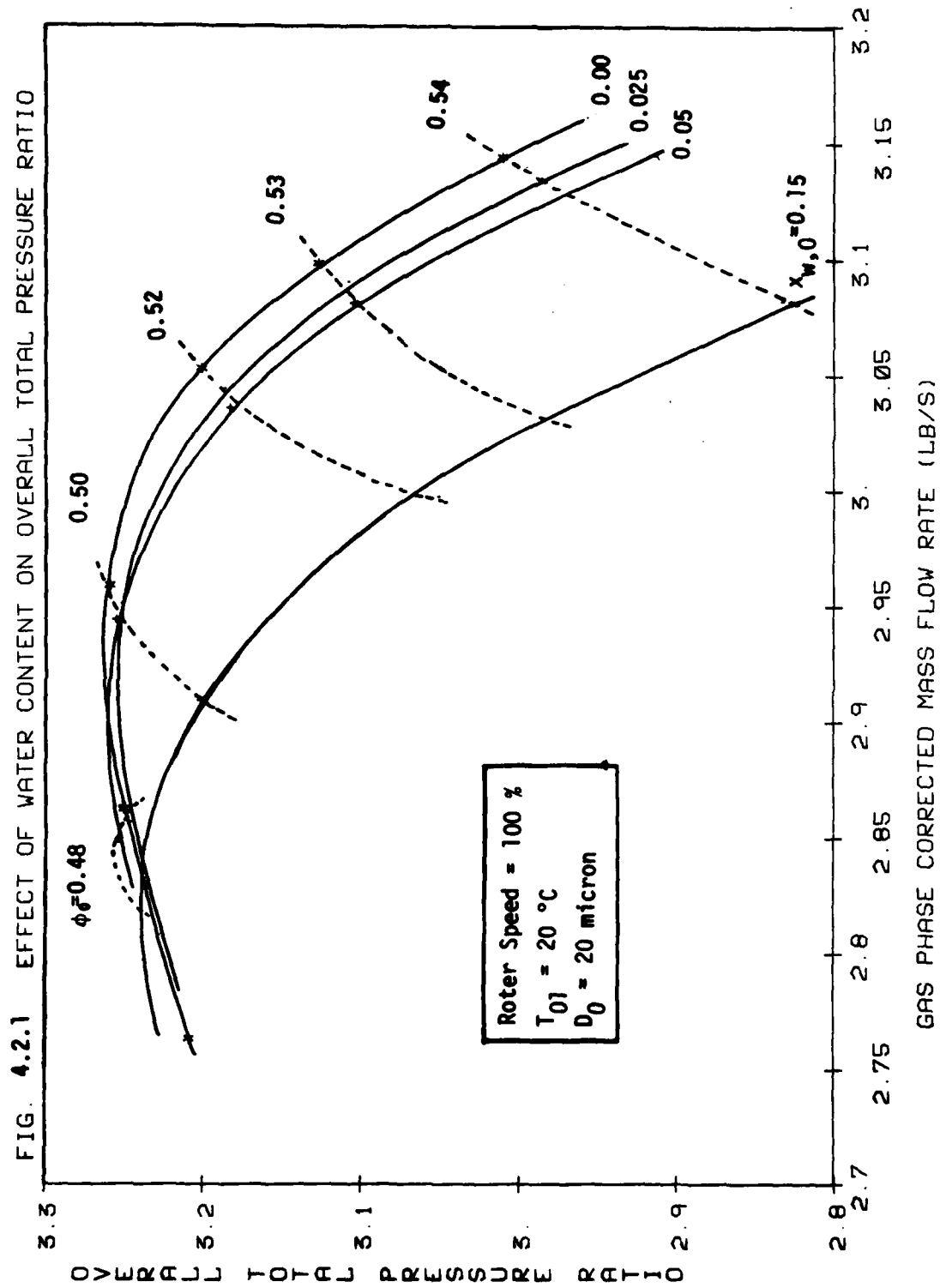


FIG. 4.2.2 EFFECT OF WATER CONTENT ON OVERALL ADIABATIC EFFICIENCY

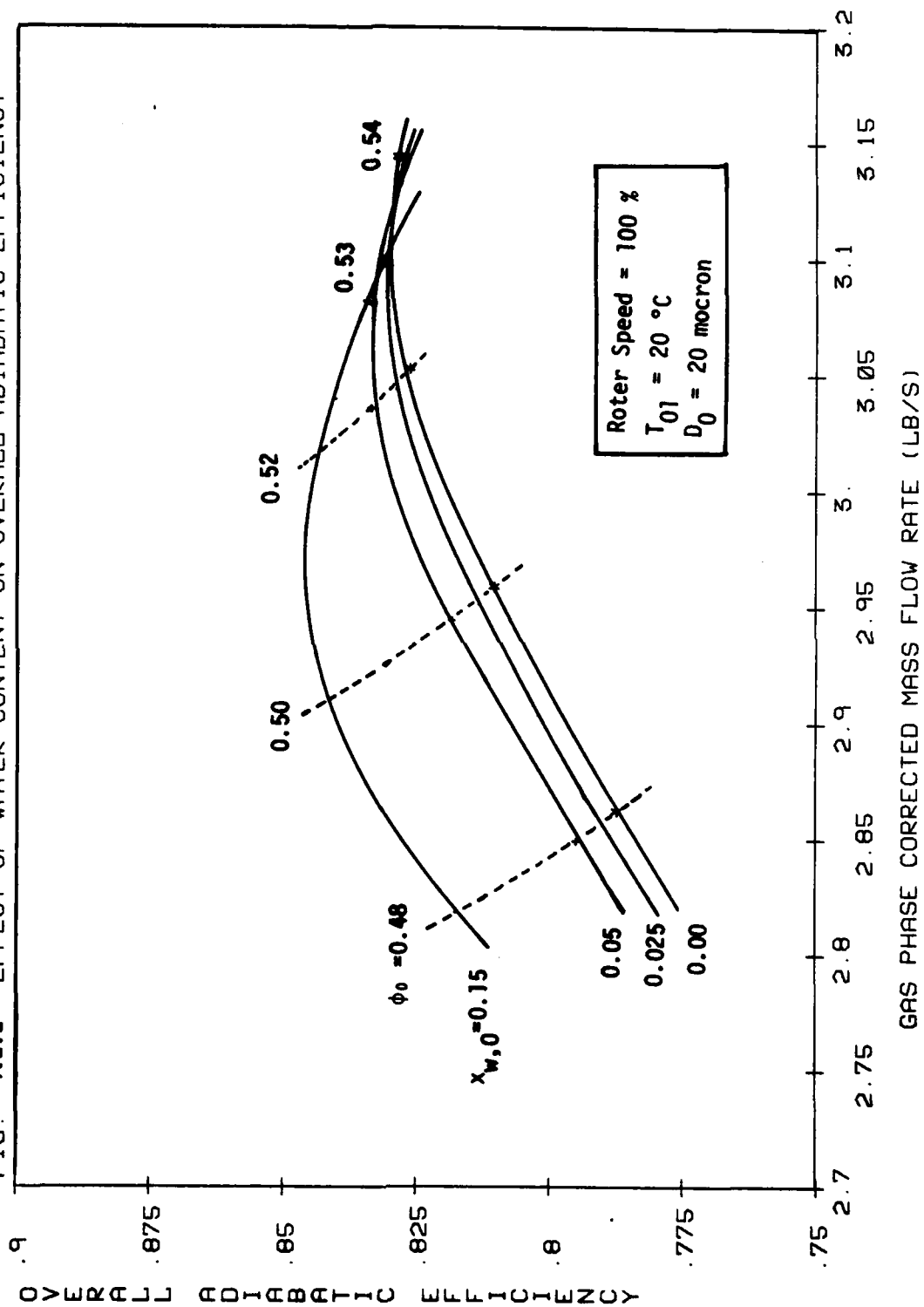


FIG. 4.2.3 EFFECT OF WATER CONTENT ON OVERALL TEMPERATURE RISE

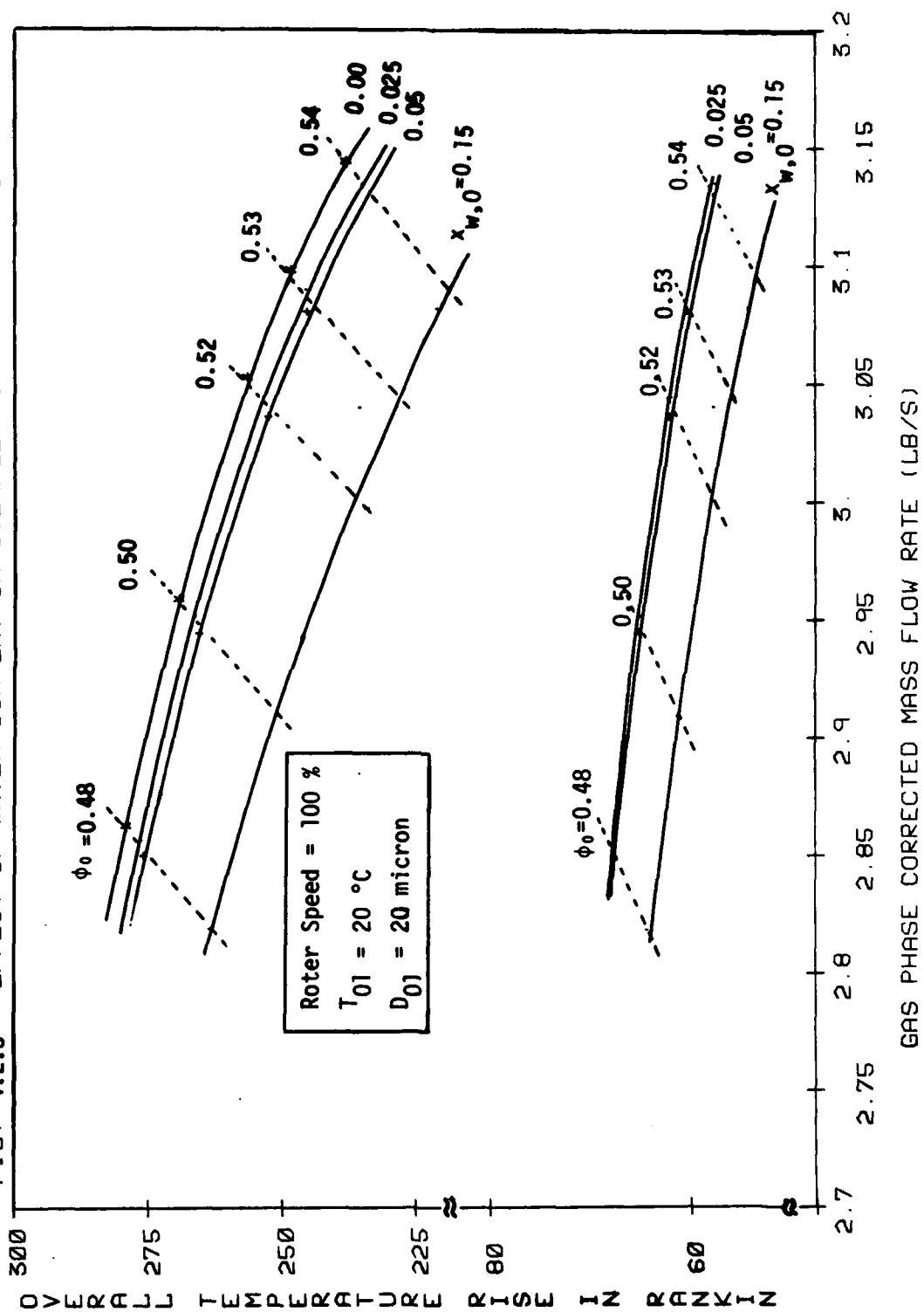


Fig. 4.2.4 CHANGE OF TEMPERATURE ALONG COMPRESSOR STAGES

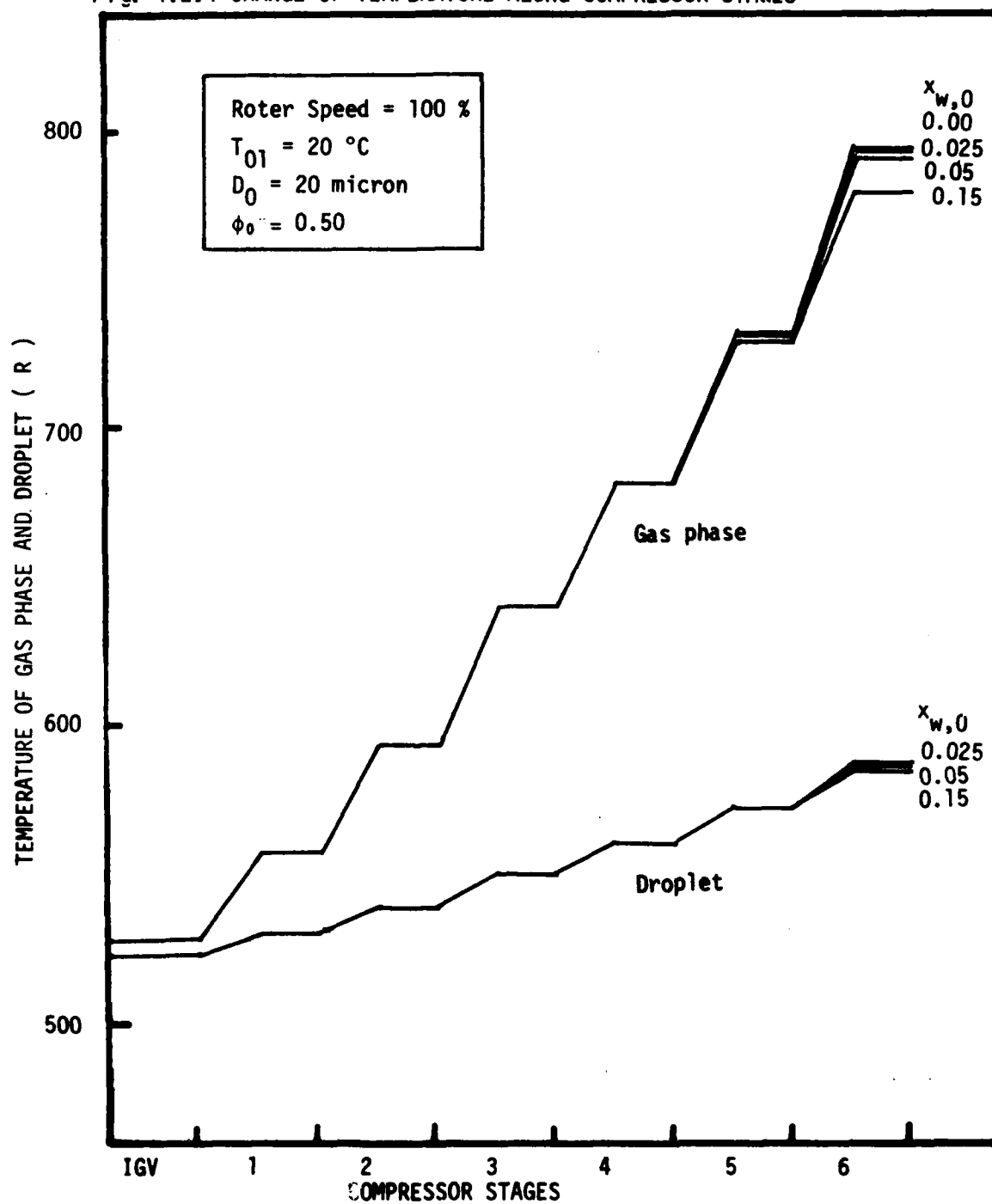


Fig. 4.2.5 CHANGE OF WATER CONTENT AT TIP ALONG COMPRESSOR STAGES

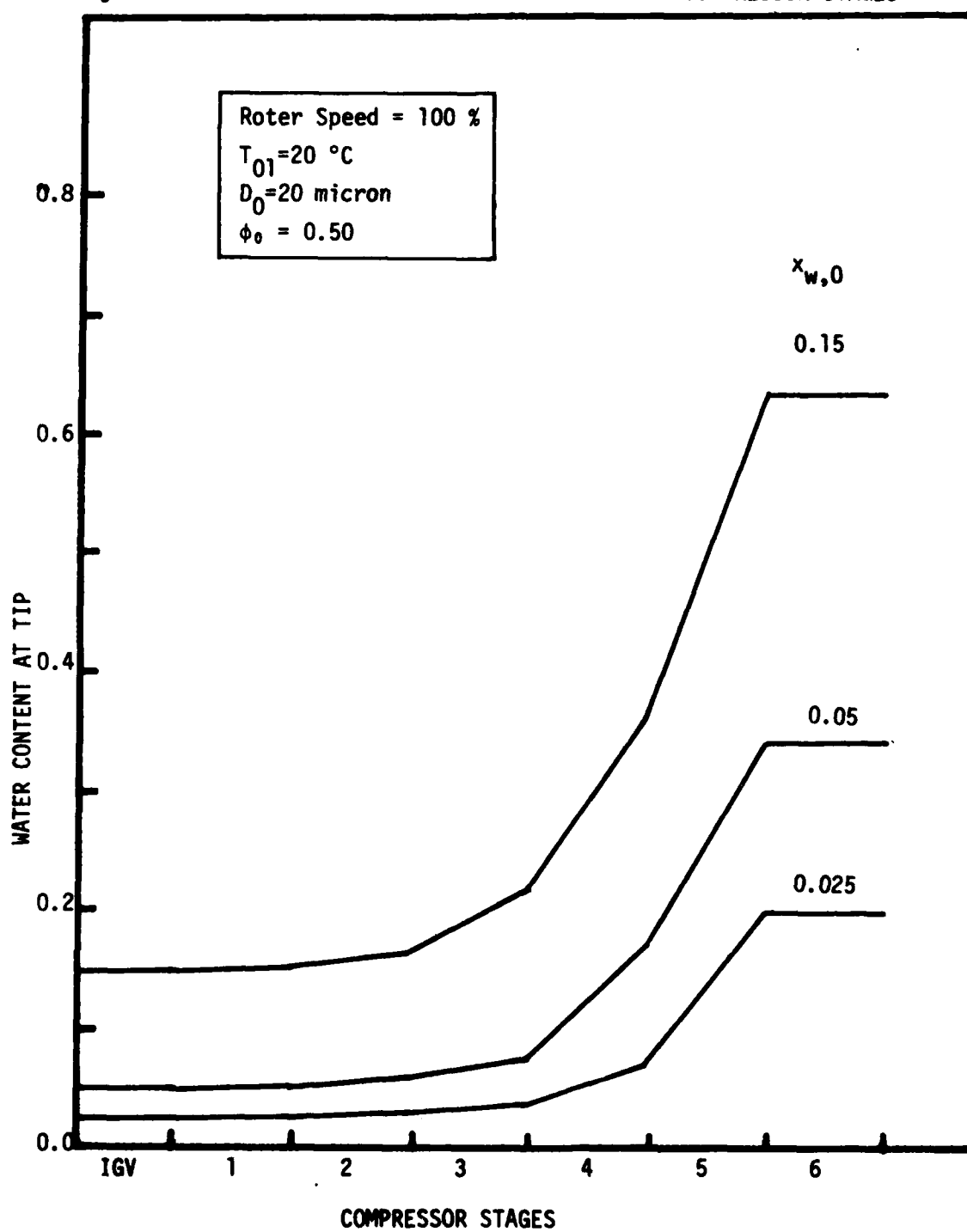


FIG. 4.2.6 EFFECT OF WATER CONTENT ON OVERALL TOTAL PRESSURE RATIO

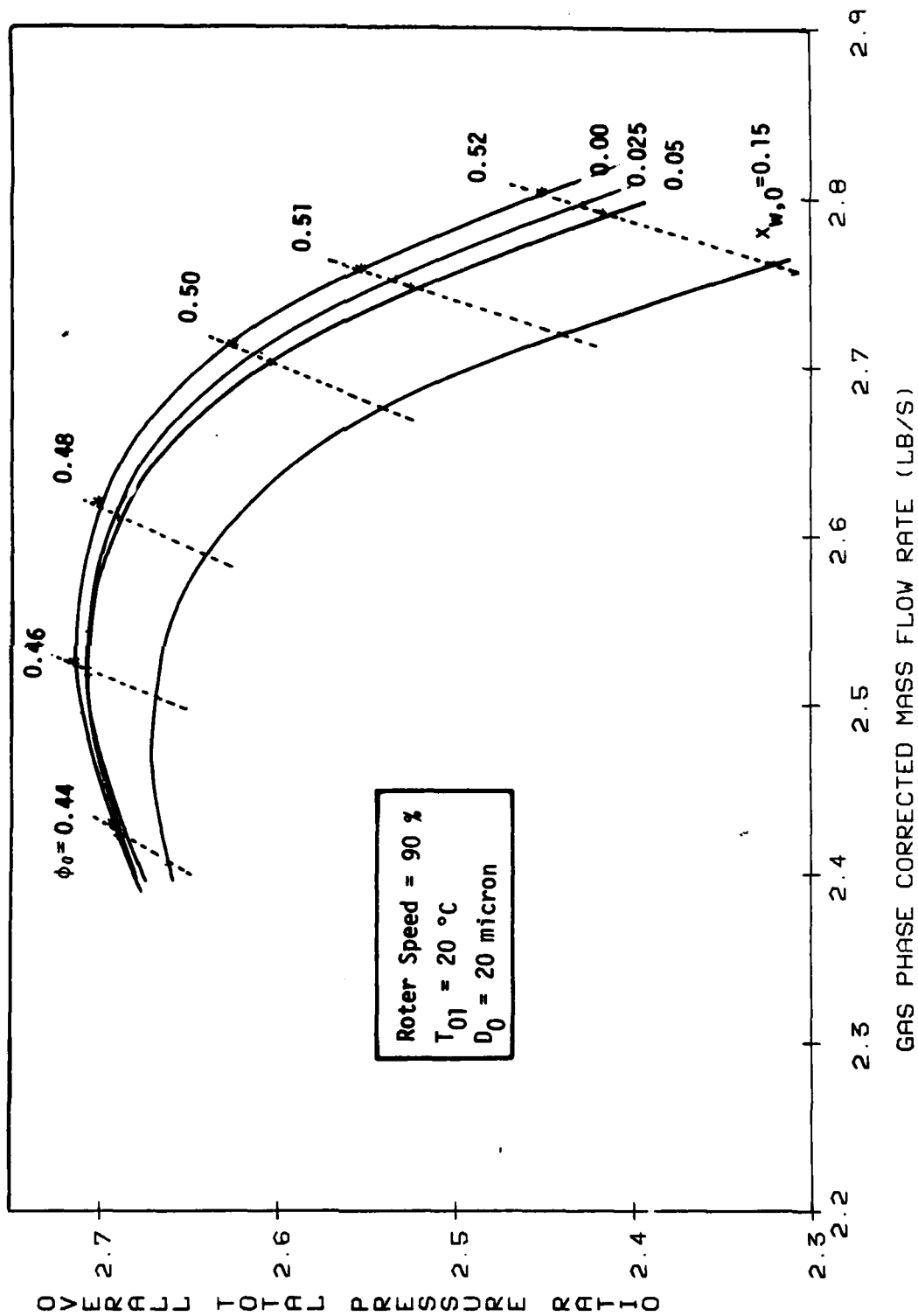


FIG. 4.2.7 EFFECT OF WATER CONTENT ON OVERALL ADIABATIC EFFICIENCY

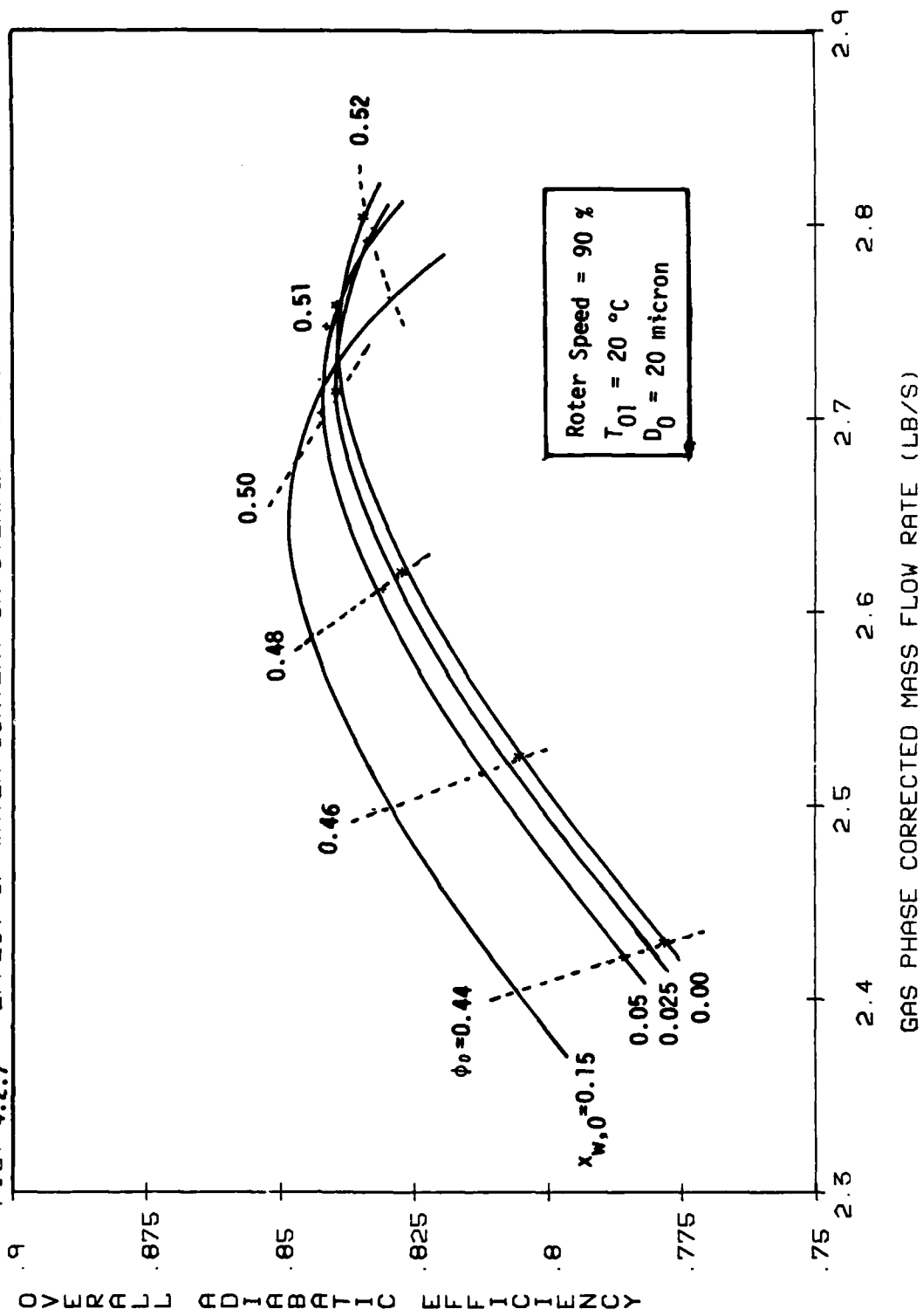


FIG. 4.2.8 EFFECT OF WATER CONTENT ON OVERALL TEMPERATURE RISE

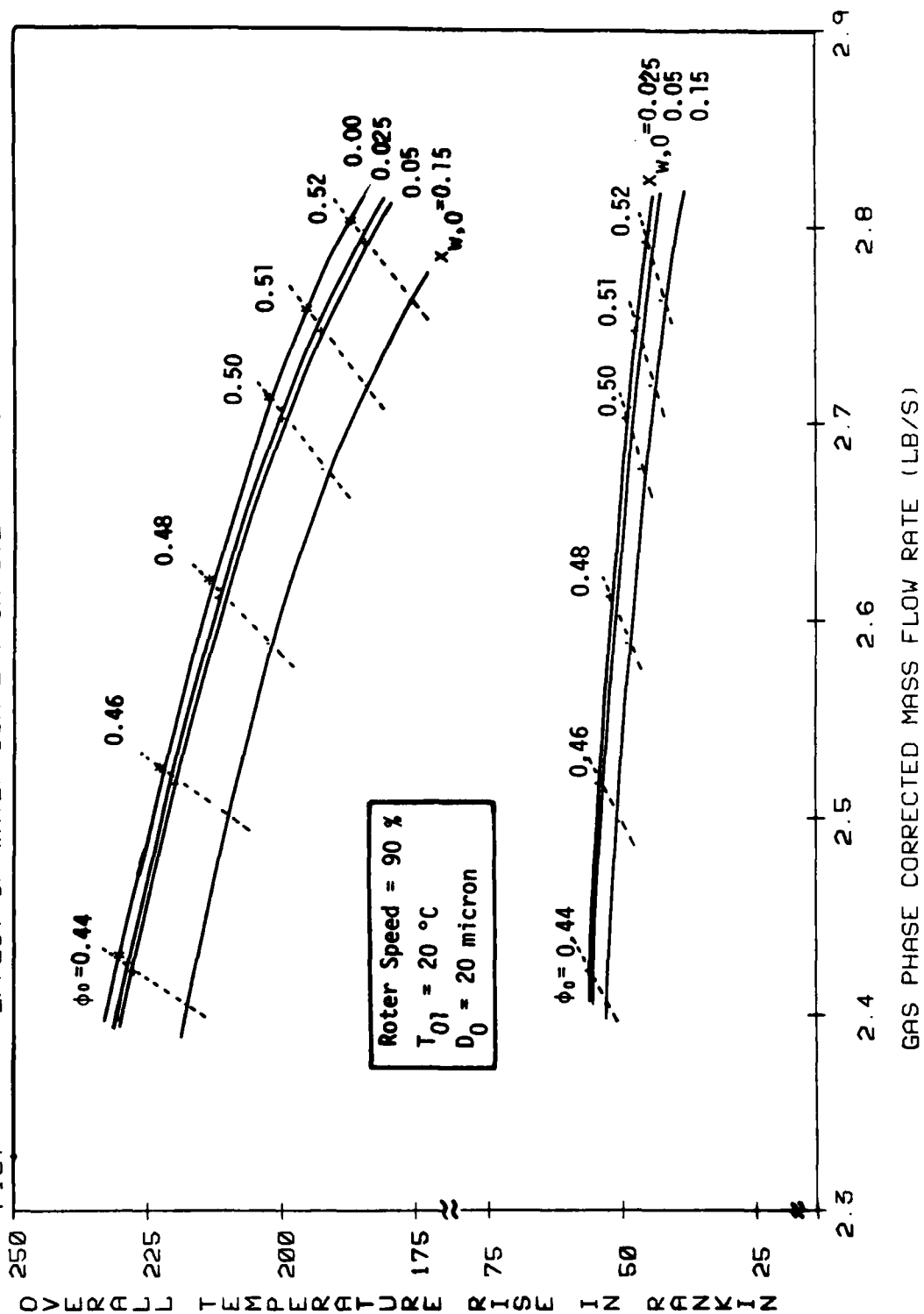


Fig.4.2.9

CHANGE OF TEMPERATURE ALONG COMPRESSOR STAGES

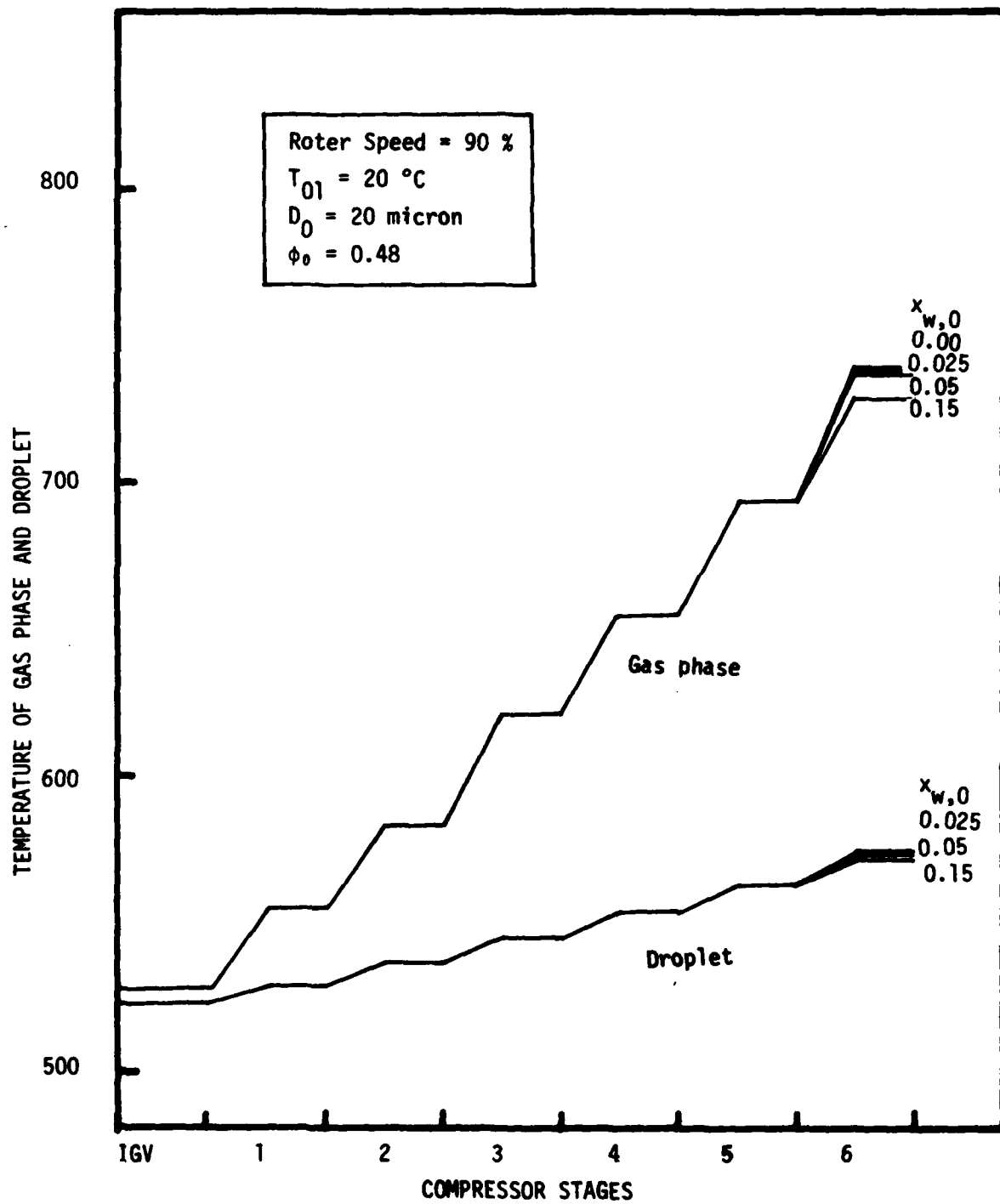
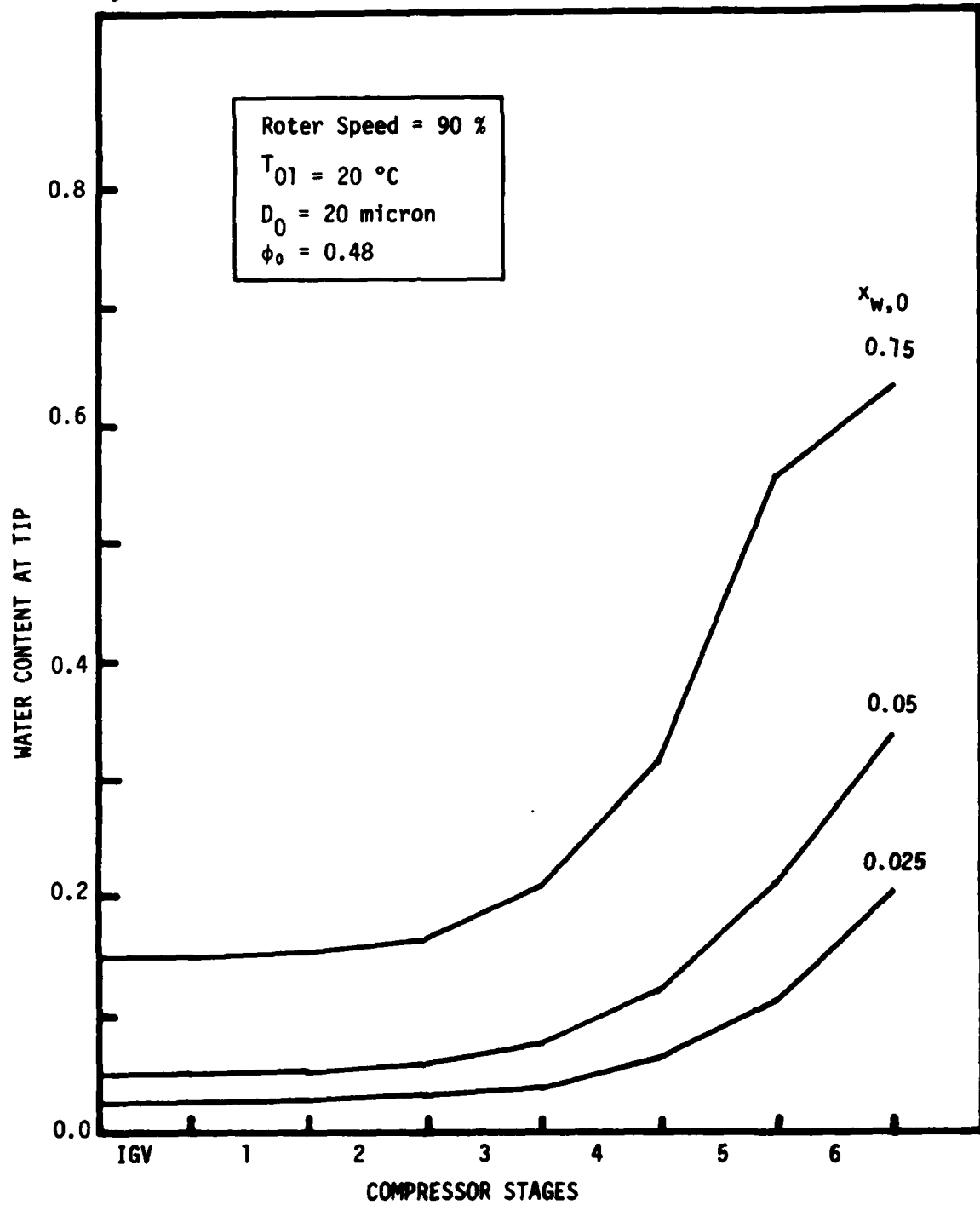


Fig. 4.2.10 CHANGE OF WATER CONTENT AT TIP ALONG COMPRESSOR STAGES



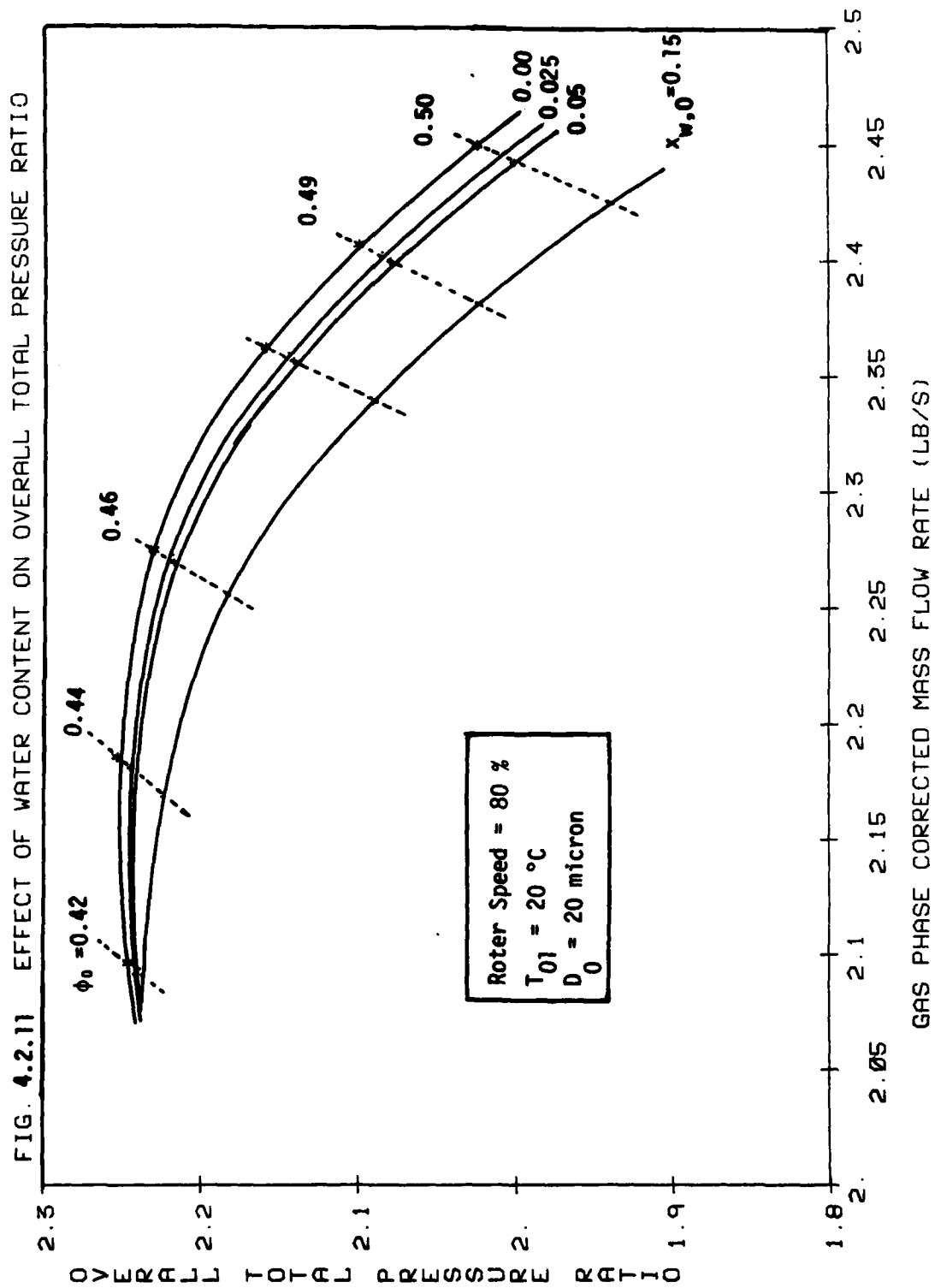


FIG. 4.2.12 EFFECT OF WATER CONTENT ON OVERALL ADIABATIC EFFICIENCY

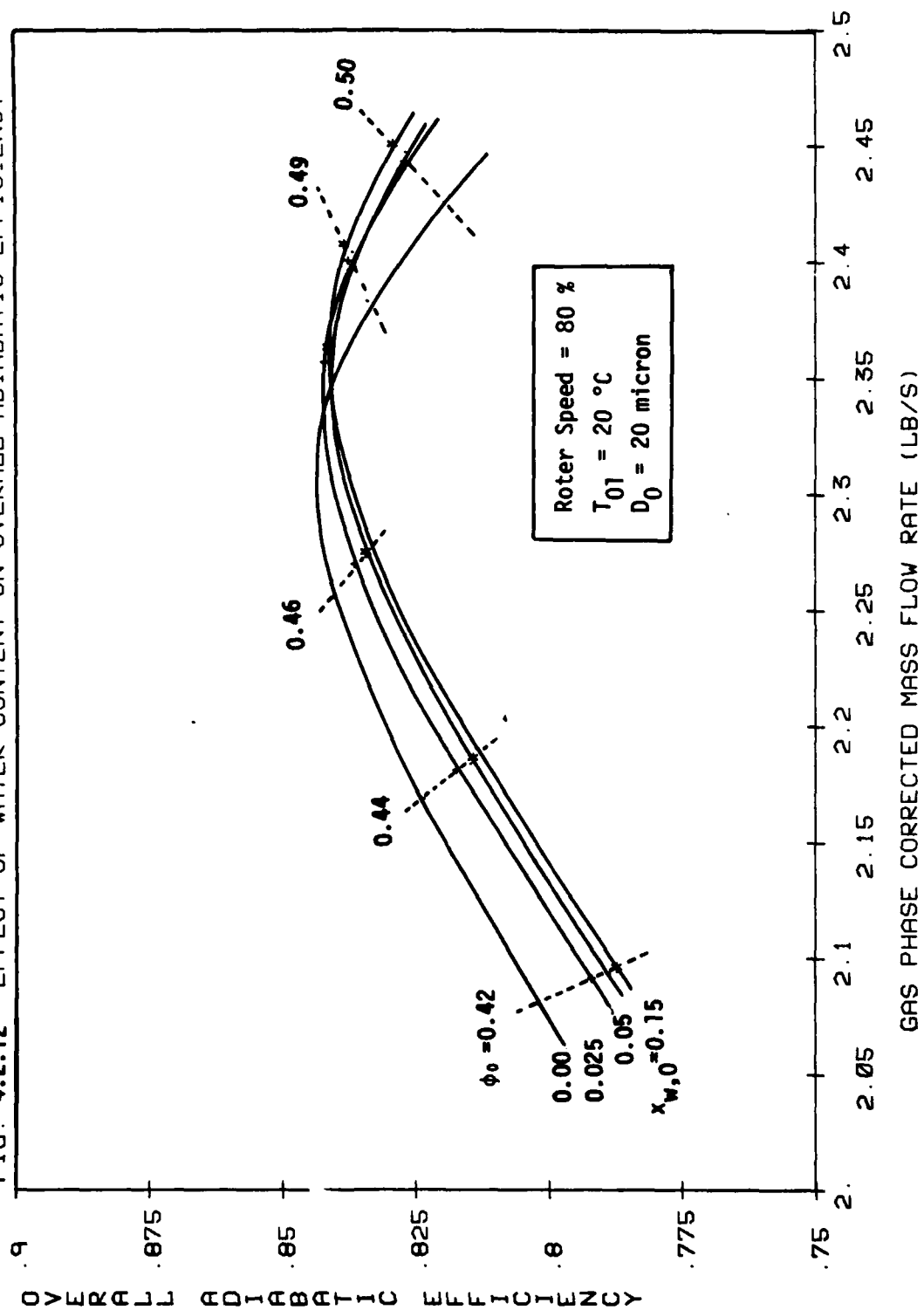


FIG. 4.2.13 EFFECT OF WATER CONTENT ON OVERALL TEMPERATURE RISE

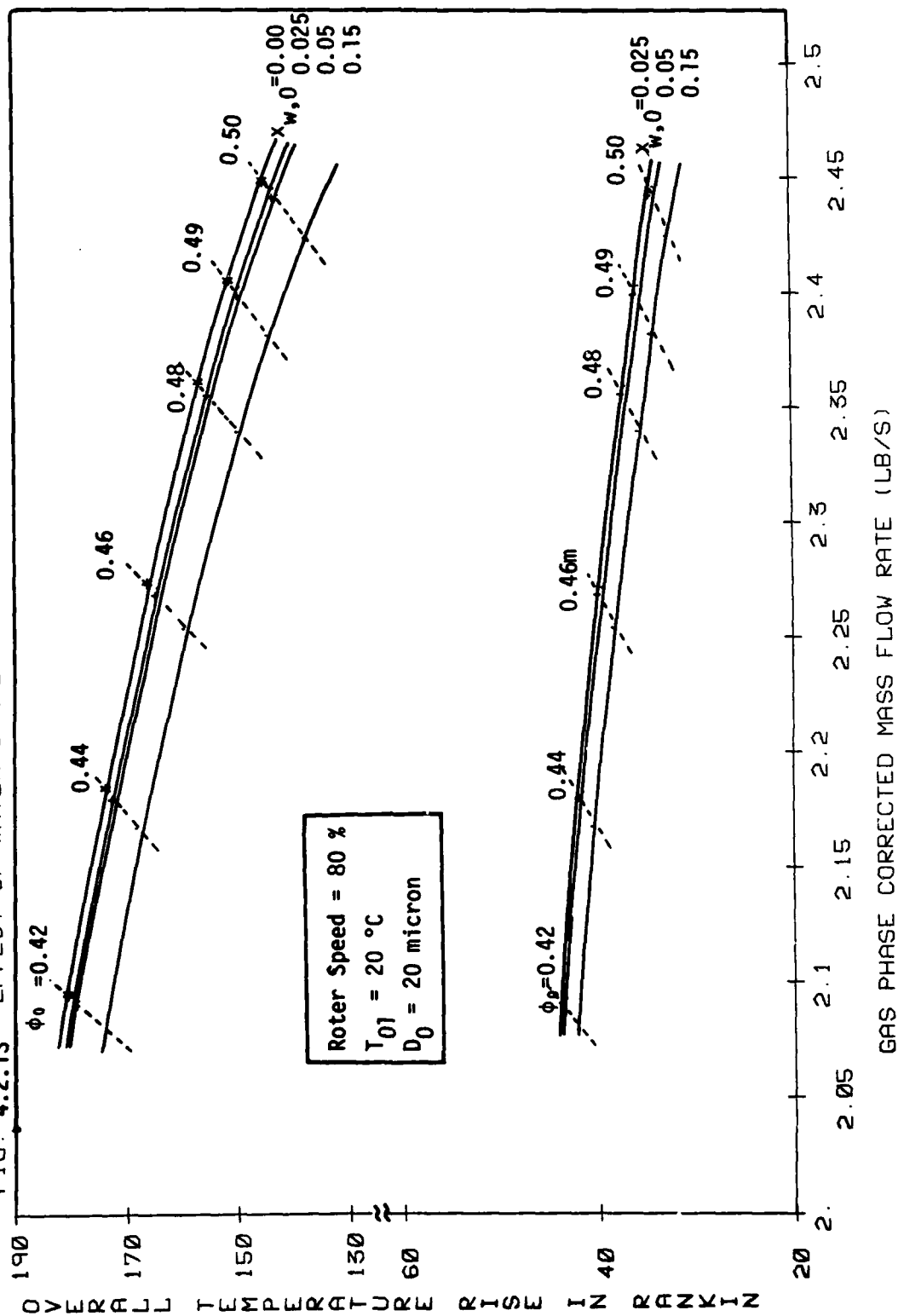


Fig. 4.2.14 CHANGE OF TEMPERATURE ALONG COMPRESSOR

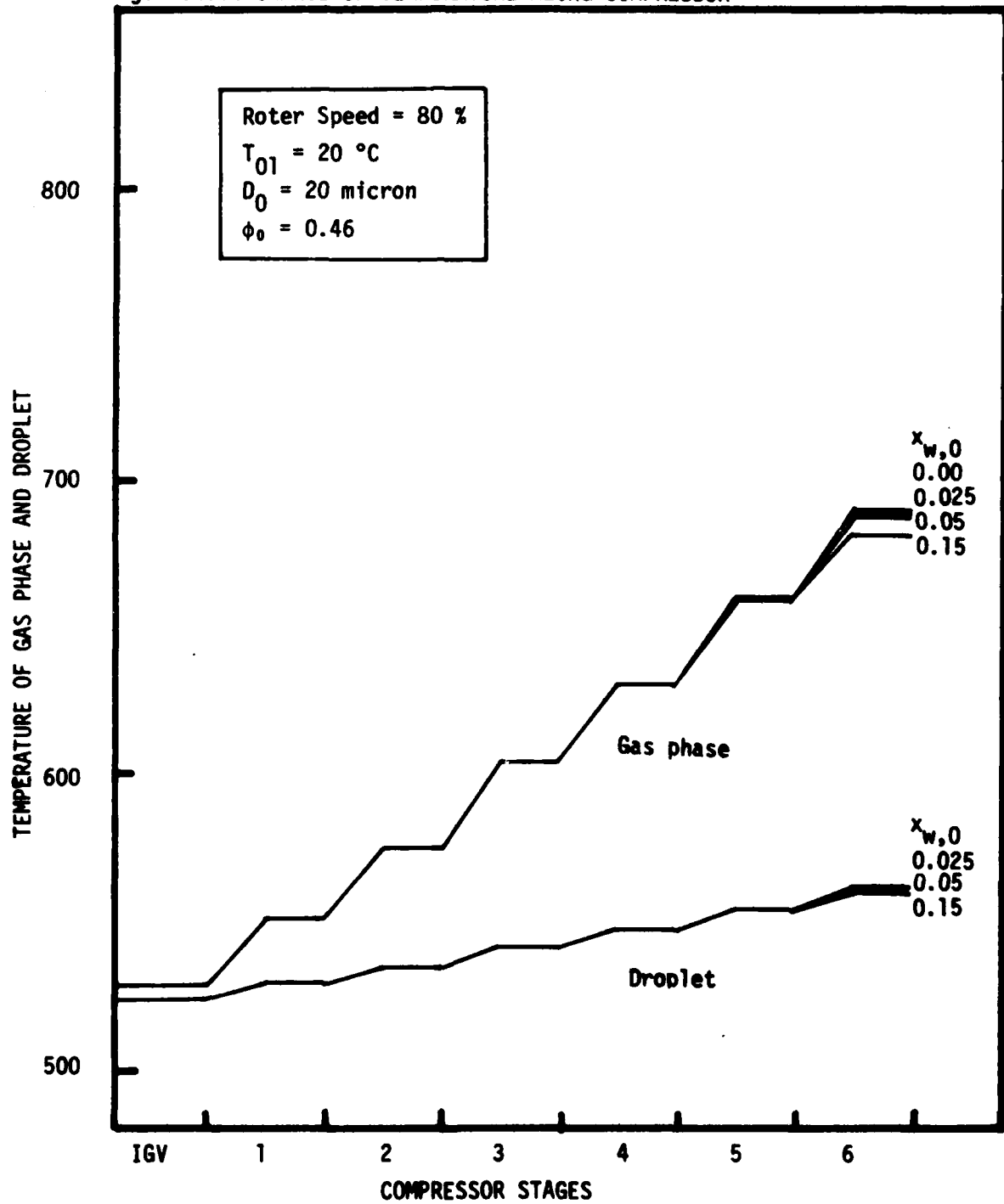


Fig. 4.2.15 CHANGE OF WATER CONTENT AT TIP ALONG COMPRESSOR

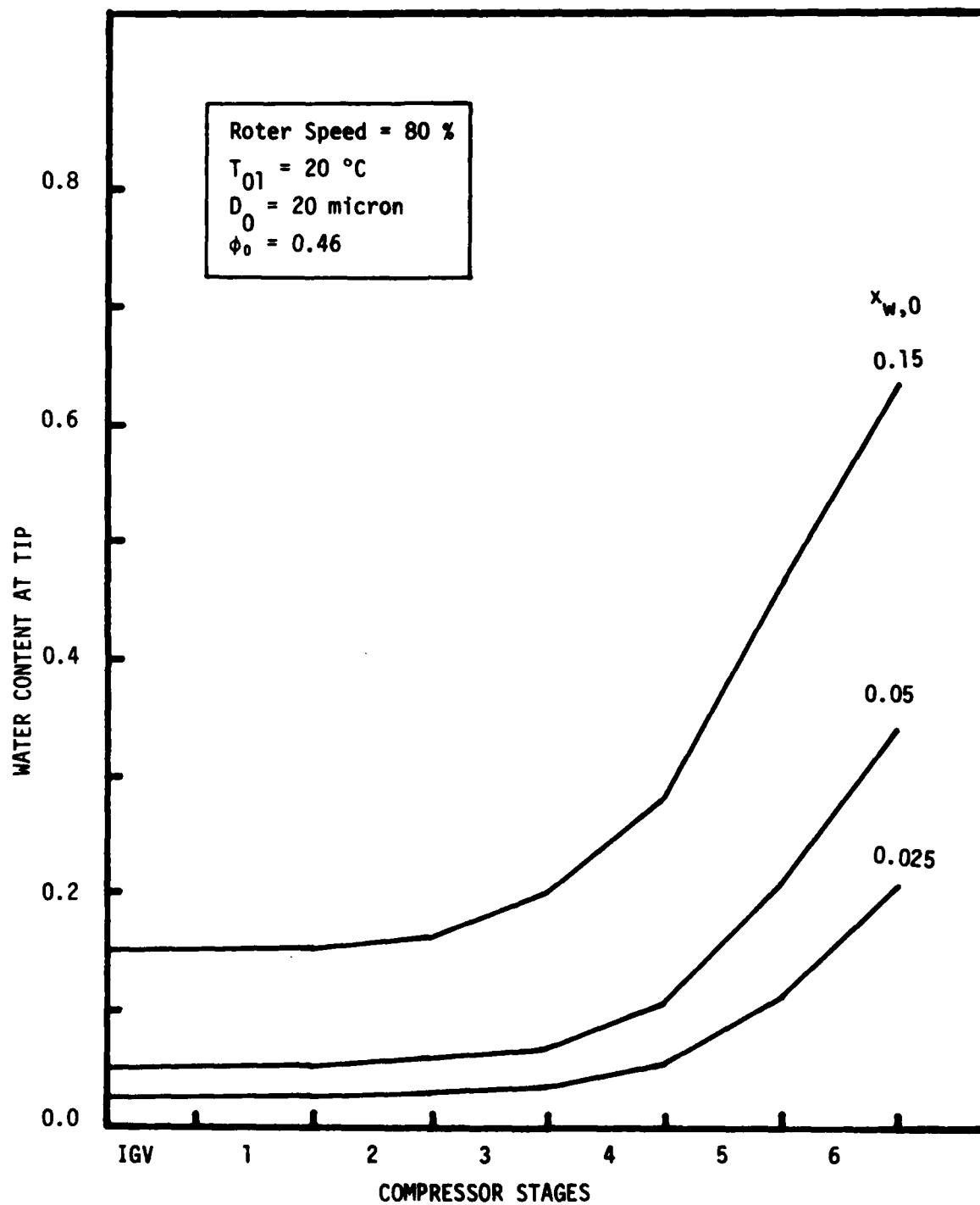
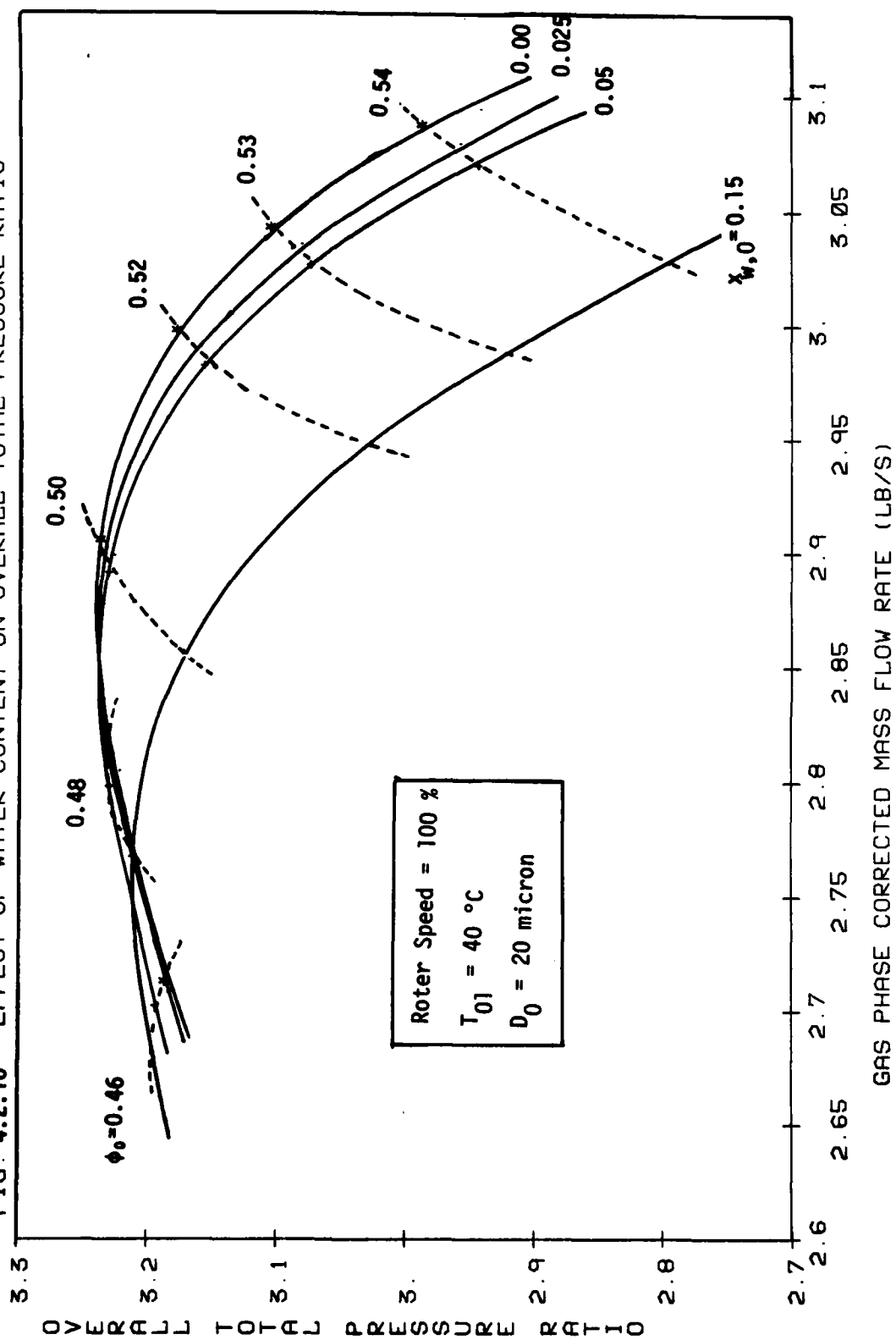


FIG. 4.2.16 EFFECT OF WATER CONTENT ON OVERALL TOTAL PRESSURE RATIO



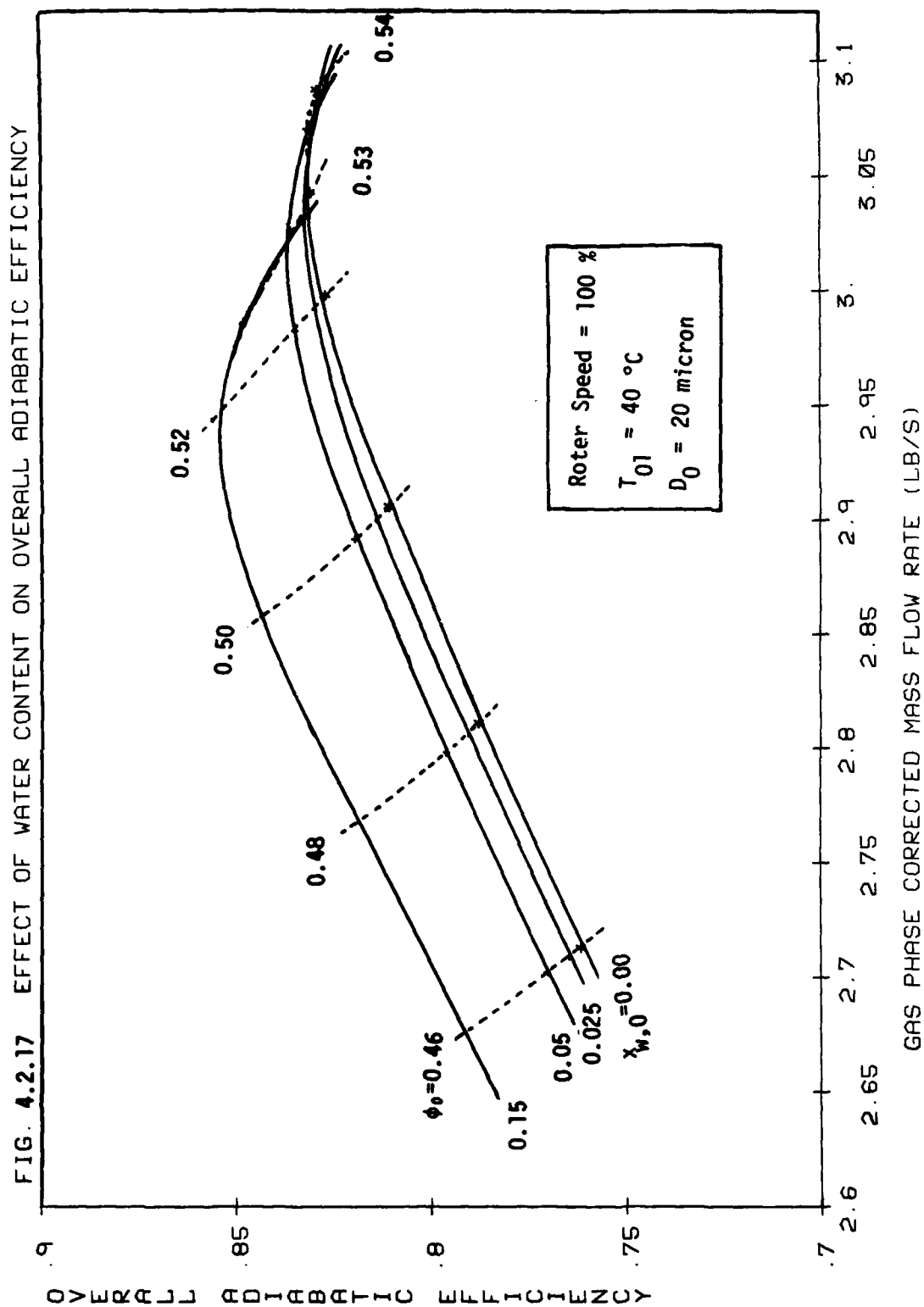


FIG. 4.2.18 EFFECT OF WATER CONTENT ON OVERALL TEMPERATURE RISE

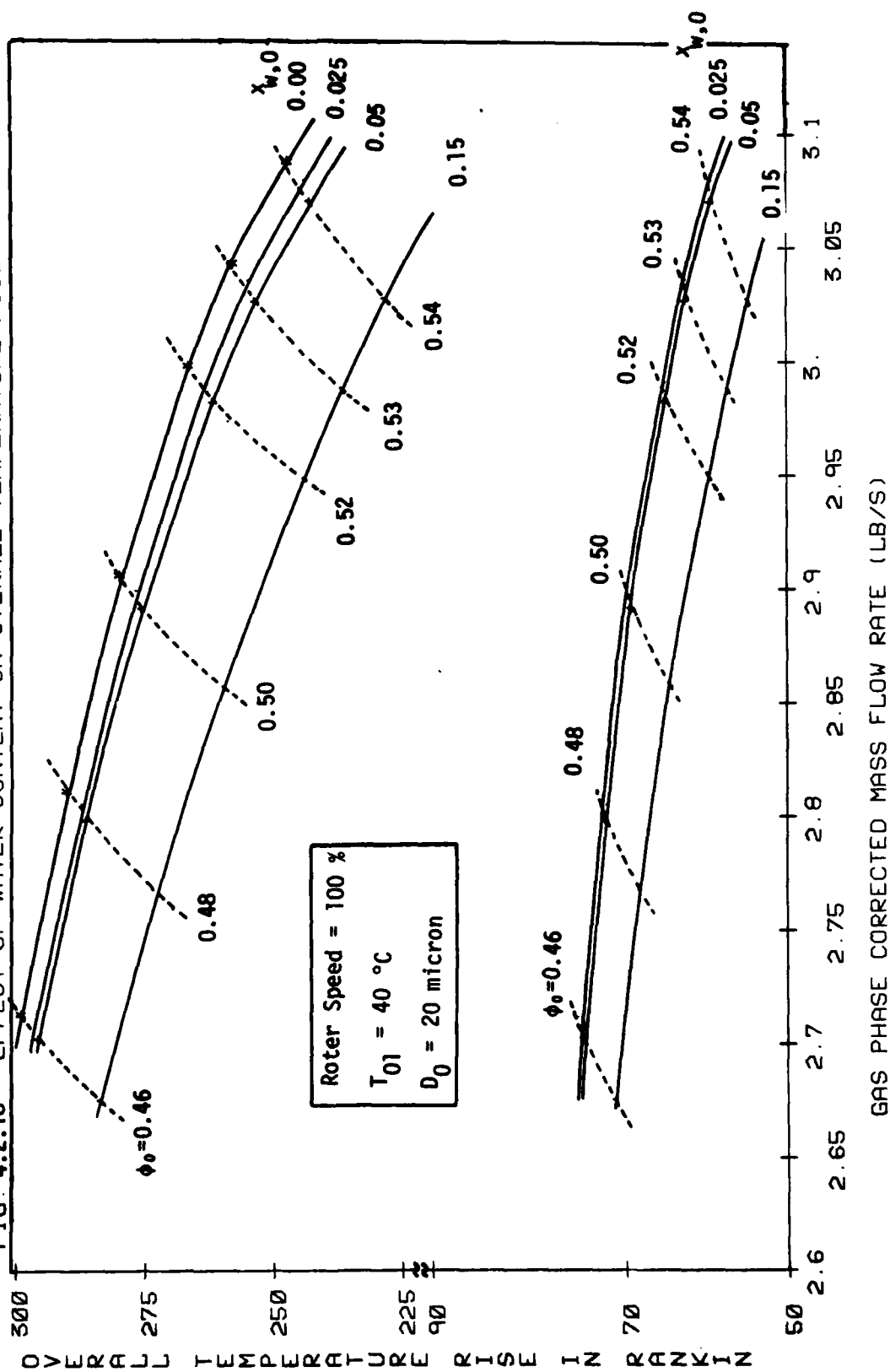


Fig. 4.2.19

CHANGE OF TEMPERATURE ALONG COMPRESSOR STAGES

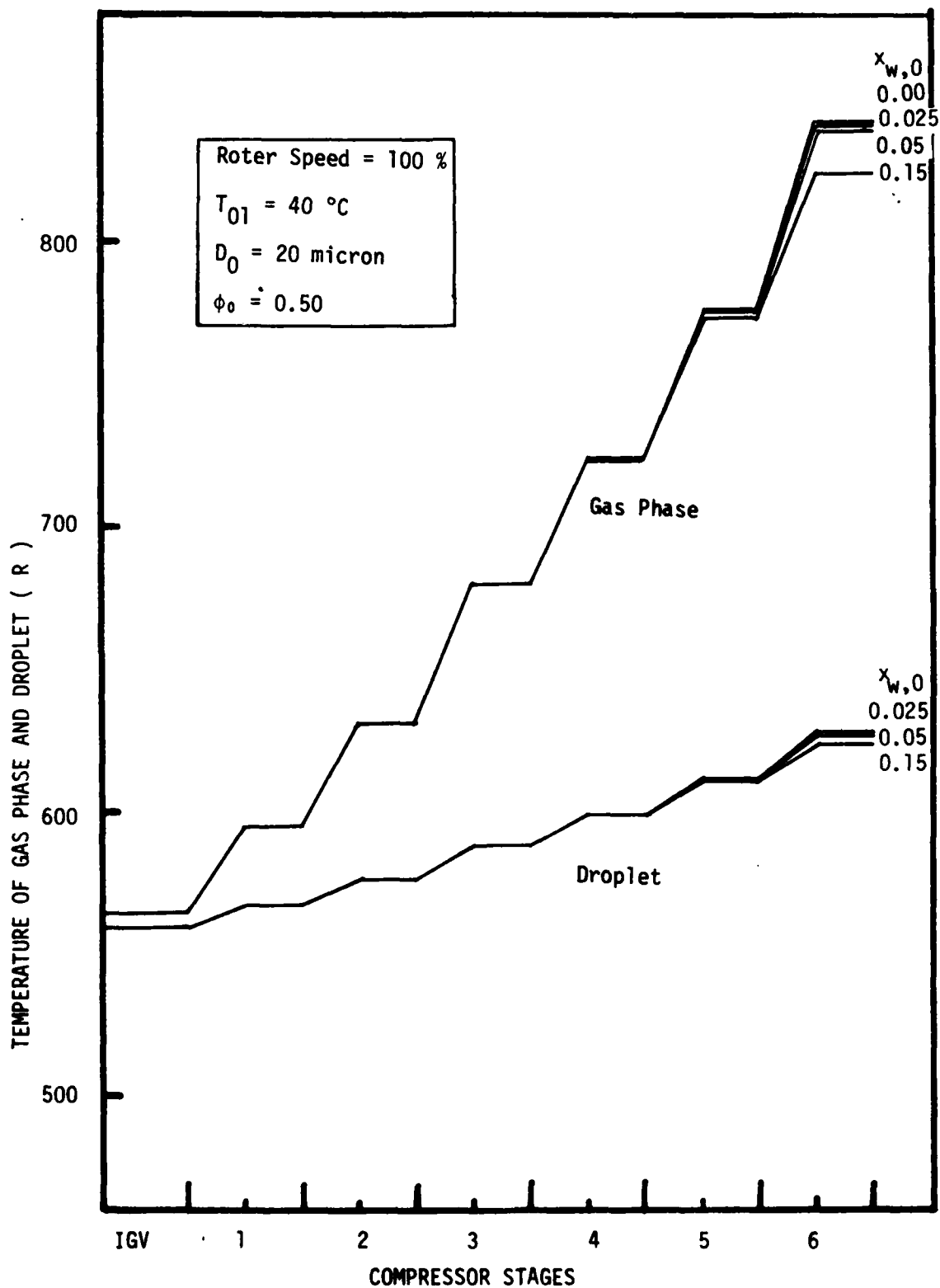


Fig. 4.2.20
CHANGE OF WATER CONTENT AT TIP ALONG COMPRESSOR STAGES

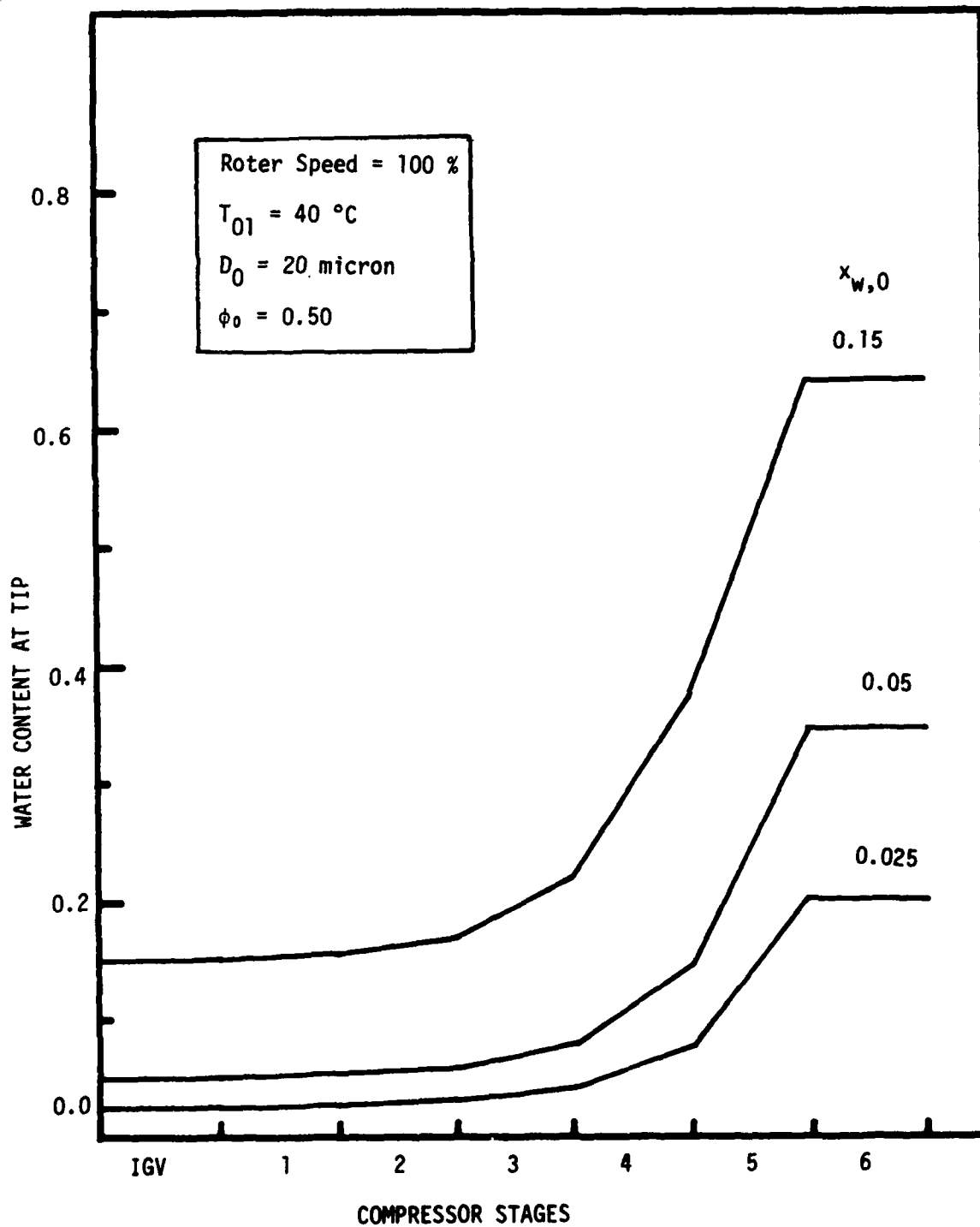


FIG 4.2.22 EFFECT OF WATER CONTENT ON OVERALL ADIABATIC EFFICIENCY

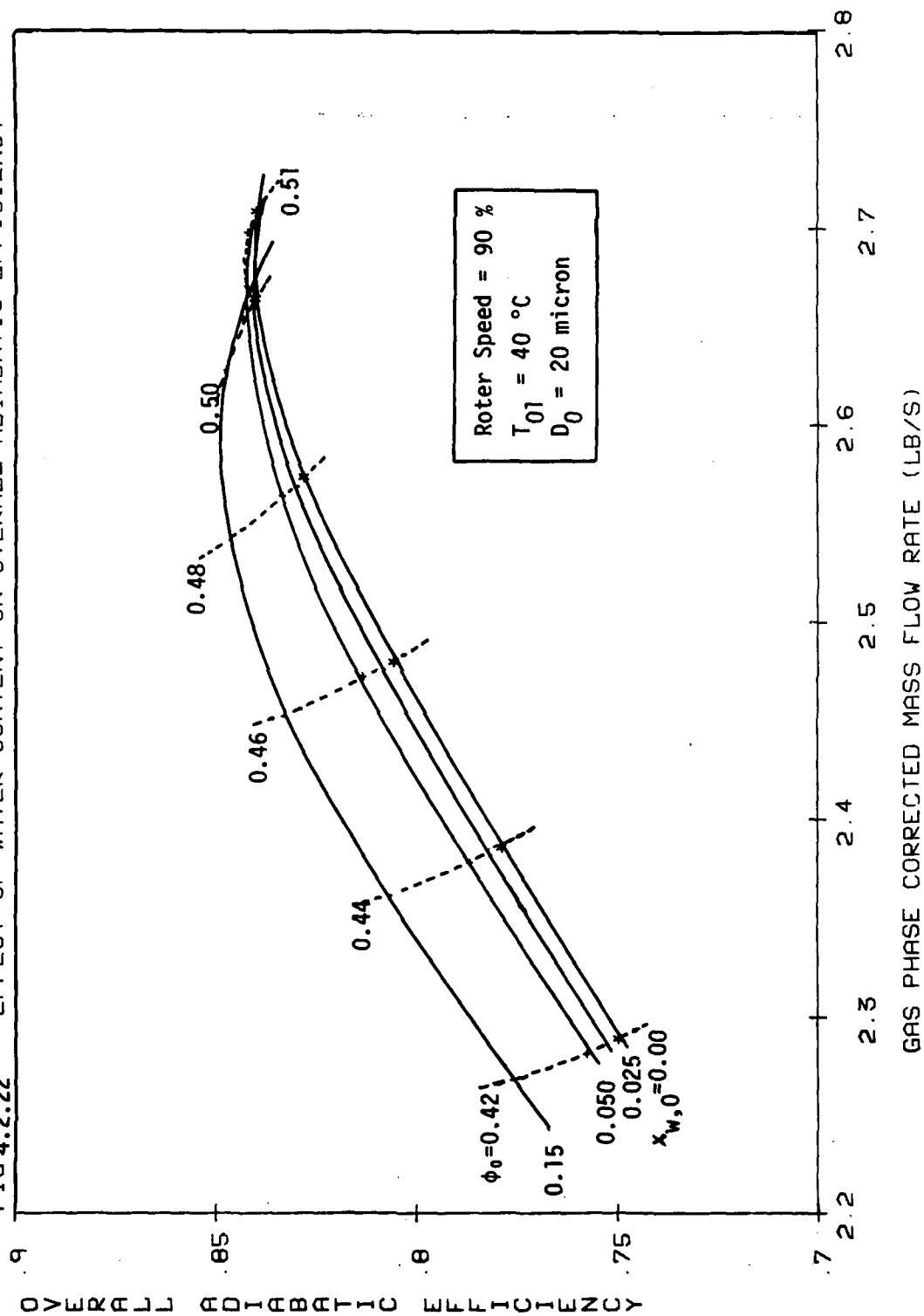
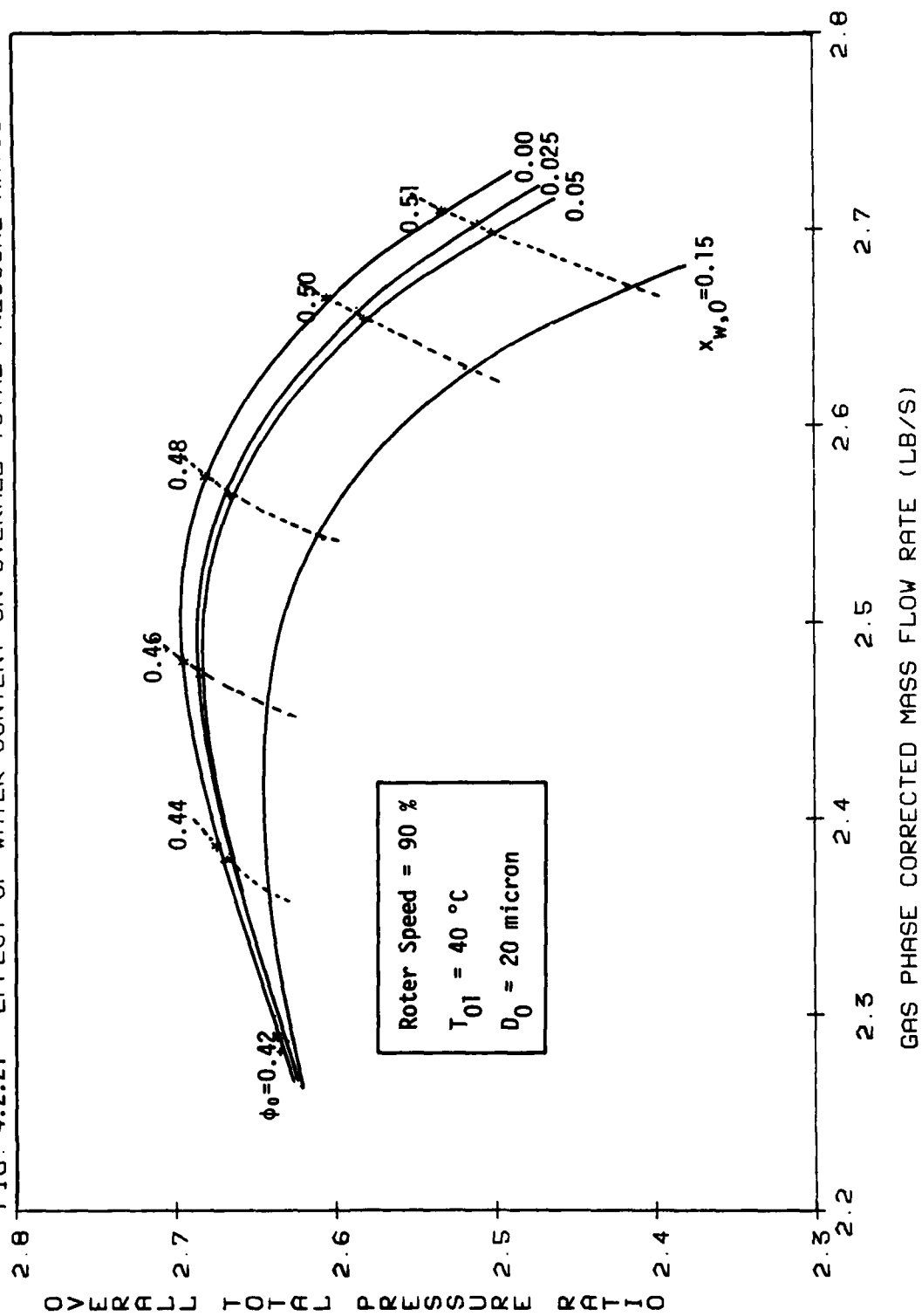


FIG. 4.2.21 EFFECT OF WATER CONTENT ON OVERALL TOTAL PRESSURE RATIO



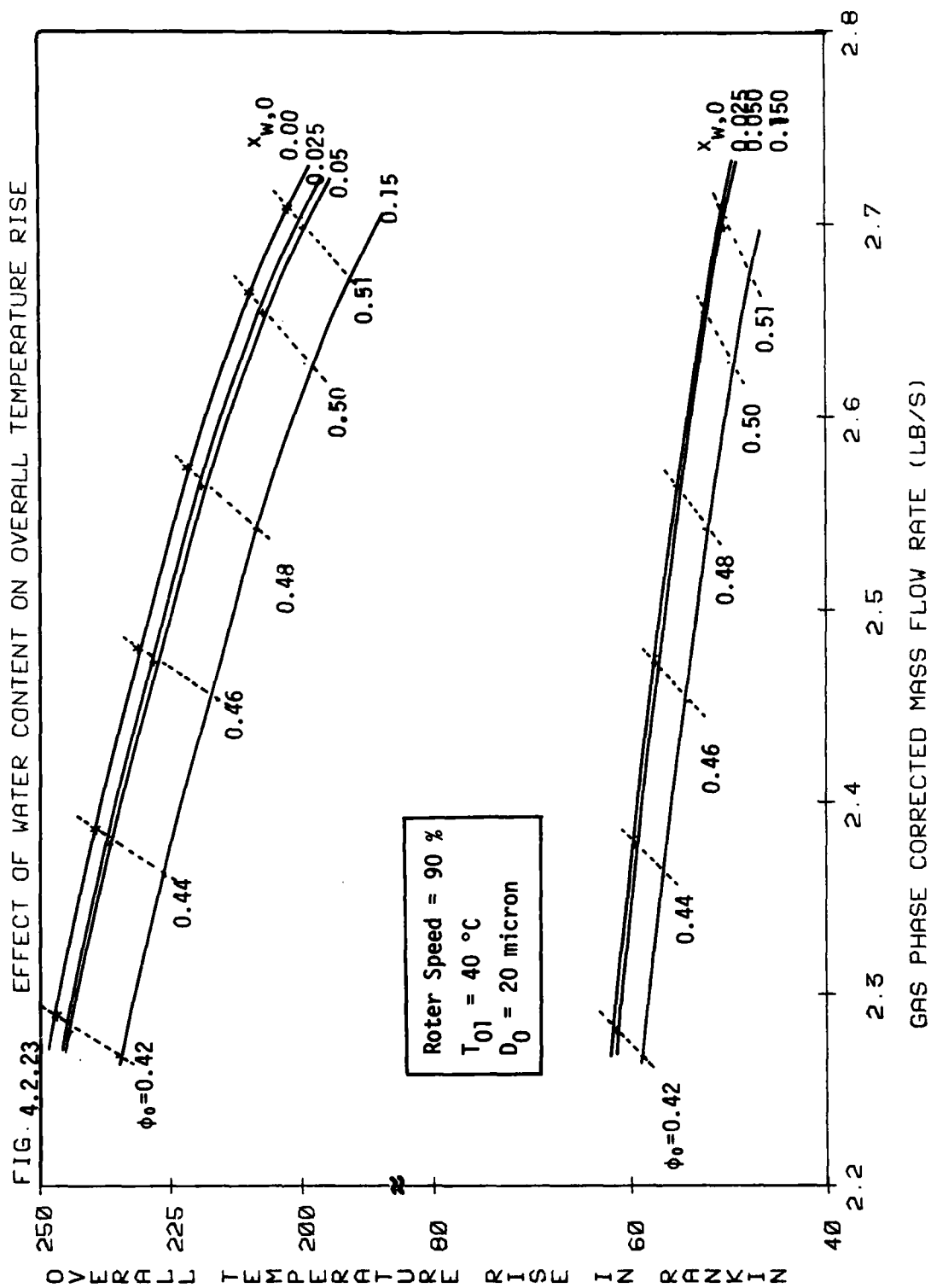


Fig. 4.2.24

CHANGE OF TEMPERATURE ALONG COMPRESSOR STAGES

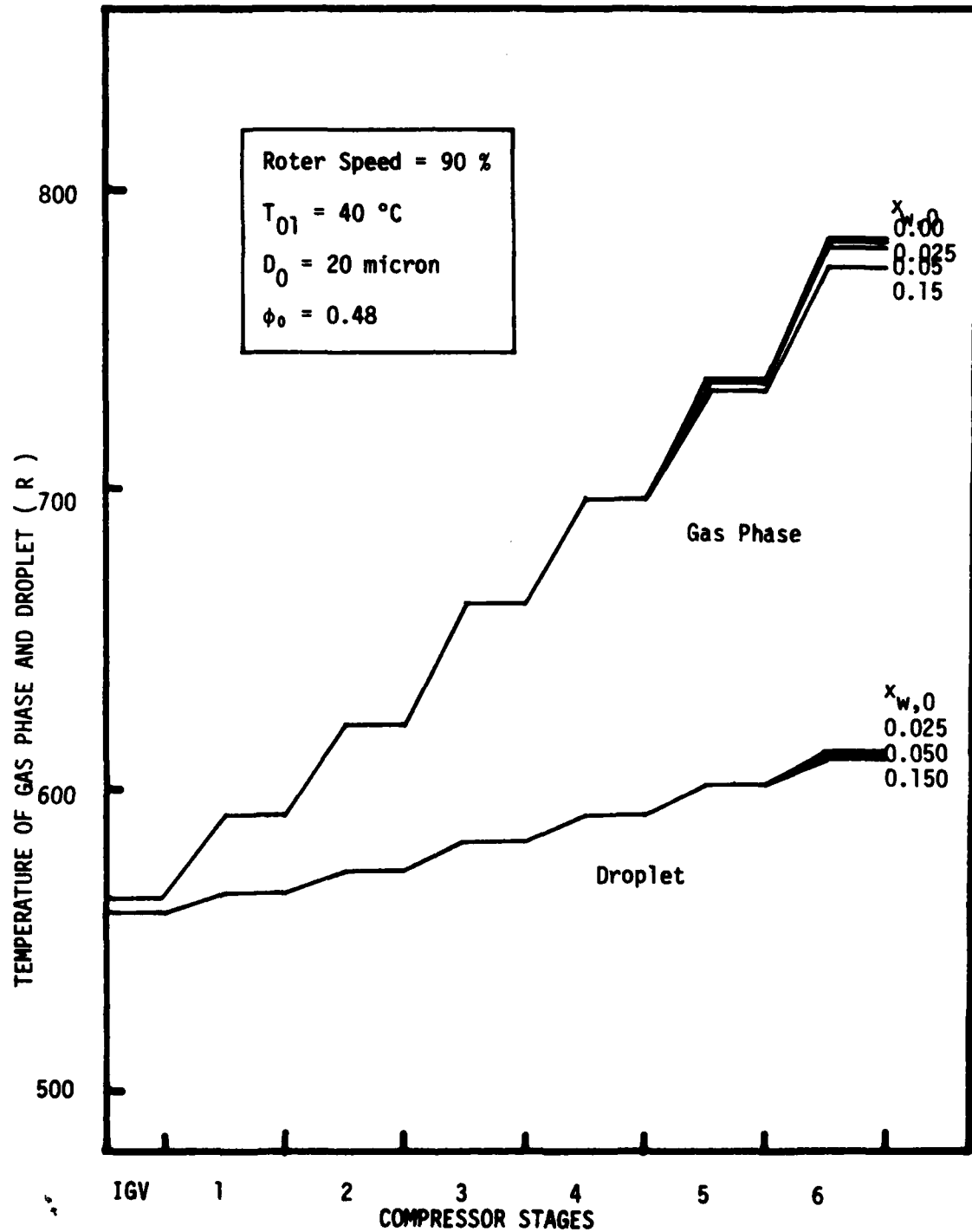
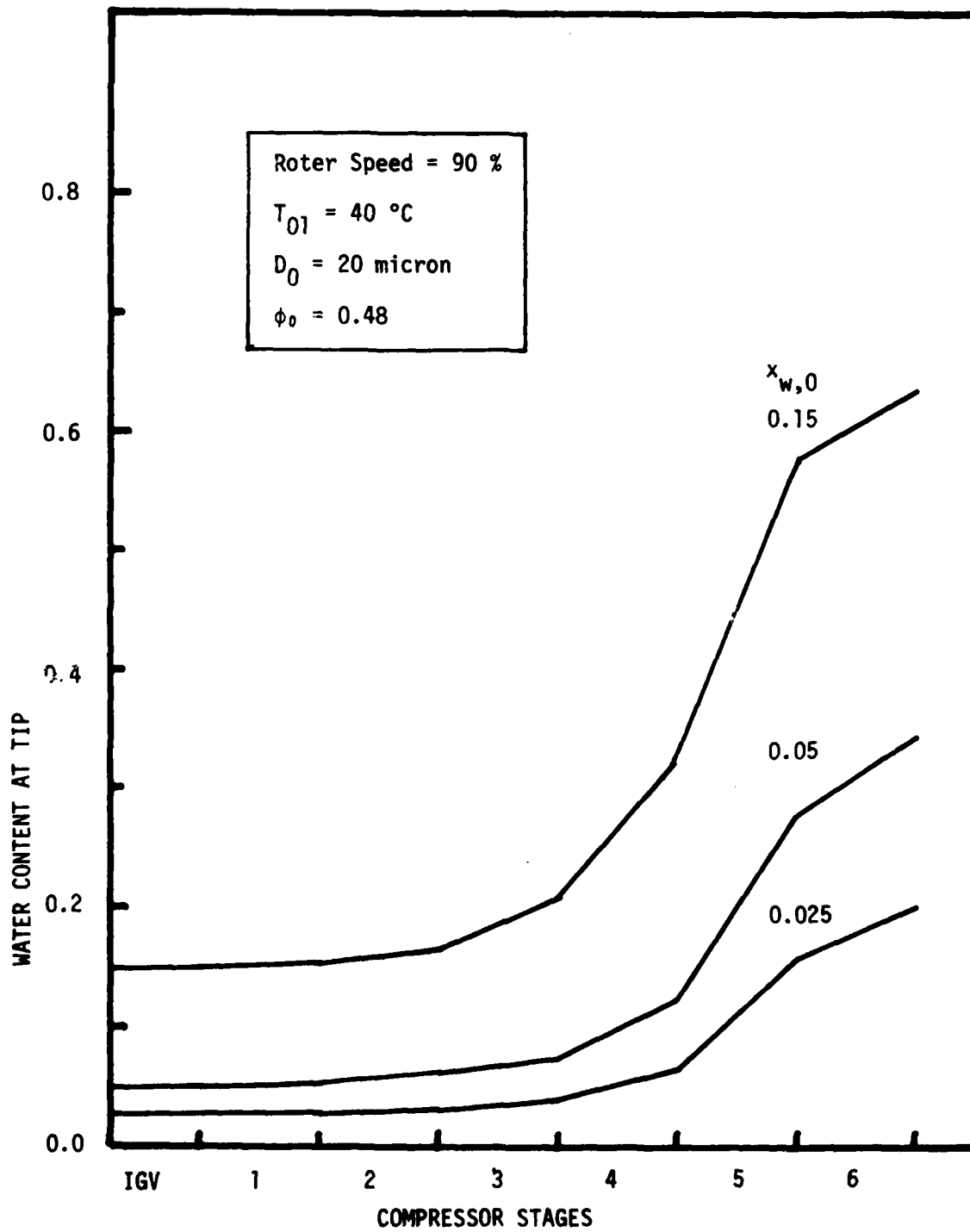


Fig. 4.2.25

CHANGE OF WATER CONTENT AT TIP ALONG COMPRESSOR STAGES



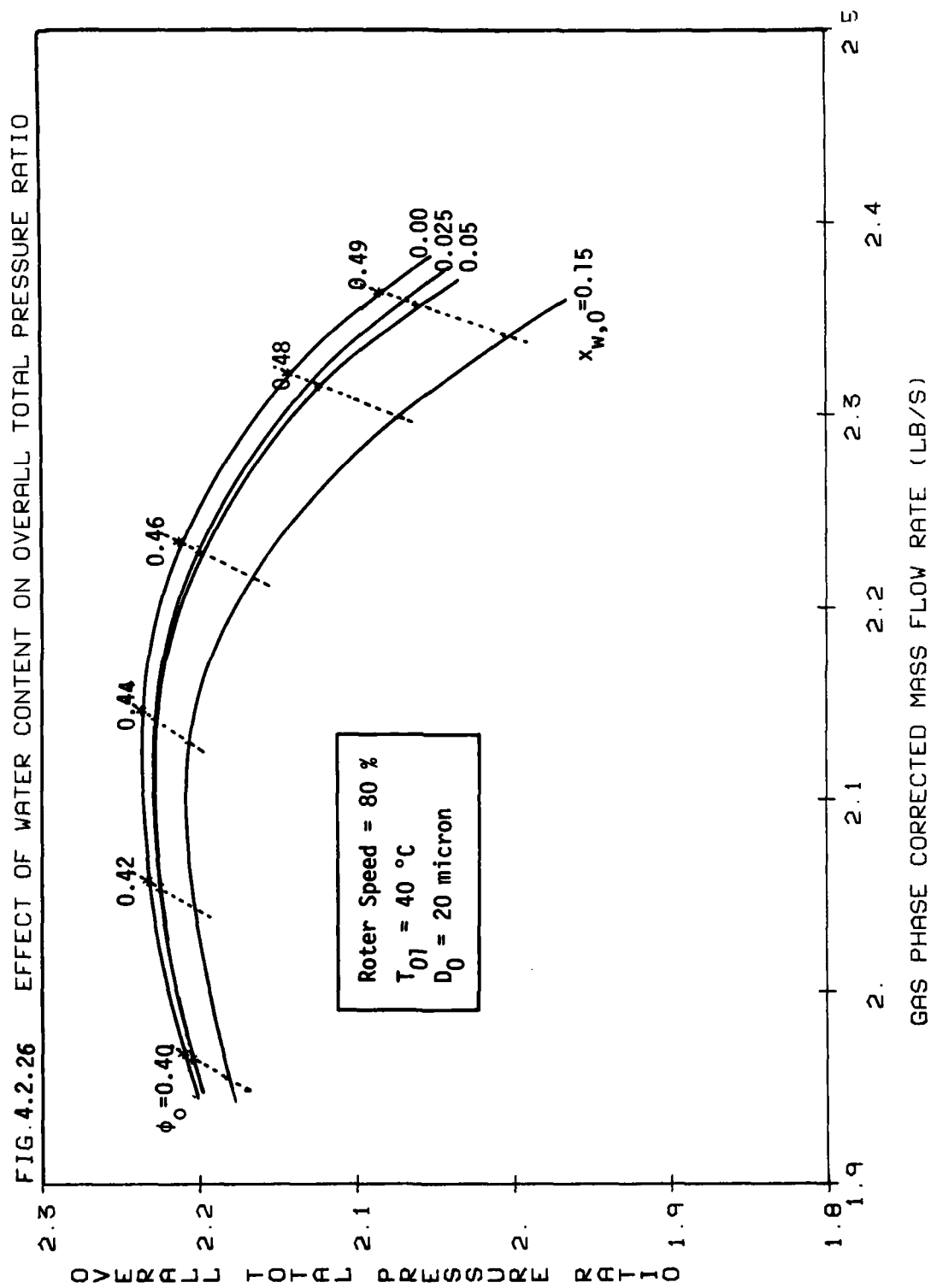


FIG. 4.2.27 EFFECT OF WATER CONTENT ON OVERALL ADIABATIC EFFICIENCY

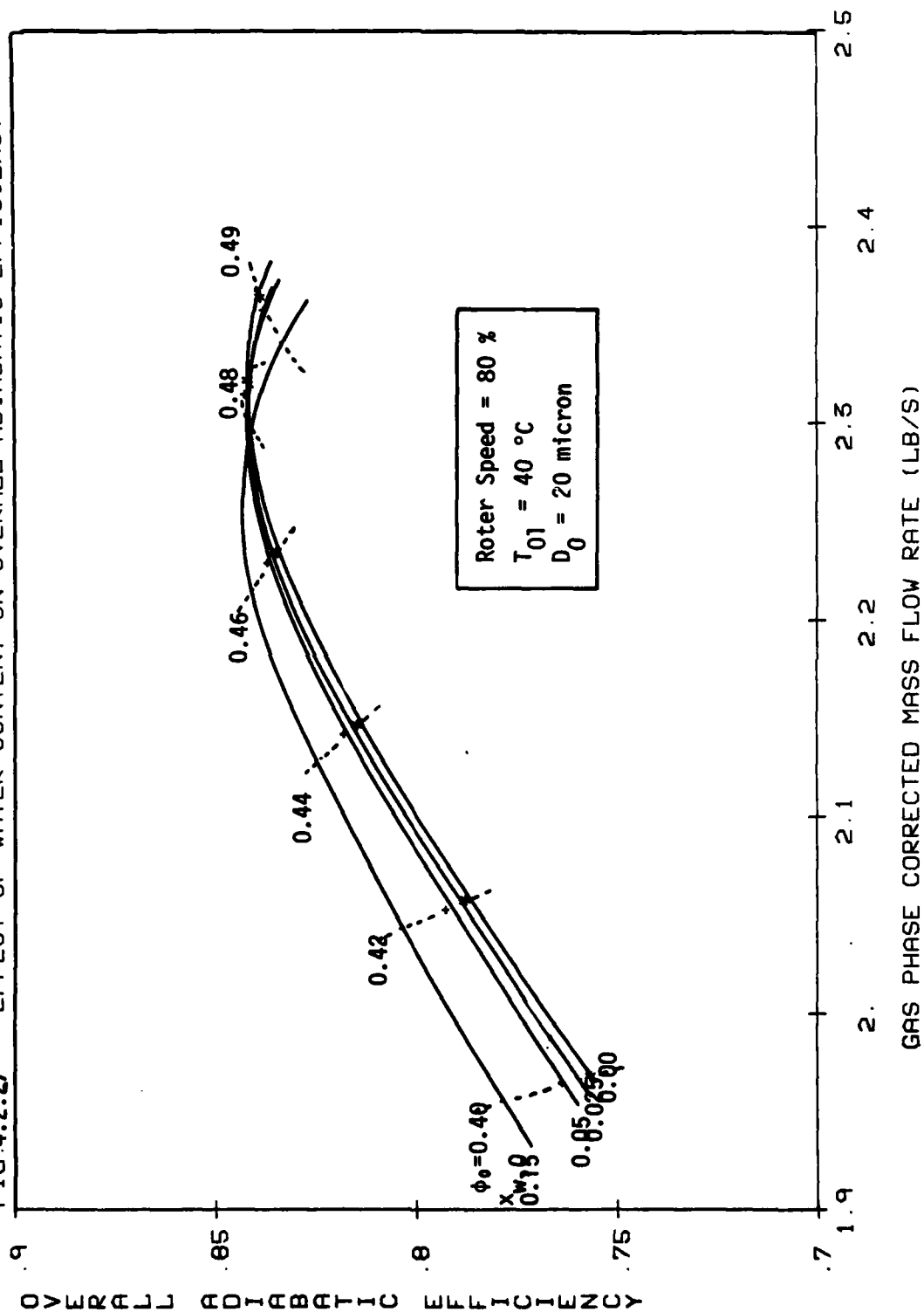


FIG. 4.2.28 EFFECT OF WATER CONTENT ON OVERALL TEMPERATURE RISE

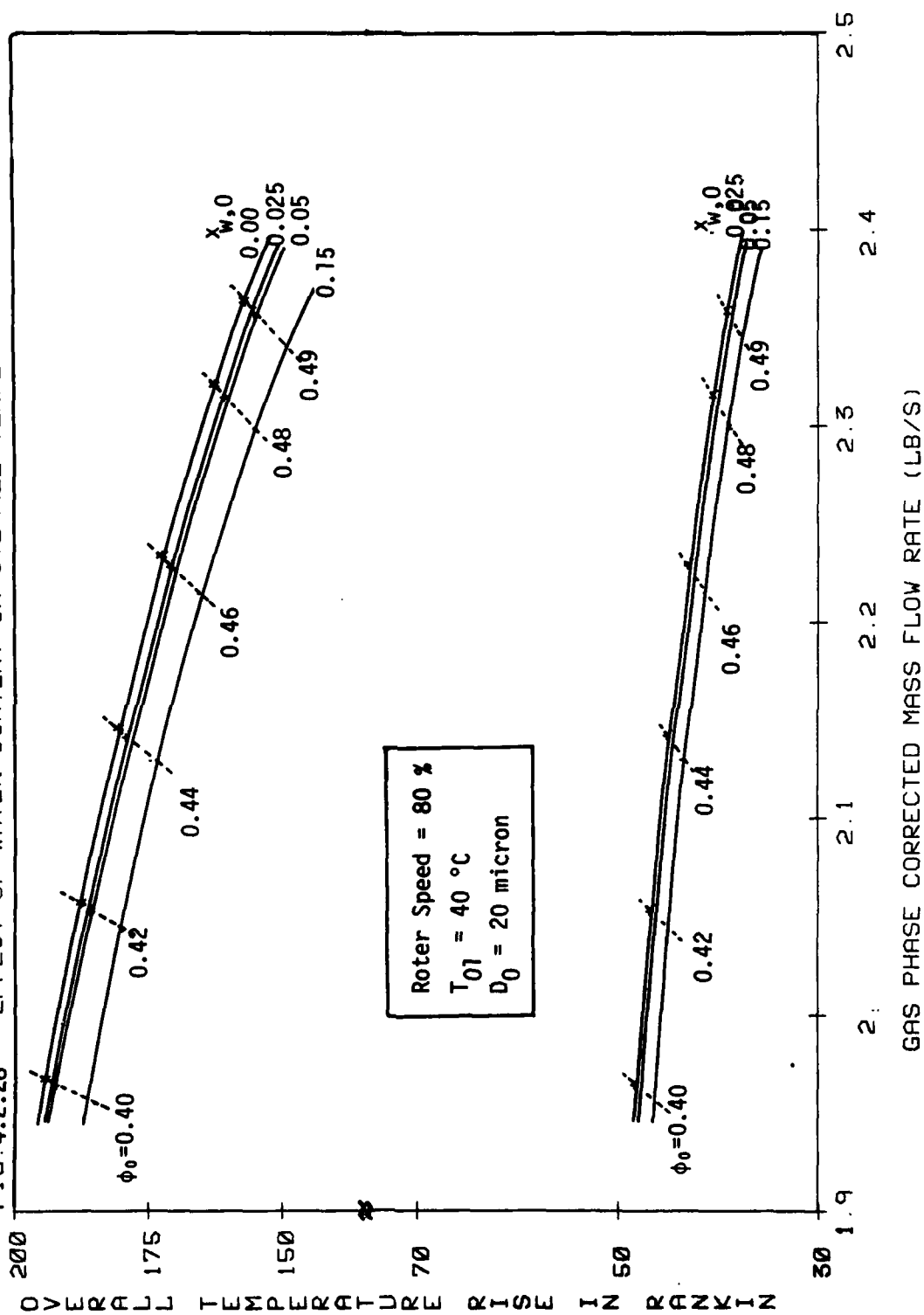


Fig. 4.2.29
CHANGE OF TEMPERATURE ALONG COMPRESSOR STAGES

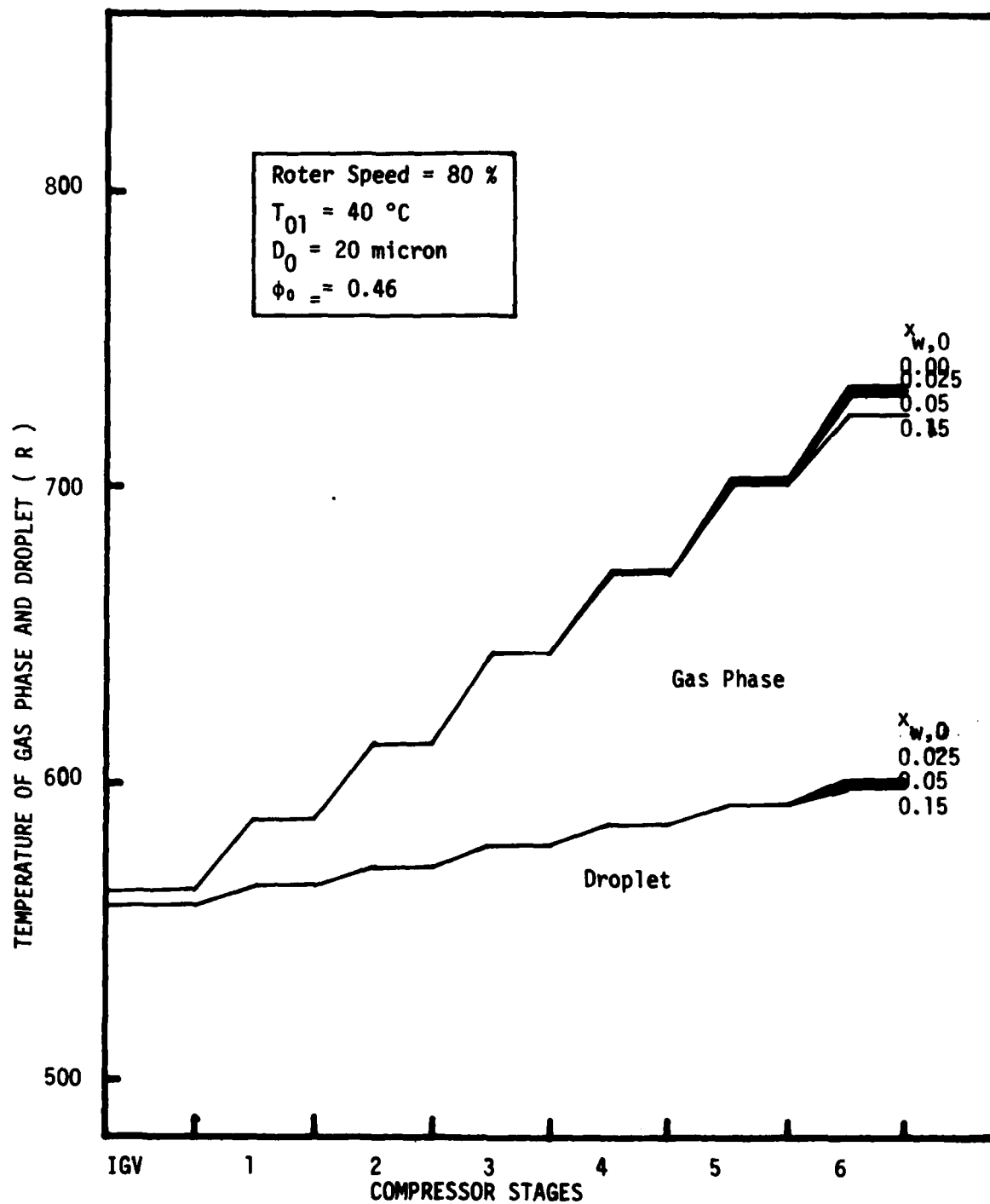


Fig. 4.2.30

CHANGE OF WATER CONTENT AT TIP ALONG COMPRESSOR STAGES

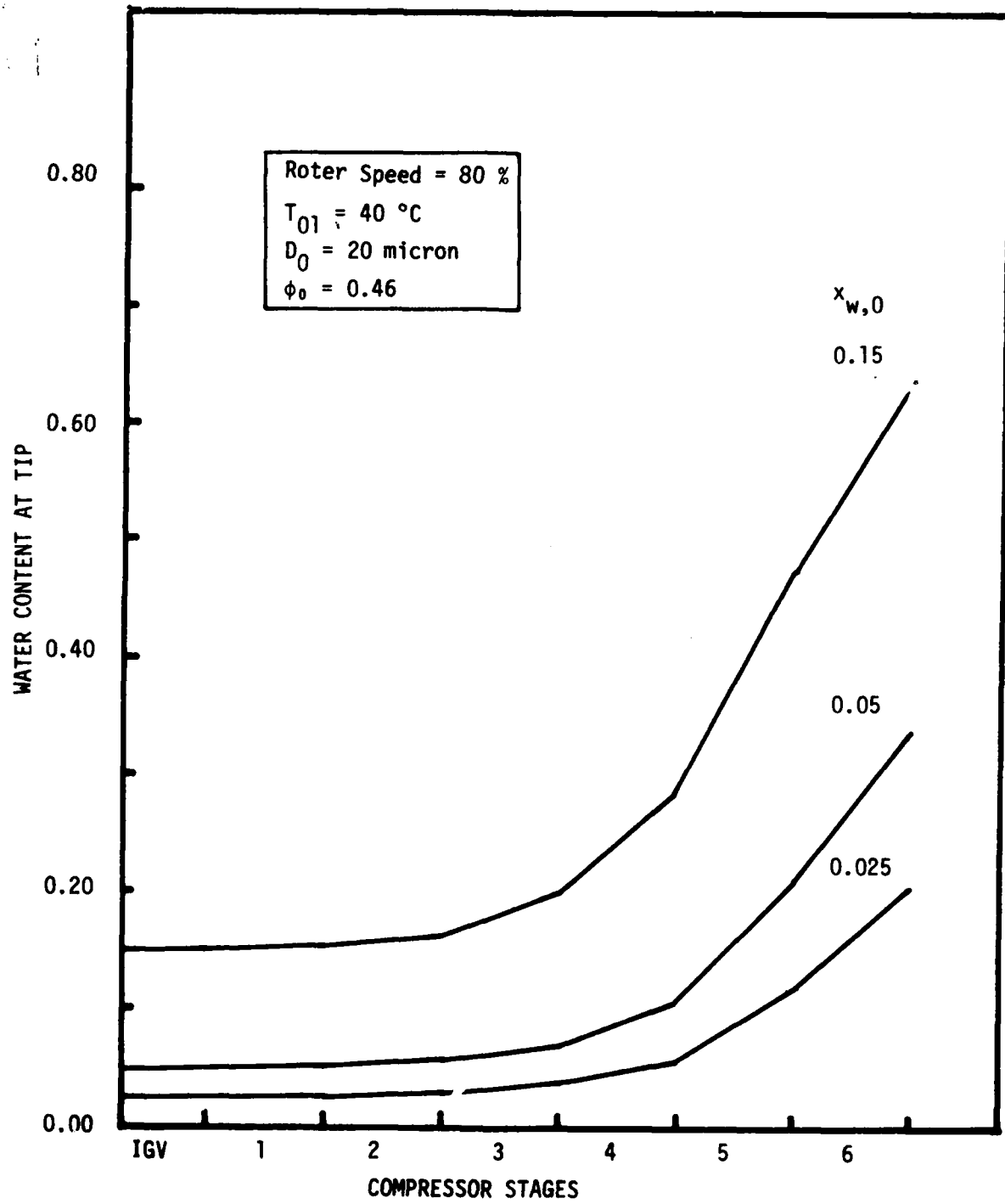


Fig. 4.3.1 Effect of Water Content on Overall Total Pressure Ratio

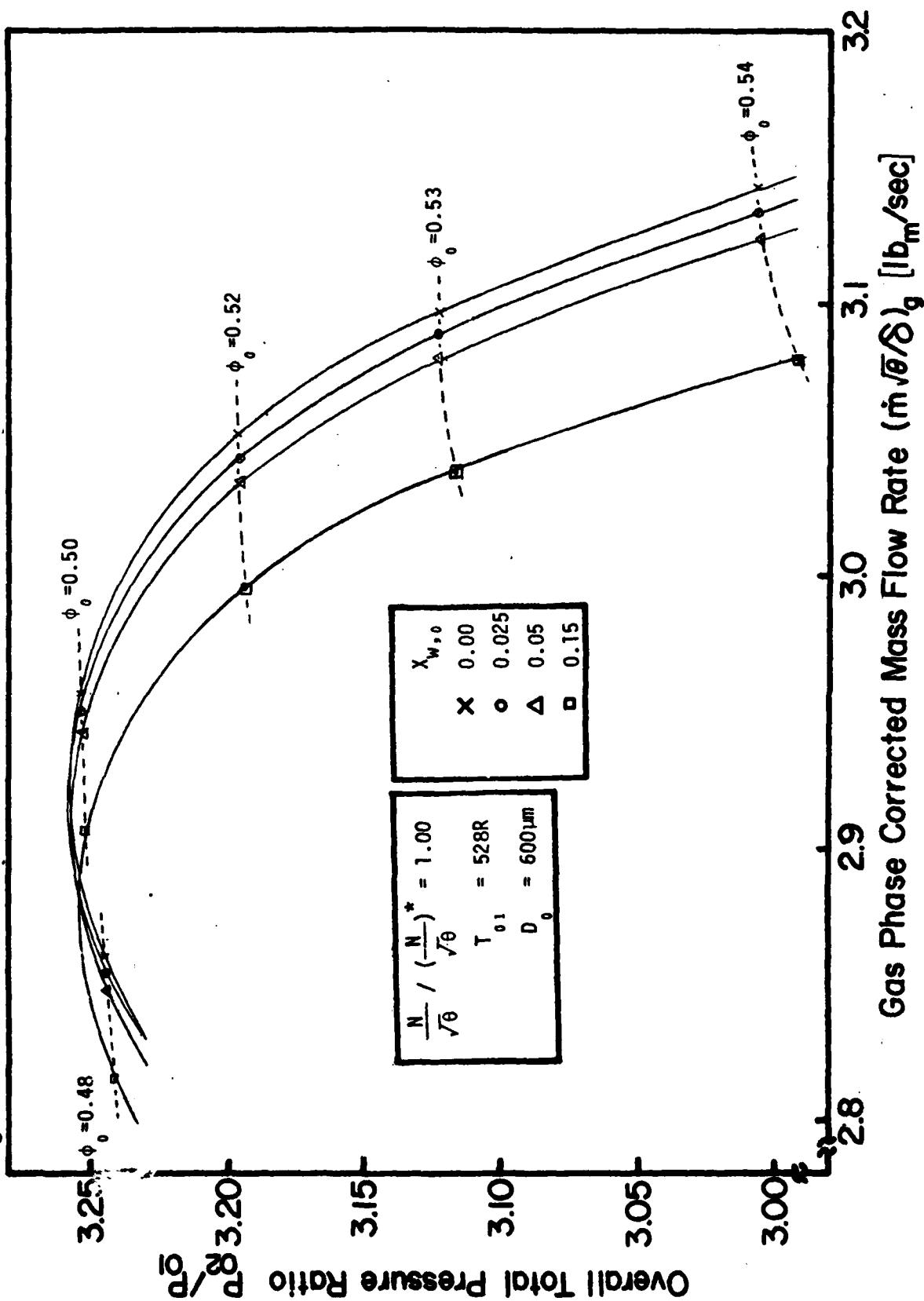


Fig.4.3.2 Effect of Water Content on Overall Adiabatic Efficiency

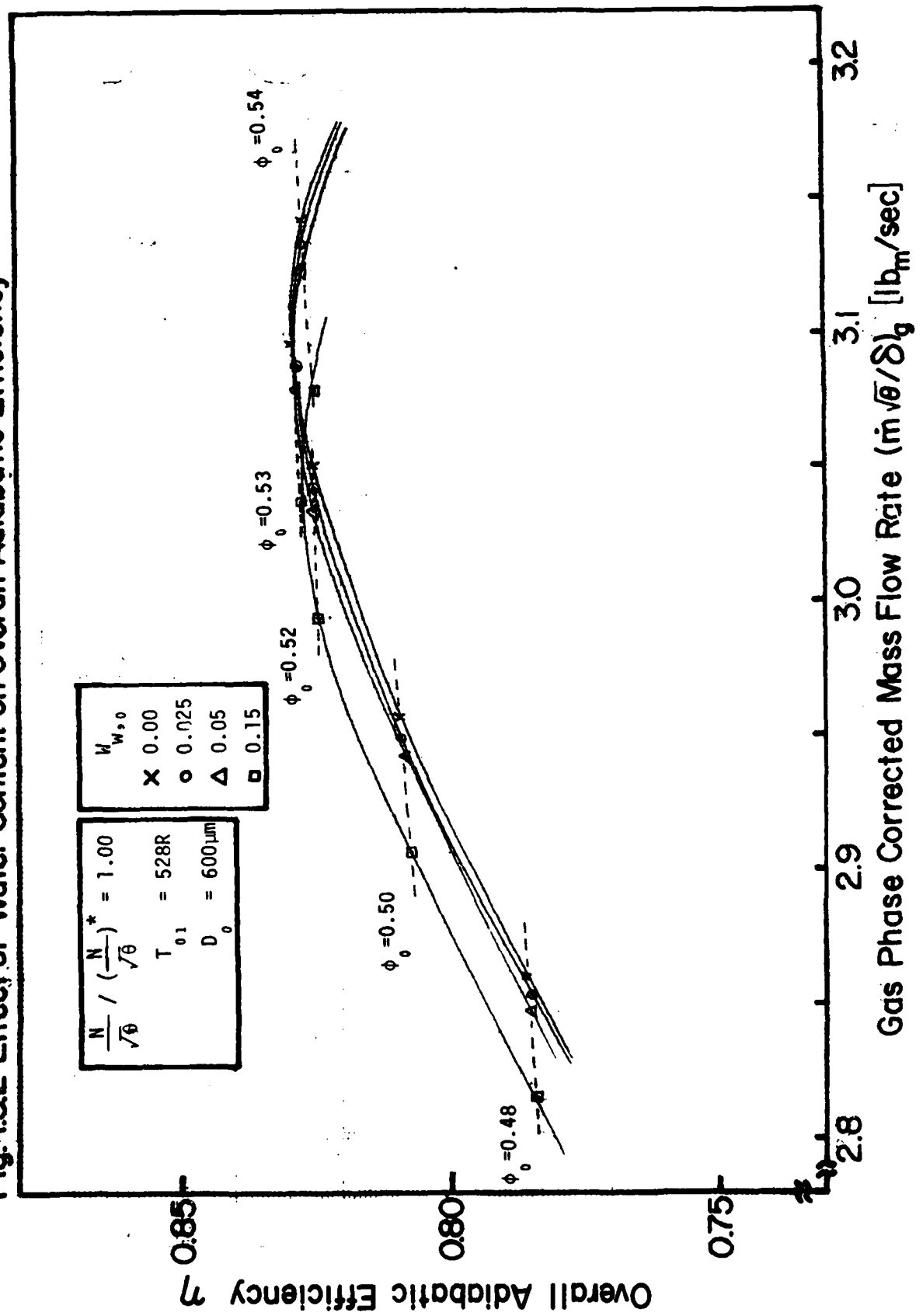


Fig.4.3.3 Effect of Water Content on Overall Temperature Rise of Gas Phase and Droplet

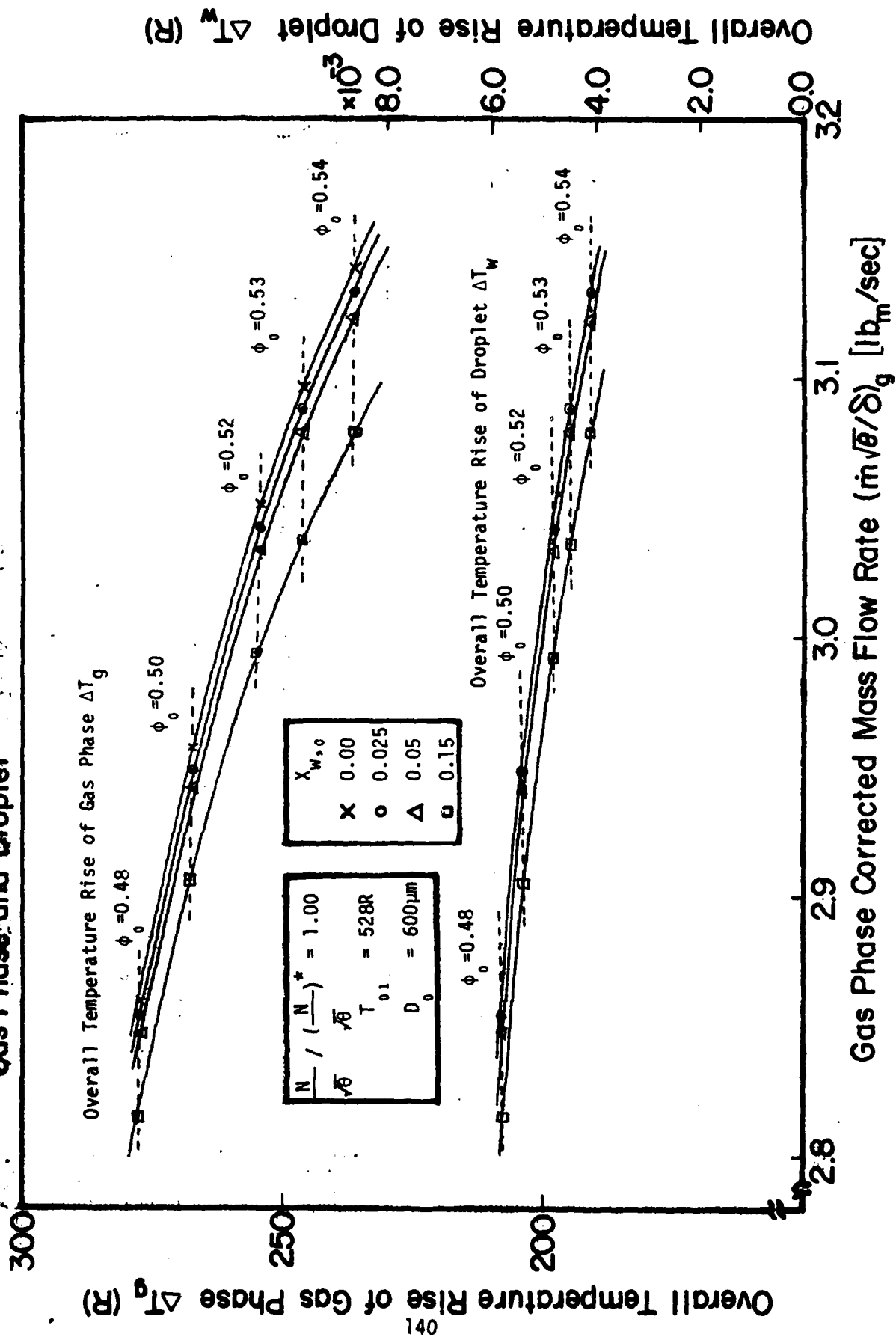


Fig.4.3.4 Temperature Change of Gas Phase and Droplet along Compressor Stages

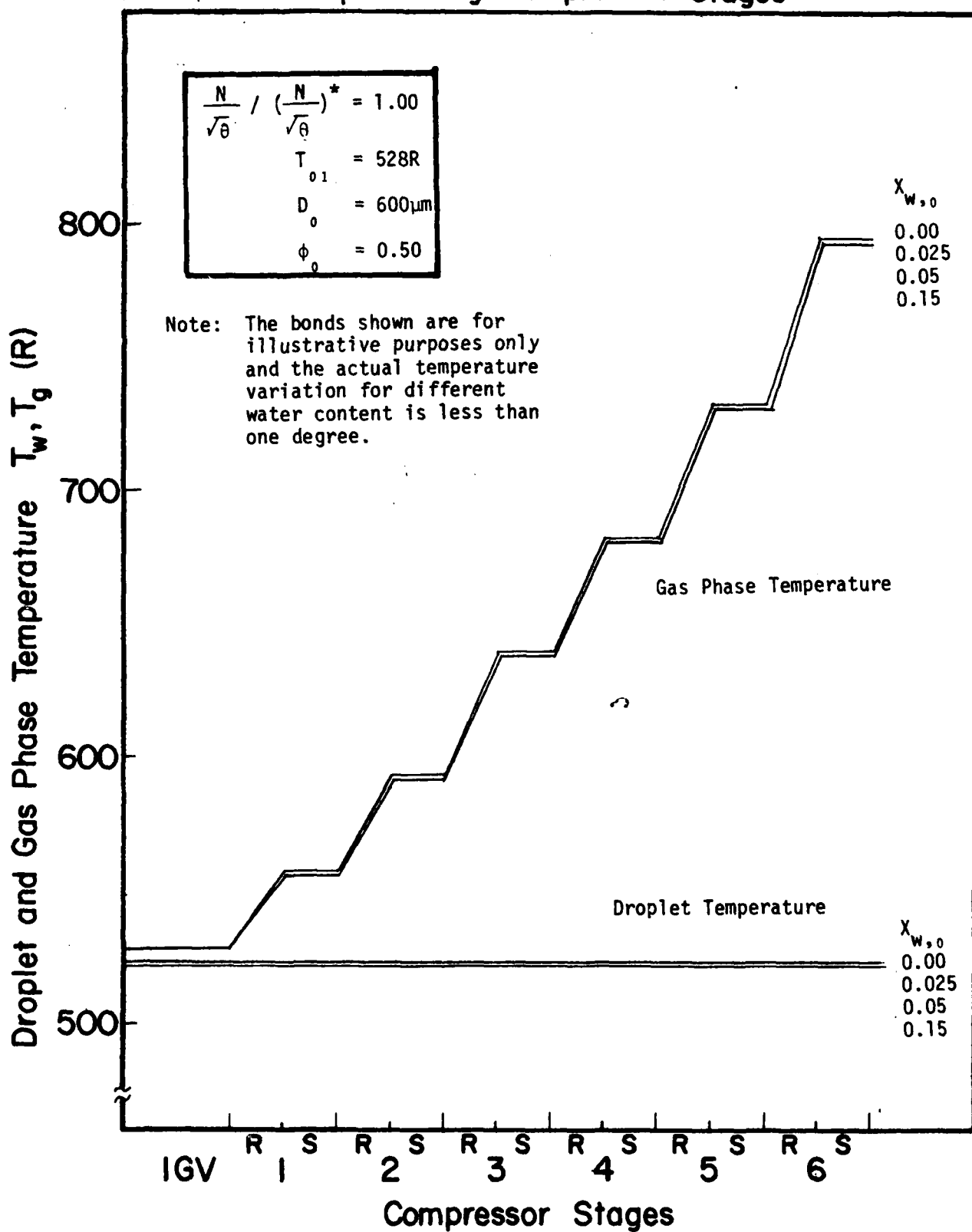


Fig.4.3.5 Change of Water Content at Tip along Compressor Stages

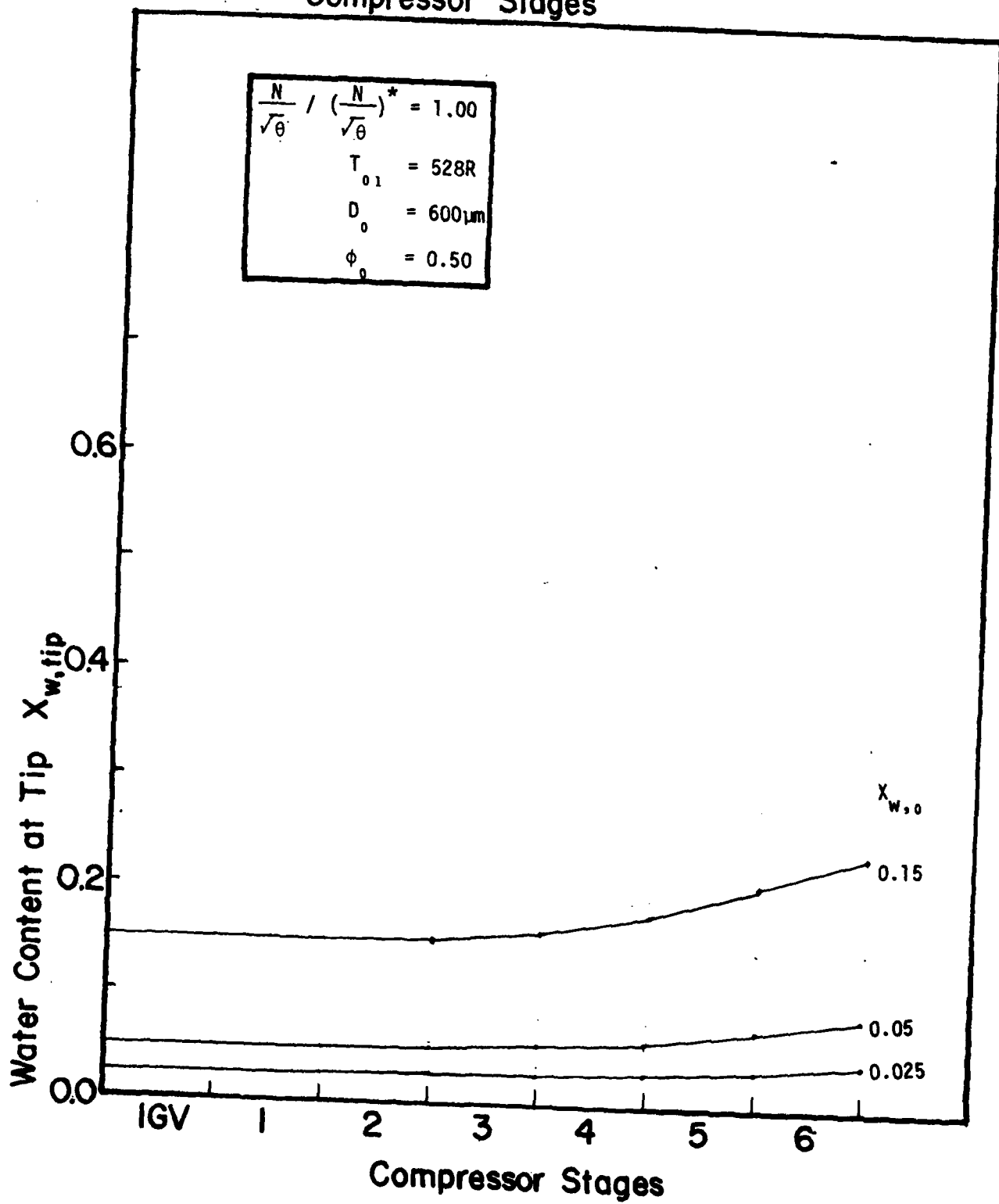


Fig. 4.3.6. Effect of Water Content on Overall Total Pressure Ratio

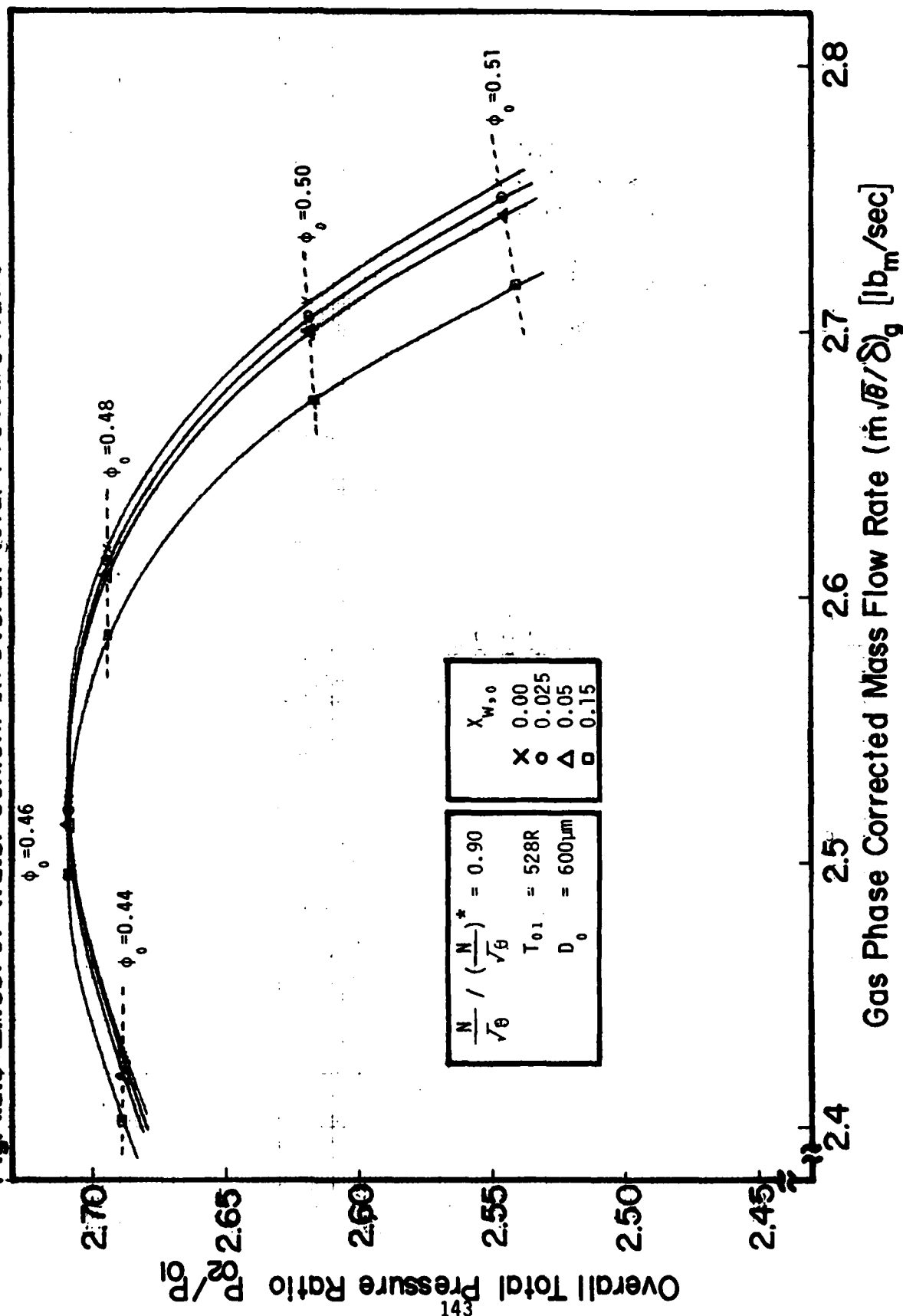


Fig.4.3.7 Effect of Water Content on Overall Adiabatic Efficiency

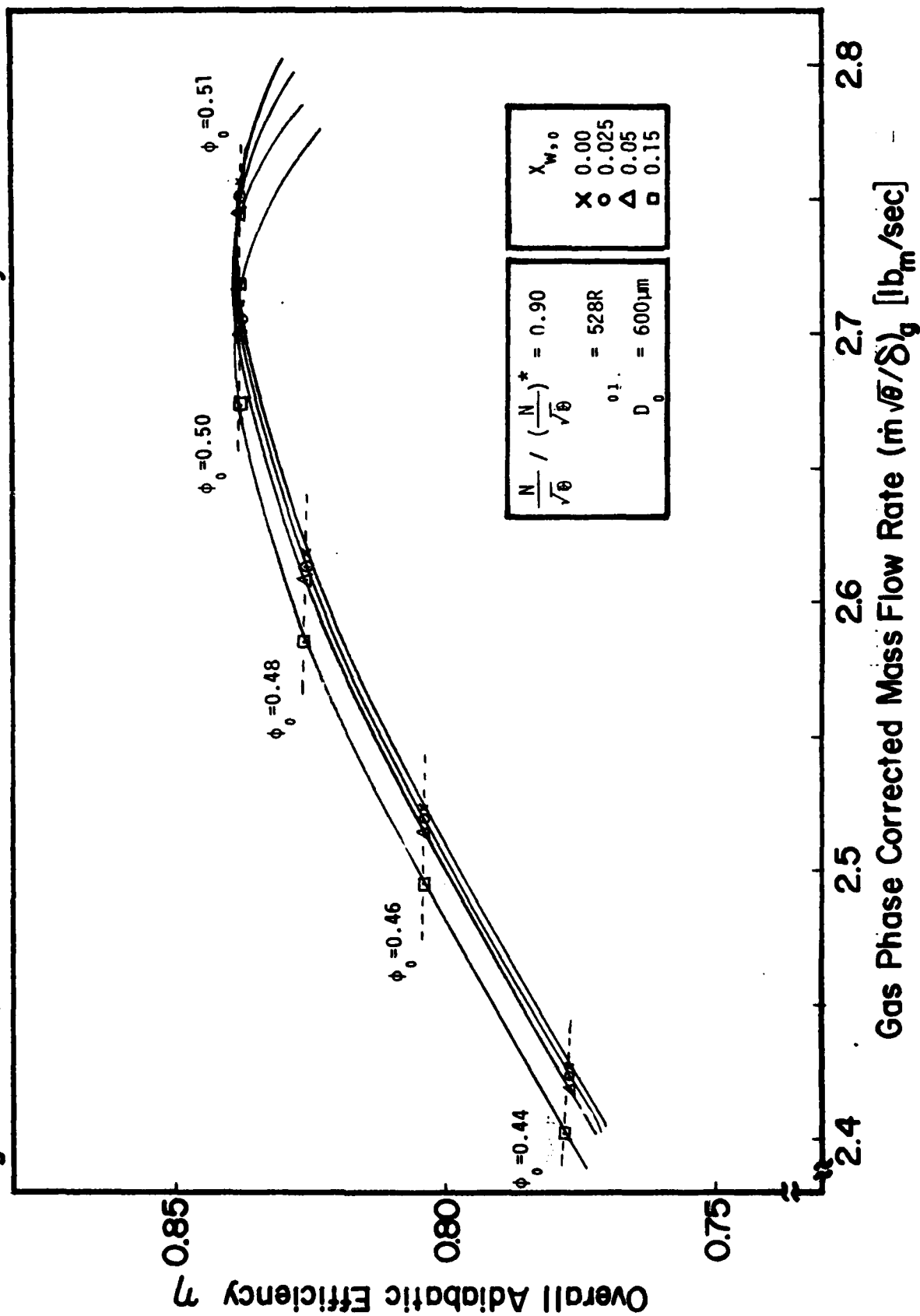


Fig.4.3.8 Effect of Water Content on Overall Temperature Rise of Gas Phase and Droplet

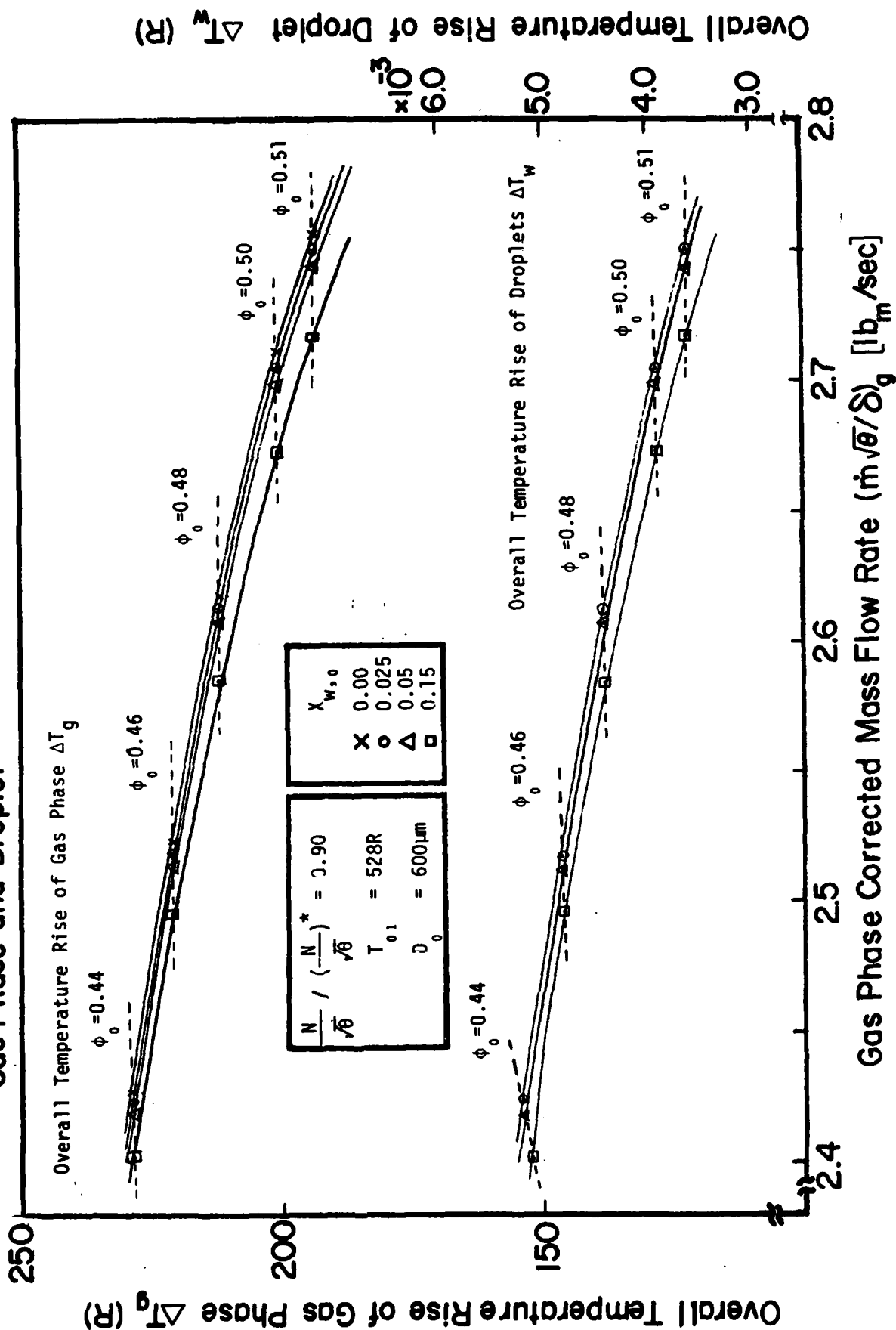


Fig.4.3.9 Temperature Change of Gas Phase and Droplet along Compressor Stages

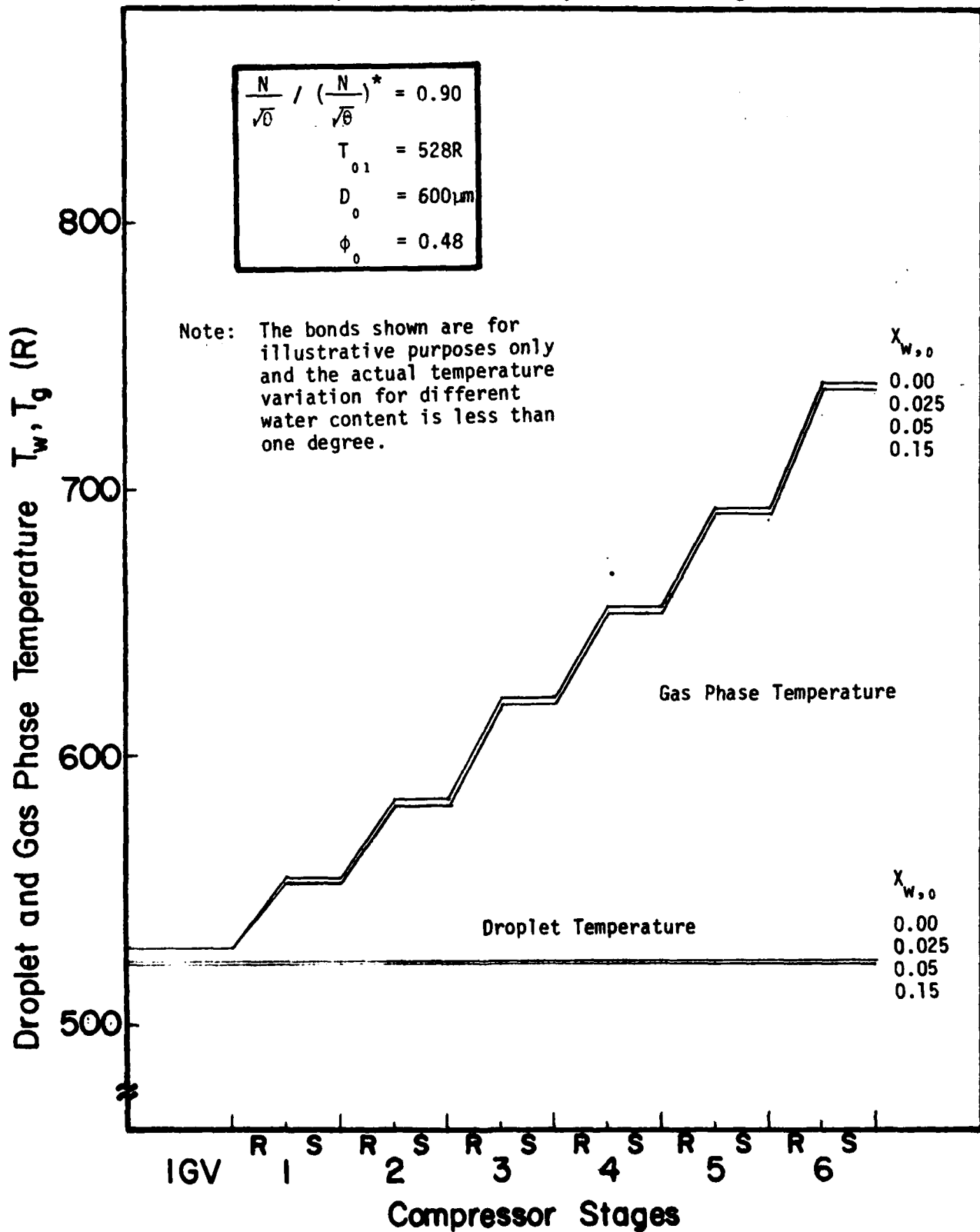


Fig.4.3.10 Change of Water Content at Tip along Compressor Stages

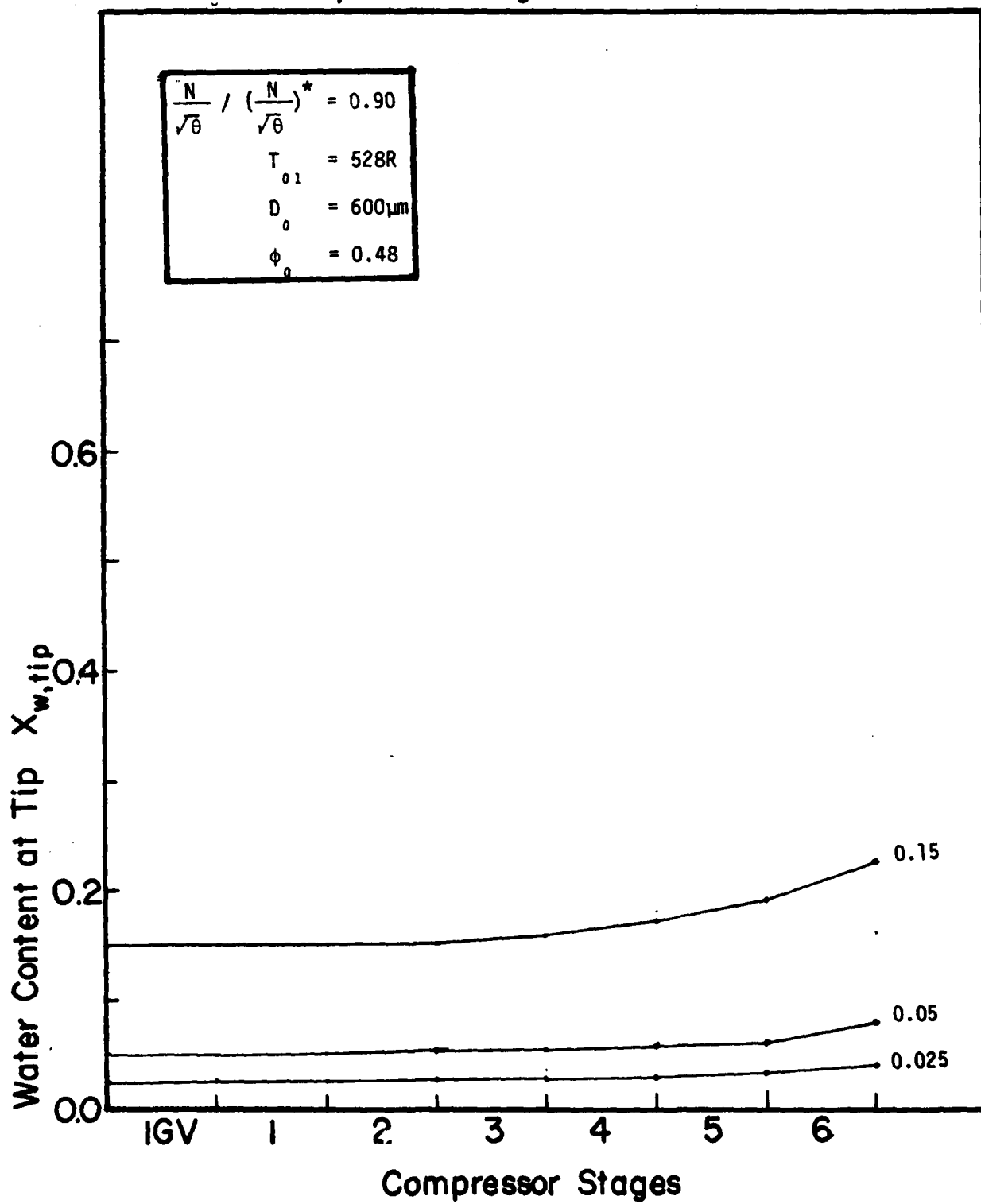


Fig.4.3.11 Effect of Water Content on Overall Total Pressure Ratio

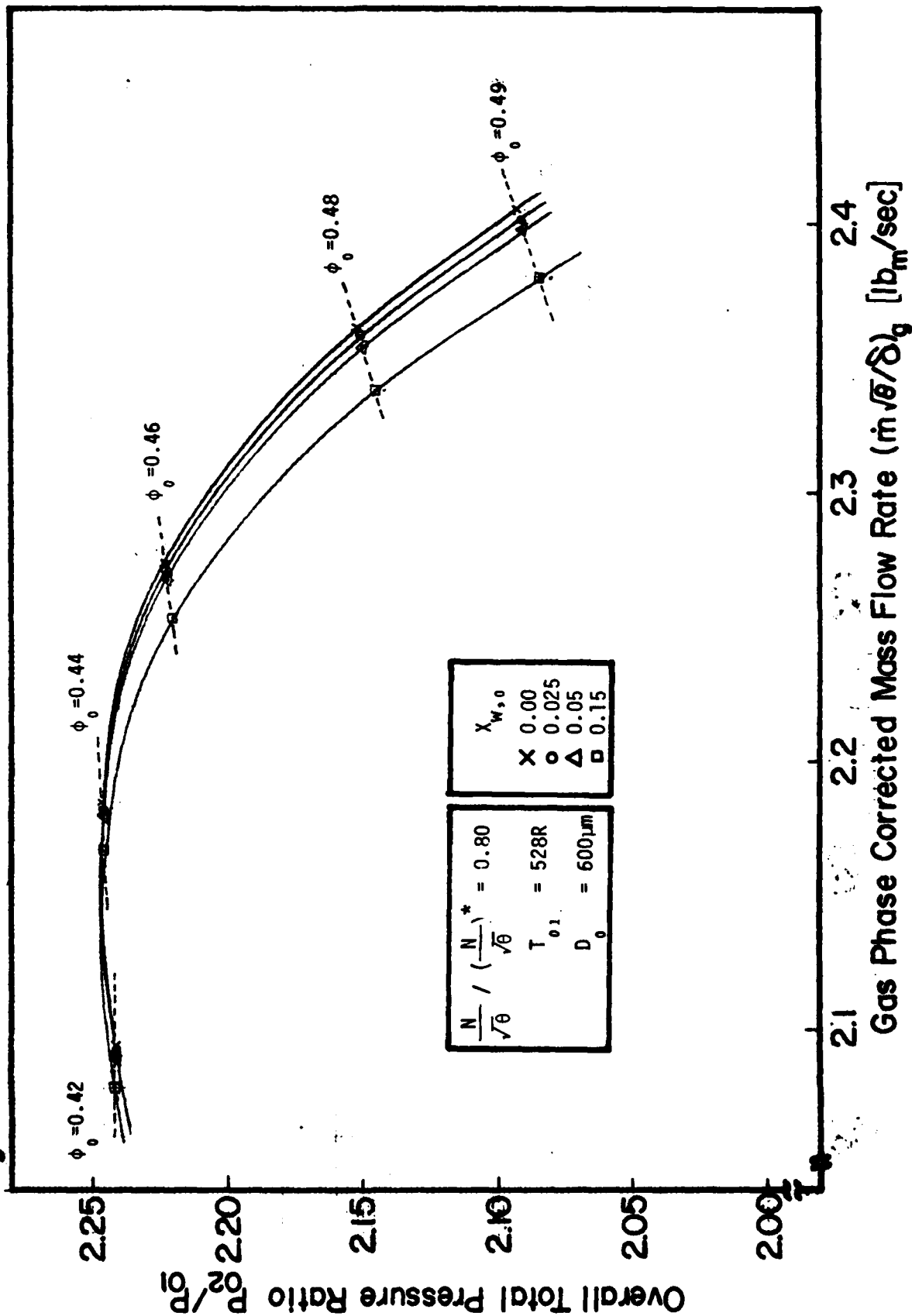


Fig.4.3J2 Effect of Water Content on Overall Adiabatic Efficiency

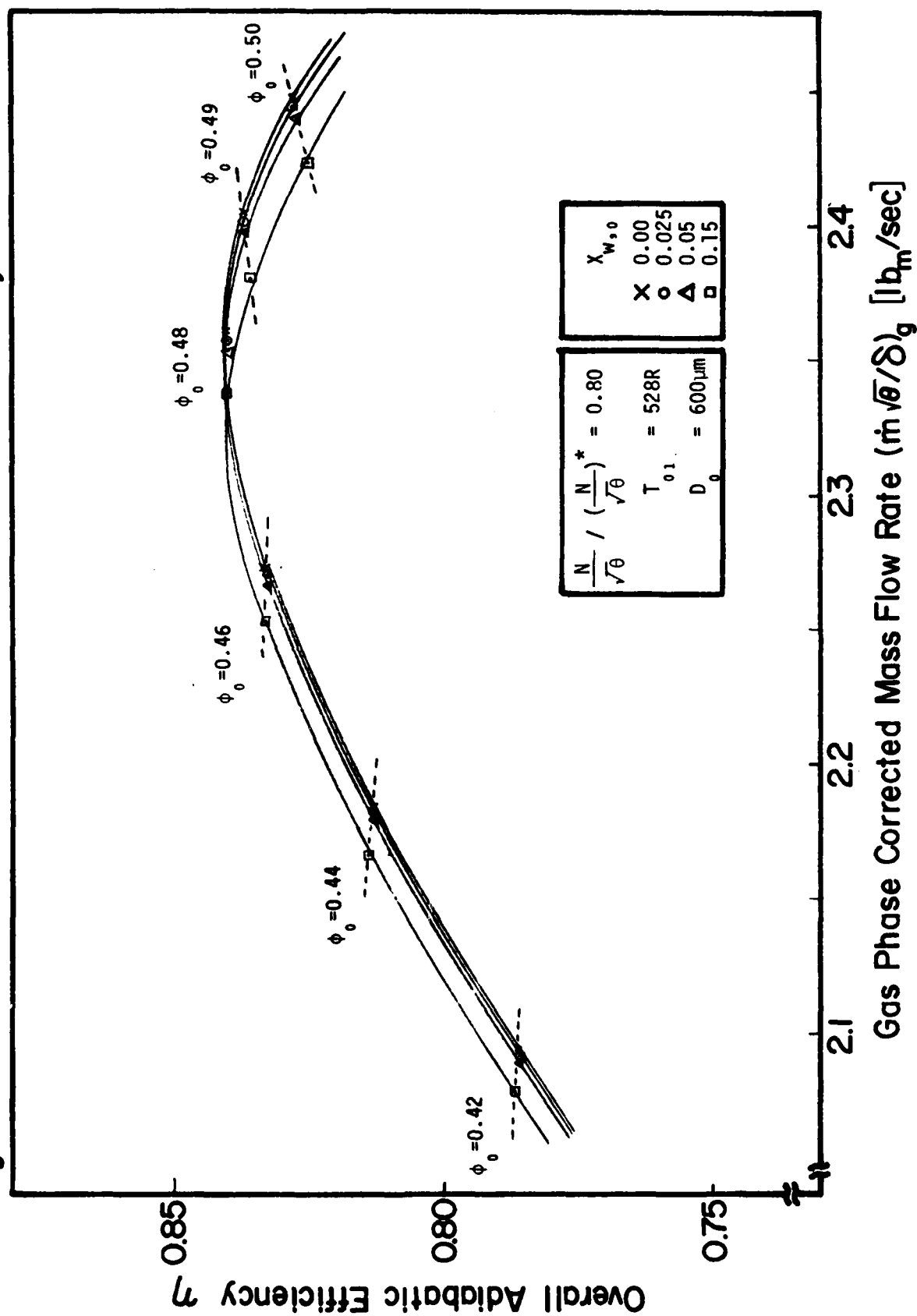


Fig.4.3.14 Temperature Change of Gas Phase and Droplet along Compressor Stages

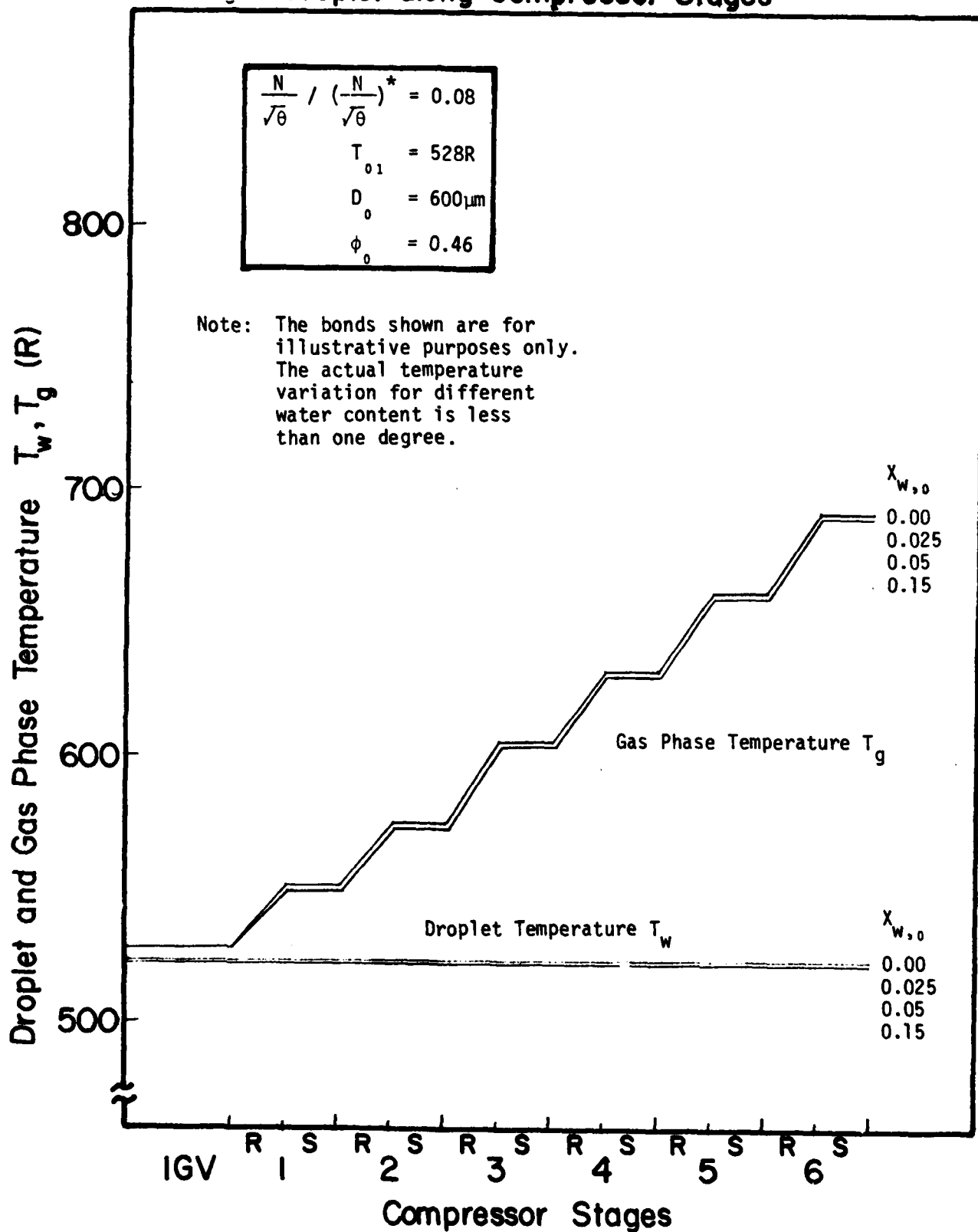


Fig.4.3.15 Change of Water Content at Tip along Compressor Stages

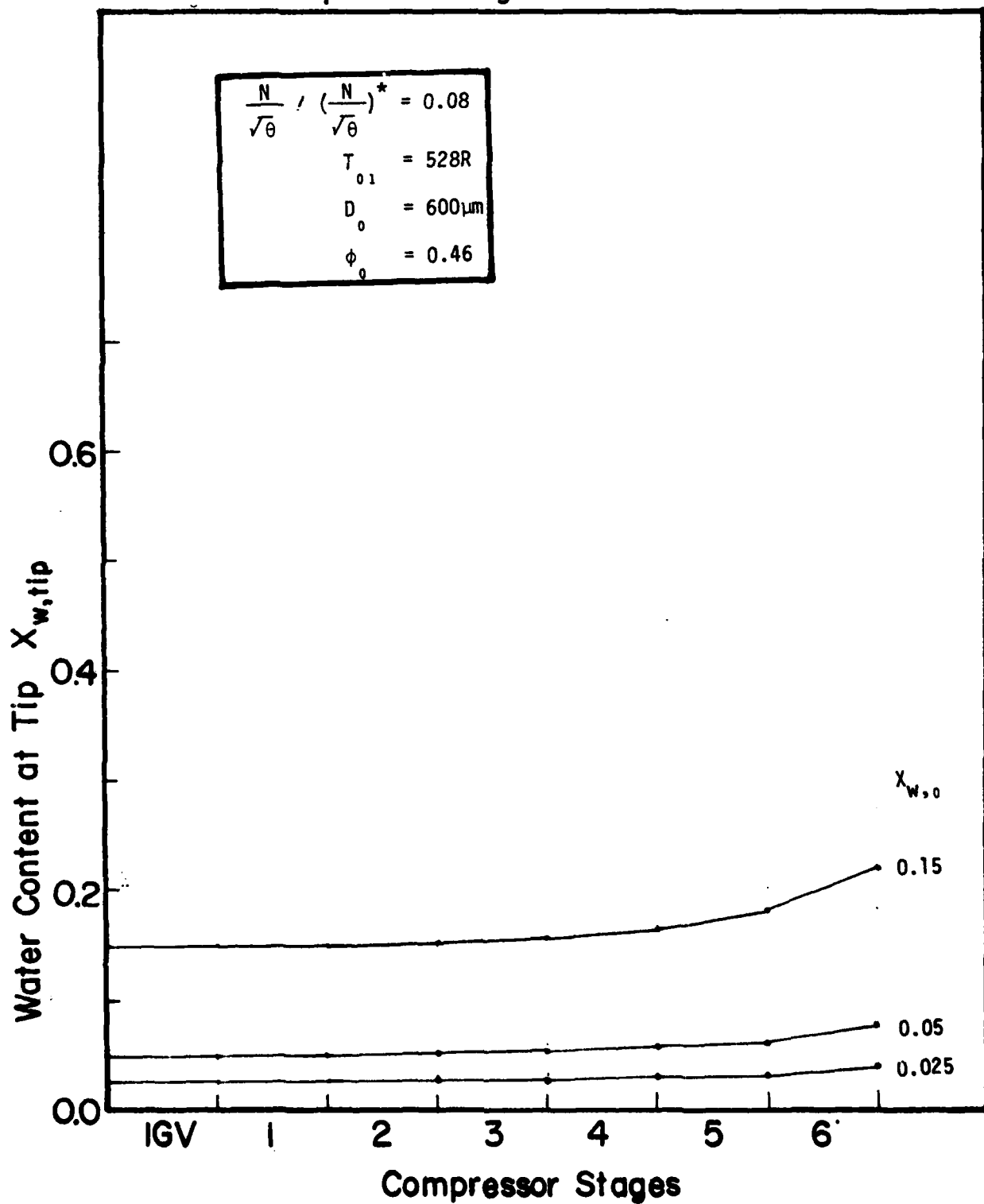


Fig. 4.3.16 Effect of Water Content on Overall Total Pressure Ratio

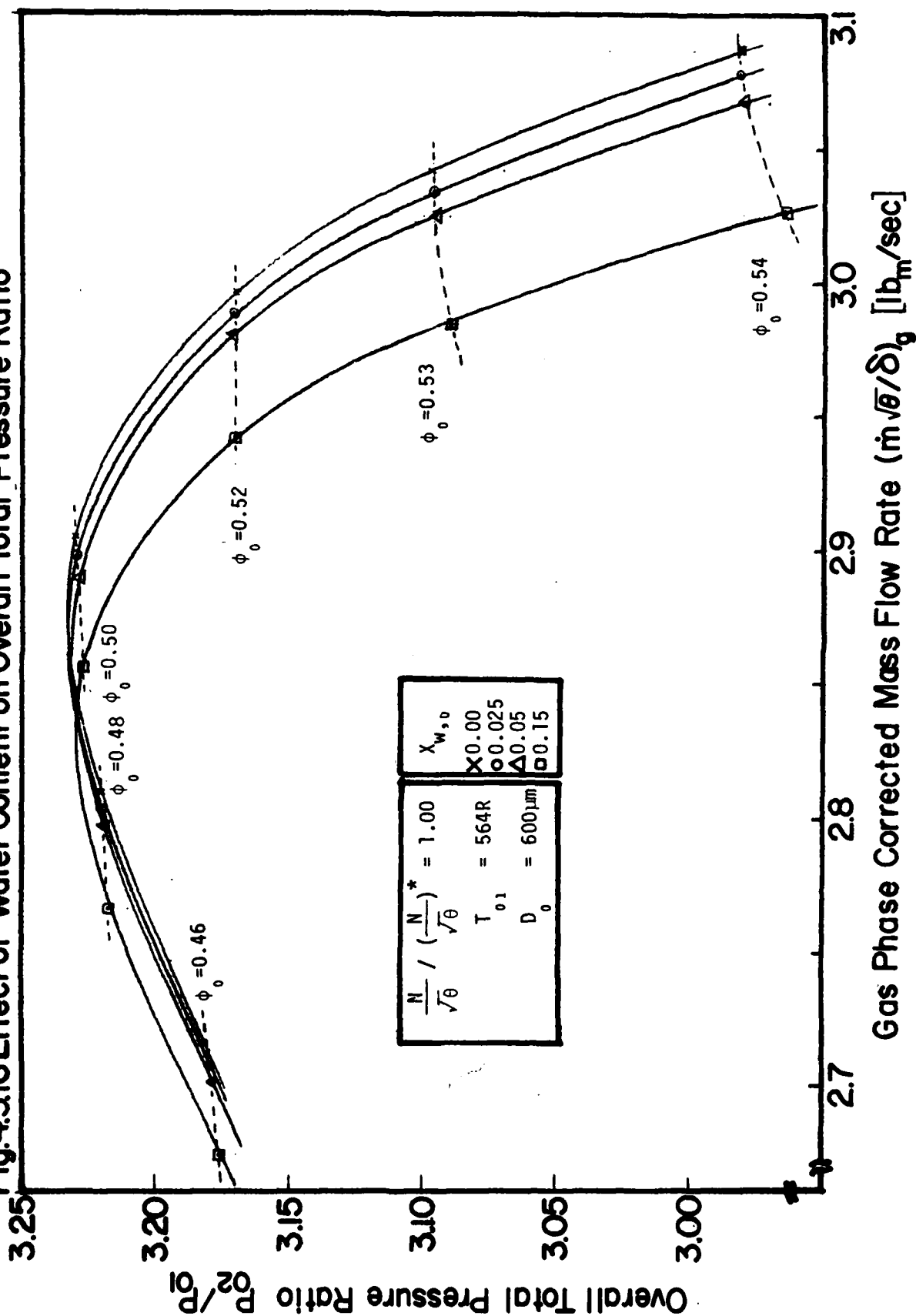
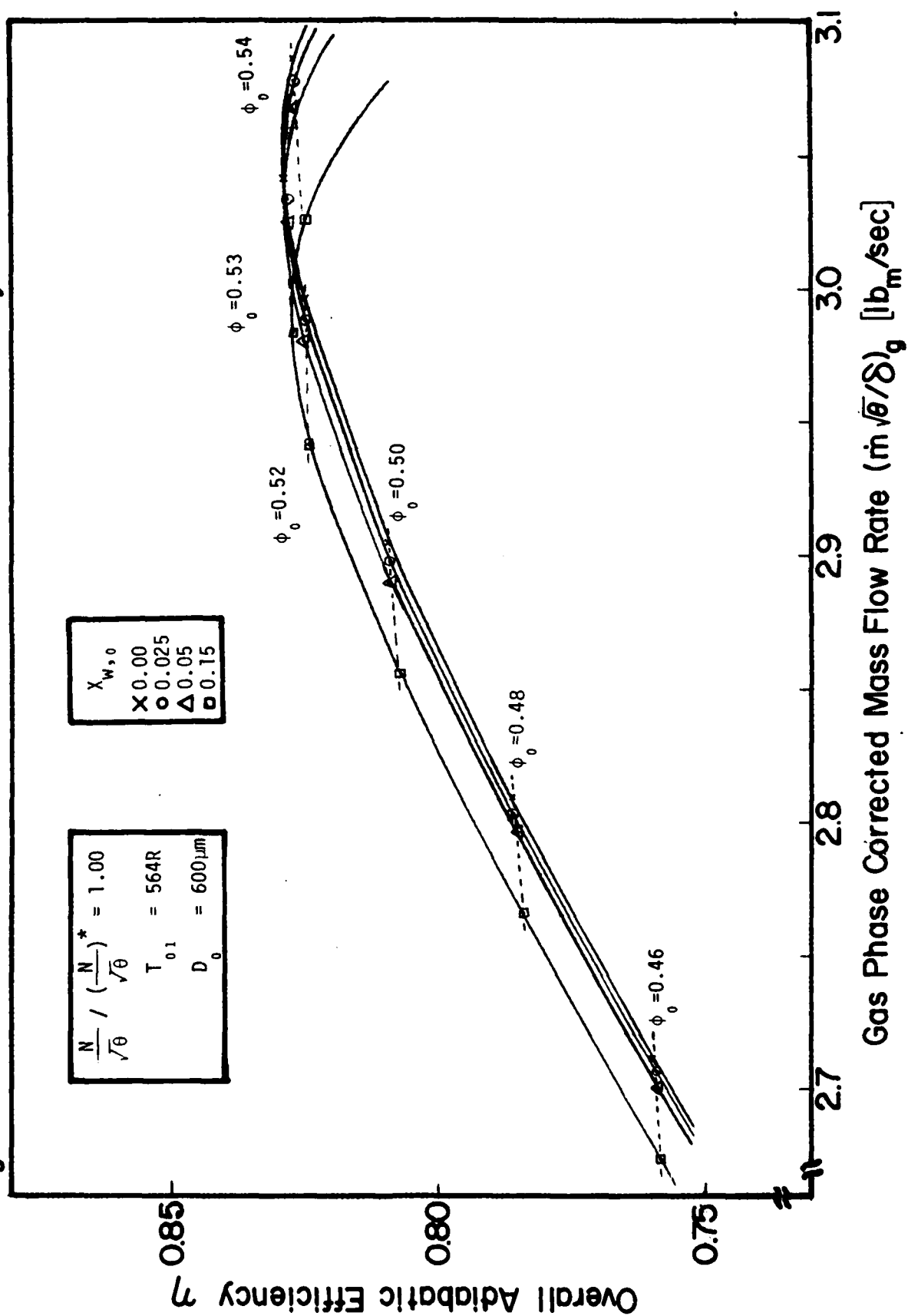


Fig.4.3.17 Effect of Water Content on Overall Adiabatic Efficiency



AD-A114 831

PURDUE UNIV LAFAYETTE IN SCHOOL OF MECHANICAL ENGINEERING F/G 21/5
EFFECT OF WATER ON AXIAL FLOW COMPRESSORS. PART II. COMPUTATION--ETC(U)
JUN 81 Y TSUCHIYA, S N MURTHY F33615-7A-C-2401

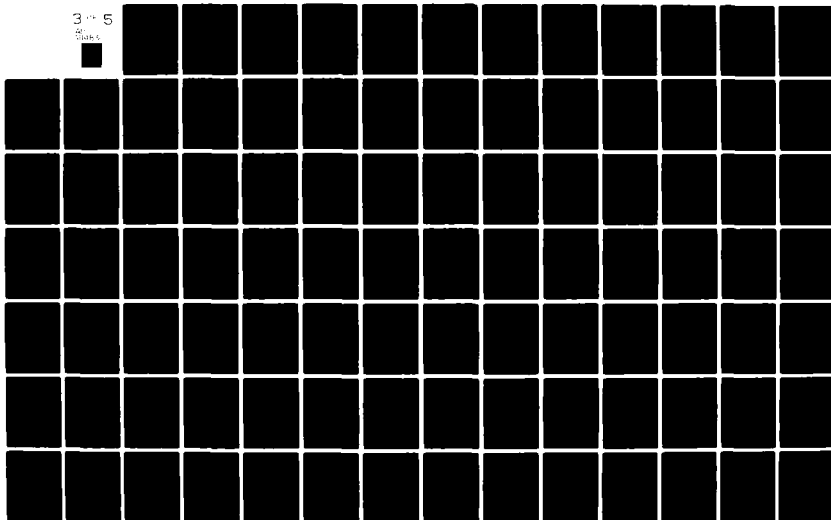
UNCLASSIFIED

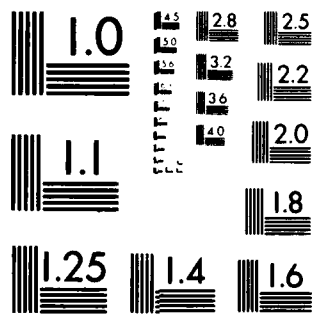
AFWAL-TR-80-2090-PT-2

NL

3 of 5

W. 10/1/81





MICROCOPY RESOLUTION TEST CHART
NATIONAL BUREAU OF STANDARDS 1963-A

Fig. 4.3.18 Effect of Water Content on Overall Temperature Rise of Gas Phase and Droplet

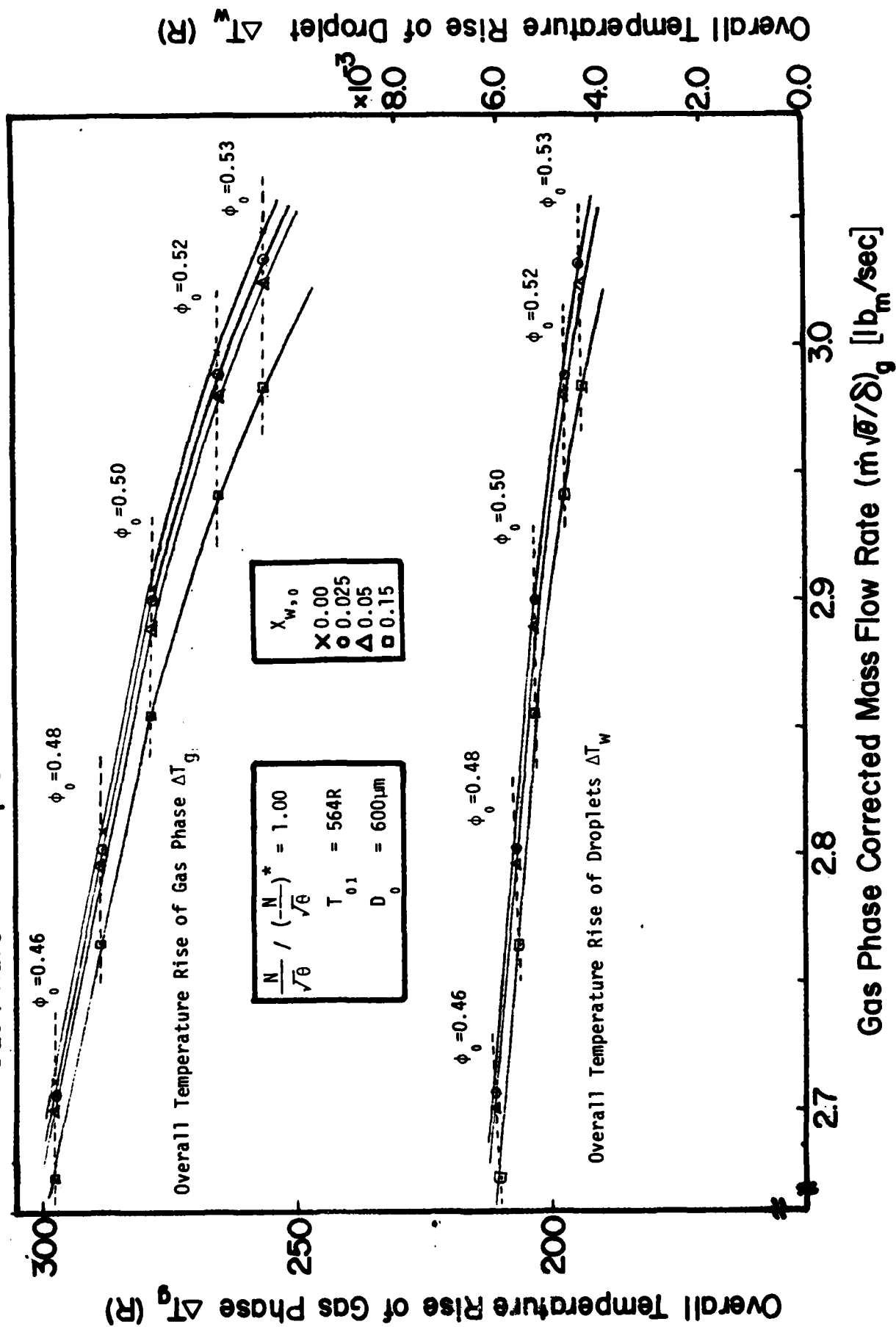


Fig.4.3.19 Temperature Change of Gas Phase and Droplet along Compressor Stages

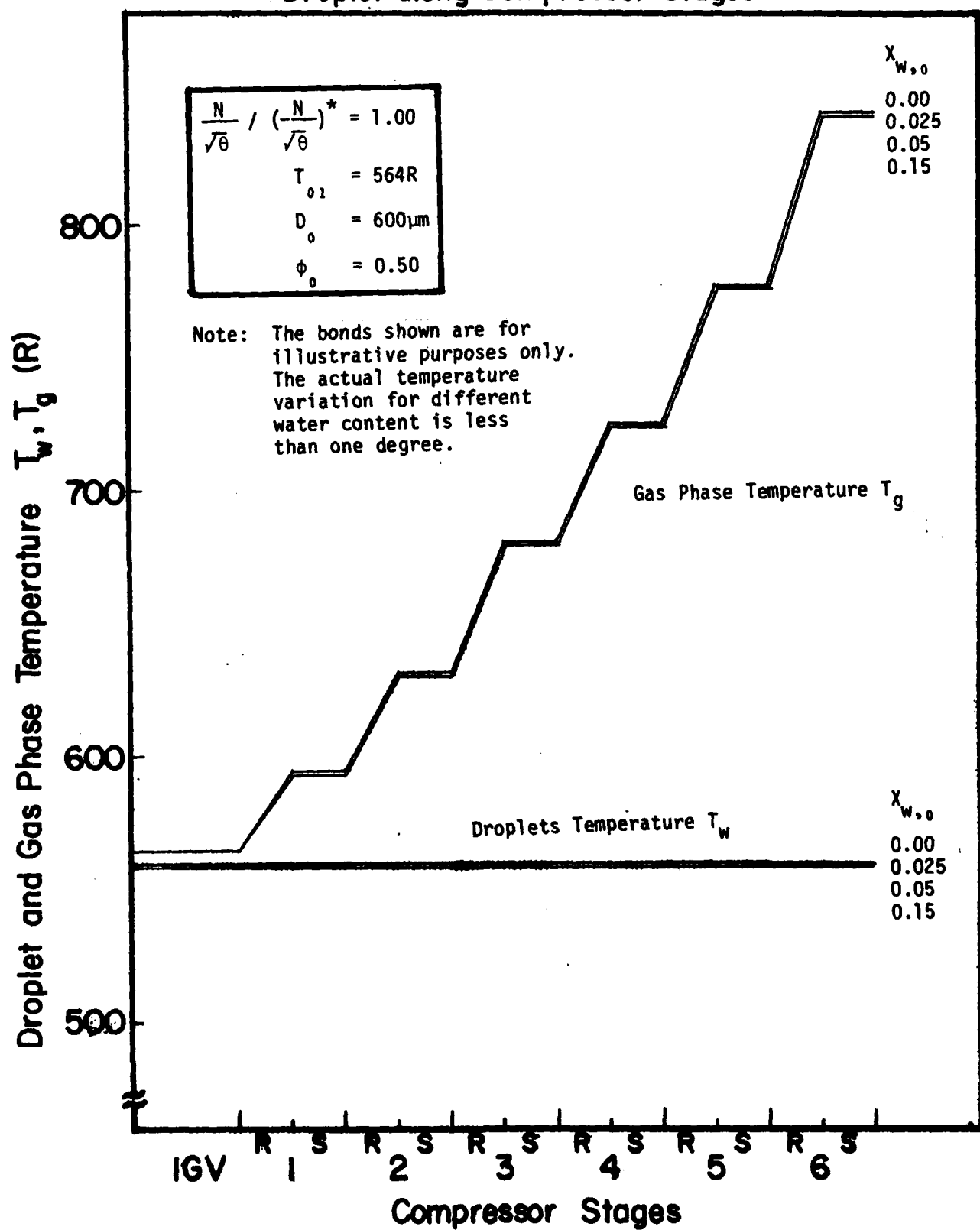


Fig.4.3.20 Change of Water Content at Tip along Compressor Stages

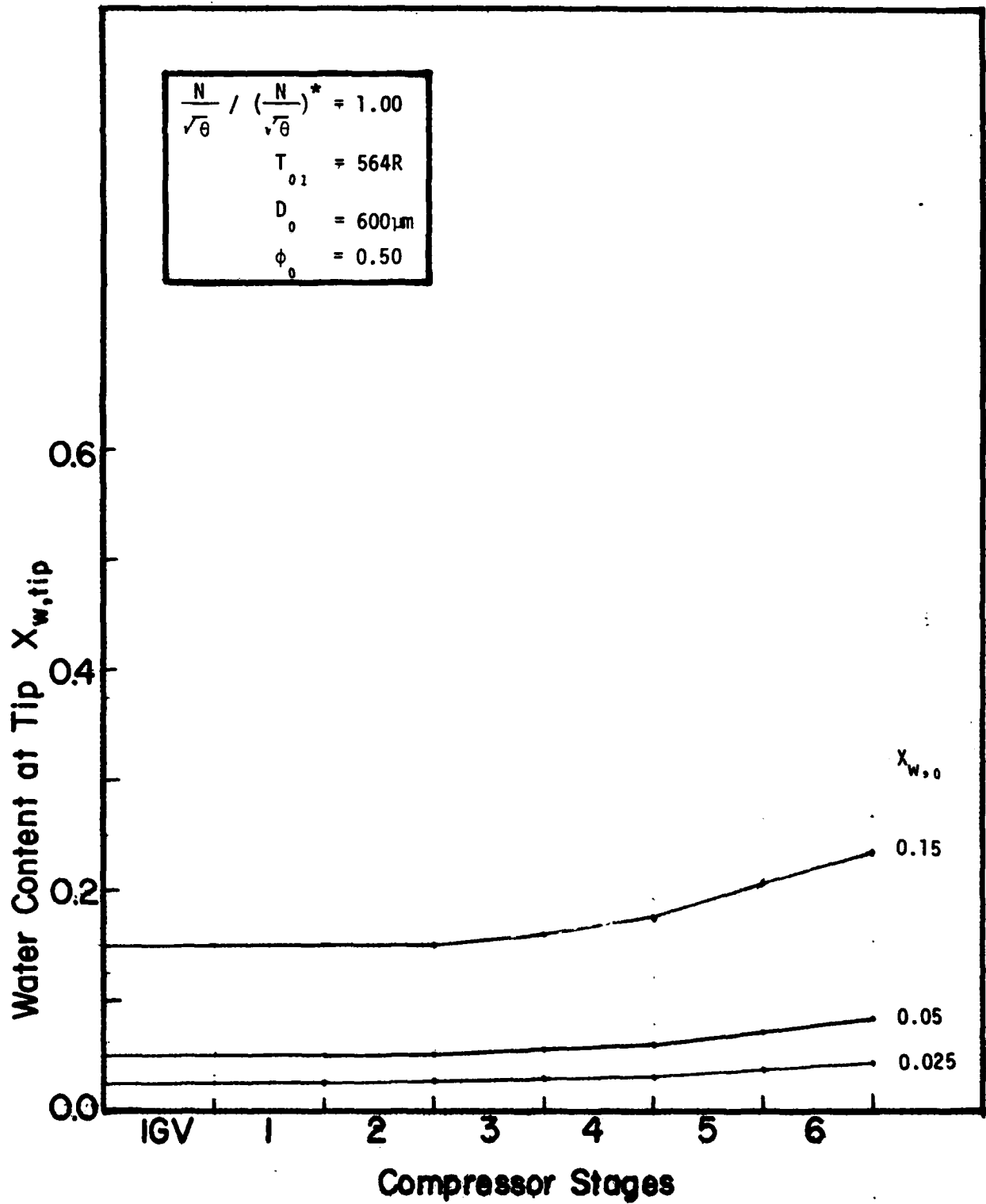


Fig.4.3.21 Effect of Water Content on Overall Total Pressure Ratio

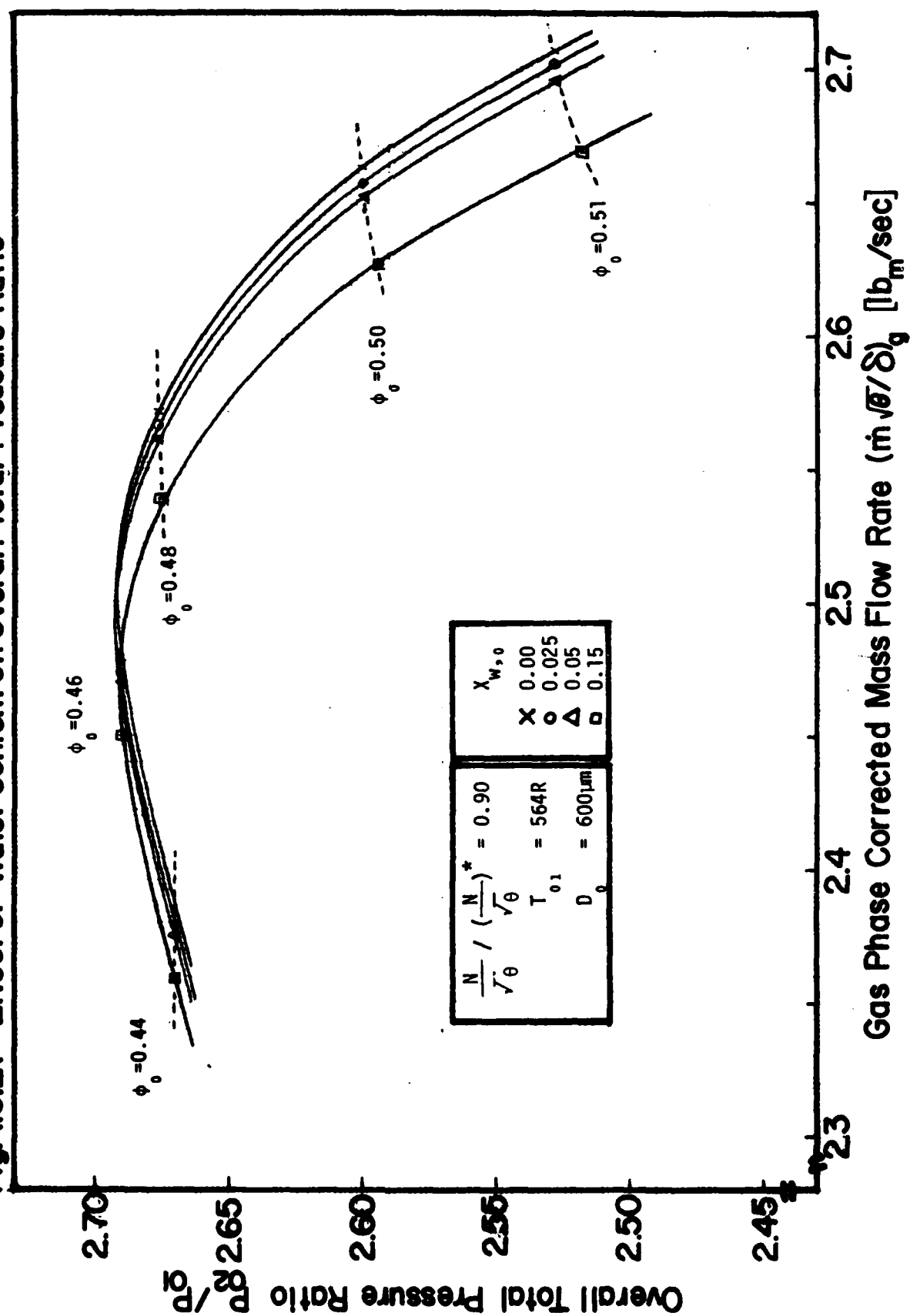


Fig. 4.3.22 Effect of Water Content on Overall Adiabatic Efficiency

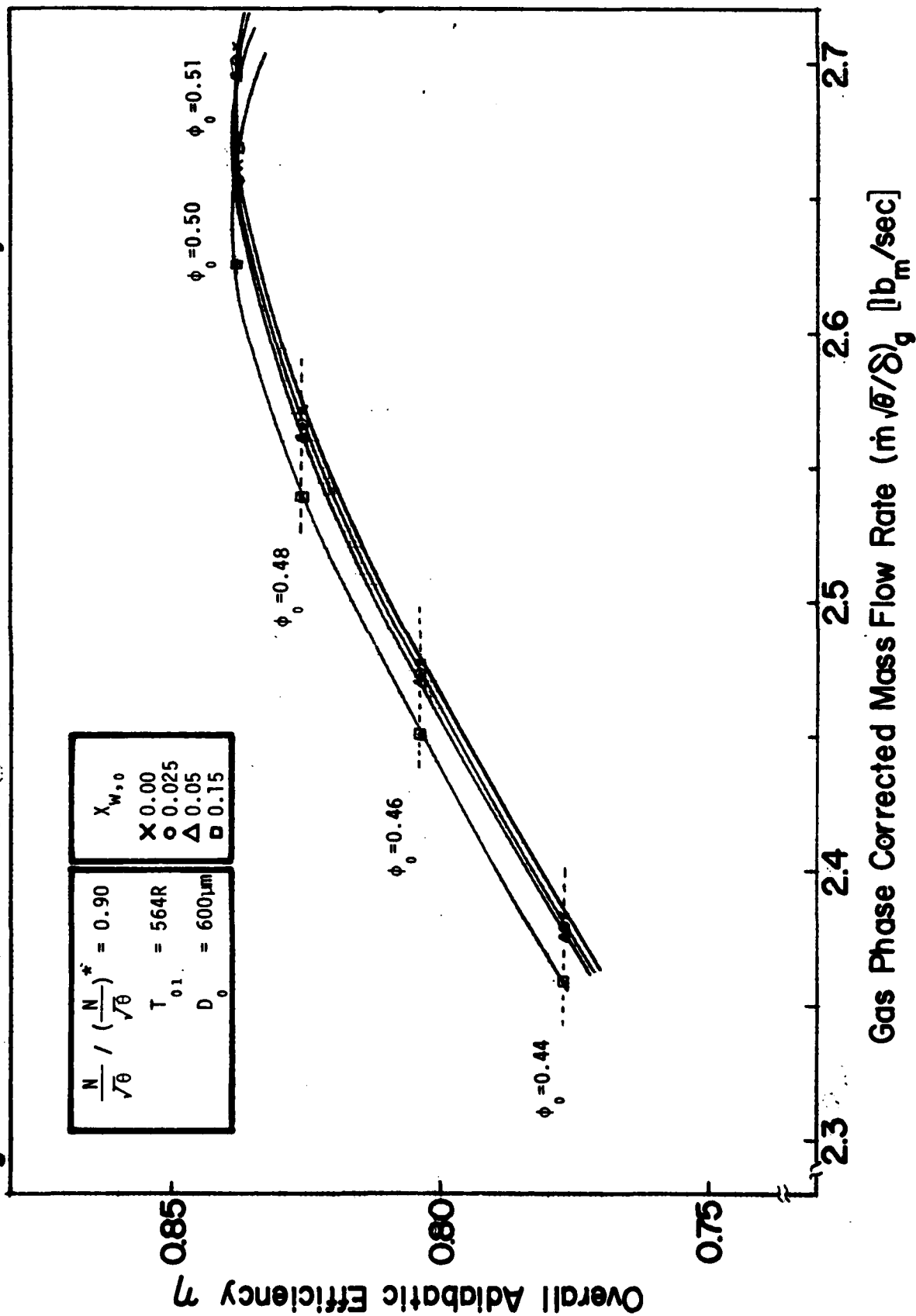


Fig. 4.3.23 Effect of Water Content on Overall Temperature Rise of Gas Phase and Droplet

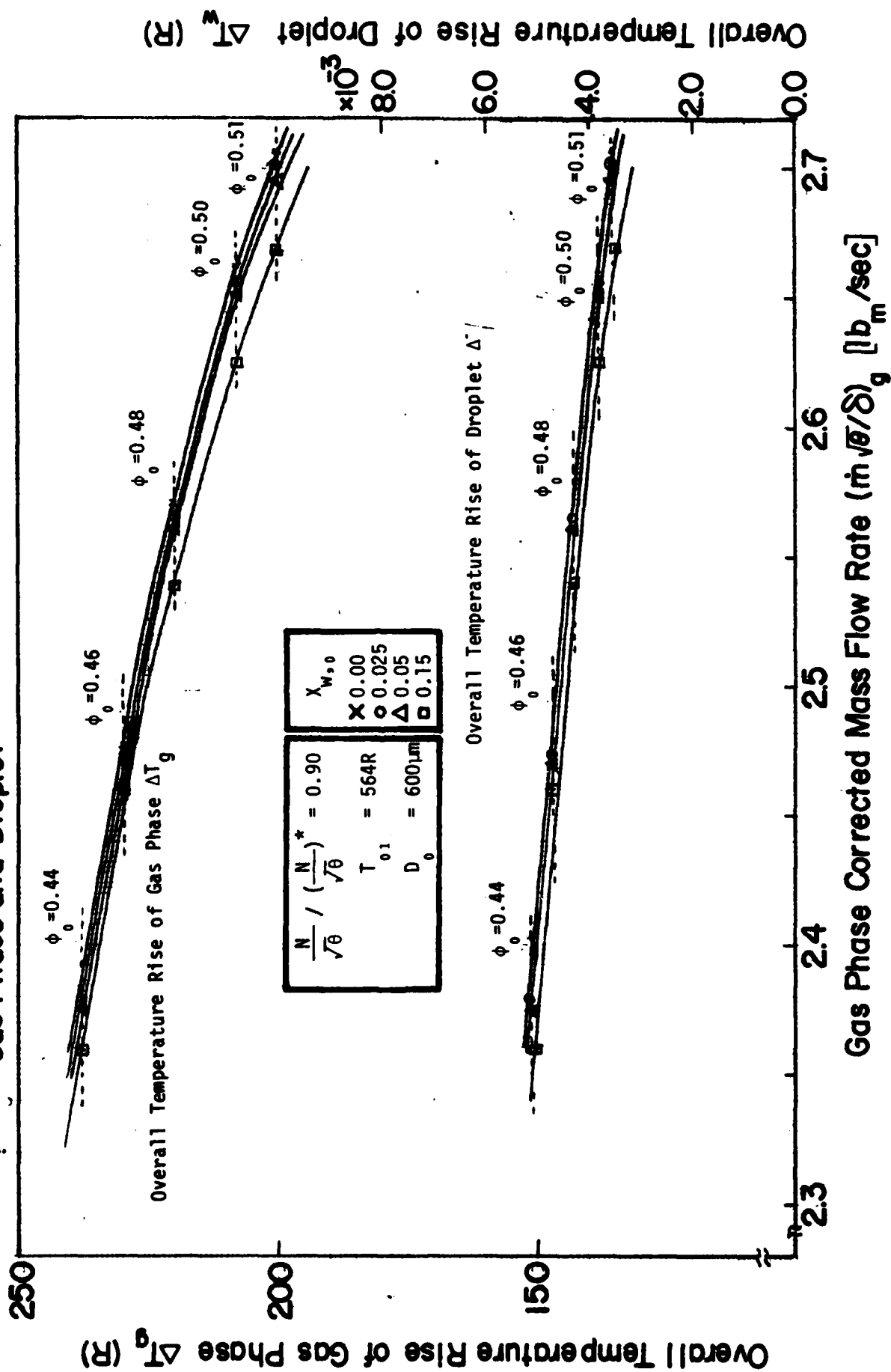


Fig.4.3.24 Temperature Change of Gas Phase and Droplet along Compressor Stages

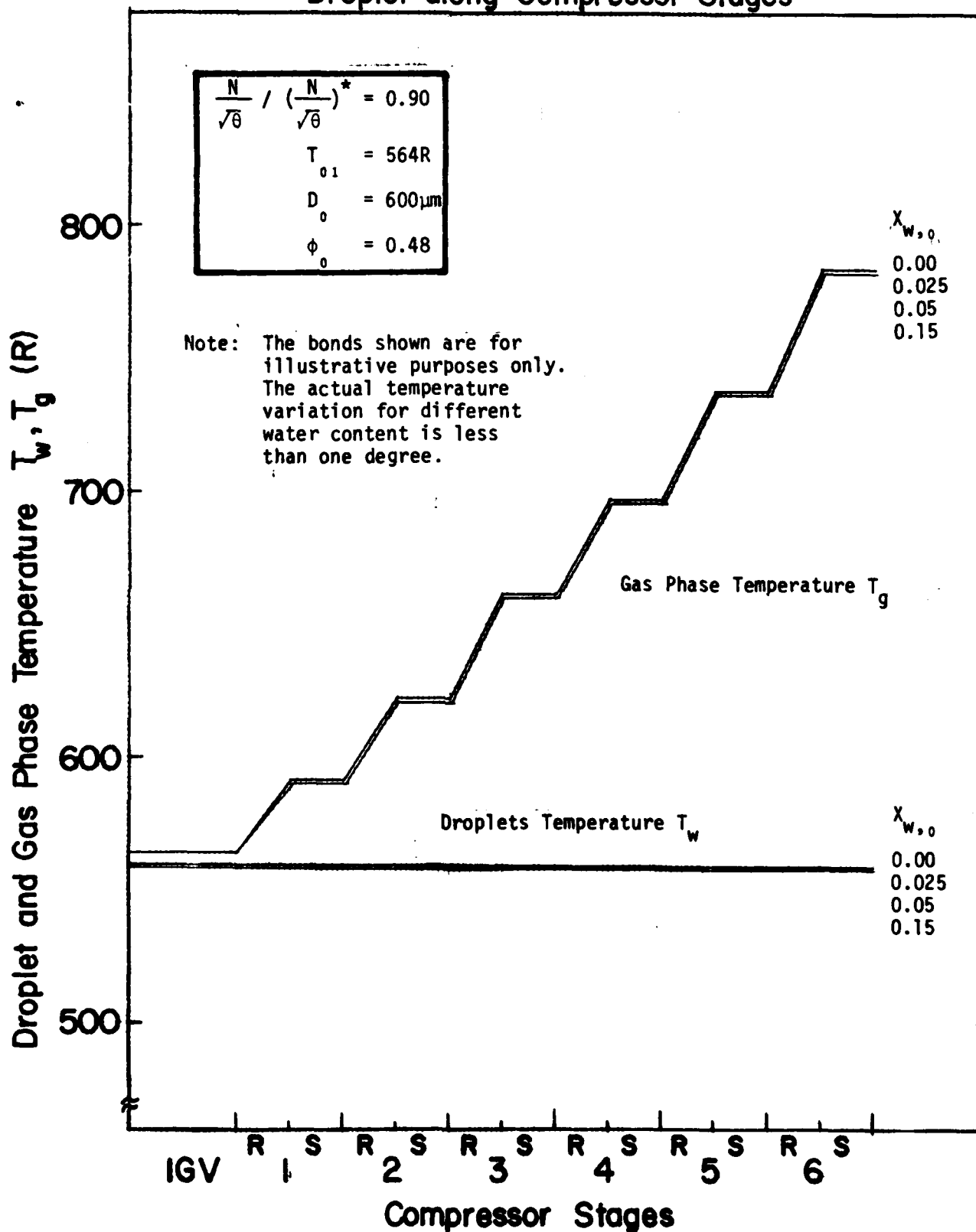


Fig.4.3.25 Change of Water Content at Tip along Compressor Stages

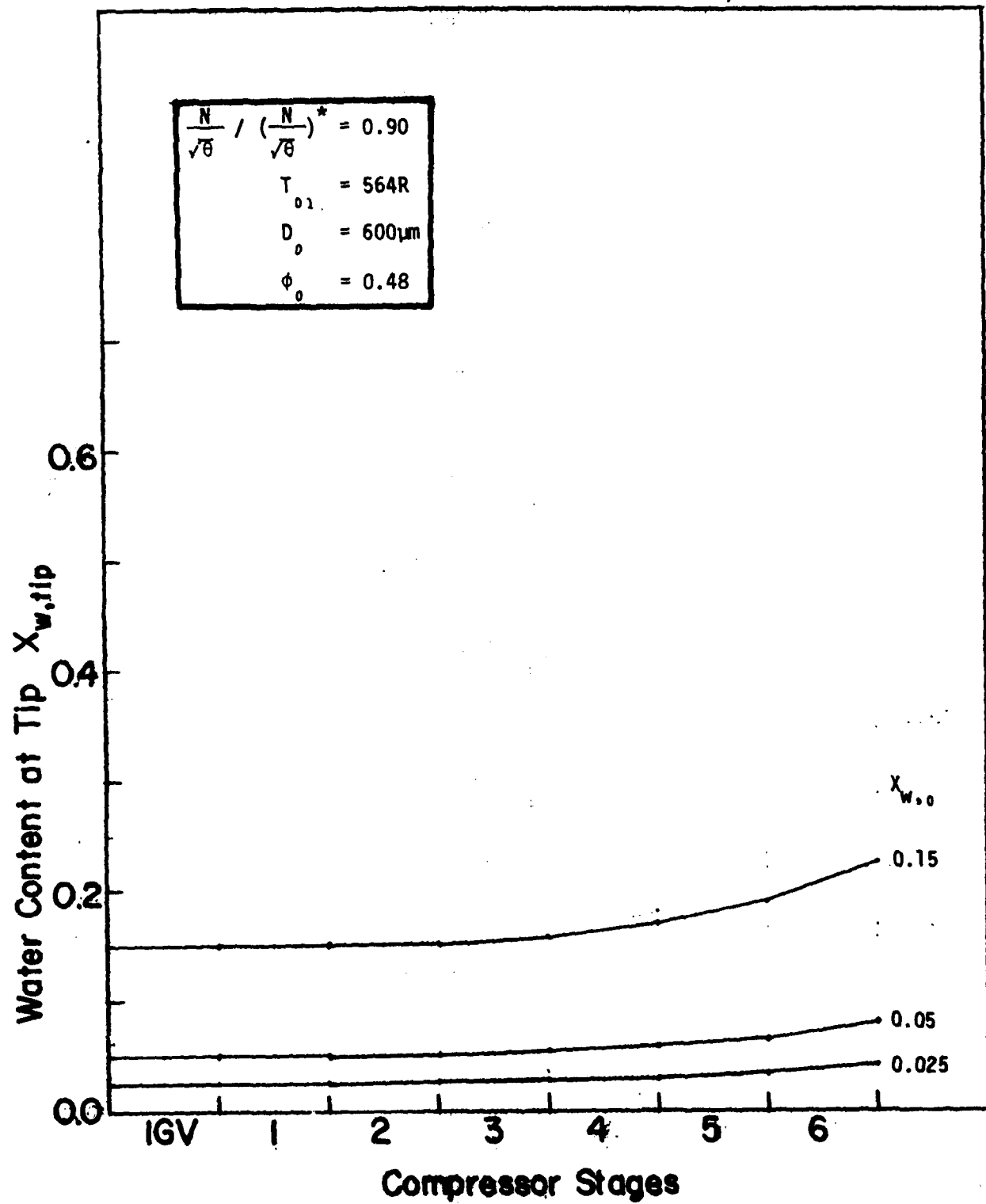


Fig.4.3.26 Effect of Water Content on Overall Total Pressure Ratio

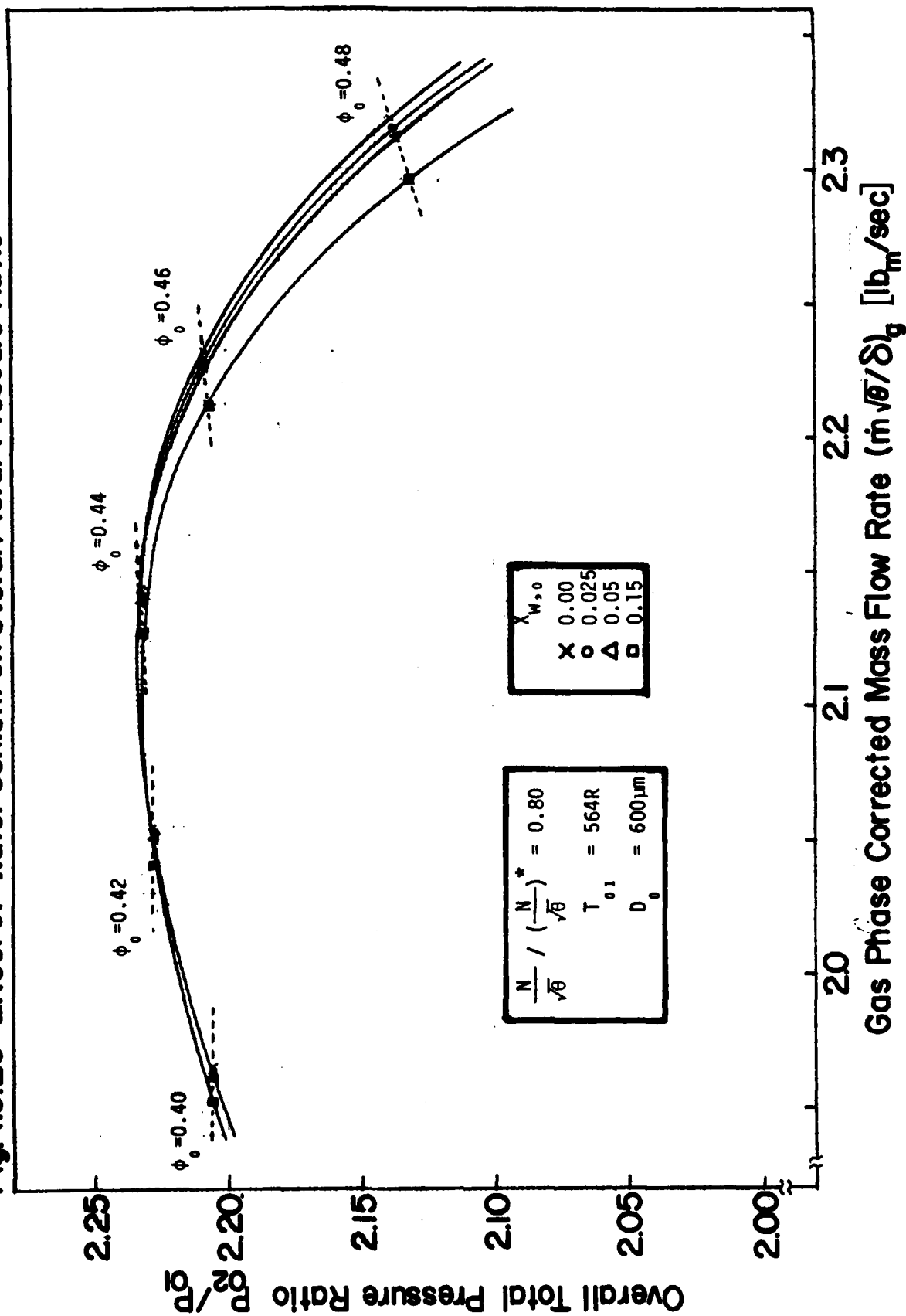


Fig. 4.3.27 Effect of Water Content on Overall Adiabatic Efficiency

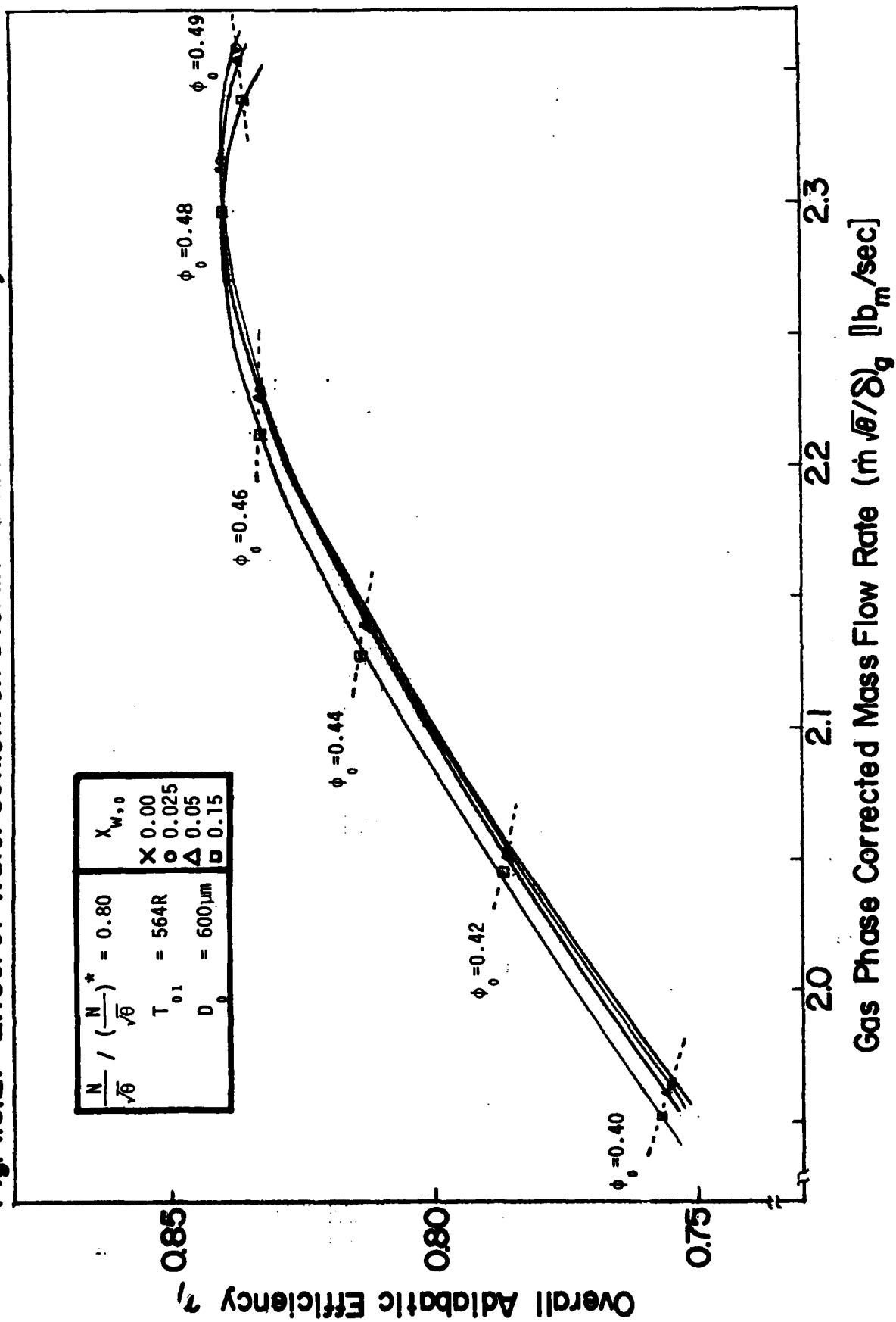


Fig. 4.3.28 Effect of Water Content on Overall Temperature Rise of Gas Phase and Droplet

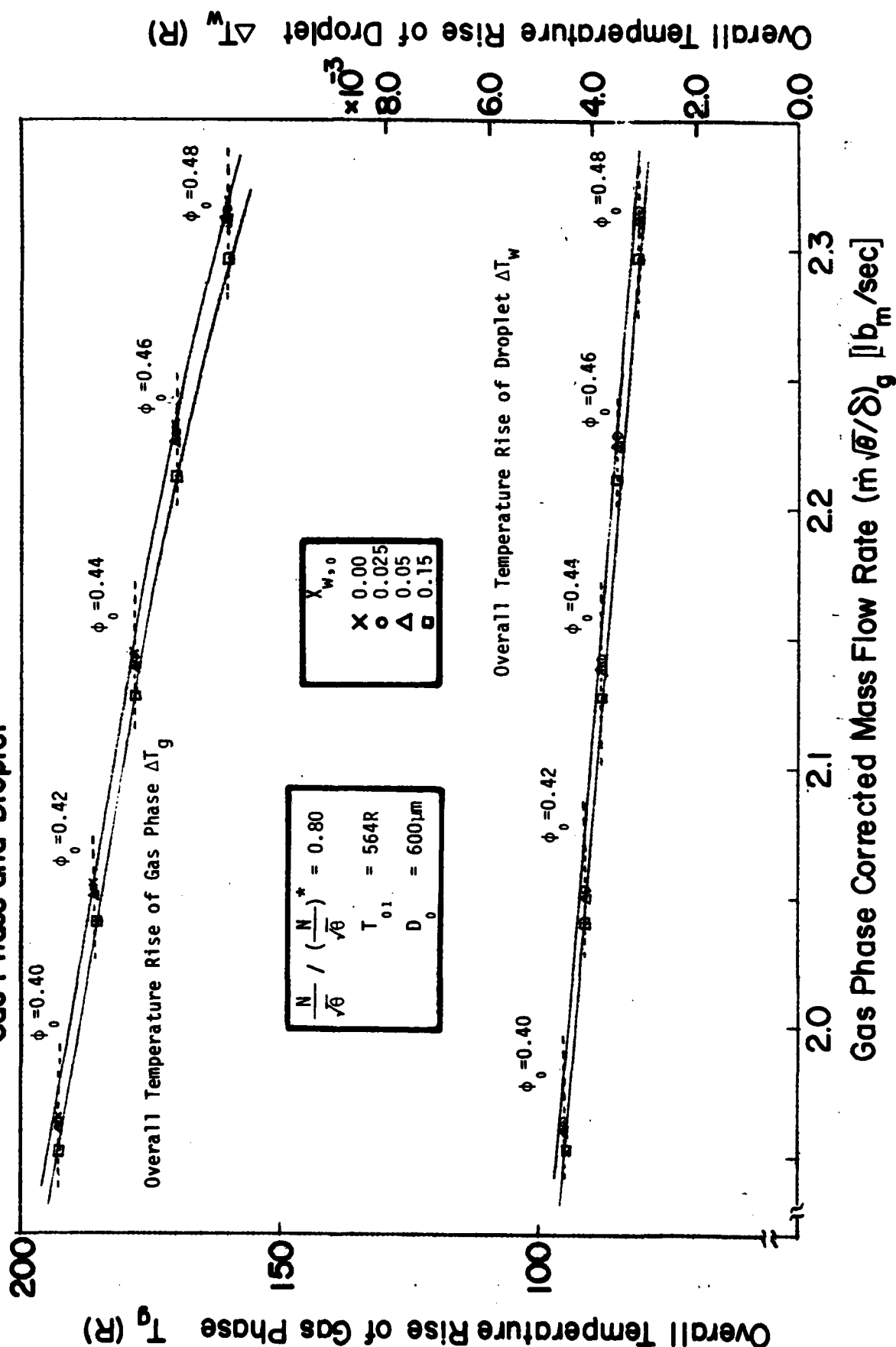


Fig.4.3.29 Temperature Change of Gas Phase and Droplet along Compressor Stages

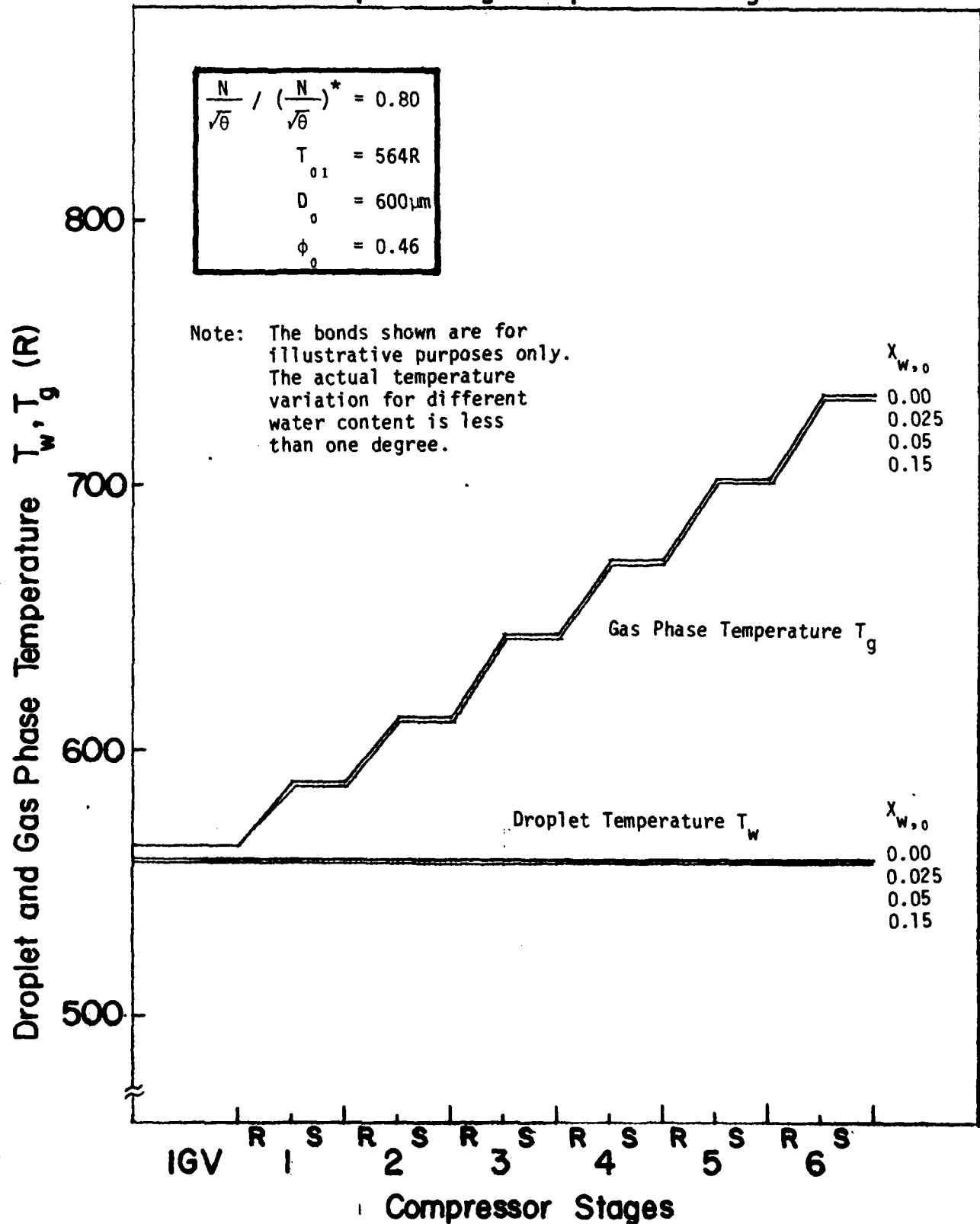


Fig.4.3.30 Change of Water Content at Tip along Compressor Stages

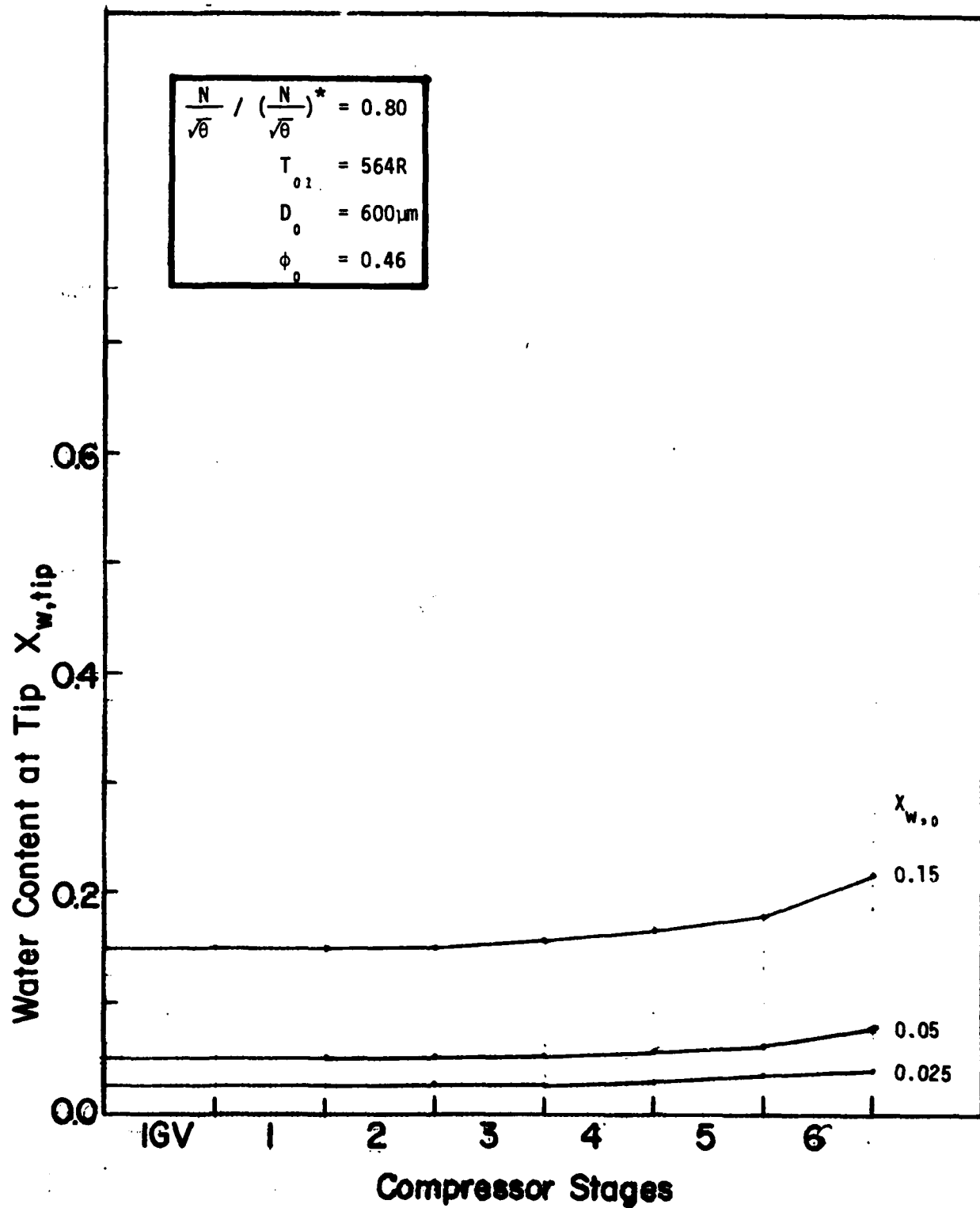


Fig.4.4.1 Effect of Location of Evaporation on Overall Total Pressure Ratio

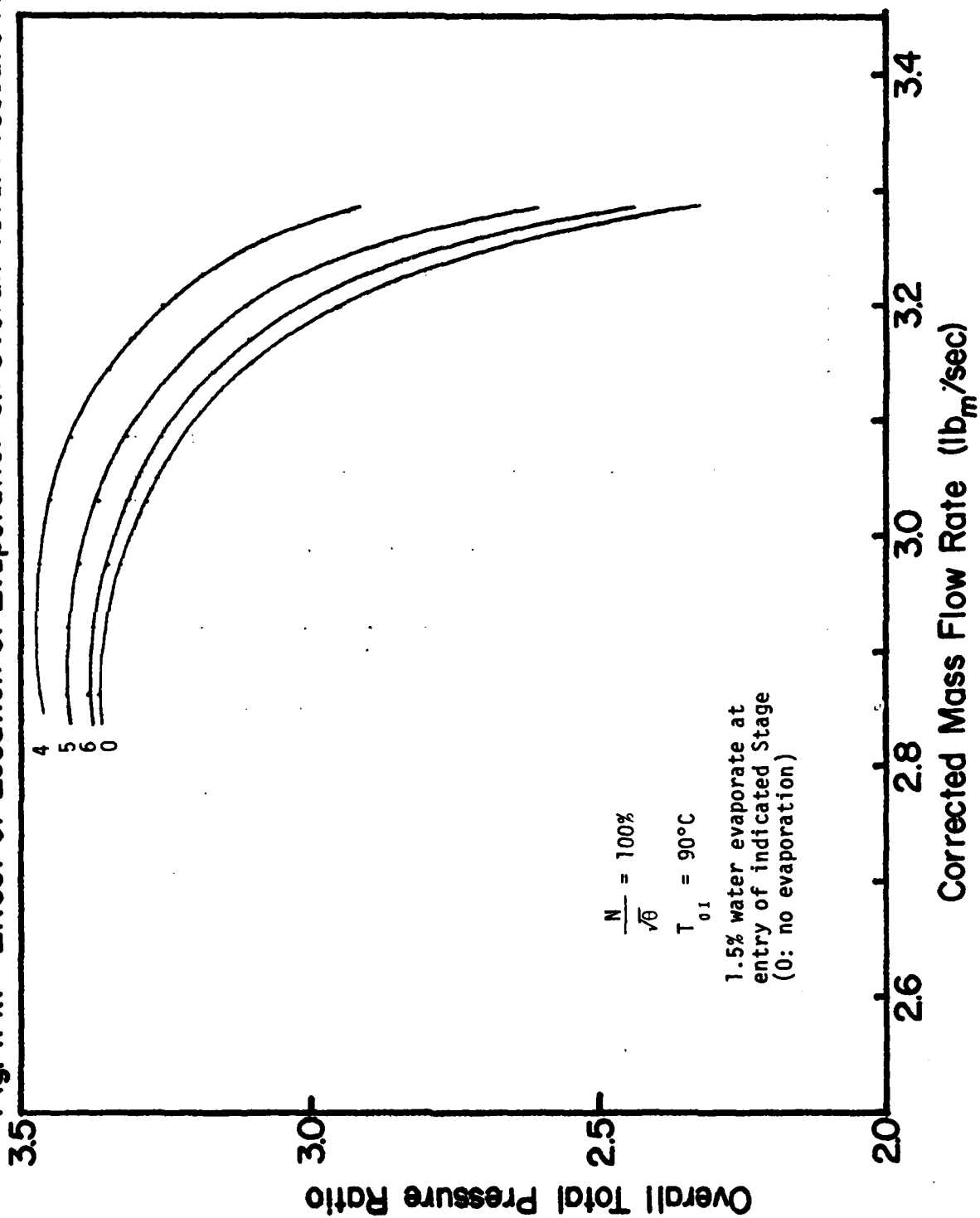


Fig.4.4.2 Effect of Location of Evaporation on Overall Adiabatic Efficiency

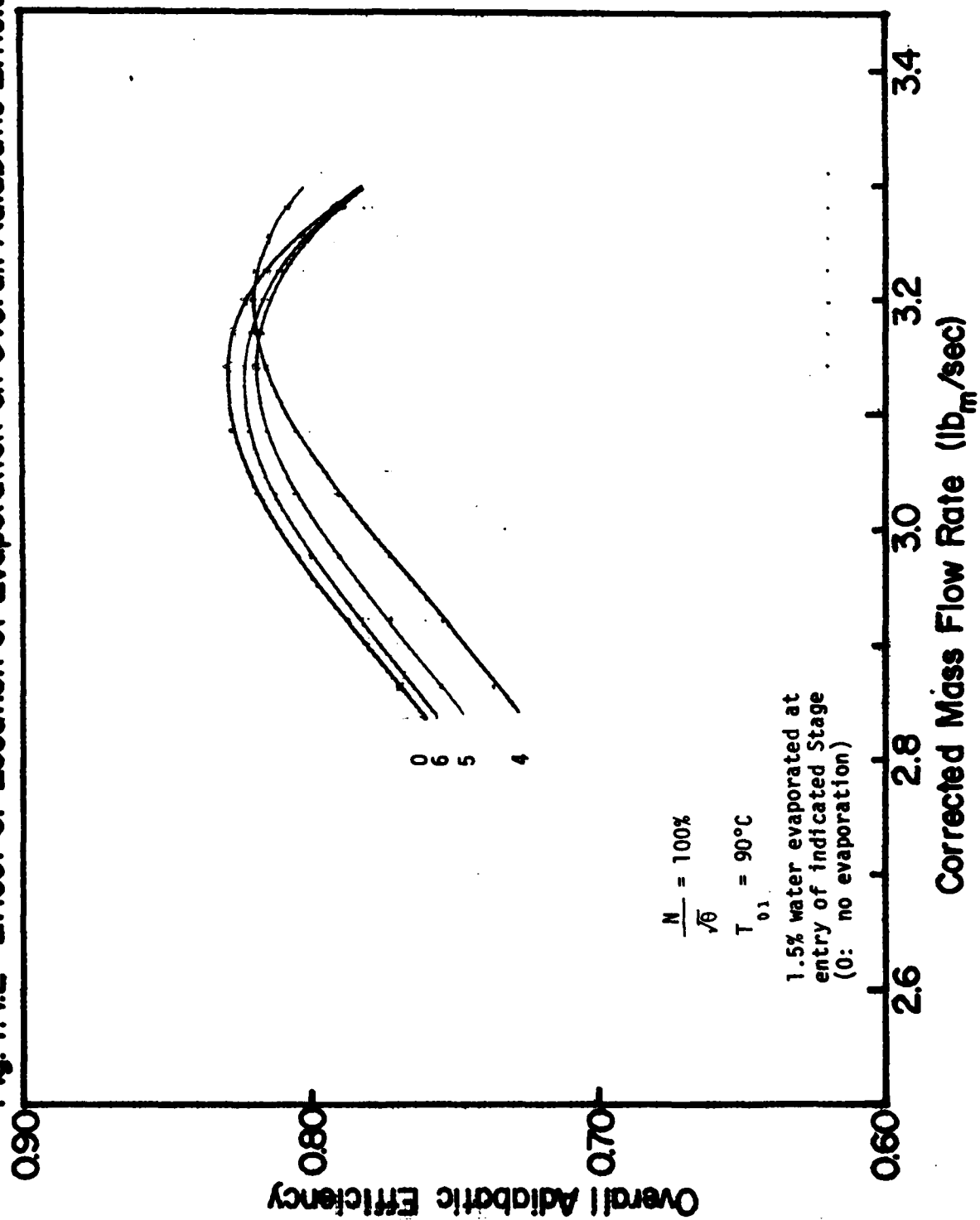


Fig.4.4.3 Effect of Location of Evaporation on Stage Total Pressure Ratio

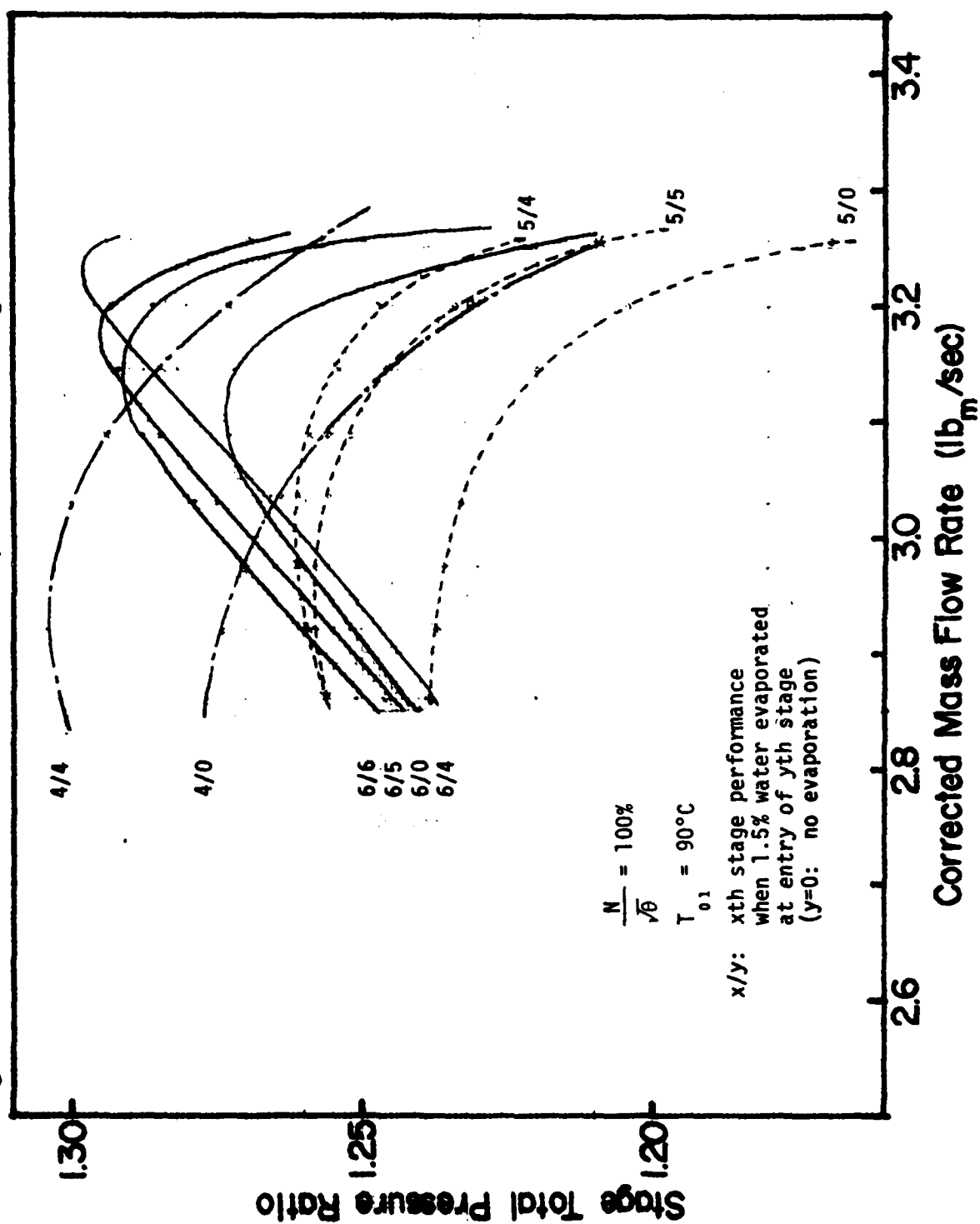


Fig.4.4.4 Effect of Location of Evaporation on Temperature Change along Compressor Stages

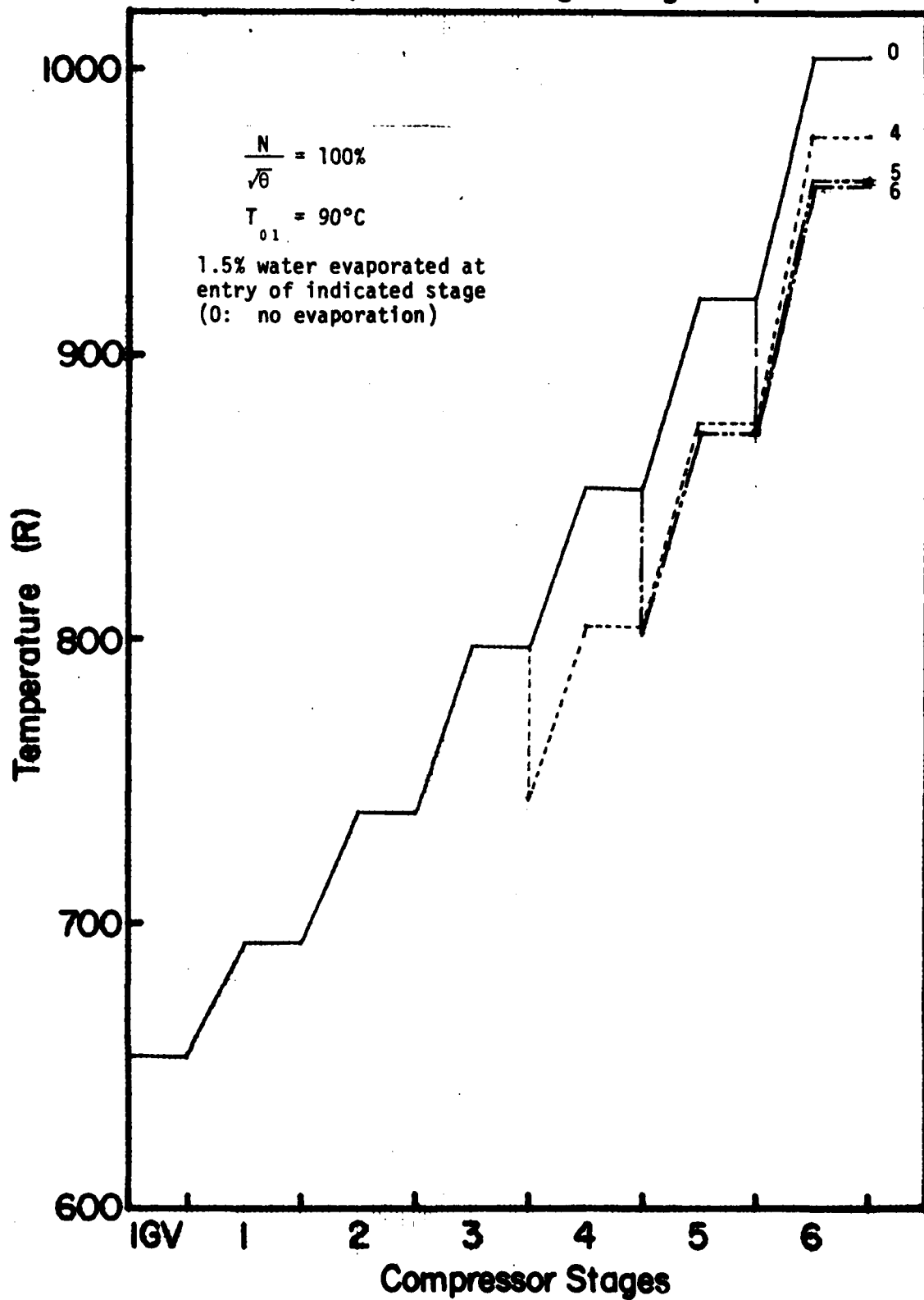


Fig. 4.4.5 Effect of Location of Evaporation on Overall Total Pressure Ratio

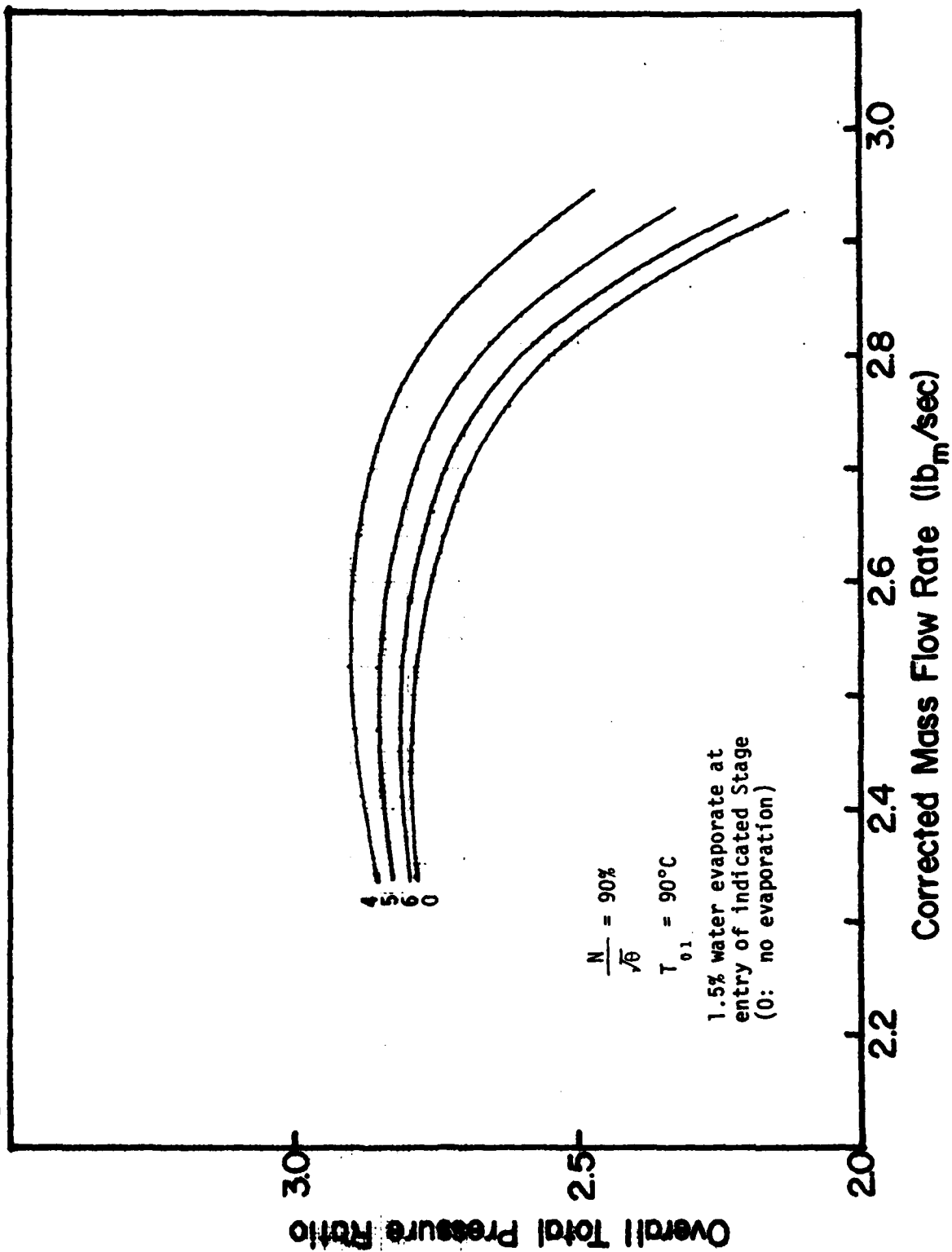


Fig.4.4.6 Effect of Location of Evaporation on Overall Adiabatic Efficiency

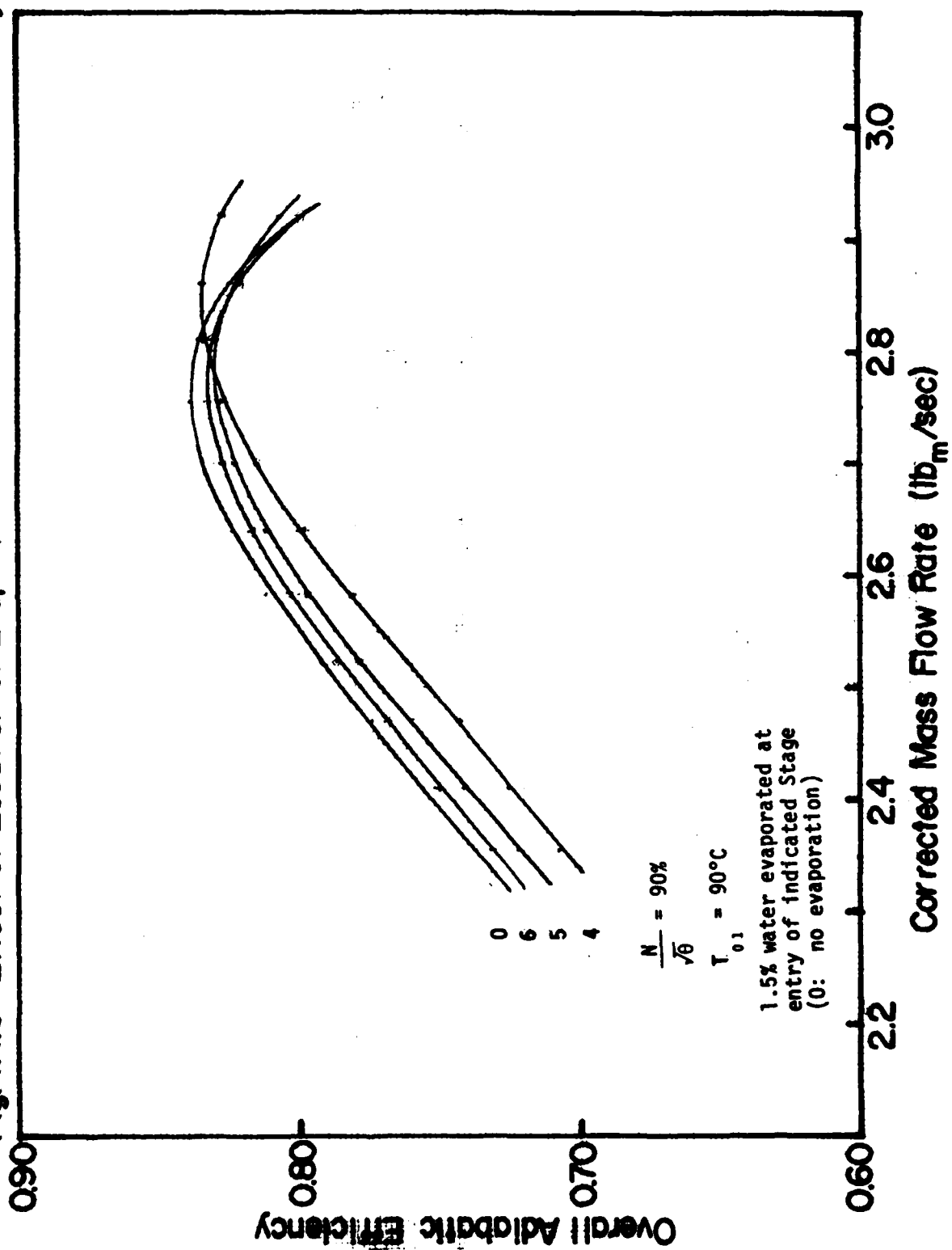


Fig.4.4.7 Effect of Location of Evaporation on Stage Total Pressure Ratio

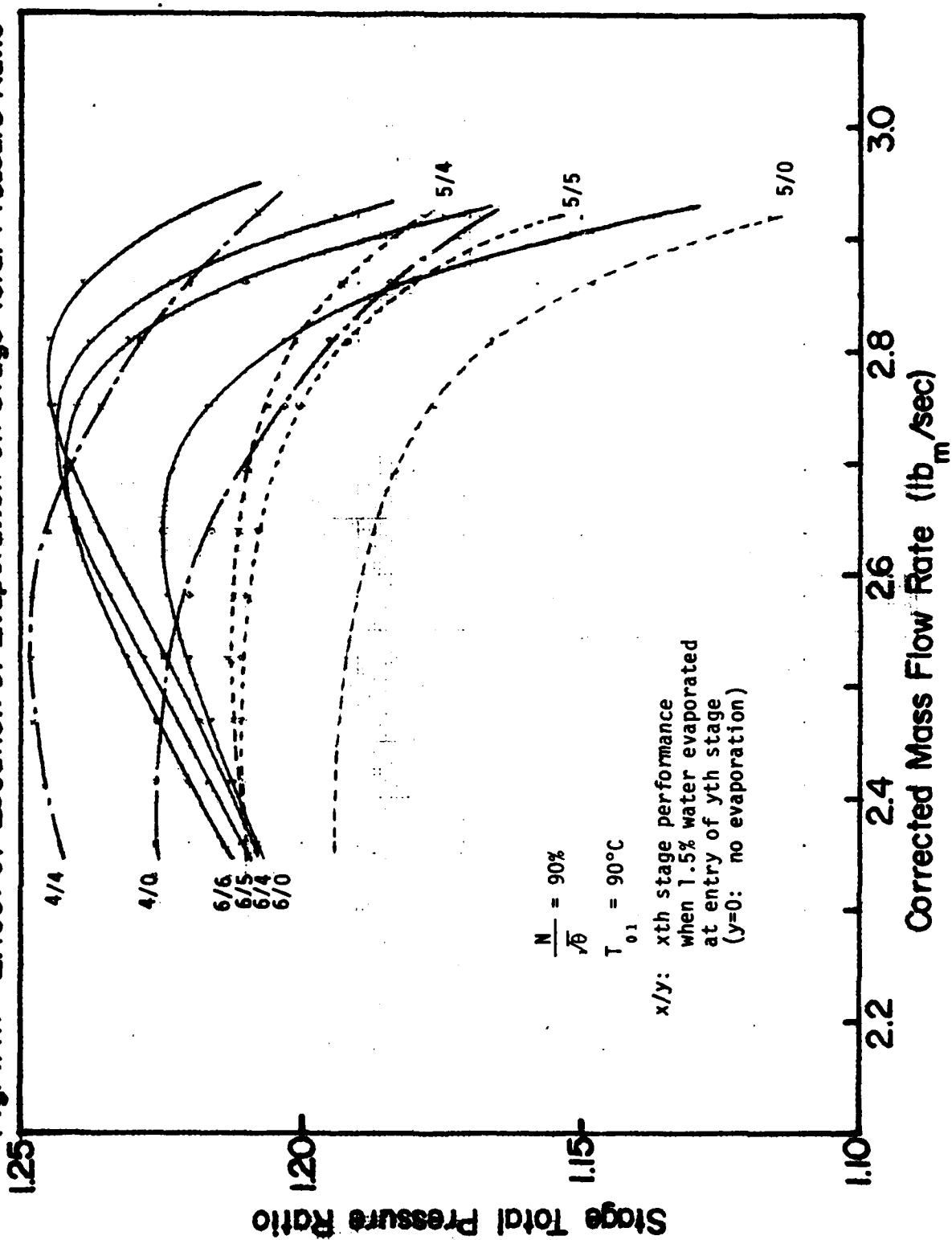


Fig.4.4.8 Effect of Location of Evaporation on Temperature Change along Compressor Stages

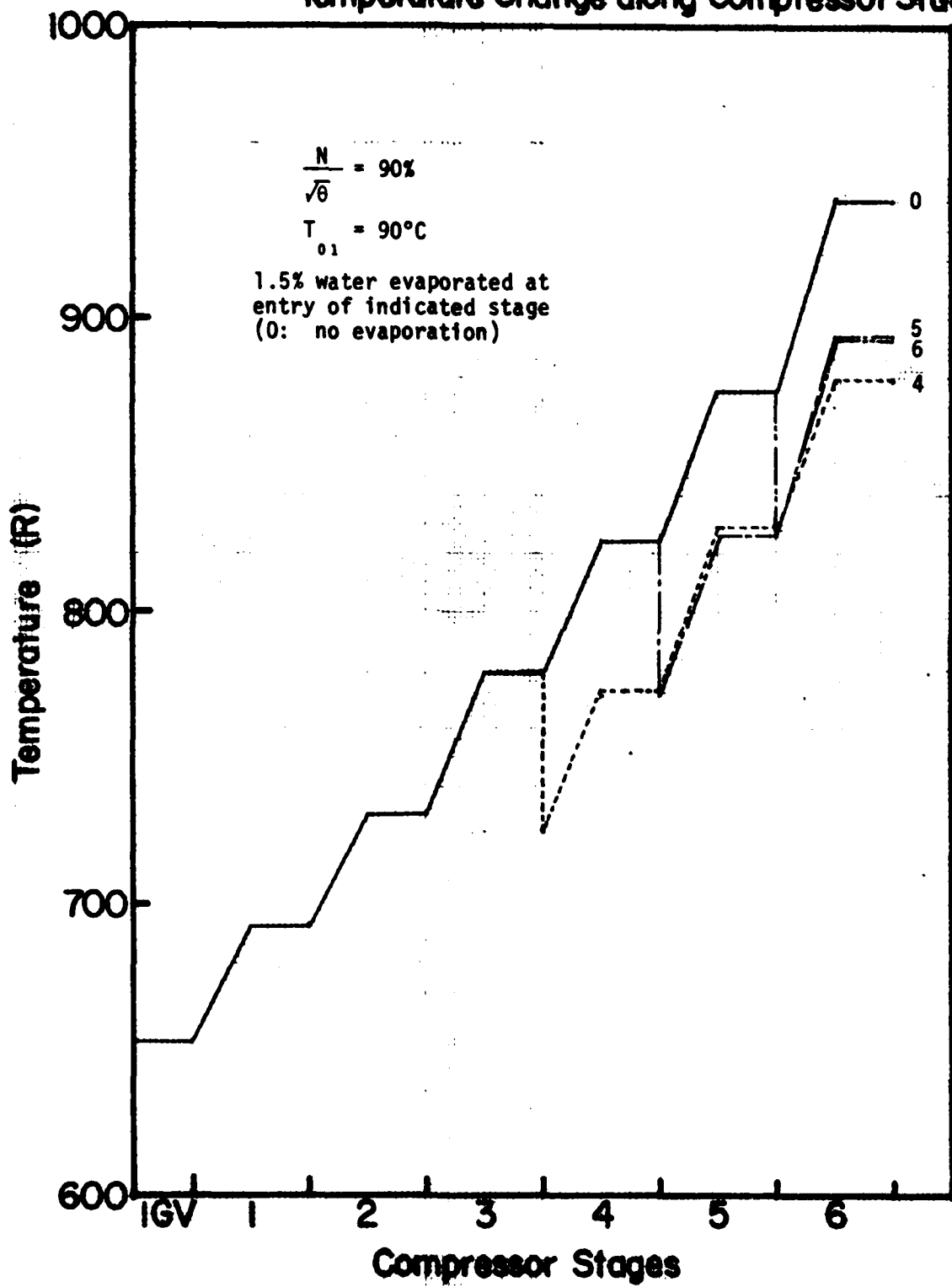


Fig.4.4.9 Effect of Location of Evaporation on Overall Total Pressure Ratio

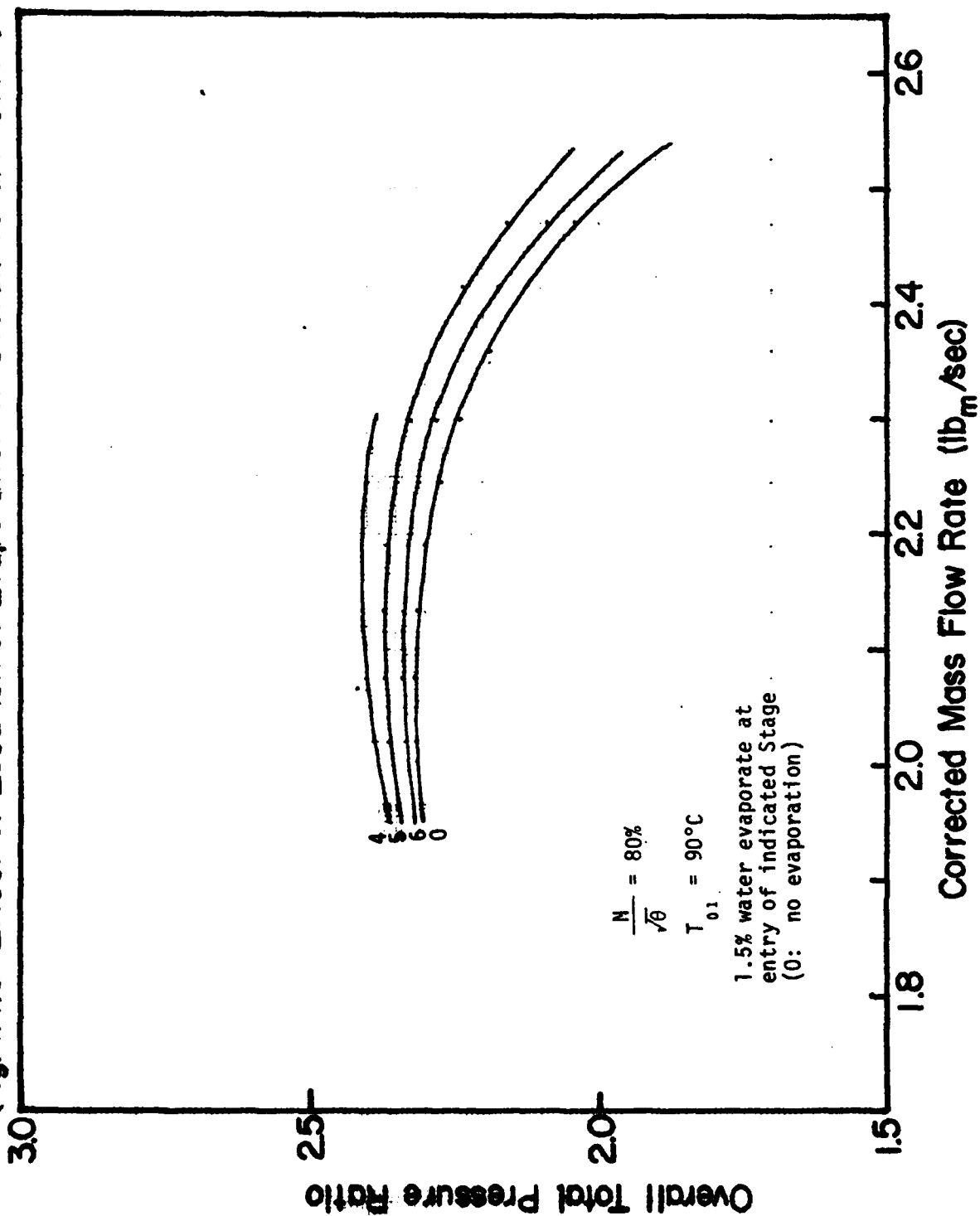


Fig. 4.4.10 Effect of Location of Evaporation on Overall Adiabatic Efficiency

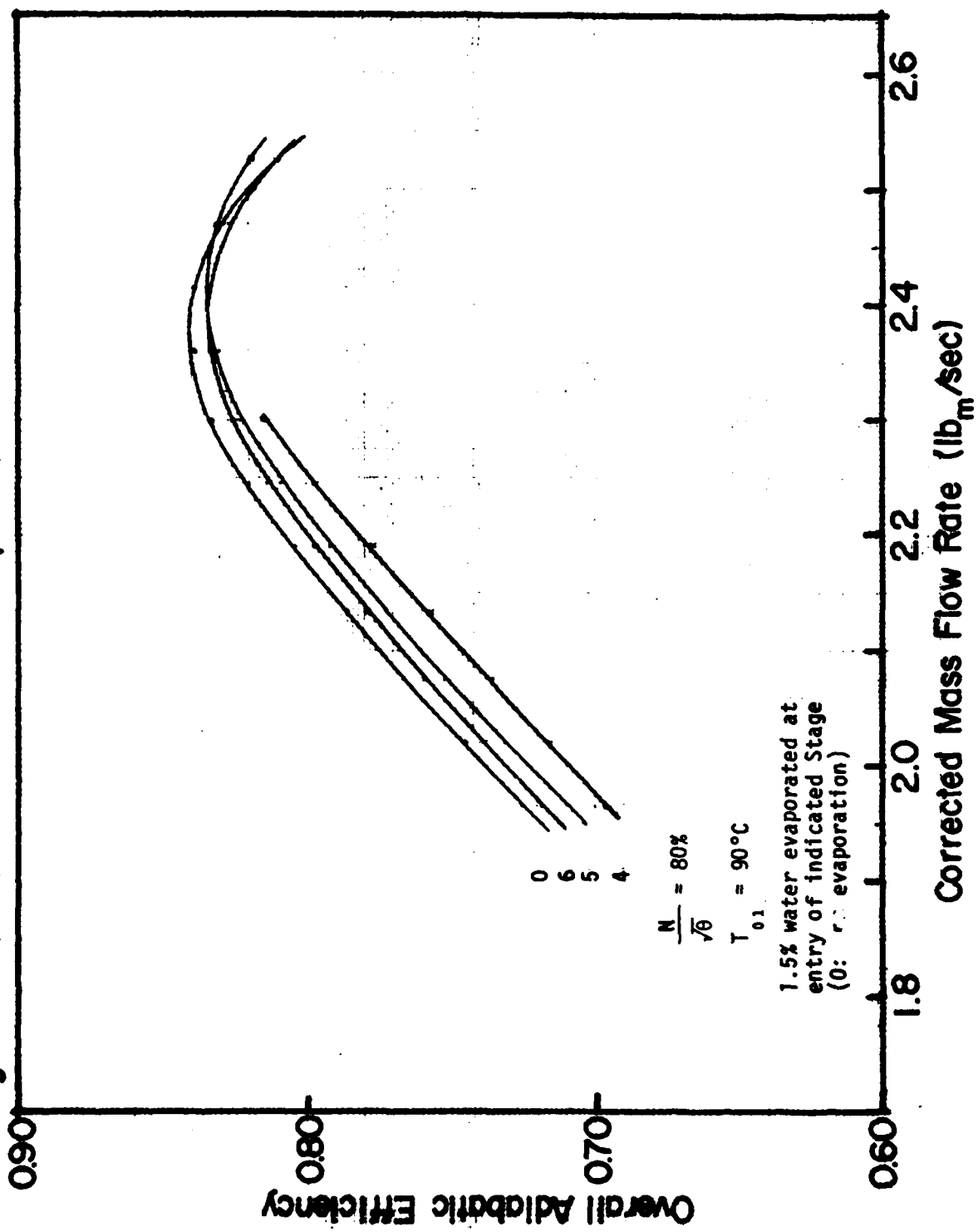


Fig.4.4.11 Effect of Location of Evaporation on Stage Total Pressure Ratio

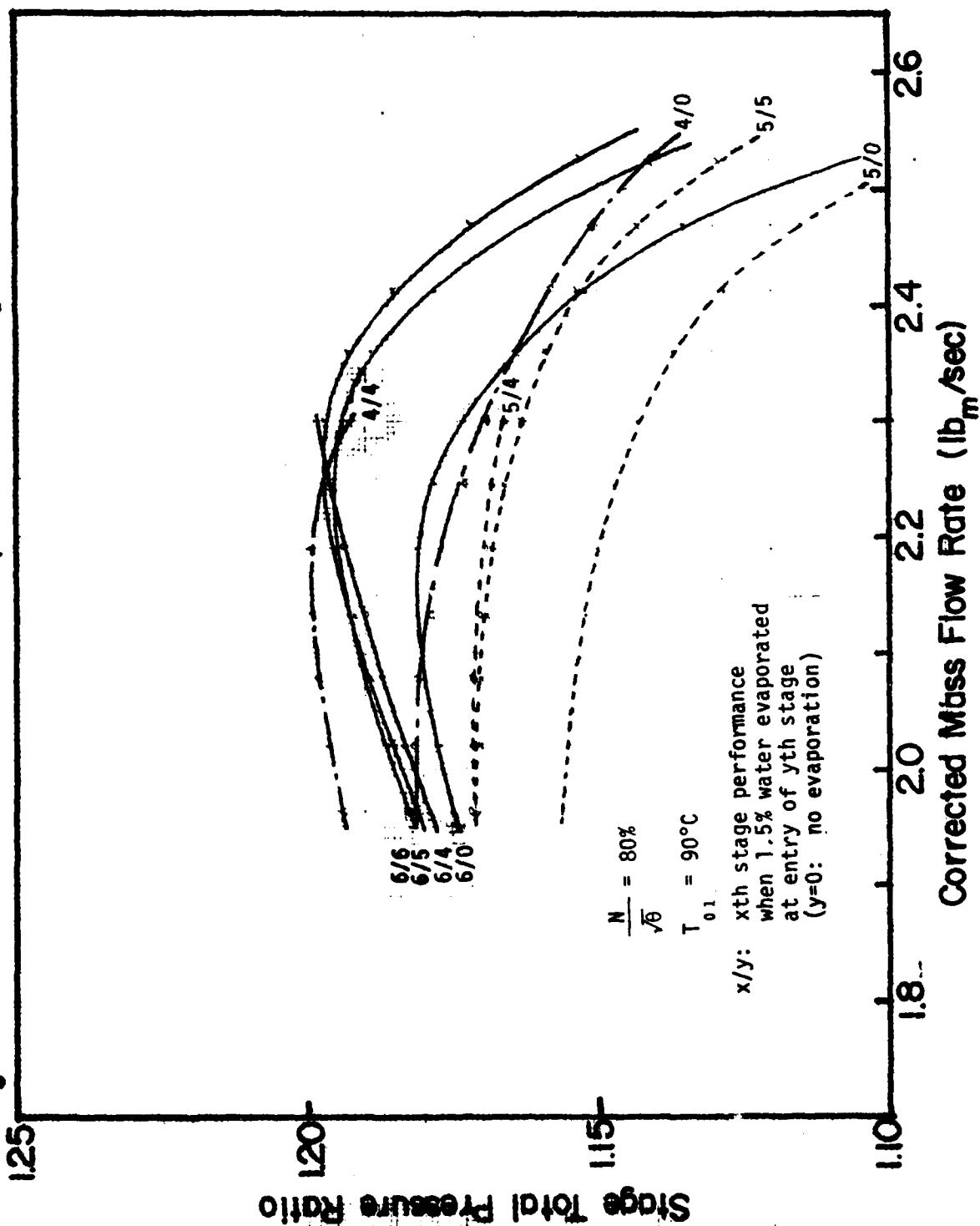


Fig.4.4.12 Effect of Location of Evaporation on Temperature Change along Compressor Stages

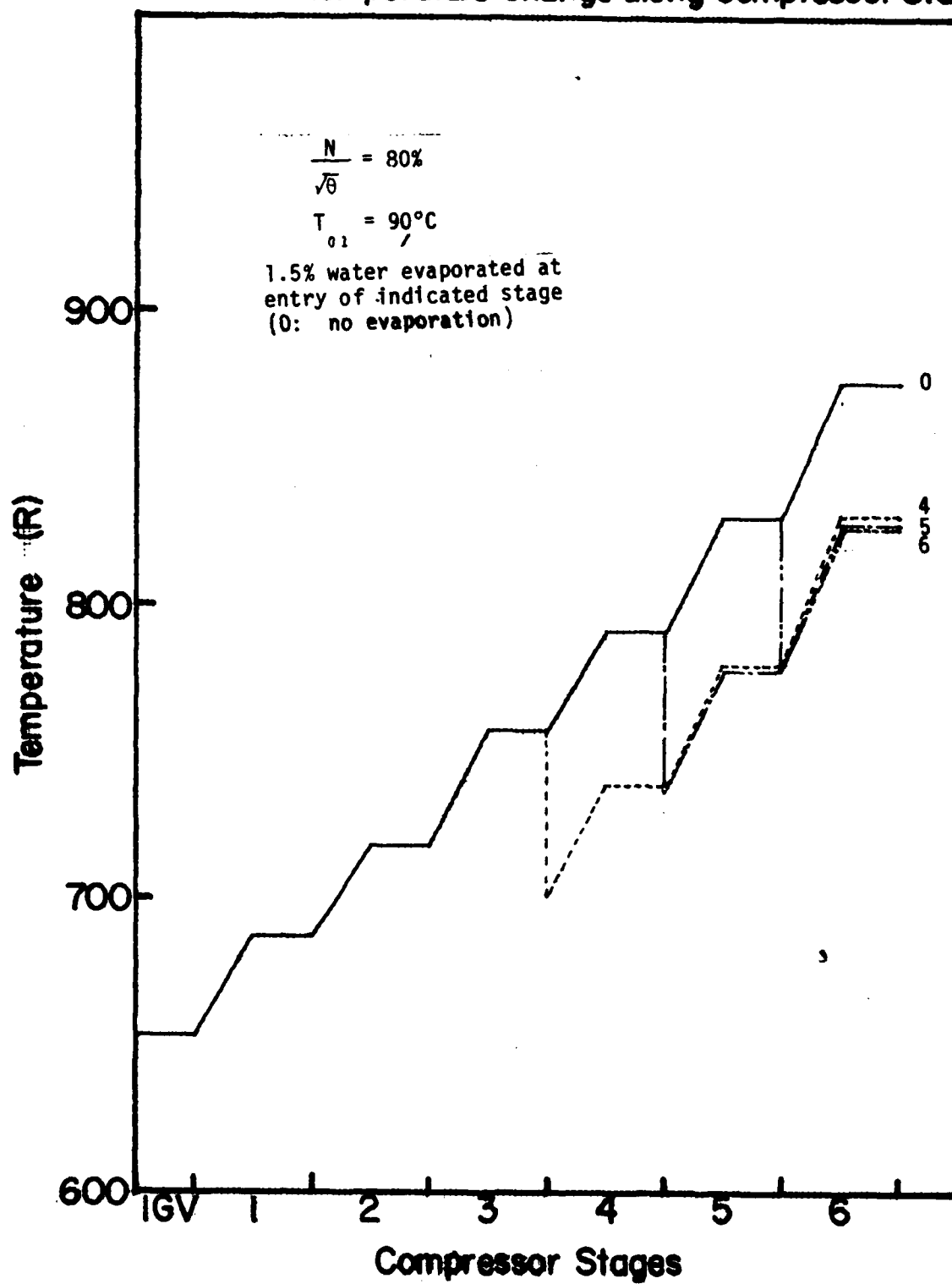


Fig.4.4.13 Effect of Location of Evaporation on Overall Total Pressure Ratio

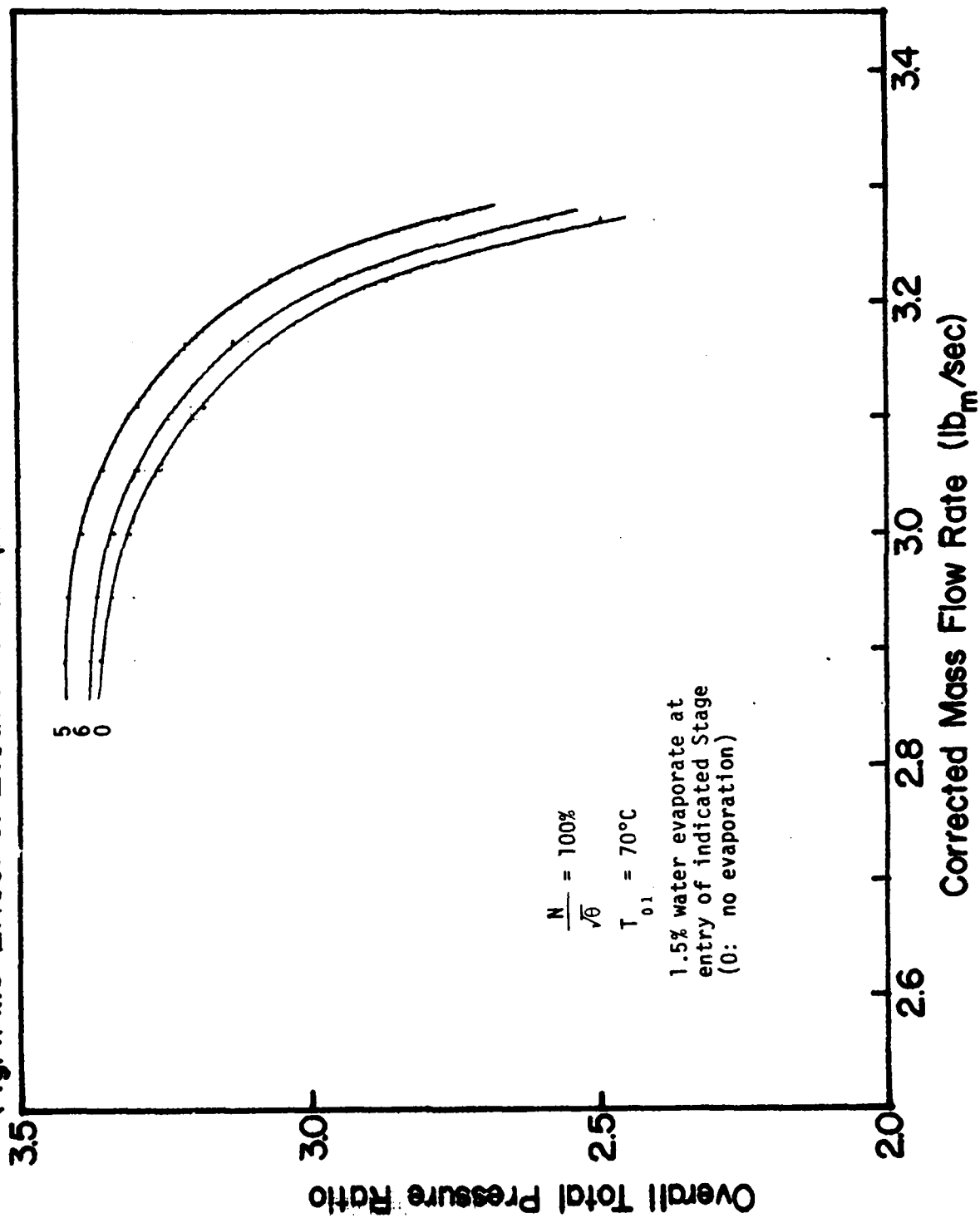


Fig.4.4.14 Effect of Location of Evaporation on Overall Adiabatic Efficiency

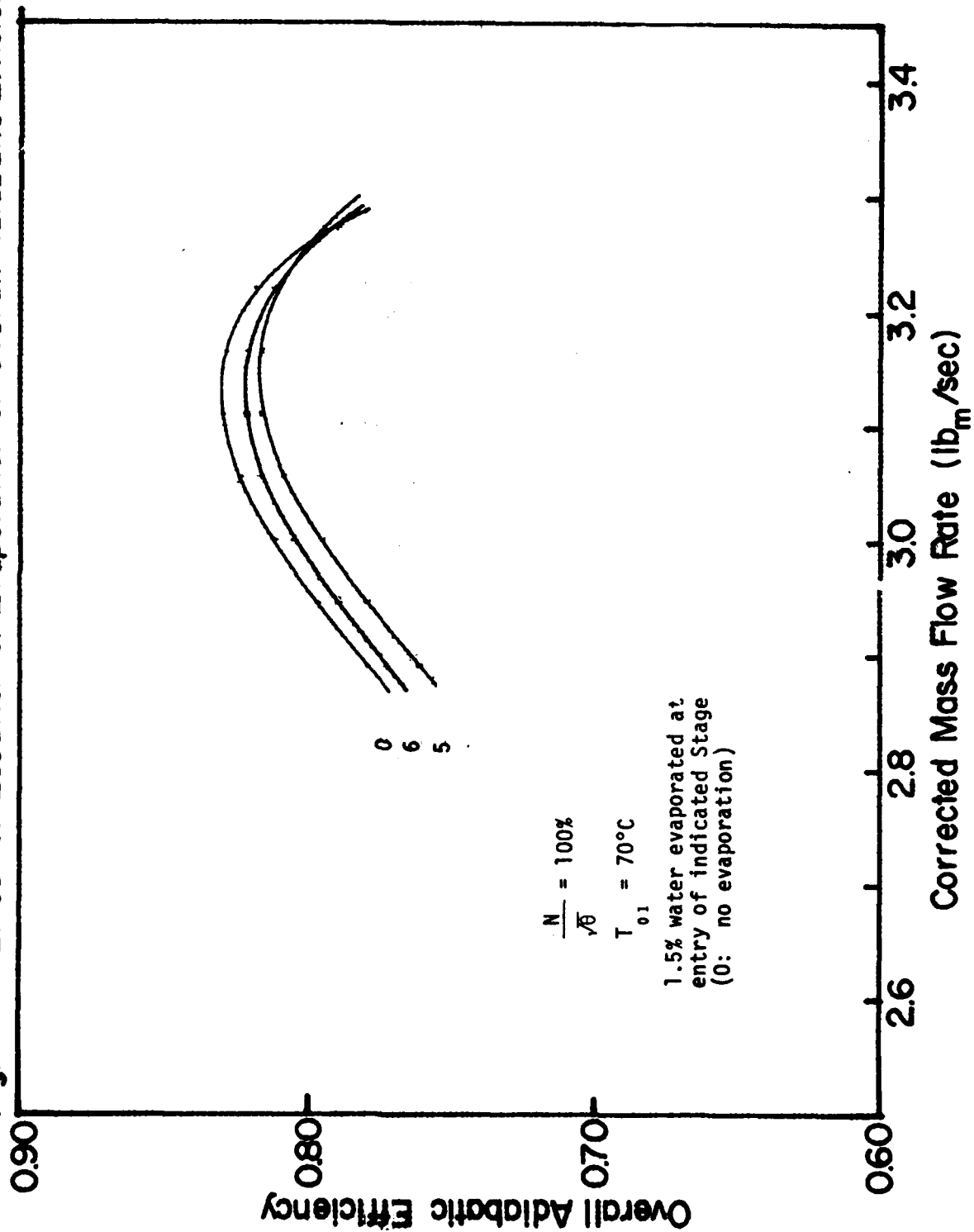


Fig.4.4.15 Effect of Location of Evaporation on Stage Total Pressure Ratio

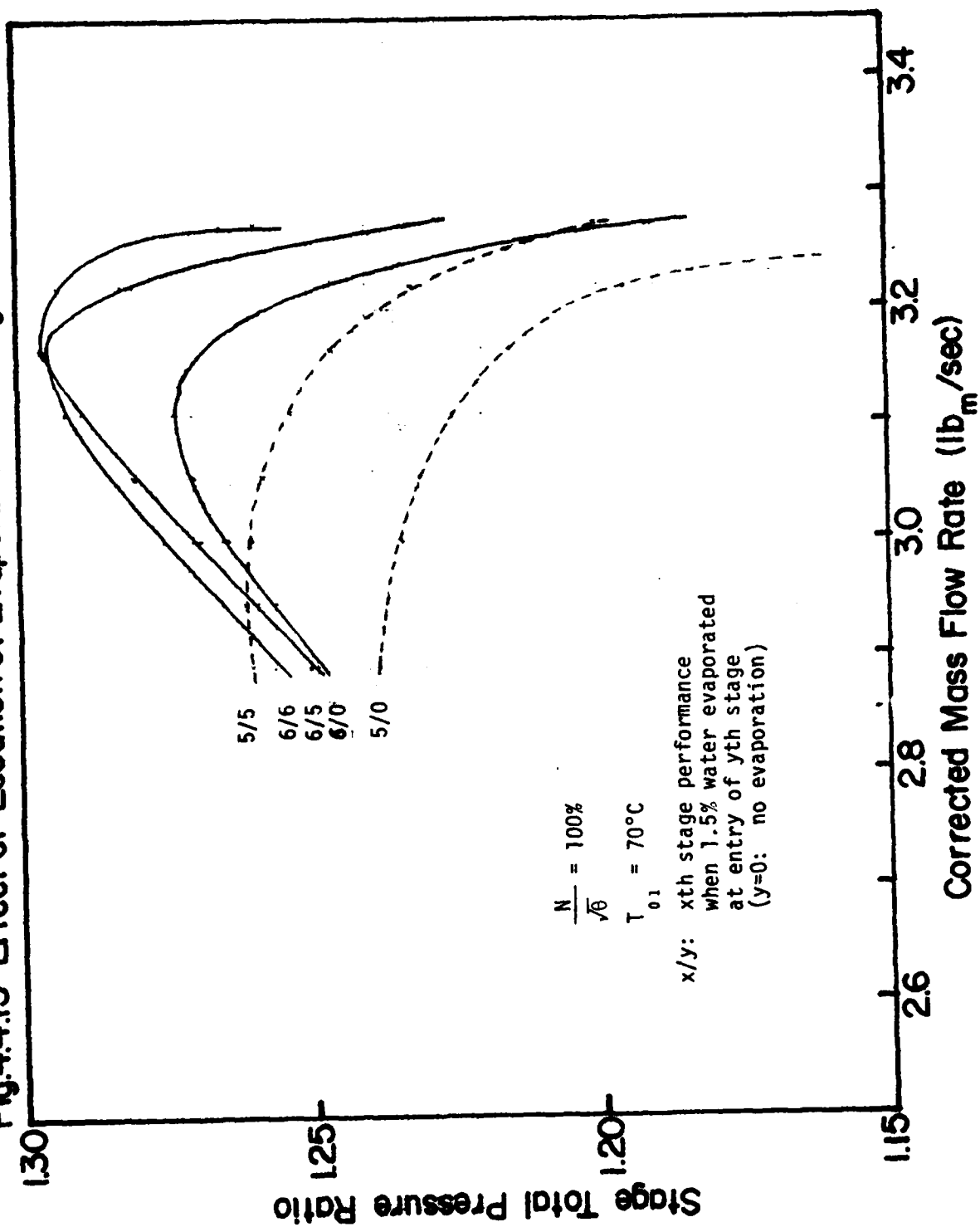


Fig.4.4.16 Effect of Location of Evaporation on Temperature Change along Compressor Stages

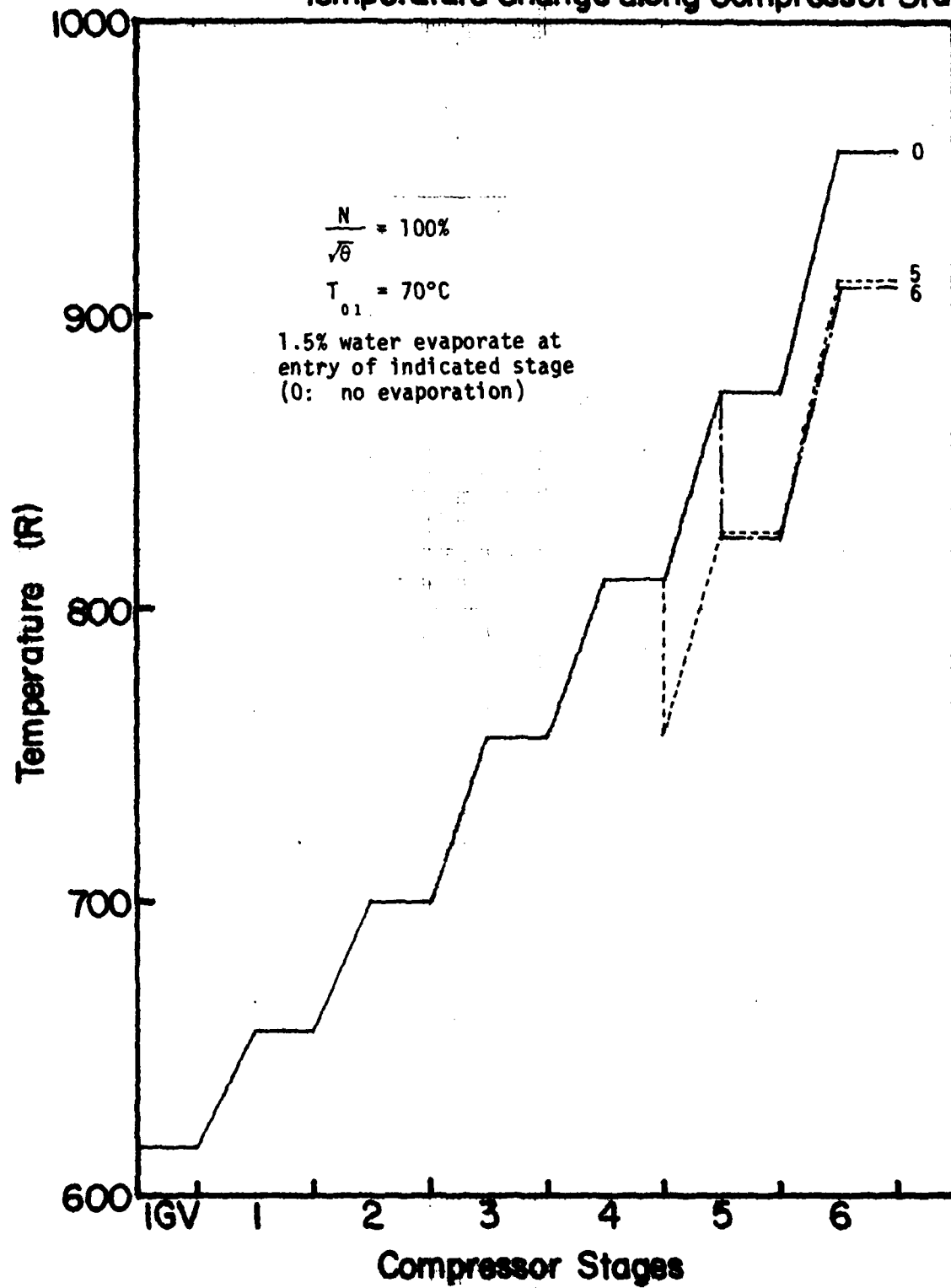


Fig.4.4.17 Effect of Location of Evaporation on Overall Total Pressure Ratio

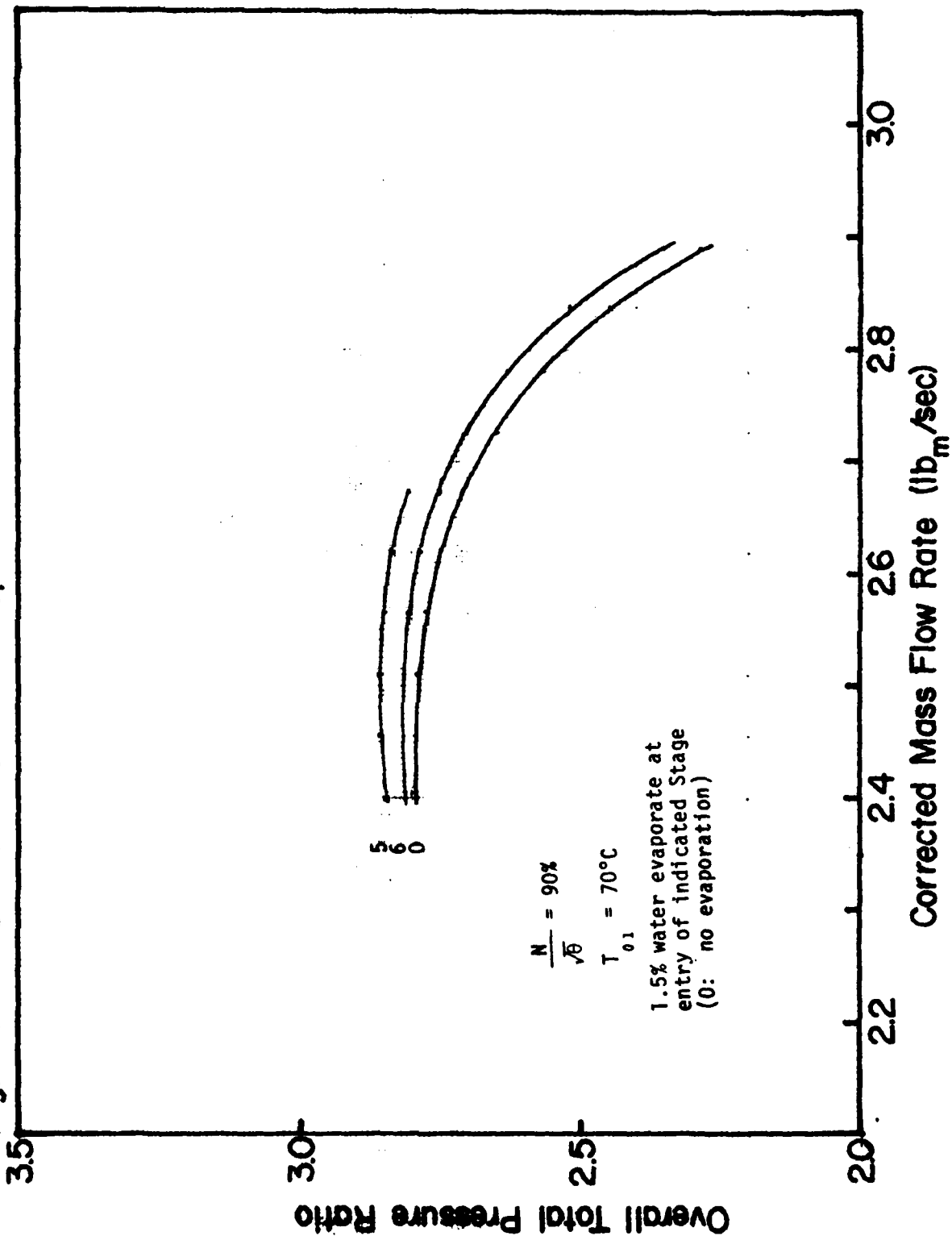


Fig.4.4.18 Effect of Location of Evaporation on Overall Adiabatic Efficiency

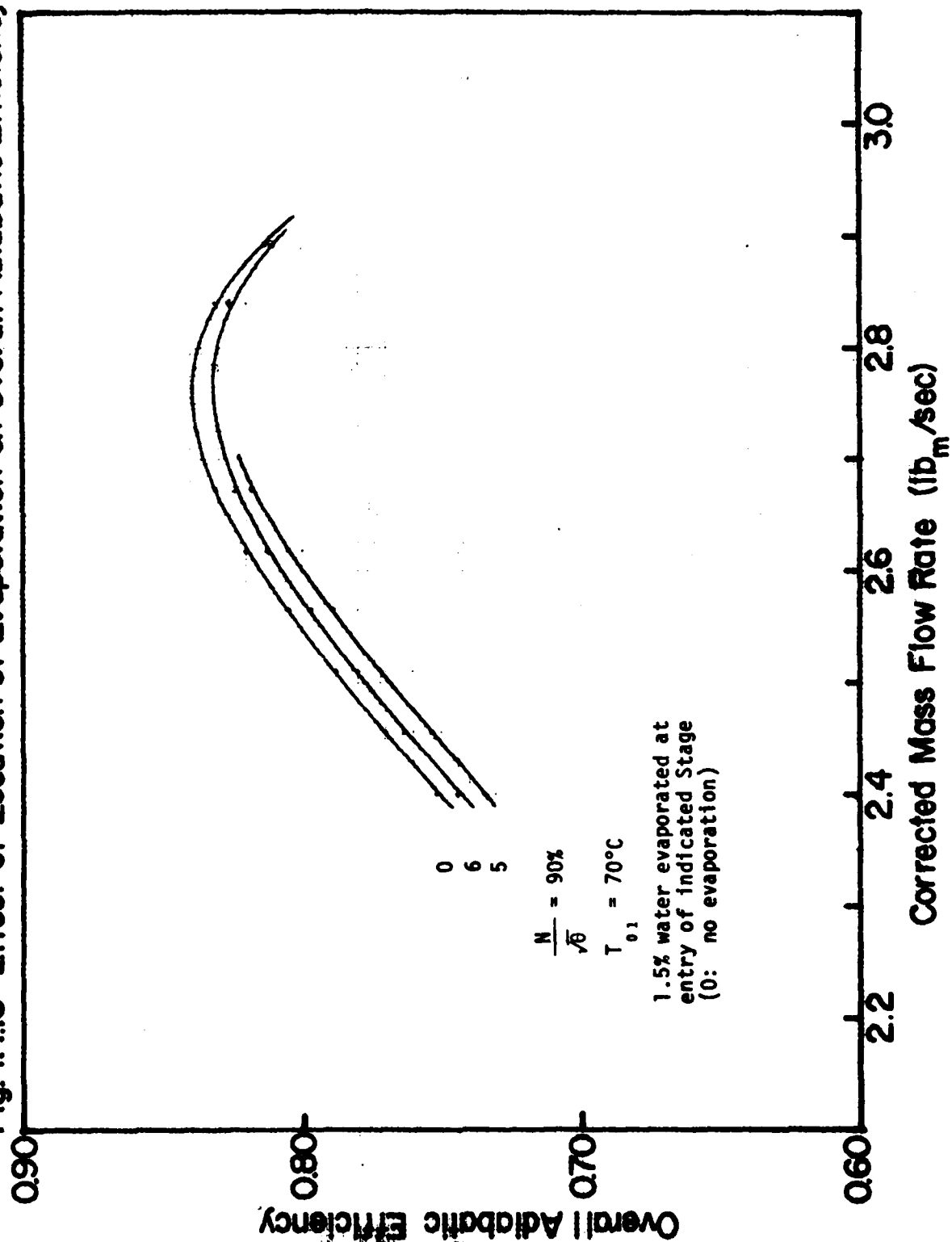


Fig.4.4.19 Effect of Location of Evaporation on Stage Total Pressure Ratio

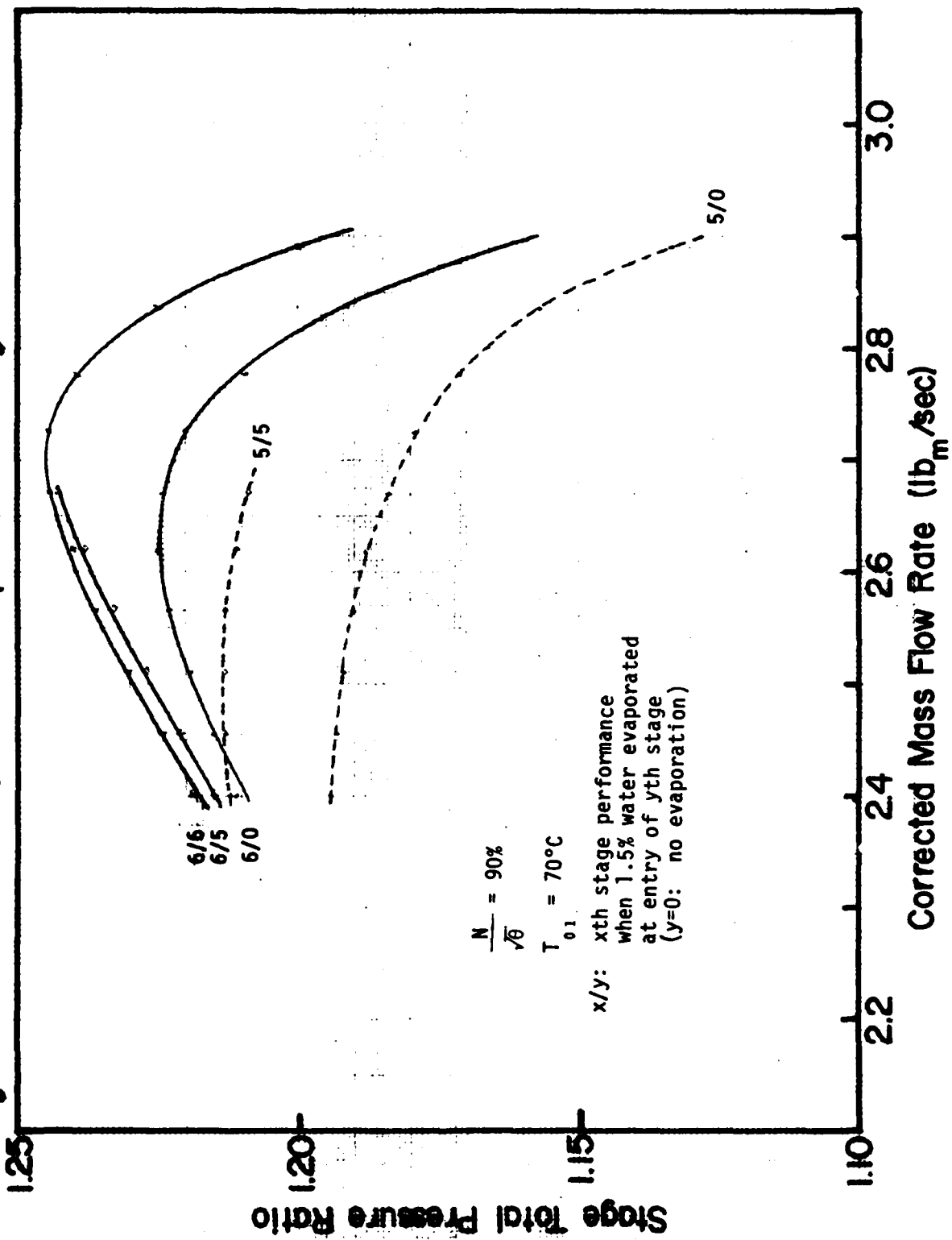


Fig.4.4.20 Effect of Location of Evaporation on Temperature Change along Compressor Stages

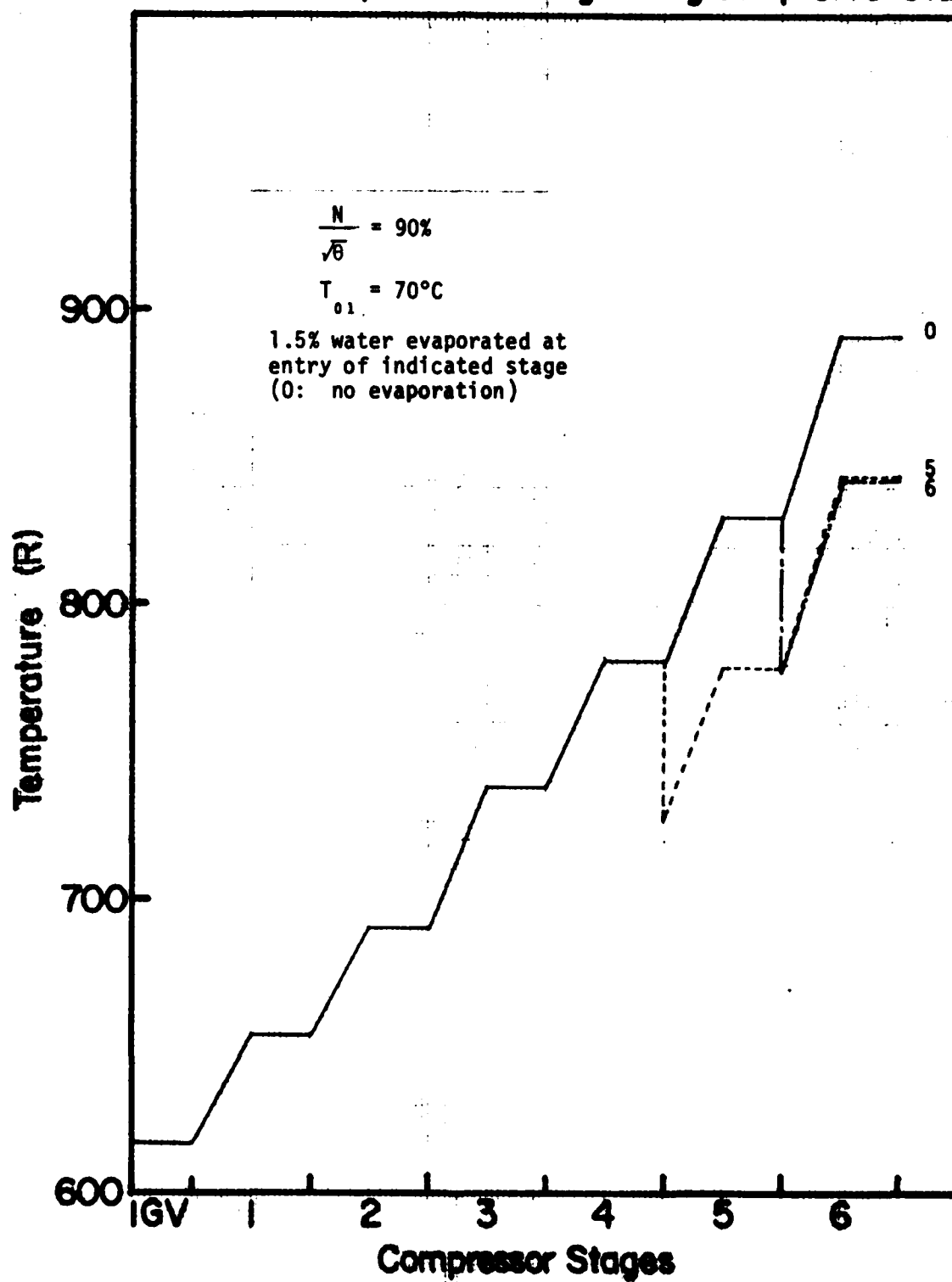


Fig.4.4.21 Effect of Location of Evaporation on Overall Total Pressure Ratio

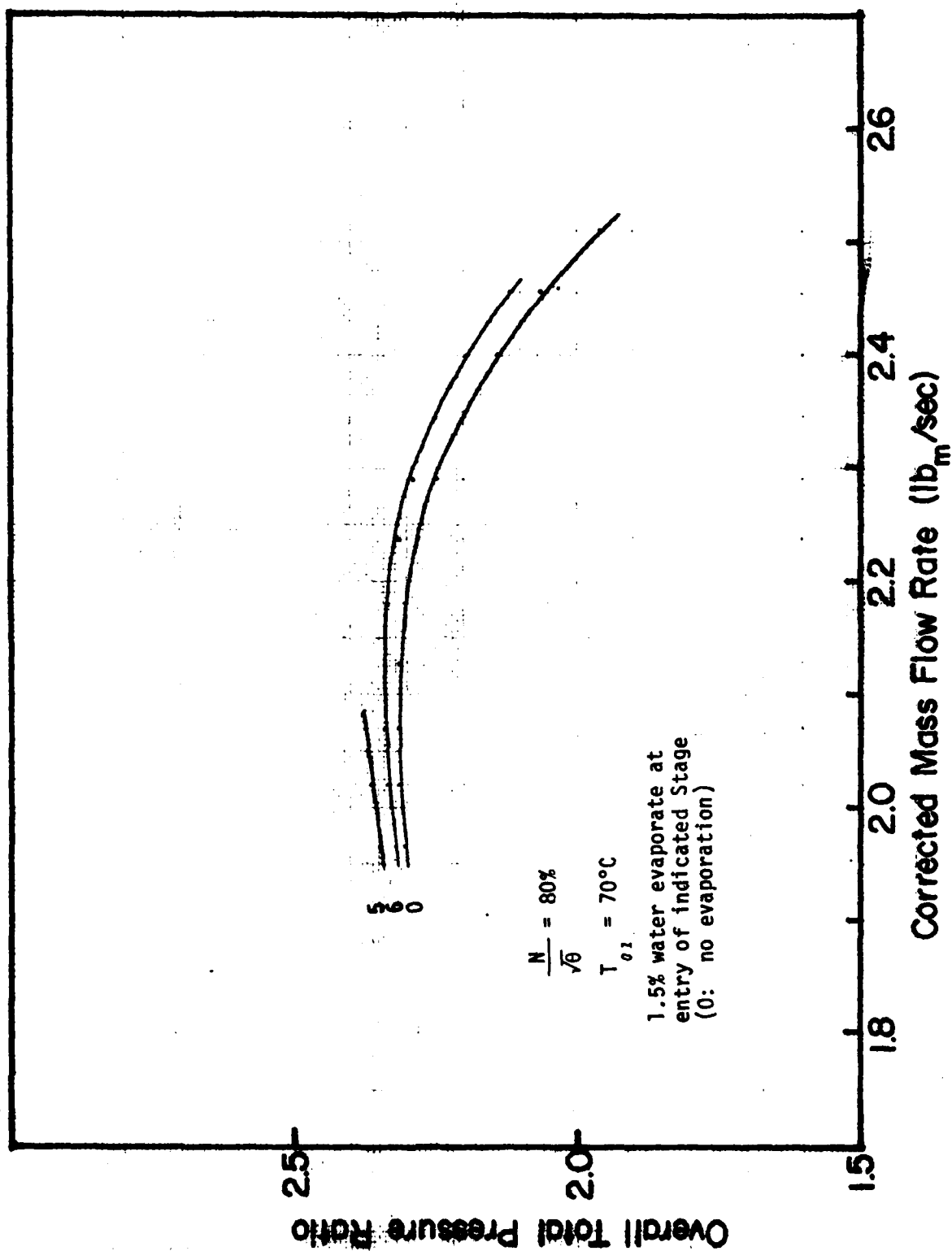


Fig. 4.4.22 Effect of Location of Evaporation on Overall Adiabatic Efficiency

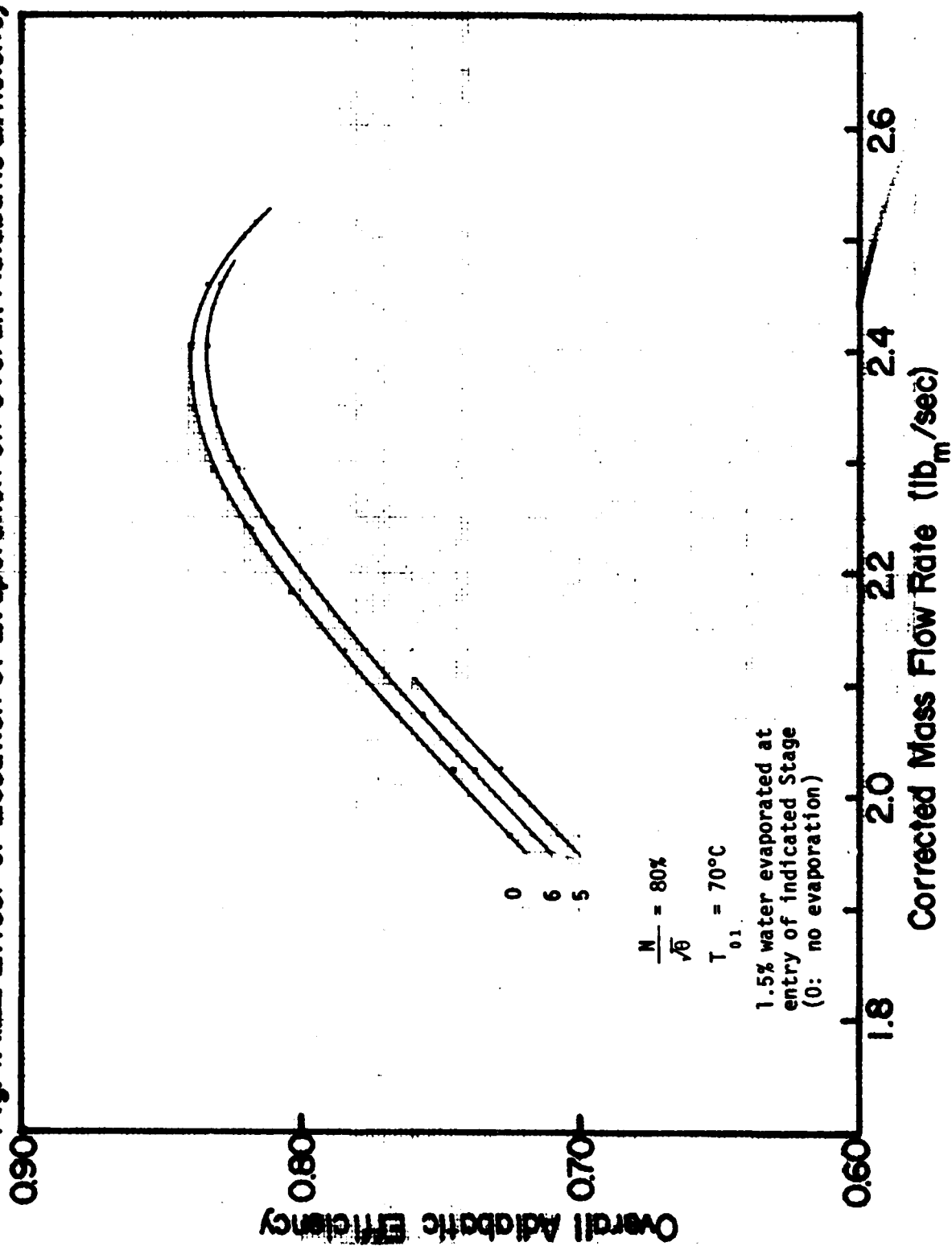


Fig.4.4.23 Effect of Location of Evaporation on Stage Total Pressure Ratio

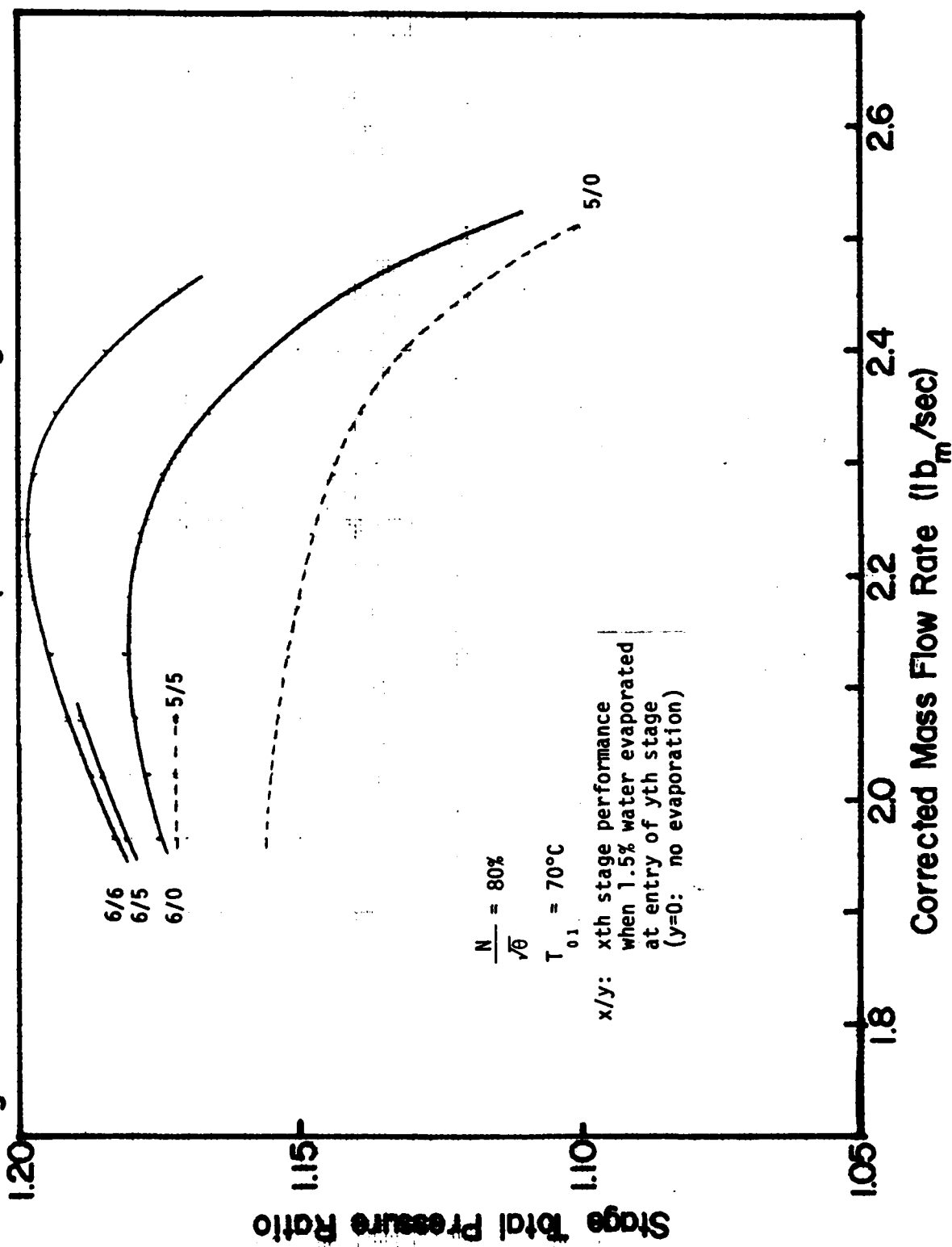


Fig.4.4.24 Effect of Location of Evaporation on Temperature Change along Compressor Stages

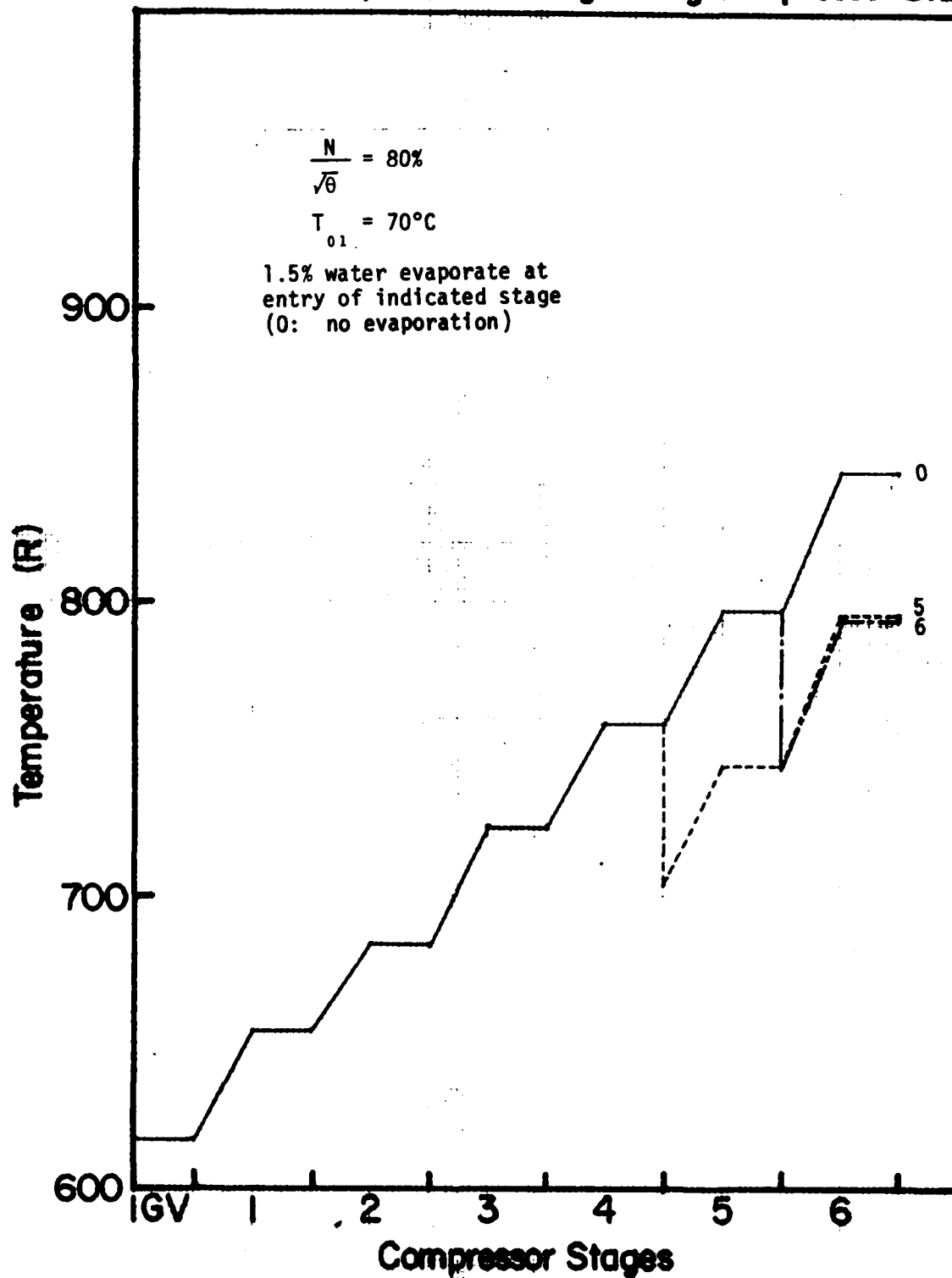


Fig.4.5.1 Effect of Evaporation on Overall Total Pressure Ratio

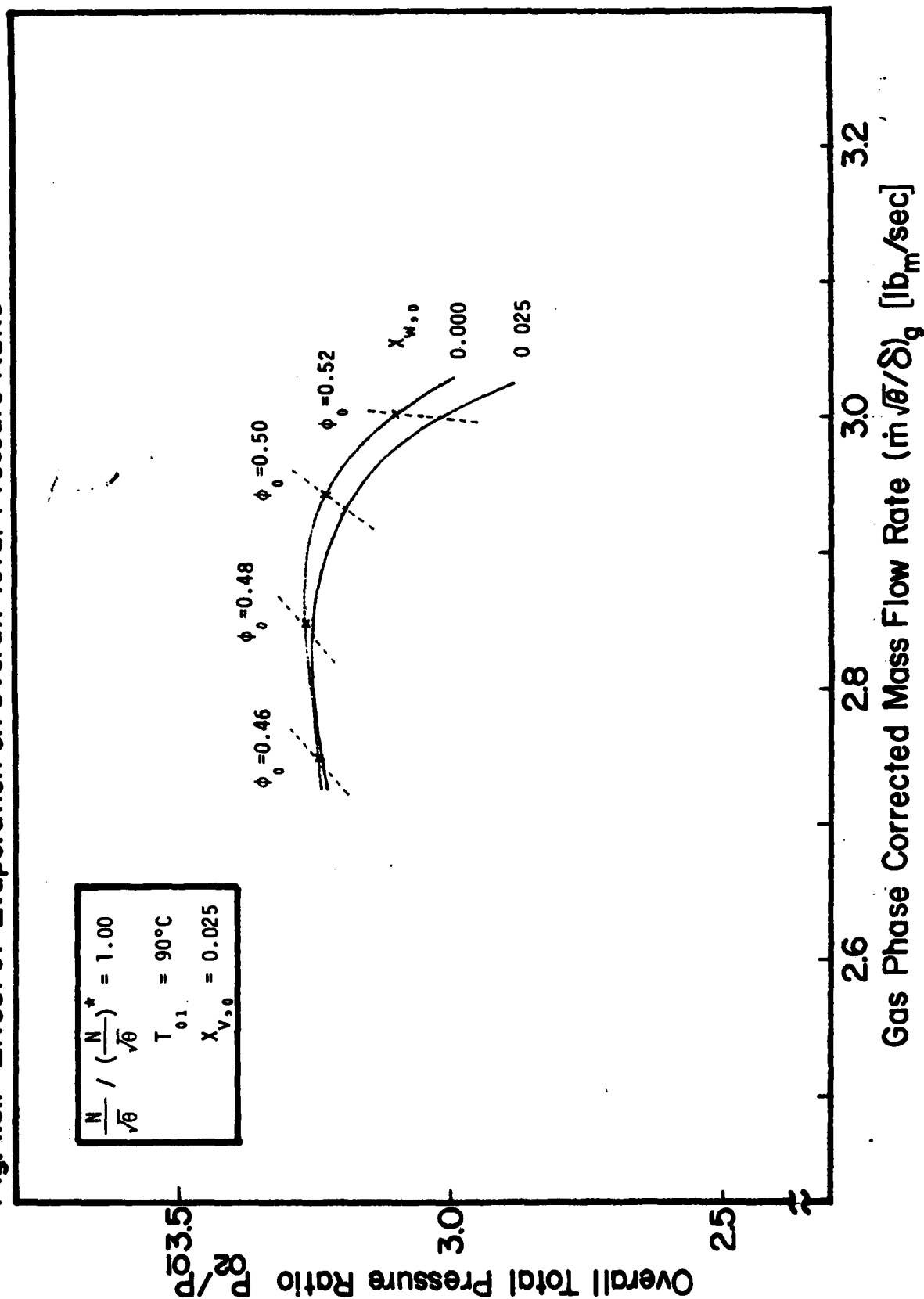


Fig.4.5.2 Effect of Evaporation on Overall Adiabatic Efficiency

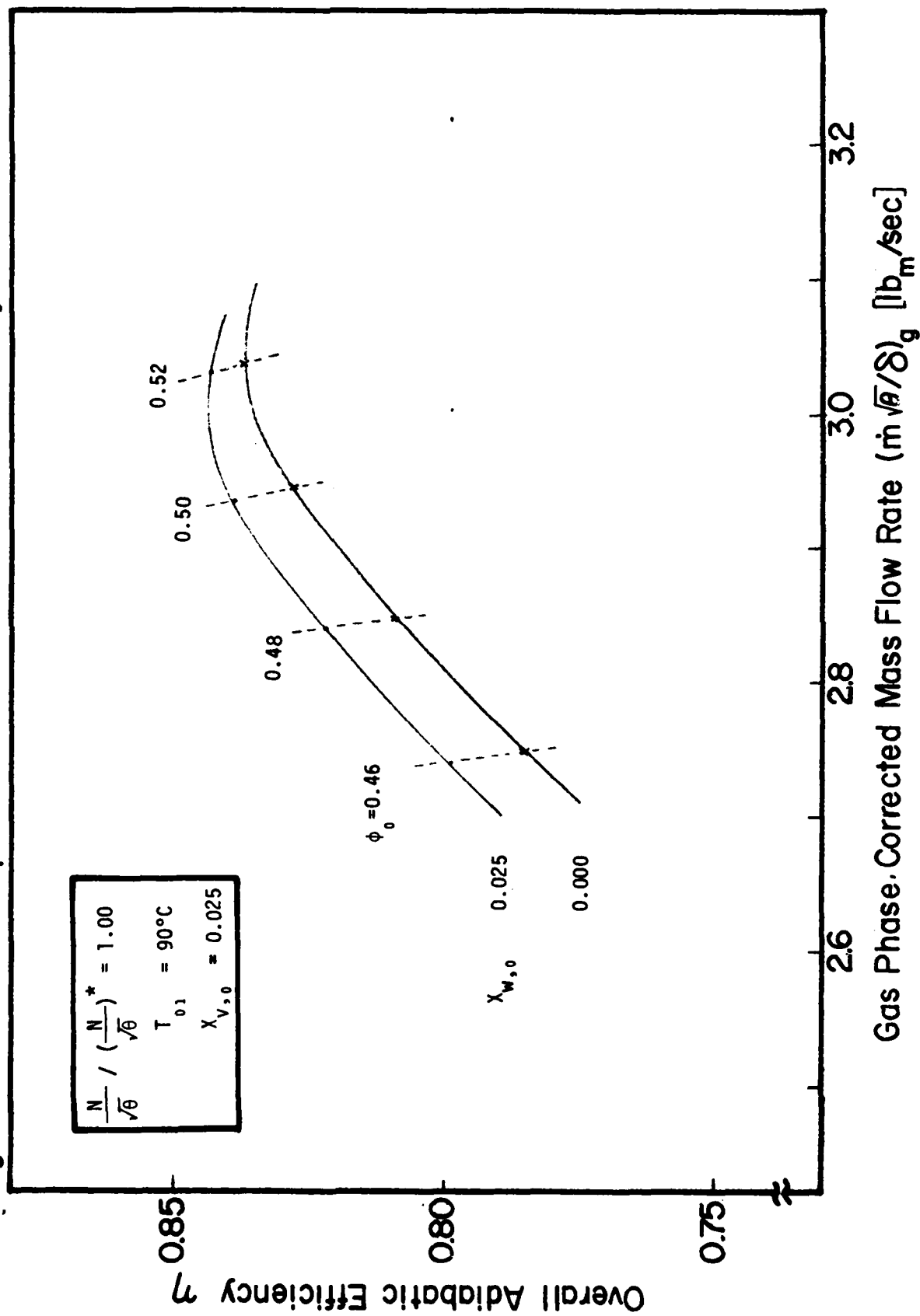


Fig.4.5.3 Effect of Evaporation on Temperature Change of Gas Phase and Droplet along Compressor Stages

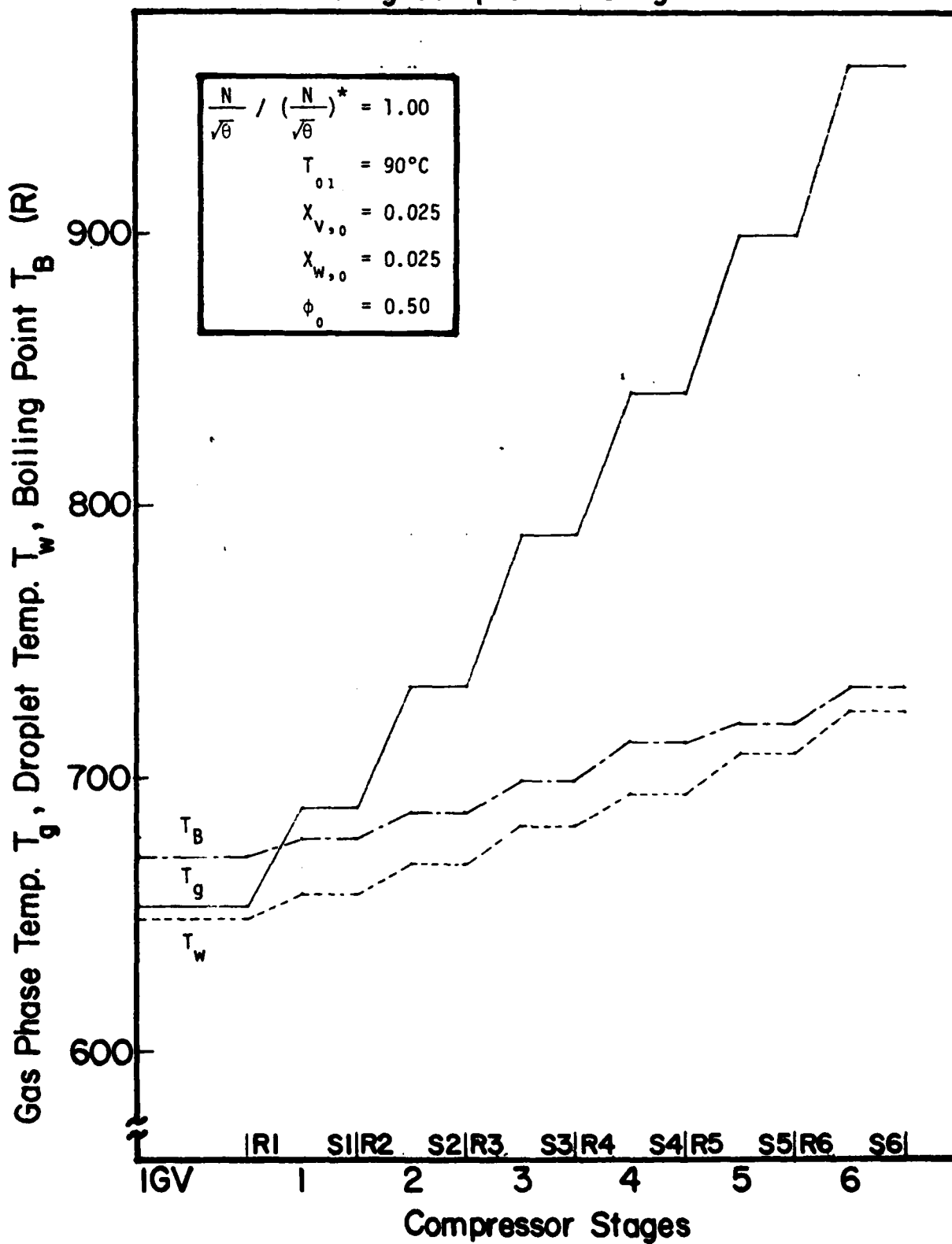


Fig.4.5.4 Effect of Evaporation on Mass Flow Rate of Liquid Phase at Tip along Compressor Stages

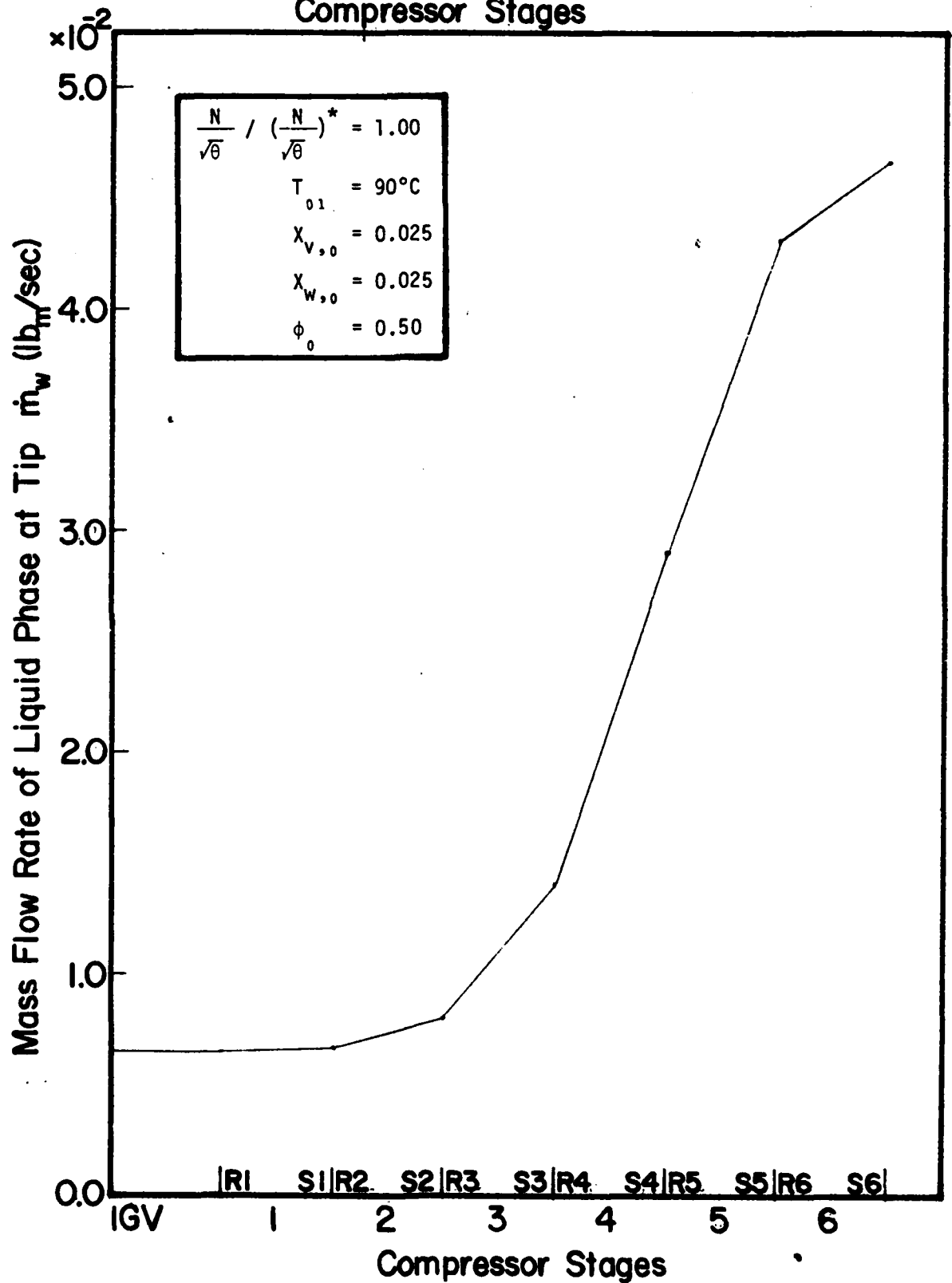


Fig.4.5.5 Effect of Evaporation on Mass Flow Rate of Gas Phase at Tip along Compressor Stages

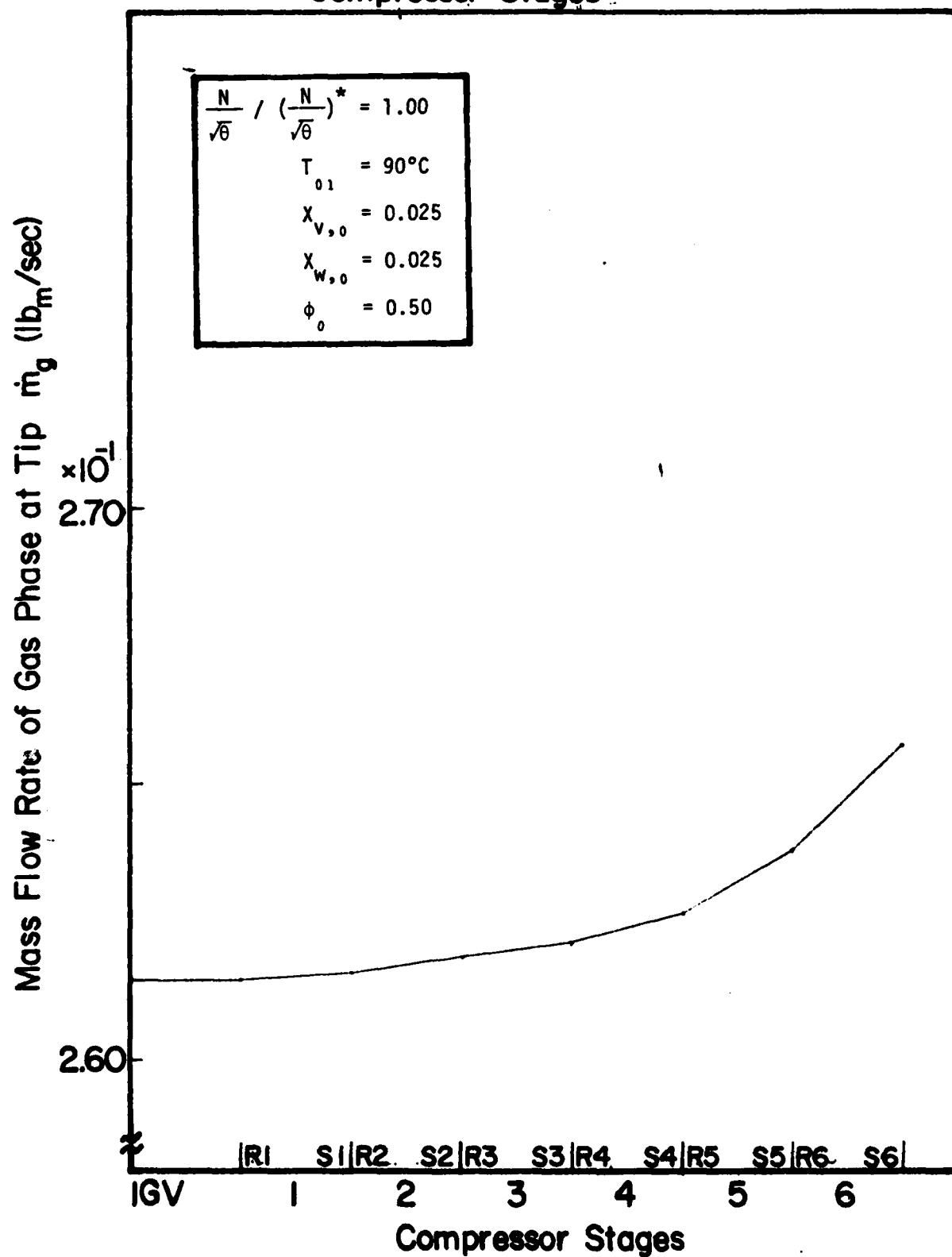


Fig.4.5.6 Effect of Evaporation on Overall Total Pressure Ratio

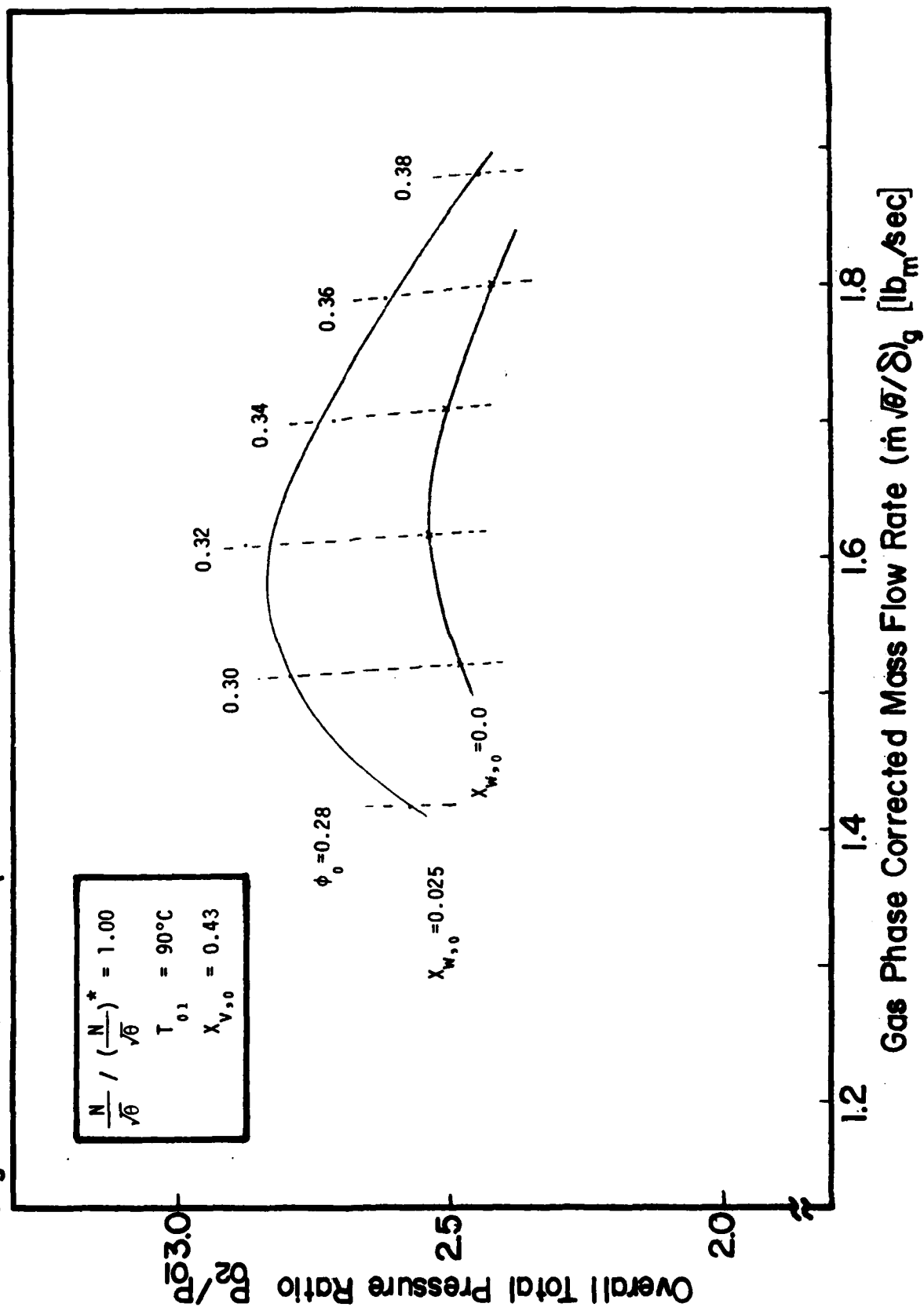


Fig.4.5.7 Effect of Evaporation on Overall Adiabatic Efficiency

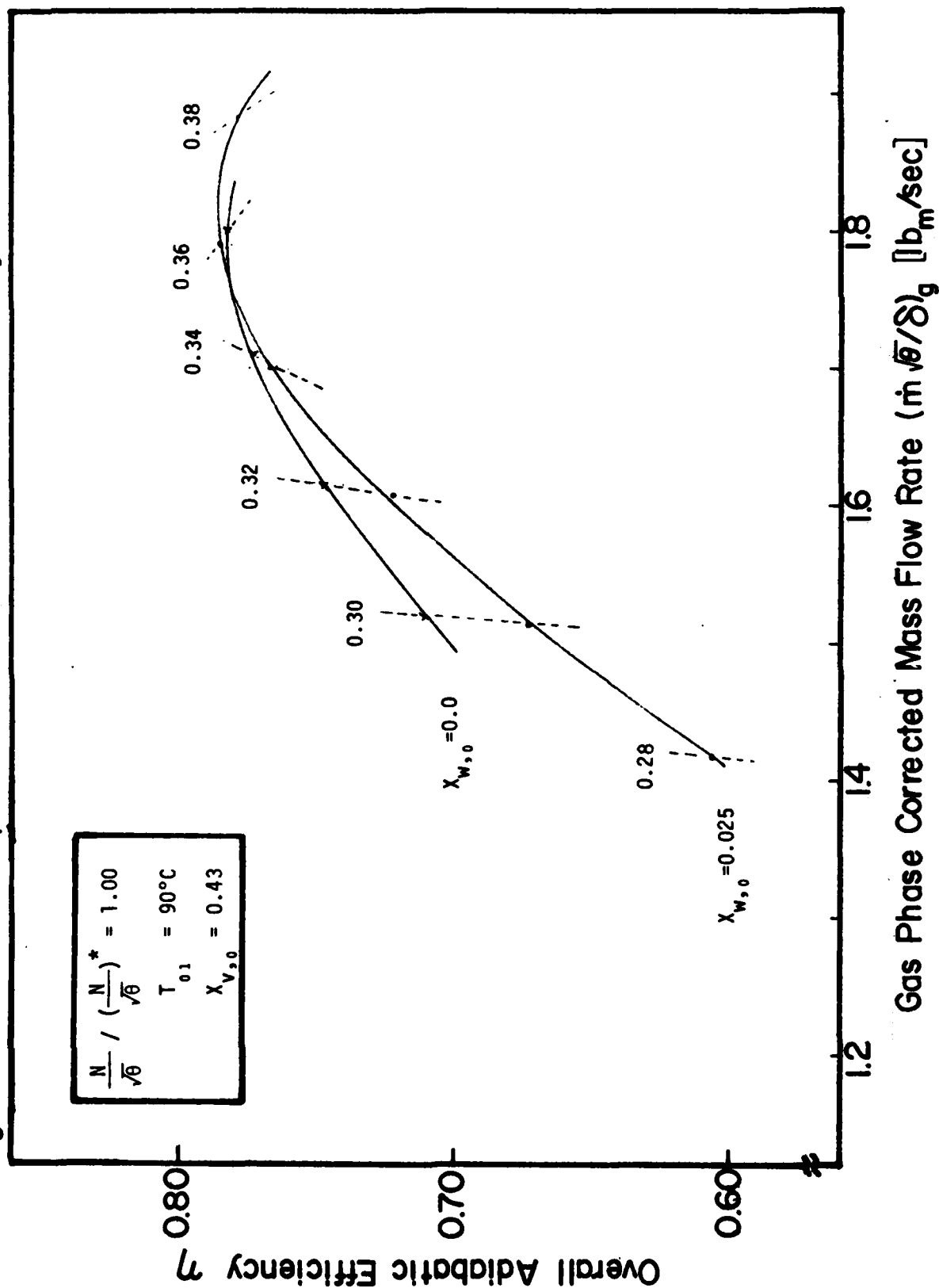


Fig.4.5.8 Effect of Evaporation on Temperature Change of Gas Phase and Droplet along Compressor Stages

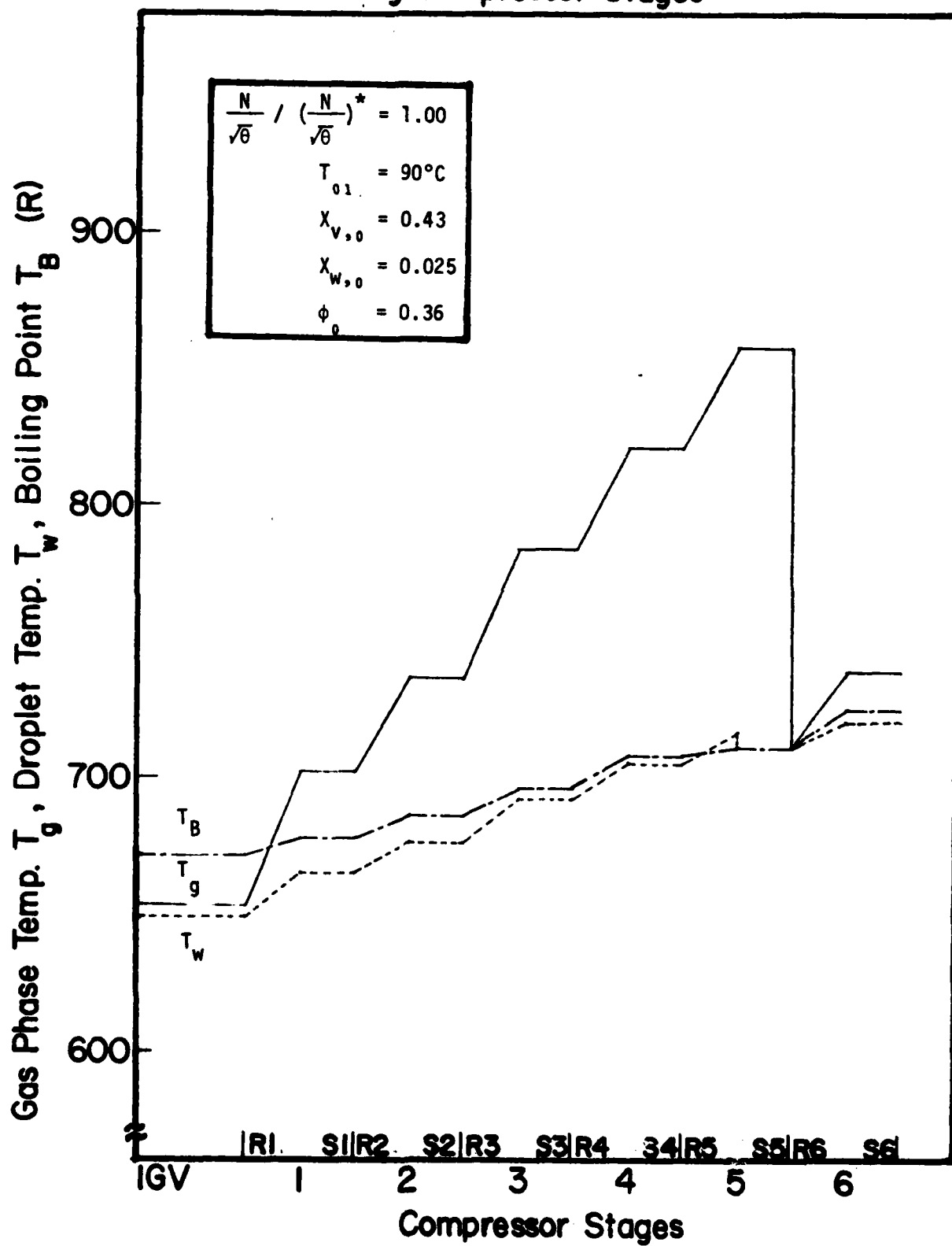


Fig.4.5.9 Effect of Evaporation on Mass Flow Rate of Liquid Phase at Tip along Compressor Stages

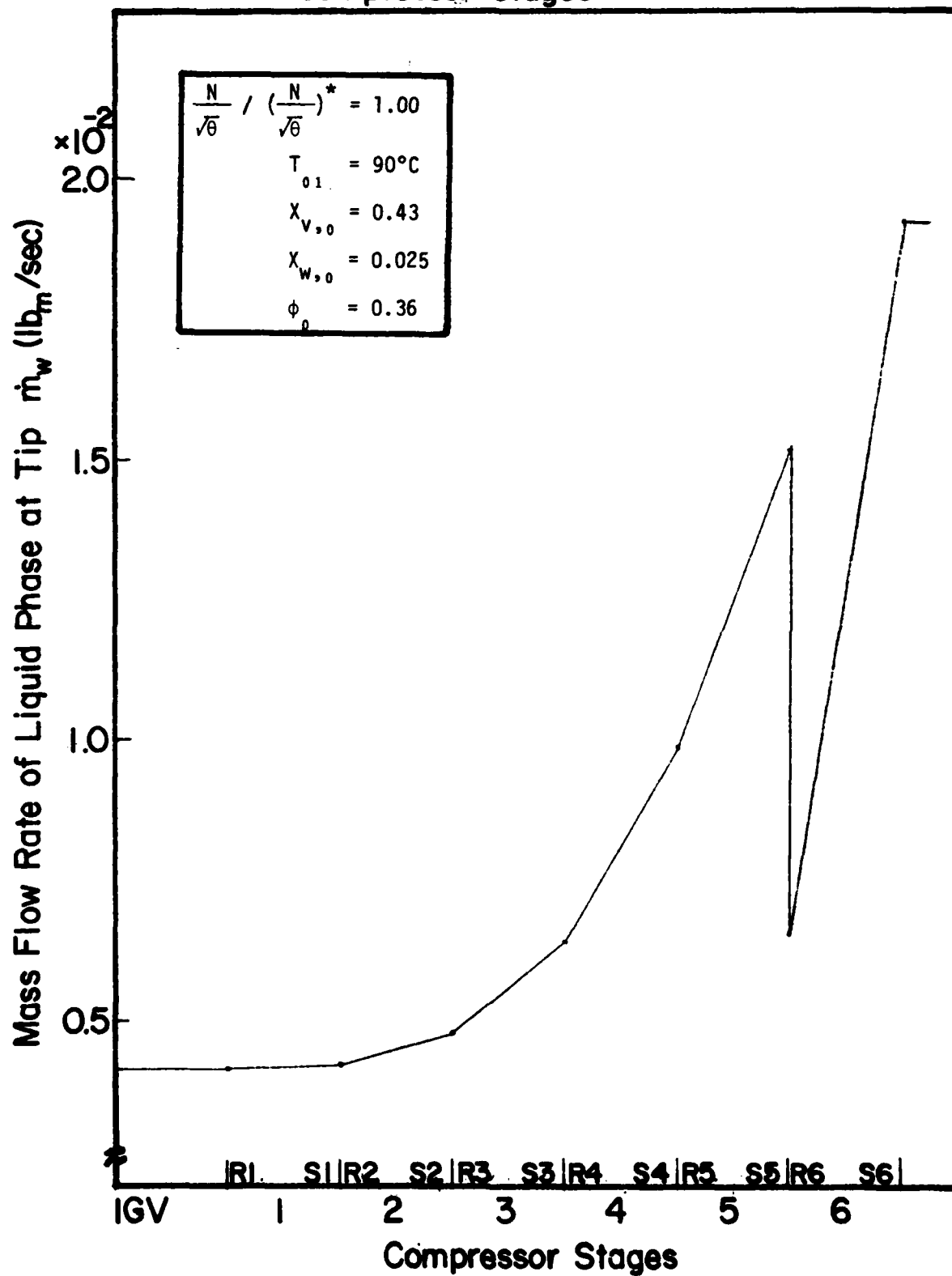


Fig.4.5.10 Effect of Evaporation on Mass Flow Rate of Gas Phase at Tip along Compressor Stages

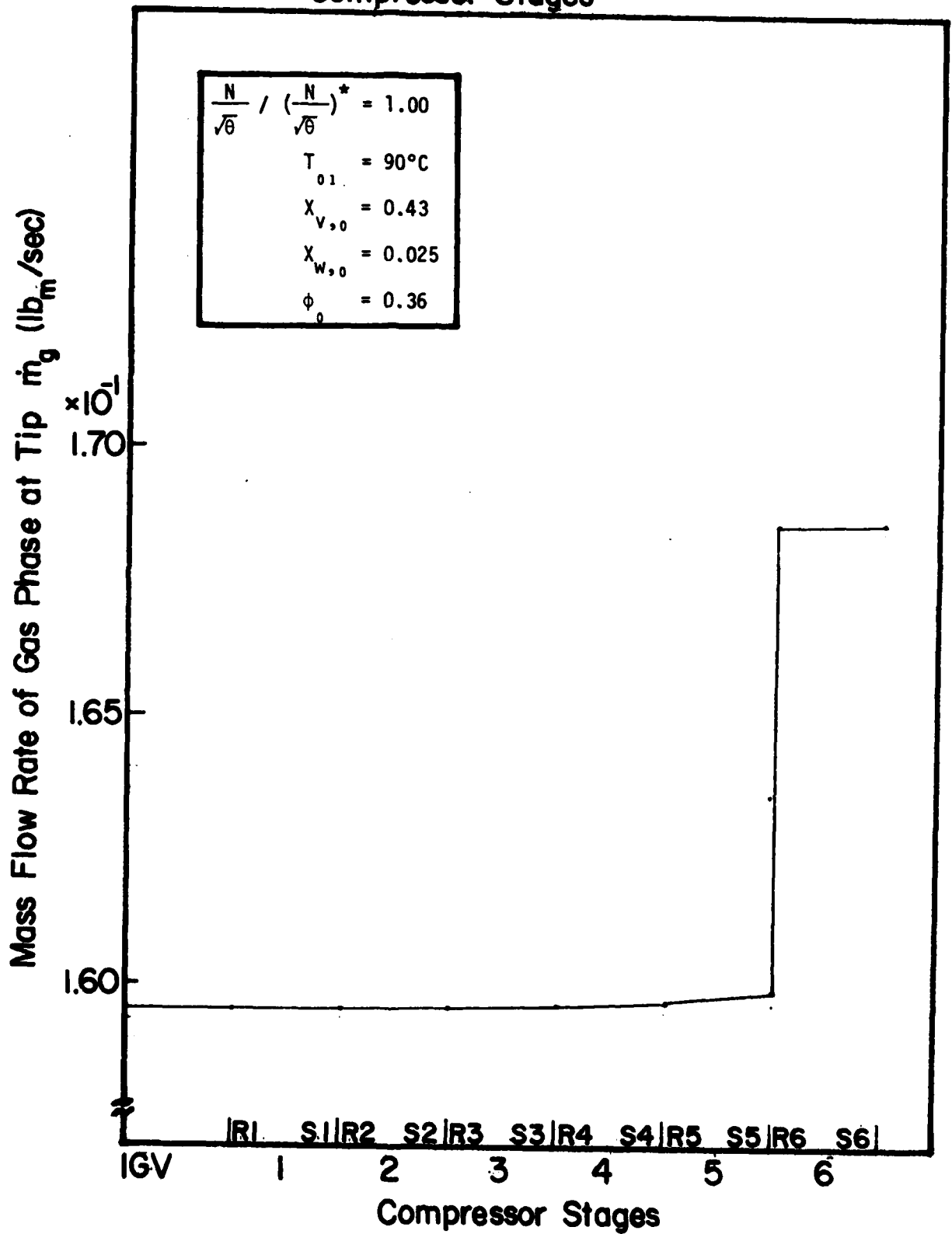


Fig.4.5.11 Effect of Evaporation on Overall Total Pressure Ratio

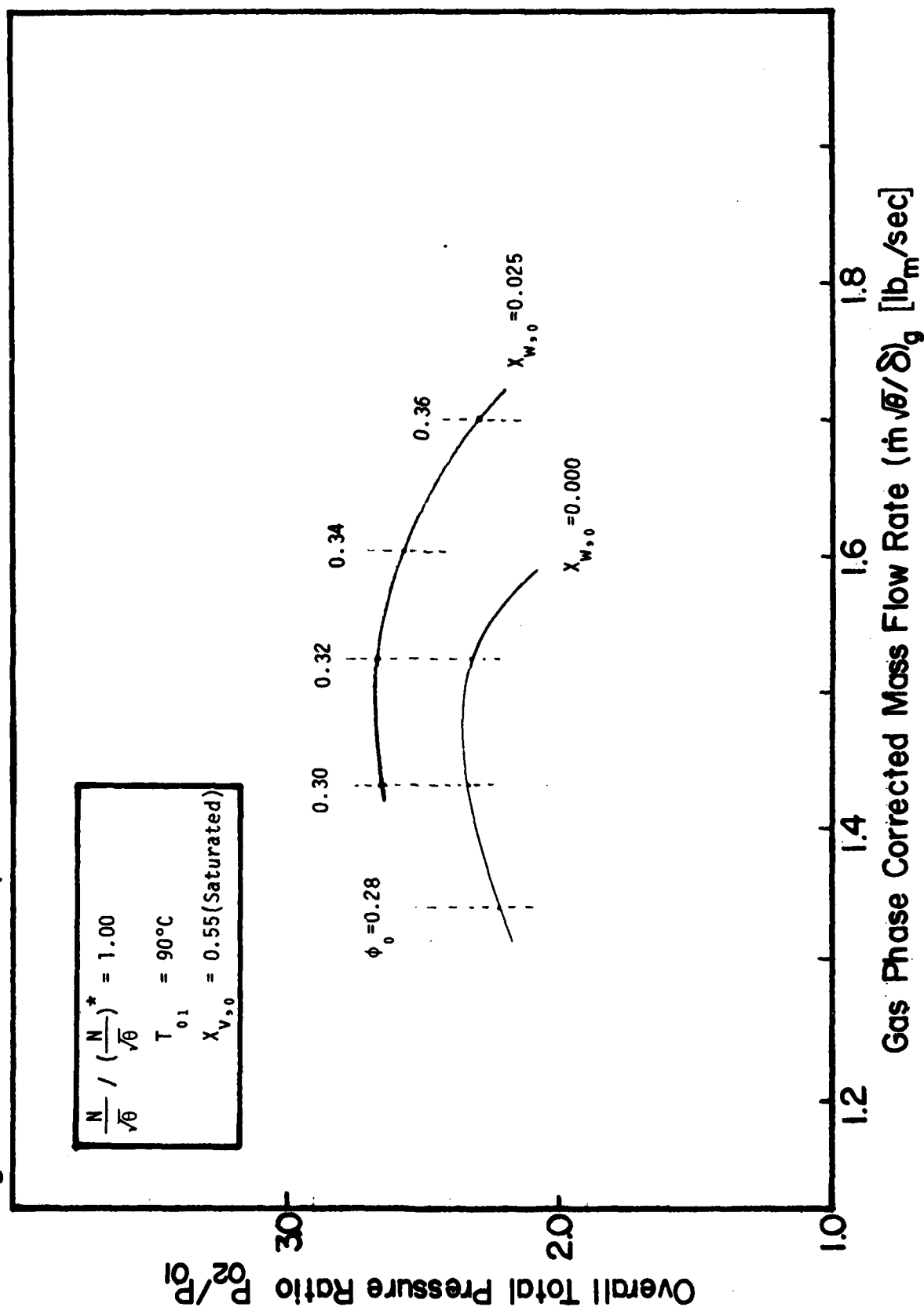


Fig.4.5.12 Effect of Evaporation on Overall Adiabatic Efficiency

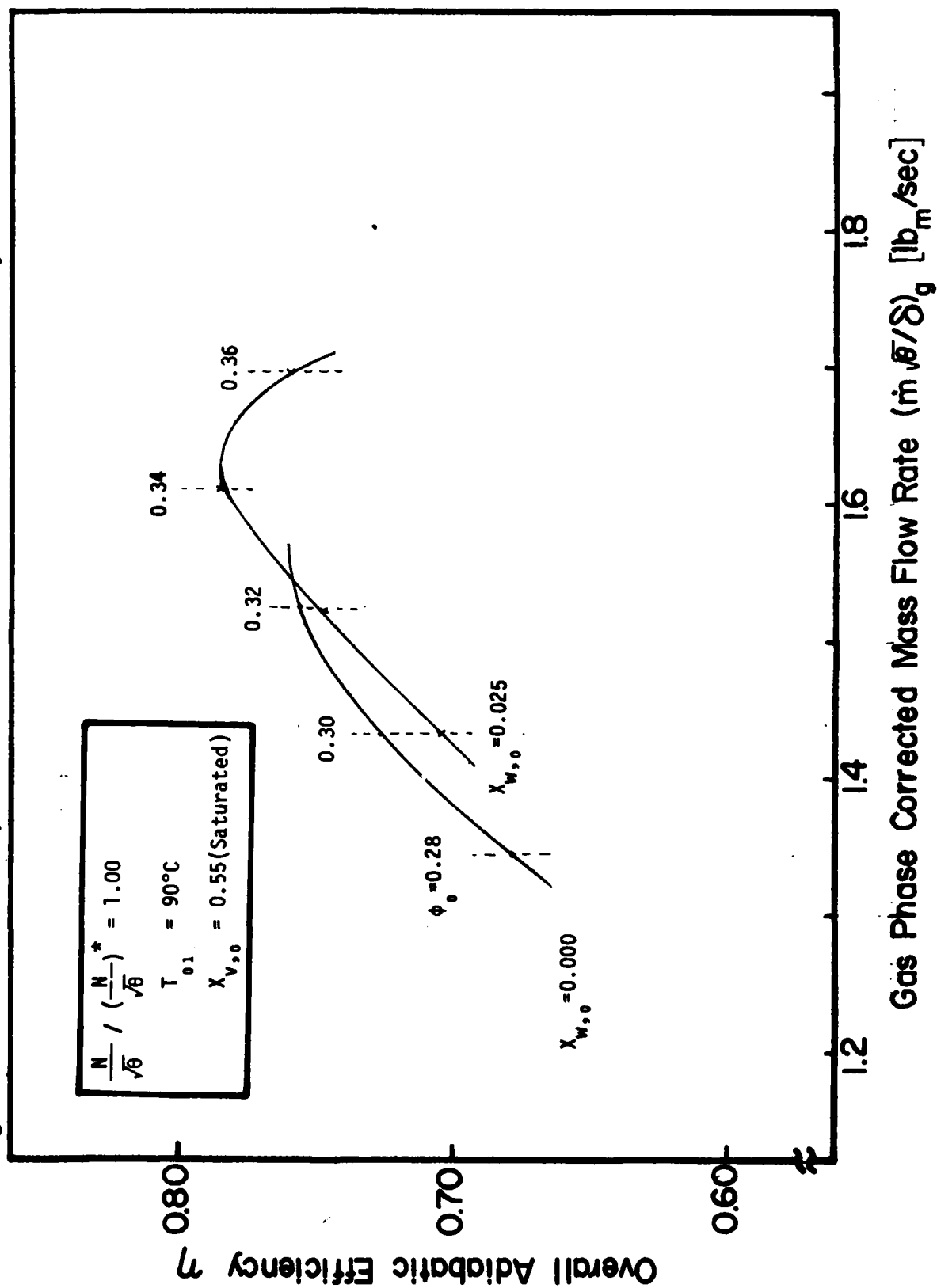


Fig.4.5.13 Effect of Evaporation on Temperature Change of Gas Phase and Droplet along Compressor Stages

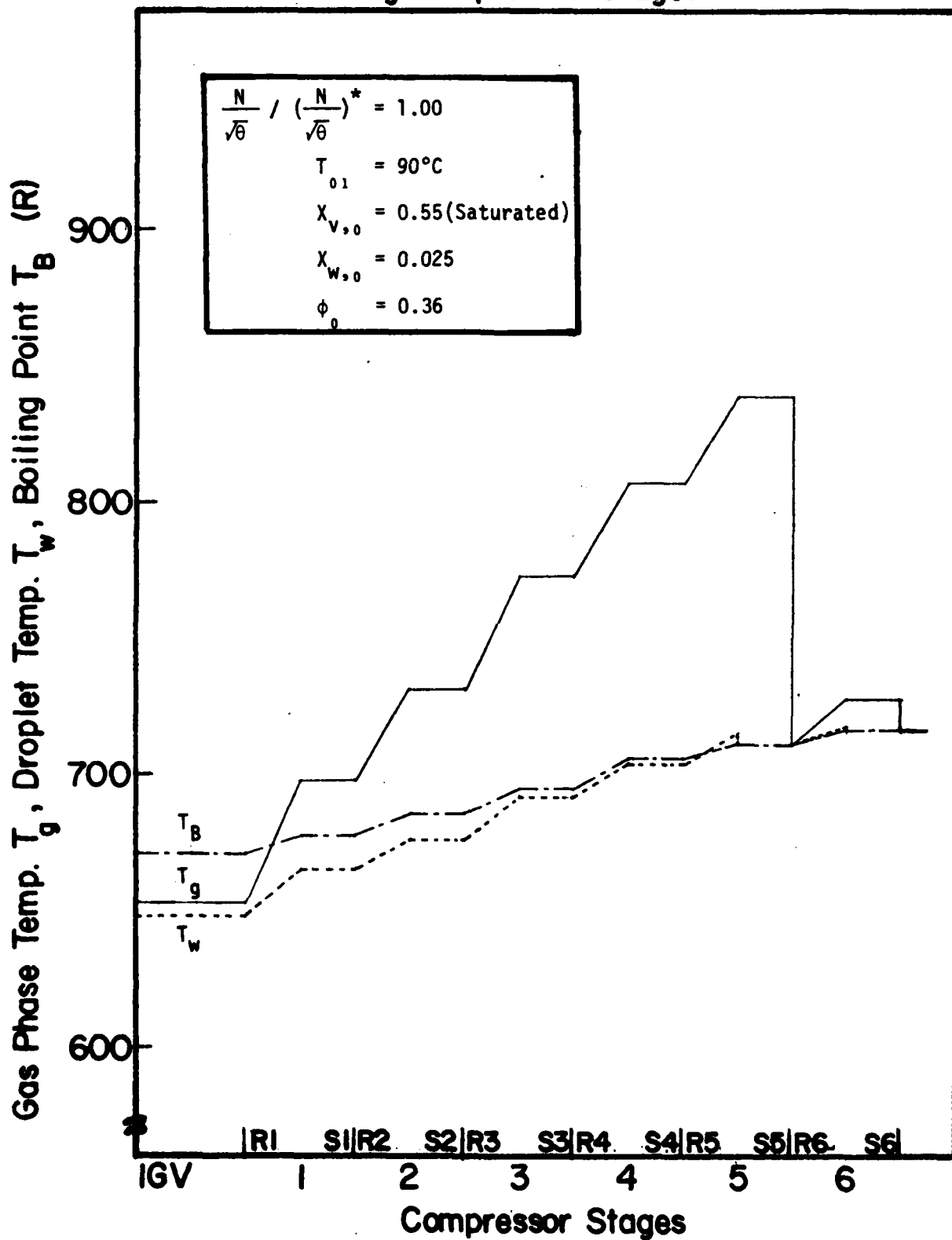


Fig.4.5.14 Effect of Evaporation on Mass Flow Rate of Liquid Phase at Tip along Compressor Stages

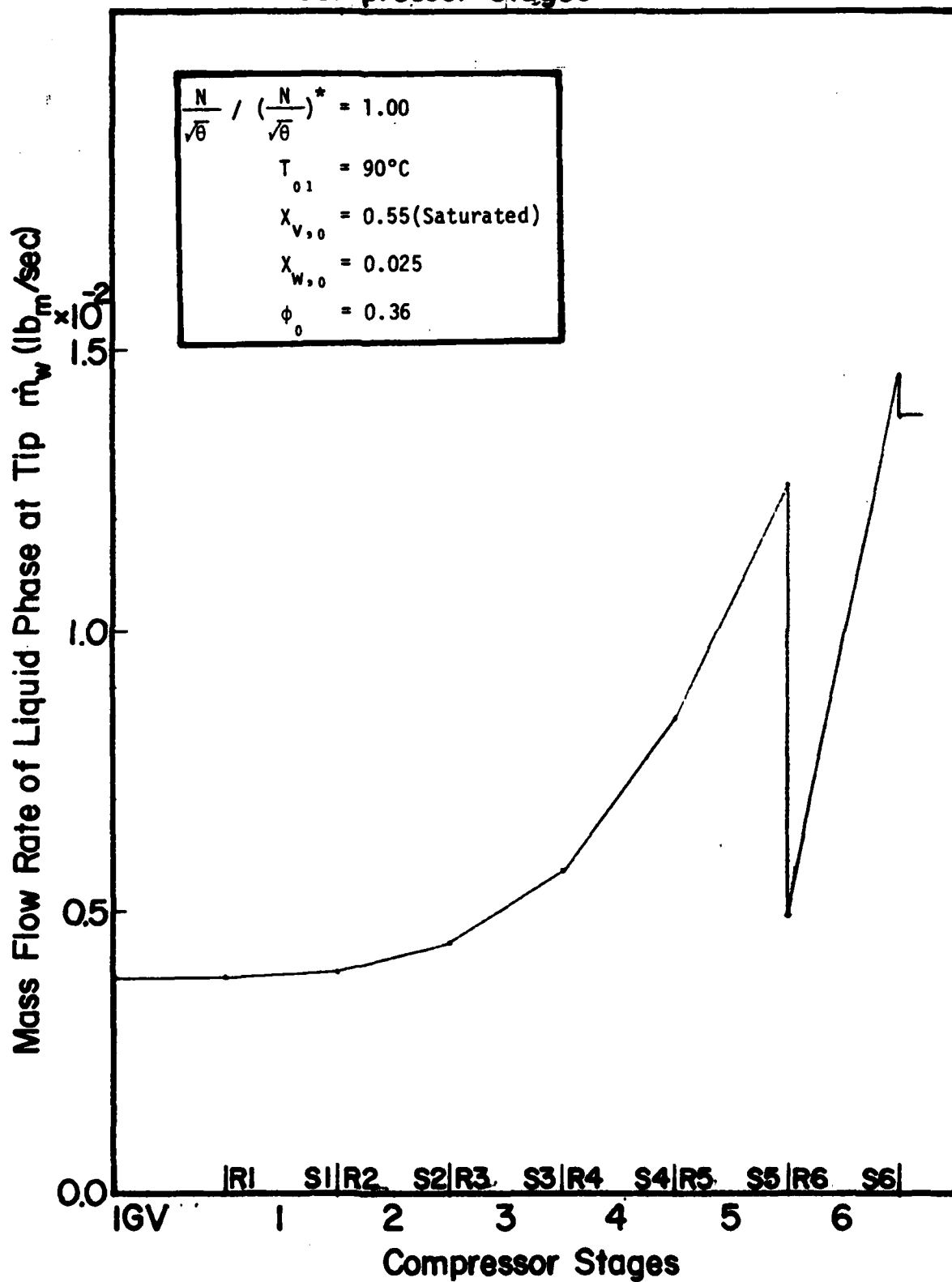


Fig.4.5.15 Effect of Evaporation on Mass Flow Rate of Gas Phase at Tip along Compressor Stages

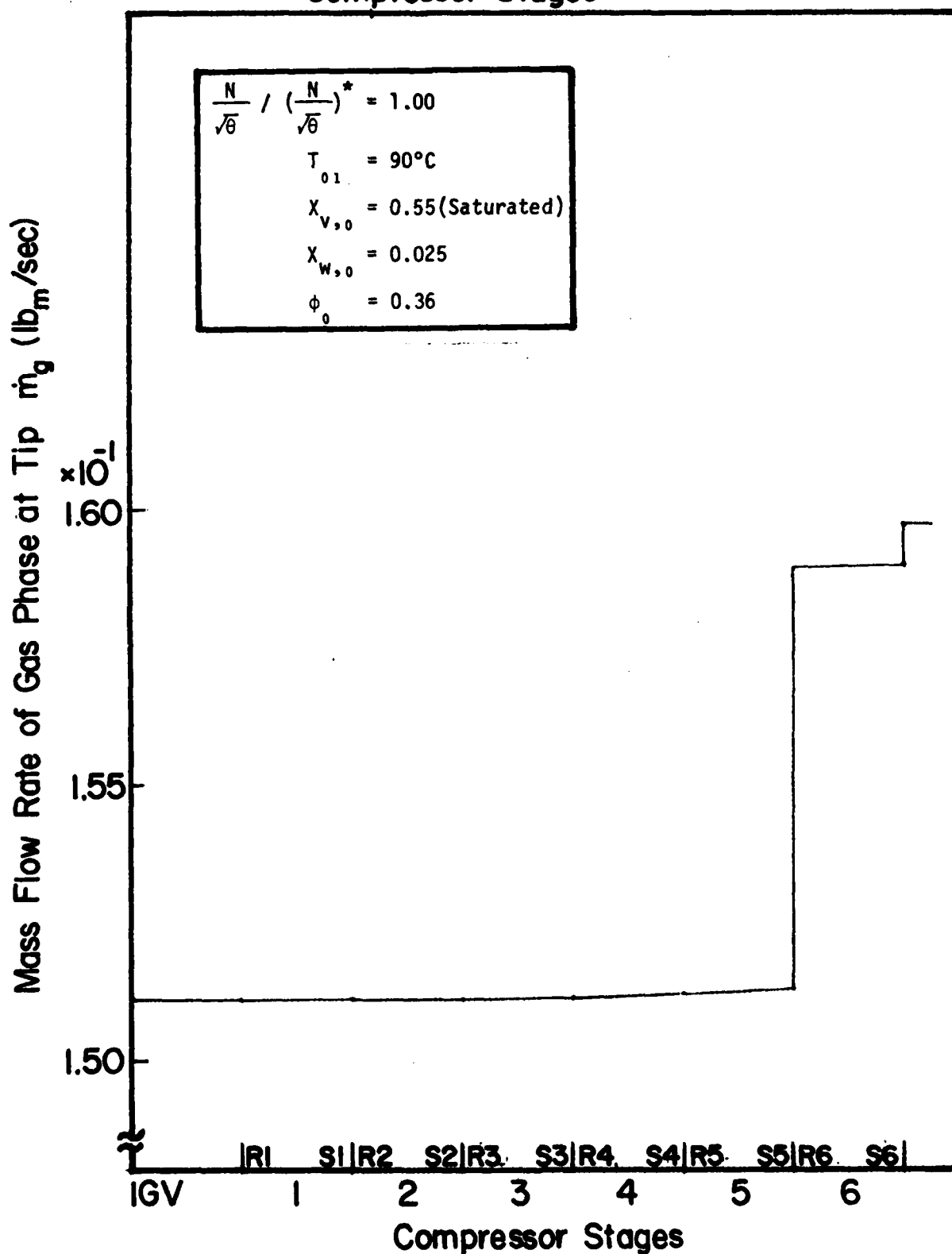


Fig.4.5.16 Effect of Evaporation on Overall Total Pressure Ratio

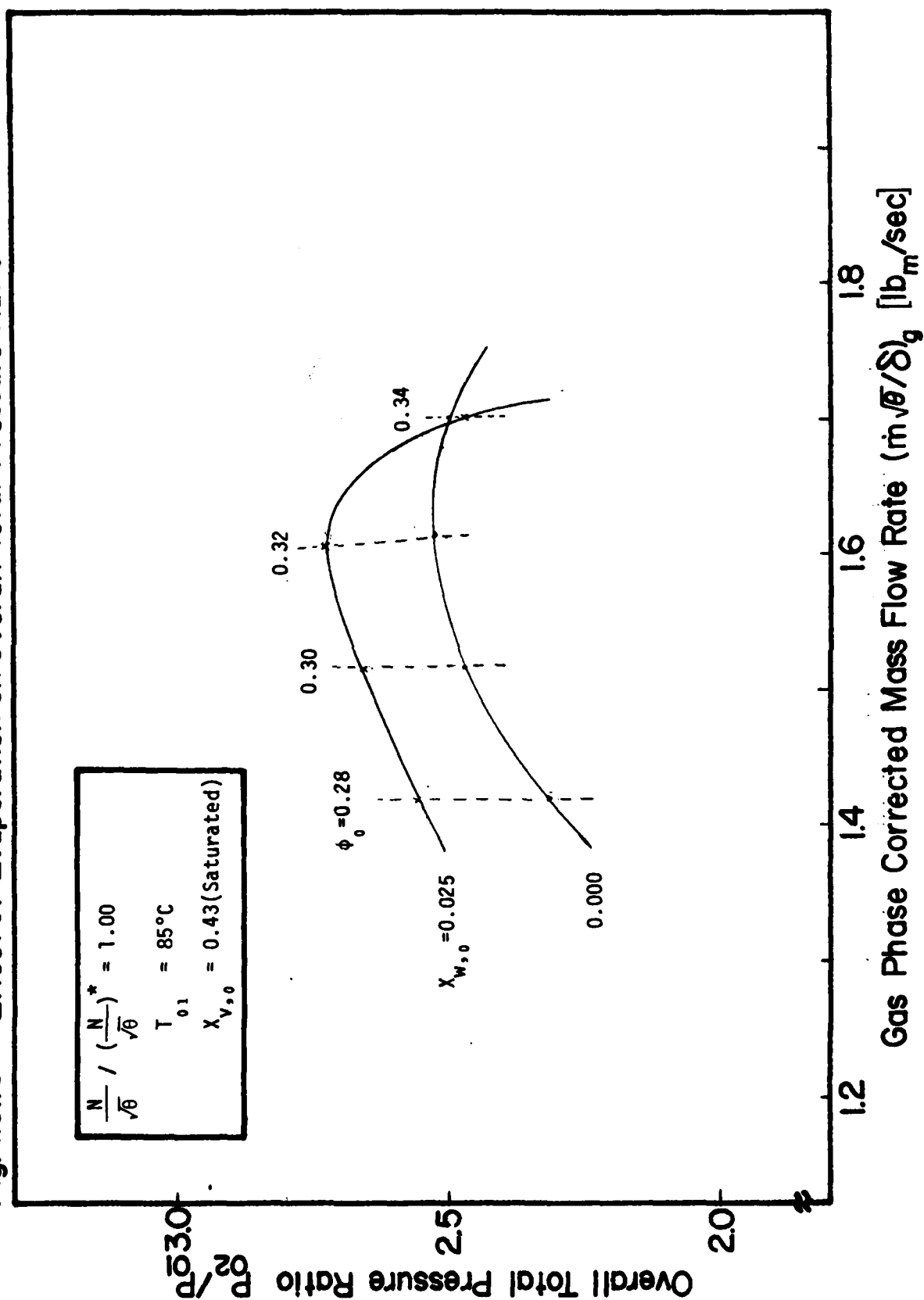


Fig.4.5.17 Effect of Evaporation on Overall Adiabatic Efficiency

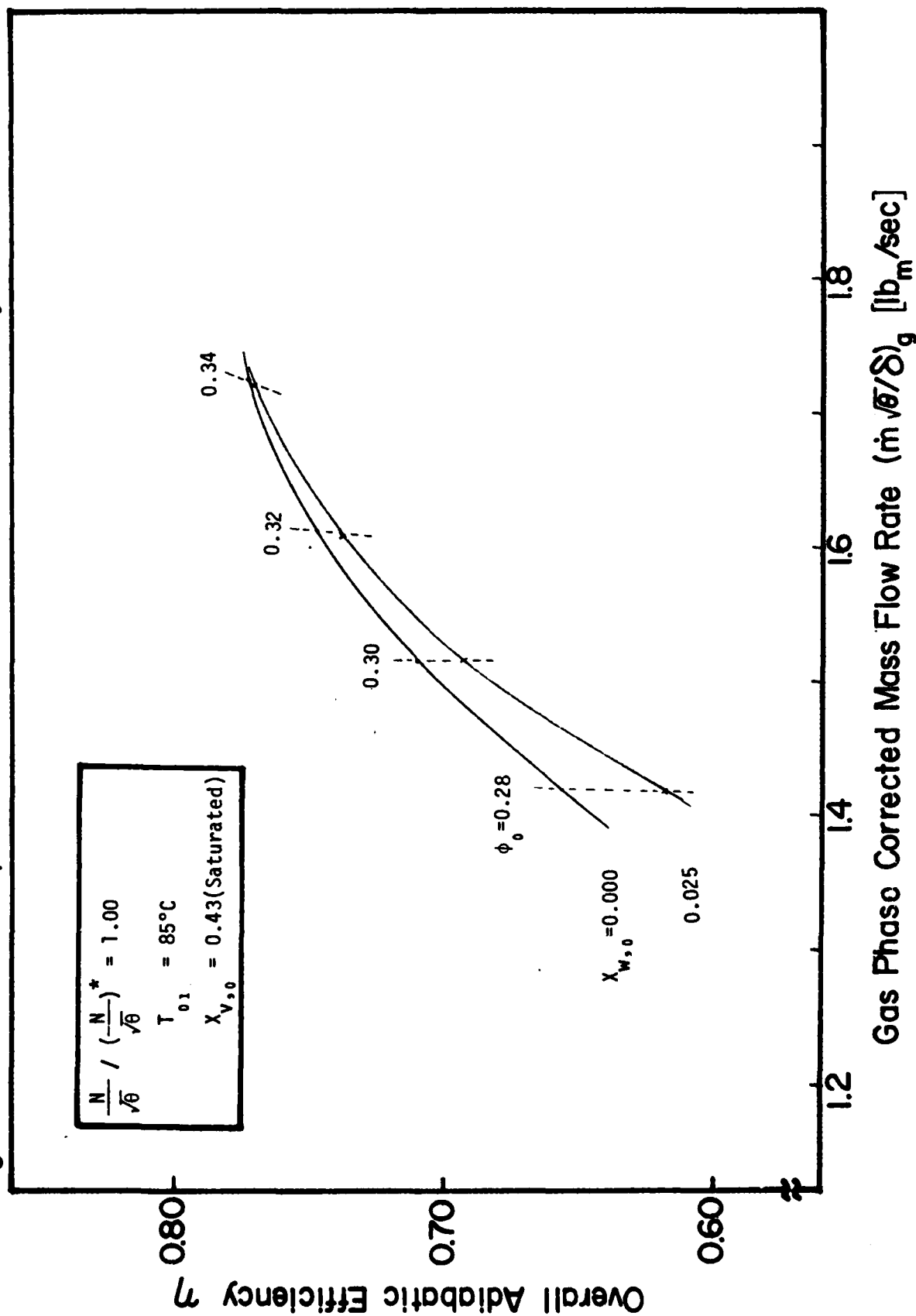


Fig.4.5.18 Effect of Evaporation on Temperature Change of Gas Phase and Droplet along Compressor Stages

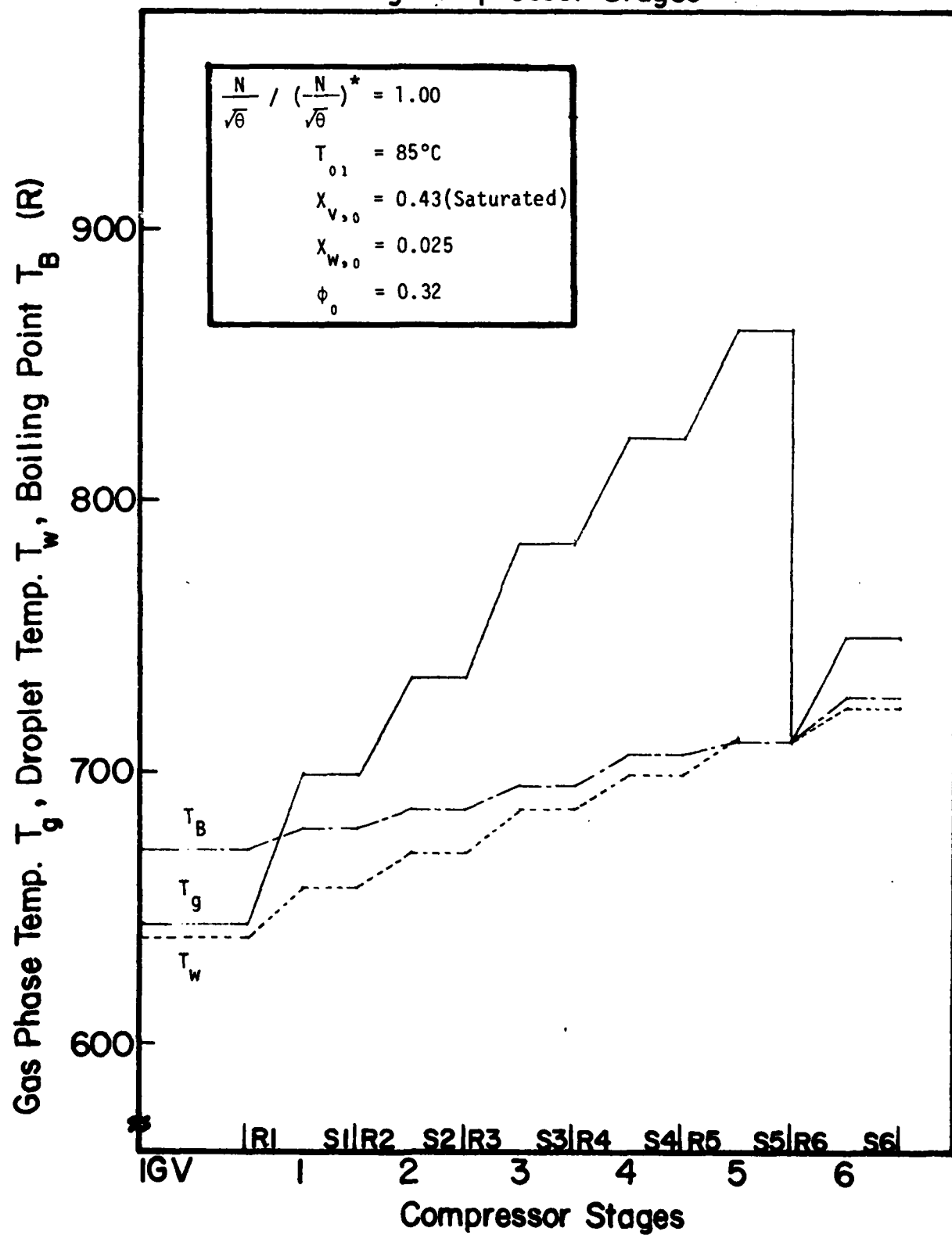


Fig.4.5.19 Effect of Evaporation on Mass Flow Rate of Liquid Phase at Tip along Compressor Stages

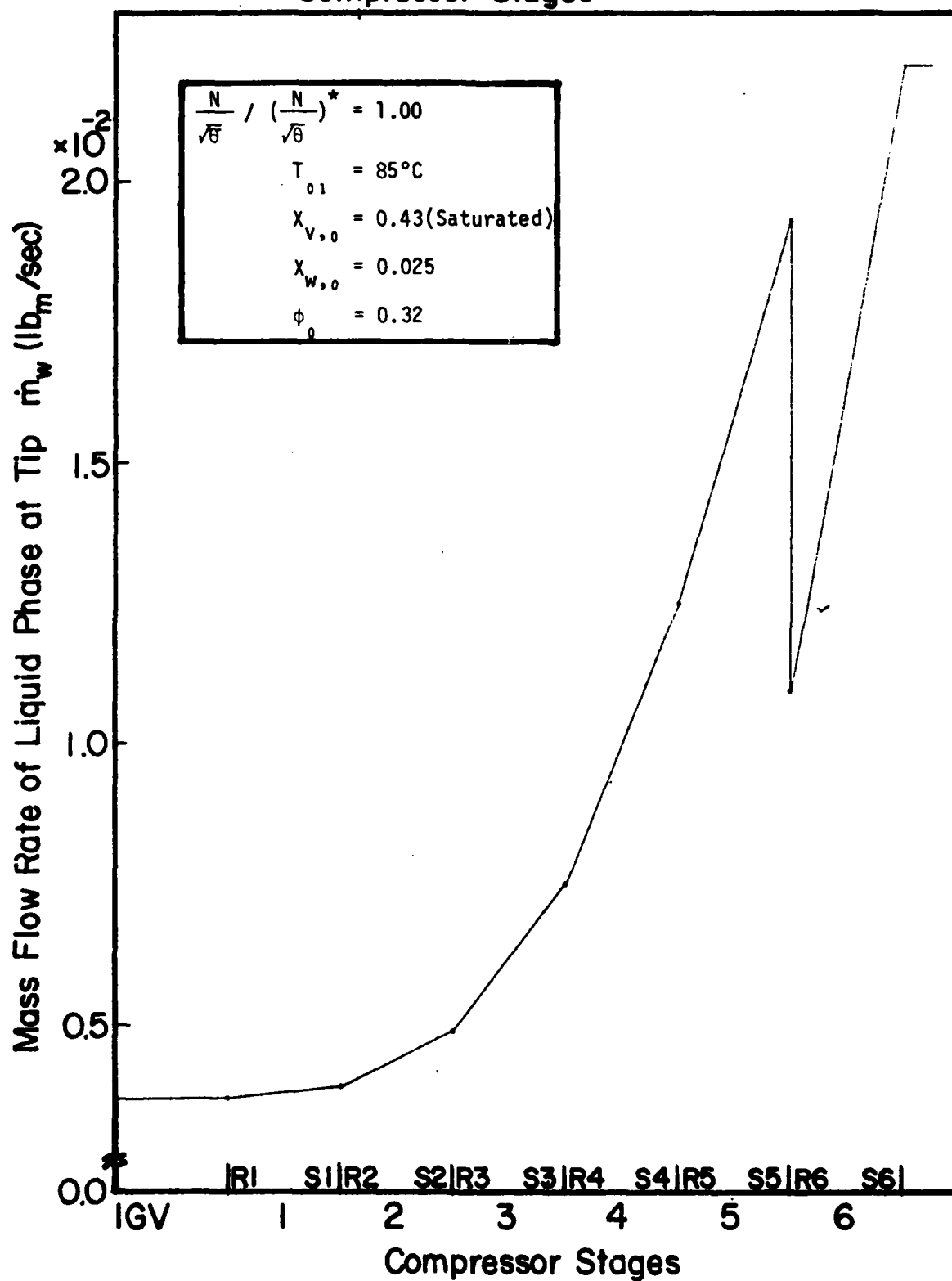


Fig.4.5.20 Effect of Evaporation on Mass Flow Rate of Gas Phase at Tip along Compressor Stages

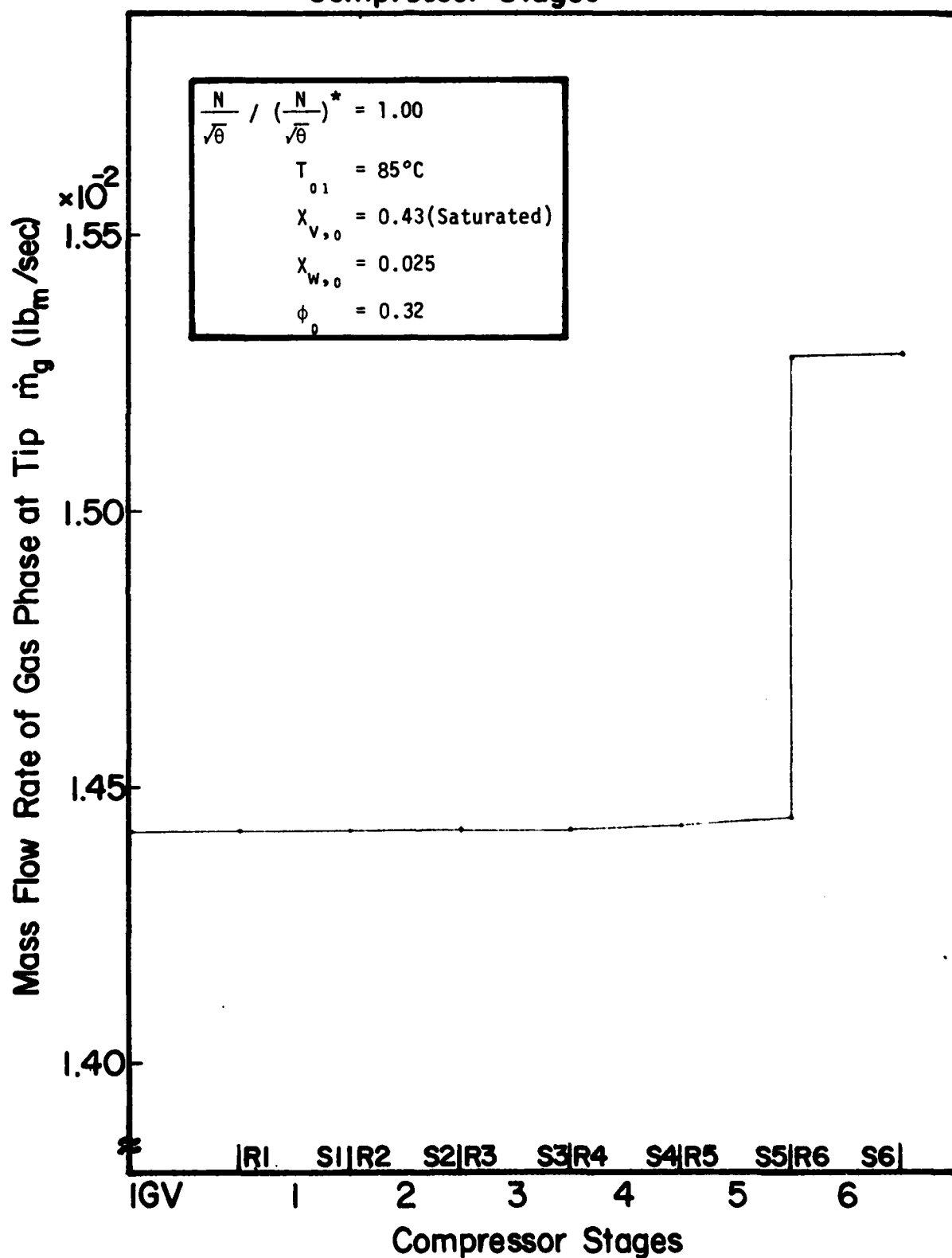


Fig.4.6.1 Effect of Water Ingestion on Overall Total Pressure Ratio

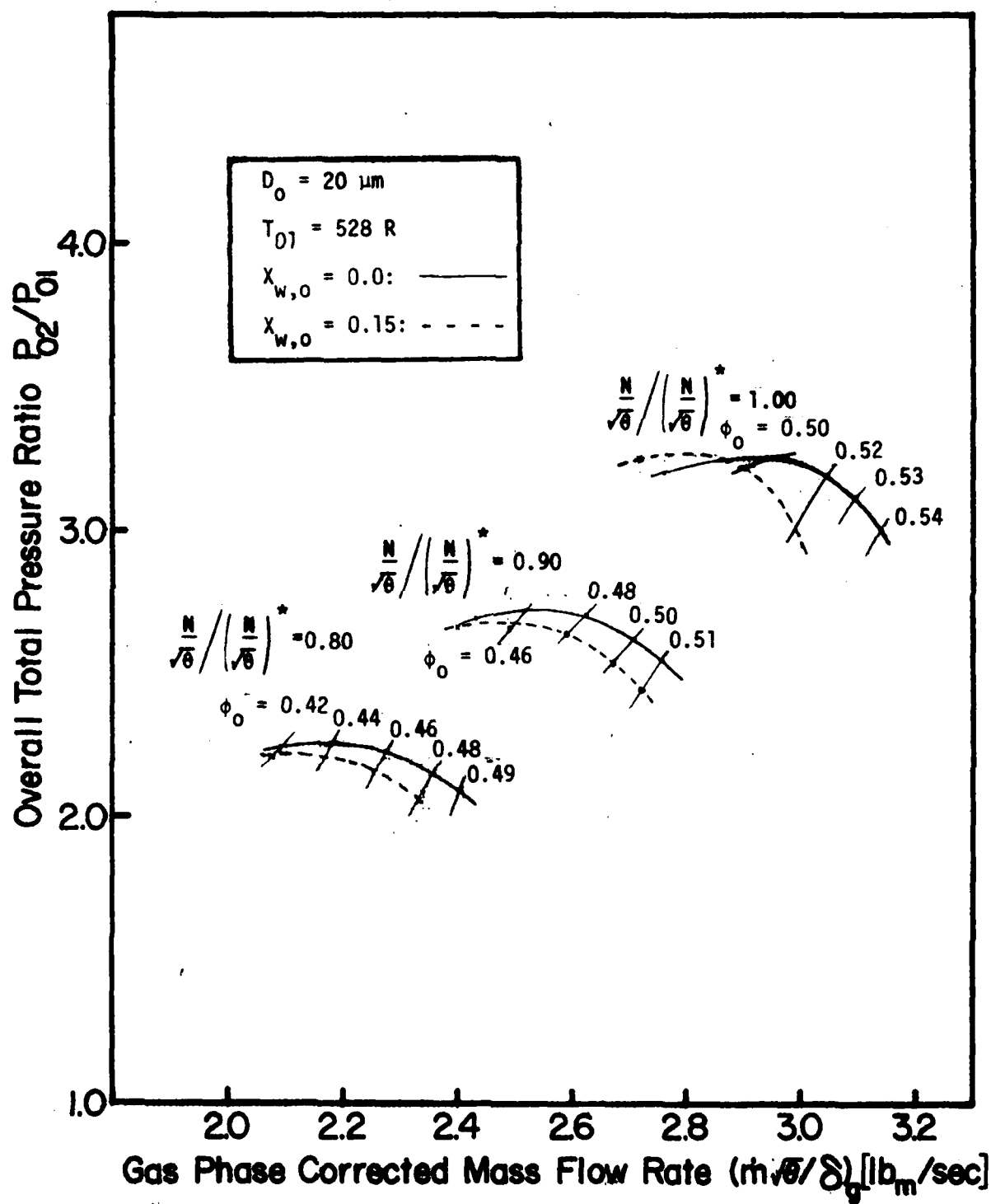


Fig.4.6.2 Effect of Water Ingestion on Overall Temperature Rise of Gas Phase

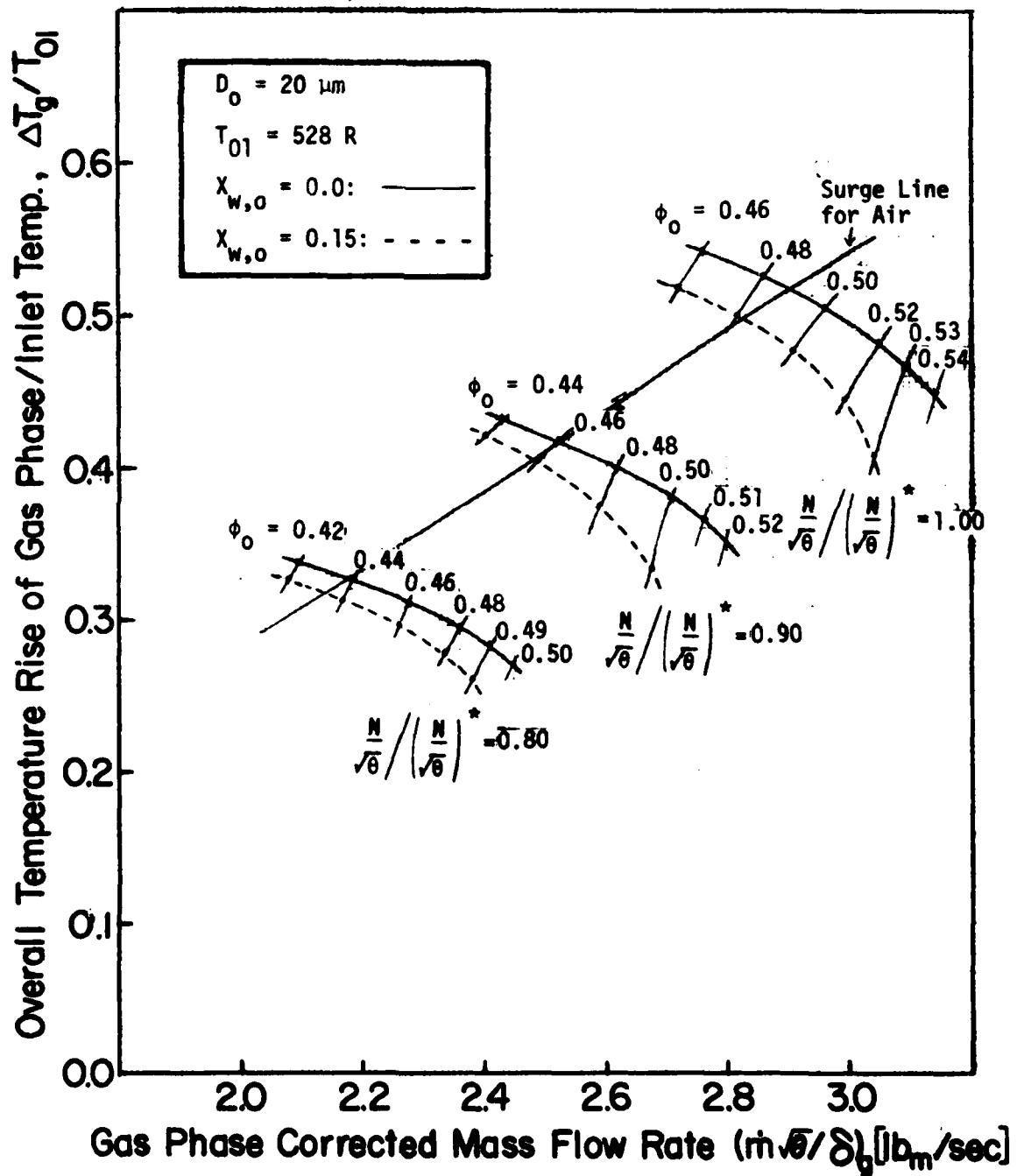


Fig.4.6.3 Effect of Water Ingestion on Overall Temperature Rise of Droplet

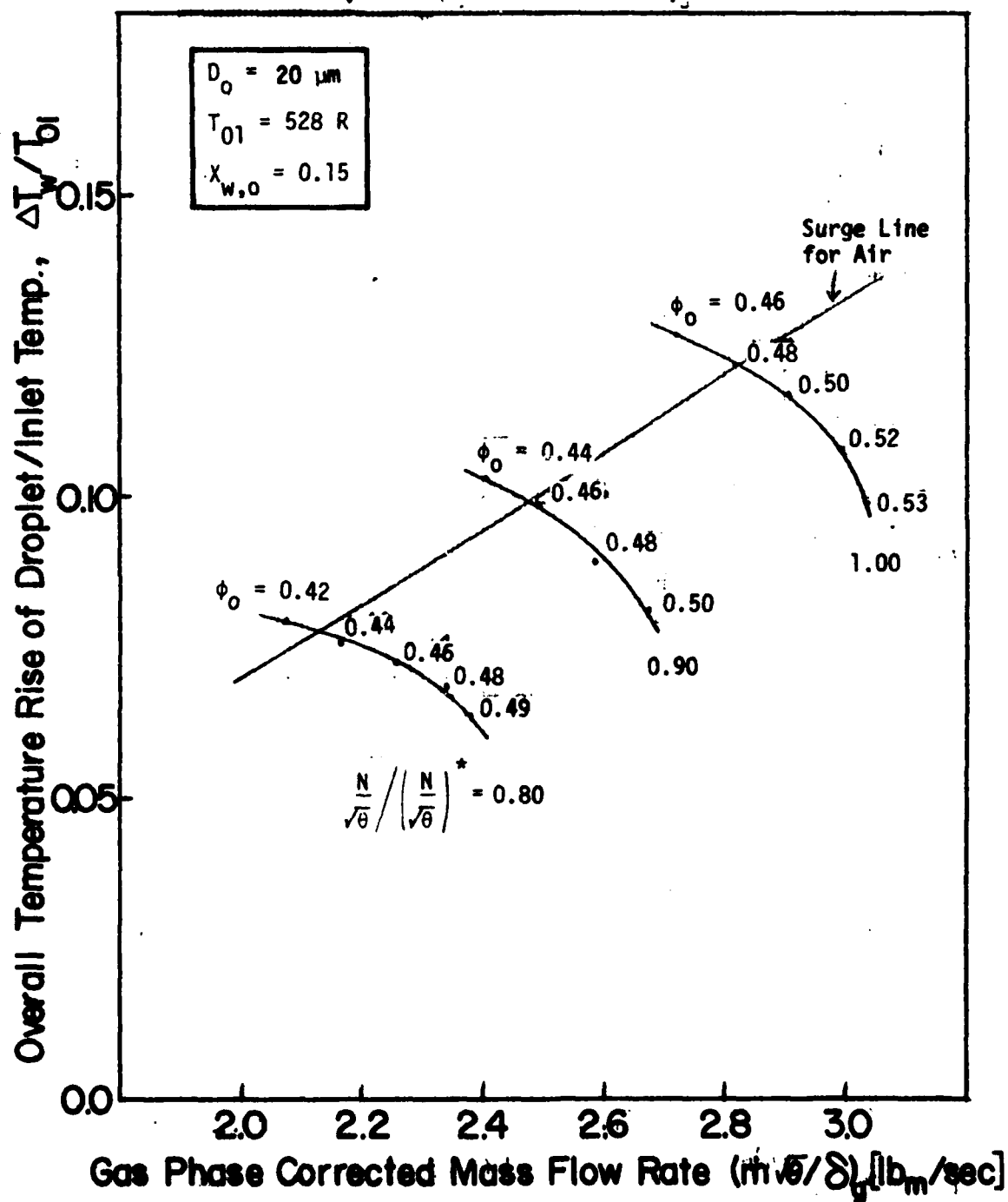


Fig.4.6.4 Effect of Water Ingestion on Work Done

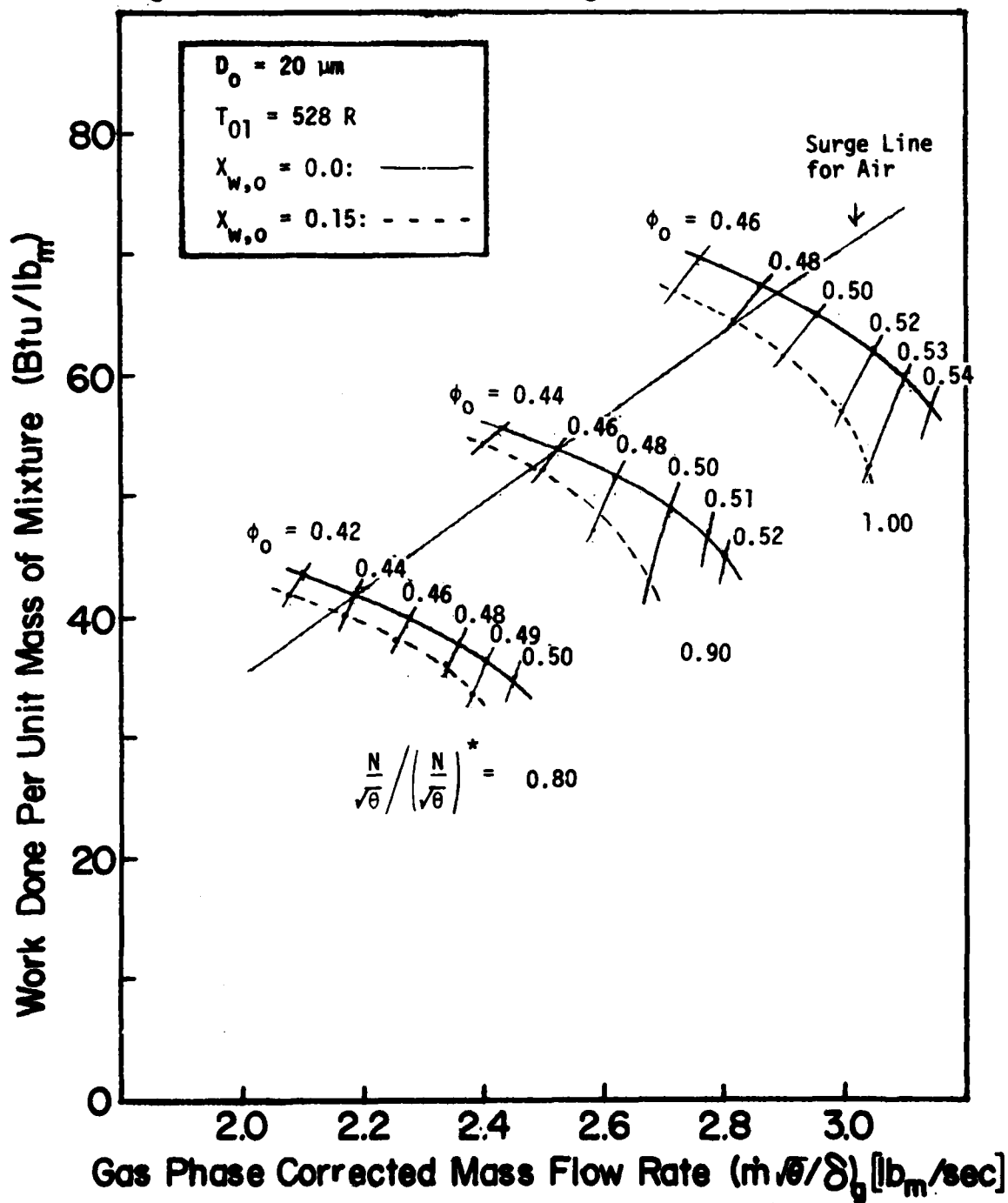


Fig.4.6.5 Effect of Water Ingestion on Overall Total Pressure Ratio

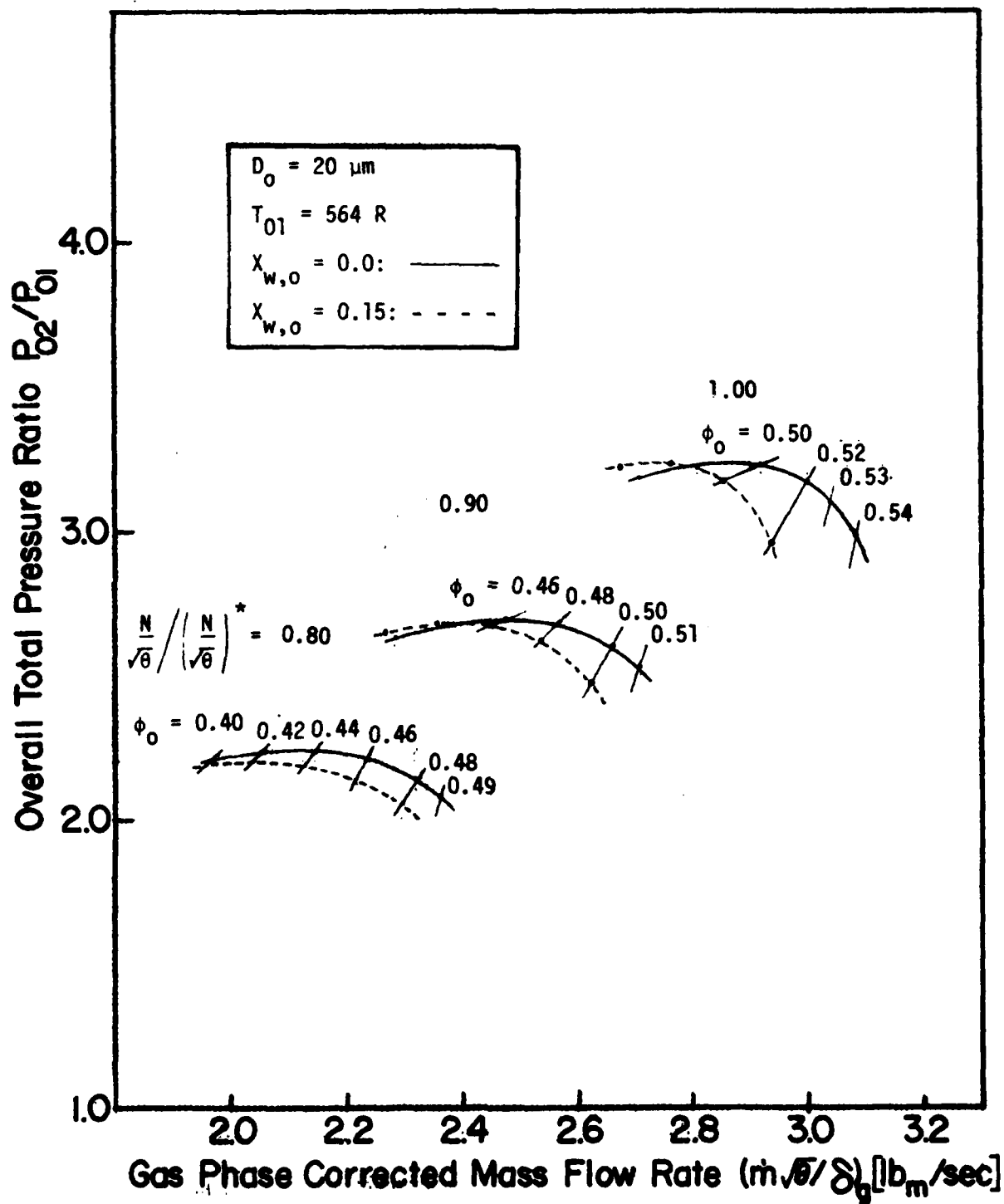


Fig.4.6.6 Effect of Water Ingestion on Overall Temperature Rise of Gas Phase

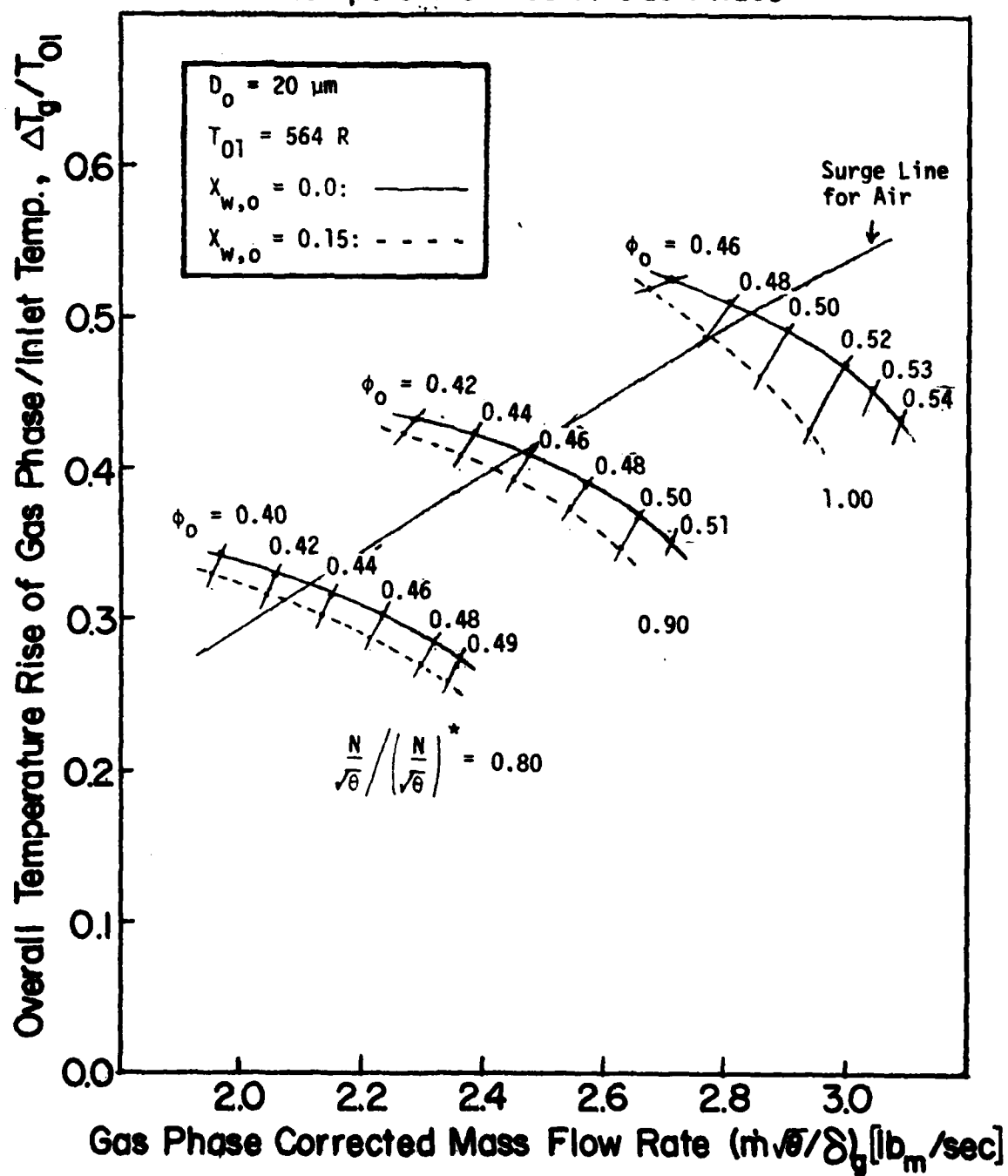


Fig.4.6.7 Effect of Water Ingestion on Overall Temperature Rise of Droplet

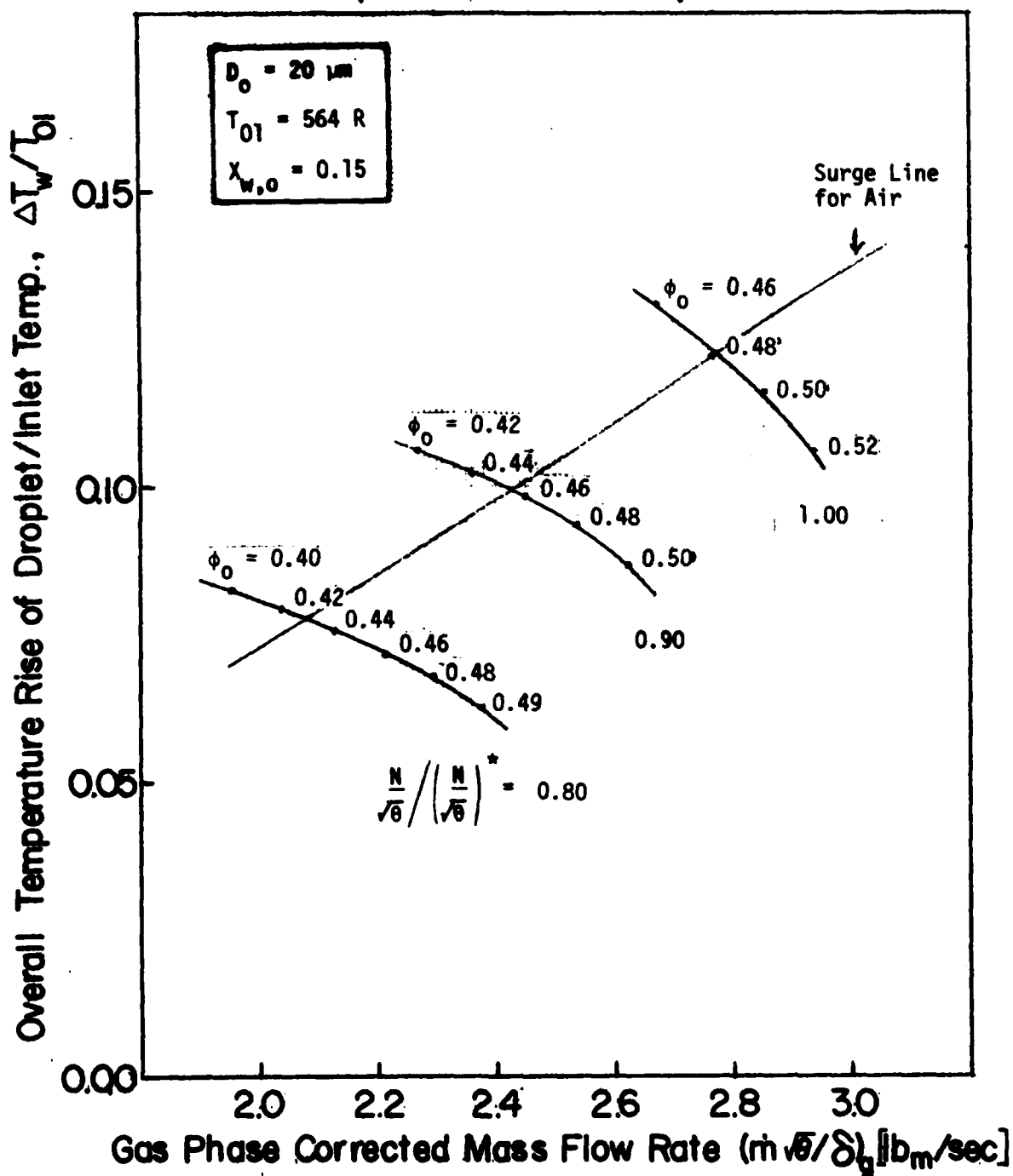


Fig.4.6.8 Effect of Water Ingestion on Work Done

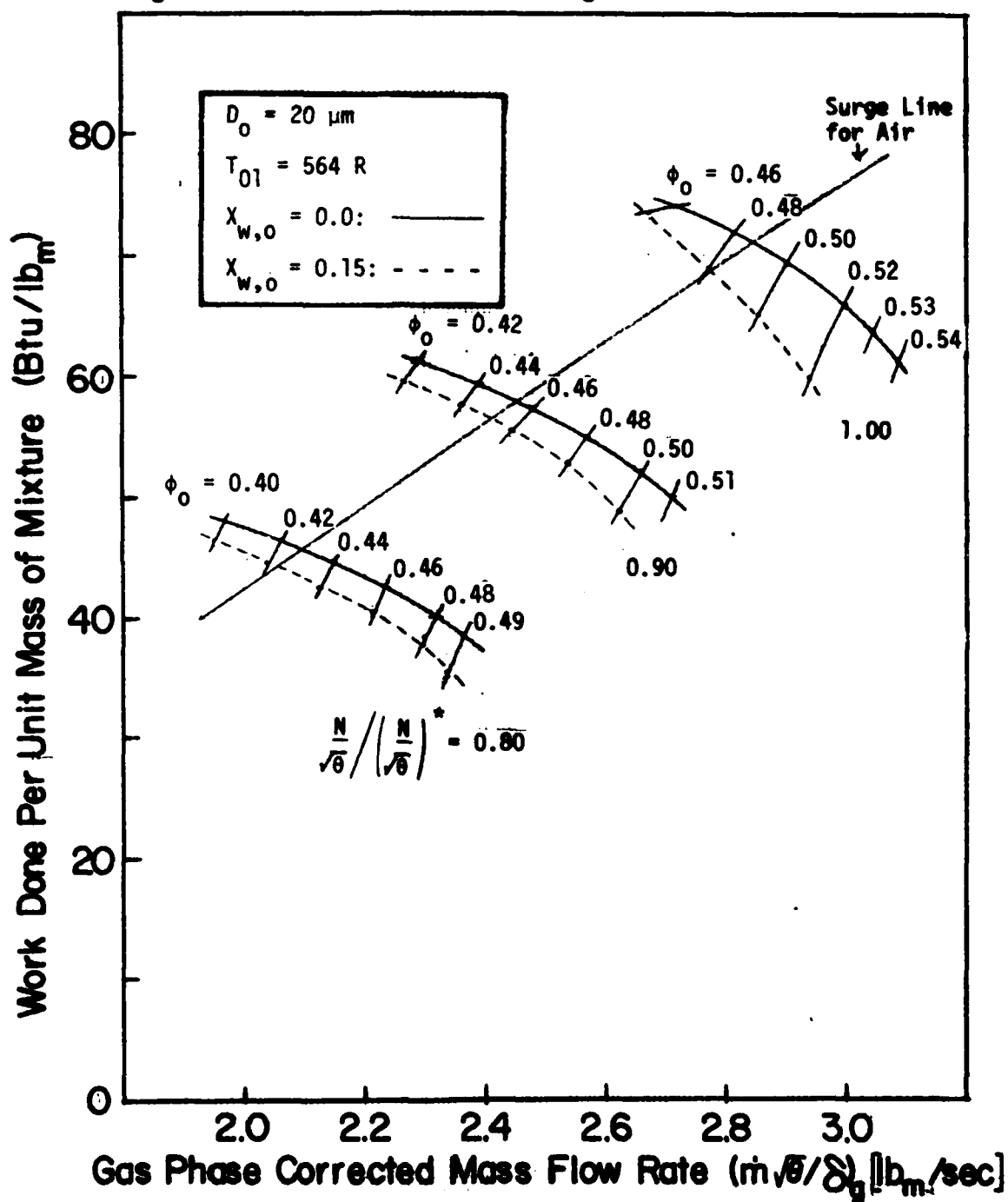


Fig.4.6.9 Effect of Water Ingestion on Overall Total Pressure Ratio

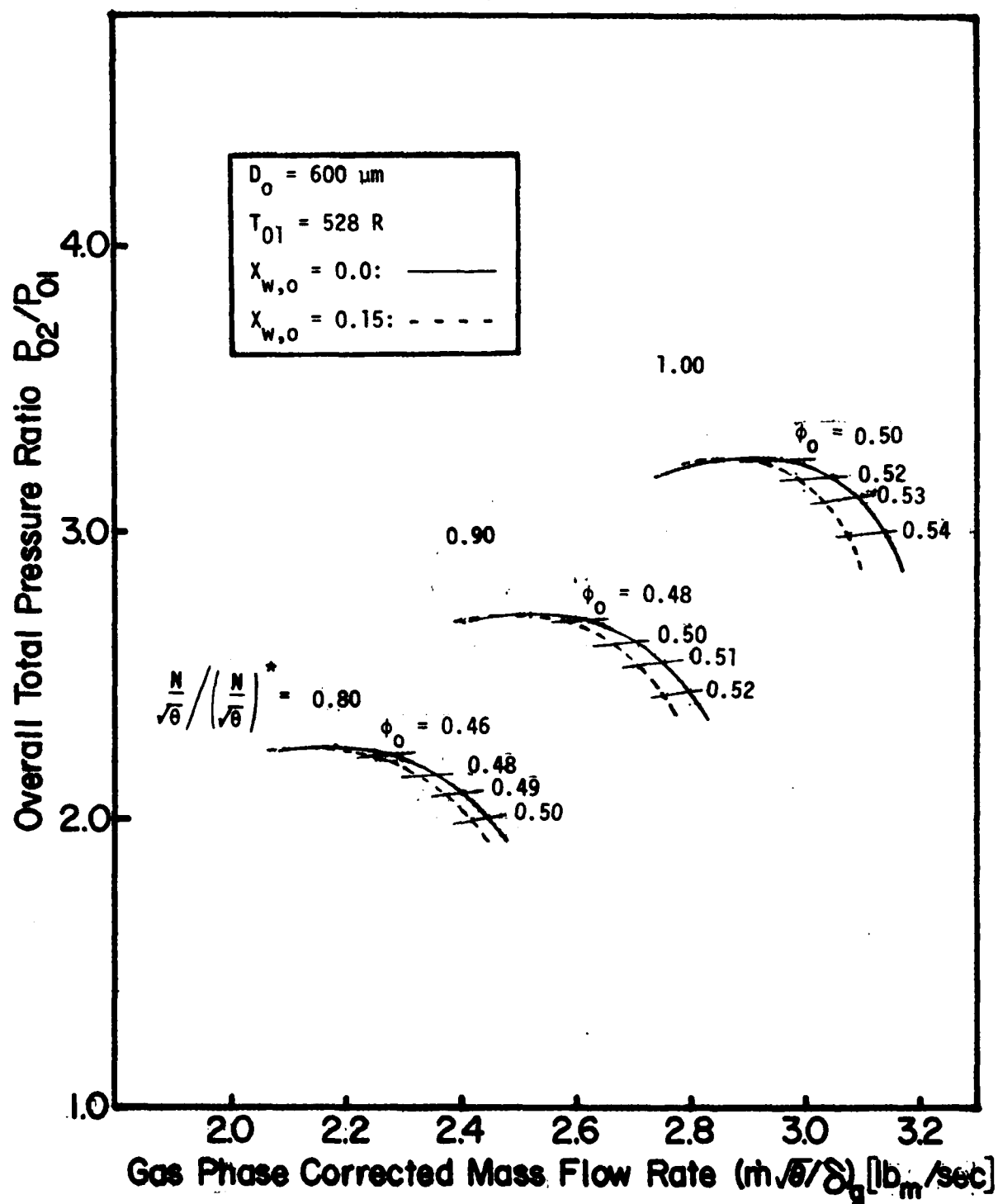


Fig.4.6.10 Effect of Water Ingestion on Overall Temperature Rise of Gas Phase

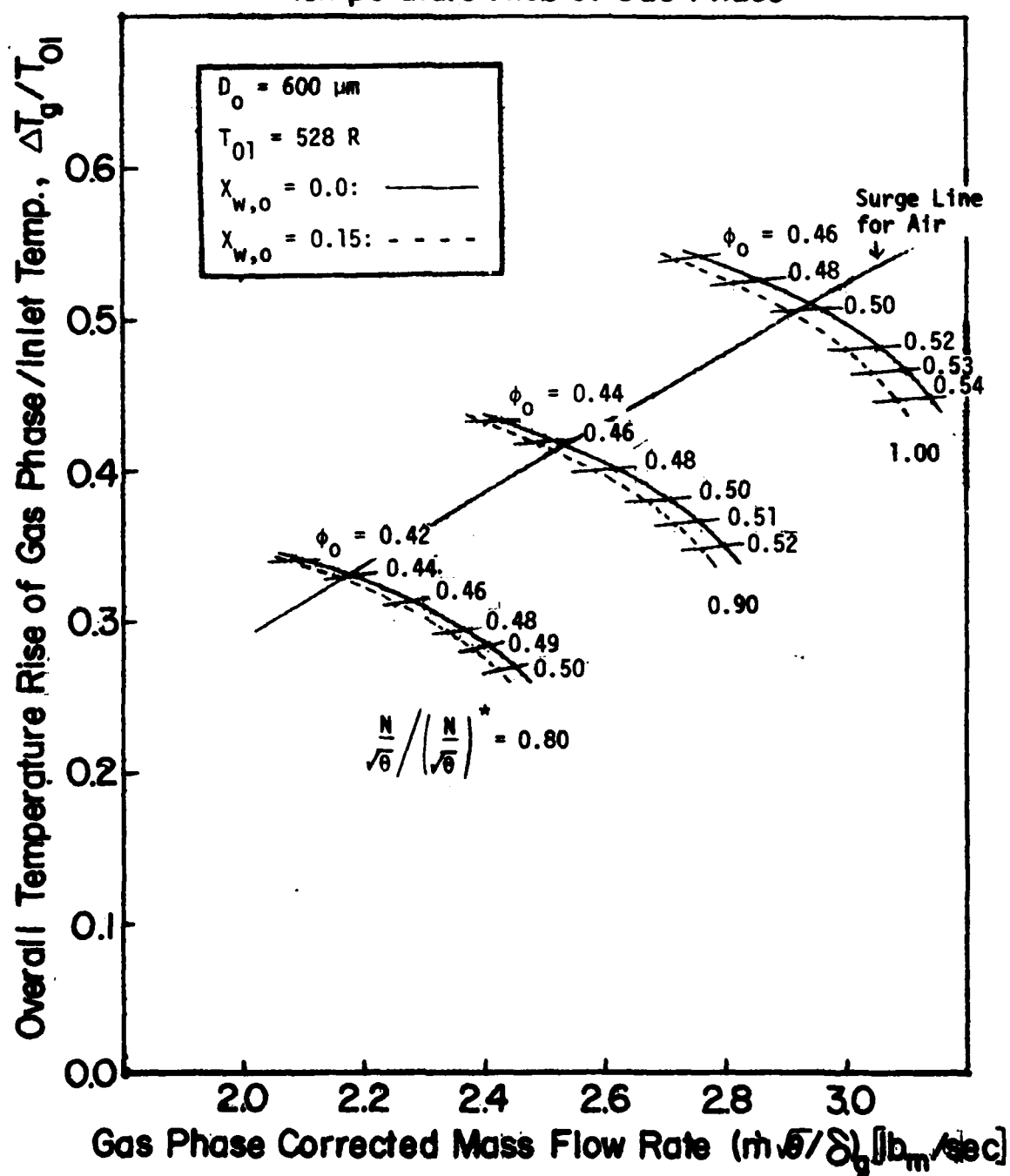


Fig.4.6.11 Effect of Water Ingestion on Overall Temperature Rise of Droplet

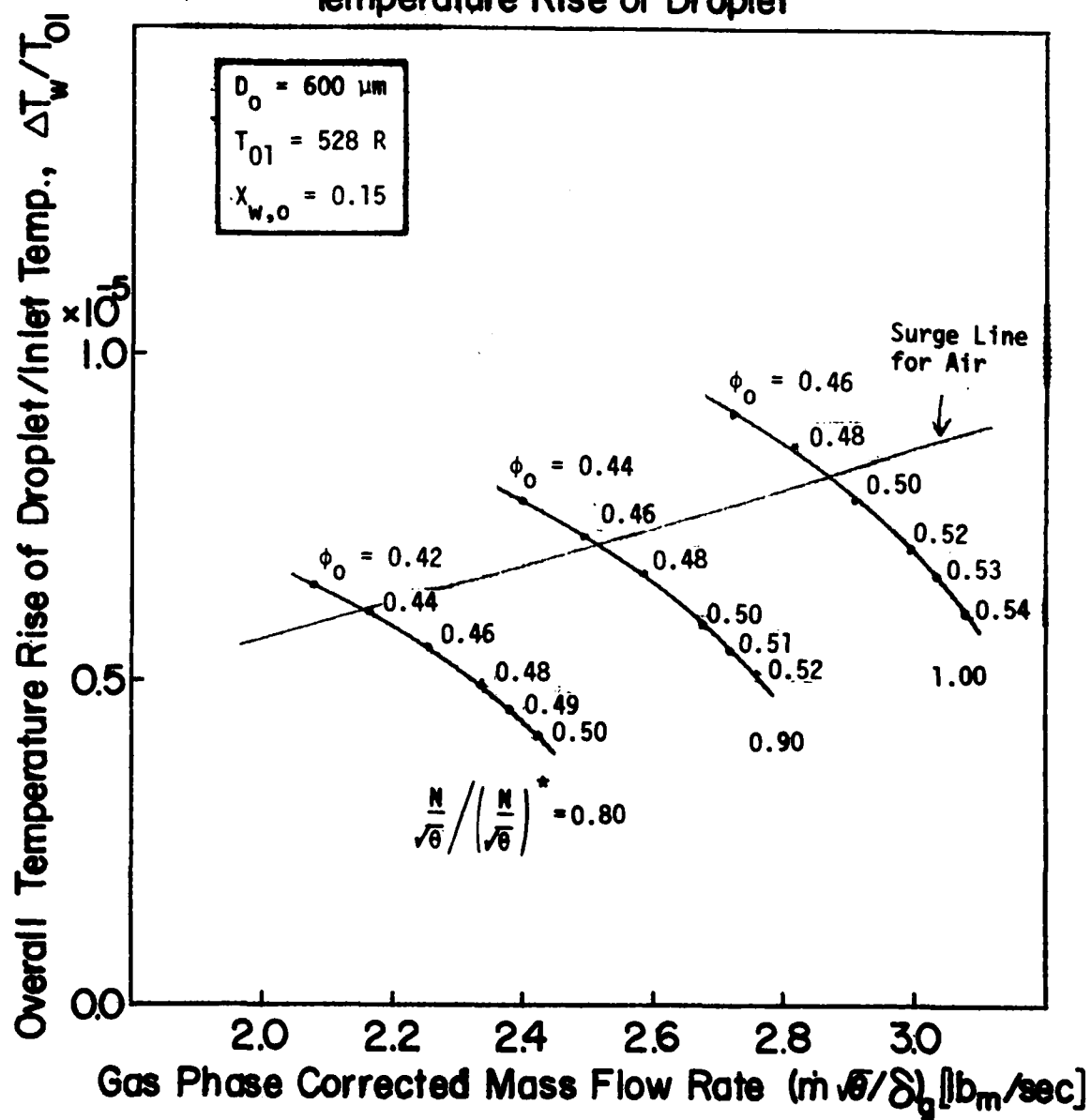


Fig.4.6.12 Effect of Water Ingestion on Work Done

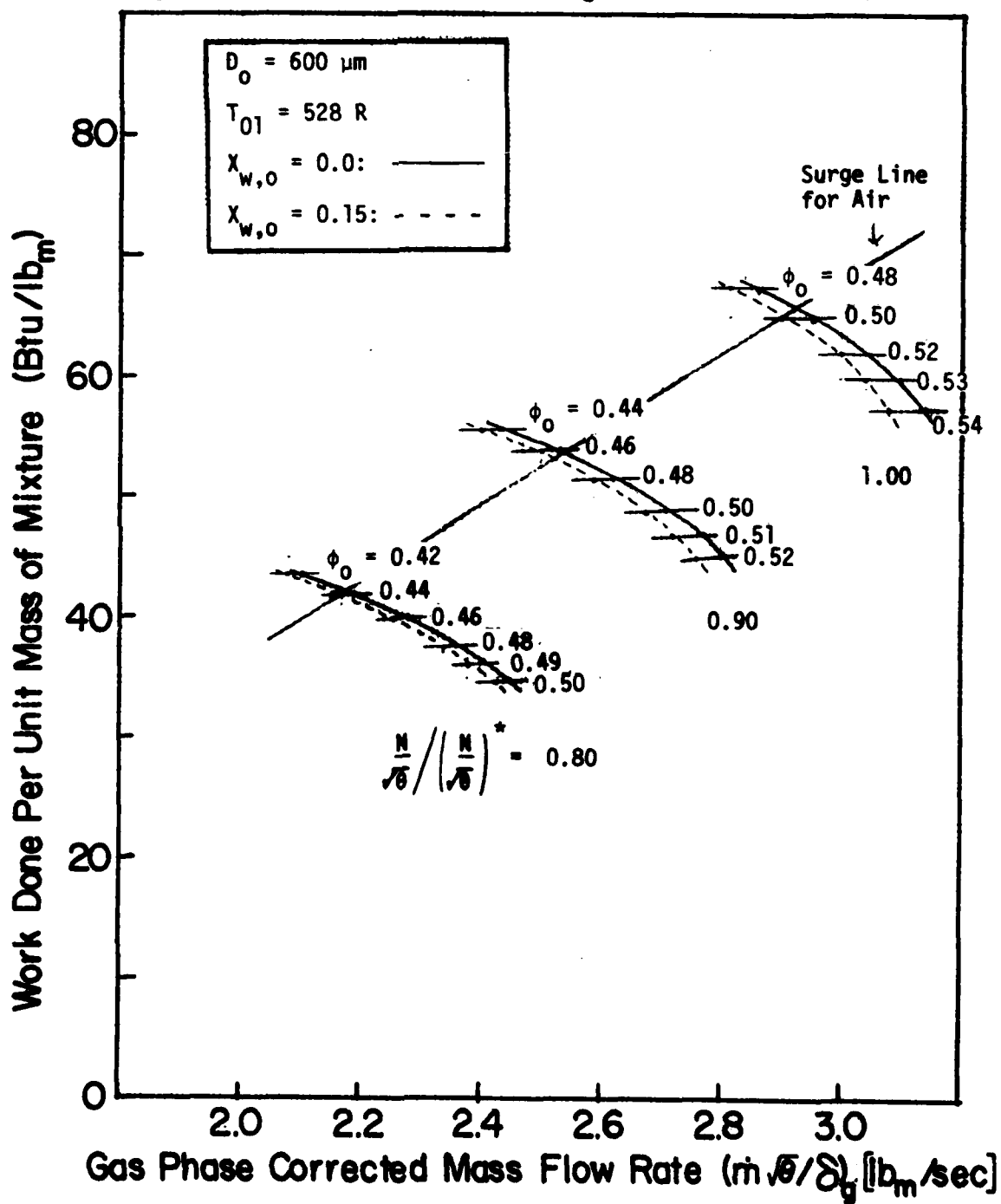


Fig.4.6.13 Effect of Water Ingestion on Overall Total Pressure Ratio

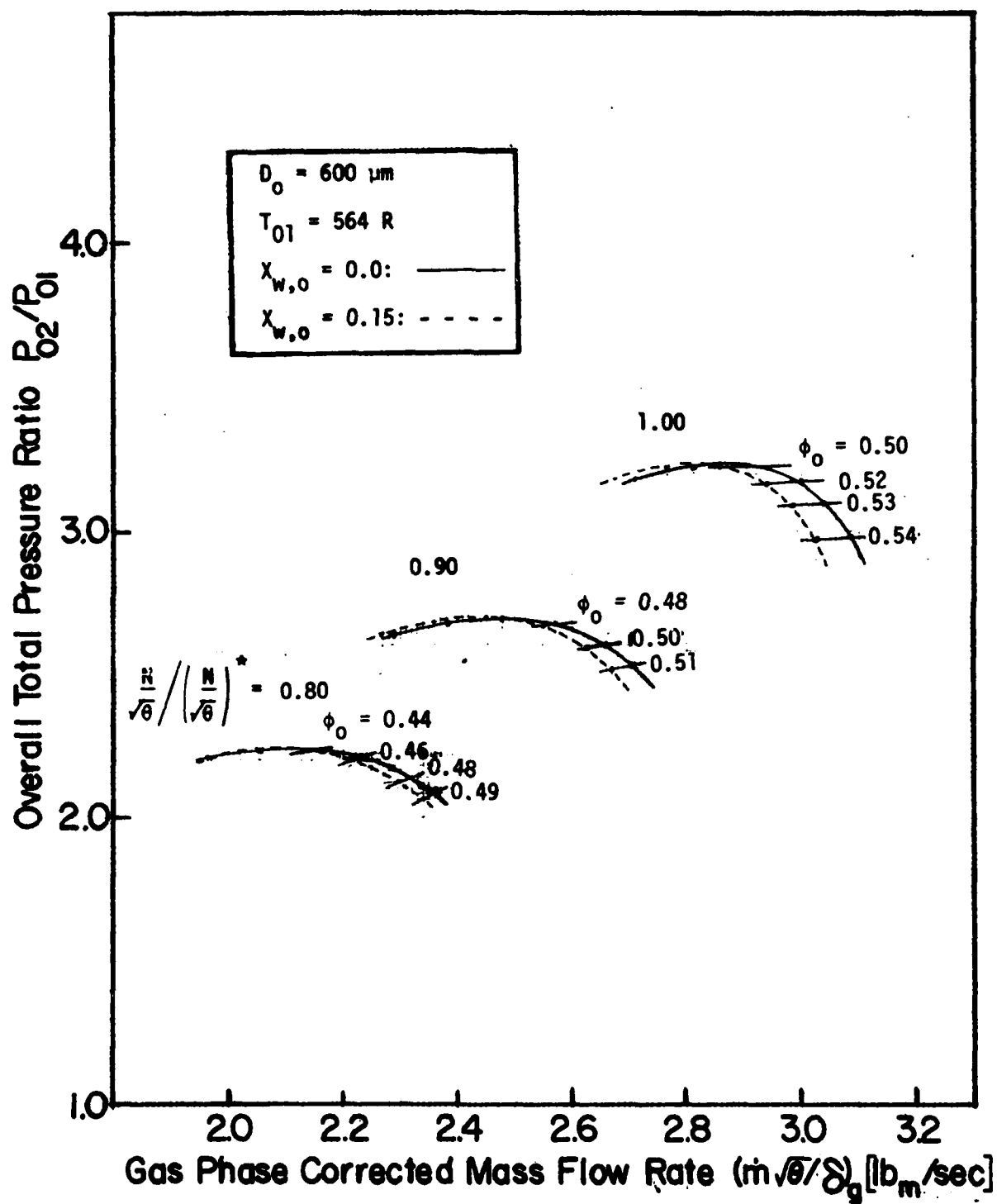


Fig.4.6.14 Effect of Water Ingestion on Overall Temperature Rise of Gas Phase

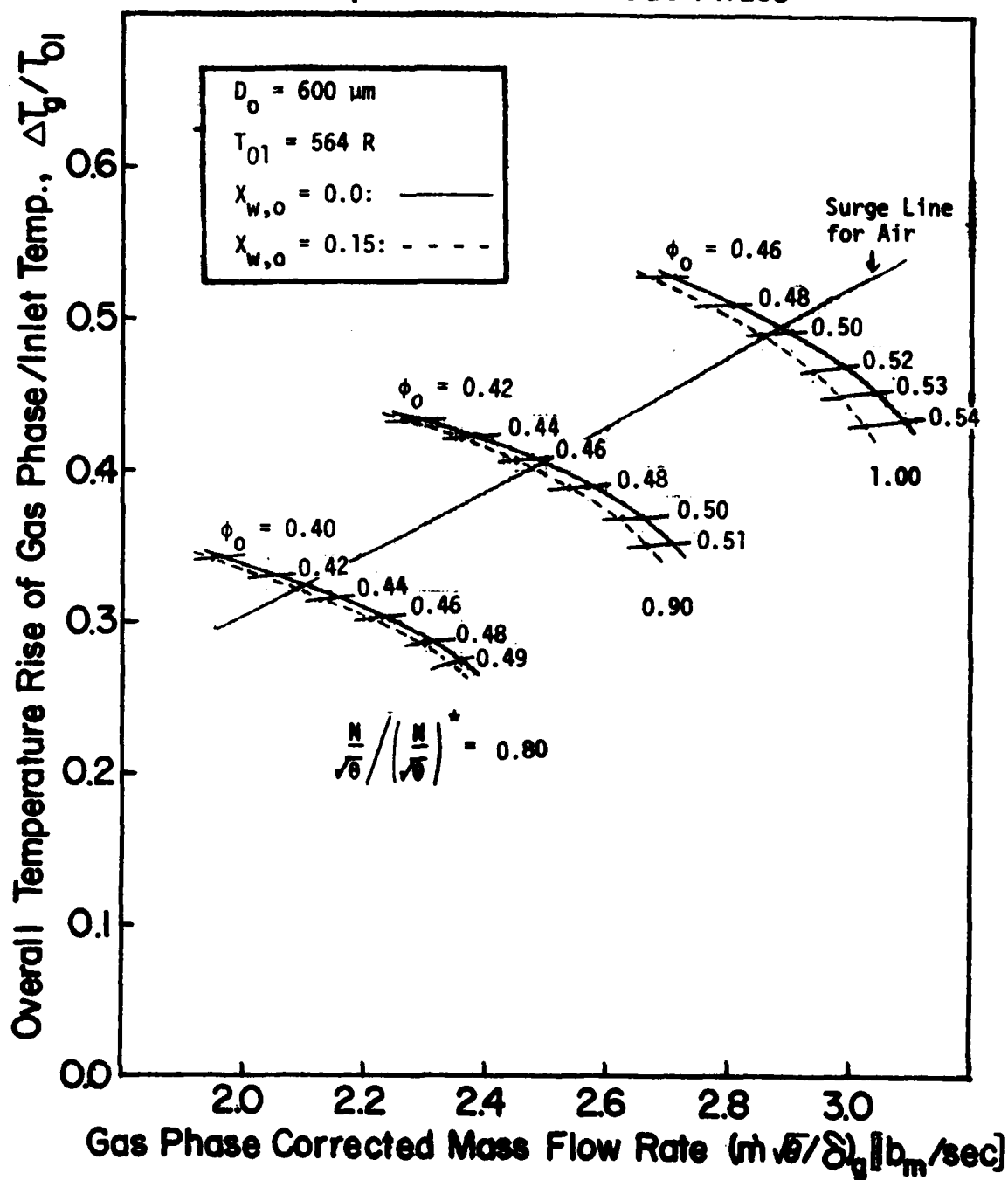


Fig.4.6.15 Effect of Water Ingestion on Overall Temperature Rise of Droplet

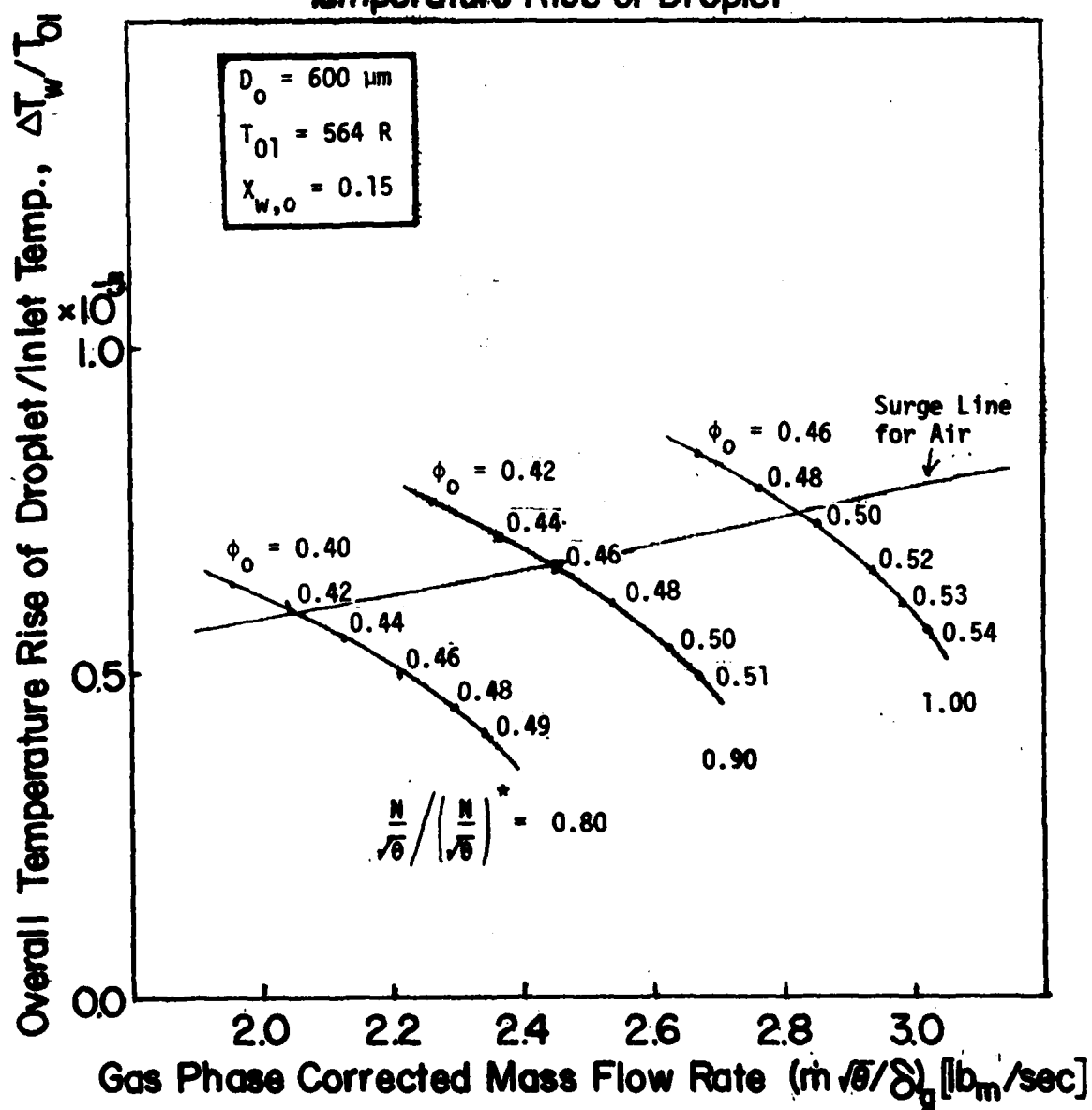


Fig.4.6.16 Effect of Water Ingestion on Work Done

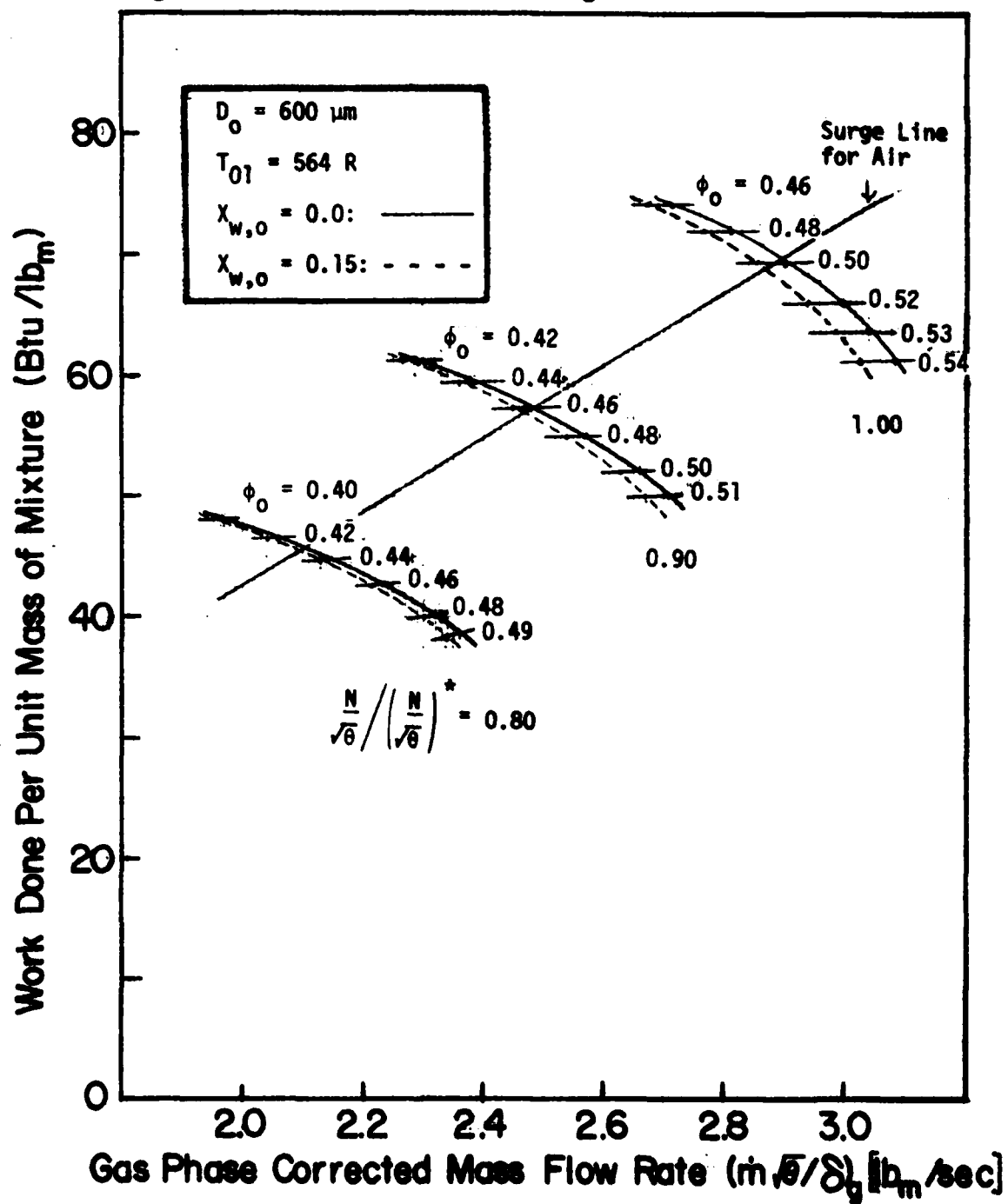


Fig.4.6.17 Effect of Initial Water Content and Flow Rates on Compressor Performance

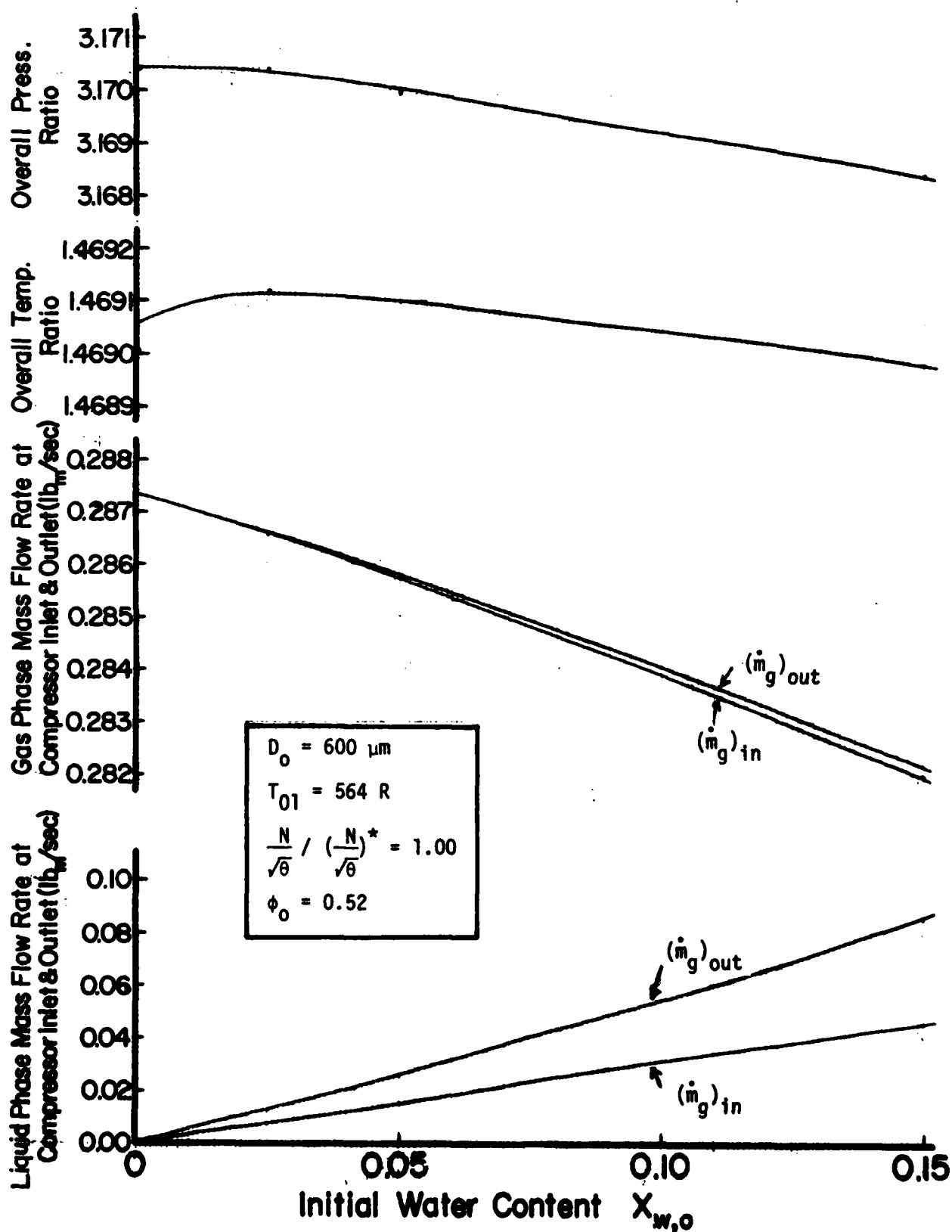
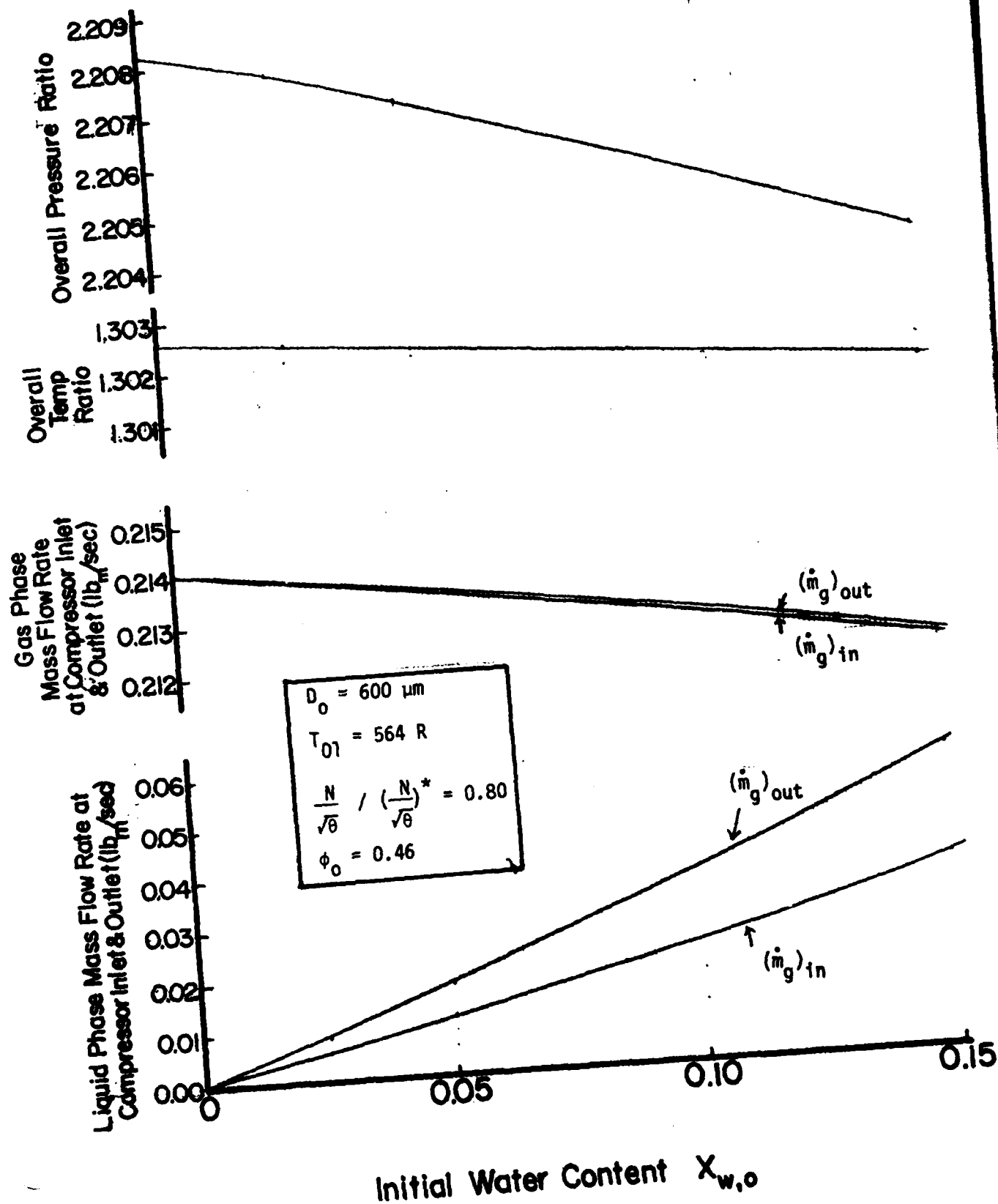


Fig.4.6.18 Effect of Initial Water Content and Flow Rates on Compressor Performance



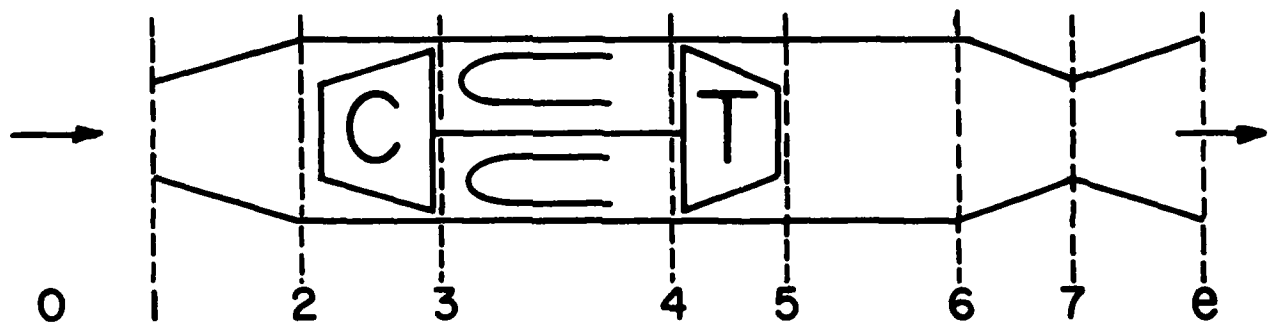


Fig. 5.1 Simple Constant Geometry Jet Engine

Fig.5.3.1 Radial Displacement of Water Droplet due to Centrifugal Effect

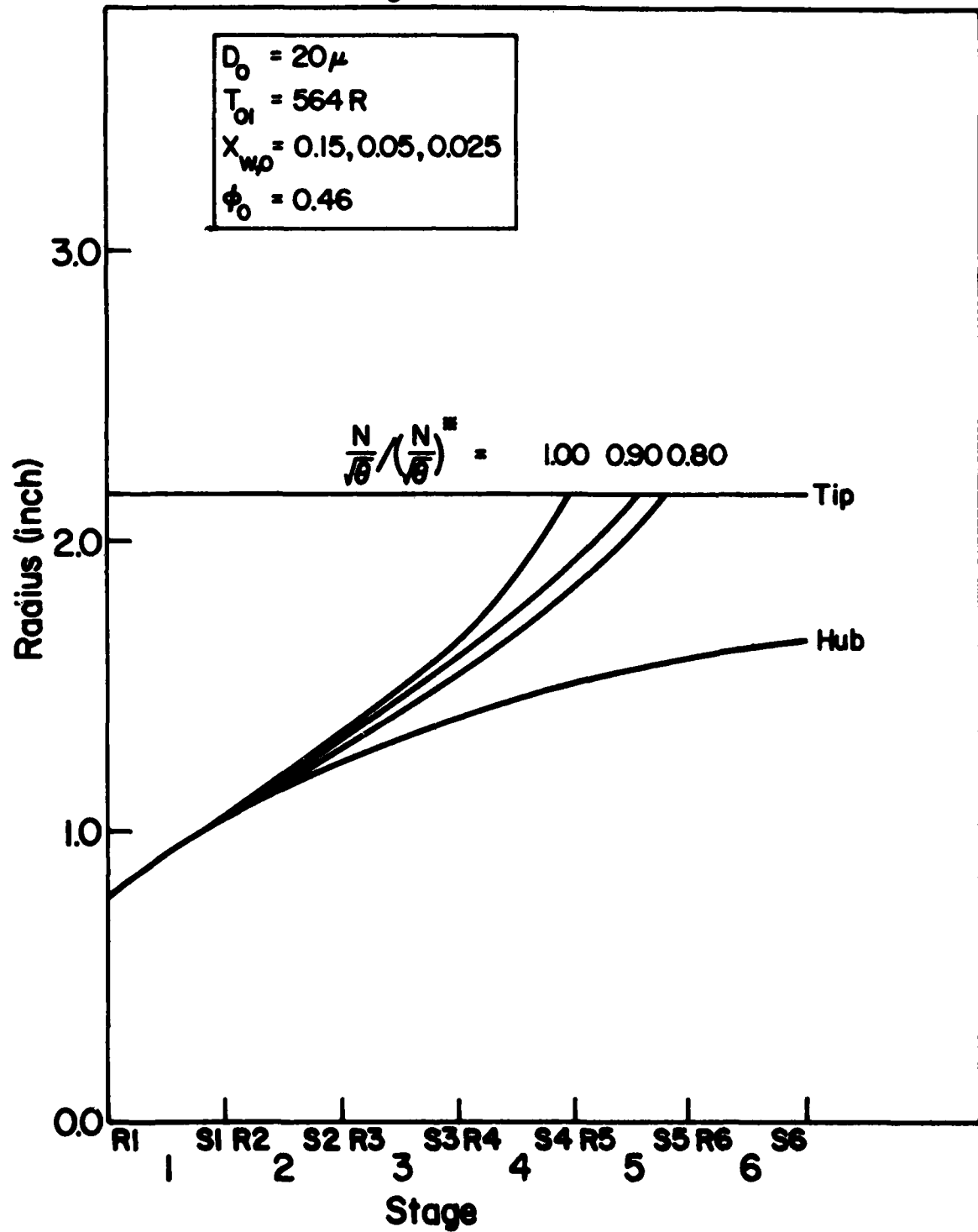


Fig.5.3.2 Radial Displacement of Water Droplet due to Centrifugal Effect

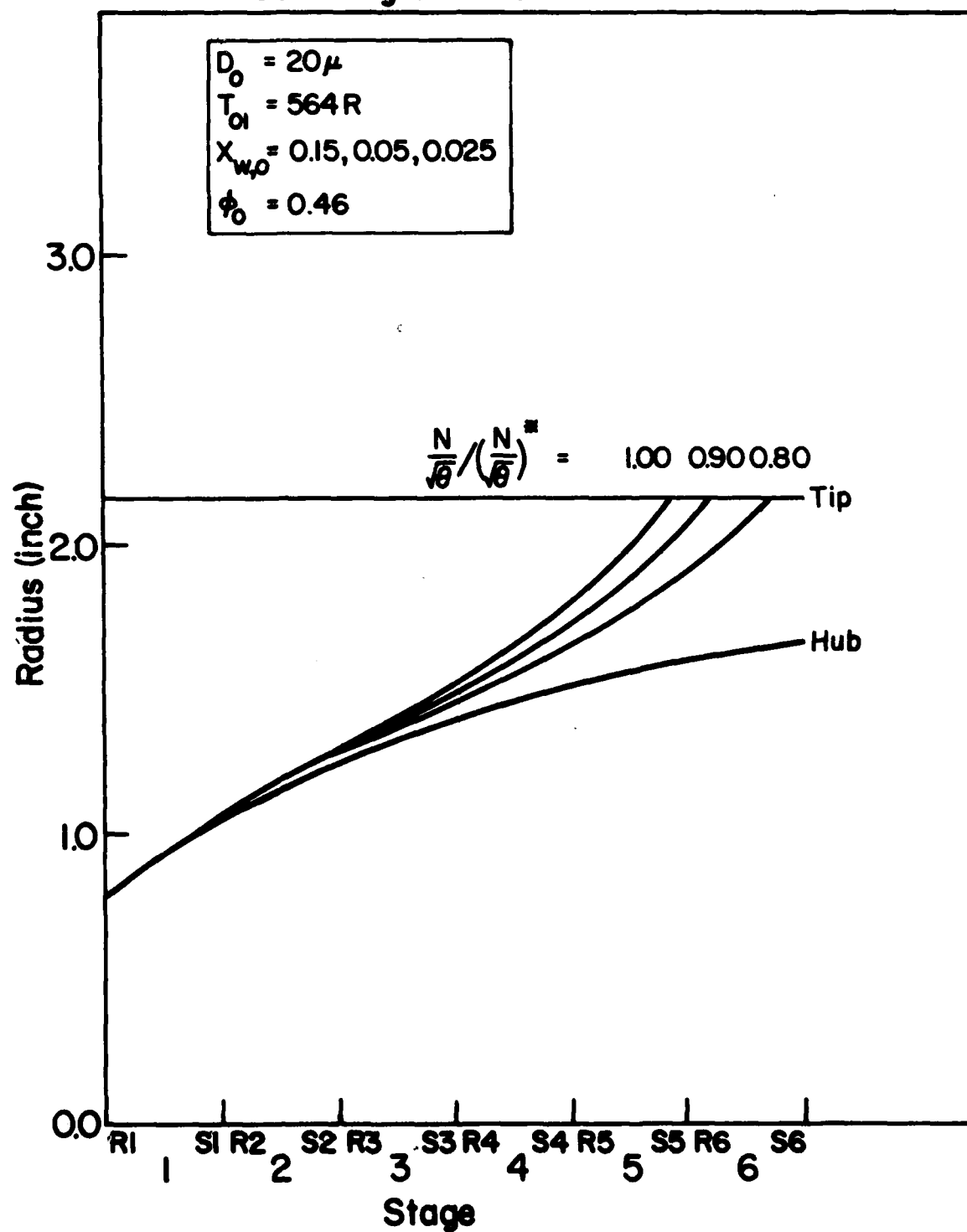


Fig.5.3.3 Change of Mass Flow Rate of Water at Hub along Compressor

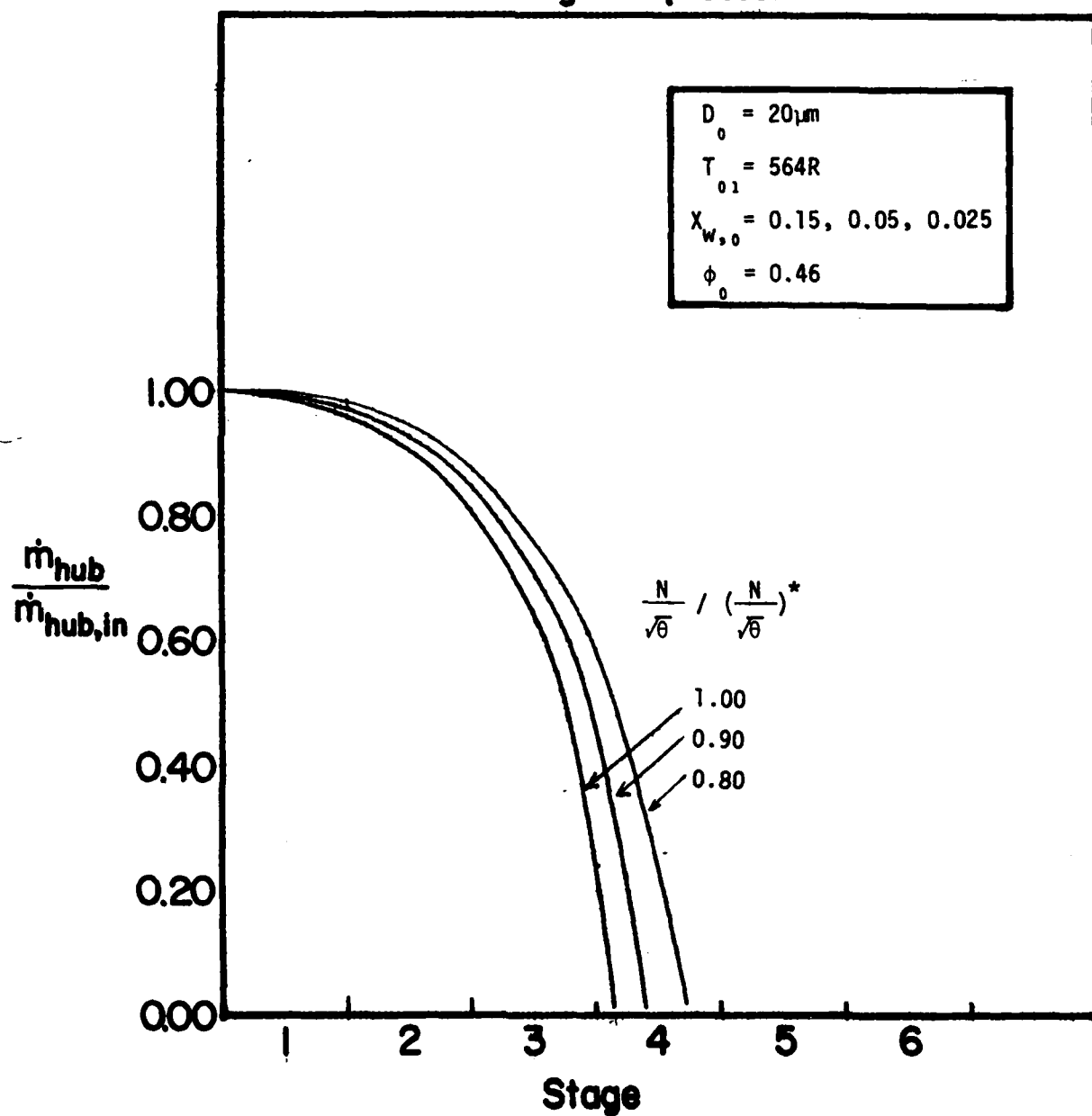


Fig.5.3.4 Change of Mass Flow Rate of Water at Hub along Compressor

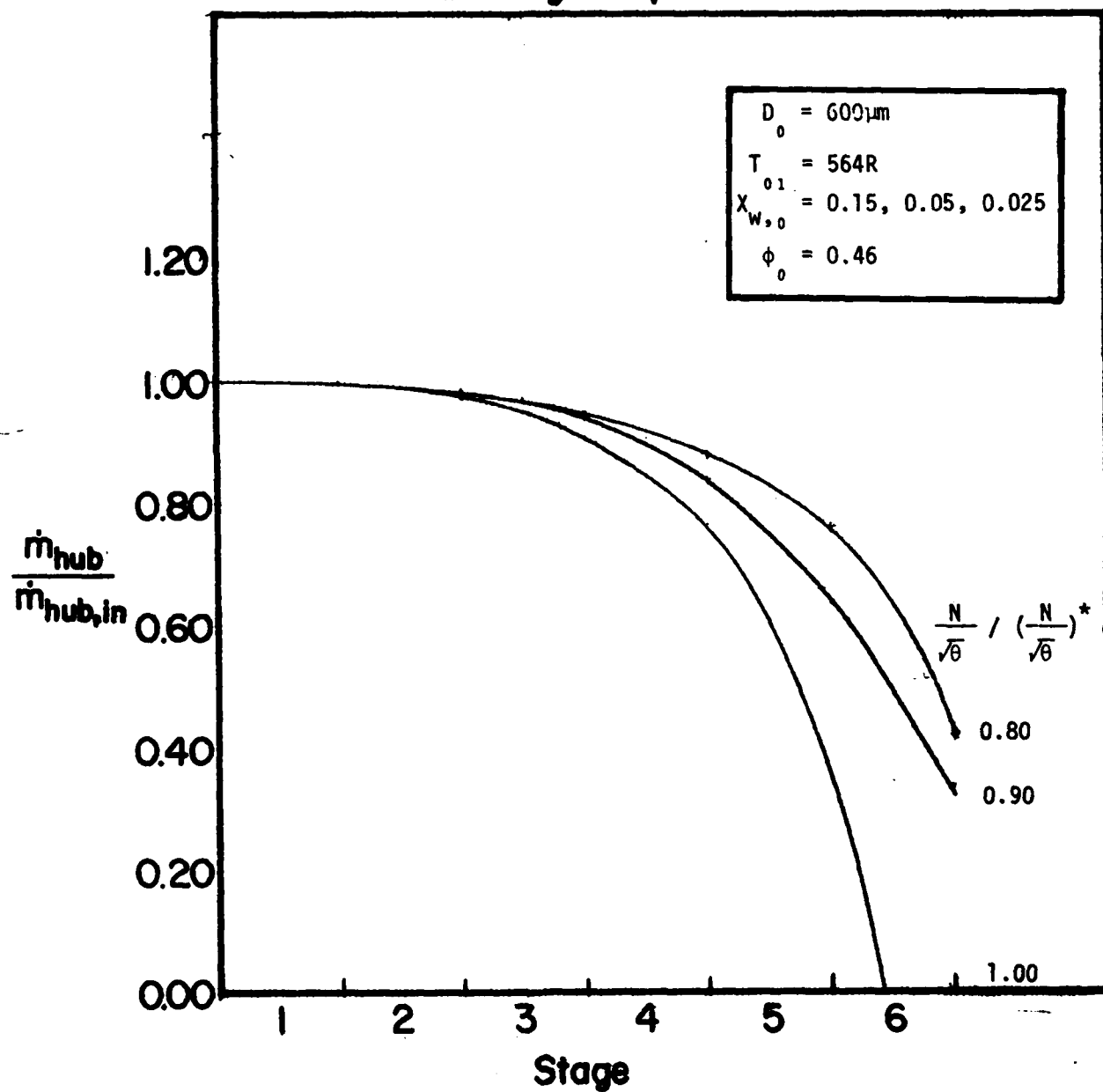


Fig. 5.3.5 Geometry of Test Compressor

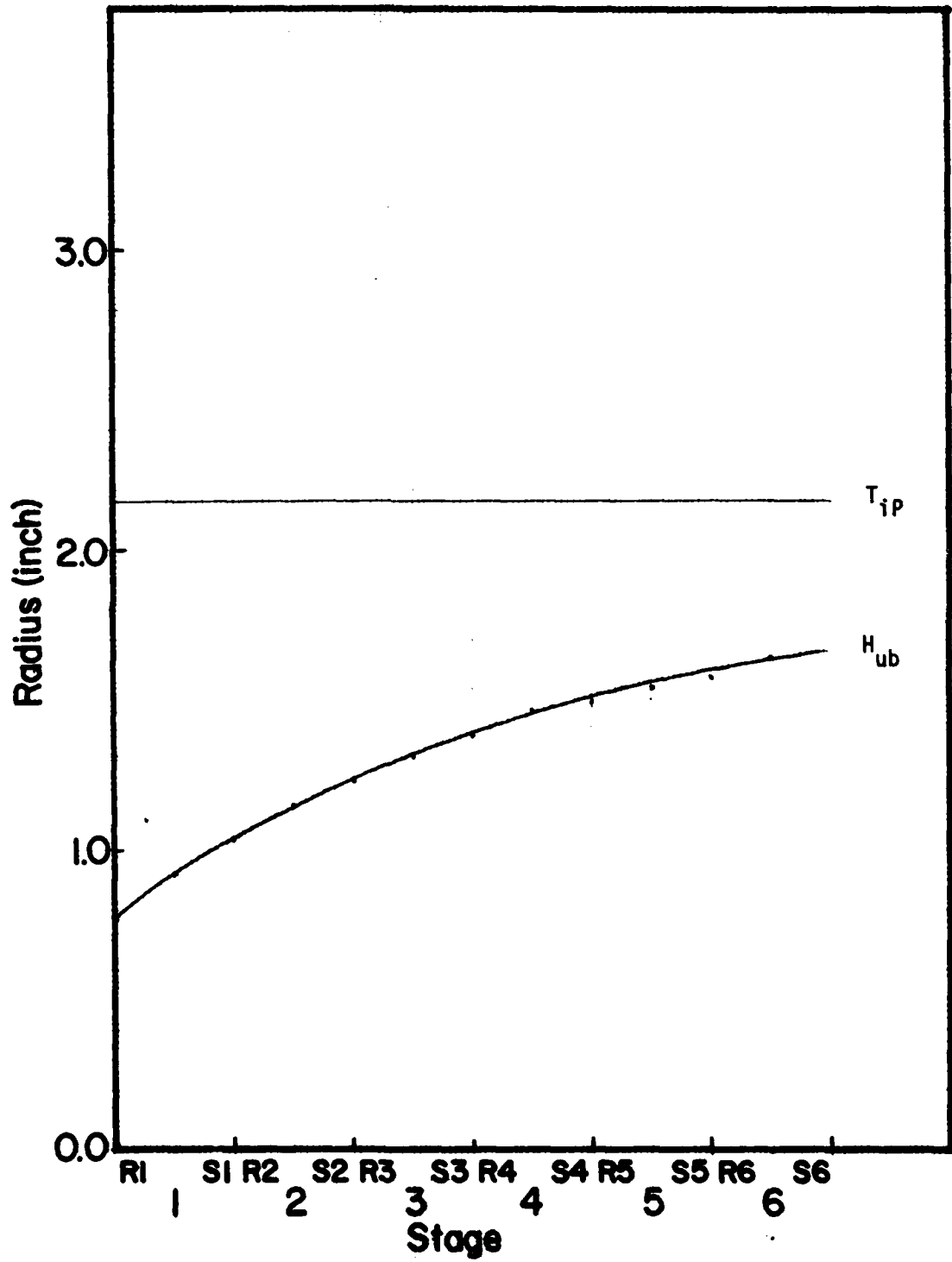
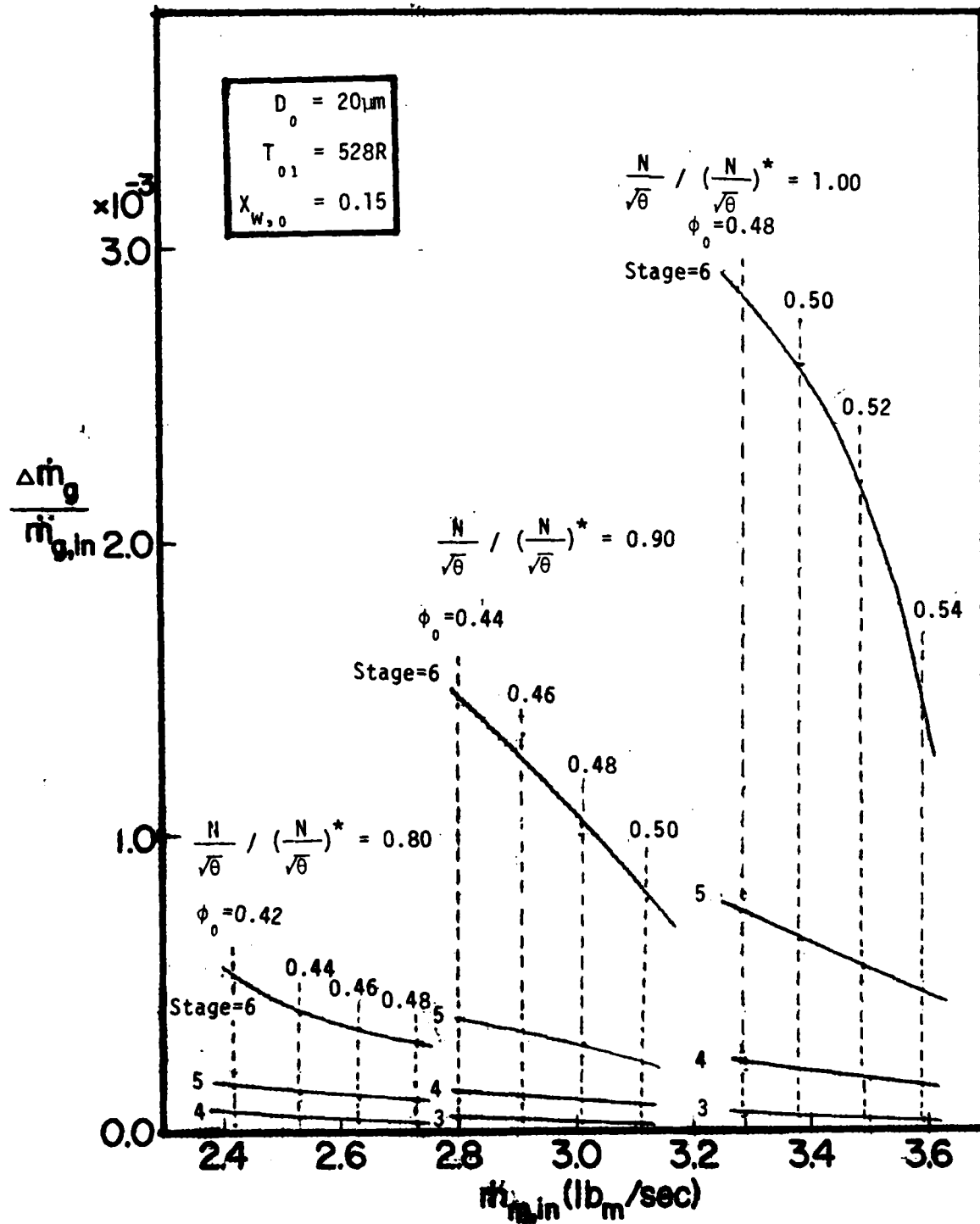


Fig.5.3.6 Variation of Mass Flow Rate of Gas Phase in Different Compressor Stages



**Fig.5.3.7 Variation of Mass Flow Rate of Gas Phase
In Different Compressor Stages**

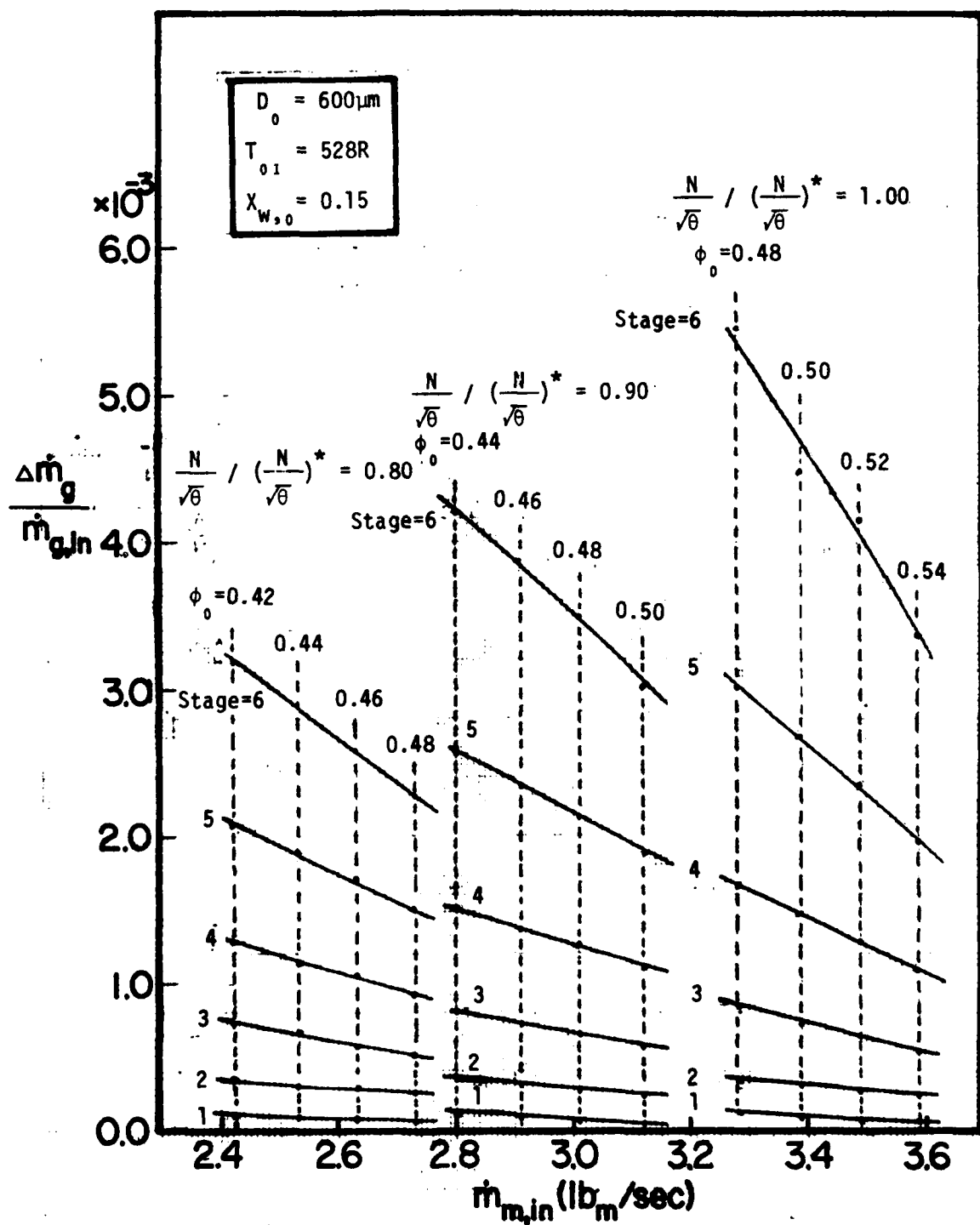


Fig.5.3.8 Variation of Mass Flow Rate of Liquid Phase in Different Compressor Stages

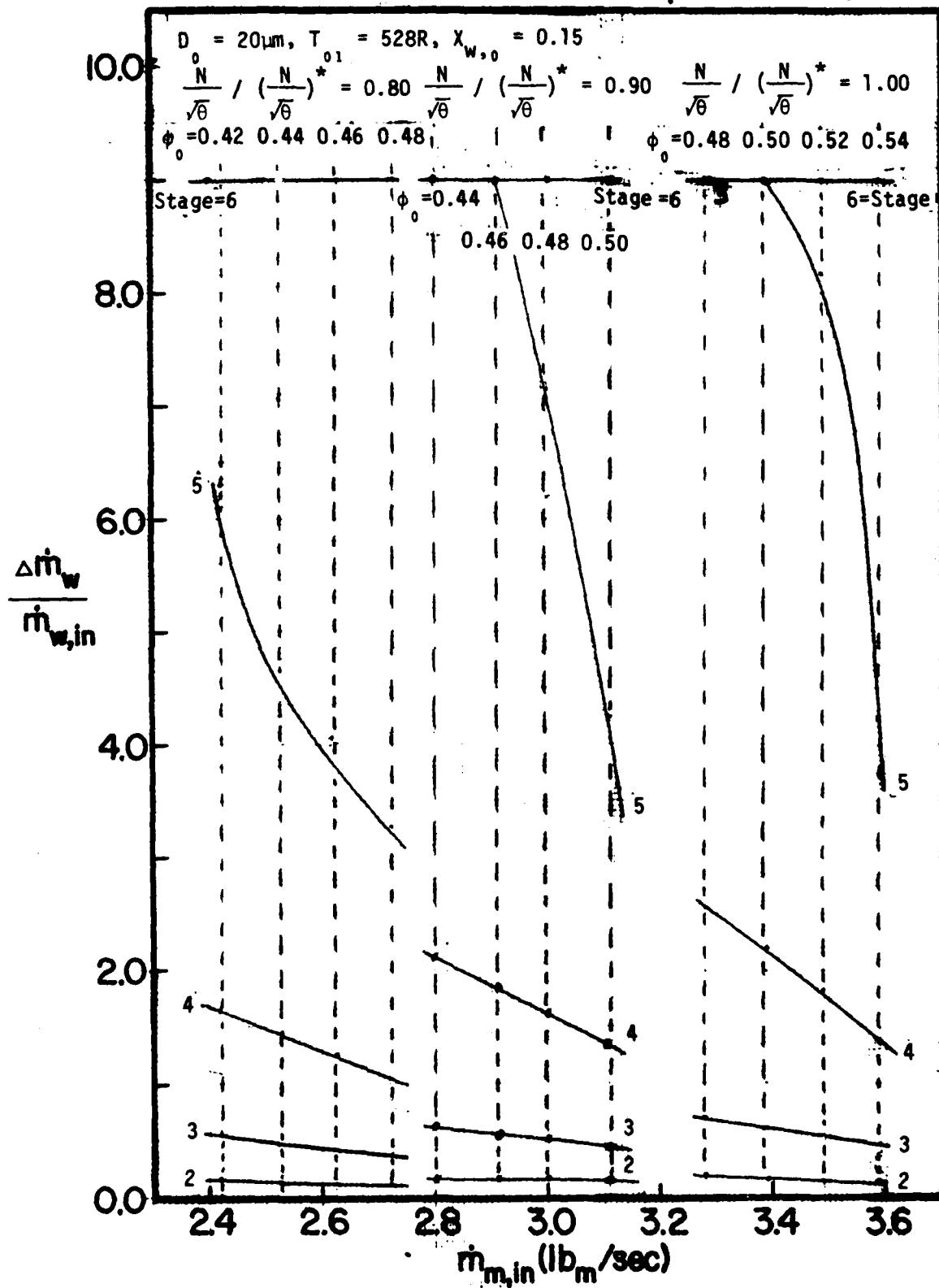
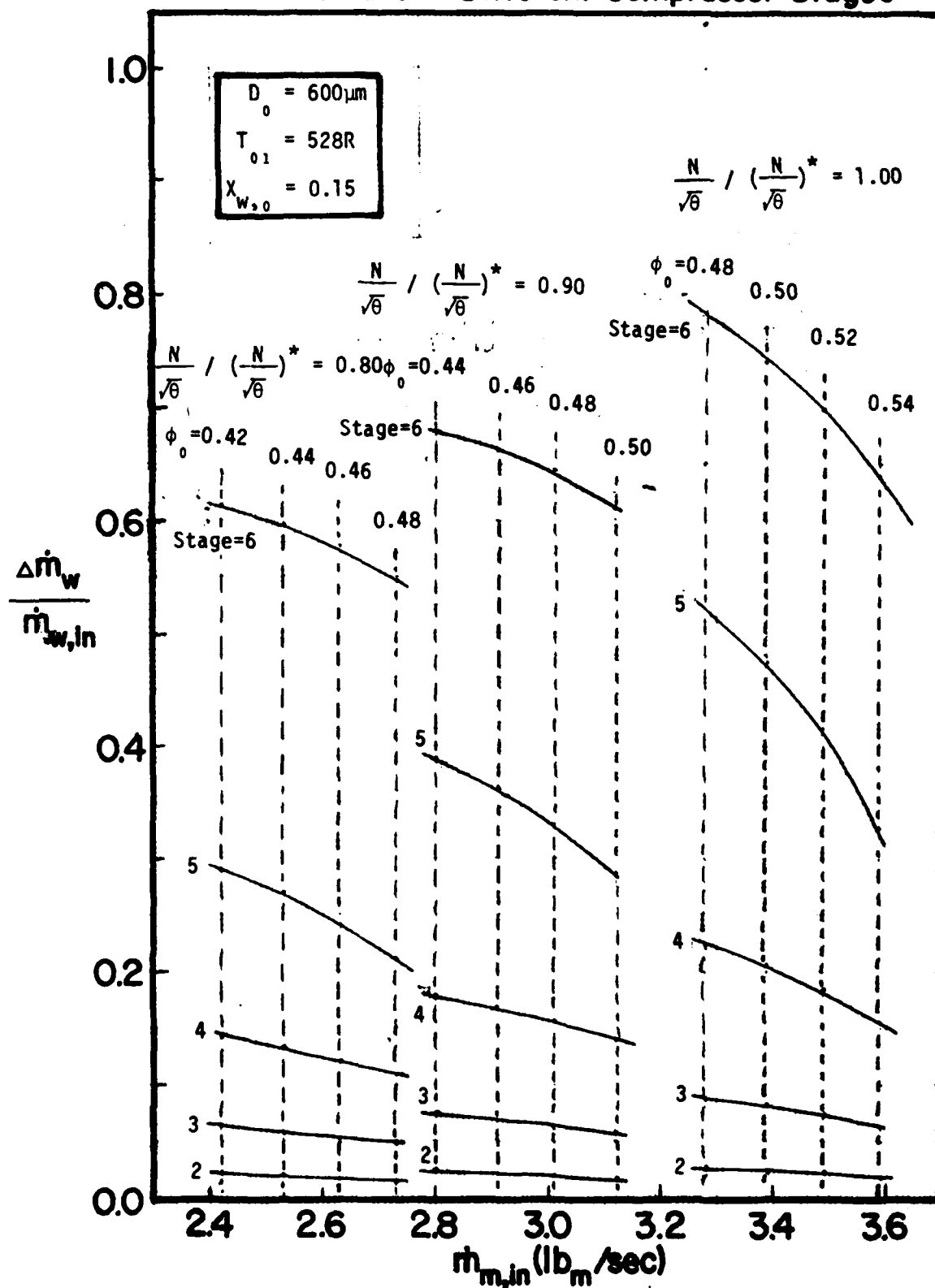


Fig.5.3.9 Variation of Mass Flow Rate of Liquid Phase in Different Compressor Stages



APPENDIX 1

DETAIL OF TEST COMPRESSOR AND DRIVE ENGINE

1. Drive Engine

A T63-A-5 engine is used to drive the Test Compressor. The specifications, limits, and performance ratings for the Drive Engine are as follows:

Design power output: 250 shp

Ram power rating: 275 shp

Design speeds:

Gas producer 51120 rpm (100%)

Power turbine 35000 rpm (100%)

Power output shaft 6000 rpm

Fuel Specification: MIL-J-5624E(JP-4)

The Drive Engine power turbine drives the Test Compressor through mechanical gearing. The power turbine speed has been increased to an output of 9,643 rpm at 100 per cent speed from the normal rating of 6,000 rpm. The Test Compressor is operated at 110 per cent (56,251.7 rpm) while the engine operates at 100 per cent or 51,120 rpm. One power turbine tachometer is used to monitor the Test Compressor speed. The ratio of the tachometer speed to the Test Compressor speed is 0.119676.

2. Test Compressor

The Test Compressor consists of the six axial stages of the ALLISON T63-A-5 engine compressor. The Test Compressor has been designed and built such that various stages of the compressor can be

assembled and tested. Thus the first two, the intermediate two or the last two stages can be tested if desired, as well as the unit with all of the six stages. Only the 6-stage unit has been used in the current tests.

The first stage of the Test Compressor is preceded by an inlet guide vane row which imparts swirl to the inlet air. The relative Mach number of the incoming air at the rotor inlet is thereby reduced as far as permissible without causing inlet blockage. The axial component features unshrouded rotors, cantilever stators, and double circular arc blading in all stages. The values of T-63 compressor design velocity diagram are presented in Table A.1.1. Table A.1.3 and A.1.4 present the hardware geometry and aerodynamic design data for rotor and stator, respectively.

Fig. A.1.1. to Fig. A.1.6 show the stage performance characteristics of Test Compressor supplied by the manufacturer. In each of the figures, the equivalent pressure ratio, ψ , equivalent temperature ratio, τ , and stage adiabatic efficiency, η , are presented in terms of flow coefficient, ϕ . The definitions of these parameters are as follows:

(i) flow coefficient: ϕ

$$\phi = V_z / U_{tip}$$

(ii) equivalent pressure ratio: ψ

$$\psi = \left\{ \left(\frac{U_{tip}^2}{T_{01} D} \right) \left(\frac{T_{01}}{U_{tip}^2} \right) \left[\left(\frac{P_{02}}{P_{01}} \right)^{\frac{\gamma-1}{\gamma}} - 1 \right] + 1 \right\}^{\frac{\gamma}{\gamma-1}}$$

(iii) equivalent temperature ratio: τ

$$\tau = \left(\frac{U_{tip}^2}{T_{01} D} \right) \cdot \left(\frac{\Delta T_{02}}{U_{tip}^2} \right)$$

TABLE A.1.1
TEST COMPRESSOR DESIGN VELOCITY DIAGRAM VALUES

Stage	1	2	3	4	5	6	
R	2.161	2.161	2.161	2.161	2.161	2.161	
U	963.5	963.5	963.5	963.5	963.5	963.5	
V_{z1}	508.4	544.1	547.0	554.9	554.1	543.7	↑
$V_{\theta 1}$	236.5	310.0	365.1	349.3	338.8	333.8	
$W_{\theta 1}$	727.0	653.5	598.4	614.2	624.7	629.9	Rotor Inlet
α_1	25.0	29.7	33.7	32.2	31.6	31.5	
β_1	54.9	50.3	47.6	47.9	48.5	49.3	
M_{1abs}	0.513	0.563	0.578	0.560	0.538	0.512	
M_{1rel}	0.812	0.765	0.713	0.707	0.692	0.658	↓
V_{z2}	507.0	554.9	551.0	554.5	548.9	544.6	↑
$V_{\theta 2}$	405.2	501.3	598.8	614.6	625.1	630.3	
$W_{\theta 2}$	558.3	462.2	364.7	348.9	338.4	333.2	Rotor Outlet
α_2	38.6	42.1	47.4	47.9	48.7	49.2	
β_2	47.8	39.8	33.6	32.2	31.7	31.5	
M_{2abs}	0.588	0.665	0.706	0.698	0.680	0.660	
M_{2rel}	0.683	0.643	0.574	0.552	0.528	0.506	↓

Note: Symbols for Table A.1.1 are provided in Table A.1.2.

TABLE A.1.2

SYMBOLS FOR TEST COMPRESSOR DESIGN VELOCITY DIAGRAM VALUES

R	Radius, inches
U	Rotor speed at R , ft/sec.
V_z	Air axial velocity, ft/sec.
V_θ	Air absolute tangential velocity, ft/sec.
W_θ	Air relative tangential velocity, ft/sec.
α	Air absolute flow angle, degrees
β	Air relative flow angle, degrees
M	Mach number

Subscript

1	rotor inlet
2	rotor outlet
abs	absolute
rel	relative

TABLE A.1.3
TEST COMPRESSOR DESIGN DATA (ROTOR)

Stage		1	2	3	4	5	6
Radius	R	2.161	2.161	2.161	2.161	2.161	2.161
Camber Angle	θ	22.6	15.9	18.0	19.7	20.9	22.0
Stagger	γ	46.1	42.3	36.5	36.1	36.0	36.3
Incidence	i	0.0	2.0	2.0	2.0	2.0	2.0
Deviation	δ	7.3	5.4	6.0	6.0	6.1	6.2
Chord	c	0.605	0.554	0.534	0.510	0.483	0.456
Solidity	σ	0.713	0.815	0.787	0.941	0.997	1.075
Max. Thickness	t	0.036	0.039	0.037	0.036	0.034	0.032
Thickness-Chord Ratio	t/c	0.060	0.070	0.070	0.070	0.070	0.070
No. of Blades	n	16	20	20	25	28	32

Note: R, c, t in [inches] and θ , γ , δ , i in [degrees]

TABLE A.1.4
TEST COMPRESSOR DESIGN DATA (STATOR)

Stage	IGV	1	2	3	4	5	6
Radius	R	2.161	2.161	2.161	2.161	2.161	2.161
Camber Angle	θ	31.7	22.4	25.6	26.2	24.4	24.7
Stagger	γ	-15.9	31.3	36.3	36.6	36.8	37.4
Incidence	i	0.0	-2.0	-2.0	-2.0	-2.0	-2.0
Deviation	δ	6.7	9.6	5.2	8.0	7.9	7.5
Chord	c	1.395	0.442	0.412	0.412	0.412	0.412
Solidity	σ	0.719	0.456	0.789	0.850	0.972	1.093
Max. Thickness	t	0.170	0.040	0.025	0.025	0.025	0.025
Thickness-Chord Ratio	t/c	0.122	0.09	0.06	0.06	0.06	0.06
No. of Blades	n	7	14	26	28	32	36

Note: R, c, t in [inches] and θ , γ , δ , i in [degrees]

Fig.A.1.1 Performance Characteristics of Test Compressor (1st Stage)

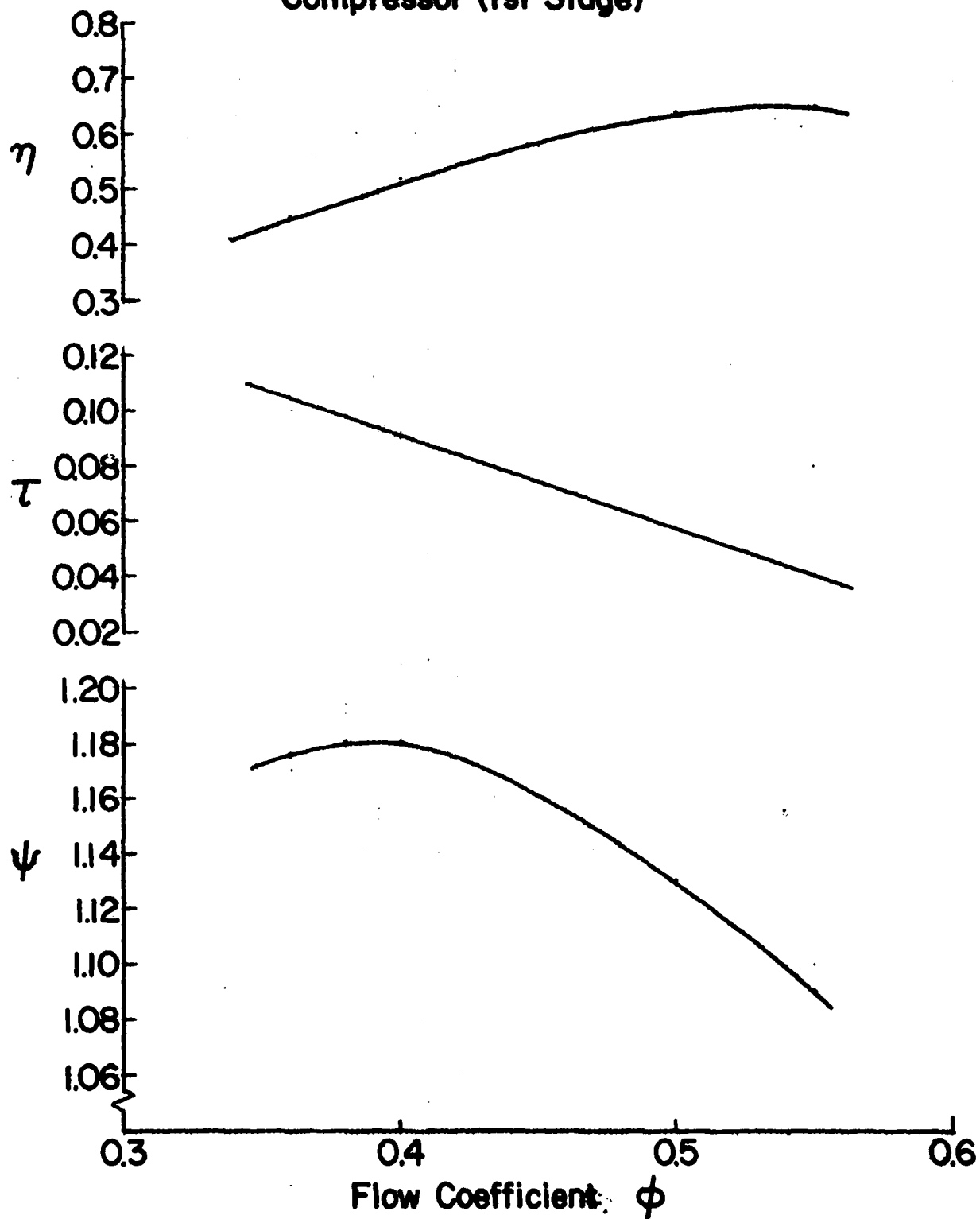


Fig.A.1.2 Performance Characteristics of Test Compressor (2nd Stage)

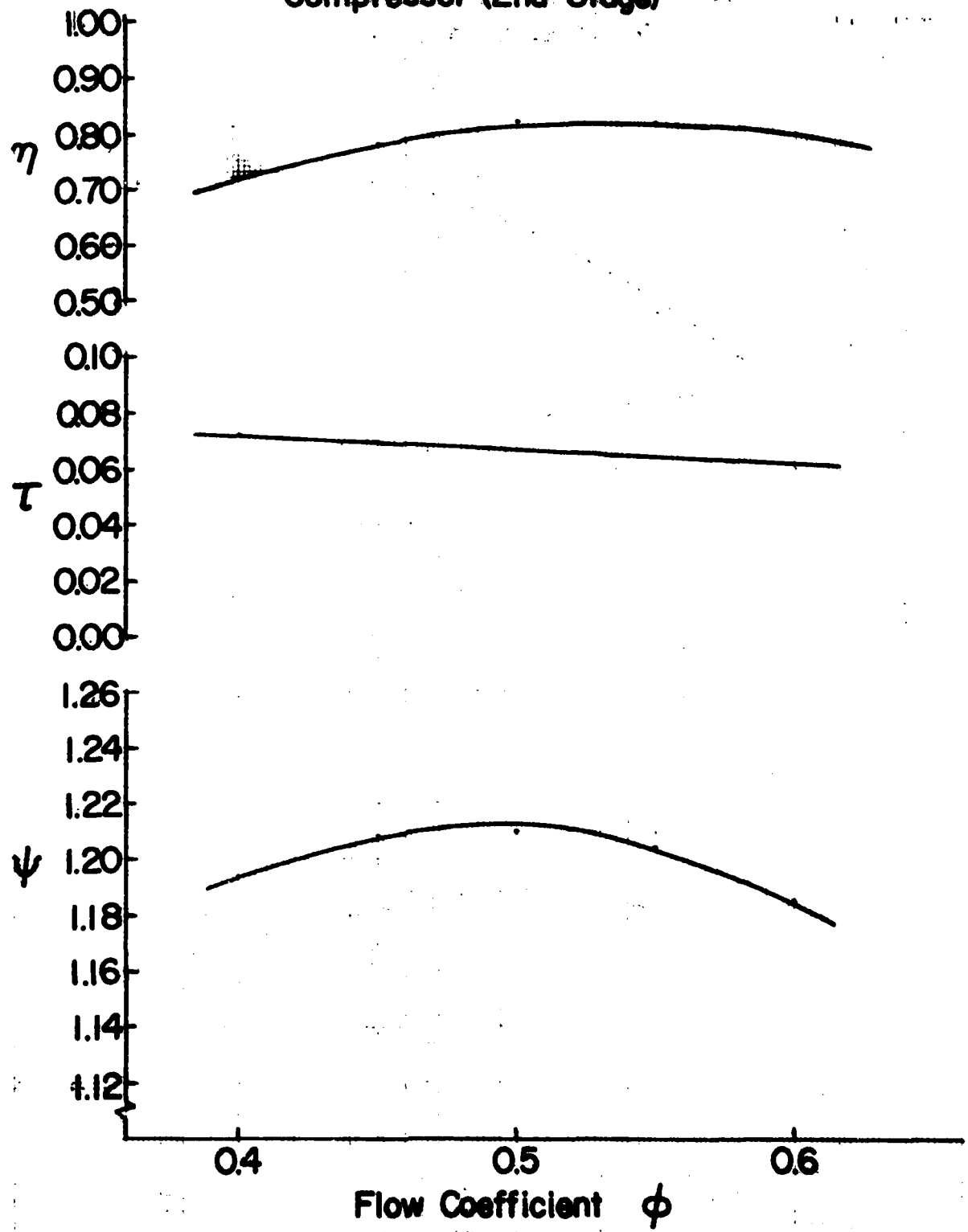


Fig.A.1.3 Performance Characteristics of Test Compressor (3rd Stage)

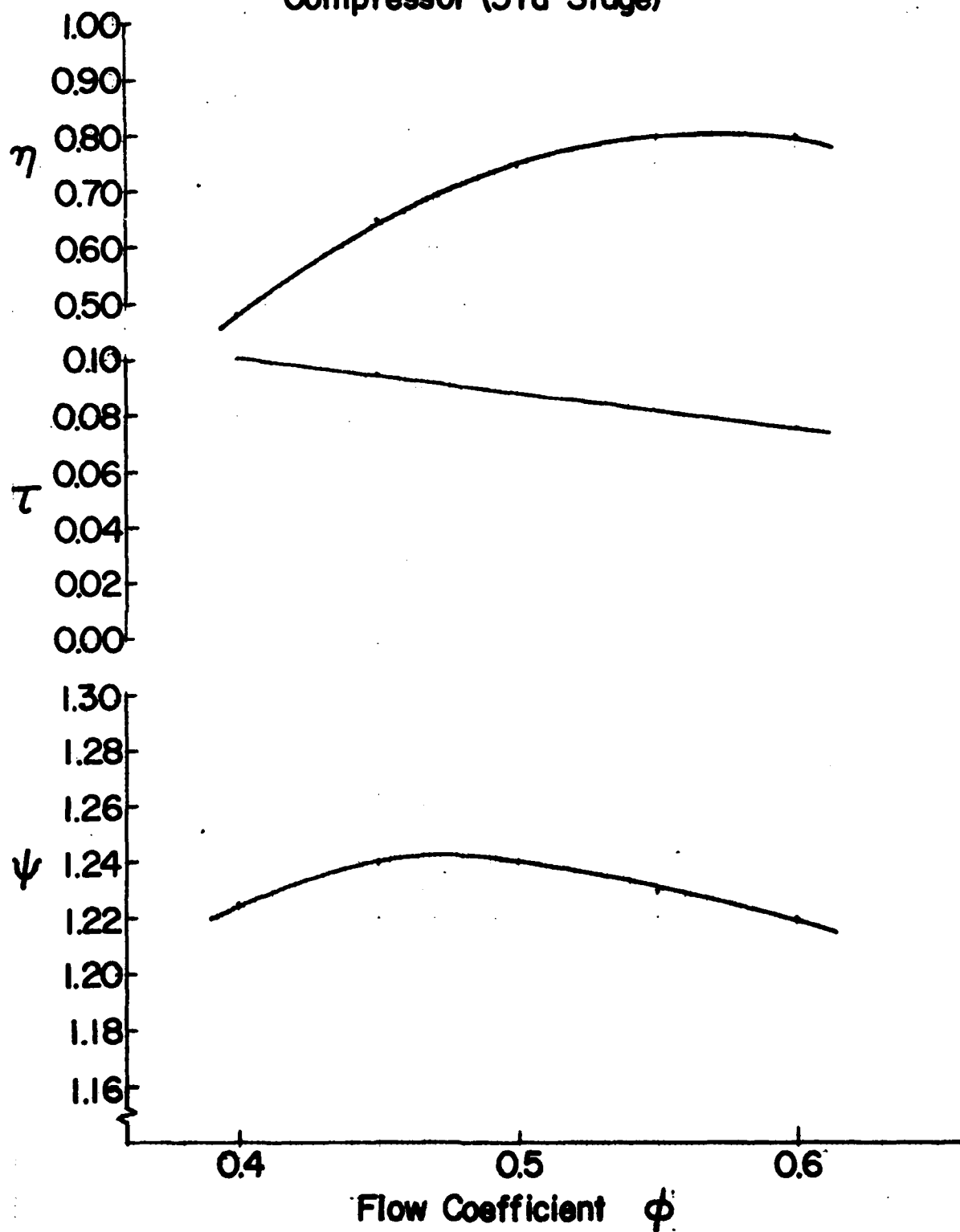


Fig.A.1.4 Performance Characteristics of Test Compressor (4th Stage)

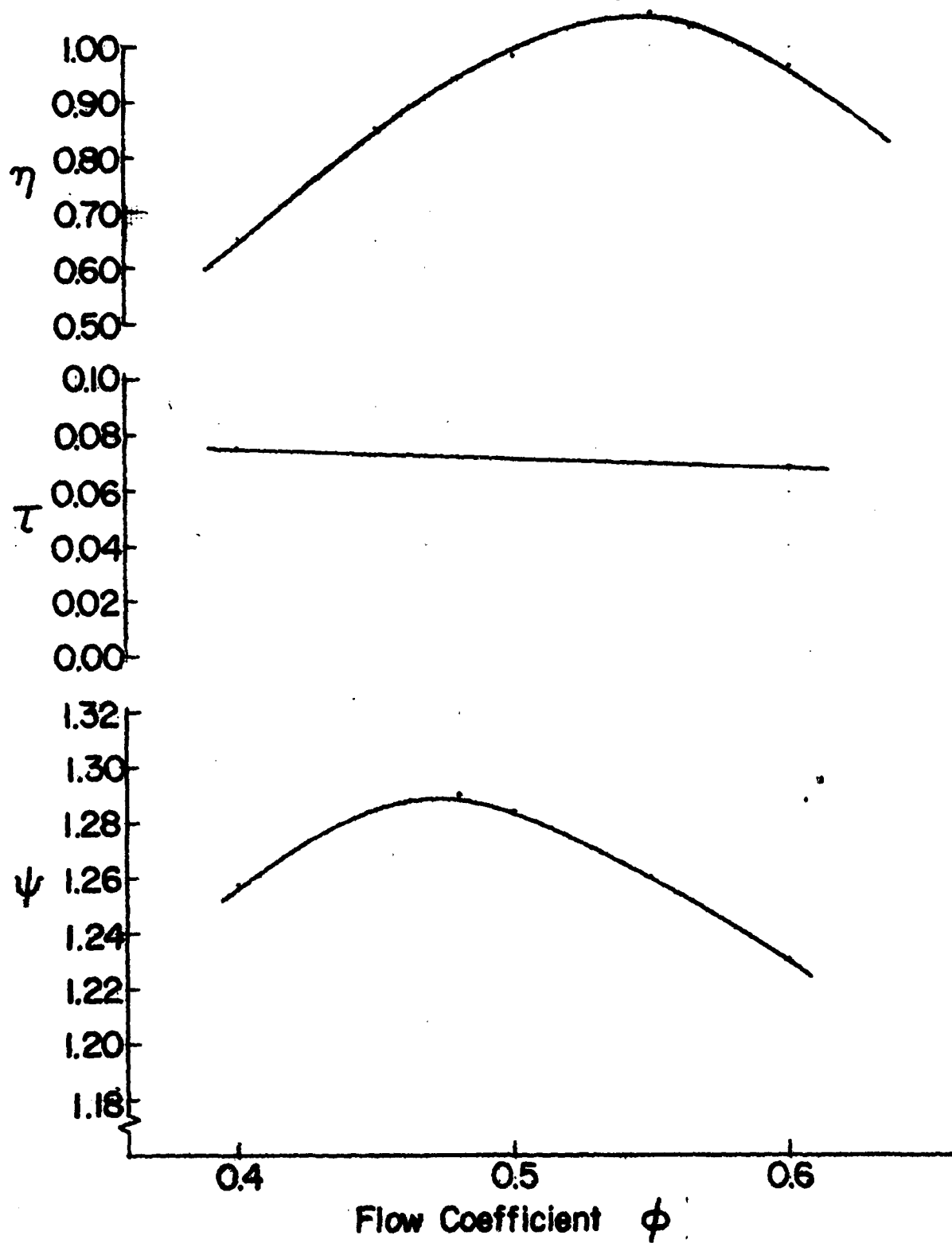


Fig.A.1.5 Performance Characteristics of Test Compressor (5th Stage)

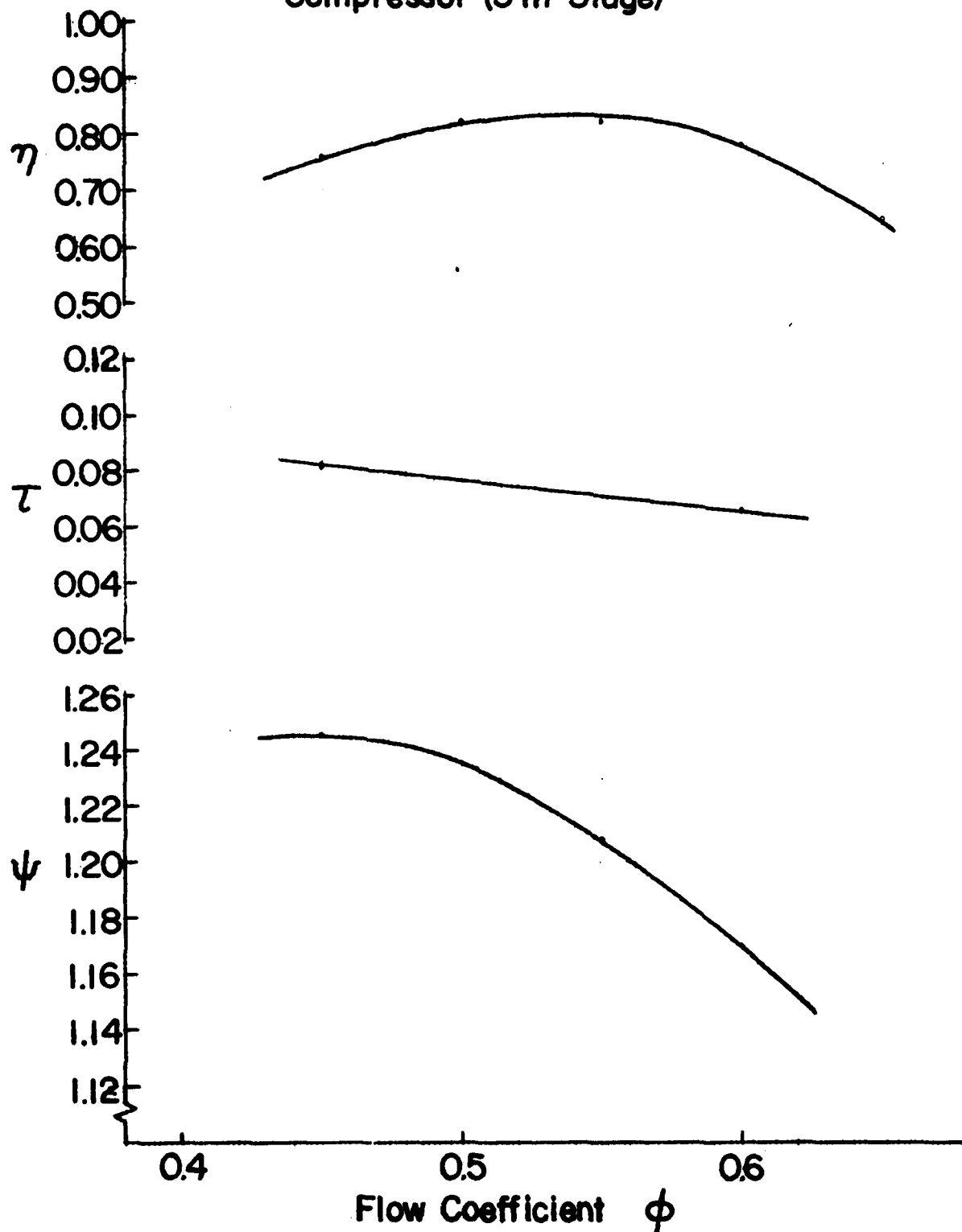
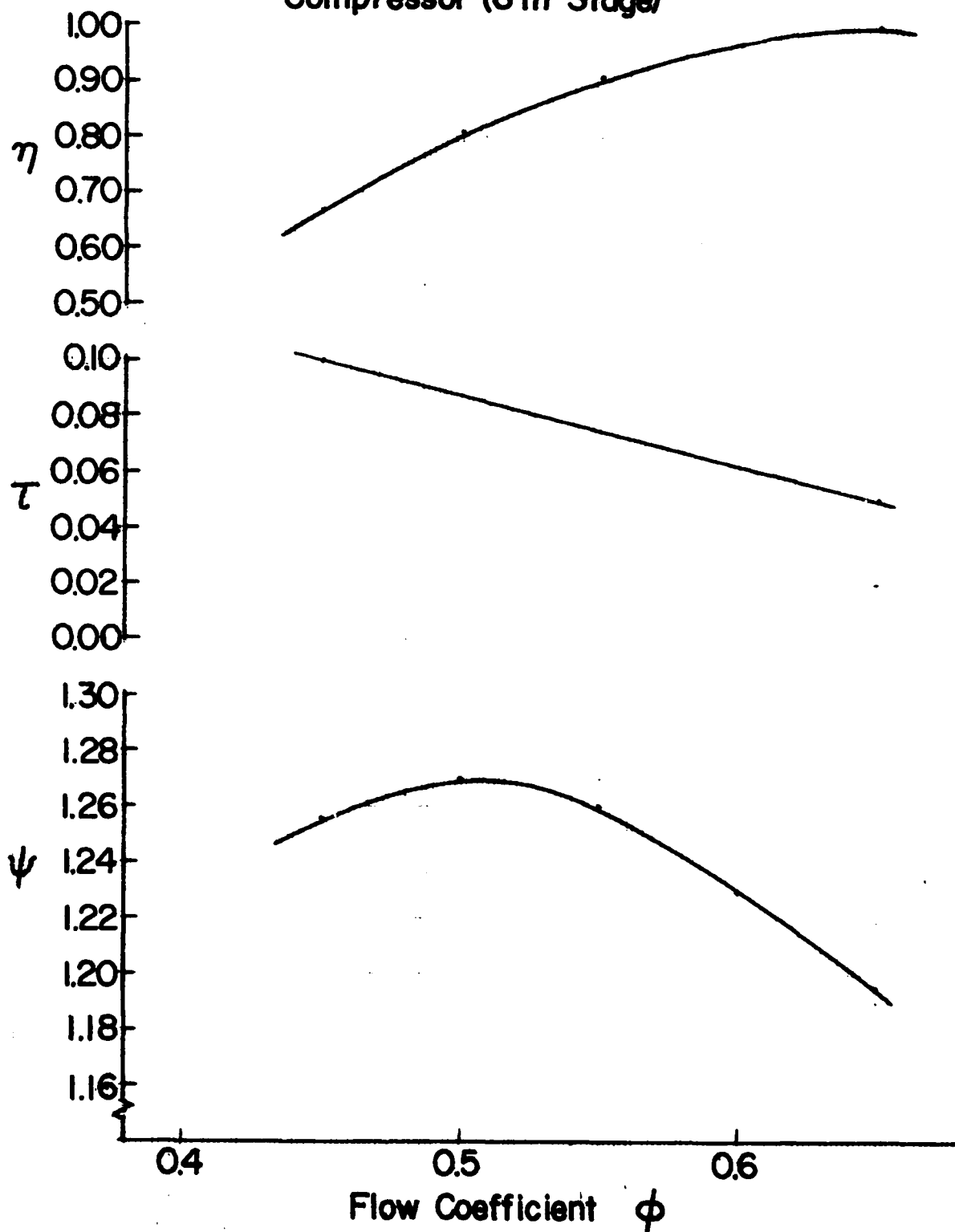


Fig.A.I.6 Performance Characteristics of Test Compressor (6th Stage)



AD-A114 831

PURDUE UNIV LAFAYETTE IN SCHOOL OF MECHANICAL ENGINEERING F/G 21/5
EFFECT OF WATER ON AXIAL FLOW COMPRESSORS. PART II. COMPUTATION--ETC(U)
JUN 81 T TSUCHIYA, S N MURTHY F33615-7A-C-2401

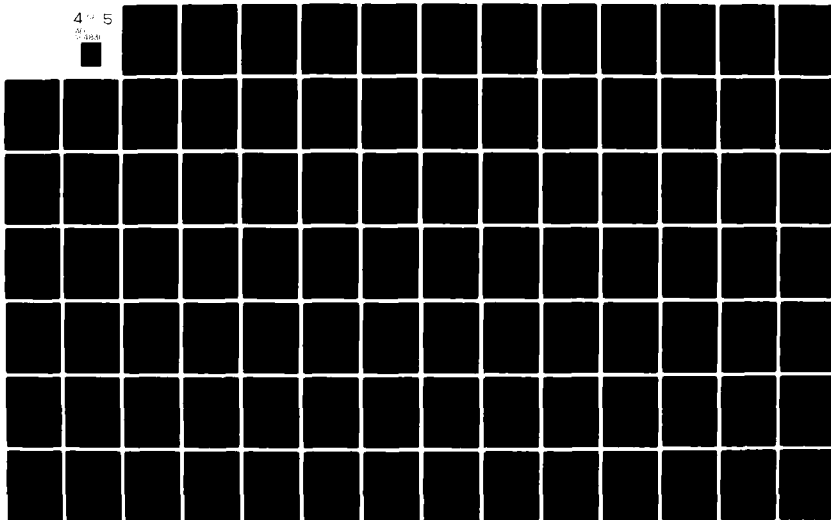
UNCLASSIFIED

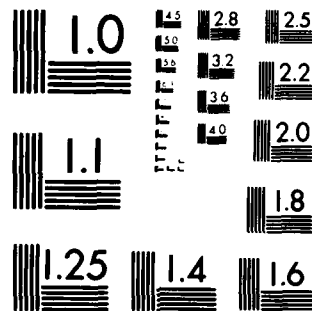
AFWAL-TR-80-2090-PT-2

NL

4 5

45.8





MICROCOPY RESOLUTION TEST CHART
NATIONAL BUREAU OF STANDARDS 1963-A

(iv) stage adiabatic efficiency: η

$$\eta = T_{01} \left[\left(\frac{P_{02}}{P_{01}} \right)^{\frac{\gamma-1}{\gamma}} - 1 \right] \frac{1}{\Delta T_0} = (\psi^{\frac{\gamma-1}{\gamma}} - 1) / \tau$$

where ΔT_0 is stage total temperature rise, P_0 total pressure, T_0 total temperature, V_z axial velocity, U_{tip} blade tip wheel speed, γ specific heat ratio. The subscripts 1 and 2 mean inlet and outlet, respectively, and D design value.

Figure A.1.7 shows overall performance characteristics of Test Compressor supplied by the manufacturer. The performance parameters are the following:

(1) Corrected mass flow rate = $\frac{\dot{m}\sqrt{\theta}}{\delta}$

where \dot{m} = mass flow rate

T_{01} = compressor inlet pressure

P_{01} = compressor inlet temperature

$\theta = T_{01}/T_{ref}$

$\delta = P_{01}/P_{ref}$

$T_{ref} = 58.7^\circ \text{F} (15.2^\circ \text{C})$

$P_{ref} = 14.7 \text{ psi} (1.0132 \times 10^5 \text{ N/m}^2)$

(2) Corrected speed = $\frac{N}{\sqrt{\theta}}$

where N = rotor speed (RPM)

(3) Overall total pressure ratio = P_{02}/P_{01}

where P_{01} = compressor inlet total pressure

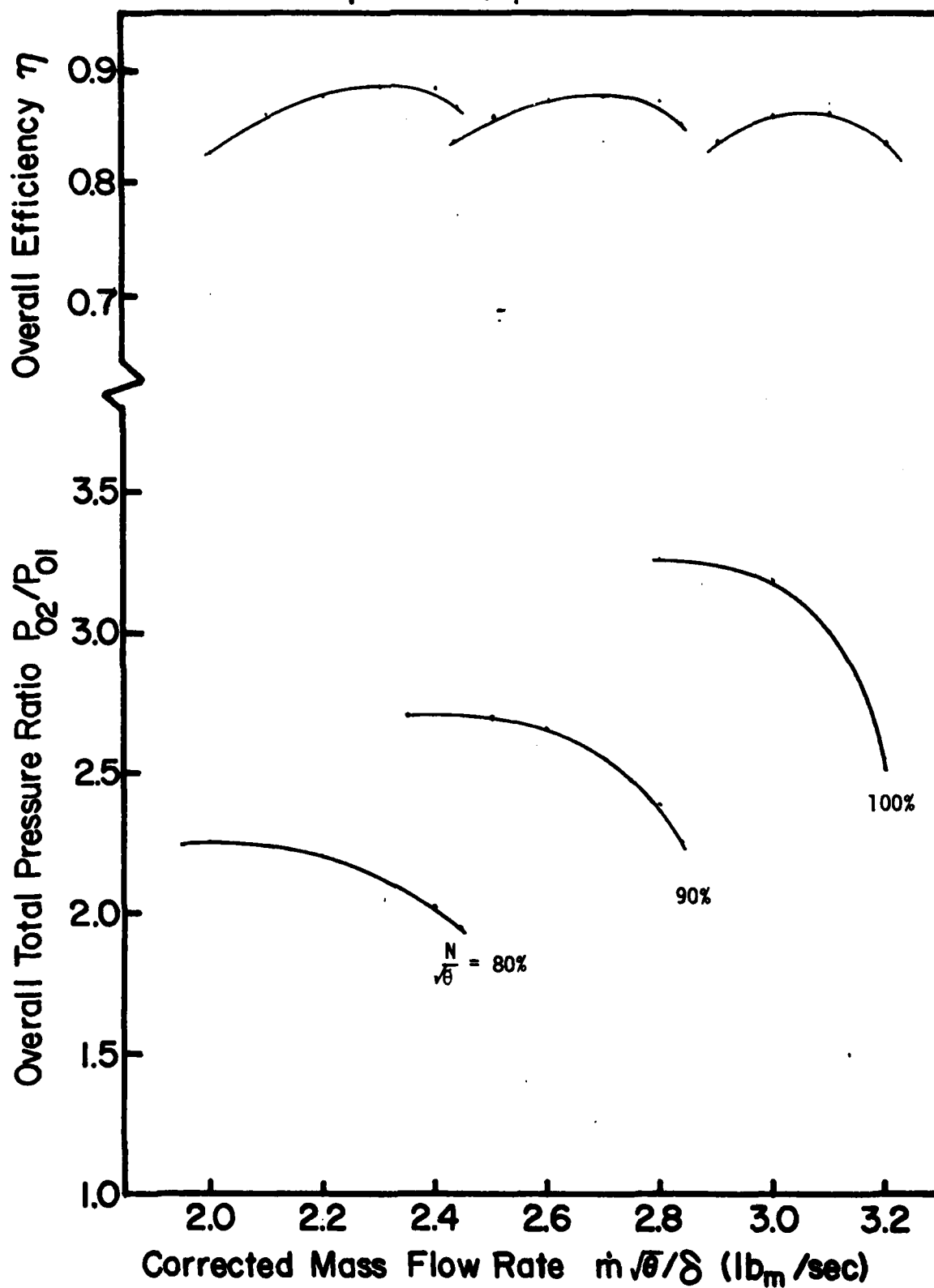
P_{02} = compressor outlet total pressure

(4) Overall adiabatic efficiency = $\eta = \frac{T_{01}}{\Delta T_0} \left[\left(\frac{P_{02}}{P_{01}} \right)^{\frac{\gamma-1}{\gamma}} - 1 \right]$

where T_{01} = compressor inlet total temperature

ΔT_0 = compressor total temperature rise

Fig.A.1.7 Performance Characteristics of Test Compressor (Overall)



P_{02}/P_{01} = overall total pressure ratio

γ = ratio of specific heats

3. Limitations

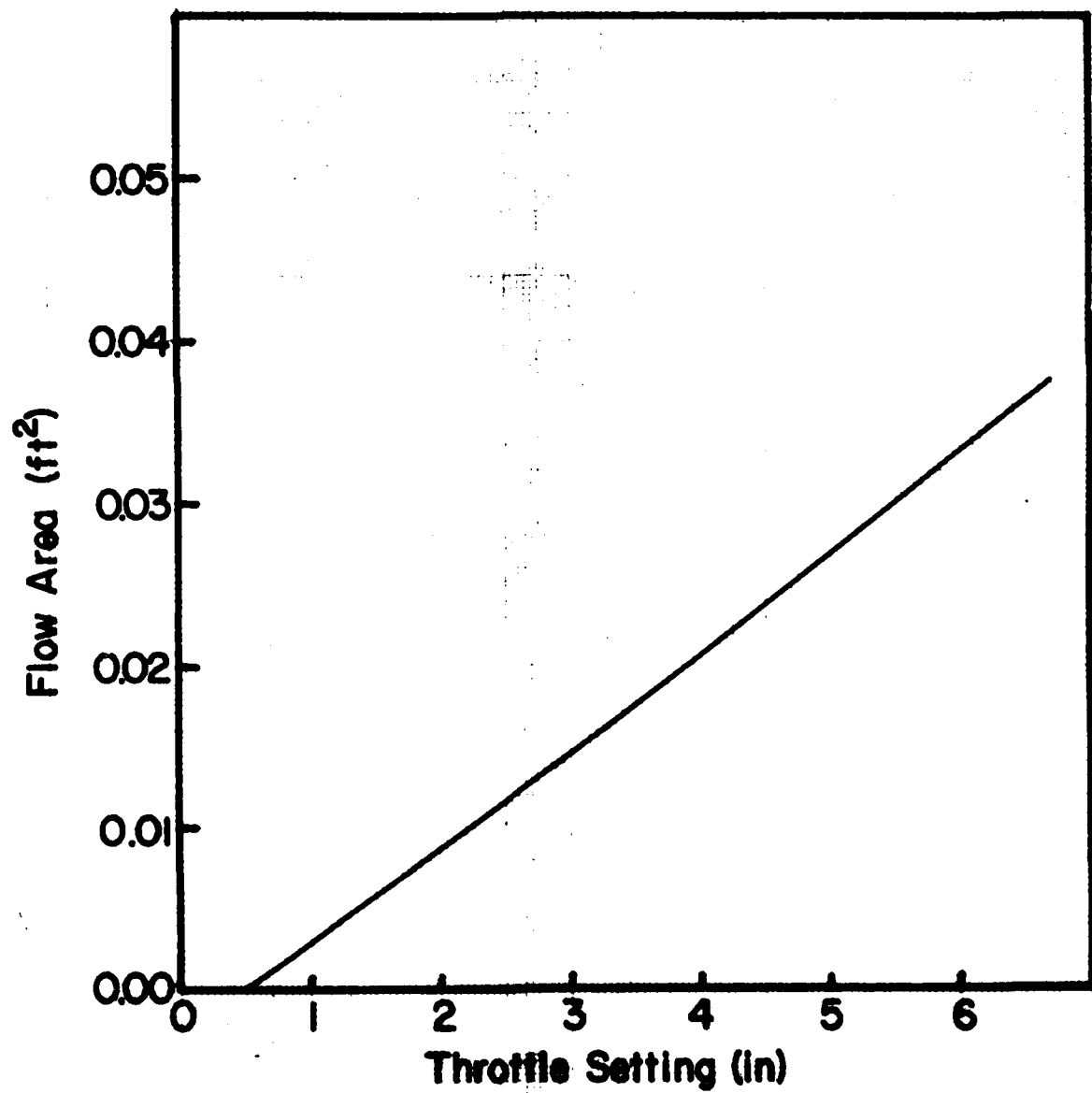
The Test Compressor is driven, through a mechanical gear train, by the power turbine of the Drive Engine. The 6-stage Test Compressor has been utilized in the past for up to 30 hours. The available life-time for further use of that Test Compressor has been uncertain.

The Test Compressor has a plastic coating on the casing that supports the stator blade rings. The mechanical and thermal strength of the coating has been uncertain since the casing was built over ten years ago and may have aged. At design point, the Test Compressor temperature rise is about 192°F, (106°C) when the inlet-air temperature is 58.7°F, (15.2°C). A casing has been replaced by a second casing during preliminary testing.

The throttle regulating the Test Compressor mass flow at any given speed of operation consists of a conical center piece that can be set at any desired location concentrically in a diverging section which is then opened to atmospheric conditions following a straight duct. The center piece can be moved utilizing an electric motor. The throttle (annulus) area that is available during center piece motion is shown in Fig.A.1.8. It is possible to set the throttle to within a tenth of an inch (about 2.0 mm) during horizontal traverse of the throttle centerpiece. At a given Test Compressor speed, a chosen throttle setting may yield one of two types of performance: (i) when it is unchoked, the pressure ratio across the throttle (the downstream pressure being related to the atmospheric pressure) determines the mass flow throughout the Test Compressor; and (ii) when the throttle area is too large for passing the mass flow through the Test Compressor with a particular set of inlet conditions, the compressor will operate under free-wheeling conditions.

The Test Compressor assembly with the gear box connecting it to the Drive Engine is such that there is no simple access to its outlet section for locating adequate instrumentation or adjusting probes to establish compressor outlet conditions. The gear box disassembly and removal of the compressor outlet ducting are required each time any access is desired to the compressor outlet section.

Fig.A.I.8 Flow Area vs Throttle Setting



3.1 Refurbishment

The Drive Engine and the Test Compressor have been refurbished in the following respects by the Detroit Diesel Allison of Indianapolis, who are the original manufacturers of both the units.

- (1) Engine fuel flow control
- (2) Drive shaft interconnecting the Drive Engine and the Test Compressor,
- (3) Test Compressor gear box,
- (4) Test Compressor bearings, and
- (5) The 6-stage assembly of Test Compressor, including balancing.

Following this refurbishment and additional work undertaken at Purdue University, proof-runs undertaken on the Drive Engine - Test Compressors installation showed feasibility of satisfactory operation of the test unit.

APPENDIX 2

EFFECTIVE DROPLET DIAMETER FOR DIFFERENT PROCESSES

1. Definition of Mean Droplet Diameter

In practice, the dispersed phase does not consist of droplets of equal size. It is often convenient to represent a spectrum of the droplet size distribution by an equivalent mono-dispersion of droplets of a mean diameter. A mean diameter is a mathematical value that represents the complete droplet size distribution. This value can be a measure of number density, diameter, surface area, or volume, each of which is of significance with respect to different aero-thermo-mechanical processes in two phase flows. A general equation that defines a mean diameter is given by (Ref. 17)

$$D_{ab} = \left\{ \frac{\int_0^{D_{\max}} D^a \frac{dN^*}{dD} dD}{\int_0^{D_{\max}} D^b \frac{dN^*}{dD} dD} \right\}^{\frac{1}{a-b}} \quad (\text{A.2.1})$$

where N^* is the cumulative number fraction of droplets below diameter D in the spectrum and a, b are integers. Depending upon the value of integers a and b , the mean diameters based on length, surface area, or volume are defined as follows using appropriate values of integers a and b in Eq. (A.2.1):

(i) linear mean diameter: D_{10}
 $a = 1, b = 0$

(ii) surface mean diameter: D_{20}
 $a = 2, b = 0$

- (iii) surface-length mean diameter: D_{21}
 $a = 2, b = 1$
- (iv) volume mean diameter: D_{30}
 $a = 3, b = 0$
- (v) volume-length mean diameter: D_{31}
 $a = 3, b = 1$
- (vi) volume-surface mean diameter (Sauter mean diameter): D_{32}
 $a = 3, b = 2.$

From the point of view of experimental determination of spray characteristics, it is useful to rewrite Eq. (A.2.1) as follows:

$$D_{ab} = \frac{\left[\sum D^a f(D) \Delta D \right]^{\frac{1}{a-b}}}{\left[\sum D^b f(D) \Delta D \right]} \quad (\text{A.2.2})$$

where $f(D)$ is the percent number of droplets with a diameter within certain size increments ΔD . A typical example of droplet distribution is shown in Table A.2.1 (Ref. 34). Using such data various mean diameters defined previously can be calculated. Fig. A.2.1 provides a comparison of mean diameters. For that Figure D_{NM} is the number median diameter on either side of which lie 50 per cent of the total number of droplets.

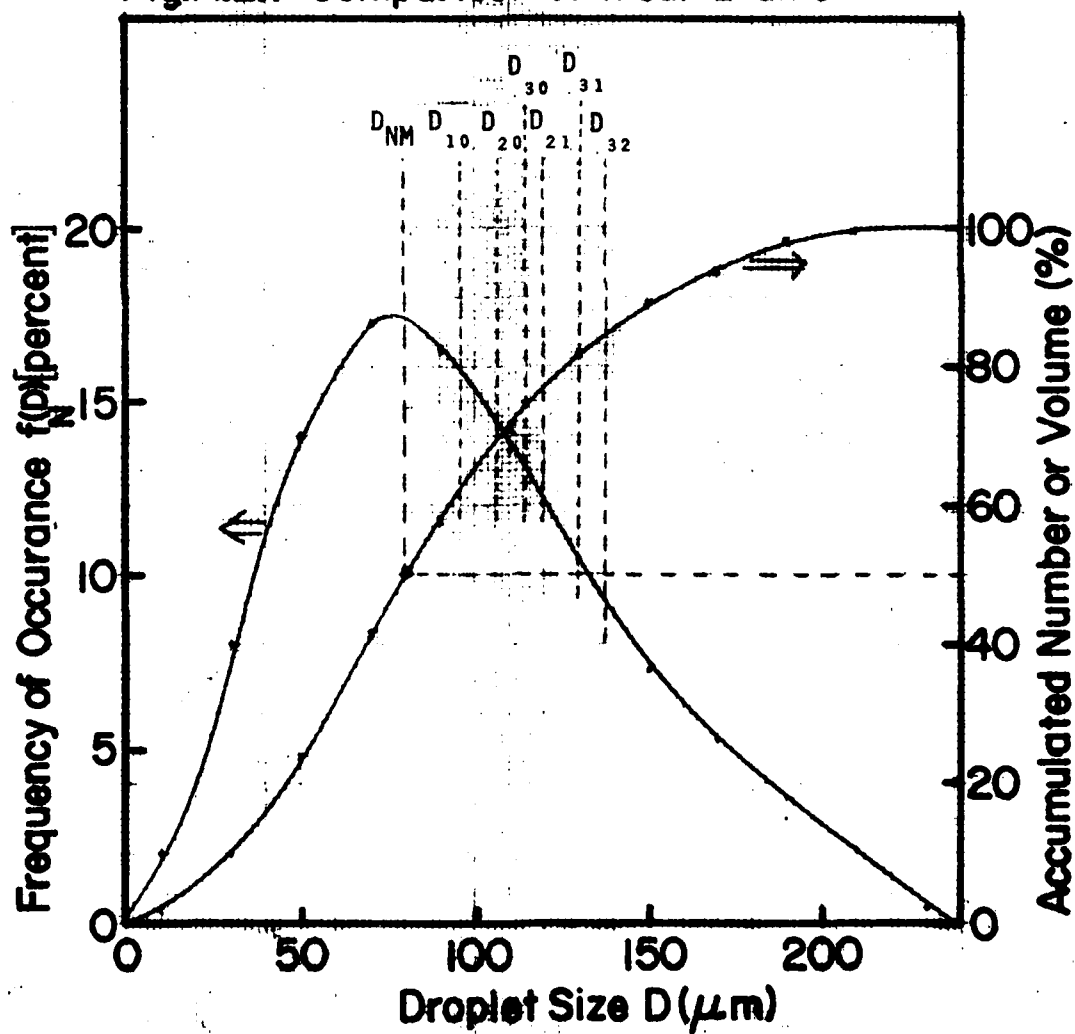
2. Effective Droplet Diameter for Different Processes

A spray can be considered in terms of an effective mono-dispersed spray that is equivalent to the given spray with respect to a chosen process. The major processes of interest are (i) heat transfer, (ii) mass transfer, (iii) drag force, (iv) centrifugal force and (v) droplet deformation and break-up. In each case it is necessary to establish an effective mean diameter of mono-dispersed spray that is equivalent to the given spray.

TABLE A.2.1
EXAMPLE OF DROPLET SIZE DISTRIBUTION

Droplet size increment ΔD (μ)	Diameter representing interval D (μ)	No. of drop-lets counted N	Occurrence $f(D)$ (percent)	$Df(D)$	$D^2f(D)$	$D^3f(D)$	Accumulated number less than D (percent)
0-20	10	10	2.0	20	200	2000	2.0
20-40	30	40	8.0	240	7200	216000	10.0
40-60	50	70	14.0	700	35000	1750000	24.0
60-80	70	86	17.2	1204	84280	5899600	41.2
80-100	90	82	16.4	1476	132840	11955600	57.6
100-120	110	68	13.6	1496	164560	18101600	71.2
120-140	130	52	10.4	1352	175760	22848800	81.6
140-160	150	36	7.2	1080	162000	24300000	88.8
160-180	170	26	5.2	804	150280	25547600	94.0
180-200	190	18	3.6	684	129960	24692400	97.6
200-220	210	10	2.0	420	88200	18522000	99.6
220-240	230	2	0.4	72	21160	4866800	100.0
		500	100	9608	1151440	1.58702x10 ⁸	

Fig.A.2.1 Comparison of Mean Diameters



(i) Heat Transfer

The heat transfer rate between the gas phase and a droplet is given by the relation,

$$\dot{q} = h\pi D^2 (T_g - T_w) \quad (\text{A.2.3})$$

where T_g and T_w are the temperatures of gas phase and droplet, respectively, and D is droplet diameter. The heat transfer coefficient, h , is given by the relation,

$$h = \frac{k}{D} \{ 2.0 + 0.6 (\text{Re})^{0.50} (\text{Pr})^{0.33} \} \quad (\text{A.2.4})$$

where k is the thermal conductivity of gas phase, Re , the Reynolds number based on relative velocity, and Pr , the Prandtl number.

For small droplets, that are assumed to follow the gas path, Eq. (A.2.3) can be written as follows:

$$\dot{q} = 2.0 k\pi D (T_g - T_w) \quad (\text{A.2.5})$$

The total heat transfer rate between the droplets and the gas phase is proportional to the number of droplets in the mixture, based on unit volume or unit mass of the mixture. If the spray consists of a mono-dispersion of droplet size equal to D_e and the number density is $(n_{\text{tot}})_e$, then the total heat transfer is proportional to $[(n_{\text{tot}})_e \cdot D_e^2]$ according to Eq. A.2.3, and is proportional to $[(n_{\text{tot}})_e \cdot D_e]$ according to Eq. A.2.5.

In a given mixture, because of the dispersion in droplet sizes, one can expect a total of (n_{tot}) droplets to be distributed over a droplet size range with a droplet size maximum of D_{max} . The effective mean diameter of an equivalent mono-dispersed spray for heat transfer, D_e , may then be written as follows using Eq. A.2.5.

$$(n_{\text{tot}})_e 2.0 k\pi D_e (T_g - T_w) = \int_0^{D_{\text{max}}} (n_{\text{tot}}) 2.0 k\pi D (T_g - T_w) \frac{dN^*}{dD} \cdot dD \quad (\text{A.2.6})$$

Now $(n_{\text{tot}})_e$ can be determined based upon the surface area of droplets or the volume of droplets as follows:

Based on surface area:

$$(n_{\text{tot}})_e = \frac{1}{D_e^2} \int_0^{D_{\text{max}}} n_{\text{tot}} D^2 \frac{dN^*}{dD} \cdot dD \quad (\text{A.2.7})$$

Based on volume:

$$(n_{\text{tot}})_e = \frac{1}{D_e^3} \int_0^{D_{\text{max}}} n_{\text{tot}} D^3 \frac{dN^*}{dD} \cdot dD \quad (\text{A.2.8})$$

The heat transfer depends upon the surface area of droplets while the change in droplet temperature due to heat transfer depends upon the droplet volume. Thus, using Eqs. (A.2.6) and (A.2.7), an effective mean diameter based on surface area can be defined by the relation, namely

$$D_e = \frac{\int_0^{D_{\text{max}}} D^2 \frac{\partial N^*}{\partial D} \cdot dD}{\int_0^{D_{\text{max}}} D \frac{\partial N^*}{\partial D} \cdot dD} = D_{21}$$

Similarly, using Eqs. (A.2.6) and (A.2.8), an effective mean diameter based on volume can be defined by the relation, namely.

$$D_e = \frac{\int_0^{D_{\text{max}}} D^3 \frac{\partial N^*}{\partial D} \cdot dD}{\int_0^{D_{\text{max}}} D \frac{\partial N^*}{\partial D} \cdot dD} = D_{31}$$

The effective mean diameter for heat transfer is then D_{21} and the effective mean diameter from the point of view of droplet temperature rise is D_{31} .

(ii) Mass Transfer

The mass transfer rate is given by the relation,

$$\dot{m} = h_m \pi D^2 (C_{wb} - C_w) \quad (\text{A.2.9})$$

where D is diameter of droplet, C_{wb} and C_w are water vapor concentration at droplet surface and in fluid flowing around droplet, respectively.

The mass transfer coefficient, h_m , is given by the relation,

$$h_m = \frac{D_v}{D} \{2.0 + 0.6(Re)^{0.50} (Sc)^{0.33}\} \quad (A.2.10)$$

$$\dot{m} = 2.0 D_v \pi D (C_{wb} - C_w)$$

Introducing the concept of effective mean diameter of mono-dispersed equivalent spray, one can write

$$(n_{tot})_e 2.0 D_v \pi D_e (C_{wb} - C_w) = \int_0^{D_{max}} (n_{tot}) 2.0 D_v \pi D (C_{wb} - C_w) \frac{\partial N^*}{\partial D} dD \quad (A.2.11)$$

Based on surface area, Eqs. (A.2.7) and (A.2.11) yield

$$D_e = \frac{\int_0^{D_{max}} D^3 \frac{\partial N^*}{\partial D} dD}{\int_0^{D_{max}} D \frac{\partial N^*}{\partial D} dD} = D_{21}$$

And based on volume, Eqs. (A.2.8) and A.2.11) yield

$$D_e = \left(\frac{\int_0^{D_{max}} D^3 \frac{\partial N^*}{\partial D} dD}{\int_0^{D_{max}} D \frac{\partial N^*}{\partial D} dD} \right)^{\frac{1}{2}} = D_{31}$$

The mass transfer rate depends upon surface area, while the change in droplet size due to mass transfer is observed as a change in droplet volume.

(iii) Drag Force

The drag force F_D , can be written as follows:

$$F_D = C_D (\pi D^2) \frac{1}{2} \rho_g W_r^2 \quad (A.2.12)$$

where D is droplet diameter, ρ_g is density of gas phase, and W_r is relative velocity between gas phase and droplet. The drag coefficient can be expressed by the relation,

$$C_D = \frac{b}{Re^n} \quad (A.2.13)$$

where Re is Reynolds number based on relative velocity and the constants b and n are given as follows:

$$\begin{aligned}
b &= 24, n = 1 && \text{for } Re < 1.9 \\
b &= 18.5, n = 0.6 && \text{for } 1.9 < Re < 500 \\
b &= 0.44, n = 0 && \text{for } 500 < Re < 200,000
\end{aligned}$$

Introducing the concept of effective mean diameter of mono-dispersed equivalent spray, one can write,

$$(n_{\text{tot}})_e C_{D_e} (\pi D_e^2) \frac{1}{2} \rho_g W_r^2 = \int_0^{D_{\text{max}}} (n_{\text{tot}})_D C_D (\pi D^2) \frac{1}{2} \rho_g W_r^2 \frac{\partial N^*}{\partial D} dD \quad (\text{A.2.14})$$

It is now useful to distinguish between large and small values of Reynolds numbers for droplets. For small Re ($Re < 1.9$), Eq. (A.2.14) becomes

$$(n_{\text{tot}})_e D_e = \int_0^{D_{\text{max}}} (n_{\text{tot}})_D \frac{\partial N^*}{\partial D} dD \quad (\text{A.2.15})$$

Based on surface area, Eqs. (A.2.7) and (A.2.15) yield

$$D_e = \frac{\int_0^{D_{\text{max}}} D^2 \frac{\partial N^*}{\partial D} dD}{\int_0^{D_{\text{max}}} D \frac{\partial N^*}{\partial D} dD} = D_{21}$$

And, based on volume, Eqs. (A.2.8) and (A.2.15) yield

$$D_e = \left(\frac{\int_0^{D_{\text{max}}} D^3 \frac{\partial N^*}{\partial D} dD}{\int_0^{D_{\text{max}}} D \frac{\partial N^*}{\partial D} dD} \right)^{\frac{1}{2}} = D_{31}$$

For large Re ($550 < Re < 20,000$), Eq. (A.2.14) becomes

$$(n_{\text{tot}})_e D_e^2 = \int_0^{D_{\text{max}}} n_{\text{tot}} D^2 \frac{\partial N^*}{\partial D} dD \quad (\text{A.2.16})$$

Based on volume, Eqs. (A.2.8) and (A.2.16) yield

$$D_e = \frac{\int_0^{D_{\text{max}}} D^3 \frac{\partial N^*}{\partial D} dD}{\int_0^{D_{\text{max}}} D^2 \frac{\partial N^*}{\partial D} dD} = D_{32}$$

For small droplets, from the point of view of drag force, the effective mean diameter is D_{31} , and for large droplets, it is D_{32} .

(iv) Centrifugal Force

The centrifugal force acting on a droplet, F_c , is given by

$$F_c = m r \omega^2 = \rho_w \left(\frac{\pi}{6} D^3 \right) r \omega^2 \quad (\text{A.2.17})$$

where ρ_w is density of droplet material, D is droplet diameter, r is radial location of droplet, and ω is angular velocity of rotor. Introducing the concept of effective mean diameter of mono-dispersed equivalent spray it follows from Eq (A.2.17) that

$$(n_{\text{tot}})_e \rho_w \left(\frac{\pi}{6} D_e^3 \right) r \omega^2 = \int_0^{D_{\text{max}}} (n_{\text{tot}}) \rho_w \left(\frac{\pi}{6} D^3 \right) r \omega^2 \frac{\partial N^*}{\partial D} dD \quad (\text{A.2.18})$$

Based on volume, Eqs. (A.2.7) and (A.2.18) yield

$$D_e = \frac{\int_0^{D_{\text{max}}} D^3 \frac{\partial N^*}{\partial D} dD}{\int_0^{D_{\text{max}}} D^2 \frac{\partial N^*}{\partial D} dD} = D_{32}$$

It may be pointed out that the centrifugal force acting on a droplet is proportional to its mass and therefore volume.

(v) Droplet Deformation and Break-up

The droplet deformation and break-up are generally related to Weber number, We . The definition of Weber number is as follows:

$$We = \frac{\rho_g W_r^2 D}{\sigma}$$

where σ is surface tension of droplet. W_r is relative velocity, D is diameter of droplet and ρ_g is density of gas phase. Introducing the concept of effective mean diameter of mono-dispersed equivalent spray, it follows that

$$(n_{\text{tot}})_e \frac{\rho_g W_r^2 D_e}{\sigma} = \int_0^{D_{\text{max}}} (n_{\text{tot}}) \frac{\rho_g W_r^2 D}{\sigma} \frac{\partial N^*}{\partial D} dD \quad (\text{A.2.19})$$

Based on surface area, Eq. (A.2 19) yields

$$D_e = \frac{\int_0^{D_{\max}} D^2 \frac{\partial N^*}{\partial D} dD}{\int_0^{D_{\max}} D \frac{\partial N^*}{\partial D} dD} = D_{21}$$

It may be pointed out that droplet break-up and deformation processes should be examined both in relation to droplet surface area since the equilibrium of a droplet depends upon the action of surface forces.

In summary, the effective diameters for equivalent mono-dispersed spray become D_{21} , D_{31} and D_{32} from the point of view of various processes. For a given spray it is possible to calculate such effective diameter values. Now, when two sprays are compared, it is in practice impossible to obtain identical values for the two sprays for all three of the effective diameters. However, the concept of effective mean diameter yields a simple and direct method of comparing two sprays for a chosen process. It appears that sprays for which D_{21} and D_{31} are nearly the same should prove equivalent for most of the processes in the current investigation.

APPENDIX 3

CHARACTERISTIC LENGTHS AND TIMES

The characteristic lengths and times may be divided into three groups as follows.

- (1) Test compressor parameters;
- (2) Spray characteristics; and
- (3) Compressor process parameters.

3.1. Test Compressor Parameters

The principal parameters of the Test Compressor are presented in Table A.3.1. They are divided into the following groups.

- (i) geometrical parameters; and
- (ii) typical times.

3.2. Spray Characteristics

The data for two injectors selected for experimental studies are presented in Table A.3.2 and A.3.3.

The relevant spray characteristics for those injectors are given in Table A.3.4 and A.3.5.

3.3. Process Parameters

There are five processes of interest during water ingestion:

- (1) equilibration of droplet and gas phase velocities,

TABLE A.3.1
CHARACTERISTIC LENGTHS AND TIMES
FOR TEST COMPRESSOR

(i) Typical Times

air residence time in a blade row	~ 0.08 msec
air residence time in a stage	~ 0.16 msec
air residence time in compressor	~ 1.3 msec
time for one revolution of rotor	~ 1.2 msec

(ii) Geometrical Parameters

Compressor inlet diameter	~ 11.4 cm
overall length of compressor	~ 20.3 cm

Rotor Blade

Stage	Height (cm)	Chord (cm)	Aspect Ratio
1	3.53	1.54	2.17
2	2.86	1.41	1.93
3	2.36	1.36	1.67
4	1.99	1.30	1.47
5	1.71	1.23	1.34
6	1.50	1.16	1.24

Stage Blade

Stage	Height (cm)	Chord (cm)	Aspect Ratio
IGV	3.53	2.83	1.25
1	3.14	1.12	2.67
2	2.59	1.05	2.35
3	2.16	1.05	1.98
4	1.77	1.05	1.68
5	1.58	1.05	1.47
6	1.32	1.05	1.41

Note: Typical times are estimated at design point operation.

TABLE A.3.2

INJECTOR CHARACTERISTICS FOR UNIJET NOZZLE*

Pressure		Capacity		Spray Angle (degree)
(psig)	(N/m ²)	(gallons per minute)	($\frac{m^3}{sec}$)	
15	2.05×10^5	0.12	7.56×10^{-6}	----
20	2.39×10^5	0.14	8.82×10^{-6}	58
30	3.08×10^5	0.17	10.71×10^{-6}	----
40	3.77×10^5	0.19	11.97×10^{-6}	59
60	5.15×10^5	0.23	14.49×10^{-6}	----
80	6.53×10^5	0.26	16.38×10^{-6}	----
100	7.91×10^5	0.30	18.90×10^{-6}	53

* 1/4 TTG1 (full cone spray pattern) manufactured by Spray System company.

TABLE A.3.3

INJECTOR CHARACTERISTICS FOR ATOMIZING NOZZLE⁺

Pressure		Capacity		Spray Angle (degree)
(psig)	(N/m ²)	(gallons per hour)	($\frac{m^3}{sec}$)	
30	3.08×10^5	5.2	5.46×10^{-6}	----
40	3.77×10^5	6.0	6.30×10^{-6}	73
60	5.15×10^5	7.3	7.67×10^{-6}	----
80	6.53×10^5	---	----	79
100	7.91×10^5	9.5	9.98×10^{-6}	----

⁺1/4 LNN6 (hollow cone spray pattern) manufactured by Spray System Company

TABLE A.3.4

SPRAY CHARACTERISTICS FOR UNIJET NOZZLE

Droplet Size (μm)	At	Pressure	Of
	10 psig (1.70×10^5 N/m^2)	40 psig (3.77×10^5 N/m^2)	100 psig (7.91×10^5 N/m^2)
$D_{n0.5}$ (number median diameter)	498	421	276
D_{10} (number mean diameter)	581	472	300
D_{20} (area mean diameter)	683	535	332
D_{30} (volume mean diameter)	781	598	362
D_{21} (area-number mean diameter)	802	607	367
D_{31} (volume-number mean diameter)	904	672	398
D_{32} (sauter mean diameter)	1020	744	432
$D_{v0.5}$ (volume median diameter)	1190	847	481

TABLE A.3.5

SPRAY CHARACTERISTICS FOR ATOMIZING NOZZLE

Droplet Size (μm)	At	Pressure	Of
	25 psig (2.74×10^5 N/m^2)	40 psig (3.77×10^5 N/m^2)	100 psig (7.91×10^5 N/m^2)
$D_{n0.5}$ (number median diameter)	80	71	62
D_{10} (number mean diameter)	91	81	68
D_{20} (area mean diameter)	104	92	77
D_{30} (volume mean diameter)	117	103	85
D_{21} (area-number mean diameter)	119	105	86
D_{31} (volume-number mean diameter)	132	117	95
D_{32} (sauter mean diameter)	147	130	105
$D_{v0.5}$ (volume median diameter)	169	148	118

- (ii) attainment of thermal equilibrium between droplets and gas phase,
- (iii) attainment of equilibrium with respect to humidity,
- (iv) attainment of equilibrium with respect to mass transfer due to evaporation, and
- (v) adjustment of droplet size based on Weber number. They may be defined as follows.

3.3.1 Relaxation Time

When some property ϕ of a medium is displaced from its equilibrium value ϕ_0 and restoration to equilibrium occurs at a finite rate, the substance is termed a relaxing medium. The simplest system is defined by the proportionality:

$$\frac{d\phi}{dt} \propto (\phi - \phi_0)$$

The system can be characterized by the constant of proportionality and may be written

$$\frac{d\phi}{dt} = -\frac{1}{\tau} (\phi - \phi_0)$$

where τ is known as the relaxation time. This equation can be integrated simply to give the familiar exponential decay of ϕ to equilibrium

$$\frac{\phi - \phi_0}{\phi_1 - \phi_0} = \exp(-t/\tau)$$

where ϕ_1 is the initial displaced value. The physical significance of relaxation time may be described as follows: It represents the time from release at ϕ_1 in which the displacement amplitude reduces to $1/e = 0.3679$ of the original value.

(i) Inertial Relaxation

Drag forces on the water droplets in the mixture tends to reduce the velocity of the gaseous phase relative to the droplets. The in equilibrium occurs when the velocities of gaseous and liquid phases are not equal.

The rate of velocity change for a droplet can be written as follows.

$$\frac{dV_w}{dt} = - \frac{1}{\tau_I} (V_w - V_g)$$

where V_w and V_g are velocities of droplet and gaseous phase. The inertial relaxation time, τ_I , is given by the following.

$$\tau_I = \frac{\rho_f D^2}{18\mu_g f}$$

where μ_g is viscosity of gaseous phase and f is the ratio of drag coefficient and Stokes' drag coefficient.

Estimated values of inertial relaxation time for several droplet sizes are presented in Table A.3.6.

(ii) Thermal Relaxation

A mixture of water droplets and air is not in thermodynamic equilibrium when the temperature of the gaseous phase differs from that of the water droplets.

The rate of temperature change for a droplet can be written as follows.

$$\frac{dT_w}{dt} = - \frac{1}{\tau_T} (T_w - T_g)$$

where T_w and T_g are temperatures of water droplet and gaseous phase. The thermal relaxation time, τ_T , is given by the following.

TABLE A.3.6

CHARACTERISTIC TIMES FOR SOME PROCESSES
DURING WATER INGESTION

(i) Inertial Relaxation

inertial relaxation time	~ 0.6*	μsec for D = 1μm
inertial relaxation time	~ 3.4*	μsec for D = 20μm
inertial relaxation time	~ 0.2 ⁺	sec for D = 600μm

(ii) Thermal Relaxation

thermal relaxation time	~ 10	μsec for D = 1μm
thermal relaxation time	~ 4	msec for D = 20μm
thermal relaxation time	~ 0.7	sec for D = 600μm

(iii) Droplet Break-Up

Droplet rupture time	~ 0.03 to 0.1	msec for D = 100μm
Droplet rupture time	~ 0.3 to 1.2	msec for D = 500μm
Droplet rupture time	~ 1 to 3	msec for D = 1000μm

*assumed relative velocity is zero.

⁺assumed relative velocity is 30 m/s.

$$\tau_T = \frac{\rho_f c_w D^2}{6 k_g} (2.0 + 0.6 Re^{0.50} \cdot Pr^{0.33})^{-1}$$

where ρ_f is density of droplet, c_w is specific heat of water, D is diameter of droplet, k_g is thermal conductivity of gaseous phase, Pr is Prandtl number, and Re is Reynolds number based on the relative velocity.

For a small droplet, since Re is small, the thermal relaxation time may be written as follows.

$$\tau_T = \frac{\rho_f c_w D^2}{12 k_g}$$

Estimated values of thermal relaxation time for several droplet sizes are presented in Table A.3.6.

3.3.2 Droplet Rupture Time

The stability of droplets moving through a gaseous atmosphere depends mainly upon the ratio of aerodynamic pressure forces tending to deform it and surface-tension forces causing its shape to remain spherical. This ratio is usually expressed by the Weber number. At low values of Weber number (slow relative speed or small droplet diameter), droplets remain nearly spherical. If the critical Weber number for break-up is sufficiently exceeded, disruption of a water droplet occurs within a very short time. The order of droplet disruption time is typically given by the following (Ref. 17)

$$\tau_{rupt} = (0.3 \sim 1) \frac{\pi}{4} \sqrt{\frac{\rho_f D^3}{\sigma}}$$

where σ is surface tension of water droplet.

Estimated values of droplet rupture time for several droplet sizes are presented in Table A.3.6.

3.3.3 Evaporation Time

(i) Droplet Evaporation with Negligible Relative Velocity with Respect to Gas Phase.

Under negligible relative velocity conditions, the evaporation time can be deduced from a heat balance over a droplet. The rate of mass transfer from a saturated surface may be expressed by the relation, namely,

$$-H_v \frac{dm}{dt} = h_c A \Delta T \quad (\text{A.3.1})$$

where

H_v = latent heat

m = mass of droplet

h_c = convection heat transfer coefficient

A = surface area of droplet

ΔT = temperature difference between droplet surface and surrounding air

Since $m = \frac{\pi}{6} D^3 \rho_d$ where ρ_d is density of droplet and D is diameter of droplet, Eq. (A.3.1) may be written as

$$dt = - \frac{H_v \rho_d}{2 h_c \Delta T} d(D) \quad (\text{A.3.2})$$

The term $(- \frac{H_v \rho_d}{2 \Delta T})$ remains constant during the evaporation (Ref.35).

Integration of Eq. (A.3.2) yields the evaporation time namely,

$$t = \frac{H_v \rho_d}{2 \Delta T} \int_{D_0}^D \frac{d(D)}{h_c} \quad (\text{A.3.3})$$

Experimental data have shown that heat transfer to a spherical droplet in still air can be expressed as

$$Nu = \frac{h_c D}{K_d} = 2.0 \quad (A.3.4)$$

Under the negligible relative velocity condition, by using Eq(A.3.4), Eq(A.3.3) becomes

$$\begin{aligned} t &= \frac{H_v \rho_d}{4K_d \Delta T} \int_0^{D_0} D \, d(D) \\ &= \frac{H_v \rho_d}{8K_d \Delta T} (D_0^2 - D^2) \\ &= \frac{H_v \rho_d}{8K_d \Delta T} D_0^2 \left\{ 1 - \left(\frac{D}{D_0} \right)^2 \right\} \quad (A.3.5) \end{aligned}$$

Equation (A.3.5) is presented graphically in Figure A.3.1.

(ii) Droplet Evaporation with Large Relative Velocity with respect to Gas Phase

The vaporization rate of a pure liquid drop may be expressed as follows (Ref.36):

$$\frac{dm}{dt} = \frac{K_a \Delta T}{H_v} \pi D \left(\frac{K_a}{K_v} \right)^{0.5} \cdot Nu \quad (A.3.6)$$

where H_v = latent heat of vaporization

D = droplet diameter

ΔT = temperature difference between droplet surface and surrounding air

K_a = thermal conductivity of air

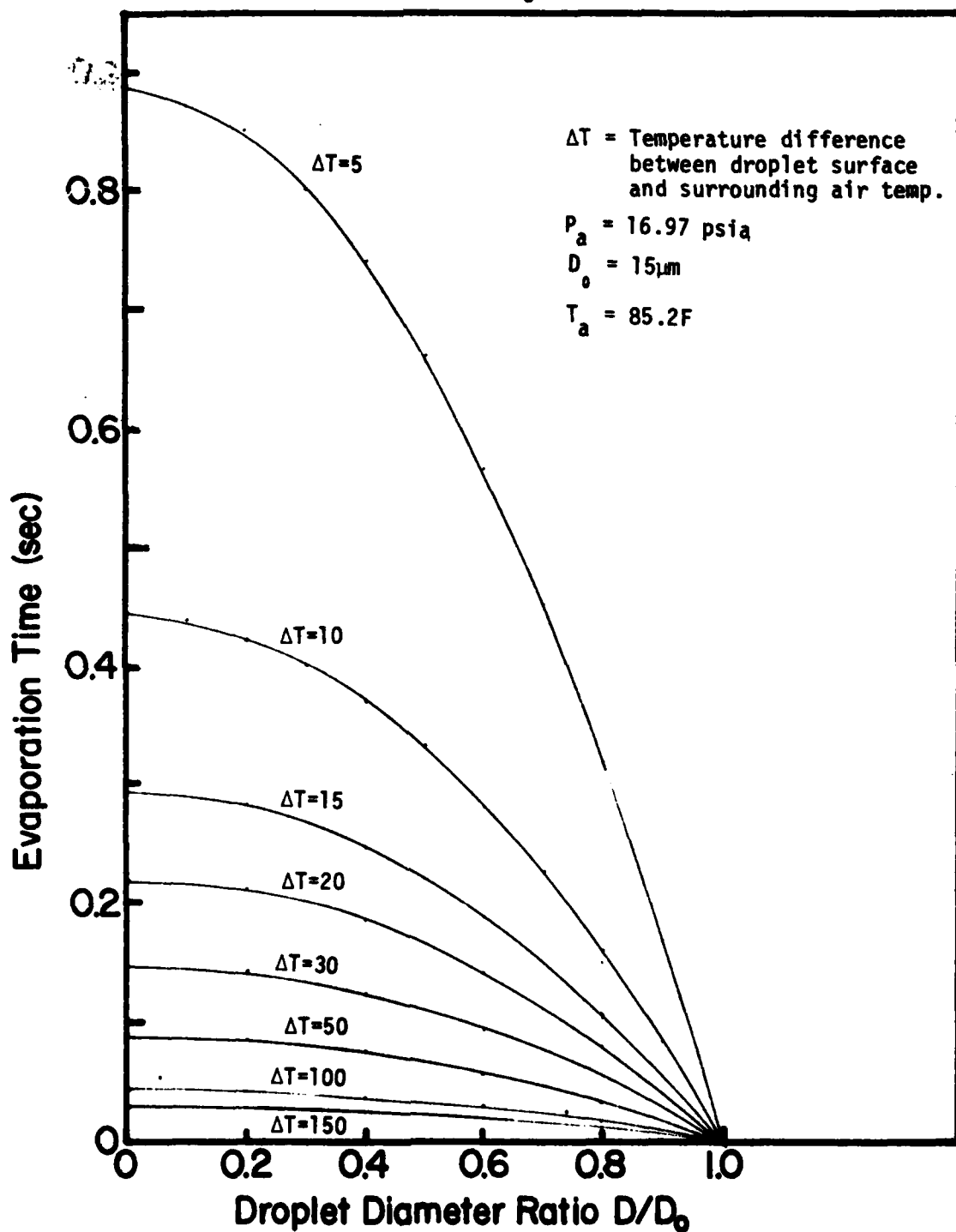
K_v = thermal conductivity of water vapor

Re = Reynolds number based on droplet diameter and relative velocity

Sc = Schmidt number

$$Nu = 2.0 + 0.303 (Re \cdot Sc)^{0.6}$$

Fig.A.3.1 Evaporation Time with Negligible
Relative Velocity Effect



In order to determine the time required for a droplet of a given diameter to vaporize completely, Eq.(A.3.6) may be rewritten as follows.

$$dt = \frac{\rho_d H_v}{4K_a \Delta T} \cdot \frac{1}{\left(\frac{K_a}{K_v}\right)^{0.5}} \cdot \frac{D d(D)}{1 + 0.152 (Re \cdot Sc)^{0.6}} \quad (A.3.7)$$

where ρ_d is density of droplet.

Integrating equation (A.3.7) yields the total evaporation time.

$$t = \int_0^{D_0} \alpha \frac{D d(D)}{1 + 0.152 (Re \cdot Sc)^{0.6}} \quad (A.3.8)$$

$$\text{where } \alpha = \frac{\rho_d H_v}{4K_a \Delta T} \cdot \frac{1}{\left(\frac{K_a}{K_v}\right)^{0.5}}$$

D_0 = droplet original diameter

From the definition of Reynolds number and Schmidt number, the term $0.152 (Re \cdot Sc)^{0.6}$ can be expressed as follows.

$$\begin{aligned} 0.152 (Re \cdot Sc)^{0.6} &= \left(\frac{D V_r \rho_a}{\mu} \cdot \frac{\bar{R} T_{av} \mu}{P_a M_{av} D_v} \right)^{0.6} \cdot 0.152 \\ &= D^{0.6} \cdot \left(\frac{V_r \rho_a \bar{R} T_{av}}{P_a M_{av} D_v} \right)^{0.6} \cdot 0.152 \\ &= \beta \cdot D^{0.6} \end{aligned}$$

$$\text{where } \beta = 0.152 \frac{V_r \rho_a \bar{R} T_{av}}{P_a M_{av} D_v}$$

V_r = relative velocity between droplet and surrounding air.

ρ_a = density of surrounding air

\bar{R} = universal gas constant

T_{av} = average temperature between droplet surface and surrounding air

P_a = pressure of surrounding air

M_{av} = average molecular weight between droplet and surrounding air

D_v = vapour diffusivity

Then Eq.(A.3.8) becomes the following.

$$t = \int_D \frac{D_0}{1 + \frac{\alpha D}{\beta D^{0.6}}} d(D)$$

or

$$t = \int_D \frac{D_0}{1 + \frac{\alpha x}{\beta x^{0.6}}} dx \quad (A.3.9)$$

Using Simpson's method, Eq.(A.3.9) can be integrated numerically. The results are presented in Figures A.3.2 to A.3.4.

3.3.4 Evaporation Time With Boiling

If the temperature of a water droplet reaches the local saturation temperature, the water droplet undergoes boiling provided there is adequate heat available in the gas phase and one has to consider the boiling heat transfer.

The vaporization rate can be calculated from Eq.(A.3.6) if the Nusselt number based on the boiling heat-transfer coefficient is used. However, the mechanism of boiling in forced convection is complex and no fundamental theory is yet available to predict the boiling heat-transfer coefficient for forced-convection boiling.

The remaining procedure for calculating evaporation time is the same as described in Section 3.3.3 of this Appendix.

Fig.A.3.2 Evaporation Time with Effect of Relative Velocity

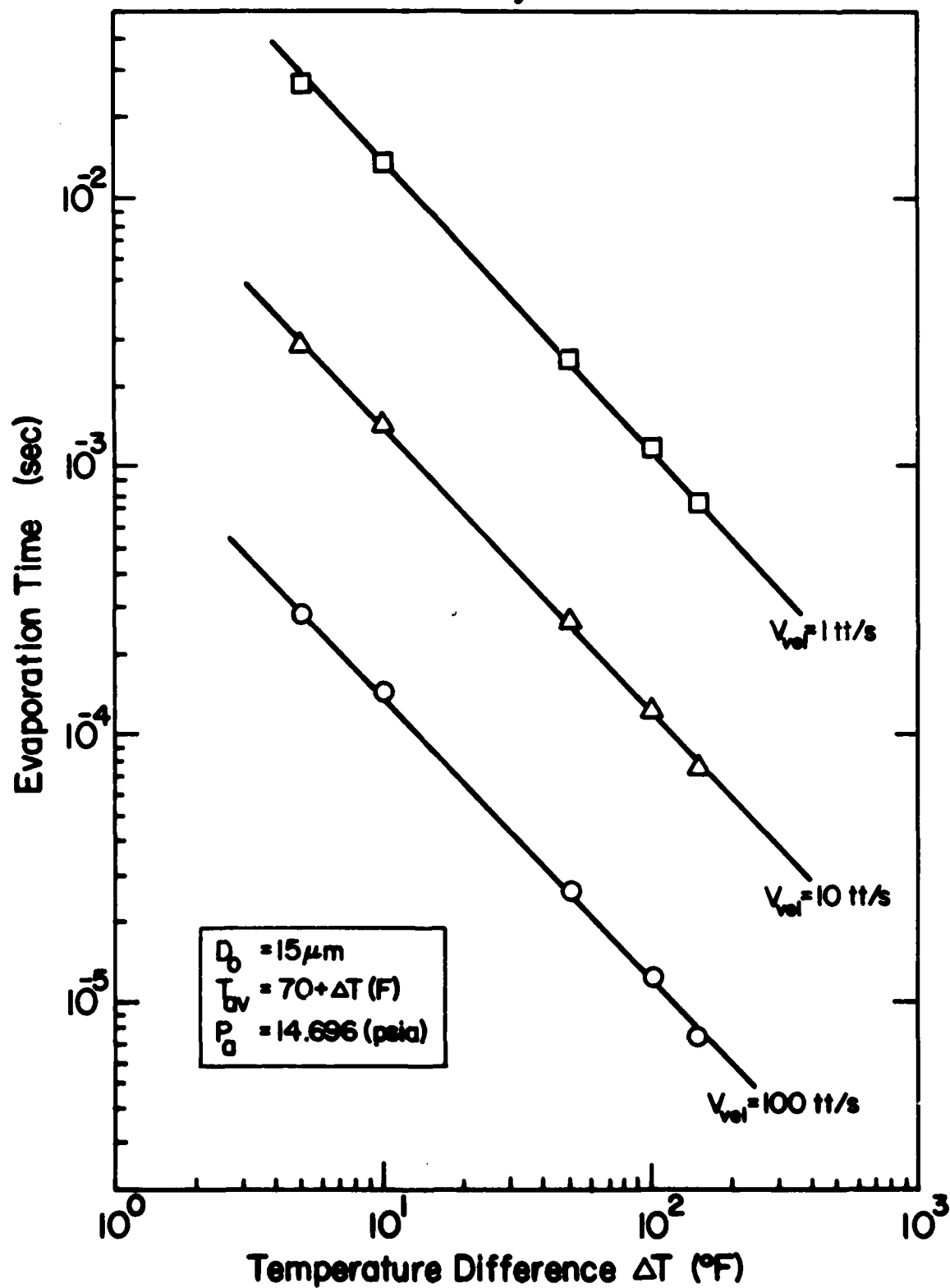


Fig.A.3.3 Evaporation Time with Effect of Relative Velocity

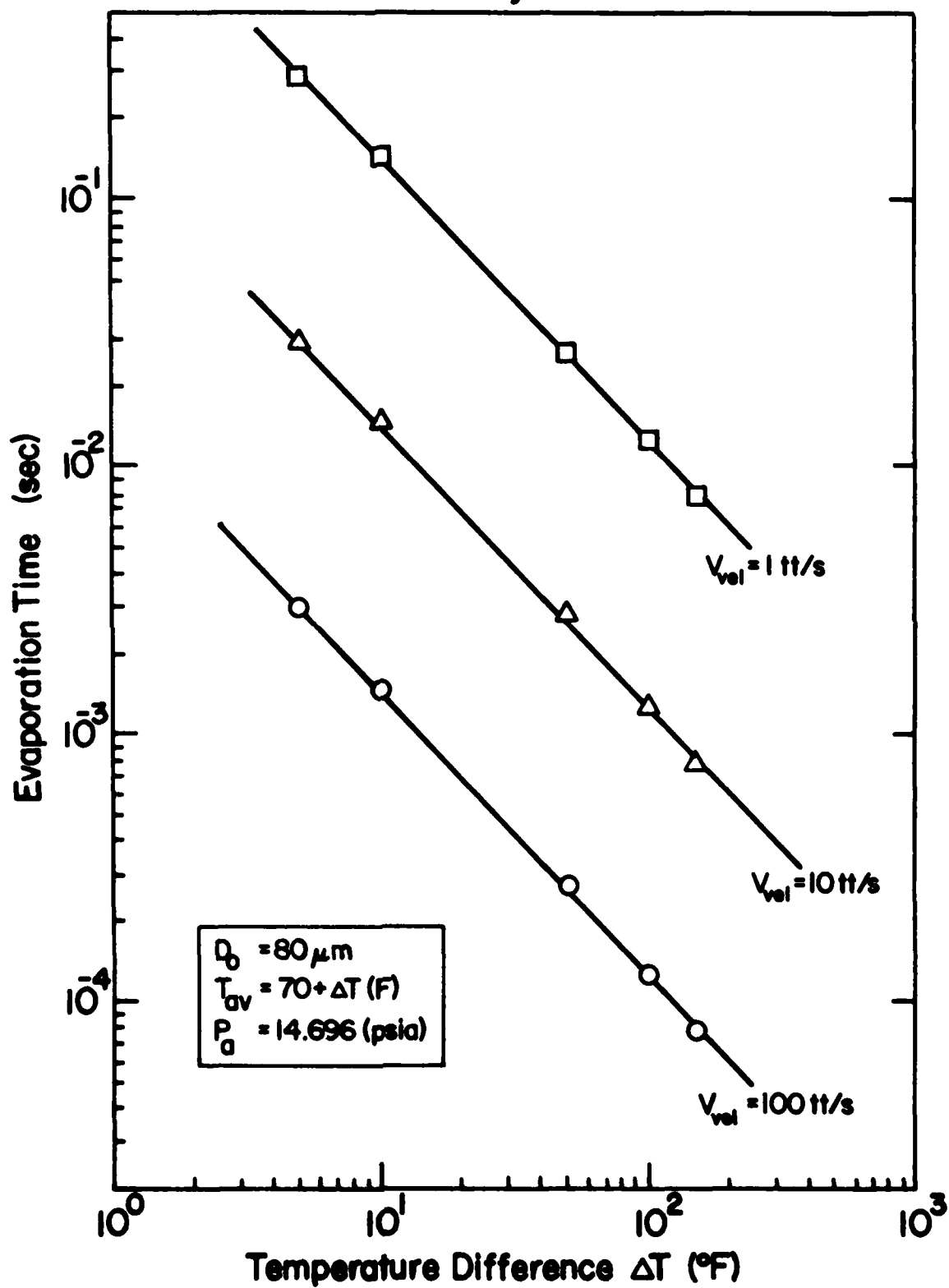
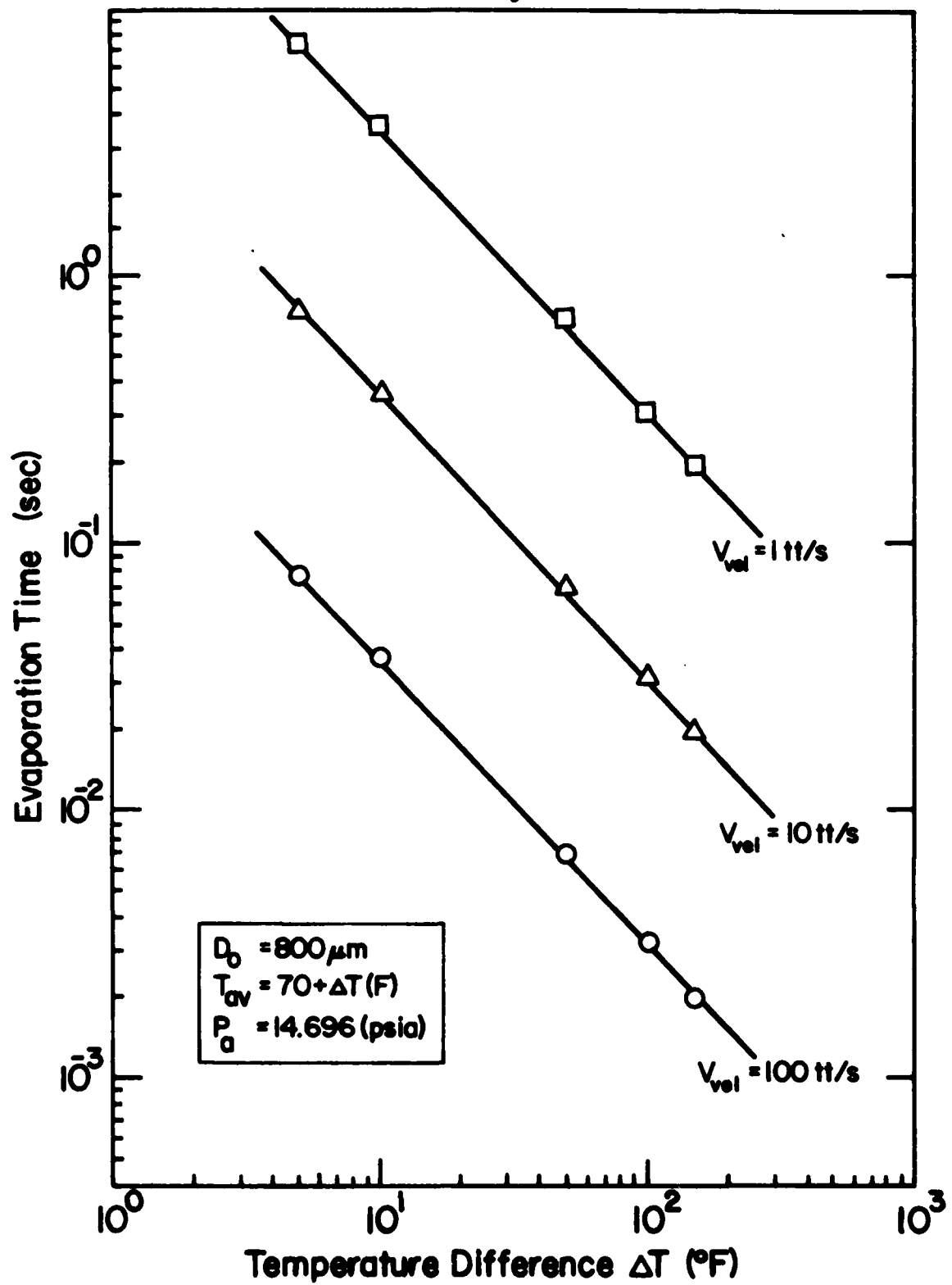


Fig.A.3.4 Evaporation Time with Effect of Relative Velocity



APPENDIX 4

AEROTHERMODYNAMIC EQUATIONS FOR TWO-PHASE FLOW IN COMPRESSORS

The aerothermodynamic equations for two-phase flow in compressors are developed based upon the following assumptions:

- (1) The two phase mixture consists of a gas phase with air and water vapor, and a liquid phase with droplets of sizes d and D . Droplets of size d (referred to hereafter as d -droplets) belong to the class of "small" droplets and those of size D (referred to hereafter as D -droplets) belong to the class of "large" droplets.
- (2) The gas phase is a perfect gas continuum. When several gases are present, they are assumed to be thoroughly mixed and in thermodynamic equilibrium.
- (3) The water droplets are finely divided so that any volume element considered contains many droplets, and the major length scale of the problem is assumed to be large compared with the droplet dimension. Then the droplets may be treated from a continuum viewpoint. However, they are supposed to be not numerous enough to contribute to pressure. While the droplet and gas are two continua, co-existing in space and interacting with each other through the transfer of heat, mass, and momentum, the droplets are sufficiently separated so that the (local) field of any droplet is independent of the field of other droplets.
- (4) Notwithstanding the assumption of continuum for droplets, momentum, heat and mass transfer arise between the gas and liquid phases.

Other features of the balance equations are discussed in the following whenever appropriate.

The balance equations for a compressor flow consist of the following.

- (i) mass balance;
- (ii) momentum balance;
- (iii) energy balance; and
- (iv) radial equilibrium or another equation to provide a means of inter-relating spanwise distributions.

In the present formulation, a radial equilibrium equation has been developed.

The compressor aerothermodynamic equations developed here are based on Refs. 11 and 30.

The equations are developed in an absolute frame of reference in Section 1 of this Appendix. The basic equations are presented using two kinds of coordinate systems, namely intrinsic and cylindrical coordinate systems. Furthermore, the equations are transformed into coordinate systems that are stationary with respect to a rotating blade row. In Section 2 of this Appendix, a description of coordinate systems is provided. In Section 3 of this Appendix, the so-called one-dimensional equations, applicable to a chosen radial location of a compressor, are derived. Finally, the application of one-dimensional equations is discussed in Section 4.

4.1 Derivation of Basic Equations

A. Mass Balance Equation

Gas phase

The balance of mass for the gaseous phase requires that the time rate of change of mass in a volume V , which moves with the substance under consideration, be equal to the rate at which water vapor is added to the volume by evaporation. This may be expressed as follows.

$$\frac{\partial}{\partial t} \iiint_V \rho'_g dV + \iint_S \rho'_g u_{gi} n_i dS = \iiint_V (\dot{m}_{ed} + \dot{m}_{eD}) dV$$

where \dot{m}_{ed} and \dot{m}_{eD} are evaporation rate per unit volume of mixture of d-droplet and D-droplet, respectively, and ρ'_g is the bulk gas density defined as mass of gas per unit volume of mixture.

Using Gauss Divergent Theorem, the above equation becomes the following:

$$\iiint_V \left\{ \frac{\partial \rho'_g}{\partial t} + \frac{\partial}{\partial x_i} (\rho'_g u_{gi}) \right\} dV = \iiint_V (\dot{m}_{ed} + \dot{m}_{eD}) dV$$

Since the above equation holds over an arbitrary volume, it must hold point by point. Hence one can obtain the differential equation, namely,

$$\frac{\partial \rho'_g}{\partial t} + \frac{\partial}{\partial x_i} (\rho'_g u_{gi}) = \dot{m}_{ed} + \dot{m}_{eD} \quad (A.4.1)$$

which is the mass balance equation for the gaseous phase per unit volume of mixture. Since the bulk density of gas phase, ρ'_g , is equal to $\alpha_g \rho_g$, where α_g and ρ_g are the volume fraction and actual density of gas phase, Eq. (A.4.1) can be written as follows.

$$\frac{\partial}{\partial t} (\alpha_g \rho_g) + \frac{\partial}{\partial x_i} (\alpha_g \rho_g u_{gi}) = \dot{m}_{ed} + \dot{m}_{eD} \quad (A.4.2)$$

Liquid phase

In a similar manner, one can develop the mass balance equation for the liquid phase. Denoting the bulk densities of d- and D-droplets by ρ'_d and ρ'_D , defined as the mass of d- and D-droplets per unit volume of mixture, and the velocity vector of the mass motion of d- and D-droplets by u_{di} and u_{Di} , the mass balance equations for d- and D-droplets per unit volume of mixture become the following.

d-droplet

$$\frac{\partial \rho'_d}{\partial t} + \frac{\partial}{\partial x_i} (\rho'_d u_{di}) = -\dot{m}_{ed} \quad (A.4.3)$$

D-droplet

$$\frac{\partial \rho_D}{\partial t} + \frac{\partial}{\partial x_i} (\rho_D u_{Di}) = - \dot{m}_{ed} \quad (A.4.4)$$

Using the relations $\rho_d' = \rho_w \alpha_d$ and $\rho_D' = \rho_w \alpha_D$, where α_d and α_D are the volume fraction of d- and D-droplets and ρ_w is the material density of water, Eqs. (A.4.3) and (A.4.4) can be written as follows.

$$\frac{\partial}{\partial t} (\rho_w \alpha_d) + \frac{\partial}{\partial x_i} (\rho_w \alpha_d u_{di}) = - \dot{m}_{ed} \quad (A.4.5)$$

$$\frac{\partial}{\partial t} (\rho_w \alpha_D) + \frac{\partial}{\partial x_i} (\rho_w \alpha_D u_{Di}) = - \dot{m}_{ed} \quad (A.4.6)$$

The continuity equation for the mixture (gas + d-droplet + D-droplet) becomes the following.

$$\frac{\partial}{\partial t} (\rho_g' + \rho_d' + \rho_D') + \frac{\partial}{\partial x_i} (\rho_g' u_{gi} + \rho_d' u_{di} + \rho_D' u_{Di}) = 0 \quad (A.4.7)$$

or

$$\frac{\partial}{\partial t} (\alpha_g \rho_g + \alpha_d \rho_w + \alpha_D \rho_w) + \frac{\partial}{\partial x_i} (\alpha_g \rho_g u_{gi} + \alpha_d \rho_w u_{di} + \alpha_D \rho_w u_{Di}) = 0 \quad (A.4.8)$$

B. Momentum Balance Equation

Gas phase

The momentum vector per unit volume of mixture is $\rho_g' u_{gi}$, and the time rate of change in the total momentum of the moving region is

$$\frac{\partial}{\partial t} \iiint_V \rho_g' u_{gi} dV + \iint_S \rho_g' u_{gi} u_{gi} n_j dS$$

Using the divergent theorem, this becomes

$$\iiint_V \left\{ \frac{\partial}{\partial t} (\rho_g' u_{gi}) + \frac{\partial}{\partial x_j} (\rho_g' u_{gi} u_{gj}) \right\} dV \quad (A.4.9)$$

The gaseous phase is acted upon by two distinct sets of forces:

(i) those imposed by the presence of the droplets; and (ii) those stresses

related to the gas phase itself. The external body force due to gravitational fields is explicitly neglected. The forces per unit volume of mixture acting upon the gaseous phase due to d- and D-droplets are denoted by F_{Igd_i} and F_{IgD_i} . Internal stresses set up within the gaseous phase are assumed to be of the same form as those which would exist in the absence of the liquid phase, since the volume fraction occupied by the liquid phase is assumed to be small. Under these conditions, the stresses in the gaseous phase may be written as follows.

$$\sigma_{ij} = \delta_{ij} \left(p + \frac{2}{3} \mu_e \frac{\partial u_{gk}}{\partial x_k} \right) + \mu_e \left(\frac{\partial u_{gi}}{\partial x_j} + \frac{\partial u_{gj}}{\partial x_i} \right) \quad (A.4.10)$$

where μ_e is the effective coefficient of viscosity. The pressure, p , is the local scalar pressure corresponding to the local temperature and density through the equation of state. Thus, the forces acting upon the volume of matter under consideration are

$$\iiint_V (F_{Igd_i} + F_{IgD_i}) dV + \iint_S \sigma_{ij} n_j dS. \quad (A.4.11)$$

Under the conditions of ordinary fluid mechanics with no internal source for gas phase, the time rate of change of momentum, Eq. (A.4.9), would be equated to the external forces, Eq. (A.4.11). However, there is an additional source of momentum in two phase flow due to the creation of gaseous medium by evaporation of the droplet. In accounting for this process, we assume that since the phase transition takes place at the surface of a droplet the mass is added to the gaseous phase at the droplet velocity. Therefore, the momentum added per unit volume of mixture due to vaporization is

$$\iiint_V (\dot{m}_{ed} u_{di} + \dot{m}_{eD} u_{Di}) dV$$

Thus, the complete relationship for the change of momentum of the gaseous phase is as follows.

$$\begin{aligned}
\iiint_V \left\{ \frac{\partial}{\partial t} (\rho'_g u_{gi}) + \frac{\partial}{\partial x_i} (\rho'_g u_{gi} u_{gi}) \right\} dV = & \iiint_V (F_{Igd_i} + F_{IgD_i}) dV \\
& + \iint_S \sigma_{ij} n_j dS \\
& + \iiint_V (\dot{m}_{ed} u_{di} + \dot{m}_{eD} u_{Di}) dV
\end{aligned}$$

Using the divergent theorem, this becomes

$$\begin{aligned}
\iiint_V \left\{ \frac{\partial}{\partial t} (\rho'_g u_{gi}) + \frac{\partial}{\partial x_i} (\rho'_g u_{gi} u_{gi}) - \frac{\partial \sigma_{ij}}{\partial x_j} - (F_{Igd_i} + F_{IgD_i}) \right. \\
\left. - (\dot{m}_{ed} u_{di} + \dot{m}_{eD} u_{Di}) \right\} dV = 0
\end{aligned}$$

Thus, the momentum balance equation for gas phase per unit volume of mixture becomes the following.

$$\begin{aligned}
& \frac{\partial}{\partial t} (\rho'_g u_{gi}) + \frac{\partial}{\partial x_i} (\rho'_g u_{gi} u_{gi}) \\
& = - \frac{\partial p}{\partial x_i} + \frac{\partial \tau_{ij}}{\partial x_j} + F_{Igd_i} + F_{IgD_i} + \dot{m}_{ed} u_{di} + \dot{m}_{eD} u_{Di} \quad (A.4.12)
\end{aligned}$$

Since $\rho'_g = \alpha_g \rho_g$, this equation may be rewritten as follows.

$$\begin{aligned}
& \frac{\partial}{\partial t} (\alpha_g \rho_g u_{gi}) + \frac{\partial}{\partial x_i} (\alpha_g \rho_g u_{gi} u_{gi}) \\
& = - \frac{\partial p}{\partial x_i} + \frac{\partial \tau_{ij}}{\partial x_j} + F_{Igd_i} + F_{IgD_i} + \dot{m}_{ed} u_{di} + \dot{m}_{eD} u_{Di} \quad (A.4.13)
\end{aligned}$$

Liquid phase

Arguments similar to those for the gas phase lead to the momentum balance equation for droplets per unit volume of mixture.

d-droplets

$$\frac{\partial}{\partial t} (\rho'_d u_{di}) + \frac{\partial}{\partial x_i} (\rho'_d u_{di} u_{di}) = - F_{Igd i} - \dot{m}_{ed} u_{di}$$

or

$$\frac{\partial}{\partial t} (\alpha_d \rho_w u_{di}) + \frac{\partial}{\partial x_i} (\alpha_d \rho_w u_{di} u_{di}) = - F_{Igd i} - \dot{m}_{ed} u_{di} \quad (A.4.14)$$

D-droplets

$$\frac{\partial}{\partial t} (\rho'_D u_{Di}) + \frac{\partial}{\partial x_i} (\rho'_D u_{Di} u_{Di}) = - F_{IGDi} - \dot{m}_{eD} u_{Di} \quad (A.4.15)$$

or

$$\frac{\partial}{\partial t} (\alpha_D \rho_w u_{Di}) + \frac{\partial}{\partial x_i} (\alpha_D \rho_w u_{Di} u_{Di}) = - F_{IGDi} - \dot{m}_{eD} u_{Di} \quad (A.4.16)$$

From Eqs. (A.4.13), (A.4.15) and (A.4.16), the momentum balance equation for mixture becomes:

$$\begin{aligned} & \frac{\partial}{\partial t} (\alpha_g \rho_g u_{gi} + \alpha_d \rho_w u_{di} + \alpha_D \rho_w u_{Di}) \\ & + \frac{\partial}{\partial x_i} (\alpha_g \rho_g u_{gi} u_{gi} + \alpha_d \rho_w u_{di} u_{di} + \alpha_D \rho_w u_{Di} u_{Di}) = - \frac{\partial p}{\partial x_i} + \frac{\partial \tau_{ij}}{\partial x_j} \end{aligned}$$

Using the mass balance equation, Eqs. (A.4.13), (A.4.15), and (A.4.16) become the following.

Gas phase

$$\begin{aligned} & (\alpha_g \rho_g) \left(\frac{\partial}{\partial t} + u_{gj} \frac{\partial}{\partial x_j} \right) u_{gi} \\ & = F_{Igd i} + F_{IGDi} - \frac{\partial p}{\partial x_i} + \frac{\partial \tau_{ij}}{\partial x_j} + \dot{m}_{eD} (u_{Di} - u_{gi}) + \dot{m}_{ed} (u_{di} - u_{gi}) \end{aligned} \quad (A.4.17)$$

Liquid phase

d-droplet

$$(\alpha_d \rho_w) \left(\frac{\partial}{\partial t} + u_{dj} \frac{\partial}{\partial x_j} \right) u_{di} = - F_{Igd i} \quad (A.4.18)$$

D-droplet

$$(\alpha_D \rho_w) \left(\frac{\partial}{\partial t} + u_{Dj} \frac{\partial}{\partial x_j} \right) u_{Di} = - F_{IgDi} \quad (\text{A.4.19})$$

C. Energy Balance Equation

Gas phase

Denoting the internal energy per unit mass of the gaseous phase by e_g , the change of energy with respect to time of the gaseous phase in a volume V at time t is

$$\begin{aligned} & \frac{\partial}{\partial t} \iiint_V \rho'_g \left(e_g + \frac{1}{2} u_{gi} u_{gi} \right) dV + \iint_S \rho'_g \left(e_g + \frac{1}{2} u_{gi} u_{gi} \right) u_{gi} n_j dS \\ &= \iiint_V \left\{ \frac{\partial}{\partial t} \left[\rho'_g \left(e_g + \frac{1}{2} u_{gi} u_{gi} \right) \right] + \frac{\partial}{\partial x_j} \left[\rho'_g \left(e_g + \frac{1}{2} u_{gi} u_{gi} \right) u_{gj} \right] \right\} dV \end{aligned} \quad (\text{A.4.20})$$

Work is done on the gaseous phase by surface stresses represented by the stress tensor, σ_{ij} , and by the force F_{Igdi} and F_{Igdj} exerted by the liquid phase. The work done on the volume V by external forces is then given by the following:

$$\begin{aligned} & \iint_S \sigma_{ij} u_{gi} n_j dS + \iiint_V F_{IgDi} u_{Di} dV + \iiint_V F_{Igdj} u_{dj} dV \\ &= \iiint_V \left\{ \frac{\partial}{\partial x_j} (\sigma_{ij} u_{gi}) + F_{IgDi} u_{Di} + F_{Igdj} u_{dj} \right\} dV \end{aligned}$$

There is an exchange of energy due to phase change. This takes place very close to the liquid surface. The kinetic energy associated with the vapor that is produced may more nearly correspond to the velocity of the droplet. Similarly, the internal energy of the vapor may be taken to correspond to the vapor internal energy at the droplet temperature, since that is the gas temperature immediately adjacent to

the droplet. Furthermore when evaporation takes place, the specific volume increases and this increase in specific volume does work against pressure. This work is given by the following.

$$p (v_g(T_p) - v_p)$$

where $v_g(T_p)$ and v_p are the specific volume of vapor and water at the local droplet temperature, respectively. Since $v_g(T_p) = [1/\rho_g(T_p)]$ and $v_p = (1/\rho_p)$, and considering that $\rho_g(T_p) \ll \rho_p$, the work done on the gas phase due to increase of specific volume may be written as follows

$$p (v_g(T_p) - v_p) = p \left(\frac{1}{\rho_g(T_p)} - \frac{1}{\rho_p} \right) \div \frac{p}{\rho_g(T_p)} \quad (\text{A.4.21})$$

When evaporation occurs, the gaseous phase has to supply latent heat to the liquid phase. Then, denoting the internal energy of water vapor at the local droplet temperature by $e_g(T_p)$, the energy change per unit time due to phase change is given by the following.

$$\begin{aligned} & \iiint_V \dot{m}_{ed} \left\{ e_g(T_D) + \frac{1}{2} u_{Di} u_{Di} + \frac{p}{\rho_g(T_D)} - \Delta H_v \right\} dV \\ & + \iiint_V \dot{m}_{ed} \left\{ e_g(T_d) + \frac{1}{2} u_{di} u_{di} + \frac{p}{\rho_g(T_d)} - \Delta H_v \right\} dV \end{aligned} \quad (\text{A.4.22})$$

Next, one has to account for the heat transfer between the gas and the liquid phases. If \dot{Q}_{gd} and \dot{Q}_{gD} represent the heat transfer rate per unit volume of mixture from the gas phase to the d- and D-droplets, the energy change due to this process is given by the expression;

$$- \iiint_V (\dot{Q}_{gd} + \dot{Q}_{gD}) dV \quad (\text{A.3.23})$$

Using Eqs. (A.4.20) to (A.4.23), the energy balance equation for the gas phase may be written as follows.

$$\begin{aligned}
& \frac{\partial}{\partial t} \{ \rho'_g (e_g + \frac{1}{2} u_{gi} u_{gi}) \} + \frac{\partial}{\partial x_j} \{ \rho'_g u_{gj} (e_g + \frac{1}{2} u_{gi} u_{gi}) \} \\
& = \frac{\partial}{\partial x_j} (\sigma_{ij} u_{gi}) + F_{Igd} u_{di} + F_{IgD} u_{Di} - \dot{Q}_{gd} - \dot{Q}_{gD} - \bar{P}_g \\
& \quad + \dot{m}_{ed} \{ e_g(T_d) + \frac{1}{2} u_{di} u_{di} + \frac{p}{\rho'_g(T_d)} - \Delta H_v \} \\
& \quad + \dot{m}_{eD} \{ e_g(T_D) + \frac{1}{2} u_{Di} u_{Di} + \frac{p}{\rho'_g(T_D)} - \Delta H_v \}
\end{aligned} \tag{A.4.24}$$

where \bar{P}_g is the external shaft work per unit time per unit volume of mixture done on the gas phase.

Liquid phase

Similarly, the energy balance equation for d- and D-droplets can be derived as follows.

d-droplet

$$\begin{aligned}
& \frac{\partial}{\partial t} \{ \rho'_d (e_d + \frac{1}{2} u_{di} u_{di}) \} + \frac{\partial}{\partial x_j} \{ \rho'_d u_{dj} (e_d + \frac{1}{2} u_{di} u_{di}) \} \\
& = - F_{Igd} u_{di} - \dot{m}_{ed} (e_d + \frac{1}{2} u_{di} u_{di}) + \dot{Q}_{gd} + \bar{P}_d
\end{aligned} \tag{A.4.25}$$

D-droplet

$$\begin{aligned}
& \frac{\partial}{\partial t} \{ \rho'_D (e_D + \frac{1}{2} u_{Di} u_{Di}) \} + \frac{\partial}{\partial x_j} \{ \rho'_D u_{Dj} (e_D + \frac{1}{2} u_{Di} u_{Di}) \} \\
& = - F_{IgDi} u_{Di} - \dot{m}_{eD} (e_D + \frac{1}{2} u_{Di} u_{Di}) + \dot{Q}_{gD} + \bar{P}_D
\end{aligned} \tag{A.4.26}$$

where \bar{P}_d and \bar{P}_D represent the shaft work per unit volume of mixture done on the d- and D-droplets, and e_d and e_D represent the internal energy of d- and D-droplets per unit mass.

The energy balance equation for the mixture can be obtained from Eqs. (A.4.24) to (A.4.26) as follows.

$$\begin{aligned}
& \frac{\partial}{\partial t} \left\{ \rho_g' (e_g + \frac{1}{2} u_{gi} u_{gi}) + \rho_d' (e_d + \frac{1}{2} u_{di} u_{di}) + \rho_D' (e_D + \frac{1}{2} u_{Di} u_{Di}) \right\} \\
& + \frac{\partial}{\partial x_j} \left\{ \rho_g' u_{gj} (e_g + \frac{1}{2} u_{gi} u_{gi}) + \rho_d' u_{dj} (e_d + \frac{1}{2} u_{di} u_{di}) + \rho_D' u_{Dj} (e_D \right. \\
& \left. + \frac{1}{2} u_{Di} u_{Di}) \right\} = \frac{\partial}{\partial t} (\sigma_{ij} u_{gi}) + \bar{P}_g + \bar{P}_d + \bar{P}_D \\
& + \dot{m}_{ed} \left\{ e_g(T_d) - e_d + \frac{p}{\rho_g'(T_d)} - \Delta H_v \right\} \\
& + \dot{m}_{eD} \left\{ e_g(T_D) - e_D + \frac{p}{\rho_g'(T_D)} - \Delta H_v \right\} \quad (A.4.27)
\end{aligned}$$

The quantities e_d and e_D represent the thermodynamic internal energy of the d- and D- droplets, and ΔH_v represents the latent heat of phase transition which is defined by the relation, namely,

$$e_p + \Delta H_v = h_g(T_p) \quad (A.4.28)$$

where e_p denotes the internal energy per unit mass and $h_g(T_p)$ is the enthalpy of the gaseous phase per unit mass at the local droplet temperature, T_p .

Using Eq. (A.4.28), the last two terms of Eq. (A.4.27) disappear and one obtains:

$$\begin{aligned}
& \frac{\partial}{\partial t} \left\{ \rho_g' (e_g + \frac{1}{2} u_{gi} u_{gi}) + \rho_d' (e_d + \frac{1}{2} u_{di} u_{di}) + \rho_D' (e_g + \frac{1}{2} u_{Di} u_{Di}) \right\} \\
& + \frac{\partial}{\partial x_j} \left\{ \rho_g' u_{gj} (e_g + \frac{1}{2} u_{gi} u_{gi}) + \rho_d' u_{dj} (e_d + \frac{1}{2} u_{di} u_{di}) \right. \\
& \left. + \rho_D' u_{Dj} (e_D + \frac{1}{2} u_{Di} u_{Di}) \right\} = \frac{\partial}{\partial x_j} (\sigma_{ij} u_{gi}) + \bar{P}_g + \bar{P}_d + \bar{P}_D. \quad (A.4.29)
\end{aligned}$$

Equations (A.4.24) to (A.4.26) may be transformed into forms that correspond more clearly to the usual energy equation for a single component gas. The left-hand side of Eq. (A.4.24) can be written in the

following manner.

L.H.S. of Eq. (A.4.24)

$$\begin{aligned}
 &= \frac{\partial}{\partial t} \left\{ \rho'_g (e_g + \frac{1}{2} u_{gi} u_{gi}) \right\} + \frac{\partial}{\partial x_j} \left\{ \rho'_g u_{gj} (e_g + \frac{1}{2} u_{gi} u_{gi}) \right\} \\
 &= \rho'_g \frac{\partial}{\partial t} (e_g + \frac{1}{2} u_{gi} u_{gi}) + \frac{\partial \rho'_g}{\partial t} (e_g + \frac{1}{2} u_{gi} u_{gi}) \\
 &\quad + \rho'_g u_{gi} \frac{\partial}{\partial x_j} (e_g + \frac{1}{2} u_{gi} u_{gi}) + \frac{\partial (\rho'_g u_{gj})}{\partial x_j} (e_g + \frac{1}{2} u_{gi} u_{gi}) \\
 &= \rho'_g \frac{\partial}{\partial t} (e_g + \frac{1}{2} u_{gi} u_{gi}) + \frac{\partial \rho'_g}{\partial t} (e_g + \frac{1}{2} u_{gi} u_{gi}) \\
 &\quad + \rho'_g u_{gj} \frac{\partial}{\partial x_j} (e_g + \frac{1}{2} u_{gi} u_{gi}) + (\dot{m}_{ed} + \dot{m}_{eD} - \frac{\partial \rho'_g}{\partial t}) (e_g + \frac{1}{2} u_{gi} u_{gi}) \\
 &= \rho'_g \left[\frac{\partial}{\partial t} (\frac{1}{2} u_{gi} u_{gi}) + u_{gj} \frac{\partial}{\partial x_j} (\frac{1}{2} u_{gi} u_{gi}) \right] \\
 &\quad + \rho'_g \frac{\partial e_g}{\partial t} + \rho'_g u_{gj} \frac{\partial e_g}{\partial x_j} + (\dot{m}_{ed} + \dot{m}_{eD}) (e_g + \frac{1}{2} u_{gi} u_{gi}) \quad (A.4.30)
 \end{aligned}$$

From Eq. (A.4.19), it follows that

$$\begin{aligned}
 \rho'_g \left(\frac{\partial u_{gi}}{\partial t} + u_{gj} \frac{\partial u_{gi}}{\partial x_j} \right) &= F_{Igd1} + F_{IgD1} + \frac{\partial \sigma_{1j}}{\partial x_j} \\
 &\quad + \dot{m}_{eD} (u_{D1} - u_{g1}) + \dot{m}_{ed} (u_{d1} - u_{g1}) \quad (A.4.31)
 \end{aligned}$$

If this equation is multiplied by u_{gi} and rearranged, the following equation is obtained

$$\begin{aligned}
 &\rho'_g \left[\frac{\partial}{\partial t} (u_{gi} u_{gi}) + u_{gj} \frac{\partial}{\partial x_j} (\frac{1}{2} u_{gi} u_{gi}) \right] \\
 &= (F_{Igd1} + F_{IgD1}) u_{g1} + \frac{\partial \sigma_{1j}}{\partial x_j} u_{g1} \\
 &\quad + \dot{m}_{eD} (u_{D1} - u_{g1}) u_{g1} + \dot{m}_{ed} (u_{d1} - u_{g1}) u_{g1} \quad (A.4.32)
 \end{aligned}$$

Substitution of Eq. (A.4.32) into (A.4.30) yields the following.

L.H.S. of Eq. (A.4.24)

$$\begin{aligned}
 &= (F_{Igd1} + F_{IgD1}) u_{g1} + \frac{\partial \sigma_{1j}}{\partial x_j} u_{g1} + \dot{m}_{eD} (u_{D1} - u_{g1}) u_{g1} \\
 &+ \dot{m}_{ed} (u_{d1} - u_{g1}) + \rho'_g \left(\frac{\partial e_g}{\partial t} + u_{gj} \frac{\partial e_g}{\partial x_j} \right) \\
 &+ (\dot{m}_{ed} + \dot{m}_{eD}) \left(e_g + \frac{1}{2} u_{g1} u_{g1} \right) \quad (A.4.33)
 \end{aligned}$$

Substituting Eq. (A.4.33) into Eq. (A.4.24), it follows that

$$\begin{aligned}
 &\rho'_g \left(\frac{\partial e_g}{\partial t} + u_{gj} \frac{\partial e_g}{\partial x_j} \right) \\
 &= \sigma_{1j} \frac{\partial u_{g1}}{\partial x_j} + F_{Igd1} u_{d1} + F_{IgD1} u_{D1} \\
 &- \dot{Q}_{gd} - \dot{Q}_{gD} + \bar{P}_g - (F_{Igd1} + F_{IgD1}) u_{g1} \\
 &+ \dot{m}_{ed} \left\{ e_g(T_d) + \frac{1}{2} u_{d1} u_{d1} + \frac{p}{\rho'_g(T_d)} - \Delta H_v \right\} \\
 &+ \dot{m}_{eD} \left\{ e_g(T_D) + \frac{1}{2} u_{D1} u_{D1} + \frac{p}{\rho'_g(T_D)} - \Delta H_v \right\} \\
 &- \dot{m}_{ed} (u_{d1} - u_{g1}) u_{g1} - \dot{m}_{eD} (u_{D1} - u_{g1}) u_{g1} \\
 &- (\dot{m}_{ed} + \dot{m}_{eD}) \left(e_g + \frac{1}{2} u_{g1} u_{g1} \right) \\
 &= \sigma_{1j} \frac{\partial u_{g1}}{\partial x_j} - \dot{Q}_{gd} - \dot{Q}_{gD} + \bar{P}_g \\
 &+ (F_{Igd1} - \dot{m}_{ed} u_{g1}) (u_{d1} - u_{g1}) + (F_{IgD1} - \dot{m}_{eD} u_{g1}) (u_{D1} - u_{g1}) \\
 &+ \text{continued}
 \end{aligned}$$

$$\begin{aligned}
& + \dot{m}_{ed} \left\{ e_g(T_d) + \frac{1}{2} u_{di} u_{di} + \frac{p}{\rho'_g(T_d)} - e_g - \frac{1}{2} u_{gi} u_{gi} - \Delta H_v \right\} \\
& + \dot{m}_{eD} \left\{ e_g(T_D) + \frac{1}{2} u_{Di} u_{Di} + \frac{p}{\rho'_g(T_D)} - e_g - \frac{1}{2} u_{gi} u_{gi} - \Delta H_v \right\}
\end{aligned}
\tag{A.4.34}$$

If the term $\sigma_{ij} \frac{\partial u_{gi}}{\partial x_j}$ is expanded, one can get the following.

$$\sigma_{ij} \frac{\partial u_{gi}}{\partial x_j} = \phi - p \frac{\partial u_{gi}}{\partial x_i}
\tag{A.4.35}$$

where ϕ is the viscous dissipation function, given by the relation,

$$\phi = \frac{4}{3} \mu_e \left(\frac{\partial u_{gi}}{\partial x_i} \right)^2 + \frac{1}{2} \mu_e \left(\frac{\partial u_{gi}}{\partial x_i} + \frac{\partial u_{gj}}{\partial x_j} \right)^2_{i \neq j}
\tag{A.4.36}$$

Substitution of Eq. (A.4.35) into (A.4.34) yields

$$\begin{aligned}
& \rho'_g \left(\frac{\partial e_g}{\partial t} + u_{gj} \frac{\partial e_g}{\partial x_j} \right) \\
& = -p \frac{\partial u_{gi}}{\partial x_i} + \phi - \dot{Q}_{gd} - \dot{Q}_{gD} + \bar{P}_g \\
& + (F_{Igd} - \dot{m}_{ed} u_{gi})(u_{di} - u_{gi}) + (F_{IGD} - \dot{m}_{eD} u_{gi})(u_{Di} - u_{gi}) \\
& + \dot{m}_{ed} \left\{ e_g(T_d) + \frac{1}{2} u_{di} u_{di} + \frac{p}{\rho'_g(T_d)} - e_g - \frac{1}{2} u_{gi} u_{gi} - \Delta H_v \right\} \\
& + \dot{m}_{eD} \left\{ e_g(T_D) + \frac{1}{2} u_{Di} u_{Di} + \frac{p}{\rho'_g(T_D)} - e_g - \frac{1}{2} u_{gi} u_{gi} - \Delta H_v \right\}
\end{aligned}
\tag{A.4.37}$$

This is an alternative form of energy equation for the gas phase.

Liquid phase

Similarly the energy equation for liquid phase can be transformed as follows.

From Eq. (A.4.14), the momentum equation for d-droplet becomes:

$$\rho'_d \left(\frac{\partial u_{di}}{\partial t} + u_{dj} \frac{\partial u_{di}}{\partial x_j} \right) = -F_{Igd i}$$

Multiplying both sides by u_{di} , one obtains,

$$\rho'_d \frac{\partial}{\partial t} \left(\frac{1}{2} u_{di} u_{di} \right) + \rho'_d u_{di} \frac{\partial}{\partial x_j} \left(\frac{1}{2} u_{di} u_{di} \right) = -F_{Igd i} u_{di}$$

Using this equation, L.H.S. of Eq. (A.4.25) becomes:

$$\begin{aligned} &= \frac{\partial}{\partial t} \left\{ \rho'_d \left(e_d + \frac{1}{2} u_{gi} u_{gi} \right) \right\} + \frac{\partial}{\partial x_j} \left\{ \rho'_d u_{dj} \left(e_d + \frac{1}{2} u_{di} u_{di} \right) \right\} \\ &= \rho'_d \left[\frac{\partial}{\partial t} \left(\frac{1}{2} u_{di} u_{di} \right) + u_{dj} \frac{\partial}{\partial x_j} \left(\frac{1}{2} u_{di} u_{di} \right) \right] \\ &\quad + \rho'_d \left(\frac{\partial e_d}{\partial t} + u_{dj} \frac{\partial e_d}{\partial x_j} \right) - \dot{m}_{ed} \left(e_p + \frac{1}{2} u_{gi} u_{gi} \right) \\ &= -F_{Igd} u_{gi} + \rho'_d \left(\frac{\partial e_d}{\partial t} + u_{dj} \frac{\partial e_d}{\partial x_j} \right) - \dot{m}_{ed} \left(e_d + \frac{1}{2} u_{di} u_{di} \right) \end{aligned}$$

Thus, Eq. (A.4.25) becomes

$$\rho'_d \left(\frac{\partial e_d}{\partial t} + u_{dj} \frac{\partial e_d}{\partial x_j} \right) = \dot{Q}_{gd} + \bar{P}_d \quad (A.4.38)$$

Similarly, Eq. (A.4.22) becomes

$$\rho'_D \left(\frac{\partial e_D}{\partial t} + u_{Dj} \frac{\partial e_D}{\partial x_j} \right) = \dot{Q}_{gD} + \bar{P}_D \quad (A.4.39)$$

D. Radial Equilibrium Equations

The entropy-enthalpy relation can be written as follows.

$$\frac{dP}{\rho} = dh - T dS$$

where dh and dS are change of enthalpy and entropy per unit mass. The energy equation for steady adiabatic flow is as follows.

$$h = H - \frac{1}{2} V^2$$

or

$$dh = dH - d\left(\frac{1}{2} V^2\right)$$

Thus we get

$$\frac{dp}{\rho} = dH - d\left(\frac{1}{2} V^2\right) - T dS$$

or

$$\frac{1}{\rho} \frac{\partial p}{\partial x_i} = \frac{\partial H}{\partial x_i} - \frac{\partial}{\partial x_i} \left(\frac{1}{2} V^2 \right) - T \frac{\partial S}{\partial x_i}$$

Gas phase

Considering the gas phase, the above equation can be written

$$\frac{1}{\rho} \frac{\partial p}{\partial x_i} = \frac{\partial H_g}{\partial x_i} - \frac{\partial}{\partial x_i} \left(\frac{1}{2} V_g^2 \right) - \frac{1}{\rho_g} T \frac{\partial S'}{\partial x_i} \quad (\text{A.4.40})$$

where $[\partial H_g / \partial x_i]$ is total enthalpy change of gas phase per unit mass of gas phase and where $[\partial S' / \partial x_i]$ is entropy rise of gas phase per unit volume of mixture.

Equation (A.4.17) is the momentum equation for the gas phase.

$$\begin{aligned} (\alpha_g \rho_g) \left(\frac{\partial}{\partial t} + u_{gj} \frac{\partial}{\partial x_j} \right) u_{gi} &= F_{Igd_i} + F_{IgD_i} - \frac{\partial p}{\partial x_i} + \frac{\partial \tau_{ij}}{\partial x_j} \\ &\quad + \dot{m}_{eD}(u_{Di} - u_{gi}) + \dot{m}_{ed}(u_{di} - u_{gi}) \end{aligned}$$

Eliminating the pressure gradient term by using Eq. (A.4.37), it follows that

$$\begin{aligned} (\alpha_g \rho_g) \left(\frac{\partial}{\partial t} + u_{gj} \frac{\partial}{\partial x_j} \right) u_{gi} \\ = F_{Igd_i} + F_{IgD_i} + \frac{\partial \tau_{ij}}{\partial x_j} + \dot{m}_{eD}(u_{Di} - u_{gi}) + \dot{m}_{ed}(u_{di} - u_{gi}) \end{aligned}$$

- continued

$$- \rho_g \frac{\partial H_g}{\partial x_i} + \frac{\partial}{\partial x_i} \left(\frac{1}{2} v_g^2 \right) + T \frac{\partial S'}{\partial x_i}$$

or

$$\begin{aligned} & (\alpha_g \rho_g) \left[\frac{\partial u_{gi}}{\partial t} + u_{gj} \frac{\partial u_{gi}}{\partial x_j} - \frac{\partial}{\partial x_i} \left(\frac{1}{2} v_g^2 \right) \right] \\ &= F_{Igd i} + F_{Igd i} + \frac{\partial \tau_{ij}}{\partial x_j} + \dot{m}_{ed} (u_{Di} - u_{gi}) + \dot{m}_{ed} (u_{di} - u_{gi}) \\ & - (\alpha_g \rho_g) \frac{\partial H_g}{\partial x_i} + T \frac{\partial S'}{\partial x_i} . \end{aligned}$$

There are three types of mechanisms causing entropy generation in gas phase, namely (i) wall shear, (ii) relative motion, and (iii) heat transfer. The entropy generated may therefore be written as follows:

- (i) Wall shear on gas phase: $T_g dS_g$
- (ii) Relative motion between gas phase and d-droplet: $T_{gd} dS_{gd}$
- (iii) Relative motion between gas phase and D-droplet: $T_{gD} dS_{gD}$
- (iv) Heat transfer between gas phase and d-droplet: dq_{gd}
- (v) Heat transfer between gas phase and D-droplet: dq_{gD}

Thus, the entropy generation term $T \frac{\partial S'}{\partial x_i}$ in Eq. (A.4.40) can be written as the sum of the foregoing.

$$T \frac{\partial S'}{\partial x_i} = T_g \frac{\partial S_g}{\partial x_i} + T_{gd} \frac{\partial S_{gd}}{\partial x_i} + T_{gD} \frac{\partial S_{gD}}{\partial x_i} - \frac{\partial q_{gd}}{\partial x_i} - \frac{\partial q_{gD}}{\partial x_i}$$

Using this relation, the radial equilibrium equation for gas phase can be written as follows.

$$\begin{aligned}
 (\alpha_g \rho_g) & \left[\frac{\partial u_{gi}}{\partial t} + u_{gj} \frac{\partial u_{gi}}{\partial x_j} - \frac{\partial}{\partial x_i} \left(\frac{1}{2} v_g^2 \right) \right] \\
 & = F_{Igd i} + F_{IgD i} + \frac{\partial \tau_{ij}}{\partial x_j} + \dot{m}_{eD} (u_{Di} - u_{gi}) + \dot{m}_{ed} (u_{di} - u_{gi}) \\
 & - (\alpha_g \rho_g) \frac{\partial H_g}{\partial x_i} + T_g \frac{\partial S_g}{\partial x_i} + T_{gd} \frac{\partial S_{gd}}{\partial x_i} + T_{gD} \frac{\partial S_{gD}}{\partial x_i} \\
 & - \frac{\partial q_{gd}}{\partial x_i} - \frac{\partial q_{gD}}{\partial x_i}
 \end{aligned} \tag{A.4.41}$$

Liquid phase

The radial equilibrium equation for liquid phase can be derived in a similar manner. For liquid phase the internal energy-entropy relation can be written as follows.

$$de = T dS$$

Using the relation, $de = dE - d(\frac{1}{2} v^2)$, it follows that

$$dE = d(\frac{1}{2} v^2) + T dS$$

or

$$\frac{dE}{dx_i} = \frac{d}{dx_i} \left(\frac{1}{2} v^2 \right) + T \frac{dS}{dx_i} \tag{A.4.42}$$

For the d-droplet, the entropy generation can be identified as follows.

- | | |
|--|------------------|
| (i) Wall shear on d-droplet: | $T_d dS_d$ |
| (ii) Relative motion between d-droplet and gas phase: | $T_{dg} dS_{dg}$ |
| (iii) Relative motion between d-droplet and D-droplet: | $T_{dD} dS_{dD}$ |

(iv) Heat transfer between d-droplet
and gas phase:

$$dq_{gd}$$

(v) Heat transfer between d-droplet
and D-droplet

$$dq_{dD}$$

Thus it follows that

$$T \frac{\partial S}{\partial x_i} = T_d \frac{\partial S_d}{\partial x_i} + T_{dg} \frac{\partial S_{dg}}{\partial x_i} + T_{dD} \frac{\partial S_{dD}}{\partial x_i} + \frac{\partial q_{dD}}{\partial x_i} + \frac{\partial q_{gd}}{\partial x_i} + \frac{\partial q_{dD}}{\partial x_i}$$

Using this, Eq. (A.4.42) becomes the following.

$$\begin{aligned} \frac{dE}{dx_i} = & \frac{d}{dx_i} \left(\frac{1}{2} V_d^2 \right) + T_d \frac{\partial S_d}{\partial x_i} + T_{dg} \frac{\partial S_{dg}}{\partial x_i} + T_{dD} \frac{\partial S_{dD}}{\partial x_i} \\ & + \frac{\partial q_{dD}}{\partial x_i} + \frac{\partial q_{gd}}{\partial x_i} \end{aligned} \quad (A.4.43)$$

Now, the momentum equation for d-droplet is given by

$$(\alpha_d \rho_w) \left(\frac{\partial u_{di}}{\partial x_i} + u_{dj} \frac{\partial u_{di}}{\partial x_j} \right) = - F_{Igd} \quad (A.4.44)$$

Multiplying Eq. (A.4.43) by $\alpha_d \rho_w$ and adding to Eq. (A.4.44), the following is obtained.

$$\begin{aligned} (\alpha_d \rho_w) \left[\frac{\partial u_{di}}{\partial t} + u_{dj} \frac{\partial u_{di}}{\partial x_j} - \frac{\partial}{\partial x_i} \left(\frac{1}{2} V_d^2 \right) \right] \\ = - F_{Igd} - (\alpha_d \rho_w) \frac{\partial E_d}{\partial x_i} + T_d \frac{\partial S_d}{\partial x_i} + T_{dg} \frac{\partial S_{dg}}{\partial x_i} + T_{dD} \frac{\partial S_{dD}}{\partial x_i} \\ + \frac{\partial q_{dD}}{\partial x_i} + \frac{\partial q_{gd}}{\partial x_i} \end{aligned} \quad (A.4.45)$$

For the D-droplet, the entropy generation can again be identified as follows:

(i) Wall shear on D-droplet: $T_D dS_D$

- | | |
|--|------------------|
| (ii) Relative motion between D-droplet and gas phase: | $T_{Dg} dS_{Dg}$ |
| (iii) Relative motion between D-droplet and d-droplet: | $T_{Dd} dS_{Dd}$ |
| (iv) Heat transfer between D-droplet and gas phase: | dq_{gD} |
| (v) Heat transfer between D-droplet and d-droplet: | dq_{dD} |

Thus, it follows that

$$T \frac{\partial S}{\partial x_i} = T_D \frac{\partial S_D}{\partial x_i} + T_{Dg} \frac{\partial S_{Dg}}{\partial x_i} + T_{Dd} \frac{\partial S_{Dd}}{\partial x_i} + \frac{\partial q_{dD}}{\partial x_i} + \frac{\partial q_{gD}}{\partial x_i}$$

Using this, Eq. (A.4.43) becomes

$$\begin{aligned} \frac{dE_D}{dx_i} = & \frac{d}{dx_i} \left(\frac{1}{2} v_D^2 \right) + T_D \frac{\partial S_D}{\partial x_i} + T_{Dg} \frac{\partial S_{Dg}}{\partial x_i} + T_{Dd} \frac{\partial S_{Dd}}{\partial x_i} \\ & + \frac{\partial q_{dD}}{\partial x_i} + \frac{\partial q_{gD}}{\partial x_i} \end{aligned} \quad (A.4.46)$$

The momentum equation for D-droplet is given by the following.

$$(\alpha_D \rho_w) \cdot \frac{\partial u_{Di}}{\partial t} + u_{Dj} \frac{\partial u_{Di}}{\partial x_j} = - F_{IgDi} \quad (A.4.47)$$

Multiplying Eq. (A.4.46) by $\alpha_D \rho_w$ and adding to Eq. (A.4.47), the following is obtained.

$$\begin{aligned} (\alpha_D \rho_w) \left[\frac{\partial u_{Di}}{\partial t} + u_{Dj} \frac{\partial u_{Di}}{\partial x_j} - \frac{\partial}{\partial x_i} \left(\frac{1}{2} v_D^2 \right) \right] \\ = - F_{IgDi} - (\alpha_D \rho_w) \frac{\partial E_D}{\partial x_i} + T_D \frac{\partial S_D}{\partial x_i} + T_{Dg} \frac{\partial S_{Dg}}{\partial x_i} \\ + T_{Dd} \frac{\partial S_{Dd}}{\partial x_i} + \frac{\partial q_{dD}}{\partial x_i} + \frac{\partial q_{gD}}{\partial x_i} \end{aligned} \quad (A.4.48)$$

E. List of Basic Equations

Mass Balance Equation

Gas phase

$$\frac{\partial \rho'_g}{\partial t} + \frac{\partial}{\partial x_i} (\rho'_g u_{gi}) = \dot{m}_{ed} + \dot{m}_{eD} \quad (\text{A.4.49})$$

Liquid phase

d-droplet:

$$\frac{\partial \rho'_d}{\partial t} + \frac{\partial}{\partial x_i} (\rho'_d u_{di}) = - \dot{m}_{ed} \quad (\text{A.4.50})$$

D-droplet:

$$\frac{\partial \rho'_D}{\partial t} + \frac{\partial}{\partial x_i} (\rho'_D u_{Di}) = - \dot{m}_{eD} \quad (\text{A.4.51})$$

Mixture:

$$\frac{\partial}{\partial t} (\rho'_g + \rho'_d + \rho'_D) + \frac{\partial}{\partial x_i} (\rho'_g u_{gi} + \rho'_d u_{di} + \rho'_D u_{Di}) = 0 \quad (\text{A.4.52})$$

Momentum Balance Equation

Gas phase

$$\begin{aligned} \frac{\partial}{\partial t} (\rho'_g u_{gi}) + \frac{\partial}{\partial x_i} (\rho'_g u_{gi} u_{gi}) = & - \frac{\partial p}{\partial x_i} + \frac{\partial \tau_{ij}}{\partial x_j} + F_{Igd_i} + F_{IgD_i} \\ & + \dot{m}_{ed} u_{di} + \dot{m}_{eD} u_{Di} \end{aligned} \quad (\text{A.4.53})$$

Liquid phase

d-droplet:

$$\frac{\partial}{\partial t} (\rho'_d u_{di}) + \frac{\partial}{\partial x_i} (\rho'_d u_{di} u_{di}) = - F_{Igd_i} - \dot{m}_{ed} u_{di} \quad (\text{A.4.54})$$

D-droplet:

$$\frac{\partial}{\partial t} (\rho_D' u_{Di}) + \frac{\partial}{\partial x_j} (\rho_D' u_{Di} u_{Dj}) = - F_{IgDi} - \dot{m}_{eD} u_{Di} \quad (A.4.55)$$

Mixture:

$$\begin{aligned} \frac{\partial}{\partial t} (\rho_g' u_{gi} + \rho_d' u_{di} + \rho_D' u_{Di}) + \frac{\partial}{\partial x_j} (\rho_g' u_{gi}^2 + \rho_d' u_{di}^2 + \rho_D' u_{Di}^2) \\ = - \frac{\partial p}{\partial x_i} + \frac{\partial \tau_{ij}}{\partial x_j} \end{aligned} \quad (A.4.56)$$

Alternative Form of Momentum Balance Equation

Gas phase

$$\begin{aligned} \rho_g' \left(\frac{\partial}{\partial t} + u_{gj} \frac{\partial}{\partial x_j} \right) u_{gi} = F_{Igd_i} + F_{IgDi} - \frac{\partial p}{\partial x_i} + \frac{\partial \tau_{ij}}{\partial x_j} \\ + \dot{m}_{ed}(u_{di} - u_{gi}) + \dot{m}_{eD}(u_{Di} - u_{gi}) \end{aligned} \quad (A.4.57)$$

Liquid phase

d-droplet:

$$\rho_d' \left(\frac{\partial}{\partial t} + u_{dj} \frac{\partial}{\partial x_j} \right) u_{di} = - F_{Igd_i} \quad (A.4.58)$$

D-droplet:

$$\rho_D' \left(\frac{\partial}{\partial t} + u_{Dj} \frac{\partial}{\partial x_j} \right) u_{Di} = - F_{IgDi} \quad (A.4.59)$$

Energy Balance Equation

Gas phase

$$\begin{aligned} \frac{\partial}{\partial t} \left(\rho_g' (e_g + \frac{1}{2} u_{gi}^2) \right) + \frac{\partial}{\partial x_j} \left(\rho_g' u_{gj} (e_g + \frac{1}{2} u_{gi}^2) \right) \\ = \frac{\partial}{\partial x_j} (\sigma_{ij} u_{gj}) + F_{Igd_i} u_{di} + F_{IgDi} u_{Di} - \dot{Q}_{gd} - \dot{Q}_{gD} + P_g \\ + \text{continued} \end{aligned}$$

$$\begin{aligned}
& + \dot{m}_{ed} \left(e_g(T_d) + \frac{1}{2} u_{di}^2 + \frac{p}{\rho_g'(T_d)} - \Delta H_v \right) \\
& + \dot{m}_{eD} \left(e_g(T_D) + \frac{1}{2} u_{Di}^2 + \frac{p}{\rho_g'(T_D)} - \Delta H_v \right)
\end{aligned} \tag{A.4.60}$$

Liquid phase

d-droplet:

$$\begin{aligned}
& \frac{\partial}{\partial t} \left(\rho_d'(e_d + \frac{1}{2} u_{di}^2) \right) + \frac{\partial}{\partial x_j} \left(\rho_d' u_{dj} (e_d + \frac{1}{2} u_{di}^2) \right) \\
& = - F_{Igd} u_{di} - \dot{m}_{ed} (e_d + \frac{1}{2} u_{di}^2) + \dot{Q}_{gd} + \overline{P}_d
\end{aligned} \tag{A.4.61}$$

D-droplet:

$$\begin{aligned}
& \frac{\partial}{\partial t} \left(\rho_d'(e_D + \frac{1}{2} u_{Di}^2) \right) + \frac{\partial}{\partial x_j} \left(\rho_D' u_{Dj} (e_D + \frac{1}{2} u_{Di}^2) \right) \\
& = - F_{IgD} u_{Di} - \dot{m}_{eD} (e_D + \frac{1}{2} u_{Di}^2) + \dot{Q}_{gD} + \overline{P}_D
\end{aligned} \tag{A.4.62}$$

Mixture:

$$\begin{aligned}
& \frac{\partial}{\partial t} \left(\rho_g'(e_g + \frac{1}{2} u_{gi}^2) + \rho_d'(e_d + \frac{1}{2} u_{di}^2) + \rho_D'(e_D + \frac{1}{2} u_{Di}^2) \right) \\
& + \frac{\partial}{\partial x_j} \left(\rho_g'(e_g + \frac{1}{2} u_{gi}^2) u_{gj} + \rho_d'(e_d + \frac{1}{2} u_{di}^2) u_{dj} + \rho_D'(e_D + \frac{1}{2} u_{Di}^2) u_{Dj} \right) \\
& = \frac{\partial}{\partial x_j} (\sigma_{ij} u_{gi}) + \overline{P}_g + \overline{P}_d + \overline{P}_D
\end{aligned} \tag{A.4.63}$$

Alternative Form of Energy Balance Equation

Gas phase

$$\begin{aligned}
& \rho_g' \left(\frac{\partial}{\partial t} + u_{gj} \frac{\partial}{\partial x_j} \right) e_g \\
& = - p \frac{\partial u_{gi}}{\partial x_i} + \phi - \dot{Q}_{gd} - \dot{Q}_{gD} + \overline{P}_g \\
& + (F_{Igd} - \dot{m}_{ed} u_{gi})(u_{di} - u_{gi}) + (F_{IgD} - \dot{m}_{eD} u_{gi})(u_{Di} - u_{gi}) \\
& + \dot{m}_{ed} \left(e_g(T_d) + \frac{1}{2} u_{di}^2 + \frac{p}{\rho_g'(T_d)} - e_g - \frac{1}{2} u_{gi}^2 - \Delta H_v \right)
\end{aligned}$$

+ continued

$$+ \dot{m}_{eD} \left(e_g(T_D) + \frac{1}{2} u_{Di}^2 + \frac{p}{\rho_g(T_D)} - e_g - \frac{1}{2} u_{gi}^2 - \Delta H_v \right) \quad (A.4.64)$$

Liquid phase

d-droplet:

$$\rho'_d \left(\frac{\partial}{\partial t} + u_{dj} \frac{\partial}{\partial x_j} \right) e_d = \dot{Q}_{gd} + \bar{P}_d - (F_{Igd} - \dot{m}_{ed} u_{gi})(u_{di} - u_{di}) \quad (A.4.65)$$

D-droplet:

$$\rho'_D \left(\frac{\partial}{\partial t} + u_{Dj} \frac{\partial}{\partial x_j} \right) e_D = \dot{Q}_{gD} + \bar{P}_D - (F_{IgD} - \dot{m}_{eD} u_{gi})(u_{Di} - u_{Di}) \quad (A.4.66)$$

Radial Equilibrium Equation

Gas phase

$$\begin{aligned} & \rho'_g \left[\left(\frac{\partial}{\partial t} + u_{gj} \frac{\partial}{\partial x_j} \right) u_{gi} - \frac{\partial}{\partial x_i} \left(\frac{1}{2} v_g^2 \right) \right] \\ &= F_{Igd} + F_{IgDi} + \frac{\partial \tau_{ij}}{\partial x_j} + \dot{m}_{ed}(u_{di} - u_{gi}) + \dot{m}_{eD}(u_{Di} - u_{gi}) \\ & - \rho'_g \frac{\partial H_g}{\partial x_i} + T_g \frac{\partial S_g}{\partial x_i} + T_{gd} \frac{\partial S_{gd}}{\partial x_i} + T_{gD} \frac{\partial S_{gD}}{\partial x_i} \\ & - \frac{\partial q_{gd}}{\partial x_i} - \frac{\partial q_{gD}}{\partial x_i} \end{aligned} \quad (A.4.67)$$

Liquid phase

d-droplet:

$$\begin{aligned} & \rho'_d \left[\left(\frac{\partial}{\partial t} + u_{dj} \frac{\partial}{\partial x_j} \right) u_{di} - \frac{\partial}{\partial x_i} \left(\frac{1}{2} v_d^2 \right) \right] \\ &= - F_{Igd} - \rho'_d \frac{\partial E_d}{\partial x_i} + T_d \frac{\partial S_d}{\partial x_i} + T_{dg} \frac{\partial S_{dg}}{\partial x_i} \\ & + T_{dD} \frac{\partial S_{dD}}{\partial x_i} + \frac{\partial q_{dg}}{\partial x_i} + \frac{\partial q_{dD}}{\partial x_i} \end{aligned} \quad (A.4.68)$$

D-droplet:

$$\begin{aligned}
 \rho_D' \left[\left(\frac{\partial}{\partial t} + u_{Dj} \frac{\partial}{\partial x_j} \right) u_{Di} - \frac{\partial}{\partial x_i} \left(\frac{1}{2} v_D^2 \right) \right] \\
 = - F_{IgDi} - \rho_D' \frac{\partial E_D}{\partial x_i} + T_D \frac{\partial S_D}{\partial x_i} + T_{Dg} \frac{\partial S_{Dg}}{\partial x_i} \\
 + T_{Dd} \frac{\partial S_{Dd}}{\partial x_i} + \frac{\partial q_{Dg}}{\partial x_i} + \frac{\partial q_{Dd}}{\partial x_i}
 \end{aligned} \tag{A.4.69}$$

F. Simplification of Basic Equations

The following assumptions are made to simplify the basic equations.

- (1) The d-droplet can be treated as part of the gas phase, except in obtaining energy balance, and velocity of d-droplet is equal to that of gas, i.e.

$$u_{di} = u_{gi}, \quad \frac{\partial S_{dg}}{\partial x_i} = 0.$$

- (2) The D-droplet does not absorb work input, i.e. $\bar{P}_D = 0$.

- (3) The flow is steady, i.e. $\frac{\partial}{\partial t} = 0$.

- (4) There is no interaction between d- and D-droplets, i.e.

$$\frac{\partial S_{dD}}{\partial x_i} = 0.$$

- (5) Heat transfer between d- and D-droplets is negligible, i.e.

$$\frac{\partial q_{dD}}{\partial x_i} = 0.$$

- (6) Effect of the viscosity can be represented by "dissipative body force, F_{Bi} ", except for the effect of the interaction between gas phase and droplets, the latter treated distinctly.

- (7) The evaporated liquid is mixed with gas phase instantaneously.

Using the above assumptions, the basic equations become simplified and are listed below without further explanation.

Continuity Equation

Gas phase (gas + d-droplet)

$$\frac{\partial}{\partial x_i} \left(\rho'_g + \rho'_d \right) u_{gi} = \dot{m}_{eD} \quad (\text{A.4.70})$$

Liquid phase

$$\text{D-droplet: } \frac{\partial}{\partial x_i} (\rho'_D u_{Di}) = - \dot{m}_{eD} \quad (\text{A.4.71})$$

Momentum Equation

Gas phase (gas + d-droplet)

$$(\rho'_g + \rho'_d) \left(u_{gj} \frac{\partial u_{gi}}{\partial x_j} \right) = F_{IgDi} - \frac{\partial p}{\partial x_i} + F_{Bi} \quad (\text{A.4.72})$$

Liquid phase

$$\text{D-droplet: } \rho'_D \left(u_{Dj} \frac{\partial u_{Di}}{\partial x_j} \right) = - F_{IgDi} \quad (\text{A.4.73})$$

Energy Equation

Gas phase (gas only)

$$\begin{aligned} \rho'_g \left(u_{gi} \frac{\partial e_g}{\partial x_i} \right) = & - p \frac{\partial u_{gi}}{\partial x_i} - \dot{Q}_{gd} - \dot{Q}_{gD} + \overline{P}_g + F_{Bi} u_i + F_{IgDi} (u_{Di} - u_{gi}) \\ & + \dot{m}_{ed} \left(e_g(T_d) + \frac{p}{\rho'_g(T_d)} - e_g - \Delta H_v \right) \\ & + \dot{m}_{eD} \left(e_g(T_D) + \frac{p}{\rho'_g(T_D)} - e_g - \Delta H_v \right) \end{aligned} \quad (\text{A.4.74})$$

Liquid phase (d- and D-droplet)

$$\rho'_d \left(u_{gi} \frac{\partial e_g}{\partial x_i} \right) + \rho'_D \left(u_{Di} \frac{\partial e_D}{\partial x_i} \right) = \dot{Q}_{gd} + \dot{Q}_{gD} + \overline{P}_d \quad (\text{A.4.75})$$

Radial Equilibrium Equation

Gas phase (gas + d-droplet)

$$\begin{aligned}
 & (\rho'_g + \rho'_d) \left[u_{gj} \frac{\partial u_{gi}}{\partial x_j} - \frac{\partial}{\partial x_i} \left(\frac{1}{2} v_g^2 \right) \right] \\
 & = F_{IgDi} - \rho'_g \frac{\partial H_g}{\partial x_i} - \rho'_d \frac{\partial E_d}{\partial x_i} \\
 & \quad + T_g \frac{\partial S_g}{\partial x_i} + T_d \frac{\partial S_d}{\partial x_i} + T_{gd} \frac{\partial S_{gd}}{\partial x_i} \\
 & \quad + T_{gD} \frac{\partial S_{gD}}{\partial x_i} - \frac{\partial q_{gD}}{\partial x_i} + F_{Bi}
 \end{aligned} \tag{A.4.76}$$

Liquid phase

D-droplet:

$$\begin{aligned}
 & \rho'_D \left[u_{Dj} \frac{\partial u_{Di}}{\partial x_j} - \frac{\partial}{\partial x_i} \left(\frac{1}{2} v_D^2 \right) \right] \\
 & = - F_{IgDi} - \rho'_D \frac{\partial E_D}{\partial x_i} + T_D \frac{\partial S_D}{\partial x_i} + T_{Dg} \frac{\partial S_{Dg}}{\partial x_i} + \frac{\partial q_{gD}}{\partial x_i}
 \end{aligned} \tag{A.4.77}$$

4.2 Description of Coordinate System

The basic equations are given using two different coordinate systems, namely, intrinsic and cylindrical coordinate systems.

(1) Intrinsic Coordinate System (Fig. A.4.1).

The m , θ , n intrinsic system is a local, right hand, orthogonal system. The m -direction lies tangent to the local streamline direction, and the θ -direction is orthogonal to the m - r plane where r is the radial vector defined in Figure A.4.1. The n -direction is normal to the m -direction in the local meridional plane.

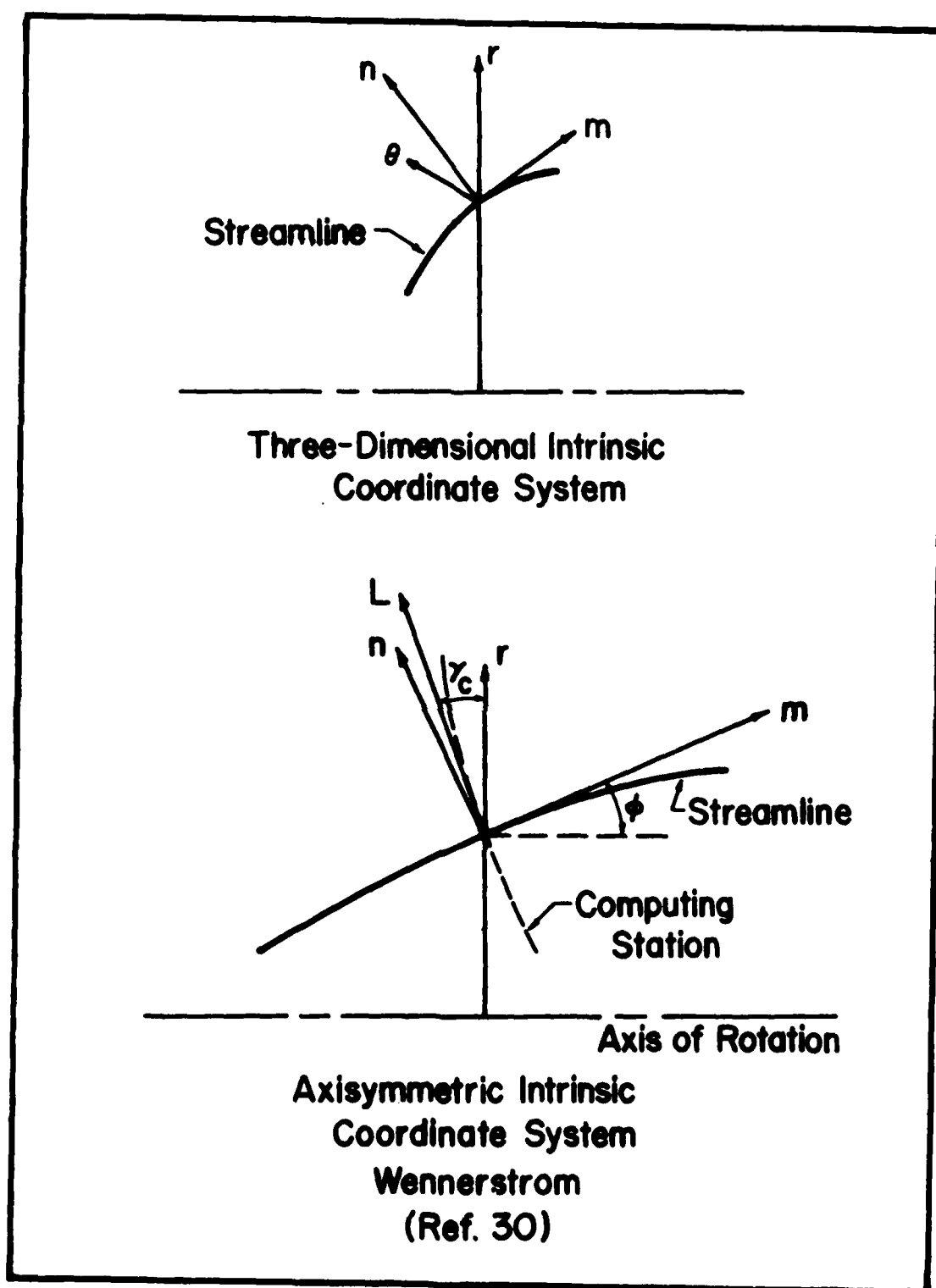


Fig. A.4.1. Intrinsic Coordinate System

(ii) Cylindrical Coordinate System (Fig. A.4.2).

The cylindrical system is fixed to the axis of rotation of the compressor. The z-direction lies along the axis of rotation and r is in the radial direction. The θ -component is in the circumferential direction defined positive with respect to a right-hand r, θ , z orthogonal coordinate system.

In many cases, it is more convenient to work in a coordinate system that is stationary with respect to a rotating blade row. Accordingly, the equations are given after transformation to a rotating frame of reference.

(1) Intrinsic Coordinates

An absolute velocity vector may be transformed to a relative velocity vector (relative with respect to a rotating system) by writing

$$\vec{V} = \vec{W} + \vec{U}$$

where \vec{V} = absolute velocity vector, \vec{W} = relative velocity vector, \vec{U} = local blade rotational velocity vector = $\vec{U}_m + \vec{U}_\theta + \vec{U}_n$, and $\vec{U}_m, \vec{U}_\theta, \vec{U}_n$ = m, θ , n components of \vec{U} , respectively.

The velocity components are given by the following.

$$\left. \begin{aligned} U_m &= f_m(U, \phi_1, \phi_2) \\ U_\theta &= f_\theta(U, \phi_1, \phi_2) \\ U_n &= f_n(U, \phi_1, \phi_2) \end{aligned} \right\}$$

where U = the magnitude of the local blade rotation velocity vector, U_m, U_θ, U_n = the magnitudes of the m, θ , n components of \vec{U} , ϕ_1 = the angle between the radius vector and the m-direction, and ϕ_2 = the angle between the radius vector and the n-direction.

Therefore, one obtains the following.

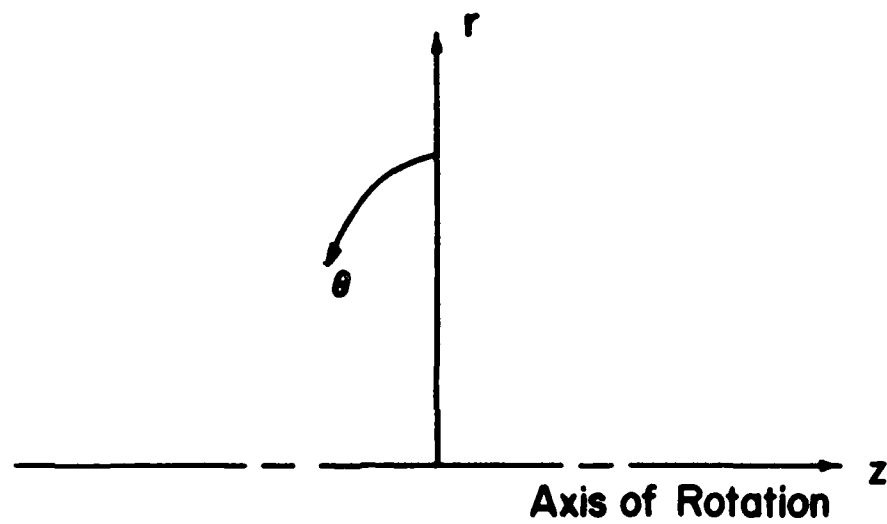


Fig. A.4.2
CYLINDRICAL COORDINATE SYSTEM

$$\left. \begin{aligned} V_{gm} &= W_{gm} + U_m \\ V_{g\theta} &= W_{g\theta} + U_\theta \\ V_{gn} &= W_{gn} + U_n = 0 \end{aligned} \right\} \quad \left. \begin{aligned} V_{pm} &= W_{pm} + U_m \\ V_{p\theta} &= W_{p\theta} + U_\theta \\ V_{pn} &= W_{pn} + U_n = 0 \end{aligned} \right\}$$

where $U_m = 0$ and $U_\theta = r\omega$, and p denotes a droplet.

(2) Cylindrical Coordinates

As in the case of the intrinsic coordinate system, the absolute and relative velocities may be related as follows. Thus,

$$\vec{V} = \vec{W} + \vec{U}$$

where $\vec{U} = \vec{U}_r + \vec{U}_\theta + \vec{U}_z$, the components in the three (r, θ, z) directions. But, $\vec{U}_r = \vec{U}_z = 0$. Therefore, $\vec{U} = \vec{U}_\theta = \omega r$, where ω = angular velocity of the rotating blade row. It follows that

$$\left. \begin{aligned} V_{gr} &= W_{gr} \\ V_{g\theta} &= W_{g\theta} + r\omega \\ V_{gz} &= W_{gz} \end{aligned} \right\} \quad \left. \begin{aligned} V_{pr} &= W_{pr} \\ V_{p\theta} &= W_{p\theta} + r\omega \\ V_{pz} &= W_{pz} \end{aligned} \right\}$$

4.3 One-Dimensional Flow Approximation

In many cases, it is sufficient to undertake compressor performance calculation at a chosen radius or spanwise location. It is then considered adequate to base the calculation on one-dimensional flow basis.

The following equations result from the one-dimensional flow approximation.

4.3.1 One-dimensional Flow Equation in Intrinsic Coordinate System

A. Mass Balance

Gas phase (gas and d-droplet)

$$\frac{1}{r} \frac{\partial}{\partial m} \left\{ r \left[(1 - \alpha_D - \alpha_d) \rho_g + \alpha_d \rho_w \right] W_{gm} \right\} = \dot{m}_{eD} \quad (\text{A.4.78})$$

Liquid phase (D-droplet)

$$\frac{1}{r} \frac{\partial}{\partial m} \left\{ r (\alpha_D \rho_w) W_{Dm} \right\} = - \dot{m}_{eD} \quad (\text{A.4.79})$$

B. Momentum Balance

Gas phase (gas and d-droplet)

n-component:

$$\left[(1 - \alpha_D - \alpha_d) \rho_g + \alpha_d \rho_w \right] \left[W_{gm} \frac{\partial W_{gn}}{\partial m} - \frac{(W_{g\theta} + r\omega)^2}{r} \frac{\partial r}{\partial m} \right] = F_{IgDn} + F_{Bn} \quad (\text{A.4.80})$$

m-component

$$\left[(1 - \alpha_D - \alpha_d) \rho_g + \alpha_d \rho_w \right] \left[W_{gm} \frac{\partial W_{gm}}{\partial m} - \frac{(W_{g\theta} + r\omega)^2}{r} \frac{\partial r}{\partial m} \right] = \frac{\partial p}{\partial m} + F_{IgDm} \quad (\text{A.4.81})$$

θ -component

$$\left[(1 - \alpha_D - \alpha_d) \rho_g + \alpha_d \rho_w \right] \left[\frac{W_{gm}}{r} \left(\frac{\partial r (W_{g\theta})}{\partial m} + 2\omega r \frac{\partial r}{\partial m} \right) \right] = F_{IgD\theta} + F_{B\theta} \quad (\text{A.4.82})$$

Liquid phase (d-droplet)

n-component:

$$(\alpha_D \rho_w) \left[W_{Dm} \frac{\partial W_{Dn}}{\partial m} - \frac{(W_{D\theta} + r\omega)^2}{r} \frac{\partial r}{\partial m} \right] = -F_{IgDn} \quad (\text{A.4.83})$$

m-component:

$$(\alpha_D \rho_w) \left[W_{Dm} \frac{\partial W_{Dm}}{\partial m} - \frac{(W_{D\theta} + r\omega)^2}{r} \frac{\partial r}{\partial m} \right] = -F_{IgDm} \quad (\text{A.4.84})$$

θ -component:

$$(\alpha_D \rho_w) \left[\frac{W_{Dm}}{r} \left(-\frac{\partial(rW_{D\theta})}{\partial m} + 2\omega r \frac{\partial r}{\partial m} \right) \right] = -F_{IgD\theta} \quad (A.4.85)$$

C. Energy Equation

Gas phase (gas only)

$$\begin{aligned} & \left[(1 - \alpha_D - \alpha_d) \rho_g \right] \left[W_{gm} \frac{\partial e_g}{\partial m} \right] \\ &= -p \frac{dW_{gm}}{dm} - \dot{Q}_{gd} - \dot{Q}_{gD} + \bar{P}_g \\ &+ \dot{m}_{ed} \left\{ e_g(T_d) + \frac{p}{\rho_g(T_d)} - e_g - \Delta H_v \right\} \\ &+ \dot{m}_{eD} \left\{ e_g(T_D) + \frac{p}{\rho_g(T_D)} - e_g - H_v \right\} \end{aligned} \quad (A.4.86)$$

Liquid phase (d- and D-droplet)

$$(\alpha_d \rho_w) \cdot \left(W_{gm} \frac{\partial e_d}{\partial m} \right) + (\alpha_D \rho_w) \left(W_{Dm} \frac{\partial e_D}{\partial m} \right) = \dot{Q}_{gd} + \dot{Q}_{gD} + \bar{P}_d \quad (A.4.87)$$

D. Radial Equilibrium Equation

Gas phase (gas and d-droplet)

n -component:

$$\left[(1 - \alpha_D - \alpha_d) \rho_g + \alpha_d \rho_w \right] \left[W_{gm} \frac{\partial W_{gn}}{\partial m} \right] = F_{IgDn} + F_{Bn} \quad (A.4.88)$$

m -component:

$$\begin{aligned} & \left[(1 - \alpha_D - \alpha_d) \rho_g + \alpha_d \rho_w \right] \left[\frac{W_{g\theta}}{r} + r\omega \left(-\frac{\partial(rW_{g\theta})}{\partial m} - 2r\omega \frac{\partial r}{\partial m} \right) \right] \\ &= F_{IgDm} + F_{Bm} - (1 - \alpha_D - \alpha_d) \rho_g \frac{\partial H_g}{\partial m} - \alpha_d \rho_w \frac{\partial E_d}{\partial m} \\ &+ T_g \frac{\partial S_g}{\partial m} + T_d \frac{\partial S_d}{\partial m} + T_{gd} \frac{\partial S_{gd}}{\partial m} + T_{gD} \frac{\partial S_{gD}}{\partial m} - \frac{\partial q_{gD}}{\partial m} \end{aligned} \quad (A.4.89)$$

θ -component:

$$\left[(1 - \alpha_D - \alpha_d) \rho_g + \alpha_d \rho_w \right] \left[\left(\frac{W_{gm}}{r} \frac{\partial(r W_{g\theta})}{\partial m} + 2r\omega \frac{\partial r}{\partial m} \right) \right] = F_{IgD\theta} + F_{B\theta} \quad (A.4.90)$$

Liquid phase (D-droplet)

n -component:

$$(\alpha_D \rho_w) \left[W_{Dn} \frac{\partial W_{Dn}}{\partial m} \right] = - F_{IgDn} \quad (A.4.91)$$

m -component:

$$(\alpha_D \rho_w) \left[\frac{W_{D\theta} + r\omega}{r} \left(- \frac{\partial(r W_{D\theta})}{\partial m} - 2r\omega \frac{\partial r}{\partial m} \right) \right] = - F_{IgDm} - (\alpha_D \rho_w) \frac{\partial E_D}{\partial m} + T_D \frac{\partial S_D}{\partial m} + T_{Dg} \frac{\partial S_{Dg}}{\partial m} + \frac{\partial q_{gD}}{\partial m} \quad (A.4.92)$$

θ -component:

$$(\alpha_D \rho_w) \left[\frac{W_{Dm}}{r} \left(\frac{\partial(r W_{D\theta})}{\partial m} + 2r\omega \frac{\partial r}{\partial m} \right) \right] = - F_{IgD\theta} \quad (A.4.93)$$

4.3.2 One-Dimensional Flow Equation in Cylindrical Coordinate System

A. Mass Balance

Gas phase (gas and d-droplet)

$$\frac{\partial}{\partial z} \left\{ \left[(1 - \alpha_D - \alpha_d) \rho_g + \alpha_d \rho_w \right] W_{gz} \right\} = \dot{m}_{eD} \quad (A.4.94)$$

Liquid phase (D-droplet)

$$\frac{\partial}{\partial z} (\alpha_D \rho_w W_{Dz}) = - \dot{m}_{eD} \quad (A.4.95)$$

B. Momentum Balance

Gas phase (gas + d-droplet)

r-component:

$$\left[(1 - \alpha_D - \alpha_d) \rho_g + \alpha_d \rho_w \right] \left[- \frac{(W_{g\theta} + r\omega)^2}{r} + W_{gz} \frac{\partial W_{gr}}{\partial z} \right] = F_{IgDr} + F_{Br} \quad (\text{A.4.96})$$

z-component:

$$\left[(1 - \alpha_D - \alpha_d) \rho_g + \alpha_d \rho_w \right] \left[W_{gz} \frac{\partial W_{gz}}{\partial z} \right] = - \frac{dp}{dz} + F_{IgDz} + F_{Bz} \quad (\text{A.4.97})$$

θ -component:

$$\left[(1 - \alpha_D - \alpha_d) \rho_g + \alpha_d \rho_w \right] \left[2W_{gr}\omega + W_{gr} \frac{W_{g\theta}}{r} + W_{gz} \frac{\partial W_{g\theta}}{\partial z} \right] = F_{IgD\theta} + F_{B\theta} \quad (\text{A.4.98})$$

Liquid phase (D-droplet)

r-component:

$$(\alpha_D \rho_w) \left[- \frac{(W_{D\theta} + r\omega)^2}{r} + W_{Dz} \frac{\partial W_{Dr}}{\partial z} \right] = - F_{IgDr} \quad (\text{A.4.99})$$

z-component:

$$(\alpha_D \rho_w) \left[W_{Dz} \frac{\partial W_{Dz}}{\partial z} \right] = - F_{IgDz} \quad (\text{A.4.100})$$

θ -component:

$$(\alpha_D \rho_w) \left[2W_{Dr}\omega + W_{Dr} \frac{W_{D\theta}}{r} + W_{Dz} \frac{\partial W_{D\theta}}{\partial z} \right] = - F_{IgD\theta} \quad (\text{A.4.101})$$

C. Energy Equation

Gas phase (gas only)

$$\begin{aligned}
 & \left[(1 - \alpha_d - \alpha_D) \rho_g \right] \left[W_{gz} \frac{\partial e_g}{\partial z} \right] \\
 & = - p \frac{dW_{gz}}{dz} - \dot{Q}_{gd} - \dot{Q}_{gD} + \bar{P}_g + F_{Bz} W_{gz} + F_{IgDz} (W_{Dz} - W_{gz}) \\
 & \quad + \dot{m}_{ed} \left\{ e_g(T_d) + \frac{p}{\rho_g(T_d)} - e_g - \Delta H_v \right\} \\
 & \quad + \dot{m}_{eD} \left\{ e_g(T_D) + \frac{p}{\rho_g(T_D)} - e_g - \Delta H_v \right\} \quad (A.4.102)
 \end{aligned}$$

Liquid phase (d- and D-droplet)

$$\begin{aligned}
 (\alpha_d \rho_w) \left(W_{gz} \frac{\partial e_d}{\partial z} \right) + (\alpha_D \rho_w) \left(W_{Dz} \frac{\partial e_D}{\partial z} \right) & = \dot{Q}_{gd} + \dot{Q}_{gD} + \bar{P}_d \\
 & \quad - F_{IgDz} (W_{Dz} - W_{gz}) \quad (A.4.103)
 \end{aligned}$$

D. Radial Equilibrium

Gas phase (gas and d-droplet)

r-component:

$$\begin{aligned}
 & \left[(1 - \alpha_D - \alpha_d) \rho_g + \alpha_d \rho_w \right] \left[W_{gz} \frac{\partial W_{gr}}{\partial z} - (W_{g\theta} + r\omega) \left(2\omega + \frac{W_{g\theta}}{r} \right) \right] \\
 & = F_{IgDr} + F_{Br} \quad (A.4.104)
 \end{aligned}$$

z-component:

$$\begin{aligned}
 & \left[(1 - \alpha_D - \alpha_d) \rho_g + \alpha_d \rho_w \right] \left[- W_{gr} \frac{\partial W_{gr}}{\partial z} - (W_{g\theta} + r\omega) \frac{\partial W_{g\theta}}{\partial z} \right] \\
 & = F_{IgDz} + F_{Bz} - (1 - \alpha_D - \alpha_d) \rho_g \frac{\partial H_g}{\partial z} - (\alpha_d \rho_w) \frac{\partial E_d}{\partial z} \\
 & \quad + T_g \frac{\partial S_g}{\partial z} + T_d \frac{\partial S_d}{\partial z} + T_{gd} \frac{\partial S_{gd}}{\partial z} + T_{gD} \frac{\partial S_{gD}}{\partial z} - \frac{\partial q_{gD}}{\partial z} \quad (A.4.105)
 \end{aligned}$$

θ -component:

$$\left[(1 - \alpha_D - \alpha_d) \rho_g + \alpha_d \rho_w \right] \left[W_{gz} \frac{\partial W_{g\theta}}{\partial z} + W_{gr} \left(2\omega + \frac{W_{g\theta}}{r} \right) \right] = F_{IgD\theta} + F_{B\theta} \quad (\text{A.4.106})$$

Liquid phase (D-droplet only)

r-component:

$$(\alpha_D \rho_w) \left[W_{Dz} \frac{\partial W_{Dr}}{\partial z} - (W_{D\theta} + r\omega) \left(2\omega + \frac{W_{D\theta}}{r} \right) \right] = - F_{IgDr} \quad (\text{A.4.107})$$

z-component:

$$\begin{aligned} (\alpha_D \rho_w) \left[- W_{Dr} \frac{\partial W_{Dr}}{\partial z} - (W_{D\theta} + r\omega) \frac{\partial W_D}{\partial z} \right] \\ = - F_{IgDz} - (\alpha_D \rho_w) \frac{dE_D}{dz} + T_D \frac{\partial S_D}{\partial z} + T_{Dg} \frac{\partial S_{Dg}}{\partial z} + \frac{\partial q_{gD}}{\partial z} \end{aligned} \quad (\text{A.4.108})$$

θ -component:

$$(\alpha_D \rho_w) \left[W_{Dz} \frac{\partial W_D}{\partial z} + W_{Dr} \left(2\omega + \frac{W_{D\theta}}{r} \right) \right] = - F_{IgD\theta} \quad (\text{A.4.109})$$

It may be pointed out that in the foregoing, the derivatives with respect to the z-direction are shown as partial derivatives, although under one-dimensional flow approximation there arise variations only in the z-direction. Since the velocity components in the r and θ directions are retained in the equations, it is felt that the partial derivative notation may be useful for clarity.

The set of Eqs. (A.4.96 - 103) may be solved numerically given the various forces and energy-exchanges involved in two phase flow through compressors. Alternatively, one may adopt the method of

obtaining the solution by a simple control volume procedure. The latter is the method adopted here.

4.4 Application of One-Dimensional Flow Model

The compressor performance is calculated based on the one-dimensional flow model in the cylindrical coordinate system as described in Section 4.3.2 of this Appendix.

A control volume is postulated that is closed thermodynamically with respect to the surroundings and extends from entry of a stage to its exit. While there is work input into the control volume, there is no other exchange of energy between the control volume and the surroundings.

The energy balance equation across the control volume is written as follows utilizing Eqs. (A.4.102) and (A.4.103).

$$\begin{aligned} \left[(1 - \alpha_d - \alpha_D) \rho_g \right] W_{gz} \frac{de_g}{dz} + \alpha_d \rho_w (W_{gz} \frac{de_d}{dz}) + \alpha_D \rho_w (W_{Dz} \frac{de_D}{dz}) \\ = - p \frac{dW_{gz}}{dz} + \bar{P} - \bar{L} \end{aligned} \quad (\text{A.4.110})$$

where \bar{P} and \bar{L} represent the total work input and total losses, respectively, per unit volume of mixture. The losses have been included with a negative sign.

The total work input, using Euler turbine equation (Ref. 23 & 24), can be represented by the relation,

$$\bar{P} = U \cdot \Delta W_{g\theta} \quad (\text{A.4.111})$$

where U is the rotational velocity of the compressor and $\Delta W_{g\theta}$ represents the change in the whirl component of gas phase (and also, small droplet) velocity relative to the rotor in the stage. In deriving

the Euler turbine equation it will be realized that the difference in radial velocity component across the rotor is considered small.

The total losses may be divided into three parts: (i) losses associated with the gas phase, L_g ; (ii) losses associated with the small droplets, L_d ; and (iii) losses associated with the large droplets, L_D . Thus,

$$\bar{L} = L_g + L_d + L_D. \quad (\text{A.4.112})$$

It is useful to introduce the concept of total enthalpy of the mixture based on relative velocity. It may be defined as follows.

$$\begin{aligned} H_{rel} = & \left[(1 - \alpha_d - \alpha_D) \rho_g \right] \left(h_g + \frac{w_g^2}{2J} \right) \\ & + \alpha_d \rho_w \left(e_d + \frac{w_g^2}{2J} \right) + \alpha_D \rho_w \left(e_D + \frac{w_D^2}{2J} \right) \end{aligned} \quad (\text{A.4.113})$$

where J is a conversion factor. The enthalpy, h , is related to internal energy, e , through the expression $dh = de + d(p/p)$. The change in total enthalpy across the stage is exactly equal to the work input. The work input is utilized in the machine (i) to produce a change in stagnation pressure, (ii) to overcome losses and (iii) to create phase change, if any. The latter is not explicit in Eq. (A.4.110) because of the gain in energy of one phase is exactly compensated by the loss in the other phase.

In view of earlier assumptions, the work input is absorbed only by the gas phase and the small (d) droplets. Therefore the energy expended in overcoming the losses, \bar{L} , is also in the nature of an energy exchange within the control volume.

If the difference in total enthalpy across the stage is denoted by \bar{H} , then it follows that

$$\bar{H} = \frac{U \cdot \Delta W_{g\theta}}{J} \quad (\text{A.4.114})$$

Denoting by \bar{H}^* , the effective enthalpy change which under isentropic conditions produces the same stagnation pressure change as the actual enthalpy change, one can write,

$$\bar{H}^* = \bar{H} - \bar{L} \quad (\text{A.4.115})$$

The stage efficiency may then be defined by the relation,

$$\eta = \frac{\bar{H} - \bar{L}}{\bar{H}}, \quad (\text{A.4.116})$$

$$\text{so that } \bar{H}^* = \eta \bar{H}. \quad (\text{A.4.117})$$

The stage stagnation pressure ratio is then given by the relation,

$$\frac{P_{02}}{P_{01}} = \left[1 + \eta \frac{\bar{H}}{H_{01}} \right]^{\frac{\gamma}{\gamma-1}} \quad (\text{A.4.118})$$

where ()₁ and ()₂ refer to the inlet and outlet conditions of the stage.

It may be noted that the efficiency refers to the stage efficiency of two phase flow.

An alternative method of correcting for losses is to obtain the stagnation pressure ratio corresponding to the actual work input and then subtracting the losses in terms of stagnation pressure loss at stage outlet. In adopting this method, it is convenient to combine the losses due to gas phase and small droplets into one group and the large droplets into a second group.

Then one can write the following.

$$\frac{P'_{02}}{P_{01}} = \left[1 + \eta' \frac{\bar{H}}{H_{01}} \right]^{\frac{\gamma}{\gamma-1}} \quad (\text{A.4.119})$$

where ()' denotes the gas and small droplets together. Correcting this for losses due to large droplets, denoted by ΔP_{0D} , one can

write the expression, namely,

$$P_{02} = P_{01} \left[1 + \eta' \frac{H}{H_{01}} \right] - \Delta P_{0D} \quad (\text{A.4.120})$$

In a similar manner, heat and mass transfer processes between the two phases can be ignored in the first instance, and then introduced at the stage exit.

4.4.1 Method of Accounting for Two Phase Effects

The two phase effects that need to be taken into account, even within the framework of one-dimensional flow analysis, are (i) losses and (ii) heat transfer from the gas to the liquid phase, and (iii) the resulting change of phase of liquid and mass transfer to the gas phase. Since the latter two processes are included only at the exit of a stage, it is sufficient to obtain a local mass and energy balance. The heat and mass transfer processes are decoupled from the compression process in the current method.

Regarding the losses, one can relate them to a change in entropy as follows. The momentum balance equations, Eqs. (A.4.96 - 98), and Eqs. (99-101), provide a convenient starting point for discussion.

Equations (A.4.96 - 98) are multiplied by W_{gr} , W_{gz} , and $W_{g\theta}$, respectively, and added. Into the resulting equation one introduces the Gibbs relations, namely,

$$\begin{aligned} T_g \cdot \nabla S_g &= \nabla h_g - \frac{1}{\rho_g} \nabla p_g \\ \text{and} \\ T_d \cdot \nabla S_d &= \nabla e_d. \end{aligned}$$

Here T_g represents the temperature of the gas phase, and T_d that of the d-droplets. The resulting equation, noting that in the absence of work input the system is closed and adiabatic, becomes the following.

$$\frac{dS_g}{dz} + \frac{dS_d}{dz} = \frac{1}{\rho'' w_{gz} T_g} \left[w_{gz} F_{Bz} + w_{g\theta} F_{B\theta} + w_{gz} F_{IgDz} + w_{g\theta} F_{IgD\theta} \right] \quad (A.4.121)$$

where $\rho'' = \left[(1 - \alpha_d - \alpha_D) \rho_g + \alpha_d \rho_w \right]$. It will be observed that w_{gr} has been assumed to be zero in this analysis. The losses in the gas phase and the d-droplets are given by the gain in entropy. The entropy change is shown distinctly for the gas and d-droplets only for convenience.

In a similar manner, the losses because of the presence of D-droplets may be written as follows.

$$\alpha_D \rho_w \cdot \frac{dS_D}{dz} = w_{gz} F_{IgDz} + w_{g\theta} F_{IgD\theta} \quad (A.4.122)$$

Eq. (A.4.122) may be combined with Eq. (A.4.121) as desired.

APPENDIX 5

MODIFICATION OF UD-0300 PROGRAM CODE

1. UD-0300 Program Code

In order to investigate the effects of utilizing mixtures of gases on the Test Compressor performance, the UD-0300 Program Code was used. The UD-0300 is a computer program that has been developed for the design and performance estimation of axial compressors. The principal feature of the program is that it enables in a single computer program the determination of the geometry of the compressor blading, details of the flow within the compressor, and the design point performance of the machine. The program consists fundamentally of three sections: two alternative means of determining blade geometry, and a computation scheme for aerodynamic performance of flow through the compressor. In one run of the program, any one section alone may be used, or the aerodynamic performance section may be used in conjunction with either or both of the blading sections. The program uses overlay; each of the main sections uses close to 130K (octal) of central memory. In the present investigation the aerodynamic section has been used to investigate the effects of using mixtures of gases in the Test Compressor.

The compressor flow computed in the aerodynamic performance section is assumed to be axisymmetric and inviscid. Provision is made in the procedure to incorporate turbulent mixing of flow and radial transfer of a blade wake. Starting with the radial equilibrium equation derived by Wennerstorm (Ref. 30), a system of flow equations is derived. The streamline curvature method is then employed to solve these equations. In this method, a number of computing stations are located at strategic points in the flow. A computing mesh is formed by the intersection of these stations with the streamlines. Their locations are iteratively

determined. An initial estimate is made of the streamline locations. The flow within the compressor is computed on the basis of this estimate and the resulting flow distribution enables a new estimate to be made. This procedure is repeated until the estimated streamline pattern is correct to within a given tolerance. The meridional velocity distribution along each computing station is found by integrating a momentum equation. The continuity equation supplies the necessary constant of integration.

A more detailed description of the UD-0300 program is available in Ref. 10.

2. Modification of UD-0300 for Mixtures of Gases

The UD-0300 code has been developed originally for use with a single fluid such as air flow through a compressor. In order to use it for mixtures of gases, it is necessary to introduce modifications to account for variable molecular weight, specific heats and acoustic speed applicable to the mixture of gases under consideration. Such modifications have been described for the case of air-steam mixture flow in Ref. 11.

The various functional expressions for thermo-physical properties of air, steam and methane are given in Appendix 11.

3. Modifications of UD-0300 for Off-design Performance Calculations

The UD-0300 program has been originally designed for design point performance calculations. In order to carry out off-design point calculations, modifications are required for the incorporation of loss coefficient corresponding to off-design flow angles and Mach number.

The total pressure loss coefficient, \bar{w} , at any inlet angle, β_1 , is defined in terms of a minimum value, \bar{w}_{\min} , a reference (or minimum loss angle, $\beta_{1\text{ref}}$, and "stalling" and "choking" inlet angles, β_{1c} and β_{1s} as follows:

$$\bar{\omega} = \bar{\omega}_{\min} \left\{ 1 - \left(\frac{\beta_1 - \beta_{1 \text{ ref}}}{\beta_{1s}(\text{or } c) - \beta_{1 \text{ ref}}} \right)^2 \right\} \quad (\text{A.5.1})$$

where β_{1s} or β_{1c} is used depending upon whether β_1 is greater or less than $\beta_{1 \text{ ref}}$. The outlet flow angle, β_2 , is varied linearly from the reference value, $\beta_{2 \text{ ref}}$, according to the rule,

$$\beta_2 = \beta_{2 \text{ ref}} + (\beta_1 - \beta_{1 \text{ ref}}) \frac{\partial \beta_2}{\partial \beta_1} \quad (\text{A.5.2})$$

According to this method, in order to perform calculations, the values for $\bar{\omega}_{\min}$, $\beta_{1 \text{ ref}}$, β_{1s} , β_{1c} , $\beta_{2 \text{ ref}}$, and $\frac{\partial \beta_2}{\partial \beta_1}$ have to be known.

Usually, the values for $\bar{\omega}_{\min}$, $\beta_{1 \text{ ref}}$, and $\beta_{2 \text{ ref}}$ are available as design point values. However, the values of β_{1s} , β_{1c} , and $\frac{\partial \beta_2}{\partial \beta_1}$ for a particular blade can be obtained only from detailed cascade tests. In order to get around this problem, the following off-design analysis scheme has been developed and used. It is based on the concept of Equivalent-Diffusion Factor, due to Lieblein (Ref 37).

Lieblein has shown that the design point loading factor, the Diffusion Factor, does not represent a suitable criterion for loading at off-design, except possibly at other minimum loss points. This is due to the fact that the basic derivation of the Diffusion Factor has been based on a flow model which corresponds to operation at or near minimum loss. He has therefore suggested a generalized loading parameter. This parameter, the Equivalent Diffusion Ratio, is based on the ratio of the maximum suction surface velocity and trailing edge velocity for a given section in cascade. Lieblein has deduced an expression which approximates this velocity ratio in terms of measured overall performance. The Equivalent Diffusion Ratio is suitable for correlation of low speed data. For the general case where the axial velocity ratio may be large, such as in a rotor or stator cascade, the Equivalent Diffusion Ratio, D_{eq} , has been defined as follows:

$$D_{\text{eq}} = \frac{\cos \beta_2}{\cos \beta_1} \left\{ 1.12 + K(1-i^*)^{1.43} + 0.61 \frac{\cos^2 \beta_1}{\sigma} (\tan \beta_1 - \tan \beta_2) \right\} \quad (\text{A.5.3})$$

where $K = 0.0117$ for the NACA 65 (A_{10}) blades and $K = 0.007$ for the C_4 circular-arc blades. The Equivalent Diffusion Ratio at minimum loss, D_{eq}^* , is obtained by dropping the term representing the incidence angle effects, that is,

$$D_{eq}^* = \frac{\cos \beta_2}{\cos \beta_1} \left\{ 1.12 + 0.61 \frac{\cos^2 \beta_1}{\sigma} (\tan \beta_1 - \tan \beta_2) \right\} \quad (A.5.4)$$

The wake momentum thickness can be expressed nondimensionally as follows.

$$\frac{\theta}{c} = \frac{\bar{w} \cos \beta_2}{2\sigma} \left(\frac{\cos \beta_2}{\cos \beta_1} \right)^2 \quad (A.5.5)$$

where c is the chord length of the blades.

At minimum loss, Eq. (A.5.5) yields

$$\left(\frac{\theta}{c} \right)^* = \frac{\bar{w}^* \cos \beta_2^*}{2\sigma} \left(\frac{\cos \beta_2^*}{\cos \beta_1^*} \right)^2 \quad (A.5.6)$$

Also, from Eq. (A.5.5), the total pressure loss coefficient, \bar{w} , can be expressed as follows.

$$\bar{w} = \left(\frac{\theta}{c} \right) \frac{2\sigma}{\cos \beta_2} \left(\frac{\cos \beta_1}{\cos \beta_2} \right)^2 \quad (A.5.7)$$

From the cascade test data, the deviation angle, δ , and the non-dimensional wake momentum thickness, $\frac{\theta}{c}$, are expressed in terms of the D_{eq} , D_{eq}^* , $\left(\frac{\theta}{c} \right)^*$, and inlet Mach number, M_1 , as follows:

$$\delta = \delta^* + [6.40 - 9.45(M_1 - 0.60)] (D_{eq} - D_{eq}^*) \quad (A.5.8)$$

$$\frac{\theta}{c} = \left(\frac{\theta}{c} \right)^* + (0.827 M_1 - 2.692 M_1^2 + 2.675 M_1^3) (D_{eq} - D_{eq}^*)^2$$

for $D_{eq} < D_{eq}^*$ (A.5.9)

$$\frac{\theta}{c} = \left(\frac{\theta}{c} \right)^* + (2.80 M_1 - 8.71 M_1^2 + 9.36 M_1^3) (D_{eq} - D_{eq}^*)^2$$

for $D_{eq} < D_{eq}^*$ (A.5.10)

Using these empirical expressions, the blade outlet and total pressure loss coefficient at off-design point can be determined as follows:

- (1) Calculate the inlet angle, β_1 , and inlet Mach number, M_1 .
- (2) Calculate the Equivalent Diffusion Ratio at minimum loss, D_{eq}^* , by Eq. (A.5.4).
- (3) Calculate the nondimensional wake momentum thickness at minimum loss, $(\frac{\theta}{c})^*$ by Eq. (A.5.5).
- (4) Assume the fluid outlet angle, $(\beta_2)_a$.
- (5) Calculate the incidence angle, i , by $i = \beta_1 - \beta_1^* + i^*$.
- (6) Calculate the Equivalent Diffusion Ratio, D_{eq} , by Eq. (A.5.3).
- (7) Calculate the deviation angle, δ , by Eq. (A.5.8).
- (8) Calculate the fluid outlet angle, $(\beta_2)_c$ by, $(\beta_2)_c = \beta_2^* - \delta^* + \delta$.
- (9) Compare the assumed value of fluid outlet angle, $(\beta_2)_a$, with the calculated value of that, $(\beta_2)_c$ to check if $|(\beta_2)_a - (\beta_2)_c| < \epsilon$ where ϵ is the desired accuracy. Iterate step (4) to step (9) until satisfactory accuracy is obtained.
- (10) Calculate the nondimensional wake momentum thickness, $\frac{\theta}{c}$, by Eq. (A.5.9) or (A.5.10).
- (11) Calculate the total pressure loss coefficient, $\bar{\omega}$, by Eq. (A.5.7).

Figure A.5.1 shows the flow chart of the overall calculation procedure to predict the fluid outlet angle and total pressure loss coefficient at off-design point.

The foregoing procedure, along with the empirical relations, Eqs. (A.5.8 - 10), has been incorporated into the UD-0300 code.

Calculations have been performed for air-methane mixture flow through the Test Compressor.

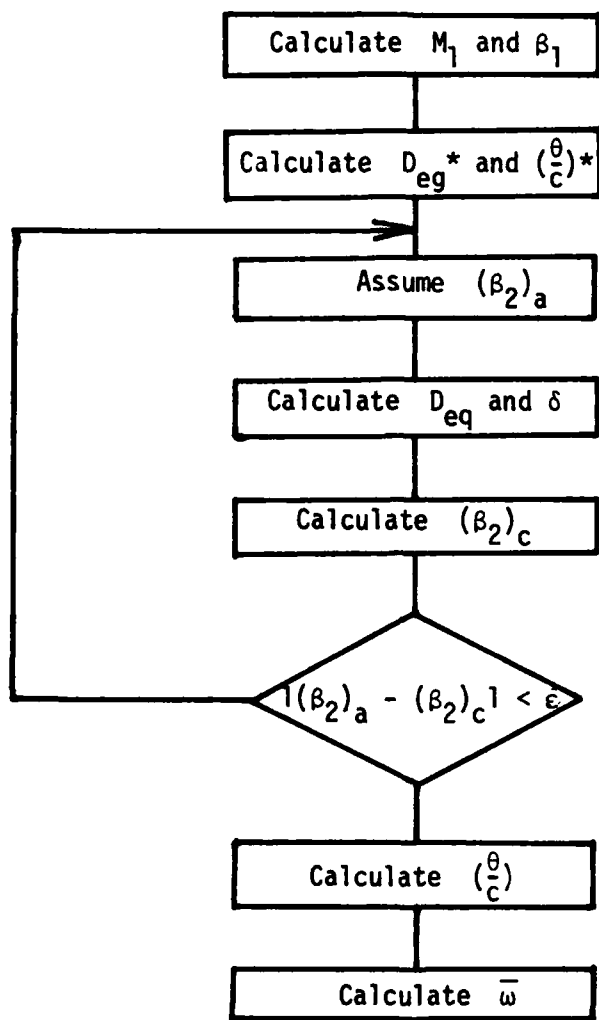


Figure A.5.1 Procedure for Prediction of Total Pressure Loss Coefficient

APPENDIX 6

CALCULATION PROCEDURE FOR AIR-METHANE MIXTURE

1. Basic Model and Assumptions

In order to investigate the effect of addition of small quantities of methane into air, a simple one-dimensional calculation has been carried out. The basic model and assumptions employed are as follows:

- (i) Methane injected at the compressor inlet is mixed with air uniformly;
- (ii) The compressor stage characteristic curves obtained during tests with air are applicable for air-methane mixture flow through the compressor;
- (iii) The thermo-physical properties for air-methane mixture are obtained utilizing the functional relations given in Appendix 11.

2. Input Data

In order to perform the calculation, the following input data are used:

- 1) compressor inlet temperature : T_{01}
- 2) compressor inlet pressure : P_{01}
- 3) blade rotational speed : N
- 4) methane content : x
- 5) initial flow coefficient : ϕ_0

3. Calculation of Mass Flow Rate

At the compressor inlet, the mass flow rate of mixture has to be determined from the initial flow coefficient, ϕ_0 . Since density has

to be based on static pressure and temperature, an iterative procedure is used as follows:

- 1) Calculate the specific heat at constant pressure for air,

$$c_{p_{\text{air}}}, \text{ and for methane, } c_{p_{\text{methane}}}, \text{ at } T_{01}.$$

- 2) Calculate the specific heat at constant pressure for the air-methane mixture.

$$c_{p_m} = (1-x)c_{p_{\text{air}}} + xc_{p_{\text{methane}}}$$

- 3) Calculate the gas constant for the air-methane mixture

$$R_m = R_u \left[\frac{(1-x)}{(mw)_{\text{air}}} + \frac{x}{(mw)_{\text{methane}}} \right]$$

where R_u = universal gas constant

$(mw)_{\text{air}}$ = molecular weight of air

$(mw)_{\text{methane}}$ = molecular weight of methane

- 4) Calculate the specific heat ratio for the air-methane mixture

$$\gamma_m = (1 - R_m/c_{p_m})^{-1}$$

- 5) Calculate the blade tip wheel speed.

$$U_{\text{tip}} = r_{\text{tip}} 2\pi N/60$$

where r_{tip} = the radius of blade tip

N = blade rotational speed (RPM)

- 6) Calculate the axial velocity

$$V_z = \phi_0 U_{\text{tip}}$$

- 7) Assume Mach number M by setting $M = M_a$

- 8) Calculate static temperature

$$T_1 = \{1 + (\gamma_m - 1)M_a^2/2\}^{-1} T_{01}$$

- 9) Calculate the acoustic speed

$$a = (\gamma_m R_m T_1 g_c)^{1/2}$$

- 10) Calculate Mach number M and set $M = M_c$

$$M = V_z/a = M_c$$

- 11) Compare the assumed Mach number, M_a , with the calculated Mach number, M_c and check if

$$|M_a - M_c| < \epsilon$$

where ϵ = desired accuracy. If the desired accuracy is obtained proceed to the next step. Otherwise, steps 7 to 11 should be repeated until the desired accuracy is obtained.

- 12) Calculate density from T_{01} and P_{01}

$$\rho_{01} = P_{01}/R_m T_{01}$$

- 13) Calculate the density based on the static properties.

$$\rho_m = \{1 + (\gamma_m - 1)M^2/2\}^{-1/(\gamma_m - 1)} \cdot \rho_{01}$$

- 14) Calculate the mass flow rate

$$\dot{m} = \rho_m V_z A$$

4. Flow Coefficient at Inlet of Each Stage

Although a flow coefficient is inputted at compressor inlet, it has to be determined at entrance to each stage. The procedure for calculation of axial velocity into different stages with a fixed mass flow is modified as follows.

- 1) From the previous stage outlet, the total temperature, T_{01} , and the total pressure, P_{01} , are known.
- 2) Calculate the density based on T_{01} and P_{01}

$$\rho_{01} = P_{01}/R_m T_{01}$$

3) Assume Mach number M_a

4) Calculate static temperature, T , and density, ρ .

$$\rho = \{1 + (\gamma_m - 1)M_a^2/2\}^{-1/(\gamma_m - 1)} \cdot \rho_{01}$$

$$T = \{1 + (\gamma_m - 1)M_a^2/2\}^{-1} \cdot T_{01}$$

5) Calculate acoustic speed

$$a = (\gamma_m R_m T g_c)^{1/2}$$

6) Calculate the axial velocity

$$V_z = \dot{m}_m / \rho A$$

7) Calculate the absolute velocity, V_1 .

$$V_1 = V_z / \cos \alpha_1$$

8) Calculate Mach number

$$M = V_1 / a = M_c$$

9) Compare the assumed Mach number, M_a , with the calculated one M_c . If M_c agrees reasonably well with M_a , proceed to the next step. Otherwise, steps 3 to 9 should be repeated until a satisfactory accuracy is obtained.

10) Calculate the flow coefficient, ϕ , at the entrance to the stage under consideration.

$$\phi = V_z / U_{tip}$$

5. Compressor Stage Characteristics

The compressor stage characteristics for the ALLISON T63-A5 axial flow compressor have been used for the performance calculation. Overall and stage characteristics, stage vector diagram, hardware geometry, and aerodynamic design data for T63-A5 axial flow compressor are presented in Appendix 1.

The equivalent pressure ratio, Ψ , equivalent temperature ratio, τ , and stage adiabatic efficiency, η , have been expressed in terms of the flow coefficient as follows:

$$\Psi = A_1 + B_1\phi + C_1\phi^2 + D_1\phi^3 + E_1\phi^4 + F_1\phi^5 + G_1\phi^6$$

$$\eta = A_2 + B_2\phi + C_2\phi^2 + D_2\phi^3 + E_2\phi^4 + F_2\phi^5 + G_2\phi^6$$

$$\tau = A_3\phi + B_3$$

The numerical values of the coefficients A_i , B_i ($i = 1, 2, 3$) and C_i , D_i , E_i , F_i , G_i ($i = 1, 2$) are presented in Table A.6.1. These three expressions have been utilized in numerical computation. Once the values of Ψ , τ , and η corresponding to ϕ are obtained, the stage outlet properties can be calculated from their definitions. Actually two of them are enough to determine the stage outlet properties. In the present calculation, the equivalent temperature rise ratio, τ , and the stage adiabatic efficiency, η , are used. The stage total temperature rise, ΔT_0 , stage and total temperature ratio, T_{02}/T_{01} , and stage total pressure ratio, P_{02}/P_{01} , are given by the following:

$$\Delta T_0 = \tau U_{tip}^2 / (U_{tip} / T_{01})_0$$

$$T_{02}/T_{01} = 1 + \Delta T_0 / T_{01}$$

$$P_{02}/P_{01} = (1 + \eta \Delta T_0 / T_{01})^{\gamma/(\gamma-1)}$$

These properties at the outlet of one stage become the inlet properties for the next stage.

6. Overall Calculation Procedures

The overall calculation procedure for air-methane mixture is summarized in the form of a flow chart in Fig. A.6.1. First for given input data, the mass flow rate is determined. This mass flow rate is constant

TABLE A.6.1
VALUES FOR COEFFICIENTS OF ψ, τ, η

1st Stage	2nd Stage	3rd Stage
A1=26.456 B1=-366.48033 C1=2161.46222 D1=-66670.16668 E1=11405.55557 F1=-10280.00001 G1=3822.22223 A2=-120.02 B2=1599.02 C2=-8730.12223 D2=25068.33336 E2=-39922.22228 F2=33466.66671 G2=-11555.55557 A3=-0.34 B3=0.226	A1=-4.285 B1=63.44567 C1=-332.95889 D1=907.0 E1=-1549.35556 F1=1095.33334 G1=-385.55556 A2=116.32 B2=-138.473334 C2=6345.80003 D2=-16503.33341 E2=2366.66677 F2=-17333.33341 G2=5333.33336 A3=-0.085 B3=0.095	A1=154.07500 B1=-1761.37834 C1=8374.33337 D1=-21034.16676 E1=29450.00013 F1=-21800.00010 G1=6666.66670 A2=-492.54 B2=5539.88003 C2=-25815.48901 D2=63806.66626 E2=-88015.33336 F2=64833.33333 G2=-19555.55565 A3=-0.1333333 B3=0.1339999
4th Stage	5th Stage	6th Stage
A1=75.43300 B1=-860.65834 C1=4090.41113 D1=-10210.83338 E1=14147.77784 F1=-10333.33338 G1=3111.11113 A2=-1182.22001 B2=13501.25673 C2=-63739.07807 D2=159216.66740 E2=-221844.44546 F2=163466.66741 G2=-49777.77800 A3=-0.04 B3=0.092	A1=-105.07400 B1=1149.70467 C1=-5145.83224 D1=12189.83339 E1=-18138.88897 F1=11320.00006 G1=-3288.88891 A2=332.04 B2=-399.84002 C2=18707.68897 D2=-46346.66688 E2=64088.88918 F2=-46933.33355 G2=14222.22229 A3=-0.1066666 B3=0.1299999	A1=-110.32400 B1=1282.14134 C1=-6136.79558 D1=15550.00007 E1=-22068.88899 F1=16586.66674 G1=-5155.33358 A2=-175.54 B2=1836.93001 C2=-7955.44448 D2=18268.33342 E2=-23411.11123 F2=15866.66675 G2=-4444.44447 A3=-0.255 B3=0.21375

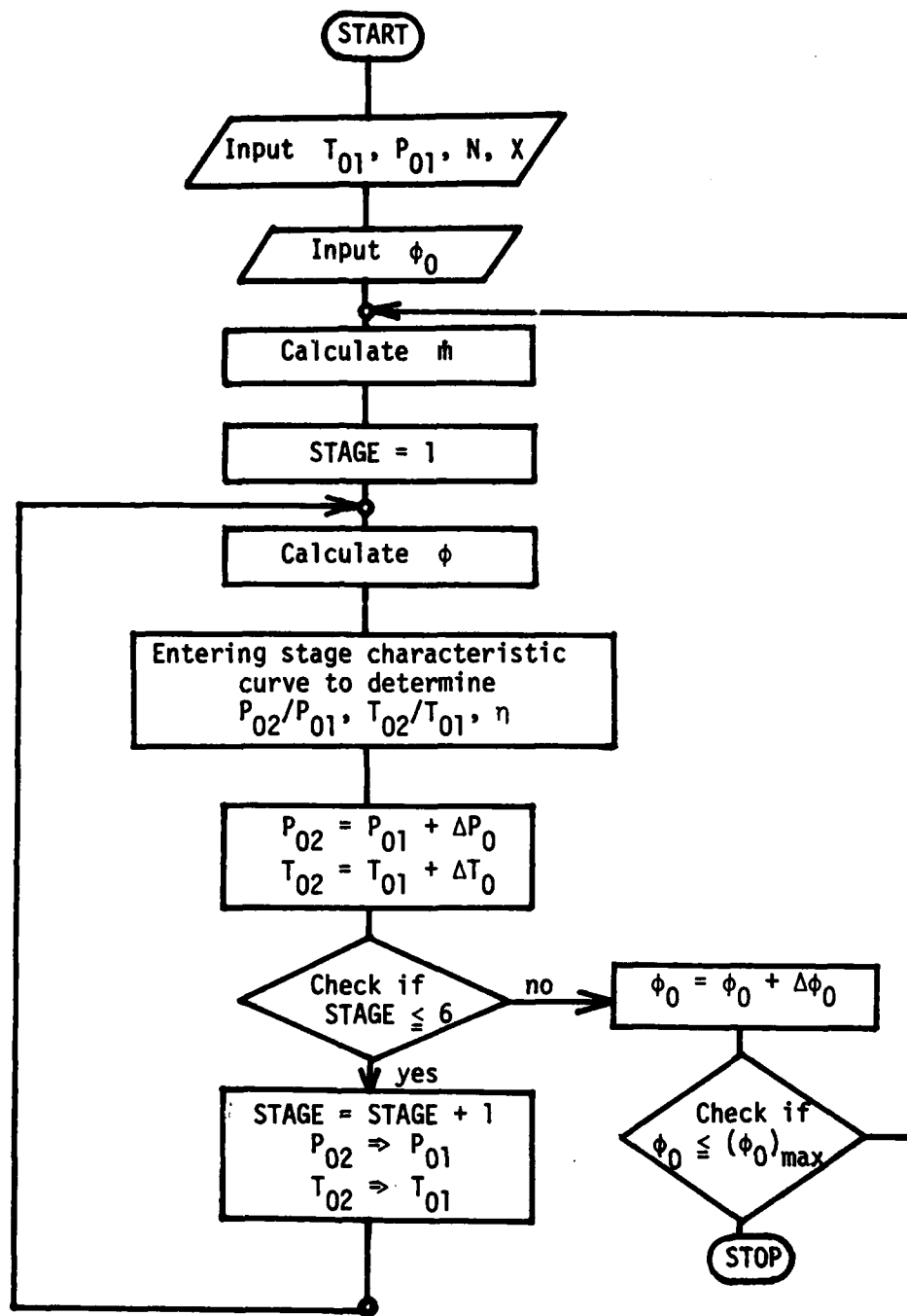


Figure A.6.1 Overall Calculation Procedure for Air-Methane Mixture

throughout the compressor. At the entrance of each stage, the flow coefficient is determined. Entering the stage characteristics curves, which are obtained by the experiment, the stage total pressure ratio, stage total temperature ratio, and stage adiabatic efficiency are obtained. These determine the stage outlet properties, which become the stage inlet properties for the next stage. The calculation is repeated until the calculations for all of the six stages are completed. Then the compressor overall performance, that is, overall total pressure ratio, overall total temperature ratio, and overall adiabatic efficiency, become determined for the chosen mass flow rate.

For other values of initial flow coefficients and speeds of rotation, the procedure has been repeated utilizing the relations postulated for the stage characteristics.

APPENDIX 7

PERFORMANCE CALCULATION PROCEDURE FOR AIR-WATER MIXTURE

FLOW WITH SMALL DROPLETS

1. Assumptions and Model Features

The assumptions introduced in modeling air-water mixture flow with small droplets are as follows.

- (1) The mixture is saturated with water vapor at the compressor inlet.
- (2) The small droplets are small enough to follow the gas phase streamlines. Hence, both the gas phase and the droplets absorb angular momentum and thus work input to the compressor.
- (3) The total number of droplets entering a blade passage may be divided into (i) those that impact a blade surface and (ii) the balance of droplets. The former in turn are divided into (a) those that rebound and (b) those that move over the blade surface.
- (4) Since the small droplets move with the gas phase, the direction of motion of the droplets is the same as that of the gas phase. The number of droplets impacting a blade surface is then proportional to the blade surface area projection normal to the gas phase velocity vector. Half of the droplets that impact the blade rebound into the flow.
- (5) The other half of the droplets impacting a blade form films or streamers running to the trailing edge of the blade, where they are re-entrained and accelerated into the flow as part of blade wakes.
- (6) The droplet size is unaffected during impact and rebound

processes. The size of the droplets that are re-entrained into the wake at the trailing edge can be predicted by consideration of the critical Weber number above which droplets can be expected to break up.

- (7) Droplets undergo a change in spanwise location due to the presence of centrifugal flow field. The spanwise motion of droplets can be calculated separately based upon radial velocity induced by the centrifugal flow field.
- (8) Drag forces between droplets and the gas phase are neglected since the relative velocity between the two phase in the case of small droplets is assumed to be small.
- (9) Heat and mass transfer processes occur between the gas and liquid phases and are accounted for at the exit of each stage.

2. Calculation Procedure

The initial and operating conditions required to perform the calculation are (i) compressor inlet temperature and pressure, (ii) blade rotational speed, (iii) initial water content, and (iv) initial flow coefficient.

The performance of a stage is then calculated as follows for given initial and operating conditions.

- (i) The stage stagnation pressure ratio is calculated utilizing experimental data obtained from air flow tests for stagnation temperature ratio and efficiency. The stagnation enthalpy rise corresponding to a chosen flow coefficient and operational rotating speed is apportioned between the liquid and gaseous phases. The liquid phase gains in temperature while both the temperature and pressure of the gaseous phase increase.
- (ii) Heat and mass transfer between the two phase are accounted for at the exit of the stage under consideration.
- (iii) Spanwise redistribution of droplets due to centrifuging is accounted for at the exit of the stage.

- (iv) Change in droplet size is accounted for at the exit of the stage.
- (v) Based on the results of calculations in steps (i) to (iv), one has all of the properties of two phase flow at the exit plane of the stage under consideration.
- (vi) In order to obtain the conditions at entry to the next stage, changes in the spacing between stages are established on the bases of one-dimensional flow taking into account area change through an iteration scheme. In carrying out this calculation, it is necessary to have the fluid outlet angle from the preceding stage. The fluid outlet angle is deduced using the concept of equivalent diffusion factor.

The calculations are then repeated for succeeding stages.

2.1 Mass Flow Rate

At the compressor inlet, the mass flow rate of mixture of air and droplets at an operating speed and at given inlet temperature and pressure is determined from the initial flow coefficient.

The mixture is a compressible fluid. The compressibility effect introduced by the presence of droplets is included by taking into consideration the acoustic speed in a droplet-laden air flow for calculating the mixture Mach number. Mass flow is related to mixture Mach number. The equation for the acoustic speed in a mixture of air and droplets is given in Appendix 11.

The mass flow rate can then be determined as follows.

- (1) Calculate the axial velocity

$$V_z = \phi_0 U_{\text{tip}}$$

- (2) Calculate the specific heat at constant pressure of air and water vapor.

- (3) Calculate the gas constant, specific heat at constant pressure, and specific heat ratio of the gas phase.

$$R_g = R_u [(1-x'_v)/(mw)_a + x'_v/(mw)_v]$$

$$c_{p_g} = x'_a c_{p_a} + x'_v c_{p_v}$$

$$\gamma_g = (1 - R_g/c_{p_g})^{-1}$$

where

$$x'_a = \dot{m}_a / (\dot{m}_a + \dot{m}_v)$$

$$x'_v = \dot{m}_v / (\dot{m}_a + \dot{m}_v)$$

- (4) Calculate the stagnation density of the gas phase.
 (5) Assume the Mach number M_a .
 (6) Calculate the static temperature of gas phase.

$$T_g = \{1 + (\gamma_g - 1)M_a^2 / 2\}^{-1} \cdot T_{01,g}$$

- (7) Calculate the acoustic speed in gas phase.

$$a_g = (\gamma_g R_g T_g)^{1/2}$$

- (8) Calculate the acoustic speed in the mixture.
 (9) Calculate the Mach number M_c .

$$M_c = V_z / a$$

- (10) Compare the assumed Mach number, M_a , with the calculated one, M_c , to check if

$$|M_a - M_c| < \epsilon$$

where ϵ is the desired accuracy. If satisfactory accuracy is obtained, proceed to the next step. Otherwise, the steps (5) to (9) should be repeated.

- (11) Calculate the static density of gas phase.

$$\rho_g = \{1 + (\gamma_g - 1)M^2/2\}^{1/(\gamma_g - 1)} \rho_{01,g}$$

- (12) Calculate the density of the mixture.

$$\rho_m = \left(\frac{x_g}{\rho_g} + \frac{x_w}{\rho_w} \right)^{-1}$$

- (13) Calculate the mixture mass flow rate.

$$\dot{m}_m = \rho_m V A$$

2.2 Flow Coefficient

Flow coefficient at the inlet of a follow-on stage is determined as follows.

- (1) From the previous stage outlet properties, the gas phase total temperature, $T_{01,g}$, and the total pressure, P_{01} , are known.
- (2) Calculate the gas constant, specific heat at constant pressure, and specific heat ratio of the gas phase.
- (3) Calculate the stagnation density of gas phase.

$$\rho_{01} = P_{01} / R_g T_{01,g}$$

- (4) Assume a value for Mach number, M_a .
- (5) Calculate the static density and static temperature of the gas phase.

- (6) Calculate the acoustic speed in the gas phase.
- (7) Calculate the acoustic speed in the mixture, a .
- (8) Calculate the density of the mixture

$$\rho_m = \left(\frac{x_g}{\rho_g} + \frac{x_w}{\rho_w} \right)^{-1}$$

- (9) Calculate the axial velocity.

$$V_z = \dot{m}_m / \rho_m A$$

- (10) Calculate the absolute velocity.

$$V_1 = V_z / \cos \alpha_1$$

where α_1 = air outlet angle of the previous stage stator.

- (11) Calculate the Mach number, M_c .

$$M_c = V_1 / a$$

- (12) Compare the assumed Mach number, M_a , with the calculated one, M_c . If M_a agrees reasonably well with M_c , proceed to the next step. Otherwise, steps (4) to (11) must be repeated.
- (13) Calculate the flow coefficient at the entrance of the stage.

$$\phi = V_z / U_{tip}$$

2.3 Compressor Stage Characteristics

The compressor stage characteristics given in Appendix 1, which apply to air flow through the compressor, have been utilized in this calculation for obtaining the stage temperature ratio and stage adiabatic efficiency for the mixture of air and droplets. It may be recalled that the stage temperature rise corresponding to a mixture flow coefficient has to be apportioned between the gas and liquid phases. The gas phase then undergoes a change in temperature and pressure while the liquid phase undergoes only a temperature change.

Utilizing the stage temperature ratio and adiabatic efficiency, one can then calculate the stage pressure ratio and the change in water temperature. In the current method of calculating stage performance for two phase flow, all of the other effects due to the presence of droplets are taken into account at the exit of the stage under consideration.

Regarding apportionment of energy input into the mixture in a stage, one proceeds as follows. The work input is expressed as follows.

$$\Delta H_0 = (\Delta H_0)_1 + (\Delta H_0)_2 + (\Delta H_0)_3 + (\Delta H_0)_4$$

where ΔH_0 = actual work input in stage;

$(\Delta H_0)_1$: work input to gas phase;

$(\Delta H_0)_2$: work input absorbed by droplets which do not impinge upon blade surface;

$(\Delta H_0)_3$: work input absorbed by water droplets which impinge upon blade surface, adhere to form a film and are re-entrained from the trailing edge; and

$(\Delta H_0)_4$: work input absorbed by droplets which impinge upon blade surface and rebound.

Defining mass fractions as follows.

x_g : mass fraction of gas phase

x_{w1} : mass fraction of water which does not impinge upon the blade surface.

x_{w2} : mass fraction of water which impinges on the blade surface and rebounds

x_{w3} : mass fraction of water which is re-entrained from the trailing edge

and noting that

$$x_g + x_{w1} + x_{w2} + x_{w3} = 1$$

AD-A114 831

PURDUE UNIV LAFAYETTE IN SCHOOL OF MECHANICAL ENGINEERING F/G 21/5
EFFECT OF WATER ON AXIAL FLOW COMPRESSORS. PART II. COMPUTATION--ETC(U)
JUN 81 T TSUCHIYA, S N MURTHY F33614-7A-C-2401

UNCLASSIFIED

AFWAL-TR-80-2090-PT-2

NL

5 5

5 5

5 5

5 5

5 5

5 5

5 5

5 5

5 5

5 5

5 5

5 5

5 5

5 5

5 5

5 5

5 5

5 5

5 5

5 5

5 5

5 5

5 5

5 5

5 5

5 5

5 5

5 5

5 5

5 5

5 5

5 5

5 5

5 5

5 5

5 5

5 5

5 5

5 5

5 5

5 5

5 5

5 5

5 5

5 5

5 5

5 5

5 5

5 5

5 5

5 5

5 5

5 5

5 5

5 5

5 5

5 5

5 5

5 5

5 5

5 5

5 5

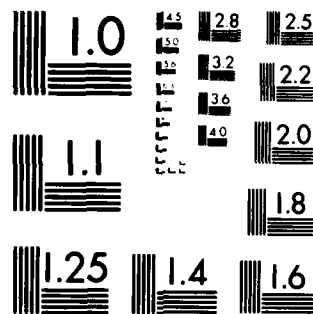
END

DATE

FILED

6 82

DTIC



MICROCOPY RESOLUTION TEST CHART
NATIONAL BUREAU OF STANDARDS 1963-A

one can express the work input fractions as follows in terms of the stage work done factor, λ .

$$(\Delta H_0)_1 = \lambda U_2 (W_{\theta 1} - W_{\theta 2}) x_g$$

$$(\Delta H_0)_2 = \lambda U_2 (W'_{\theta 1} - W'_{\theta 2}) x_{w1}$$

where $W_{\theta 1}$ and $W'_{\theta 1}$ are relative inlet wheel velocities of the gas phase and water droplets which not impinge upon the blade surface, respectively, and $W'_{\theta 2}$ and $W_{\theta 2}$ are the same velocities at outlet. Also, from physical considerations, the angular momentum change of water which impinges on the surface and adheres to form films and is finally re-entrained from the trailing edge can be considered to be negligible. Therefore,

$$(\Delta H_0)_3 = 0.$$

Then, $(\Delta H_0)_4$ can be calculated by writing

$$(\Delta H_0)_4 = \Delta H_0 - (\Delta H_0)_1 - (\Delta H_0)_2$$

The total work input, ΔH_0 , is calculated from the stage performance curves. In the present analysis, since we are considering small droplets, the velocity lag between gas phase and water droplet can be considered to be negligible. Accordingly, $W'_{\theta 1}$ and $W'_{\theta 2}$ can be set to be the same as $W_{\theta 1}$ and $W_{\theta 2}$.

From $(\Delta H_0)_1$, $(\Delta H_0)_2$, $(\Delta H_0)_3$, and $(\Delta H_0)_4$, the total temperature rise can be calculated for each phase.

2.4 Adjustment of Droplet Size

The size of droplet which is re-entrained into the wake at the blade trailing edge is calculated as follows.

- (1) Assume a value for the droplet diameter, d .
- (2) Calculate the stability number, SN.

$$SN = \mu_f^2 / \rho_g \sigma d g_c$$

(3) Calculate the critical Weber number

$$We_{crit} = 12 [1 + (SN)^{0.36}]$$

(4) Calculate the largest stable droplet diameter

$$d_{max} = \frac{We_{crit} \sigma g_c}{\rho_g V_g^2}$$

(5) Compare the assumed droplet diameter with the calculated droplet diameter. Repeat until satisfactory agreement is obtained.

The size of all the droplets can be adjusted on the basis of the above in the inter-blade row spacing.

2.5 Calculation of Centrifugal Force Effect

Three forces act on a droplet moving through a fluid: (1) the external force consisting of gravitational and centrifugal forces; (2) the buoyancy force, which acts parallel to the external force, but in the opposite direction; and (3) the drag force, which appears whenever there is relative motion between the droplet and the fluid, and acts parallel to the direction of motion but in the opposite direction. In the present case, the direction of motion of a droplet relative to the fluid is not parallel to the direction of the external and buoyant forces, and therefore the drag force makes an angle with the other two forces. However, under the one-dimensional approximation, the lines of action of all forces acting on the droplet are co-linear and therefore the forces may be added in obtaining a balance of momentum, as follows.

$$\frac{m}{g_c} \frac{du}{dt} = F_e - F_b - F_D$$

where F_e , F_b and F_D are the external, buoyancy and drag forces, respectively.

The external force can be expressed as the product of mass and

acceleration, a_e , of the droplet due to this force, and therefore,

$$F_e = \frac{m}{g_c} a_e$$

In the present case, because of the large rotor speeds, the centrifugal acceleration is far larger than the gravitational acceleration.

$$a_e = r\omega^2$$

where r is the radius and ω , the angular velocity. The acceleration can also be written as follows.

$$a_e = V_\theta^2/r$$

where V_θ is the circumferential velocity of the droplet. For droplets passing through a rotor blade passage, the circumferential component of the relative velocity, W_θ , should be used in place of V_θ . When there is a large change in whirl velocity between the inlet and the outlet of a blade row, a mean value of velocity may be more applicable.

The buoyancy force is, by Archimedes' principle, the product of the mass of the fluid displaced by the droplet and the acceleration from the external force. The mass of fluid displaced is $(m/\rho_w)\rho_g$, where ρ_w is the density of water and ρ_g is the density of the surrounding fluid. The buoyancy force is then given

$$F_b = m \rho_g a_e / \rho_w g_c$$

The drag force is expressed by the relation,

$$F_d = C_D \frac{\rho_g u^2}{2 g_c} A_p$$

where C_D is the drag coefficient and A_p is the projected area of the droplet measured in a plane perpendicular to the direction of motion of the droplet. The drag coefficient C_D can be used in a general form as follows.

$$C_D = b_1 / \text{Re}^n$$

where Re is the Reynolds number based on relative velocity between gas and droplet. The constants b_1 and n are as follows.

$$\begin{array}{lll}
 b_1 = 24.0, & n = 1.0 & \text{when } Re < 1.9 \\
 b_1 = 18.5, & n = 0.6 & \text{when } 1.9 < Re < 500 \\
 b_1 = 0.44, & n = 0.0 & \text{when } 500 < Re < 200,000.
 \end{array}$$

The equation of droplet motion then becomes the following:

$$\frac{du}{dt} = A/r - B u^{2-n}$$

where

$$A = (W_\theta)_{ave}^2 (1 - \rho_g/\rho_w),$$

$$B = 3 \mu^n b_1 \rho_g^{1-n} / 4 \rho_w D^{1+n},$$

D being the average droplet diameter. Over a small time interval, the equation of motion can be written as follows:

$$\Delta u = (A/r - B u^{2-n}) \Delta t$$

This equation can be used to determine the radial location of a droplet in a stage as follows:

- (1) Select the initial values for u_1 and r_1 .
- (2) Calculate the Reynolds number to determine the values of b_1 and n .
- (3) Calculate A and B.
- (4) Calculate the change of u during time interval Δt .
- (5) Calculate the new velocity u_2 .

$$u_2 = u_1 + \Delta u$$

- (6) Calculate the change in location of droplet in terms of Δr .

$$\Delta r = (u_1 + u_2)/2.0 \cdot \Delta t$$

- (7) Calculate the new radial location.

$$r_2 = r_1 + \Delta r$$

- (8) Repeat the calculation for new values of u_2 and r_2 and progressively extend the calculation.

The time interval should be sufficiently small in order to obtain reasonable accuracy. As stated in Section 2.1.3 in Chapter II of this Report, the length between the leading and trailing edges of a blade is divided into ten steps. The time interval Δt is then given by the relation, namely

$$\Delta t = \frac{\text{chord}}{V} \times \frac{1}{10}$$

where V is the velocity of moisture in the blade passage.

2.6 Heat Transfer to Droplets

The heat transfer rate can be determined from the following equation

$$\frac{dh}{dt} = h_h A (T_g - T_w)$$

where h_h is the heat transfer coefficient, A , the droplet surface area, T_w , the droplet surface temperature, and T_g , the temperature of the surrounding gas. The heat transfer coefficient can be expressed as follows:

$$h_h = \frac{k_a}{D_d} Nu$$

where k_a is the thermal conductivity of air, and Nu , the Nusselt number. The Nusselt number can be expressed in terms of the dimensionless groups as follows:

$$Nu = 2.0 + 0.6 (Re)^{0.50} (Pr)^{0.33}$$

where Re is the Reynolds number based on the relative velocity between the droplet and the surrounding air, and Pr is Prandtl number.

After calculating the temperature rise of the water and gas phases due to the work done by the rotor, the heat transfer calculation is carried out as follows:

- (1) Calculate the average droplet diameter, D_d .

- (2) Calculate the number of droplets, N_d .

$$N_d = \frac{\dot{m}_w}{\rho_w \frac{4}{3}\pi \left(\frac{D_d}{2}\right)^3} \cdot \frac{\Delta z}{V_z}$$

where \dot{m}_w is the mass flow rate of water phase, ρ_w , the density of water, V_z , the axial direction velocity, and Δz , the axial length of one stage.

- (3) Calculate the droplet surface area, A .
 (4) Calculate the Nusselt number, Nu .
 (5) Calculate the heat transfer coefficient, h_h .
 (6) Calculate the stage outlet temperature for droplet and gas without heat transfer, that is

$$T_{g2} = T_{g1} + (\Delta T_g)_{wk}$$

$$T_{w2} = T_{w1} + (\Delta T_w)_{wk}$$

where $(\Delta T_g)_{wk}$ and $(\Delta T_w)_{wk}$ are the temperature rise of gas and water due to work done by rotor.

- (7) Calculate the amount of heat transferred from the gas to the droplet.

$$\Delta H = h_h A (T_{g2} - T_{w2})$$

- (8) Calculate the temperature rise of the droplet and the temperature drop of the surrounding gas.

$$(\Delta H_g)_{ht} = \Delta H / \dot{m}_g c_s$$

$$(\Delta H_w)_{ht} = \Delta H / \dot{m}_w c_w$$

where c_w is the specific heat for water and c_s is the humid heat for air-water mixture.

- (9) Calculate the stage outlet temperature for droplet and gas.

$$T_{g2} = T_{g1} + (\Delta T_g)_{wk} - (\Delta T_g)_{ht}$$

$$T_{w2} = T_{w1} + (\Delta T_w)_{wk} + (\Delta T_w)_{ht}$$

- (10) Using the temperature calculated in step (9), repeat the steps (7) to (9) until a desired accuracy is obtained.

2.7 Mass Transfer to Droplets

The mass transfer rate can be calculated by the following equation

$$\frac{dm}{dt} = h_m A (C_{wb} - C_w)$$

where h_m is the mass transfer coefficient, A , the droplet surface area, C_{wb} , the water vapor concentration at droplet surface, and C_w , the water vapor concentration in fluid flow around droplet.

Since the density represents the mass concentration, and the vapor is almost a perfect gas, the mass transfer rate can be expressed in terms of vapor pressure as follows:

$$\frac{dm}{dt} = h_m A (\rho_{wb} - \rho_w)$$

or

$$\frac{dm}{dt} = h_m A \left(\frac{P_{wb}}{T_{wb}} - \frac{P_w}{T_w} \right) \frac{1}{R_v}$$

where R_v is the gas constant for water vapor, P_{wb} , the vapor pressure at droplet surface, P_w , the vapor pressure in fluid flowing around droplet, T_{wb} , the vapor temperature at droplet surface, and T_w , the vapor temperature in fluid flowing around droplet.

The surface area, A , for the droplet cloud is given by the relation,

$$A = \pi D_d^2 N_d$$

where D_d is the average droplet diameter, and N_d , the number of droplets.

The mass transfer coefficient, h_m , is expressed as follows.

$$h_m = \frac{D_v}{D_a} Sh$$

where D_v is the diffusion coefficient, and Sh , the Sherwood number.

A semi-empirical equation for the diffusion coefficient in gases is given by

$$D_v = 435.7 \frac{T^{3/2}}{p(V_A^{1/3} + V_B^{1/3})^2} \left(\frac{1}{M_A} + \frac{1}{M_B} \right)^{1/2}$$

where D_v is in square centimeters per second, T is in degree Kelvin, p is the total system pressure in newtons per square meter, and V_A and V_B are the molecular volumes of constituents A and B as calculated from the atomic volumes. M_A and M_B are the molecular weights of constituents A and B. For water-air systems, the numerical values of V_A , V_B , M_A and M_B are given as follows:

$$V_A = V_{air} = 29.9$$

$$M_A = M_{air} = 28.9$$

$$V_B = M_{water} = 18.8$$

$$M_B = M_{water} = 18.0$$

When the relative velocity between a single droplet and the surrounding fluid approaches zero, the following relationship is used to determine the mass transfer rate: $Sh = 2.0$.

Mass transfer rates increase with increase in relative velocity between the droplet and the surrounding air due to the additional mass transfer caused by the convection in the boundary layer around the droplet. The mass transfer coefficient from a spherical droplet can be expressed in terms of dimensionless groups as follows:

$$Sh = 2.0 + k(Re)^x(Sc)^y$$

where Re is the Reynolds number based on relative velocity, which expresses the ratio of inertial force to viscous force, and Sc is the Schmidt number, which expresses the ratio of kinetic viscosity to molecular diffusivity.

There is much discussion over the values of x , y , and k . The form most widely applied is the Ranz and Marshall equation which is

$$Sh = 2.0 + 0.6 (Re)^{0.50} (Sc)^{0.33}$$

The procedure for determining the mass transfer rate is as follows.

- (1) Calculate the Sherwood number, Sh .
- (2) Calculate the diffusion coefficient, D_v .
- (3) Calculate the average droplet size, D_d .
- (4) Calculate the mass transfer coefficient, h_m .
- (5) Calculate the total number of droplets, N_d .
- (6) Calculate the total surface area for all droplets.
- (7) Calculate the water vapor pressure at droplet surface, P_{wb} , based on the droplet surface temperature, T_s .
- (8) Assume the vapor pressure, p_w , and set $p_w = (p_w)_a$.
- (9) Calculate the mass transfer rate, $\frac{dm}{dt}$.
- (10) Calculate the new value of water mass flow rate.

$$\dot{m}_w = \dot{m}_w - \frac{dm}{dt}$$

- (11) Calculate the new value of vapor mass flow rate.

$$\dot{m}_v = \dot{m}_v + \frac{dm}{dt}$$

- (12) Calculate the specific humidity, W .

$$W = \dot{m}_v / \dot{m}_a$$

where \dot{m}_a is the air mass flow rate.

- (13) Calculate the vapor pressure.
- (14) Compare the calculated value, $(p_w)_c$, with the assumed value, $(p_w)_a$.

If $(p_w)_c$ agrees reasonably well with the assumed value $(p_w)_a$, proceed to step (15). Otherwise, steps (8) to (14) should be repeated.

- (15) Using the determined p_w , the mass transfer rate is calculated.

Also, the specific humidity can be determined by the following equation:

$$W = 0.6219 \frac{P_w}{P - P_w}$$

3. Overall Calculation Procedures

1. Input Data

- (i) compressor inlet temperature: T_{01}
- (ii) compressor inlet pressure: P_{01}
- (iii) rotational speed : N
- (iv) initial water content: $x_{w,0}$
- (v) initial droplet size: D_0
- (vi) initial flow coefficient: ϕ_0

2. Axial velocity: $V_z = U_{tip} \phi_0$

3. Specific humidity for saturated air at T_{01} W_s

4. Water mass fraction: x_w

5. Vapor mass fraction: $x_v = \frac{W_s}{1 + W_s} (1 - x_w)$

6. Dry air mass fraction: $x_a = 1.0 - x_w - x_v$

7. Density of mixture: ρ_m

8. Mass flow rate of mixture: $\dot{m}_m = \rho_m V_z A$

9. Mass flow rate of air: $\dot{m}_a = \dot{m}_m x_a$

10. Mass flow rate of vapor: $\dot{m}_v = \dot{m}_m x_v$

11. Mass flow rate of water: $\dot{m}_w = \dot{m}_m x_w$

12. Impingement, rebound, and re-entrainment for IGV
13. Nominal droplet size
14. Density at rotor inlet: ρ
15. Axial velocity at rotor inlet: V_z
16. Flow coefficient at rotor inlet: $\phi = V_z/U_{tip}$
17. Entering the Compressor map with ϕ to get adiabatic efficiency η , and temperature rise ΔT_0 .
18. Total input energy: $\Delta H_{in} = c_{p_a} \Delta T_0$
19. Energy absorbed by gas phase: $\Delta H_g = \Delta H_{in} x_g$
20. Energy absorbed by droplet: $\Delta H_w = \Delta H_{in} x_w$
21. Temperature rise of gas phase due to rotor work: $(\Delta T)_{work}$
22. Temperature rise of droplet due to rotor work: $(\Delta T_w)_{work}$
23. Pressure ratio:

$$\frac{P_{02}}{P_{01}} = \left\{ 1 + \eta \frac{(\Delta T_g)_{work}}{T_{01}} \right\}^{\gamma/(\gamma-1)}$$
24. Stage outlet pressure: $P_{02} = \left(\frac{P_{02}}{P_{01}} \right) P_{01}$
25. Construct velocity triangle
26. Impingement, rebound, re-entrainment for rotor
27. Nominal droplet size at rotor outlet
28. Centrifugal effect in the rotor
29. Impingement, rebound, re-entrainment for stator
30. Nominal droplet size at stator outlet

31. Stage outlet pressure
32. Heat transfer calculation to find (ΔT_g) Heat Transfer, and (ΔT_w) Heat transfer
33. Temperature of gas phase at stage outlet:

$$T_{g2} = T_{g1} + (\Delta T_g)_{\text{work}} - (\Delta T_g)_{\text{Heat Transfer}}$$

34. Temperature of droplet at stage outlet:

$$T_{w2} = T_{w1} + (\Delta T_w)_{\text{work}} + (\Delta T_w)_{\text{Heat Transfer}}$$

35. Mass transfer calculation
36. Mass fraction of water x_w , mass fraction of vapor x_v .
37. Specific humidity:
38. Adjust droplet size based on mass transfer rate
39. Make the outlet properties be inlet properties for the next stage
40. Repeat steps 14 - 39 until the calculation of the last stage is finished.

$$W = \dot{m}_w / \dot{m}_a$$

APPENDIX 8

PERFORMANCE CALCULATION PROCEDURE FOR AIR-WATER MIXTURE

FLOW WITH LARGE DROPLETS

1. Assumptions and Model Features

Referring to Appendix 7, Section 1 therein has been devoted to a discussion of assumptions and model features for the case of small droplets. In the case of large droplets, all of the assumptions for the case of small droplets apply except the following.

Item (2): The large droplets are not expected to follow the gas phase streamlines and hence do not share the work input with the gas phase.

Item (4): The large droplets move with substantial relative velocity with respect to the gas phase and have equal probability of motion in all directions. However, regarding the latter aspect, the droplets are divided into two subclasses with a direction of motion for each class, specified with respect to the gas phase velocity vector. The number of droplets impacting on the blade surface is then proportional to the blade surface area projection normal to the velocity vectors for the two subclasses of droplets.

Item (7): Centrifugal force action is confined to those droplets that impact the blade but do not rebound back to the gas stream.

Except for modifications arising with respect to the foregoing, the rest of the assumptions are the same as in the case of small droplets.

2. Calculation Procedure

The initial and operating conditions required to perform the calculation are (i) compressor inlet temperature and pressure, (ii) blade rotational speed, (iii) initial water content, and (iv) initial flow coefficient.

The performance of the stage is then calculated in the same manner as in the case of small droplets (Appendix 7, Section 2) except for the following: large droplets only affect the gas phase mass flow and no part of the work input goes directly into the large droplets.

2.1 Mass Flow Rate

At the compressor inlet, the mass flow rate of mixture of air and droplets at an operating speed and at given inlet temperature and pressure is determined from the initial flow coefficient.

The procedure for calculating the gas and liquid mass flow rates corresponding to a value of flow coefficient is the same as that described in Appendix 7, Section 2.1.

2.2 Flow Coefficient

Flow coefficient at the inlet of a follow-on stage is determined in the case of large droplets in the same manner as in the case of small droplets utilizing the procedure given in Appendix 7, Section 2.2.

2.3 Compressor Stage Characteristics

The compressor stage characteristics, given in Appendix 1, which apply to air flow through the compressor, have been utilized in this calculation for obtaining the stage temperature ratio and stage adiabatic efficiency for the gaseous phase. Droplets do not share in the work input. Accordingly, utilizing the terminology of Appendix 7, Section 2.3, the work input is simply expressed as follows.

$$\Delta H_0 = (\Delta H_0)_1 .$$

2.4 Droplet Classification

The large droplets are divided as stated in Chapter III, Section 3.3.2, into two subclasses, each subclass with an assigned direction of motion and a total number of droplets.

Referring to Fig. A.8.1, the two subclasses are shown as (1) and (2) which have direction of motion given by γ_1 , and γ_2 relative to the gas phase velocity vector. The total number of droplets in subclass (1) is proportional to angle $2\gamma_1$ and those in subclass (2) is proportional to angle $2\gamma_2$ or $(180 - 2\gamma_1)$. The relative velocity between the gas phase and droplets of subclass (1) is given by the difference between V_{g1} and the component of V_{p1} (the velocity of droplets of subclass (1) in the direction of V_{g1}). Similarly, the relative velocity between the gas phase and the droplets of subclass (2) is given by the difference between V_{g1} and the component of V_{p2} in the direction of V_{g1} . Thus, for droplets of subclass (1), the relative velocity is given by the relation,

$$V_{g1} - V_{p1} \cos \gamma_1$$

and for droplets of subclass (2), the relative velocity is given by the relation,

$$V_{g1} - V_{p2} \cos \gamma_2$$

In Fig. A.8.1, the blade outlet conditions are also shown. As at the blade inlet section, the relative velocities between the gas phase and droplets of subclasses (1) and (2) may be written as follows.

$$V_{g2} - V_{p1} \cos \delta_1 \quad \text{for subclass (1), and}$$

$$V_{g2} - V_{p2} \cos \delta_2 \quad \text{for subclass (2),}$$

where δ_1 is the inclination of the mean velocity vector for subclass (1) and δ_2 , the inclination of the mean velocity vector for subclass (2), both of them measured with respect to the gas phase velocity vector at outlet, designated V_{g2} . Once again, at the outlet section, the

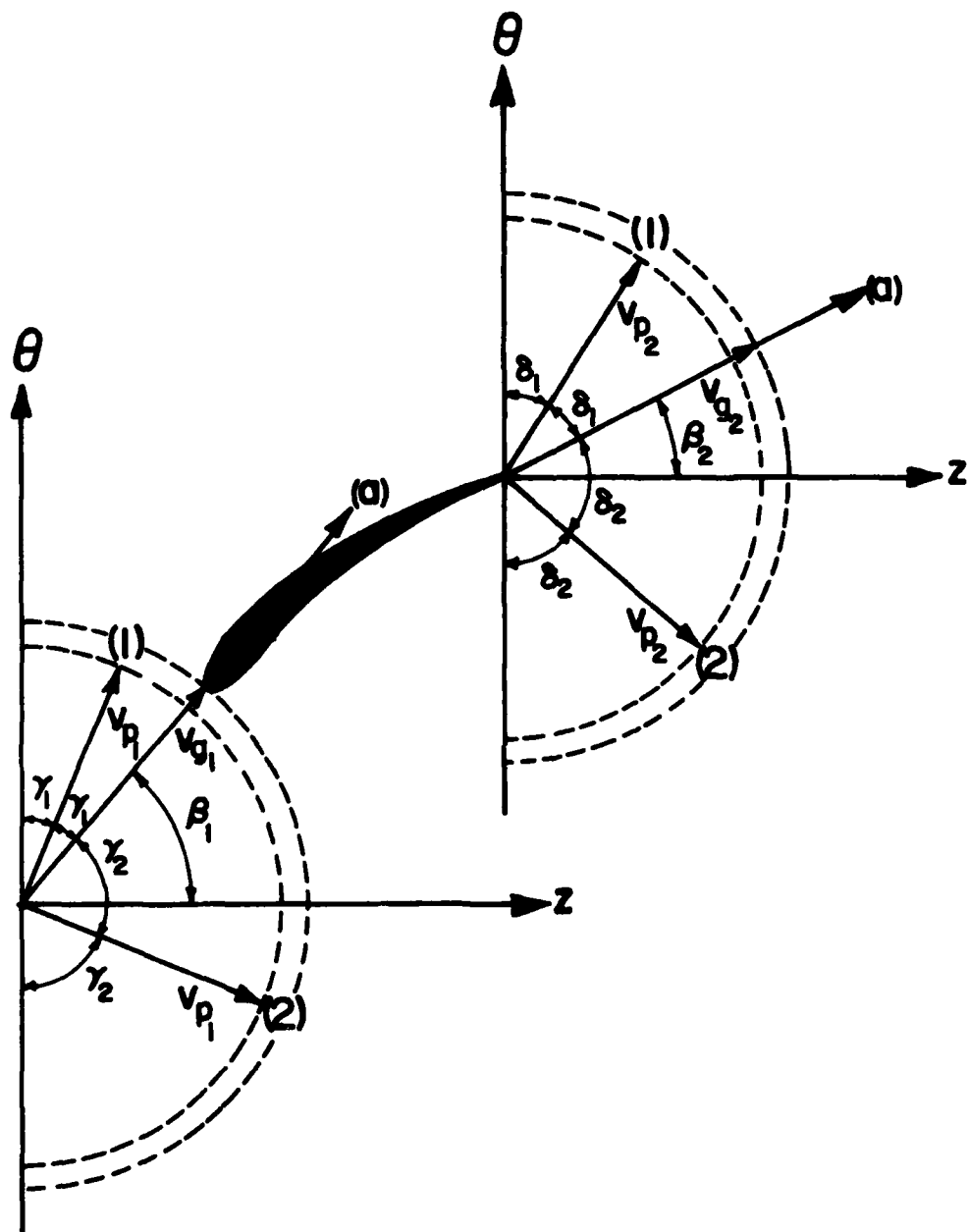


Fig.A.8.1 Model for Motion of Large Droplet

number of droplets in subclass (1) is proportional to angle $2\delta_1$, and the number of droplets in subclass (2) is proportional to angle $2\delta_2$ or $(180 - 2\delta_1)$. It is clear that the total number of droplets is divided into two new subclasses at the outlet, based on the directions of motion of droplets relative to the gas phase velocity. The two subclasses at the outlet are the output from the blade row for the given initial and operating conditions.

2.5 Droplet Drag

The droplet drag losses are included as additional two phase flow losses at stage exit. They are based on droplet drag which is a function of droplet Reynolds number based on droplet diameter and droplet relative velocity with respect to the gas phase. The droplet relative velocities for the two subclasses of droplets has been discussed in the previous section.

2.6 Adjustment of Droplet Size

The size of droplets at the exit plane of a blade row of stage is calculated based on Weber number in the same manner as described in Appendix 7, Section 2.4 for the case of small droplets.

The readjusted droplet size becomes part of the initial conditions for the next row along with the identification of the two subclasses for droplets at the exit plane of the previous row of blades.

2.7 Calculation of Centrifugal Force Effect

In the case of large droplets, because of the general independence of droplet motion with respect to gas phase motion, centrifugal force action has to be confined to what arises on the surface of rotor blades for droplets that impact on them and are not rebound. Droplets in the free stream through the blade passages are unaffected by the whirl component of gas phase velocity.

With this qualification, centrifugal force action, resulting in

spanwise redistribution of droplets at the exit of a stage, is calculated for large droplets in the same manner as for small droplets, as described in Appendix 7, Section 2.5.

2.8 Heat and Mass Transfer Effects

Heat transfer to droplets and mass transfer from droplets to gas phase are calculated for large droplets in the same manner as for the case of small droplets, according to the procedure outlined in Appendix 7, Sections 2.6 and 2.7.

These processes are taken into account at the exit of a stage as additional two phase flow effects.

3. Overall Calculation Procedures

1. Input data

- (i) compressor inlet temperature: T_{01}
- (ii) compressor inlet pressure: P_{01}
- (iii) rotational speed: N
- (iv) initial water content: $x_{w,0}$
- (v) initial droplet size: D_0
- (vi) initial flow coefficient: ϕ_0

- 2. Axial velocity: $V_z = U_{tip} \phi_0$

- 3. Specific humidity for saturated air at T_{01} : W_s

- 4. Water mass fraction: x_w

- 5. Vapor mass fraction: $x_v = \frac{W_s}{1 + W_s} (1 - x_w)$

- 6. Dry air mass fraction: $x_a = 1.0 - x_w - x_v$

- 7. Density of mixture: ρ_m

8. Mass flow rate of mixture: $\dot{m}_m = \rho_m V_z A$
9. Mass flow rate of air: $\dot{m}_a = \dot{m}_m x_a$
10. Mass flow rate of vapor: $\dot{m}_v = \dot{m}_m x_v$
11. Mass flow rate of water: $\dot{m}_w = \dot{m}_m x_w$
12. Impingement, rebound and re-entrainment for IGV
13. Nominal droplet size
14. Density at rotor inlet: ρ
15. Axial velocity at rotor inlet: V_z
16. Flow coefficient at rotor inlet: $\phi = V_z/U_{tip}$
17. Entering the Compressor map with ϕ to get adiabatic efficiency, η , and temperature rise ΔT_0
18. Total input energy: $\Delta H_{in} = c_{p_a} \Delta T_0$
19. Energy absorbed by gas phase: $\Delta H_g = \Delta H_{in}$
20. Energy absorbed by droplet: $\Delta H_w = 0$
21. Temperature rise of gas phase due to rotor work: $(\Delta T)_{work}$
22. Temperature rise of droplet due to rotor work: $(\Delta T)_{work} = 0$
23. Pressure ratio:

$$\frac{P_{02}}{P_{01}} = \left\{ 1 + \eta \frac{(\Delta T)_{work}}{T_{01}} \right\}^{\gamma/(\gamma-1)}$$
24. Stage outlet pressure: $P_{02} = \left(\frac{P_{02}}{P_{01}} \right) P_{01}$
25. Construct velocity triangle
26. Impingement, rebound, re-entrainment for rotor

27. Nominal droplet size at rotor outlet
28. Drag for rotor flow
29. Centrifugal effect in the rotor
30. Impingement, rebound, re-entrainment for stator
31. Nominal droplet size at stator outlet
32. Drag for stator flow
33. Total drag and associate pressure loss
34. Stage outlet pressure
35. Heat transfer calculation to find (ΔT_g) Heat Transfer and (ΔT_w) Heat Transfer
36. Temperature of gas phase at stage outlet:

$$T_{g2} = T_{g1} + (\Delta T_g)_{\text{work}} - (\Delta T_g)_{\text{Heat Transfer}}$$

37. Temperature of droplet at stage outlet:

$$T_{w2} = T_{w1} + (\Delta T_w)_{\text{Heat Transfer}}$$

38. Mass transfer calculation
39. Mass fraction of water x_w , mass fraction of vapor x_v .

40. Specific humidity:

$$W = \dot{m}_w / \dot{m}_a$$

41. Adjust droplet size based on mass transfer rate
42. Make the outlet properties be inlet properties for the next stage

43. Repeat steps 14 to 42 until the calculation of the last stage is finished.

APPENDIX 9

CALCULATION PROCEDURE FOR LOCAL INJECTION AND INSTANTANEOUS EVAPORATION OF WATER

1. Model and Assumptions

- (1) Water is injected into the compressor at the correct temperature at chosen locations in the compressor to undergo instantaneous evaporation locally. Consequently there is an instantaneous reduction in fluid temperature and increase in the gas phase mass content. All of the water injected (1.5 per cent in all of the cases discussed here) is assumed to undergo evaporation. The aero-mechanical effects due to the presence of water droplets are therefore entirely left out of account except for the evaporation process.
- (2) Both prior to and after the evaporation of water, the performance of various stages of the compressor is based on air flow data. In estimating the performance of a stage with air-stream mixture, account is taken of changes in molecular weight and ratio of specific heats.

2. Calculation Procedures

A. Pre-Evaporation

- (1) Select compressor inlet temperature T_{01} , pressure P_{01} , rotation speed N , and mass flow rate \dot{m} .
- (2) Calculate stagnation density from P_{01} and T_{01} .

$$\rho_0 = P_{01} / RT_{01}$$

(3) Assume Mach number M_a .

(4) Calculate static density, ρ , and static temperature T .

$$\rho = \rho_0 \left(1 + \frac{\gamma-1}{2} M_a^2 \right)^{-1/(\gamma-1)}$$

$$T = T_0 \left(1 + \frac{\gamma-1}{2} M_a^2 \right)^{-1}$$

(5) Calculate axial velocity V_z .

$$V_z = \dot{m} / \rho A$$

(6) Calculate Mach number, M_c .

$$M_c = V / \sqrt{\gamma R T_g}$$

(7) Compare the calculated value M_c with the assumed value M_a .
If M_c agrees reasonably well with M_a proceed to Step (8).
Otherwise, Steps (3) to (6) have to be repeated.

(8) Calculate rotor tip speed U_{tip}

$$U_{tip} = r_{tip} 2\pi N / 60$$

(9) Calculate flow coefficient

$$\phi = V_z / U_{tip}$$

(10) Obtain from stage characteristic curves the corresponding pressure rise coefficient, ψ , and stage efficiency η .
Hence calculate the stage outlet total pressure and total temperature.

B. Evaporation and Post-Evaporation

Evaporation can occur at the entry of a specified stage when the

following conditions are satisfied.

- (1) stage inlet temperature is higher than the local boiling point of water; and
- (2) inlet temperature is high enough to supply the required latent heat of evaporation of water.

Then, the inlet temperature drops by an amount given by

$$\Delta T = x_w H_v / c_p$$

where x_w is water content, and H_v is latent heat of vaporization. Also, the mass flow increases by the amount of water undergoing evaporation.

When the changes in temperature and mass flow are accounted for at the stage where evaporation takes place, the performance of various succeeding stages can be calculated as in pre-evaporation stages.

APPENDIX 10

CALCULATION PROCEDURE FOR AIR-WATER DROPLET

MIXTURE FLOW WITH EVAPORATION

1. Assumptions and Model

- 1) The water droplets belong to the category of small droplets.
- 2) The inlet temperature of the mixture is sufficiently high to permit evaporation of (at least) part of the water at some stage in the compressor.

2. Calculation Procedure

The calculation procedure up to the location where water begins to undergo change of phase is the same as that described in Appendix 7.

The calculation procedure following the location where water undergoes evaporation is the same as that described in Appendix 9, part (B) of Calculation Procedure.

APPENDIX 11

FUNCTIONAL EXPRESSIONS FOR THERMO-PHYSICAL PROPERTIES

1. Properties of Air, Steam, and Methane

A. Specific Heat at Constant Pressure

The specific heat at constant pressure for various gases can be calculated by writing (Ref. 38)

$$c_p = (a + bT^1 + cT^2 + dT^3 + eT^4)R$$

where c_p = specific heat at constant pressure [J/kg-K], T = temperature [K], and R = gas constant [J/kg-K].

Values of coefficients a , b , c , d , and e are presented in Table A.11.1 for air, steam and methane.

B. Molecular Weight, Gas Constant and Specific Heat Ratio

Molecular weight, gas constant, and mean value of specific heat ratio for air, steam, and methane employed in the calculations are presented in Table A.11.2. Utilizing these, one can calculate the properties for mixtures of gases.

C. Saturation Vapor Pressure

The saturation vapor pressure p_s , can be related to the saturation vapor temperature, T_s , by the following equation (Ref. 39):

$$\log_{10} p_s = A - B/T_s$$

Table A.11.1
COEFFICIENT FOR c_p CALCULATION

	a	b	c	d	e
Air	3.65359	-1.33736×10^{-3}	3.29421×10^{-6}	-1.91142×10^{-9}	0.275462×10^{-12}
Steam	4.07013	-1.10845×10^{-3}	4.15212×10^{-6}	-2.96374×10^{-9}	0.807021×10^{-12}
Methane	3.82619	-3.97946×10^{-3}	24.5583×10^{-6}	-22.7329×10^{-9}	6.96270×10^{-12}

Table A.11.2
MOLECULAR WEIGHT, GAS CONSTANT, AND SPECIFIC HEAT RATIO

	Molecular Weight mw	Gas Constant R $\left[\frac{\text{lb}_f\text{-ft}}{\text{lb}_m\text{-R}} \right]$	Gas Constant R $\left[\frac{\text{J}}{\text{kg-K}} \right]$	Specified Heat Ratio γ
Air	28.964	53.352	287.056	1.400*
Steam	18.016	85.774	461.495	1.294**
Methane	16.043	96.322	518.251	1.304*

* At 25 °C atmospheric pressure, ** at 110 °C, atmospheric pressure.

The constants A and B are given as follows:

$$\begin{array}{lll} A = 5.97780 & B = 2224.4 & \text{when } 20^\circ \text{C} < T_s < 100^\circ \text{C} \\ A = 5.64850 & B = 2101.1 & \text{when } 100^\circ \text{C} < T_s < 200^\circ \text{C} \\ A = 5.45142 & B = 2010.8 & \text{when } 200^\circ \text{C} < T_s < 350^\circ \text{C} \end{array}$$

where p_s is in $[\text{Kg/cm}^2]$ and T_s is in $[^\circ\text{K}]$.

D. Temperature of Boiling and Dew Point

In order to find the local boiling point and dew point, the following simple relationships can be used.

$$T_{\text{boil}} = B / (A - \log_{10} p)$$

$$T_{\text{dew}} = B / (A - \log_{10} p_w)$$

where p is local mixture pressure, and p_w is local vapor pressure.

The constants A and B are the same as those of the saturation temperature-saturation pressure equation in part C.

E. Specific Humidity

The specific humidity is defined as follows (Ref. 40):

$$W = 0.6219 \frac{p_w}{p - p_w}$$

where p_w = vapor pressure and p = mixture pressure.

The specific humidity can, also, be calculated from the relation

$$W = \frac{\dot{m}_v}{\dot{m}_a}$$

where \dot{m}_v and \dot{m}_a are mass flow rate of vapor and dry air, respectively.

F. Saturation Specific Humidity

The saturation specific humidity, W_s , is defined as specific humidity corresponding to saturation vapor pressure, p_s . Thus,

$$W_s = 0.6219 \frac{P_s}{p - P_s}$$

Figure A.11.1 shows the relation between temperature and saturation specific humidity.

G. Latent Heat for Vaporization

The latent heat for vaporization can be expressed in terms of temperature for any specified temperature range. In the present investigation, the temperature range of interest is 100 ~ 400 °F (38 ~ 205 °C). In this temperature range, the latent heat for vaporization, H_v , may be written as follows

$$H_v = aT + b$$

where units of H_v and T are [Btu/lb_m] and [F], respectively, and $a = -0.6840909$, $b = 1115.3272$. Figure A.11.2 shows the relation between latent heat for vaporization and temperature in the chosen range (Ref. 41).

2. Acoustic Speed in Droplet-Laden Air

The acoustic speed in droplet-laden air flow is given by the following relation (Ref. 22):

$$a = \left[\{ (1 - \sigma_v) \rho_g + \sigma_v \rho_w \} \left\{ \frac{1 - \sigma_v}{\rho_g a_g^2} + \frac{\sigma_v}{\rho_w a_w^2} \right\} \right]^{-1/2}$$

where a = acoustic speed in a droplet-laden air flow

a_g = gas phase acoustic speed

a_w = liquid phase acoustic speed

ρ_g = density of gas phase

ρ_w = density of liquid phase

σ_v = particulate liquid volume fraction

x_w = particulate liquid mass fraction

$\sigma_v = x_w \rho_g / [\rho_w - x_w (\rho_w - \rho_g)]$

Fig.A.11.1 Saturation Specific Humidity vs Temperature

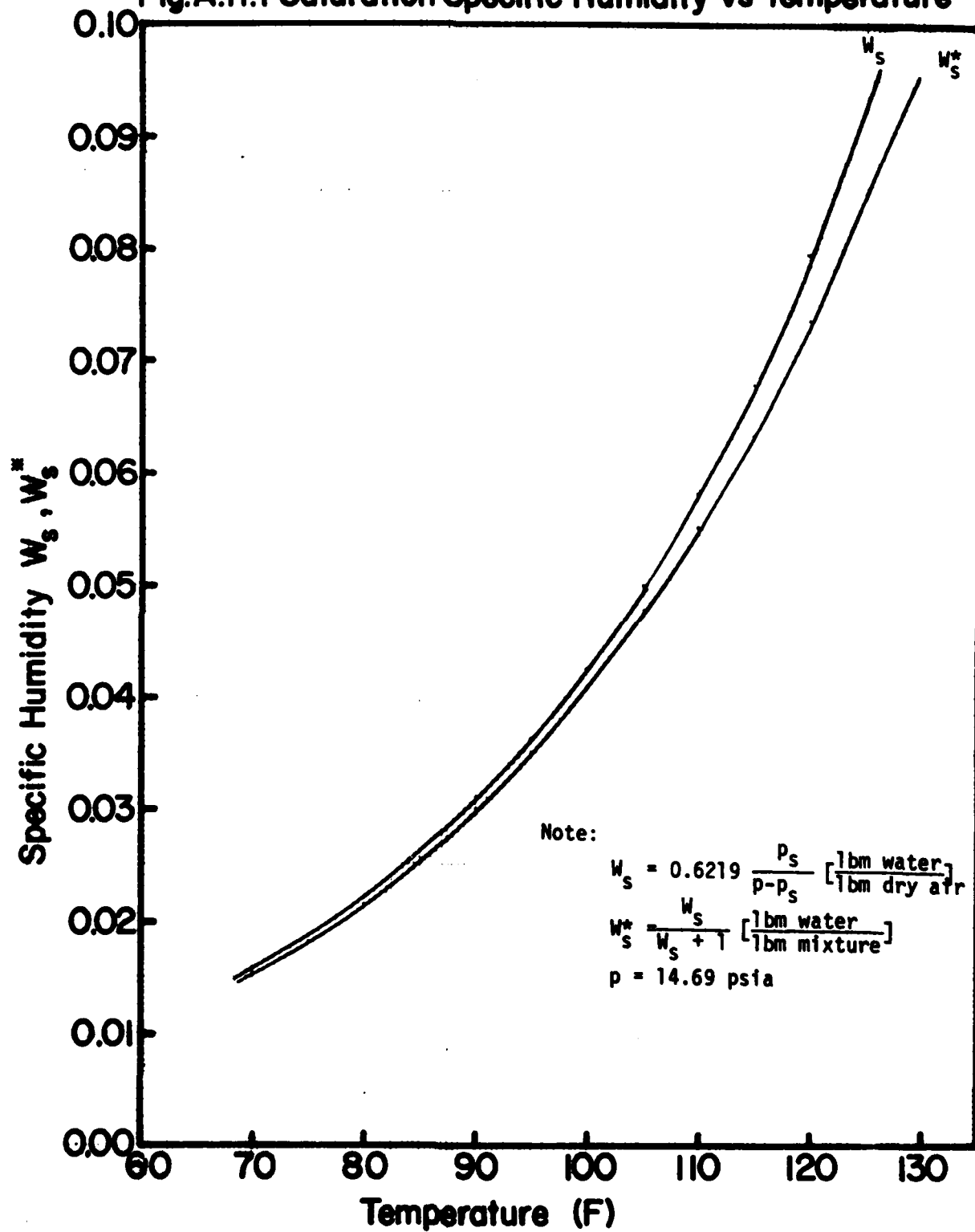
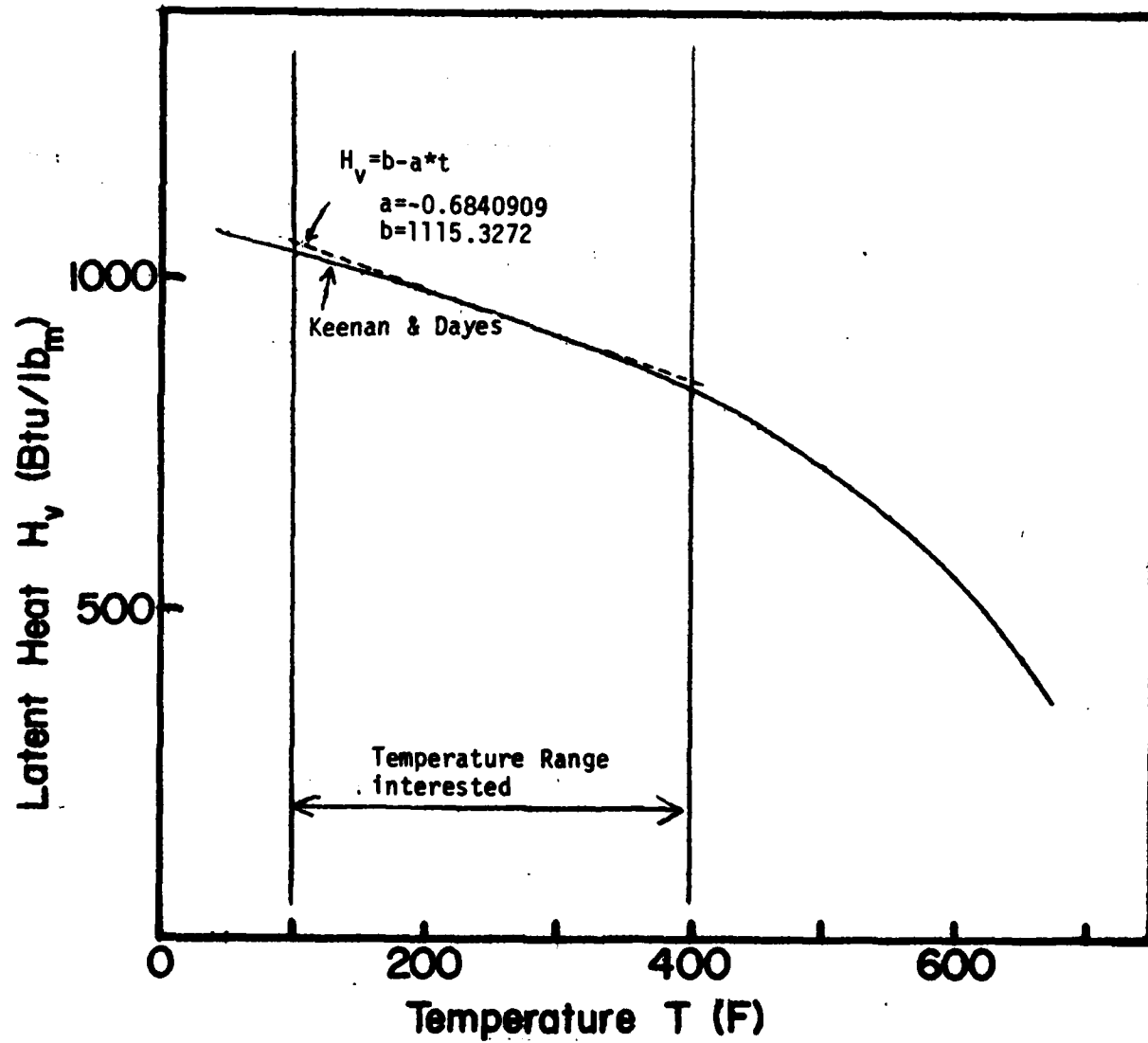


Fig.A.II.2 Latent Heat vs Temperature



LIST OF REFERENCES

1. Willenborg, J.A., et al., "F-111 Engine Water Ingestion Review," F-111 System Program Office, Wright-Patterson Air Force Base, Dayton, Ohio, October 31-November 10, 1972.
2. Useller, J.W., et al., "Effect of Heavy Rainfall on Turbojet Aircraft Operation," Aeronautical Engineering Review, February, 1955.
3. MacGregor, C.A. and Bremer, R.J., "An Analytical Investigation of Water Ingestion in the B-1 Inlet," Rockwell International, NA-73-181, June, 1973.
4. (a) "Concorde Complete Flooded Runway Tests," Aviation Week and Space Technology, p. 22, October 4, 1971.
(b) "Board Assays Crash of DC-9 in Storm," Ibid, pp. 63-67, July 24, 1978.
(c) "Storm Traced in Southern DC-9 Crash," Ibid, pp. 59-61, July 31, 1978.
(d) "Damage Assessed in Southern Crash," Ibid, pp. 59-63, August 7, 1978.
(e) "Thrust Loss Cited in Southern Accident," Ibid, pp. 55-58, August 21, 1978.
(f) "Board Urges Improved Thunderstorm Reporting," Ibid, pp. 63-64, August 28, 1978.
5. Papadaes, B.S. and Taylor, D.W., "A Review of Sea Loiter Aircraft Technology," AIAA Paper No. 76-876, September, 1976.
6. Pfeifer, G.D. and Maier, G.P., "Engineering Summary of Powerplant Icing Technical Data," Federal Aviation Administration Report No. FAA-RD-77-76, July, 1977.
7. Danielson, K. and Huggins, A.W., "Raindrop Size Distribution Measurement of High Elevation Continental Cumuli," Conference on Cloud Physics, pp. 305-310, October, 1974.
8. Fowler, M.G., et al., "Cloud Droplet Measurements in Cumuliform and Stratiform Clouds," Ibid, pp. 296-299, October, 1974.

9. Kissel, G.J., "Rain and Hail Extremes at Altitude," AIAA Paper No. 79-0539, February, 1979.
10. Hearsey, R.M., "A Revised Computer Program for Axial Compressor Design," Wright-Patterson Air Force Base Aerospace Research Laboratories, ARL TR 75-0001, Volume I and II.
11. (a) Murthy, S.N.B., et al., "Water Ingestion Into Axial Flow Compressors," Report No. AFAPL-TR-76-77, Air Force Systems Command, Wright-Patterson Air Force Base, August, 1976.
(b) Murthy, S.N.B., et al., "Analysis of Water Ingestion Effects in Axial Flow Compressors," Report No. AFAPL-TR-78-35, Air Force Systems Command, Wright-Patterson Air Force Base, June, 1978.
12. Grant, G. and Tabakoff, W., "Erosion Prediction in Turbomachinery Resulting from Environmental Solid Particles," Jr. of Aircraft, Volume 12, No. 5, pp. 471-478, May, 1975.
13. Tabakoff, W., et al., "Effect of Solid Particles on Turbine Performance," Transaction of the ASME, Jr. of Engineering for Power, pp. 47-52, January, 1976.
14. Marble, F.E., "Nozzle Contours for Minimum Particle-Lag Loss," AIAA Journal, Volume 1, No. 12, pp. 2793-2801, December, 1963.
15. Korkan, K.D., et al., "Particle Concentrations in High Mach Number Two-Phase Flows," AIAA Paper No. 74-606, July, 1974.
16. Hoffman, J.D., "An Analysis of the Effects of Gas-Particle Mixtures on the Performance of Rocket Nozzles," Ph.D Thesis, Purdue University, January, 1963.
17. Moore, M.J. and Sieverding, C.H., Two-Phase Steam Flow in Turbines and Separators, McGraw-Hill, New York, 1976.
18. Gardner, G.O., "Events Leading to Turbine Blade Erosion," Proc. Inst. Mech. Eng., Vol. 178, Pt. 1, No. 23, pp. 593-624, 1964.
19. Keller, H., Erosionskorrosion on Heissdampfturbinen VGB Kraftwerkstechnik, 1974, Heft 5.
20. Diagnostics and Engine Condition Monitoring, AGARD-CP-165, June 1975.

21. "Distortion Induced Engine Instability," Advisory Group for Aerospace Research and Development, Lecture Series, AGARD-LS-72, December, 1974.
22. Collier, J.G. and Wallis, G.B., Two-Phase Flow and Heat Transfer, Vol. II, p. 405, Dept. of Mechanical Engineering, Stanford University, Stanford, California, 1967.
23. Horlock, J.H., Axial Flow Compressors, Butterworths, London, 1966.
24. Shepherd, D.G., Principles of Turbomachinery, The MacMillan Company, New York, 1956.
25. Pfeifer, G.D., "Aircraft Engine Icing Technical Summary," AGARD Conference Proceedings, AGARD-CP-236, pp. 9-1 to 9-17, April, 1978.
26. Bongrand, J., "Etude Theorique et Experimentale de L'influence de Divers Parametres Sur le Givrage D'un Profil," AGARD Conference Proceedings, AGARD-CP-236, p. 10-1, April, 1978.
27. Soo, S.L., "Boundary Layer Motion of a Gas-Solids Suspension," Proceedings of Interaction Between Fluids and Particles, pp. 50-63, Instn. Chem. Engrs., London, October, 1961.
28. Boysan, F. and Swithenbank, J., "Spray Evaporation in Recirculating Flow," Presented at 17th International Symposium on Combustion, Leeds, 1978.
29. Wallis, G.B., One-Dimensional Two-Phase Flow, pp. 376-377, McGraw-Hill, New York, 1969.
30. Wennerstorm, A.J., "On the Treatment of Body Forces in the Radial Equilibrium Equation of Turbomachinery," Air Force Aero Propulsion Laboratory, Report No. ARL 75-0052, April, 1974.
31. Evans, R.L., "Some Turbulence and Unsteadiness Effects in Turbomachinery," pp. 485-516 in Turbulence in Internal Flows, edited by S.M.B. Murthy, Hemisphere Publishing Corporation, Washington, 1976.
32. "Through-flow Calculations in Axial Turbomachinery," Advisory Group for Aerospace Research & Development, Conference Proceeding, AGARD-CP-195, October, 1976.
33. Taylor, E.S., Dimensional Analysis for Engineers, Clarendon Press, Oxford, 1974.
34. Masters, K., Spray Drying, p. 41, John Wiley & Sons, New York, 1976.
35. Ibid, p. 294.

36. Ingebo, R.D., "Vaporization Rates and Heat-Transfer Coefficients for Pure Liquid Drops," NACA TN 2368.
37. Lieblein, S., "Loss and Stall Analysis of Compressor Cascades," Jr. of Basic Engineering, Transaction of the ASME, September, 1959.
38. Zucrow, M.J. and Hoffman, J.D., Gas Dynamics, Vol. 1, pp. 55-57, John Wiley & Sons, New York, 1976.
39. Watanabe, I., Thermodynamics, p. 55, Kyoritsu Publishing Company, Tokyo, 1968.
40. Bosnjakovic, F. and Blackshear, P.L., Technical Thermodynamics, p. 2, Holt, Rinehart and Winston, New York, 1965.
41. Keenan, J.H. and Keyes, F.G., Thermodynamic Properties of Steam, John Wiley & Sons, New York, 1936.

DATE
ILME
—8